USE OF A CONTINOUS STIRRED TANK REACTOR FOR THE STUDY OF AQUEOUS AEROSOL CHEMISTRY

Thesis by

Carol Leslie Jones Adkins

In Partial Fulfillment of the Requirements

for the Degree of

Doctor of Philosophy

California Institute of Technology

Pasadena, California

1988

(Submitted August 13, 1987)

ACKNOWLEDGEMENTS

I want to thank my advisors, Professors John Seinfeld and Rick Flagan, for their help and guidance during my stay at Caltech. Between the two of them, they make a really "crack" advising team! In particular, I want to thank them for taking the time to talk to me and raise my spirits when I thought the equipment would never work and I was doomed never to graduate. This project has been a long one but I've learned quite a bit about fixing broken instruments, the necessity of a good calibration and robust data inversion routine, and most importantly, the value of "hanging-in-there."

I received financial support in the form of a National Science Foundation fellowship and a Haagen-Smit/Tyler fellowship. Financial aid was also received in the form of a grant from the US Environmental Protection Agency. For this help I am grateful.

I've had the pleasure of sharing a lab with a group of great folks — Gidi Sageev Grader, Brian Wong, Yiannis Levendis, Ranajit Sahu, Jin Jwang Wu, Pratim Biswas, and Hung Nguyen. We've had some good times crooning tunelessly to the radio, getting crazy late at night in the lab, planning equipment schedules, talking about this and that, etc. The technical discussions I've had with Professor Jim Morgan, Mark Cohen, and Sonia Kreidenweis-Dandy have been a great help in understanding the rather murky subjects of mixing rules and activity coefficients. It's always nice to discover that you aren't the only person who finds a "scientific topic" to be, rather, a philosophical issue. Sharing an office and some good times with Jennifer Stern has been a real pleasure. I also want to acknowledge the help offered by Leonard Montenegro, John Lee, and Tom Dunn in dealing with the electrical side of my equipment.

My life at Caltech would have been considerably less fun if it hadn't been for the support and friendship of Malina Hills, Julia Lester and Jackie Shanks.

Our "ladies' lunches" every Thursday at the Athenaeum have been a regular fixture in my life these last several years. The subject of conversation was typically untechnical and always interesting.

My family has always been very important to me. The regular letters from my grandmothers and the weekly calls from the folks made me feel wanted, cared for and loved. Mom, Daddy, Sharon, Larry (and the dogs, of course) — thanks for everything!

Finally, and most importantly, I want to thank my husband, Doug Adkins. Meeting and marrying Doug was a side benefit of coming to Caltech that I hadn't expected when I accepted admission! It's unfortunate that we didn't finish our theses at the same time, but he's waited patiently, a thousand miles away in New Mexico, while I finished my work. Now we can finally start our life together.

ABSTRACT

Atmospheric aerosol chemistry is important in areas ranging from urban air pollution to cloud formation. It has long been supposed that droplet-phase reactions account for a significant fraction of the atmospheric conversion of SO_2 to sulfate. Among such reactions is the manganese-catalyzed aqueous-phase oxidation of SO_2. Whereas the role of aqueous phase SO_2 oxidation in the dilute solutions characteristic of fog and cloud droplets (diameter $> 10\ \mu m$) has been reasonably well established, the role of comparable reaction in submicron aerosols is uncertain. In this thesis a reactor system is developed to carry out gas-aerosol reactions under humid, ambient-like conditions. The apparatus consists of a continuous stirred tank reactor (CSTR) in which the growth of the aqueous aerosol is measured. Absence of mass transfer limitation, coagulation, and nucleation ensure that particle growth is direct evidence of reaction. Special care is taken to minimize size biasing of the aqueous aerosol in the electrostatic classifier used to measure the reactor feed and effluent distributions. Aerosol behavior in the reactor is modeled assuming an ideal CSTR and, given the solution thermodynamics and equilibrium chemistry, the effluent distribution can be predicted using one of the proposed reaction rate mechanisms.

Experiments were performed using a pure $MnSO_4$ or a $MnSO_4$-Na_2SO_4 mixture feed aerosol. The relative humidity ranged from 86 to 94% and 0.1 ppm $< p_{SO_2} <$ 50 ppm. The slow, approximately constant reaction rate of Bronikowski and Pasiuk-Bronikowska (1981) ($R \sim 2 \times 10^{-4}\ M\,s^{-1}$) was found to best predict the observed growth over the entire range of operating conditions. The various rate expressions proposed for this system in the literature resulted in varying estimates of growth. When reactor conditions were similar to those at which the rate expression was determined, the agreement between the predicted and observed distributions improved. This indicates that use of a rate expression beyond its specified range may result in erroneous predictions.

TABLE OF CONTENTS

LIST OF FIGURES

LIST OF TABLES

CHAPTER 1
INTRODUCTION

Heterogeneous atmospheric reactions are currently recognized as a significant contributor to the overall chemistry of SO_2 in the atmosphere (e.g., Hidy (1982), McMurry and Wilson (1983)). However, the study of these reactions in the atmosphere is complicated by the influence of transport and mixing processes, particle deposition, and gas-phase reaction chemistry. To date, the most common method of assessing the relative importance of heterogeneous reactions with respect to overall atmospheric chemistry has been via theoretical modeling (e.g., Hoffmann and Jacob (1984), Saxena and Seigneur (1987), Middleton et al. (1982), Pilinis and Seinfeld (1987)), in which various reaction rate expressions, initial concentrations, and source emission rates are set for the species of interest.

The kinetic rate expressions governing heterogeneous reactions are typically determined by either droplet- or bulk-phase studies. In this context droplets refer to particles ranging in size from cloud droplets ($\sim$ 20 μm diameter) to aqueous aerosol particles (0.1 $-$ 1.0 μm diameter). Detailed rate expressions are difficult to obtain from droplet-phase studies because of the increased complexity, and thus uncertainty, associated with performing these experiments. Each piece of equipment required to generate, react, and measure the aerosol must be characterized and its operating conditions controlled — droplet-phase studies are by nature large experiments. Indeed, one need only observe the range of concentrations, pH, ionic strength, etc., studied in the bulk as opposed to droplet-phase studies to conclude that control and variability of experimental conditions are more readily achieved in classical bulk-phase kinetic experiments (Penkett, 1986). On the other hand, the applicability of bulk-phase studies to atmospheric droplet chemistry, particularly to that of aerosols, may be compromised because of the presence of microphysical

processes (Jaeschke, 1986).

Aerosols, fogs and clouds that participate in heterogeneous reactions are typically aqueous, or have an aqueous layer around a solid core. Consequently, the droplets are sensitive to changes in relative humidity — whether these changes occur in the ambient or experimental atmosphere, or in the instruments used to study the system. It is, in fact, the maintenance and control of humidity in the experimental system that is the chief cause of much of the uncertainty associated with aqueous droplet-phase reaction rate studies. The ambient relative humidity and particle size determine the equilibrium concentration of solute in an aqueous droplet, and thus affect the rate of any heterogeneous reactions occurring. If droplet size is being measured, the system relative humidity must be maintained within the measuring instrument or significant size biasing is possible.

This thesis will address the study of heterogeneous reactions in the aerosol phase. Atmospheric models that include heterogeneous reactions include reaction rate expressions that are presumed to adequately represent the chemistry occurring. Therefore, the approach used in this work was not the determination of yet another reaction rate expression, but rather an assessment of the ability of the proposed rate expressions to correctly predict the extent of reaction. The methods typically used to study aerosol-phase reaction are determination of the composition of collected filter samples, measurement of the reactant gas consumption, or measurement of particle growth. Collected filter samples are particularly prone to artifact formation, yet afford the only available opportunity to determine the average aerosol composition. The measurement of reactant gas consumption requires sensitive instrumentation and adequate time/space resolution in the reactor; however, it is possible to follow very slow reactions using this method. If particle growth is used to determine the extent of reaction, it is necessary to ensure that condensation is the only mechanism by which growth occurs. Growth measurements are susceptible to size biasing in the measurement instruments, and sufficient time for

growth must be allowed. Particle growth is a parameter often measured in field studies and was therefore used as evidence of heterogeneous reaction in this study.

A reactor system was designed and constructed for the purpose of measuring particle growth as a result of reaction. A well-characterized, ideal continuous stirred tank reactor with a mean residence time of one hour is the basis of the system. Special attention was focused on the aerosol measurement instruments and care was taken to minimize size biasing as a result of humidity changes within the instrument. A model of the aerosol behavior within the reactor was used to predict the reactor effluent size distribution given the input feed distribution and a proposed reaction rate expression. These calculations required modeling the solution thermodynamics and chemical equilibrium. The measured effluent aerosol from the reactor and the results predicted by the various proposed rate expressions were compared in order to assess whether or not the rate expression adequately described the reaction system.

The chemical system studied in this work is the aqueous-phase, manganese-catalyzed oxidation of SO_2 to S(VI). There have been a number of studies done on this system, both in the aerosol and bulk phase; however, the form of the reaction rate expression is still uncertain. Comparing the reactor aerosol size distributions predicted by the various rate expressions to those experimentally measured provides the ability to assess the compatibility of the theories and the measurements under realistic atmospheric conditions.

The apparatus constructed for the aerosol growth experiments is described in Chapter 2. Calibration and characterization of the various components of the experimental apparatus are discussed in Chapter 3. A review of the literature concerning the S(IV)-manganese reaction system, both aerosol and bulk phase, is the subject of Chapter 4. Chapter 5 contains the measured size distributions under a variety of conditions along with a discussion of mass transfer limitation of the observed reaction rate. The predicted aerosol size distributions, including the

chemistry and thermodynamics used in the calculations, are presented in Chapter 6. Finally, a summary and recommendations for future work are given in Chapter 7.

CHAPTER 2
DESCRIPTION OF THE REACTOR SYSTEM

The reactor system described in this chapter was designed to measure the growth of a humid aerosol when exposed to a reactive gas in a controlled atmosphere. The basic design was patterned after the continuous stirred tank reactor system described by Crump et al. (1983a) and is shown in Figure 2.1. While the system described here was used to measure the growth of a liquid $MnSO_4$ aerosol in an SO_2-containing atmosphere, this apparatus could be used to study growth in a variety of humid aerosol/gas systems with minor modification, e.g., the $CuSO_4/SO_2$, $MnCl_2/SO_2$ or $(NH_4)_2SO_4/NO_2$ systems. Naturally, the gas-phase analysis instrument will have to be specific to the gas contaminant being studied. Also, if the aerosol of interest does not deliquesce into a liquid solution drop (e.g., if the solute forms a colloidal suspension when rehumidified) then the method of aerosol generation will have to be modified.

Aerosol is generated using an atomizer of the type described by Liu and Lee (1975). A liquid solution is fed to the atomizer by one of two Sage Instruments (model 355) syringe pumps. The feed lines from both syringes are joined at a tee prior to entering the atomizer. In this way, there is no interruption of the liquid flow — when one syringe is finished delivering the solution, the second pump is switched on. Both syringe pumps have been calibrated and set to deliver 0.25 cm^3/min liquid to the atomizer. During calibration it was found that once 40 ml of fluid had been delivered from a 60 ml syringe, the pump could not maintain a constant liquid flowrate. Therefore, the syringes are changed once 20 ml of solution remain. Air at $2.55 \times 10^5\,Pa_g$ (37 psig) from a clean air generation system (see Figure 2.2) passes through an 0.029 cm (0.0115 inch) orifice and atomizes the liquid solution. Approximately 3 ℓpm of air flows through the orifice at this pressure.

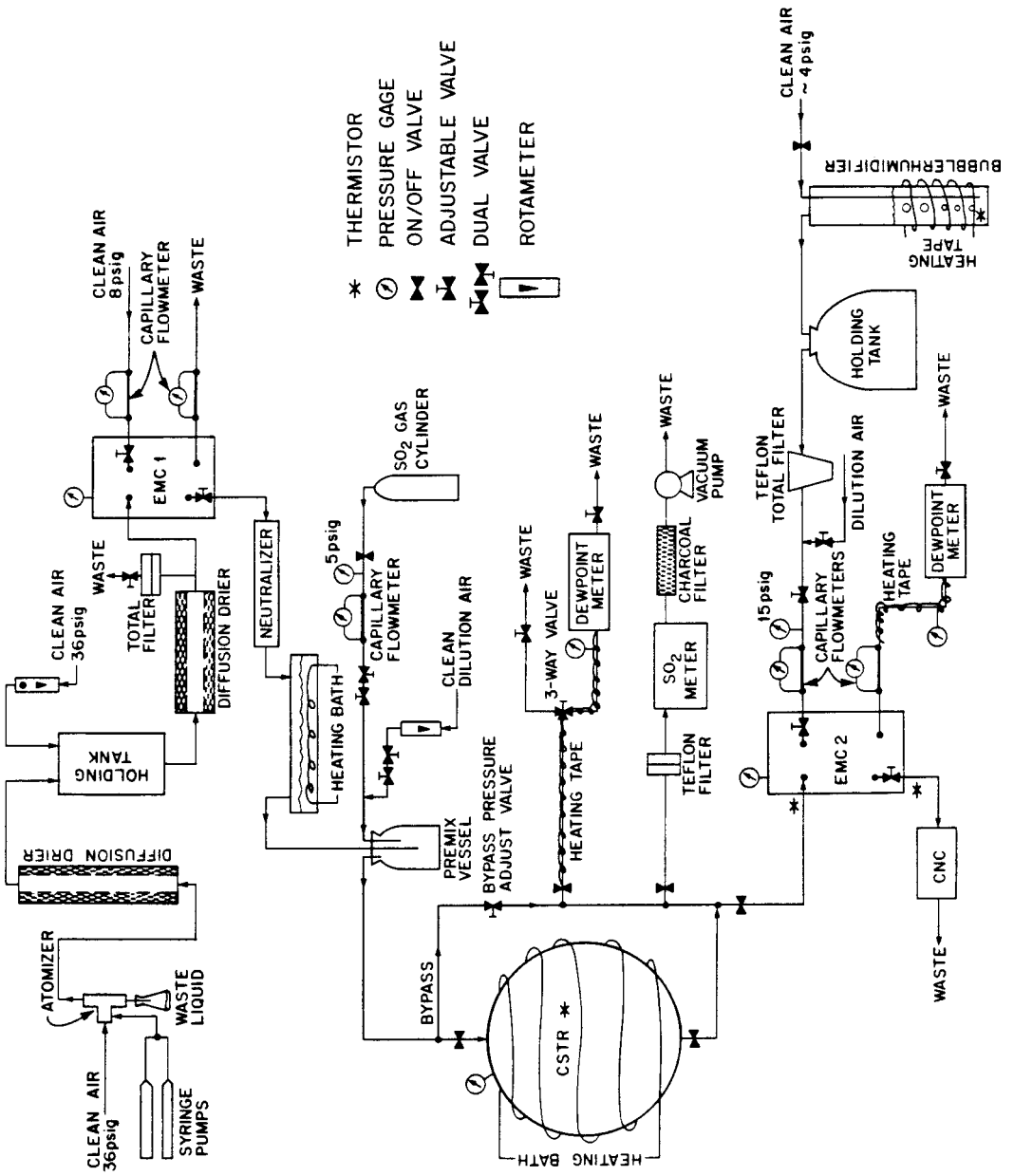

Figure 2.1 The reactor system. (14.7 psi = 1.013×10^5 Pa)

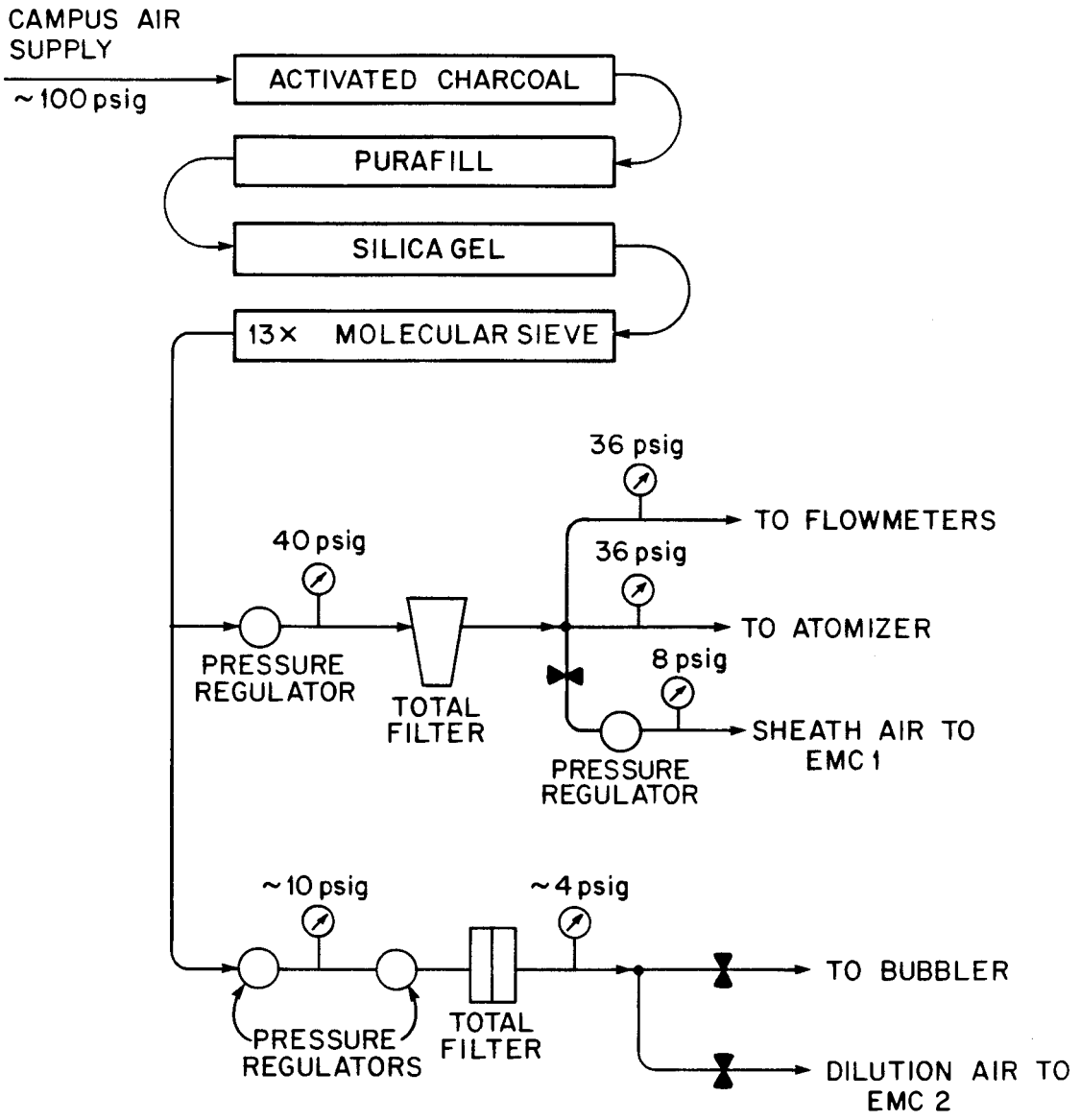

Figure 2.2 The air cleaning system. (14.7 psi = 1.013×10^5 Pa)

Waste liquid, formed by aerosol impaction on the atomizer wall, is collected in a flask below the atomizer. A length of stiff bus wire is placed in the atomizer drain tube to eliminate liquid plugs by breaking the surface tension.

After leaving the atomizer, the wet aerosol and humid air pass through a meter long diffusion drier where the air is dried. This air has a measured relative humidity of 10%. In order to smooth out any fluctuations in flow due to the syringe pumps, the air/particle mixture is fed to an 11 liter holding tank. It is possible to add dilution air at this point if it is desired. The aerosol then flows through a second diffusion drier (46 cm long) as it leaves the holding tank.

Because an atomizer generates a very broad, flat aerosol distribution, the aerosol is now sent to a TSI Model 3071 Electrostatic Classifier. This classifier (EMC1) is set and maintained at a constant voltage and constant flowrates during the course of an experiment. Approximately 2 of the 3 ℓpm of aerosol-containing air are fed to the classifier. The remaining volume is vented to the atmosphere after passing through a total filter. The sheath air for this classifier (10 ℓpm) comes from the clean air generation system and is metered using a calibrated capillary. The excess air from EMC1 is also metered using the pressure drop across a capillary. It is convenient to operate the classifier "balanced" — the sheath and excess flowrates being equal. Overall classifier pressure is measured using a Magnehelic differential pressure gage. In the classifier the aerosol flow passes through a ^{85}Kr neutralizer. Because the aerosol is charged with a Boltzmann equilibrium distribution, it also acquires a mobility distribution. The mobility of a particle is a function of its size and charge. For a given set of operating conditions, a known mobility range will be allowed to pass through the classifier. A set of discrete diameters, corresponding to the same mobility but to different particle charges, make up the output distribution. Thus, EMC1 serves not only to sharpen the aerosol size distribution, but to reduce the overall number concentration from about 10^6 to 10^4 particles/cm^3 as well. Given sheath, excess, and aerosol flowrates of 10, 10, and 2 ℓpm, respectively, the

voltage is set so as to give particles (corresponding to a single charge) that are approximately 0.15 μm in diameter when humid.

All valves, vessels and lines following EMC1 are either stainless steel, glass, or teflon. Deposition of charged particles in teflon lines is significantly higher than that predicted solely on the basis of diffusional deposition (Liu et al., 1985). Because the aerosol leaves EMC1 charged, a significant number of particles would be lost in the lines if the particles are not decharged. Therefore, the aerosol flows through a second ^{85}Kr neutralizer immediately after leaving the classifier and once again acquires a Boltzmann equilibrium distribution of charge. Since a higher fraction of the particles are now neutrally charged, particle loss to the walls is reduced.

The aerosol is humidified by passing the flow over a pool of water. A heating bath is used to circulate constant temperature water through coils in the water to maintain the pool at a desired temperature. Additional details about the humidifier can be found in Crump (1983). As the air reaches saturation, the aerosol deliquesces and becomes liquid. The humidity in the reactor downstream is controlled by the temperature of this humidifying water bath, the temperature of the reactor and the subsequent addition of dilution air. All lines, valves, and vessels following the humidifier are insulated.

SO_2 is added to the humidified aerosol in a 1 liter premix vessel. Dilution air can also be added to this vessel for humidity control. The SO_2 used in these experiments comes from either a 10, 100, or 1000 ppm gas cylinder supplied by Scott-Marrin, Inc. depending upon the final reactor concentration desired. The accuracy of the SO_2 concentration analysis is listed as $\pm 2\%$ in each case. A calibrated capillary is used to meter the gas.

After leaving the premix vessel, the aerosol is sent either to the measuring instruments for an analysis of the reactor feed, or to the reactor and then the instruments. The reactor is a spherical 118 liter, pyrex vessel. It has five ports —

one on top, three on the upper half and one on the bottom. All ports are fitted with teflon flanges. The feed line, effluent line and a temperature probe are introduced in the radial side ports. Reactor pressure is measured at the bottom port. Constant temperature water from a heating bath is run through copper coils that are wound loosely about the vessel to help maintain a constant temperature. The reactor is supported in a plywood box lined with 1 inch thick styrofoam. The styrofoam has been painted black. The upper half of the reactor is completely enclosed while the lower half is lined with glass wool and painted styrofoam. The plywood enclosure serves three purposes. First, it helps maintain a constant reactor temperature. Second, it protects the reactor. And third, it ensures that the reaction of interest will not be influenced by any potential photochemistry. No mechanical mixing devices are used. Crump et al. (1983b) experimentally verified that for a 2 ℓpm flowrate this vessel behaves like an ideally mixed continuous stirred tank reactor. Relying only on convective mixing has the added advantage that no additional deposition surfaces are present. The ideal behavior of the reactor was confirmed by monitoring the approach of the effluent humidity to the feed humidity as a function of time. Figure 2.3 shows the approach to steady state characteristic of an ideal CSTR. After $\sim$ 6 hours the effluent value was 99% of the feed value of 92%.

The reactor feed or effluent is divided into three branches for analysis of the SO_2, water content and the aerosol size distribution. Approximately 0.56 ℓpm are drawn through a 47 mm teflon filter into a Monitor Labs Model 8850 Fluorescent SO_2 Analyzer. This instrument uses a pulsed fluorescence technique to determine the SO_2 concentration. The teflon filter is changed often and the aerosol loading has no discernible effect on the SO_2 reading. This instrument typically measures SO_2 concentrations less than 10 ppm. However, it has been reset and calibrated to measure between 0.1 and 100 ppm within $\pm$5%. A high relative humidity ($\leq$ 95%) has no noticeable effect on the instrument; the measured SO_2 concentration is within several percent of the expected value.

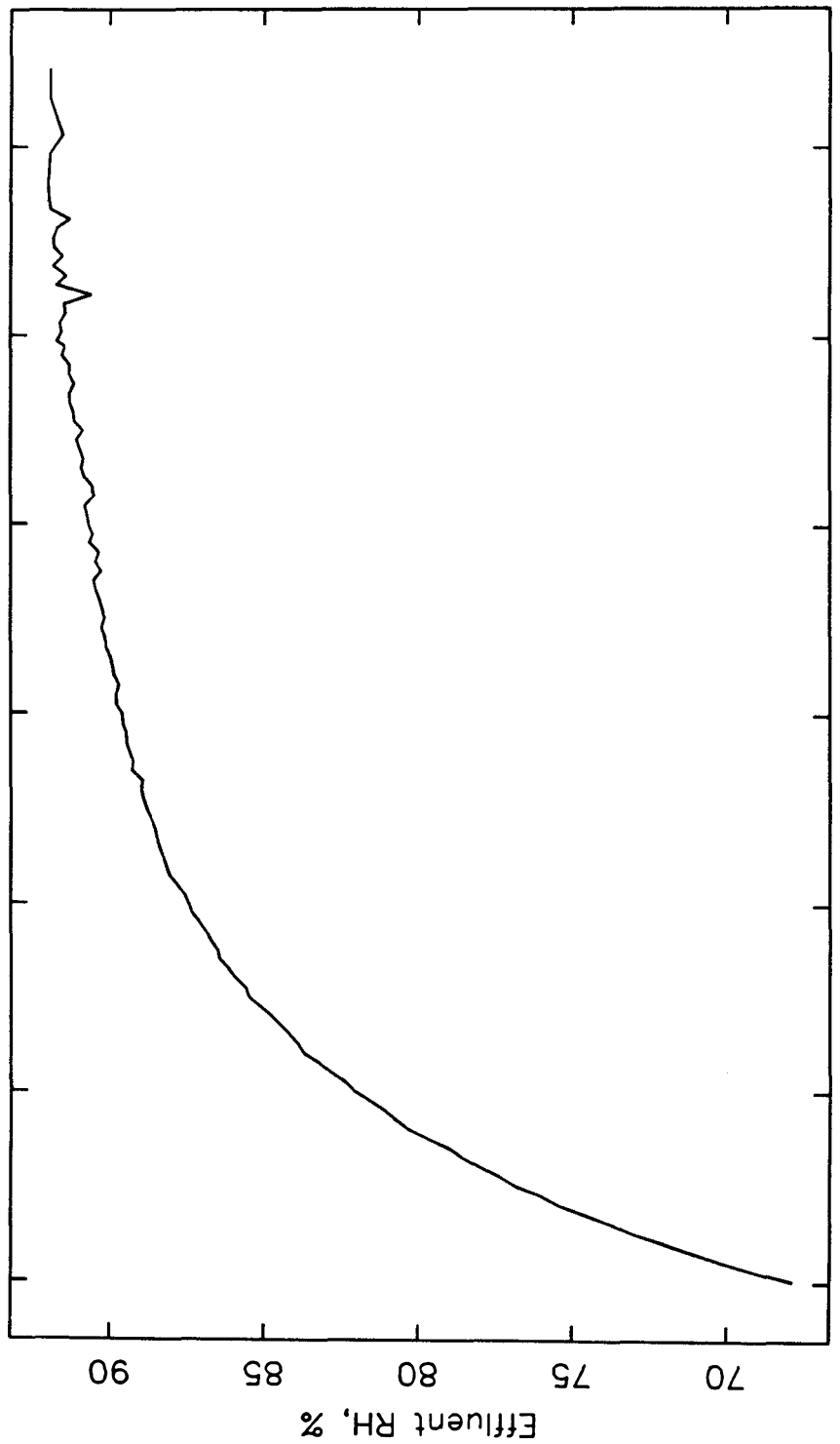

Figure 2.3 Reactor effluent humidity as a function of time. Feed humidity = 92%.

Of the remaining flow to be analyzed, about 1 ℓpm flows to an EG&G 911 Dew-All Digital Humidity Analyzer. This instrument can be bypassed by switching a three-way valve so that the waste flow is fed to the exhaust lines. While the reactor system is coming to steady state, the valves to all the measuring instrument lines are closed. Only the valve to the waste line remains open. When steady state is reached, the instrument line valves are opened and the three-way valved switched to pass the flow to the dew point meter. In this way, instrument exposure to the corrosive atmosphere is minimized. Heating tape has been wrapped around the instrument feed line to lower the humidity of the air mixture. The EG&G 911 meter does not measure humidity, but rather the dew point temperature, using the chilled mirror/condensation method. This method is particularly suited to a "dirty" environment and high moisture content. The instrument has been calibrated and it is estimated that the error in relative humidity is less than $\pm 1\%$. The meter also has an ambient temperature probe that is currently used to measure the temperature in the reactor. Again, the probe has been calibrated and is accurate to within $\pm 0.03°C$. The pressure of the system immediately upstream of the dew point meter is measured using a Magnehelic pressure gage.

Finally, the remaining reactor effluent or feed volume is sent to a TSI Model 3071 Electrostatic Classifier (EMC2) so the aerosol size distribution can be measured. This classifier is set up identically to EMC1 except that the sheath, excess, and sample flowrates are 7, 7, and 0.3 ℓpm, respectively. Instead of remaining at one fixed voltage, the center rod voltage is scanned from 0 to 10000 volts in order to generate a "mobility distribution," which can later be inverted to a size distribution. Aerosol that passes through the classifier at each voltage is counted using a TSI Model 3020 Condensation Nuclei Counter (CNC). This instrument can measure particles down to 0.02 μm in diameter at concentrations greater than 0.1 particles/cm^3. These minimum conditions are easily satisfied by the reactor aerosol. Also, because the aerosol number concentration at each voltage is less than 1000 particles/cm^3, the CNC operates in "count" mode — measuring the particle

concentration directly by counting the frequency with which particles pass through the sensing chamber.

Water vapor has the potential to introduce error into the particle counting because it dilutes the butanol in the CNC. However, Agarwal and Sem (1980) demonstrated that when a CNC was operated in the auto-drain mode (butanol is automatically replaced every 4 hours) at 65% relative humidity and less than 1000 particles/cm^3, there was no error in the measured concentration after 24 hours of continuous operation. While the current reactor system is operating at considerably higher humidities (> 85%), the average scan time of 2 hours adds less water to the system than does operation at 65% for 4 hours. Also, the butanol is changed before every voltage scan. Therefore, the assumption that relative humidity does not affect the CNC's counting capability is justified in this case.

When measuring the size of a humid aerosol, it is possible that the sizing instrument will bias the distribution. Relative humidity changes within the instrument can be caused by, for example, hygroscopic filters, pressure changes in nozzles, and heating due to electric dissipation (see Appendix A). Because an electrostatic classifier requires the addition of sheath air, the potential for size biasing does exist. The problem, however, is easily remedied by humidifying the sheath air to the same humidity as in the CSTR. The glass fiber total particulate filters supplied with the classifier for use in the sheath and excess air lines are also extremely hygroscopic and were removed. In the reactor system the sheath air is humidified by bubbling it through a water column. To counter the large evaporative cooling effect involved in humidifying 7 ℓpm of air, the water column is heated using a heating tape, which is controlled to maintain approximately room temperature. The humidified air then flows to a 50 liter tank to dampen some of the flow oscillations produced by the bubbles. Submicron water particles produced by the bursting bubbles are filtered out as the air passes through a teflon total filter. At this point, just prior to entering the classifier, the pressure of the air is checked

and any dilution air necessary is added. The capillary flowmeter is calibrated for an initial pressure of 1.03×10^5 Pa_g (15 psig).

The excess flow from the classifier is metered using a calibrated capillary. The air flow is heated to reduce its humidity, and then sent to an EG&G Model 880 Dew Point Hygrometer. This is a dew point meter of the same type as the newer Model 911. The system pressure is measured immediately upstream of the dew point meter. This dew point meter was calibrated against the model 911 in order to assure that the two instruments read the same dew point temperature given air with the same moisture content.

As can be seen in Figure 2.1, thermistors have been placed at various points about the system — in the CSTR, at the aerosol inlet to EMC2, at the aerosol outlet of EMC2, and in the bubbler humidifier. Room temperature is also measured using a thermistor. As mentioned above, the bubbler humidifier temperature is referenced to room temperature to control the water column temperature. The output from these thermistors is fed to a Digital PDP-11 computer equipped with a Sinetrac Series Model ST-LSI A/D-D/A 12-bit Computer Peripheral board. In addition, the voltage output from the two dew point meters, the EG&G 911 ambient temperature sensor output, and the voltage corresponding to the SO_2 concentration from the SO_2 analyzer are also monitored by the computer.

CHAPTER 3
CHARACTERIZATION OF THE REACTOR SYSTEM

Before an experimental system can be used to measure an unknown, it is first necessary to understand how the system responds to a known input. There are four major areas of measurement in the reactor system — temperature, relative humidity, SO_2 content, and particle size. Instruments used in the reactor system that require special attention are thermistors, dew point meters, an SO_2 analyzer, and electrostatic mobility classifiers. The calibration/characterization of these instruments will be discussed in this chapter.

§3.1 Thermistors

Figure 2.1 shows where thermistors are located in the reactor system. Each thermistor is sheathed in a stainless steel tube. Four thermistors were calibrated — thermistor #4 (room temperature), thermistor #5 (EMC2 aerosol inlet temperature), thermistor #6 (EMC2 sample outlet temperature), and the EG&G 911 ambient temperature sensor (CSTR temperature). A Neslab Model RTE-8DD digital refrigerated circulating bath was used for the calibration. The bath's operation specifications claim a temperature stability of $\pm 0.02°C$ which was consistent with the variation observed during the calibrations. The thermistors were placed in the center of the bath reservoir in close proximity, but not touching. A thermometer (-1 to 51°C with 0.1° divisions) was also placed in the reservoir. The voltage output of each thermistor was fed to the A/D board of a PDP-11 computer. In this way any voltage offset associated with the computer was included in the calibration. Calibration data were taken for the range 15 to 30°C. Once the bath temperature and thermistor voltages were stable, thermistor voltages were sampled for 30 minutes by the A/D and the bath thermometer readings recorded. The voltage

Table 3.1

Calibration Results

Instrument	Formula	Uncertainty Estimate
Room temperature thermistor # 4	$T = 9.94V + 0.144$	$\pm 0.04°C$
EMC2 inlet temperature thermistor # 5	$T = 9.91V + 0.122$	$\pm 0.04°C$
EMC2 outlet temperature thermistor # 6	$T = 9.88V + 0.159$	$\pm 0.04°C$
CSTR temperature EG&G 911	$T = 9.99V - 39.55$	$\pm 0.04°C$
Dew point temperature EG&G 911	$T_{DP} = 10.21V - 40.54$	$\pm 0.03°C$
Dew point temperature EG&G 880	$T_{DP} = 16.41V - 42.84$	$\pm 0.15°C$
Sheath flowrate EMC1	$Q_{std} = 1.670\Delta P_c + 4.761$	$\pm 2\%$
Excess flowrate EMC1	$Q_{std} = 2.243\Delta P_m + 4.903$	$\pm 2\%$
Sample flowrate EMC1	$Q_{std} = 6.94V - 14.92$	$\pm 1.3\%$
Sheath flowrate EMC2	$Q_{std} = 1.29\Delta P_c + 3.170$	$\pm 0.8\%$
Excess flowrate EMC2	$Q_{std} = 14.85\Delta P_m + 2.670$	$\pm 0.8\%$
SO_2 Monitor 10-100 ppm, 10 ppm scale	$ppm = 0.0392 + 10.041V$ $-0.0734\mathrm{V}^2 + 0.00659\mathrm{V}^3$	$\pm 5\%$
SO_2 Monitor 0.1-2.5 ppm, 0.25 ppm scale	$ppm = 0.294V - 0.053$	$\pm 5\%$

data were time-averaged and a linear least-squares regression performed on the temperature versus voltage data for each thermistor. The calibration results are presented in Table 3.1. The voltage standard deviation was approximately ± 0.004 V, corresponding to a temperature variation of $\pm 0.04°C$. Inasmuch as the thermometer used had 0.1° divisions, 0.03°C was the resolution one would expect. The importance of the absolute accuracy of the thermometer will be discussed in the next section.

§3.2 Dew Point Meters

Calibrating the dew point meters posed a more difficult problem than calibrating the thermistors. The EG&G dew point meter uses the chilled mirror dew point condensation method and the air being measured has to flow over the mirror/temperature sensor. In order to "balance" the optical/thermal circuit in the meter, the mirror surface is heated to remove the condensate. At high humidity it is possible that the mirror condensate will not evaporate into the nearly saturated air. When this occurs, a large liquid drop forms on the mirror and dew point temperature readings are meaningless. This problem can be avoided if the air is heated prior to entering the sample chamber; the humidity of the air is lowered without affecting the moisture content. Better control is also achieved since the system responds more quickly to a change in the mirror temperature.

The possibility of using a saturated solution (e.g., the humidity over a saturated solution of $NH_4H_2PO_4$ at 25°C is 93%) to generate a standard of known humidity was considered. However, the idea was discarded primarily because of the flow needs of the sensor. Since using a known humidity standard was impractical, it was decided that the sensor would be calibrated for temperature. By removing a transistor from the cooling circuit, the sensor becomes a simple linear platinum resistance thermometer. Copper coils, through which 1 ℓpm air flowed, were placed in the reservoir of the Neslab circulating bath. The complete sen-

sor housing assembly was removed from the back of the EG&G 911 hygrometer, placed in a plastic container, connected to the air line, and submerged in the bath reservoir. In order to decrease the time required for the sensor housing to reach a steady-state temperature, the plastic container was filled with brass Swagelok ferrules. The same thermometer was used to measure the bath temperature as was used in the thermistor calibration. The 0 to 10 V output from the EG&G 911 meter, corresponding to the "dew point" temperature, was monitored by the computer. Bath temperatures ranging from 15 to 30°C were set and 5 to 8 hours were allowed for the system to reach thermal equilibrium for each setting. The voltages for each bath temperature were averaged together and then a linear least-squares regression was performed on the data. The resulting calibration equation for the EG&G 911 dew point temperature is given in Table 3.1. The standard deviation for the voltages was, in all cases, less than 0.001 V. This value is less than the $\pm$ 0.0024 V resolution of a 12-bit A/D, which corresponds to a temperature change of 0.02°C. However, because the thermometer resolution is only $\pm$ 0.03°C, this more conservative estimate of the uncertainty was assumed.

The EG&G 911 sensor was now calibrated for temperature and the relationship between this calibration and the desired dew point temperature calibration had to be determined. Perhaps the major difference between these two measurements is that the dew point measurement is a dynamic, interactive process involving the heating and cooling of the sensor, while simple temperature measurement is a static process. There are several potentiometers in the cooling control loop that can be adjusted to vary 1) the current delivered to the cooler in the sensor, 2) the gain in the control circuit, and 3) the light reduction necessary before the cooler current is cut (i.e., the thickness of the condensate layer on the mirror that interrupts the optical signal). In order to study the sensitivity of the dew point temperature determination to these parameters, humid air was passed to the hygrometer and its dew point measured. The potentiometers mentioned above were then scrambled, reset, and the dew point measured again. This was repeated five times, and each

time the same dew point temperature was reached. Therefore, it was assumed that the dew point temperature determination is relatively insensitive to the details of the condensate formation and the temperature calibration for the sensor was equivalent to the dew point temperature calibration.

Because the EG&G 880 dew point hygrometer would be used to match the moisture content in the excess air of the second classifier to that in the reactor as measured by the 911, the 880 was calibrated with respect to the 911. In other words, the EG&G 911 hygrometer would be a standard for the system. The model 880 hygrometer is an older, analog model of the 911. The principal differences between the two instruments are that the 880 sensor uses a nonlinear thermistor and the 880 circuits produce a "noisier" voltage output than the 911. Humid air was run through the EG&G 911 hygrometer and then directly into the 880 meter. Since measuring the dew point temperature is an equilibrium phenomenon, the first meter should have no effect on the second meter, since the moisture content of the air will remain constant. The flow lines leading to the instruments were wrapped with heating tape to lower the relative humidity of the air. The voltage output from the model 880 is on the order of tens of millivolts. Since the A/D voltage range is 0 to 10 V, an amplifier was used to raise the dew point meter voltage by a factor of 100. The amplifier was used during the calibration so that any voltage offset incurred with its use was included in the results. Again, the voltage output from both meters was monitored by the computer. Dew points ranging from 18 to 24°C were measured. The standard deviation of the EG&G 880 voltage was approximately ± 0.009 V. This result was approximately $2\frac{1}{2}$ times greater than the standard deviation of the 911 voltages and was due to the noisier circuits in the 880. A linear fit to the data was generated and is presented in Table 3.1. The voltage uncertainty corresponds to an uncertainty of 0.15°C in temperature.

There are several additional factors that could affect the dew point determination. The first of these factors is that insoluble contaminants on the mirror can

reduce the amount of light to the photoconductor. This does not change the final equilibrium temperature but can affect the rate of sensor cooling. Rebalancing the meter should compensate for this up to a point. Cleaning the sensor regularly eliminates the problem. The presence of soluble contaminants is a second factor that can affect the dew point temperature. Because the dew point is the temperature at which the condensate is in equilibrium with the water vapor, anything affecting this equilibrium will alter the dew point temperature reading. In the reactor system, soluble contamination is caused by aerosol particles impacting and dissolving into the condensate, and by the equilibrium established between the SO_2 and the condensate. Calculations estimating the effects of this contamination (see Appendix B) indicate that they are insignificant for the reactor system.

Another factor must be considered when using the measured dew point to calculate the relative humidity. This is pressure. If a dew point temperature measured at pressure P_1 is used to calculate the relative humidity at pressure P_2, a pressure correction must be made. Although the dew point is the *temperature* at which the air is saturated, it is more revealing to think of it as a measure of the water vapor *pressure*. Relative humidity is the ratio of the system water vapor to the saturated water vapor pressure at the system temperature T,

$$\mathrm{RH} \equiv \frac{P_{\mathrm{H_2O}}}{P^{sat}_{\mathrm{H_2O}}(T)} = \frac{P^{sat}_{\mathrm{H_2O}}(T_{DP})}{P^{sat}_{\mathrm{H_2O}}(T)}. \tag{1}$$

Assuming the vapor to be ideal, Dalton's law of partial pressures can be used to show the pressure dependence of the dew point temperature,

$$P_{\mathrm{H_2O}} = P^{sat}_{\mathrm{H_2O}}(T_{DP}). \tag{2}$$

The saturated water vapor pressure is represented by a fit to Antoine's equation,

$$\ln P^{sat}_{\mathrm{H_2O}}(T) = -\frac{5313.88}{T} + 20.988 \quad (\mathrm{mmHg}). \tag{3}$$

If it is assumed that no water vapor is lost and only the system pressure changes

from P_1 (case 1) to P_2 (case 2), then the following expressions can be written to describe the dew point temperature and relative humidity changes with pressure

$$\frac{1}{T_{DP_2}} = \frac{1}{T_{DP_1}} + \frac{1}{5313.88} ln\left(\frac{P_1}{P_2}\right) \tag{4}$$

$$\mathrm{RH}_2 = \left(\frac{P_2}{P_1}\right) \mathrm{RH}_1. \tag{5}$$

Figures 3.1 and 3.2 show the dew point temperature and relative humidity changes, respectively, to be expected for several pressure ratios ($\Delta P = P_2/P_1$). Pressure is monitored about the reactor system (see Figure 2.1 for the exact locations) so that the necessary corrections can be made. The ratio of pressure between two points in the reactor system typically fell between 1.0001 and 1.001, resulting in a 0.01% change in dew point and 0.1% in the relative humidity. While the correction is minor in this case, it is important to remember that the dew points might need to be corrected for pressure variations in an experimental apparatus.

The final factor to be considered is the possibility that the thermometer used in the thermistor and dew point temperature calibrations was not accurate. Even though the thermometer gave an exact reading of 0°C in an ice/water slurry, the temperature at 21 – 23°C (a typical dew point and system temperature range) could be off by several tenths of a degree. If this was true, then one would expect *all* temperatures to be off by the same amount. The correct dew point temperature would be $T'_{DP} = T_{DP} + \delta T$ and the correct system temperature $T' = T + \delta T$. For values of $(T - T_{DP}) = 0.5 - 2°\mathrm{C}$, $T = 22 - 24°\mathrm{C}$, and typical thermometer corrections of $\delta T = 0.1 - 0.5°\mathrm{C}$, the difference between $\mathrm{RH}(T, T_{DP})$ and $\mathrm{RH}(T', T'_{DP})$ is insignificant. Therefore, the exact accuracy of the thermometer is unimportant and the calculated relative humidity unaffected.

§3.3 SO_2 Analyzer

The Monitor Labs SO_2 analyzer comes from the factory with an operating

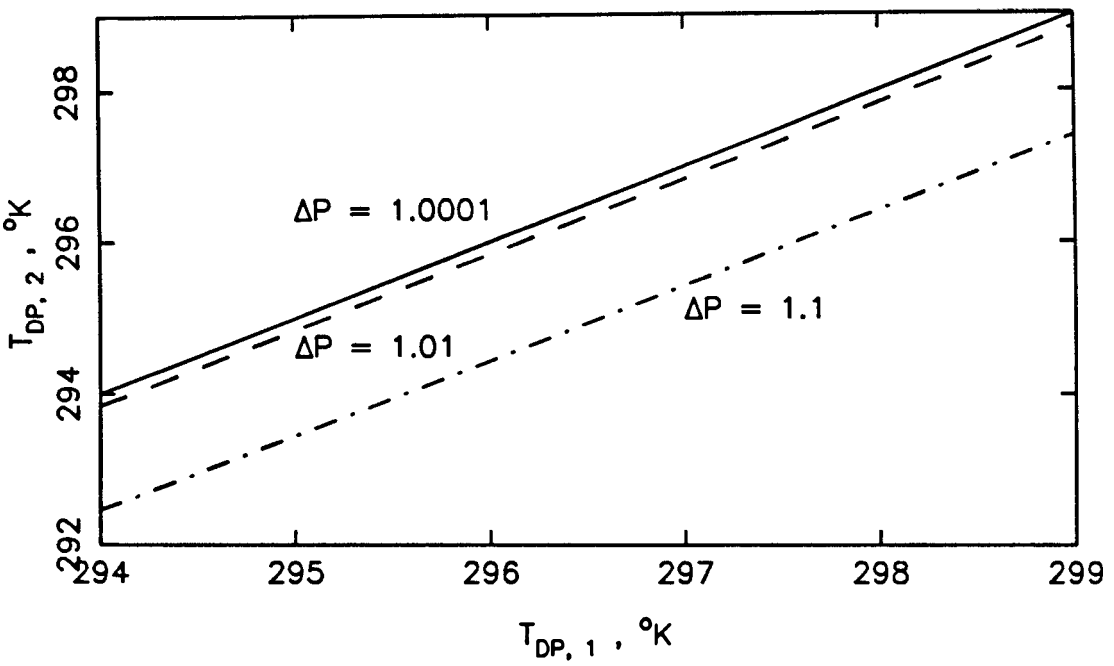

Figure 3.1 Dew point temperature shift as a result of a pressure shift.

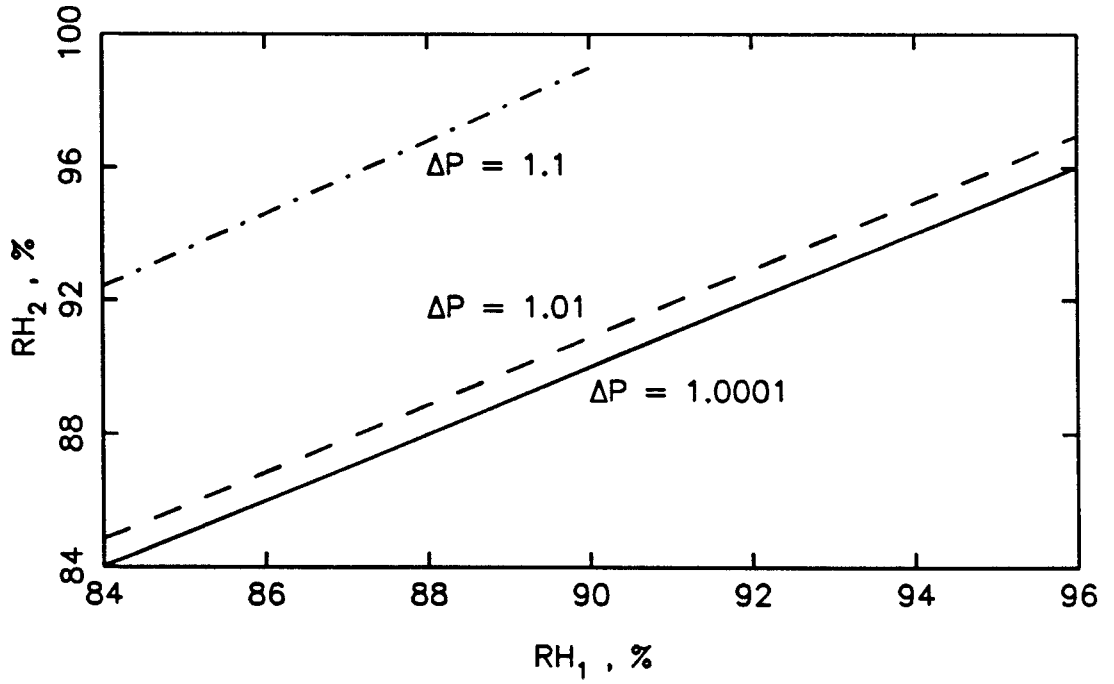

Figure 3.2 Relative humidity shift as a result of a pressure shift.

range of 0 to 10 ppm and a lower detection limit of 0.001 ppm. However, by adjusting the coarse SO_2 gain potentiometer, it was possible to raise the operating limit by a factor of 10. Because it was not known how this would affect the instrument's operation, the meter required calibration.

Before the SO_2 calibration could be done, a system of obtaining known SO_2 concentrations was constructed. The lab had three cylinders of SO_2 gas (10, 100, and 1000 ppm) and it was decided to make use of these. A flowrate of 0.56 ℓpm was required by the SO_2 meter and the range 0.1 to 100 ppm needed to be calibrated. Glass capillaries were used to meter the flow. These capillaries were calibrated at a set inlet pressure (3.45×10^4 Pa = 5 psig) and the time for the pressure in a known volume to go from P_1 to P_2 was measured. Capillary lengths of 5, 10, 20, and 30 cm were used and flowrates ranging from 0.01 to 1.0 ℓpm were obtained. The error associated with the capillary flow measurement was $\pm 1.5\%$.

With the calibrated capillaries, it was possible to calibrate the SO_2 analyzer. The 100 ppm $\pm 2\%$ SO_2 cylinder was used to calibrate the 10 to 100 ppm range and the 10 ppm $\pm 2\%$ cylinder for the 0.1 to 2.5 ppm range. The SO_2 gas was diluted with varying amounts of ultrapure air (< 0.001 ppm SO_2) and fed to the instrument. The 0 to 10 (100) ppm scale was calibrated for concentrations over 10 ppm and the 0.25 (2.5) ppm scale for those concentrations less than 2.5 ppm. A 0 to 10 volt output corresponding to the analog meter was fed to the computer. At least 30 minutes were allowed for the instrument to reach steady state after each concentration change. The results collected by the computer were averaged and fit to two curves — one for the high, 10 to 100 ppm, concentration range, and one for the low, 0.1 to 2.5 ppm, range. These equations are presented in Table 3.1. A conservative estimate of the error in the measured SO_2 concentration — a result of error in the generated "reference" concentration and voltage error in the data acquisition — is $\pm 5\%$. Each time the instrument was used for an experiment, the zero and span settings were adjusted to give the same voltage readings for 0,

10, and 100 ppm that were obtained in the calibration. Once this was done, the calibration curve was reproducible for all intermediate concentrations.

§3.4 Electrical Mobility Classifier (EMC)

Recently there has been considerable interest in using the electrical mobility classifier (EMC) to measure aerosol size distributions (e.g., Hoppel (1978), Liu et al. (1978), Hagen and Alofs (1983), Ten Brink et al. (1983), Kousaka et al. (1985), and Rader and McMurry (1986)). This is due to the recent development of better condensation nuclei counters (CNCs), and the relative ease with which a classifier can be operated and the data inverted. Classifiers are used for two purposes in the reactor system: first, to generate a nearly monodisperse dry feed aerosol and second, to measure the humid reactor feed and effluent aerosol distributions. It is for this second purpose that the classifier must be characterized. In this section the basic governing equations of the classifier will be reviewed, the data inversion method will be discussed, and the experimental calibration and verification will be presented.

§3.4.1 Instrument Description and Operation

A schematic of the electrical mobility analyzer is given in Figure 3.3. The device consists of a center rod at high negative voltage and a grounded concentric outer cylinder. The aerosol flow, Q_a, passes through a ^{85}Kr bipolar neutralizer before entering the classifier. The center rod is sheathed by a flow Q_c of clean air while the aerosol flows along the outer cylinder wall. Ideally, the flow between the concentric cylinders is laminar and there is no mixing between the aerosol and sheath air flows. As it flows down the length of the cylinder wall, a particle of mobility z_p (mobility will be defined later), carrying a positive charge, is attracted towards the negative voltage rod. Those aerosol particles having a specific mobility range, $\overline{z}_p + \Delta z_p$ to $\overline{z}_p - \Delta z_p$, will reach the center rod and flow through the slit

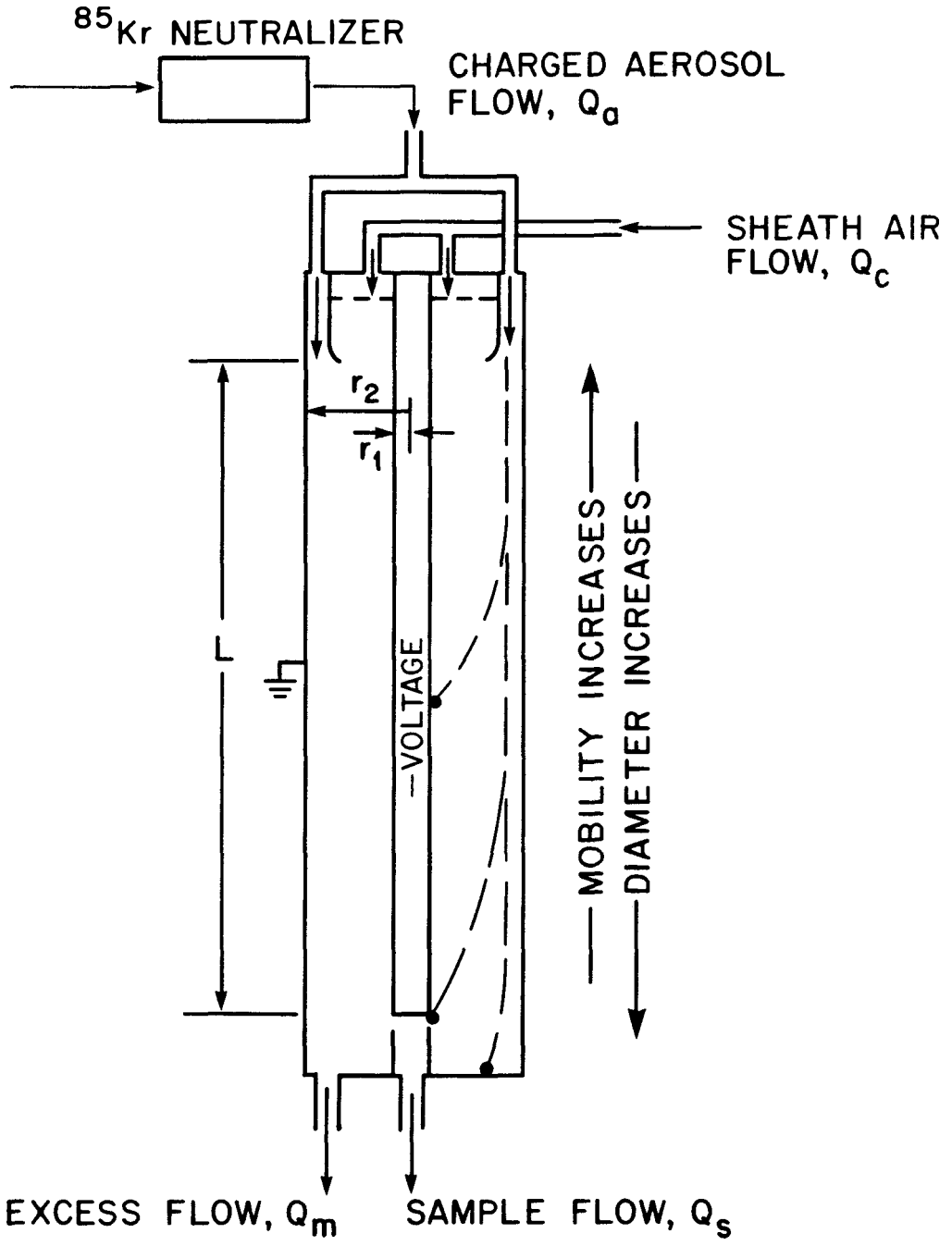

Figure 3.3 Schematic of an electrostatic mobility classifier (EMC).

at its base out of the classifier at a rate Q_s. The remaining, or excess flow (Q_m), passes out of the classifier and is used to measure the relative humidity in the instrument. Details of the various aspects of the operation of the classifier will be discussed later.

The equations governing the behavior of the classifier were developed by Knutson and Whitby in 1975. They assumed that 1) space and image charges are negligible, 2) the air flow is laminar and axisymmetric, and 3) particle diffusion is insignificant. Kousaka et al. (1985) found that particle loss in the classifier as a result of diffusion becomes significant only for particle sizes less than 0.015 μm. Conceptually, diffusion can be thought of as the "smearing" of a given particle mobility over a range of trajectories. Some of those particles expected to pass through the classifier will be lost because they either impacted on the rod before the slit or passed into the excess flow. Stolzenburg and McMurry (1985) and Kousaka et al. (1985) have studied classifier behavior when particle diffusion is a significant process.

Given that particle diffusion is indeed negligible, Knutson and Whitby's (1975) trapezoidal "classifier transfer function" (see Figure 3.4) describes the probability that an aerosol particle having mobility z_p will pass through the classifier and leave in the sample flow. The transfer function Ω is a function of the flowrates, the classifier geometry (rod length L, rod radius r_1, and cylinder radius r_2), and the center rod voltage V. The mean mobility is

$$\overline{z}_p = (Q_c + Q_m)/(4\pi\Lambda V), \tag{6}$$

where $\Lambda = L/\ln(r_2/r_1)$, and the $\frac{1}{2}$-width is given by

$$\Delta z_p = (Q_s + Q_a)/(4\pi\Lambda V). \tag{7}$$

Clearly, the sheath and excess flow "position" the mobility band pass while the sample and aerosol flows determine its shape. The EMC mobility resolution is a function only of flowrate such that,

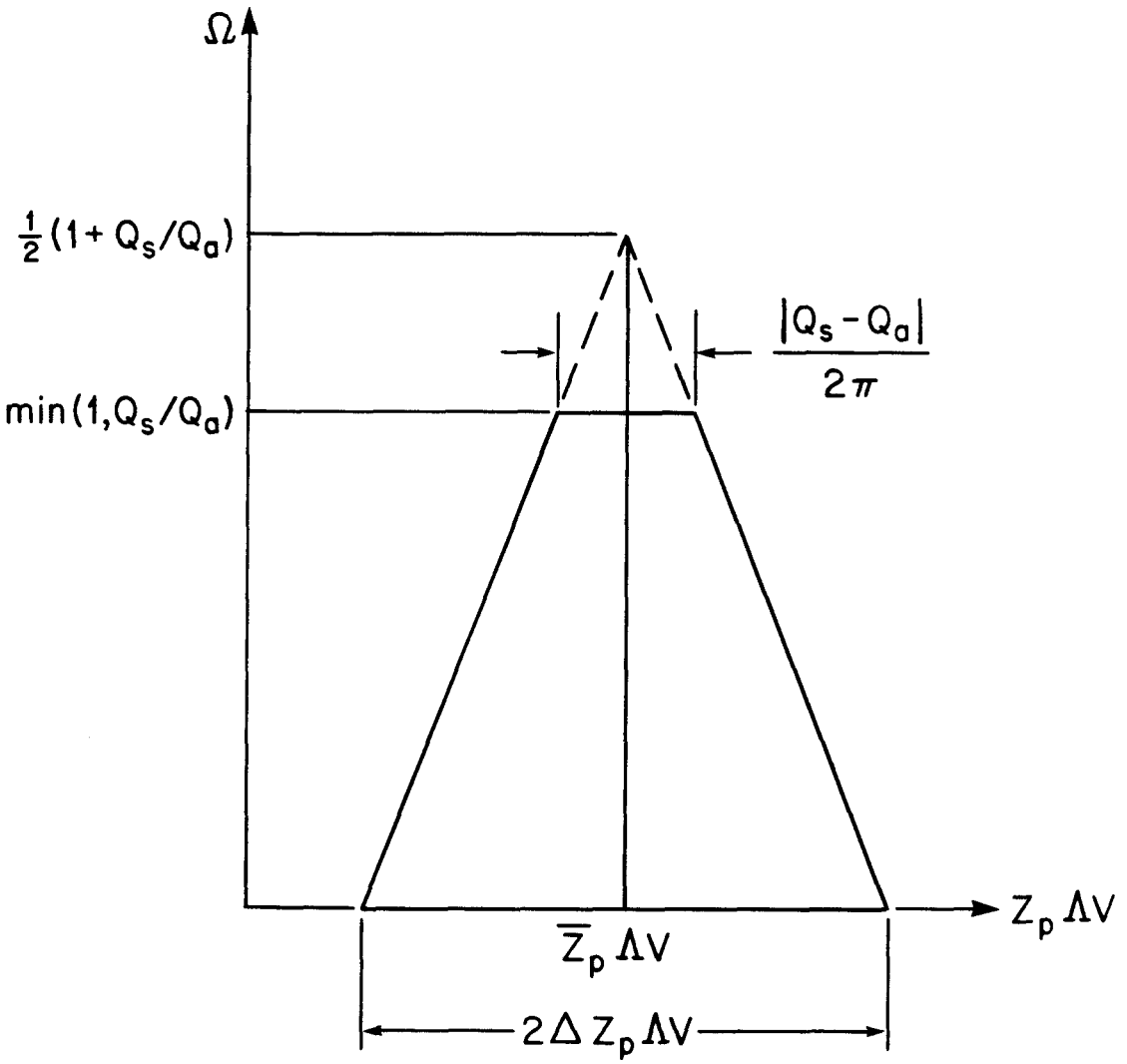

Figure 3.4 Classifier transfer function.

$$\frac{\Delta z_p}{\overline{z}_p} = \frac{Q_s + Q_a}{Q_c + Q_m}. \tag{8}$$

Mobility resolution increases as the flowrate ratio decreases. Flowrates are typically chosen so that the ratio is less than 0.1. As Kousaka et al. (1985) point out, if $Q_s = Q_a$, then at best only one-half of the particles having a mobility between $\overline{z}_p + \Delta z_p$ to $\overline{z}_p - \Delta z_p$ will exit the classifier because of the triangular shape of the transfer function. This accounts for the "diluting" effect of running an aerosol through an EMC.

But what is mobility? Mobility is a physical property of a *charged* aerosol in an electric field. An electric field will have no effect on neutral particles. Mobility is defined as the ratio of the particle's terminal velocity to the field strength and is a measure of the effect of the electric field on particle velocity. A particle of size D_p (μm) having charge ν has a mobility z_p ($\mathrm{cm^2\,V^{-1}\,s^{-1}}$) of

$$z_p = \frac{10^{11}\nu e C(D_p)}{3\pi\mu D_p} = \frac{\nu e D}{kT}, \tag{9}$$

where $C(D_p)$ is the slip correction

$$C(D_p) = 1 + 2.492\left(\frac{\lambda}{D_p}\right) + 0.84\left(\frac{\lambda}{D_p}\right)\exp(-0.43D_p/\lambda), \tag{10}$$

and e is the elementary unit of charge (1.6×10^{-19} C), μ is the air viscosity ($\mathrm{g\,cm^{-1}\,s^{-1}}$), D is the diffusion coefficient of the particle ($\mathrm{cm^2\,s^{-1}}$), k is Boltzmann's constant ($\mathrm{J\,K^{-1}}$), T (K) is the absolute temperature, and λ (μm) is the mean free path of air. In general, mobility is proportional to the charge and inversely proportional to the particle diameter, so it is possible for a larger particle carrying multiple charges to have the same mobility as a smaller singly charged particle. This fact is particularly important when considering the operation and data inversion of the electrical *mobility* classifier.

Given the mobility resolution of Equation (8), the corresponding diameter resolution can be calculated using Equation (9).

$$\frac{\Delta D_p}{\overline{D}_p} = -\frac{\Delta z_p}{\overline{z}_p}\left(\frac{\overline{z}_p/\overline{D}_p}{\partial z_p/\partial D_p}\right) = -\beta\frac{\Delta z_p}{\overline{z}_p} \tag{11}$$

The factor β is shown as a function of diameter in Figure 3.5. As the diameter increases, the diameter resolution approaches that of the mobility. However, for small diameters the resolution approaches one-half of the mobility resolution. Thus, choosing the appropriate operating flowrates, and hence the mobility resolution, is a critical factor in obtaining an adequate size resolution.

§3.4.2 Flowrate Selection

Choosing the operating flowrates for a classifier depends much on the use for which it is intended. If the instrument is used to measure size distributions, then the two factors that need to be considered are 1) the diameter range to be measured and 2) the desired resolution. As indicated above, the range of diameters allowed through the classifier will be determined by the sheath and excess flowrates, while the resolution is determined by the aerosol and sample flows. For the purposes of this discussion, consider that $Q_c = Q_m$ and $Q_s = Q_a$. In other words, the instrument flows are "balanced" and the transfer function Ω assumes a triangular shape.

In the case of EMC2, the classifier used to measure the size distributions from the reactor system, the sample flowrate is set by the condensation nuclei counter (CNC). The CNC counts the particles out of the classifier and requires 0.3 ℓpm of flow. From Equation (8), the sheath flowrate must, therefore, be greater than or equal to 3 ℓpm. A classifier typically has a voltage range of 0 to approximately 11000 V. In the standard TSI instrument, it is difficult to precisely set the voltage at values less than 1000 V. The voltage adjustment potentiometer is overly sensitive at the low voltages. Therefore, it is wise to choose a sheath air flowrate so that

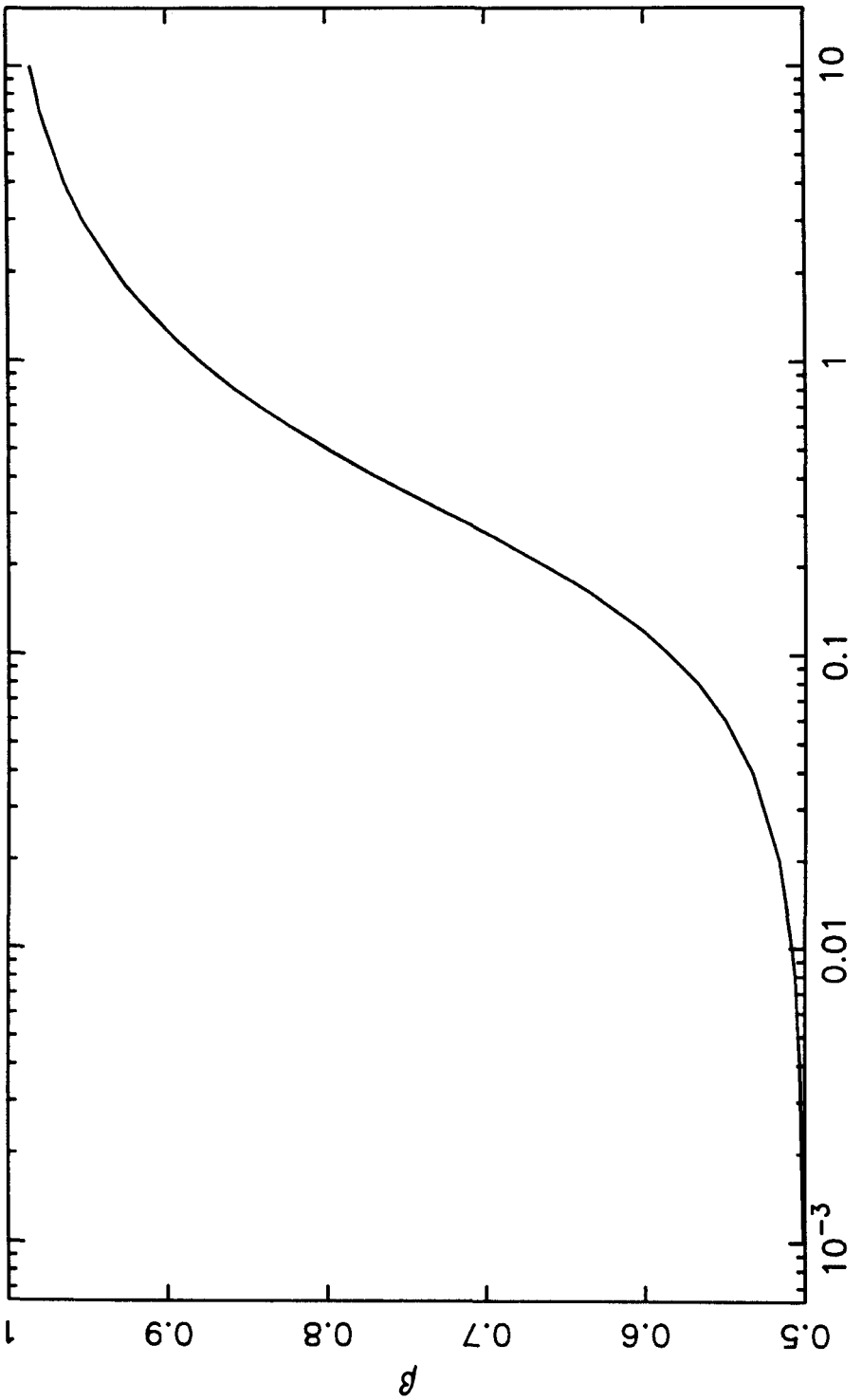

Figure 3.5 Ratio of diameter to mobility resolution as a function of diameter.

the smallest expected diameter corresponds (singly charged) to a voltage over 1000 V. It was also observed that for humidities over 85%, voltages much over 8000 V were unstable. Again, the sheath air flowrate should be chosen so that the largest particle diameter expected (singly charged) is collected at a voltage less than 8000 V.

The sheath air flowrate selection should be based on the diameters corresponding to singly charged particles for two reasons — 1) the ratio of singly to multiply charged particles is always greater than one, and 2) a particle of size D_p having charge ν will have mobility $\overline{z}_p$ at voltage $V_\nu = V_1/\nu$. In other words, multiply charged particles are collected at voltages less than that corresponding to the singly charged particle. Diameter (at $\overline{z}_p$, $\nu = 1$) as a function of the rod voltage is plotted in Figure 3.6 for sheath/excess air flowrates ranging from 5 to 9 ℓpm. The sample/aerosol flowrate was assumed to be 0.3 ℓpm in all cases. Also shown are the expected diameter ranges. The particles that will be measured (humid) are expected to range from 0.1 to 0.4 μm in diameter. Given this diameter spread it is apparent from Figure 3.6 that sheath air flowrates greater than 8 ℓpm will make classifying the largest particles impossible if an upper voltage limit of 8000 V is imposed. On the other hand, using flowrates less than 7 ℓpm does not take full advantage of the entire available voltage range. The mobility resolution is also decreased. Therefore, the best sheath air flowrate to use in measuring the size distributions from the reactor system is 7 ℓpm. For $Q_c = Q_m = 7$ ℓpm and $Q_s = Q_a = 0.3$ ℓpm, the mobility resolution is 0.043 and the diameter resolution ranges from 0.025 to 0.032 for a given voltage. These flowrates will be used in the following discussion of the data inversion problem.

§3.4.3 Data Inversion Algorithm and Verification

The basic inversion problem for most instruments, including the classifier, can be described by a Fredholm integral of the first kind

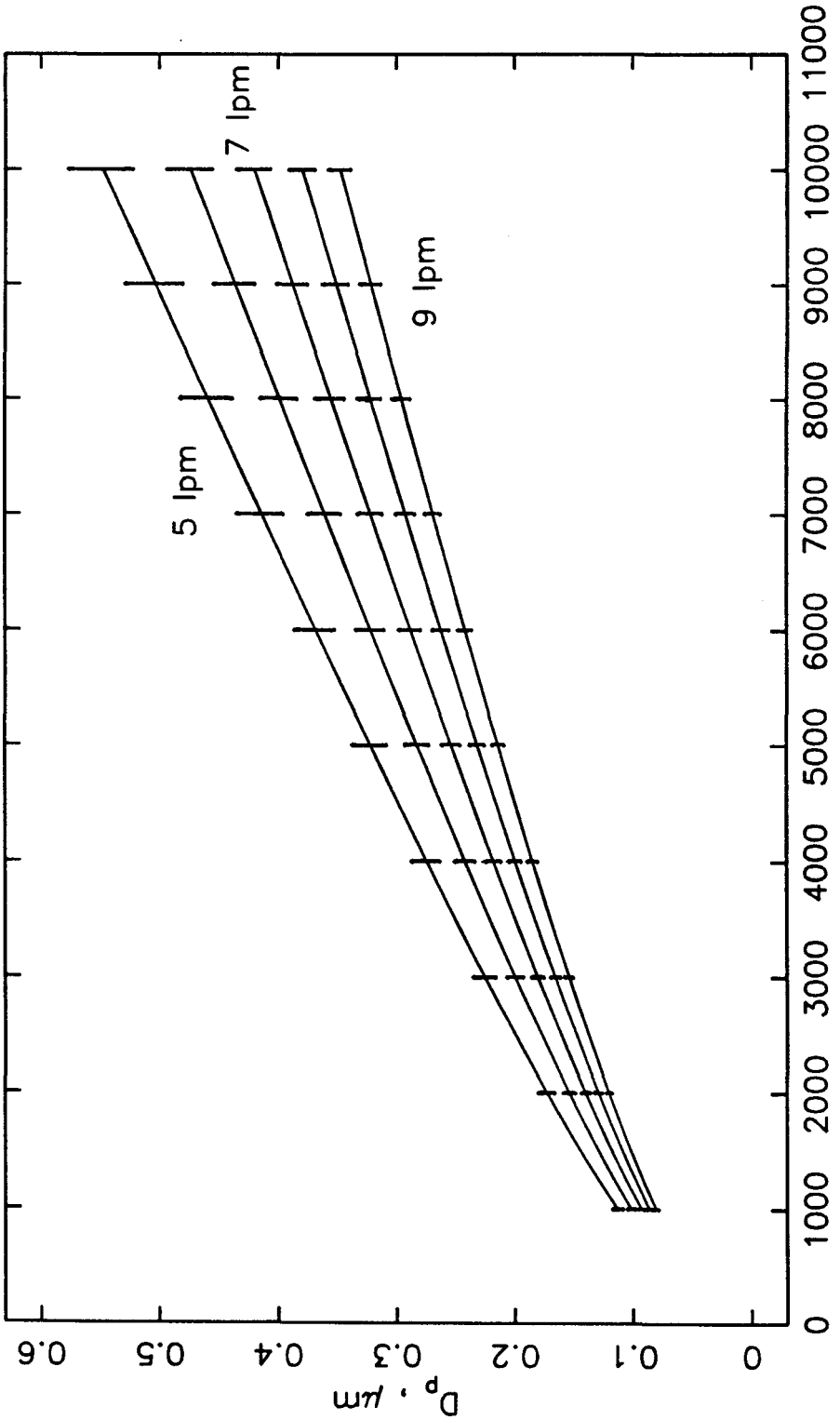

Figure 3.6 Diameter ($\tilde{z}_p$, $\nu = 1$) as a function of voltage for various sheath air flowrates. $Q_s = 0.3$ ℓpm.

$$R(V) = \int_0^\infty K(V, D_p)\, n(D_p)\, dD_p, \tag{12}$$

where $R(V)$ is the actual experimental data (e.g., the CNC number counts at a given voltage V), $K(V,\ D_p)$ is the kernel function describing the instrument response at voltage V to a particle size D_p, and $n(D_p)$ is the size distribution dN/dD_p. The kernel functions for the classifier may be written explicitly given the transfer function Ω, the charge distribution $\phi(\nu,\ D_p)$, and the flowrates,

$$K(V, D_p) = \frac{Q_a}{Q_s} \sum_{\nu=1}^{\infty} \phi(\nu, D_p)\, \Omega(z_p \Delta V), \tag{13}$$

where

$$\Omega(v) = \begin{cases} 0 & v < v_1, \\ \min(1, Q_s/Q_a)(v - v_1)/(v_2 - v_1) & v_1 \le v < v_2, \\ \min(1, Q_s/Q_a) & v_2 \le v < v_3, \\ \min(1, Q_s/Q_a)(v_4 - v)/(v_4 - v_3) & v_3 \le v < v_4, \\ 0 & v \ge v_4, \end{cases} \tag{14}$$

and

$$\begin{aligned} v_1 &= (Q_c + Q_m - Q_s - Q_a)/4\pi, \\ v_2 &= (Q_c + Q_m - |Q_s - Q_a|)/4\pi, \\ v_3 &= (Q_c + Q_m + |Q_s - Q_a|)/4\pi, \\ v_4 &= (Q_c + Q_m + Q_s + Q_a)/4\pi. \end{aligned} \tag{15}$$

The primary difficulty in inverting classifier data is dealing with the multiple charging. The response at a voltage may be due to several different particle sizes bearing charge +1, or +2, etc. Therefore, before the discussion concerning the data inversion continues, it is appropriate to take a brief look at the charge distribution.

As mentioned earlier, a ^{85}Kr neutralizer is used to charge the aerosol. The radioactivity ionizes the air, which in turn charges the aerosol. This type of charging is called bipolar in that both positively and negatively charged aerosol is generated in addition to the neutral fraction. Knowing the aerosol charge distribution $\phi(\nu,\ D_p)$ is important since charge determines a particle's mobility and hence, the voltage at which the particle will pass through the classifier. A number of experimental

studies (Liu and Pui (1974a), Liu and Pui (1974b), and Kousaka et al. (1981)) have indicated that this method of charging particles produces a Boltzmann equilibrium change distribution for particle sizes greater than 0.1 μm and a sufficiently long residence time in the neutralizer. The Boltzmann distribution gives $\phi(\nu, D_p)$, the fraction of particles size D_p with charge ν to be

$$\phi(\nu, D_p) = \frac{1}{\sqrt{2\pi\sigma^2}} \exp(-\nu^2/2\sigma^2), \tag{16}$$

where $\sigma^2 = D_p kT/2e^2$, k is the Boltzmann constant, T is the absolute temperature, and e is the elementary unit of charge. Note that this functional form predicts equal numbers of positively and negatively charged particles. Because the negative and positive ions produced in the charger have a different properties, Hoppel and Frick (1986) have calculated that the ratio of ion densities is crucial in determining the ratio of positively to negatively charged aerosol. Experimentally, Liu and Pui (1974a) found a slightly negative median charge (approximately one-half), although they concluded that the Boltzmann distribution adequately described their data. The results of Kousaka et al. (1981), on the other hand, indicate completely symmetric charging had occurred. Inasmuch as the bipolar charger used in the reactor experiments is identical to the type used by Liu and Pui (1974a), it was assumed that the charge distribution produced by the ^{85}Kr neutralizer was a Boltzmann equilibrium distribution. To determine if this assumption was reasonable, the ratios of singly to doubly, singly to triply and doubly to triply charged (positively) aerosol were estimated from some voltage scans made of various sizes of polystyrene latex (PSL) particles. For instance, assuming that the 0.27 μm PSL is monodisperse (the standard deviation is actually 0.006 μm) — $\phi_1/\phi_2 \sim 1.99$, $\phi_2/\phi_3 \sim 3.16$, and $\phi_1/\phi_3 \sim 6.3$. A Boltzmann distribution gives $\phi_1/\phi_2 = 1.87$, $\phi_2/\phi_3 = 2.85$, and $\phi_1/\phi_3 = 5.3$. The assumption of a Boltzmann distribution appears, therefore, to be within reason. It should be noted that the validity of this expression for particle diameters less than 0.1 μm has been questioned by a number of researchers and the experiments yield ambiguous results

(e.g., Kousaka et al. (1983), Liu and Pui (1974a), Hoppel and Frick (1986)).

Hoppel's (1978) classifier data inversion was used because it is a particularly robust iterative method. Data are inverted on the mobility scale to give the total number of particles in successive mobility intervals. The method proposed by Hagen and Alofs (1983) is conceptually more attractive because it works on the diameter scale. However, a matrix inversion must be performed and problems were encountered when actual experimental data were used. Both Hoppel's and Hagen and Alofs' inversion routines require that a set of specifically prescribed voltages be used. Since voltage V_j corresponds to a specific mean mobility $\overline{z}_{p_j}$ for a given a set of classifier operating flowrates, the voltages must be chosen so that the entire mobility range is spanned by adjoining non-overlapping mobility intervals,

$$\frac{V_{j+1}}{V_j} = \frac{Q_c + Q_m + Q_s + Q_a}{Q_c + Q_m - Q_s - Q_a}. \tag{17}$$

Thus, the classifier flowrates and the chosen initial voltage determine the sequence of voltages that can be used in one inversion run. The inversion program is typically run several times with different starting voltages in order to generate a complete number distribution. Hoppel's method will be briefly outlined here.

Every mobility range $\overline{z}_{p_j}$ to $\overline{z}_{p_{j+1}}$ corresponds to a set of discrete particle diameters. The number of particles counted by the CNC for this range can be written as the sum of the number of singly, doubly, triply, etc., charged particles:

$$\Delta N^{CNC}\left(\overline{z}_{p_{j+1}} - \overline{z}_{p_j}\right) = \sum_{\nu=1}^{\infty} \Delta N^{\nu}\left(\frac{\overline{z}_{p_{j+1}}}{\nu} - \frac{\overline{z}_{p_j}}{\nu}\right), \tag{18}$$

where superscript ν indicates the number of charges and $\overline{z}_p/\nu$ is the mobility a ν-charged particle would have if it were singly charged. The particle diameter is calculated from Equation (9) for a *singly* charged particle with mobility $\overline{z}_p/\nu$. This is equivalent to calculating the diameter for a particle with mobility $\overline{z}_p$ and charge ν. Initially, all particles in the mobility range are assumed to be singly charged.

$$\Delta N_I^1 \left(D_p(\overline{z}_{p_{j+1}}) - D_p(\overline{z}_{p_j})\right) = \Delta N^{CNC} \left(D_p(\overline{z}_{p_{j+1}}) - D_p(\overline{z}_{p_j})\right) \qquad (19)$$

The Roman numeral subscript indicates this is a first approximation. If the charge distribution $\phi(\nu, D_p)$ is known, a first estimate of the total number of particles — positively charged, negatively charged, and neutral — in this mobility interval can be made:

$$\Delta N_I^{total} \left(D_p(\overline{z}_{p_{j+1}}) - D_p(\overline{z}_{p_j})\right) = \frac{\Delta N_I^1 \left(D_p(\overline{z}_{p_{j+1}}) - D_p(\overline{z}_{p_j})\right)}{\phi(1, \overline{D}_{p_j})}, \qquad (20)$$

where $\overline{D}_{p_j}$ is the diameter corresponding to the average mobility in the $\overline{z}_{p_j}$ to $\overline{z}_{p_{j+1}}$ range. This overestimates ΔN_I^{total} for the interval. The total number estimate is now used to predict the number of multiply charged particles contributing to the mobility interval,

$$\begin{aligned} \Delta N_I^{\nu} \left(D_p(\frac{\overline{z}_{p_{j+1}}}{\nu}) - D_p(\frac{\overline{z}_{p_j}}{\nu})\right) \\ = \phi(\nu, \overline{D}_{p_j}) \, \Delta N_I^{total} \left(D_p(\overline{z}_{p_{j+1}}) - D_p(\overline{z}_{p_j})\right), \end{aligned} \qquad (21)$$

and the number of singly charged particles is recalculated, using

$$\begin{aligned} \Delta N_{II}^1 \left(D_p(\overline{z}_{p_{j+1}}) - D_p(\overline{z}_{p_j})\right) = \Delta N^{CNC} \left(D_p(\overline{z}_{p_{j+1}}) - D_p(\overline{z}_{p_j})\right) \\ - \sum_{\nu=2}^{\infty} \Delta N_I^{\nu} \left(D_p(\frac{\overline{z}_{p_{j+1}}}{\nu}) - D_p(\frac{\overline{z}_{p_j}}{\nu})\right). \end{aligned} \qquad (22)$$

A new estimate of the total number in the mobility range is given by

$$\Delta N_{II}^{total} \left(D_p(\overline{z}_{p_{j+1}}) - D_p(\overline{z}_{p_j})\right) = \frac{\Delta N_{II}^1 \left(D_p(\overline{z}_{p_{j+1}}) - D_p(\overline{z}_{p_j})\right)}{\phi(1, \overline{D}_{p_j})}. \qquad (23)$$

This iteration process (Equations (21) – (23)) is continued until some convergence criterion is met. The criterion used here is that distribution total particle number must converge to a constant value

Table 3.2

Lognormal Distribution Parameters for Inversion Test

D_p, μm	N_{tot}, #/cm^3	σ
0.16	10000	1.05
0.21	2000	1.08
0.27	500	1.08

$$N_i^{total} = \sum_{j=1}^{\infty} \Delta N_i^{total} \left(D_p(\overline{z}_{p_{j+1}}) - D_p(\overline{z}_{p_j}) \right), \tag{24}$$

before the final distribution is reached.

The standard method for verifying an inversion routine is to generate the instrument response to a lognormal distribution and then invert this generated data. The temperature and pressure were set at typical reactor system values of 23°C and 740 mmHg, respectively. As discussed earlier, values of $Q_c = Q_m = 7$ ℓpm and $Q_s = 0.3$ ℓpm were set for the flowrates. Table 3.2 gives the parameters for the trimodal lognormal aerosol distribution assumed, one similar to those produced by the reactor system. Equations (12) through (16) were used to generate the response, or "CNC," data corresponding to a set of classifier voltages and the resulting "voltage scan" was fit with a spline function (see Figure 3.7). With a scan spline fit it is possible to estimate the CNC response to any voltage. Thus, given any initial voltage and the classifier operating conditions, the voltage sequence required by the inversion routine can be determined and the corresponding CNC number counts calculated.

The generated CNC data were inverted using Hoppel's technique. As can be

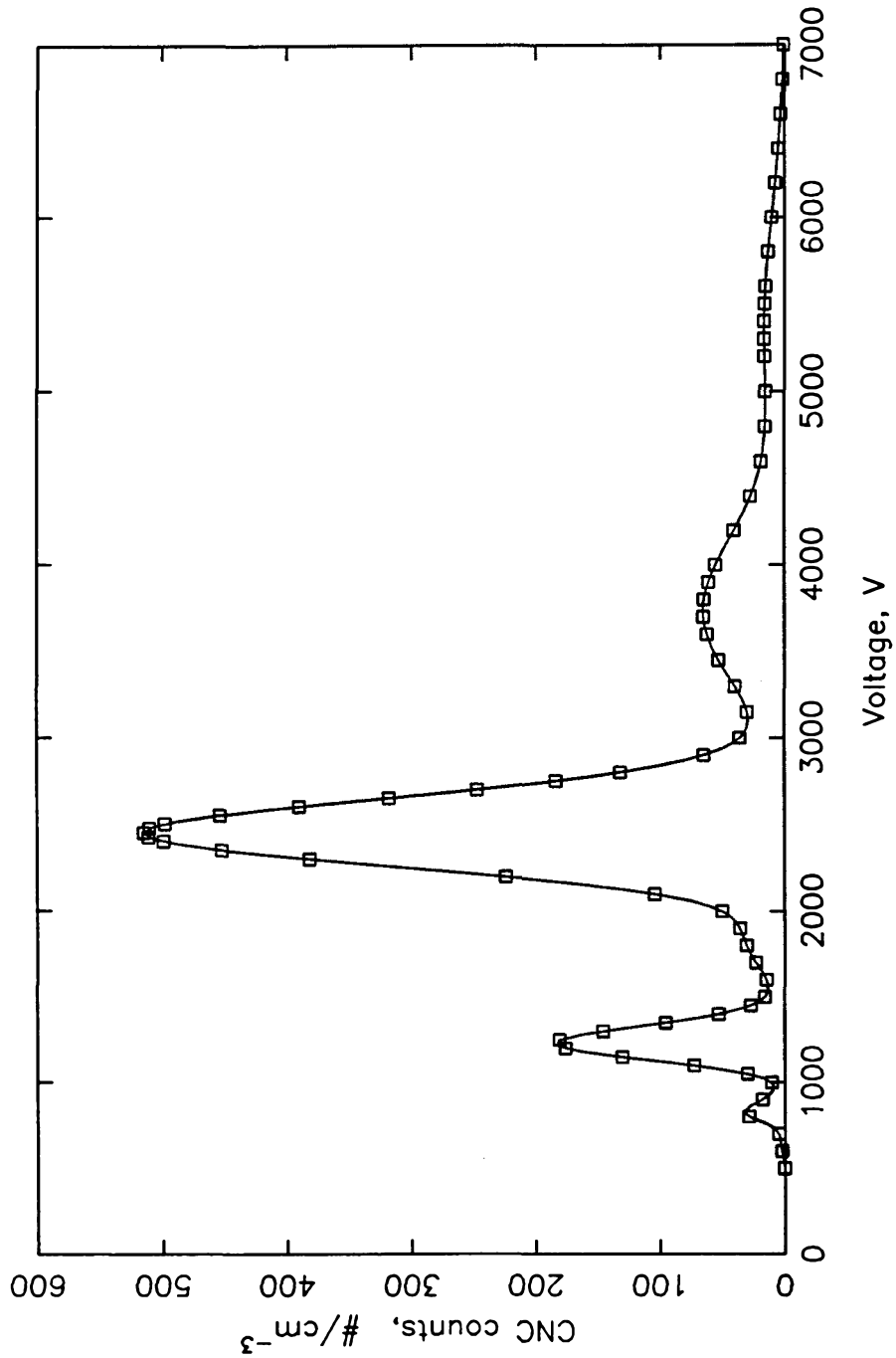

Figure 3.7 Generated voltage scan (□) and spline fit (————) for a trimodal lognormal distribution. $T = 23°C$, $P = 740$ mmHg, $Q_c = Q_m = 7$ ℓpm, and $Q_s = 0.3$ ℓpm. $D_{p1} = 0.16$ μm, $N_{tot_1} = 10000/\text{cm}^3$, $\sigma_1 = 1.05$; $D_{p2} = 0.21$ μm, $N_{tot_2} = 2000/\text{cm}^3$, $\sigma_2 = 1.08$; and $D_{p3} = 0.27$ μm, $N_{tot_3} = 500/\text{cm}^3$, $\sigma_3 = 1.08$.

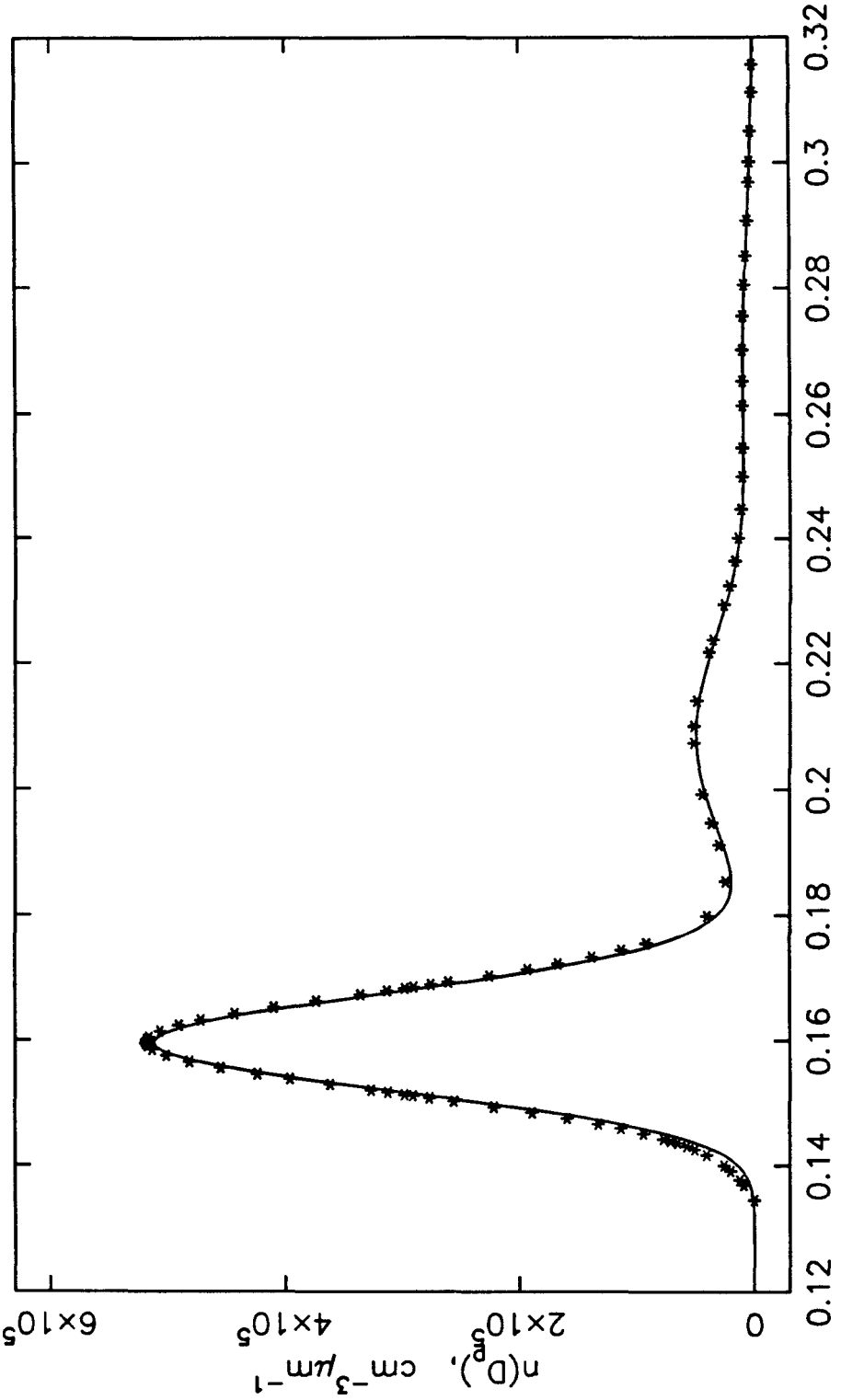

Figure 3.8 Lognormal distribution (———) and inversion result for the generated CNC data (*).

seen in Figure 3.8, the inversion recovered the initial trimodal lognormal distribution. A comparison of the inversion result and the actual distribution is presented in Table 3.3. The accuracy with which the peak diameters are determined by the inversion depends on how carefully the voltage scans (or initial voltages) are chosen. Different scans should be tried, to see if the peak position changes. The scan that correctly predicts the peak is the one that includes the voltage corresponding to the mobility of the peak diameter. The inversion routine is better able to predict the peak diameters than the peak heights. Nonetheless, the agreement is still impressive, given the small geometric standard deviation (σ) of the test distribution. Kousaka et al. (1985) point out that as the standard deviation approaches one and/or the peak diameter increases, values of $Q_s/Q_c < 0.1$ are necessary to obtain adequate inversion results. The small error in peak diameter is important since the reactor system experimental results hinge on size distribution shifts.

The inversion routine performs well when given ideal CNC data, but actual experimental data will have some scatter. In order to test the inversion routine under more realistic conditions, two sources of error were considered: 1) random

Table 3.3

Comparison of Test Lognormal Distribution and Inversion Results

	Test	Inversion	% Error
D_{p_1}, μm	0.1596	0.1595	0.063
$n(D_{p_1})$, $cm^{-3}\mu m^{-1}$	511,765	518,809	1.37
D_{p_2}, μm	0.2088	0.2087	0.047
$n(D_{p_2})$ $cm^{-3}\mu m^{-1}$	49,562	51,669	4.25
Total number, #/cm^3	12,500	13,197	5.58

error was added to the CNC number counts generated above; and 2) small changes were made in the flowrates. Not enough numerical tests were made to constitute a true statistical survey; however, the general response of the routine to different error sources was determined.

The CNC response at classifier voltage V generated for the trimodal lognormal test distribution (see Table 3.2) was considered to be the mean value of a random, normally distributed parent population of CNC readings. The standard deviation associated with this parent population was defined as a given percentage of the mean, or $\sigma_i = \alpha C_j$. This type of uncertainty is known as relative error. A random, normally distributed number (see Press et al. (1986)) with a mean of zero and a variance of one was used to generate a new CNC value having some level of error. These new CNC values were input to the inversion routine. For each level of relative error studied, 5, 10, and 20%, ten runs of the inversion routine were made. Figures 3.9a-c present the distributions resulting from the inversion of the error-containing CNC concentrations plotted along with the original test case (0% error). The plots indicate that while increasing error affects the magnitude of the size distribution, there was no accompanying shift along the diameter axis. This was anticipated since the diameter range is determined solely by the classifier flowrates and voltage, and not by the CNC concentrations. However, the location of the distribution peak *could* be affected by the CNC concentrations if the added random error significantly shifted the maximum concentration along the voltage axis.

The results of the numerical analysis are presented in Table 3.4. Again, in interpreting these results it should be remembered that only 10 runs were made: enough to observe general trends, but not enough to be statistically significant. All of the observed parameters — primary peak diameter D_{p_1}, secondary peak diameter D_{p_2}, and total number concentration — vary from the ideal case (0% error) by less than one percent regardless of the level of relative error. There is

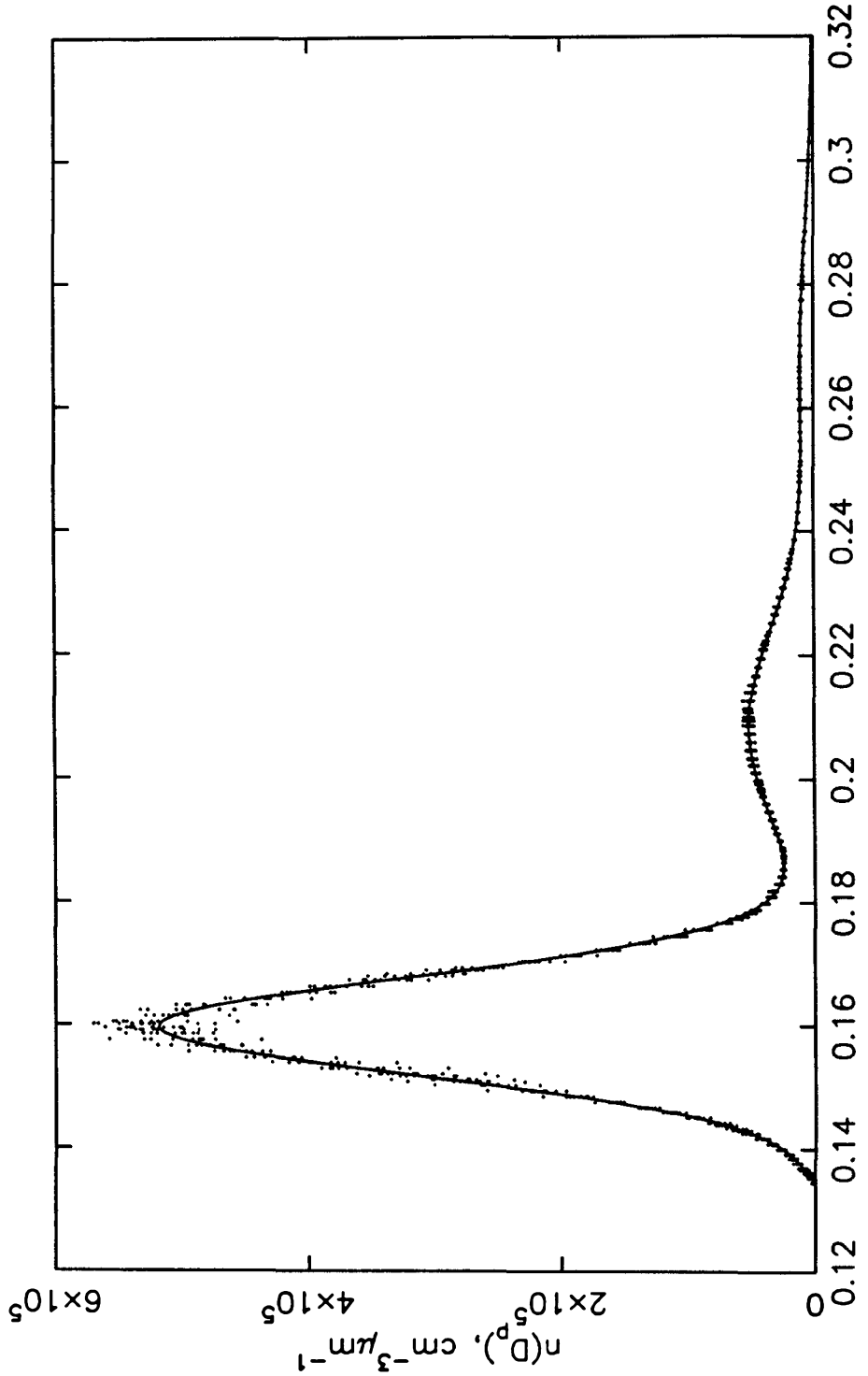

Figure 3.9a Inversion results for CNC data having various levels of relative error. $\sigma_j = (5\%)C_j$. $Q_c = Q_m = 7.0$ ℓpm, $Q_e = 0.3$ ℓpm.

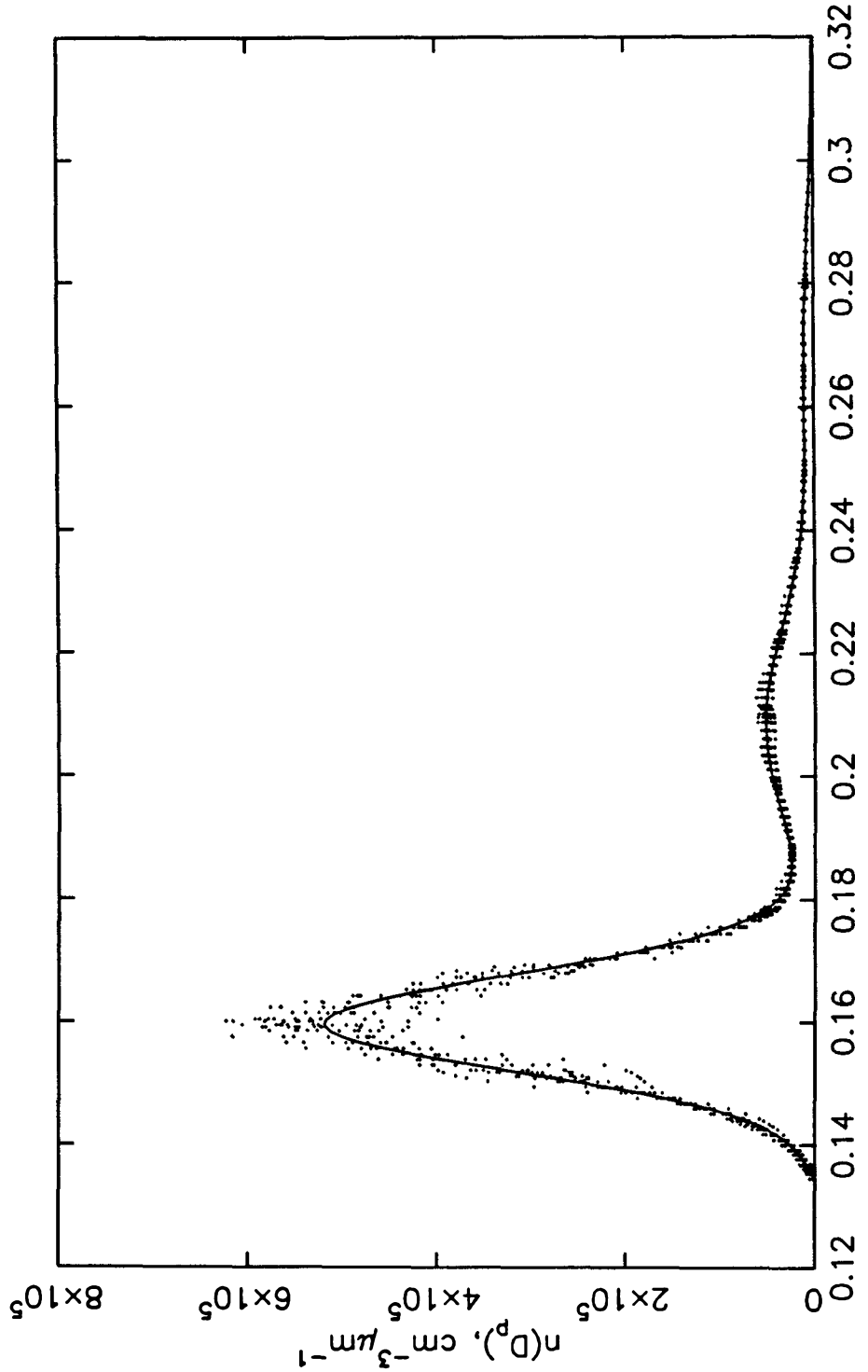

Figure 3.9b Inversion results for CNC data having various levels of relative error. σ_j = (10%)C_j. $Q_c = Q_m = 7.0$ ℓpm, $Q_s = 0.3$ ℓpm.

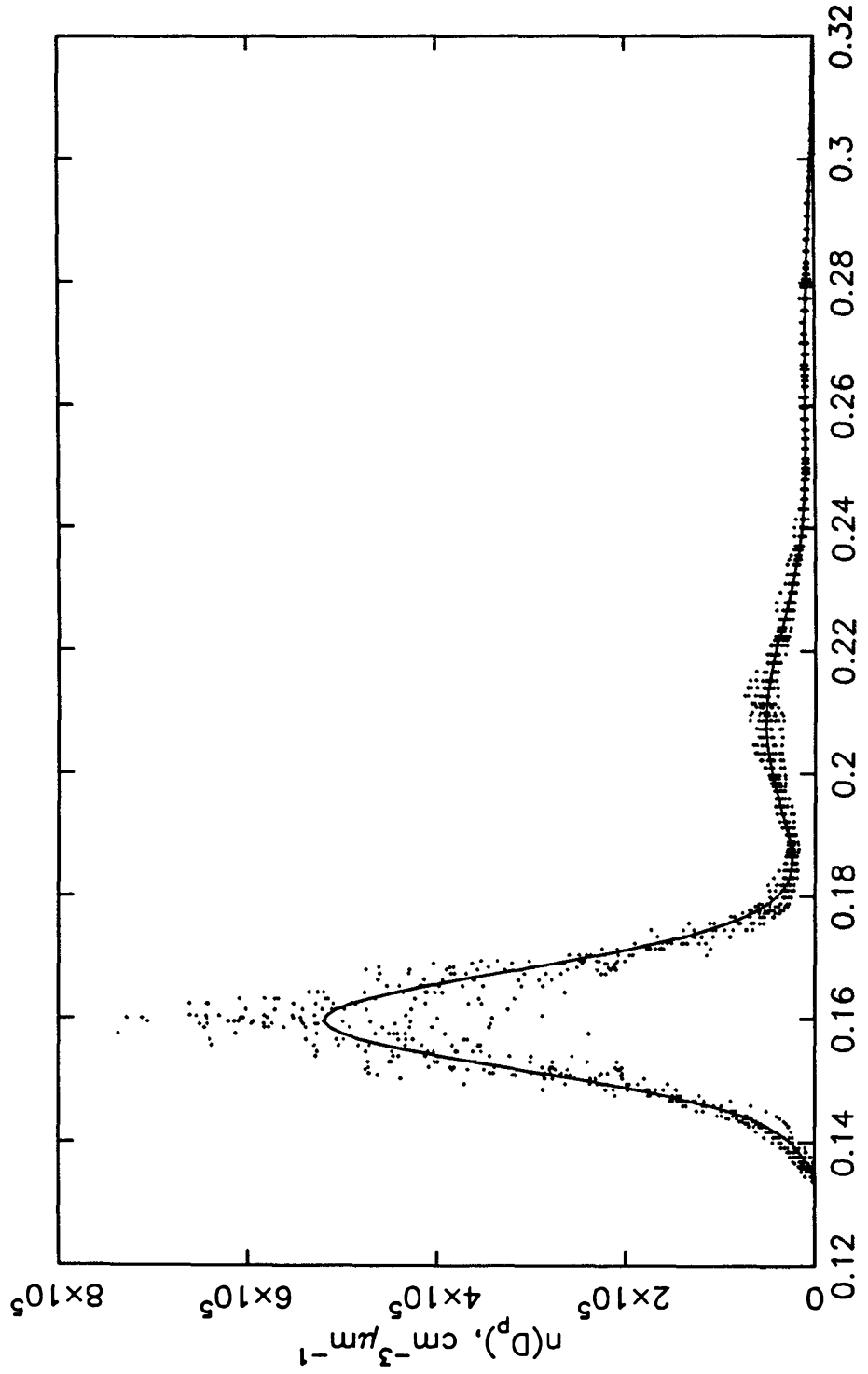

Figure 3.9c Inversion results for CNC data having various levels of relative error. $\sigma_j = (20\%)C_j$. $Q_c = Q_m = 7.0$ ℓpm, $Q_s = 0.3$ ℓpm.

Table 3.4

Inversion Results For Various Levels of Relative Error in the CNC Concentrations

	0%	5%	10%	20%
D_{p_1} (μm)	0.1595	0.1599	0.1595	0.1597
$\sigma_{Dp,1}$ (%)	–	0.43	0.72	0.68
D_{p_2} (μm)	0.2087	0.2086	0.2104	0.2104
$\sigma_{Dp,2}$ (%)	–	1.5	1.7	1.8
Total no. (#/cm^3)	13,197	13,158	13,103	13,111
σ_{tot} (%)	–	1.3	2.6	4.7

a slight increase in the standard deviation associated with the observed mean as the error level is increased. Thus, one can conclude that the inversion routine is relatively insensitive to random error in the input CNC concentrations with regard to determining the peak diameter.

The effect of flowrate perturbations on the inversion was studied by varying the sheath, excess, and sample air flowrates. The CNC number concentrations generated for the trimodal lognormal distribution (Q_c= Q_m= 7 ℓpm and Q_s= 0.3 ℓpm) were used in this sensitivity study. This is equivalent to "measuring" the CNC data at a particular set of flowrates and inverting them at another. The effect of flowrate error is considerably more complicated than the effect of CNC number concentration error. Of the four classifier operating flowrates — sheath, excess, aerosol, and sample — only three are independent. Therefore, given that $Q_c = Q_{c,0} + \delta Q_c$, $Q_m = Q_{m,0} + \delta Q_m$, and $Q_s = Q_{s,0} + \delta Q_s$, the aerosol flowrate will be,

$$Q_a = Q_{a,0} + (\delta Q_c + \delta Q_m + \delta Q_s). \tag{25}$$

Because mobility is determined by the classifier operating conditions, changing the flowrates results in a mobility shift. This ultimately causes a shift of size distribution along the diameter axis. These shifts in the mobility and its range can be written as follows:

$$\overline{z}_p = \left(1 + \frac{\delta Q_c + \delta Q_m}{Q_{c,0} + Q_{m,0}}\right) \overline{z}_{p,0}, \tag{26}$$

and

$$\Delta z_p = \left(1 + \frac{\delta Q_s + \delta Q_a}{Q_{s,0} + Q_{a,0}}\right) \Delta z_{p,0}. \tag{27}$$

An increase in either the sheath or excess flowrate causes an increase in the mean mobility and a corresponding decrease in diameter. Similarly, a decrease in either flowrate causes a positive shift along the diameter axis. Perturbations in the sheath and excess flowrates cause equal but opposite perturbations in the aerosol flowrate for a constant sample flowrate. For example, an increase in the sheath flowrate results in a decrease in the mobility range, or increased mobility resolution, while an excess flowrate increase causes decreased mobility resolution. It should be remembered that while the effect on the mean mobility is similar, changing the excess and sheath flowrates are completely different processes. A change in the sheath flowrate merely increases or decreases the aerosol flowrate (as determined by Equation (25)). There is no effect on the total flow through the classifier. On the other hand, changing the excess flowrate results in both a different aerosol flowrate and a different total flow. A change in the sample flowrate does not shift the distribution significantly because it alters only the mobility range of Equation (27).

The inversion program was run for $\pm$ 0.1 and $\pm$ 0.2 ℓpm ($\pm$ 1.4 and 2.9% respectively) perturbations in the sheath and excess flowrates. Only one flowrate per run was changed from the initial case Q_c= Q_m= 7 ℓpm, Q_s= 0.3 ℓpm. The sheath and excess flowrates were then held constant while the sample flowrate

was perturbed ± 0.01 ℓpm (± 3.3%). The inversion results are plotted in Figures 3.10a-c, and the accompanying data are presented in Table 3.5.

As expected, the peak diameters increased with decreasing sheath or excess flowrate and decreased for increasing flowrate. However, the increases and decreases were not symmetrical and not identical for both sheath and excess flow. A decrease of 2.9% in either the sheath or excess flowrate resulted in a 1.2% increase in the primary peak diameter. On the other hand, an increase of 2.9% in either the sheath or excess flowrate corresponded to an 0.8 and 0.5% decrease in peak diameter, respectively.

Although identical sheath and excess flowrate changes affect the mean mobility identically, the effect on the mobility range is quite different. One would not expect similar sheath and excess flowrate changes to result in identical distributions. This is particularly apparent in the predicted total particle number concentrations. Sheath air flowrates ranging from 6.8 to 7.2 ℓpm resulted in total number concentrations ranging from 9,594 to 19,875 particles/cm^3, respectively tively. On the other hand, excess air flowrates ranging from 6.8 to 7.2 ℓpm gave total number concentrations from 19,174 to 10,061 particles/cm^3, respectively. Given the Fredholm inversion integral and the classifier kernel function (Equations (12) and (13)), a first-order explanation for this phenomenon is apparent. If the size distribution is defined as $n(D_p) = N_{total}\, n'(D_p)$, the Fredholm integral can be rewritten as

$$R(V) = \left(\frac{Q_a}{Q_s}\right) N_{total} \sum_{\nu=1}^{\infty} \int_0^{\infty} \phi(\nu, D_p)\, \Omega(z_p \Lambda V)\, n'(D_p)\, dD_p. \qquad (28)$$

Since the CNC data, or $R(V)$ values, are identical in every case, a change in N_{total} compensates for a change in Q_a/Q_s. For instance, increasing the sheath air flowrate decreases the aerosol flowrate; the ratio Q_a/Q_s decreases resulting in an increased value of N_{total}. This explanation is an oversimplification inasmuch as the shifted mobility scale alters the charge distribution ϕ and transfer function Ω under the integral. Therefore, an increase or decrease in the flow ratio Q_a/Q_s does cause a

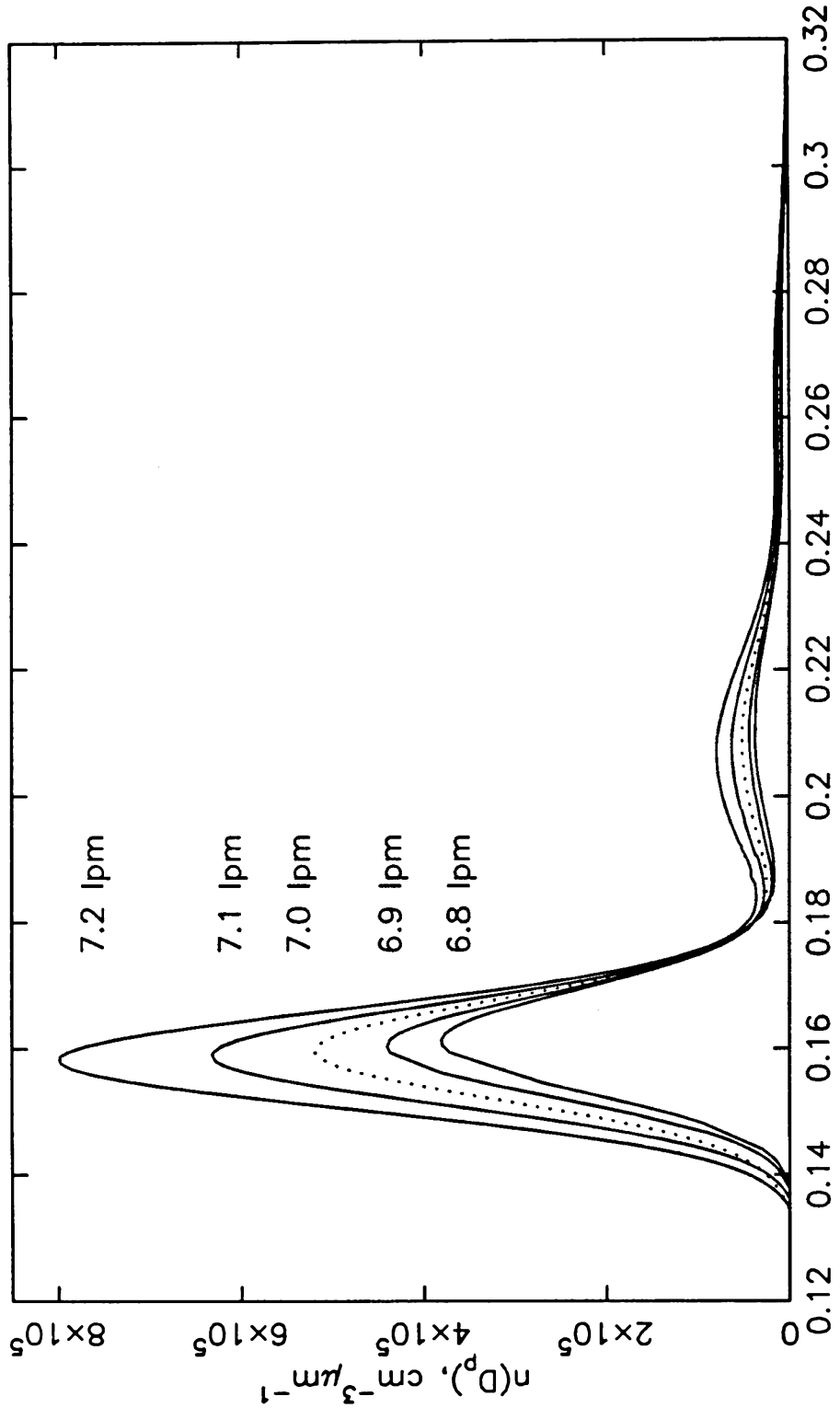

Figure 3.10a Inversion results for flowrate variations. Q_c= 6.8 - 7.2 ℓpm, Q_m= 7.0 ℓpm, Q_s= 0.3 ℓpm.

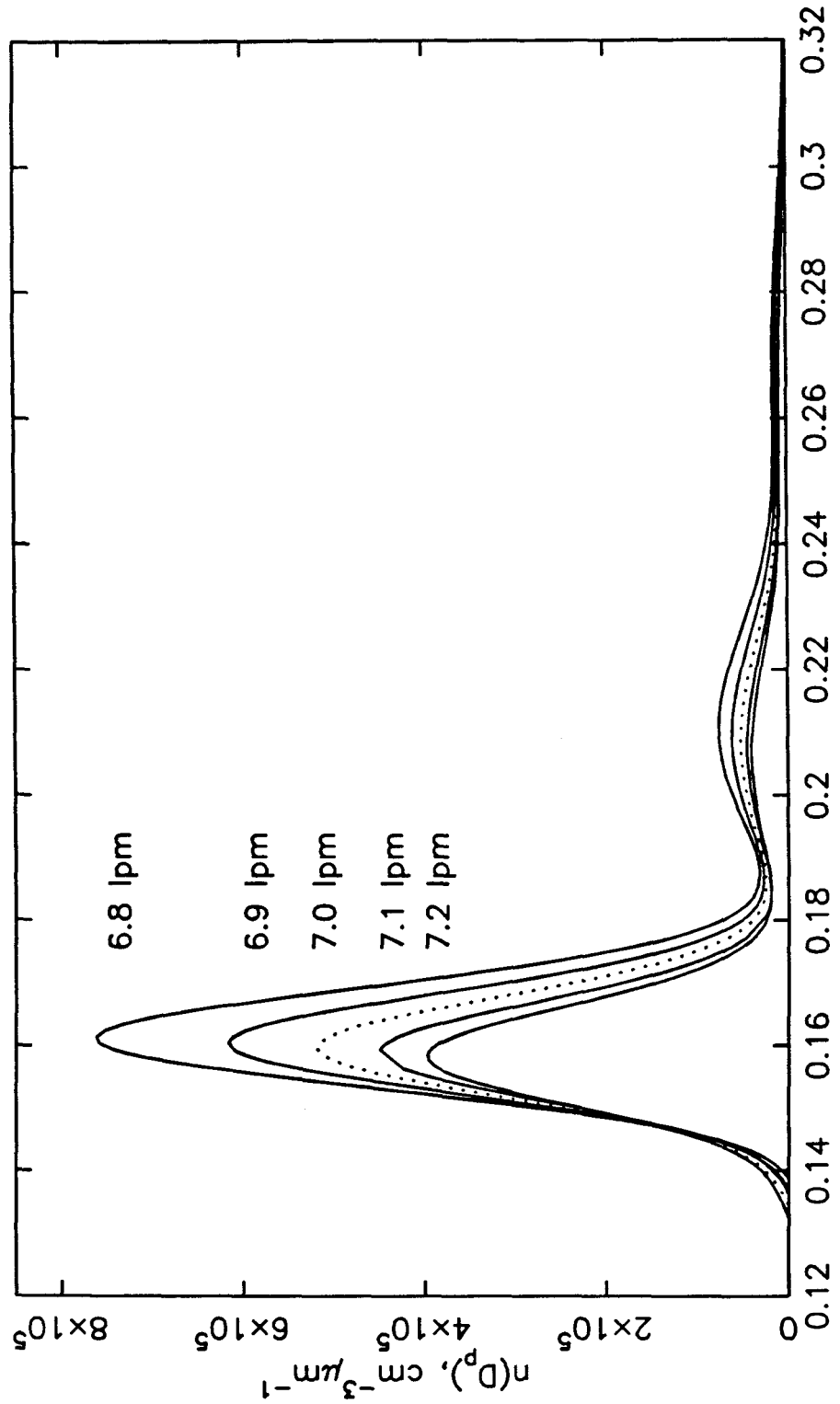

Figure 3.10b Inversion results for flowrate variations. Q_c= 7.0 ℓpm, Q_m= 6.8 - 7.2 ℓpm, Q_s= 0.3 ℓpm.

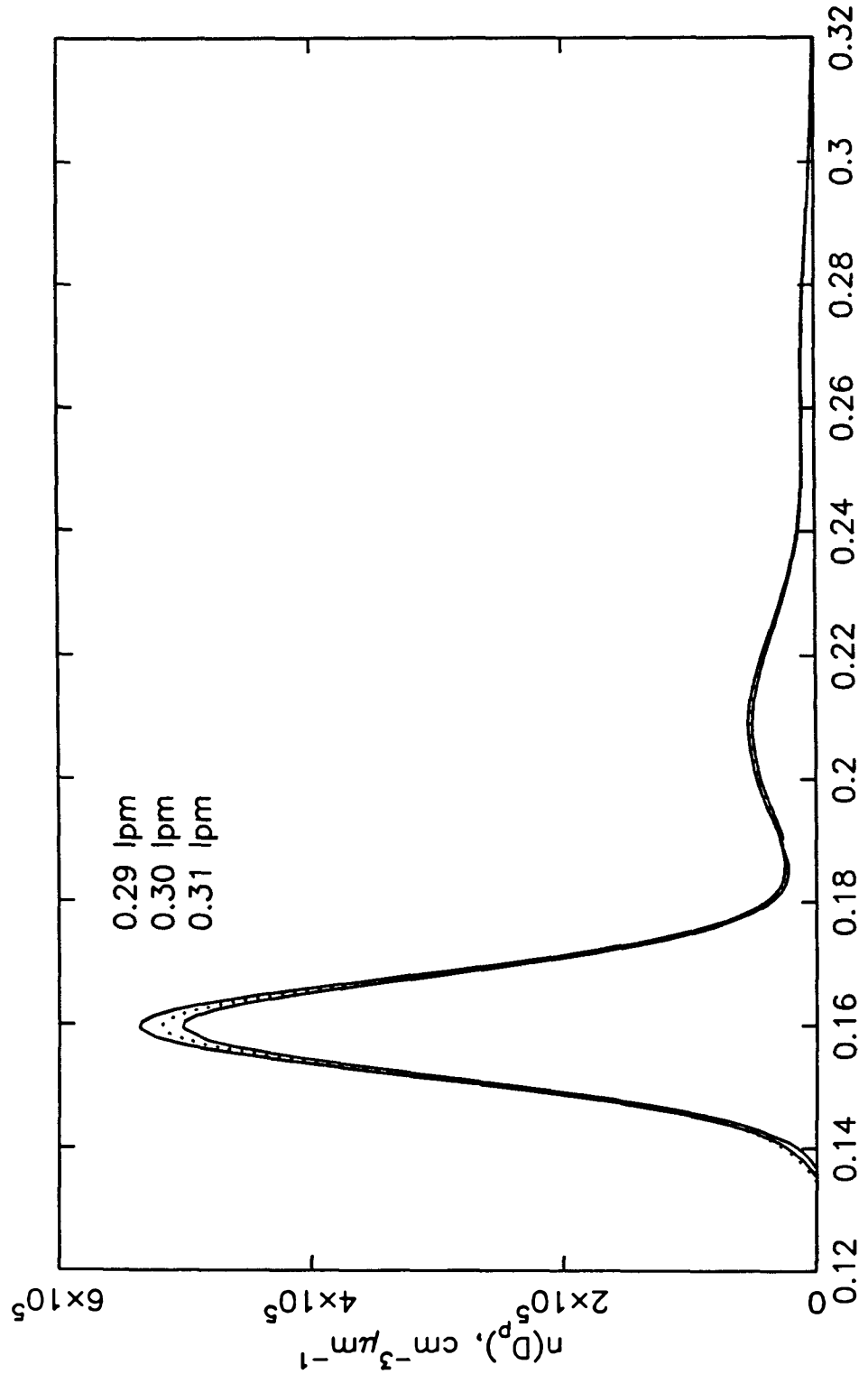

Figure 3.10c Inversion results for flowrate variations. Q_c= 7.0 ℓpm, Q_m= 7.0 ℓpm, Q_s= 0.29 - 0.31 ℓpm.

Table 3.5

Inversion Results For Flowrate Variations

Q_c (ℓpm)	Q_m (ℓpm)	Q_s (ℓpm)	D_{p_1} (μm)	D_{p_2} (μm)	Total no. (#/cm^3)
6.8	7.0	0.30	0.1614	0.2110	9,594
6.9	7.0	0.30	0.1604	0.2104	11,065
7.0	7.0	0.30	0.1595	0.2087	13,197
7.1	7.0	0.30	0.1591	0.2077	15,716
7.2	7.0	0.30	0.1583	0.2065	19,875
7.0	6.8	0.30	0.1614	0.2108	19,174
7.0	6.9	0.30	0.1603	0.2097	15,557
7.0	7.0	0.30	0.1595	0.2087	13,197
7.0	7.1	0.30	0.1593	0.2083	11,188
7.0	7.2	0.30	0.1587	0.2068	10,061
7.0	7.0	0.29	0.1593	0.2092	13,586
7.0	7.0	0.30	0.1595	0.2087	13,197
7.0	7.0	0.31	0.1593	0.2090	12,594

decrease or increase in the particle total number concentration, although the actual value is influenced by other factors.

Three conclusions can be drawn from these numerical exercises. First, Hoppel's inversion is capable of inverting ideal CNC number concentration data corresponding to a sharp, trimodal, lognormal distribution. The peak diameters were located to within 0.0001 μm and error in the total number concentration amounted to 5.6%. Second, 5 – 20% random relative error in the CNC data did not significantly affect the inversion routine. The primary peak diameter was within 0.2% for all error values, while the secondary peak diameter was within 0.1% for 5% error and within 1% for 20% or less error. Total number estimation remained within the 5.6% limit for the ideal case. Third, flowrate error has a much greater effect on the inversion results than does CNC error. Limiting the sheath and excess flowrates to 6.9 - 7.1 ℓpm ($\pm$ 1.4%) results in the determination of the primary peak diameter to within a 0.5% accuracy and the total number to within 20%. Positive deviations cause smaller errors in the location of the peak diameter than do negative deviations. The errors associated with sample flowrate perturbations are minimal.

§3.4.4 Calibration

Because classifier flowrate has a large effect on the success of the data inversion, the flowmeters on both classifiers (EMC1 and EMC2) were calibrated. The thermal mass sheath and excess flowmeters supplied with each classifier were replaced by capillary flowmeters. EMC1 would be operated with the flowrates set at Q_c= Q_m= 10 ℓpm and Q_s= 2 ℓpm to generate the dry monodisperse feed aerosol. The original thermal mass meter was used to measure the sample flowrate. Actual flowrate values were less critical for this instrument; a stable, constant flow was all that was required. A constant pressure of 5.5×10^4 Pa (8 psig) was maintained at the inlet of the sheath air capillary. The sheath and excess air were calibrated by measuring the time required for a known volume to flow through a Singer Model

DTM-325 dry test meter. A bubble flowmeter was used to calibrate the sample air flowmeter. A linear fit to the data for each of the three flowmeters is presented in Table 3.1. Note that Q_c and Q_m are functions of the pressure drop across the capillary and Q_s is a function of the meter voltage. The error is estimated to be $\pm$ 2% for the sheath and excess capillary meters, and $\pm$ 1.3% for the sample meter.

The sheath and excess flowmeter calibrations for EMC2 were far more critical than for EMC1. Classifier EMC2 is used to measure the size distributions in the reactor system. Flowrates of $Q_c = Q_m = 7$ ℓpm and $Q_s = 0.3$ ℓpm were chosen for the various reasons discussed in the preceding text. The sample flowrate was set by the pump in the CNC. The same method of calibration was used as for the meters of EMC1, although longer times and larger volumes were used to minimize the error. A pressure of 1.03×10^5 Pa (15 psig) was maintained at the inlet to the sheath air capillary. Both dry and humidified air ($\sim$ 90%) air were used for the calibration. No difference was observed in the results even though the viscosity of saturated air is estimated to be approximately one percent less than that of dry air (Hirschfelder et al., 1964). The calibration formulas are presented in Table 3.1. Flowrate error is determined to be $\pm$ 0.8% — the longer measuring times and extra care taken with EMC2 resulting in a 50% reduction in the error as compared to EMC1. Therefore, the error expected in the measured peak diameter as a result of flowrate fluctuations in EMC2 should be less than 0.5%.

Checking the response of an instrument to PSL (polystyrene latex) particles is a standard method of aerosol instrument calibration. Three different PSL sizes — 0.14 $\pm$ "?" μm (no standard deviation was given by the manufacturer), 0.198 $\pm$ 0.0036 μm, and 0.27 $\pm$ 0.006 μm — were fed to EMC1 and EMC2. Both classifiers were operated at the nominal flowrates of $Q_c = Q_m = 7$ ℓpm and $Q_s = 0.3$ ℓpm. In some cases, two scans were taken for the same PSL size using the same instrument. These measurements were made (on different days) for the purpose of checking the reproducibility of the size distribution. The size distributions are plotted on a

scale of zero to one in Figures 3.11, 3.12, and 3.13. The peak diameters and the corresponding classifier are listed in Table 3.6.

The diameter agreement between the classifiers for each size is excellent. However, the measured peak diameter is different than the specified mean PSL diameter. In the case of the 0.198 μm PSL, the measured diameter is smaller by 0.005 μm. This amounts to a 2.5% error — more than would be due to the flowrates, the inversion method, or the CNC concentrations. One might initially suspect an error in the voltage readings. In the past, EMC1 had needed electrical repairs and the voltage circuit was reset. Any bias in the voltage reading that would have resulted from a systematic error in the factory calibration was eliminated. Another explanation could be systematic, not random, error in the flowrates. However, this would lead either to consistently high or consistently low diameter estimations. The results in Table 3.6 show this was not the case.

The final possibility considered was that the PSL, which was several years old, had "aged" and was no longer the specified size. Since measuring the size of PSL using an electron microscope involves special techniques to prevent the swelling or shrinking of the particle upon irradiation (see Bradford and Vanderhoff, 1955), a different tack was taken. If the same diameter was measured with a completely different set of classifier operating conditions, this would indicate that the measured diameters were indeed correct. Any possible bias associated with the operating conditions would have been eliminated. In general, the flowrates $Q_c = Q_m = 10$ ℓpm and $Q_s = 2$ ℓpm will not measure a size distribution with the same accuracy as the flowrates $Q_c = Q_m = 0.7$ ℓpm and $Q_s = 0.3$ ℓpm, particularly not as sharp a distribution as that of the PSL ($\sigma \sim 1.03$). However, the peak diameter in either case should be the same given the same initial aerosol. This was verified by generating CNC data corresponding to a lognormal distribution ($D_{p_g} = 0.193$ μm, $\sigma = 1.03$, and $N_{total} = 10000$ particles/cm^3) for both sets of flowrates. The peak diameter of this distribution was 0.1928 μm. Inversion of the 7/7/0.3 ℓpm data

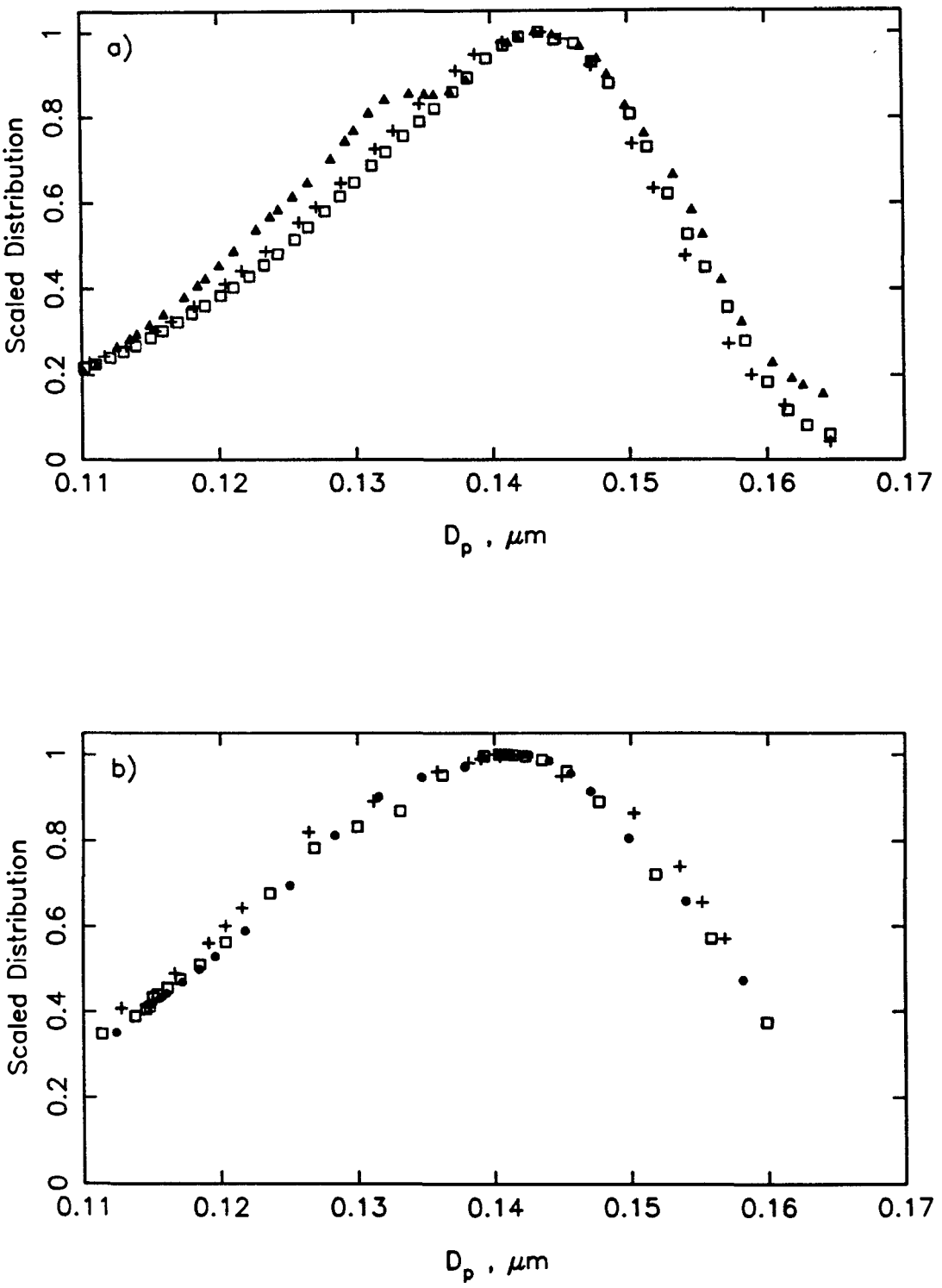

Figure 3.11 Inversion results for $0.14 \pm ?$ μm PSL. Figure a): Q_c= Q_m= 7.0 ℓpm, Q_s= 0.3 ℓpm; EMC1 (□), EMC2(a) (+), EMC2(b) (▲). Figure b): Q_c= Q_m= 10 ℓpm, Q_s= 2 ℓpm; EMC1(a) (□), EMC1(b) (•), EMC2 (+).

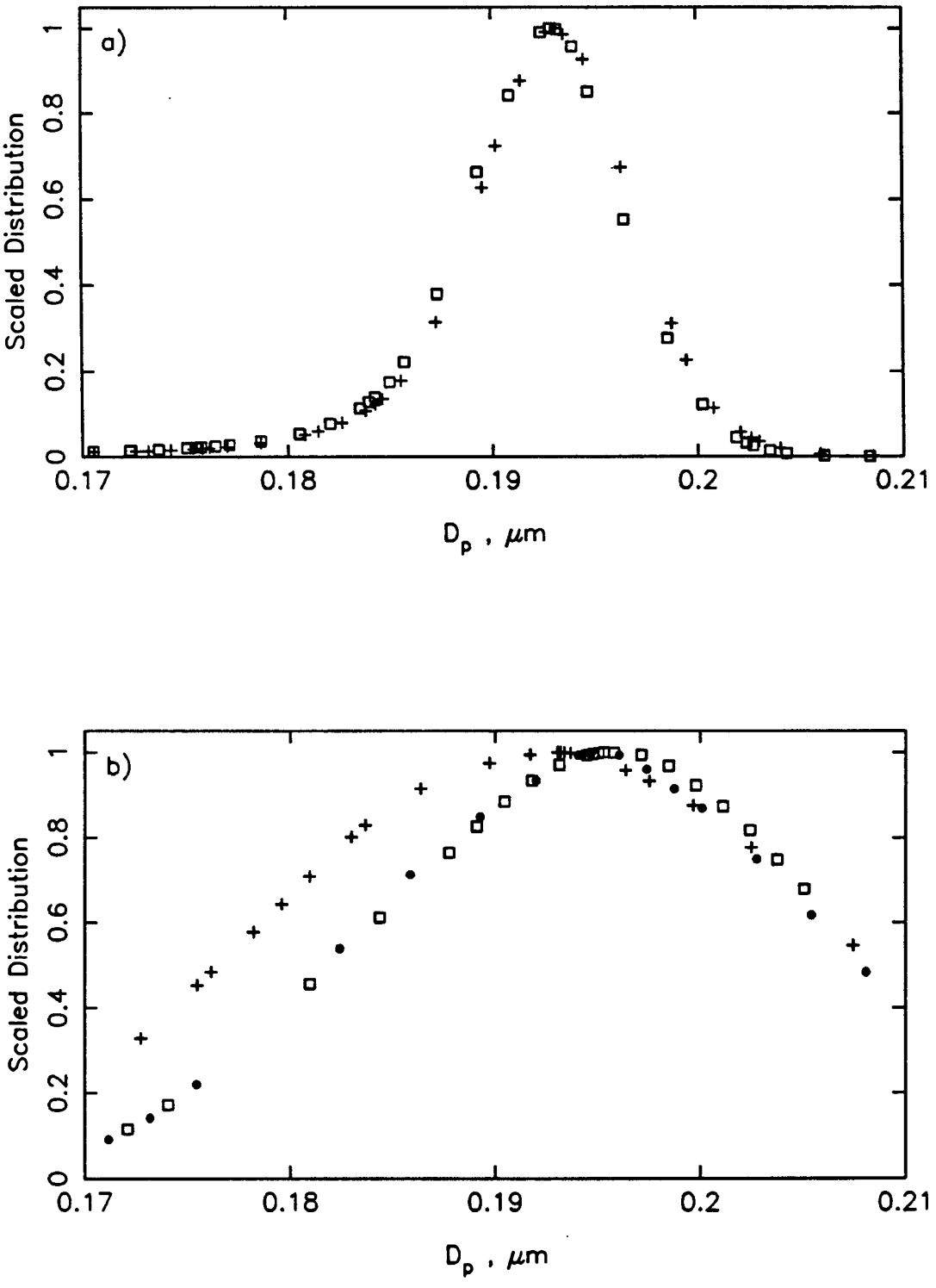

Figure 3.12 Inversion results for 0.198 ± 0.0036 μm PSL. Figure a): $Q_c = Q_m = 7.0$ ℓpm, $Q_s = 0.3$ ℓpm; EMC1 (□), EMC2 (+). Figure b): $Q_c = Q_m = 10$ ℓpm, $Q_s = 2$ ℓpm; EMC1(a) (□), EMC1(b) (•), EMC2 (+).

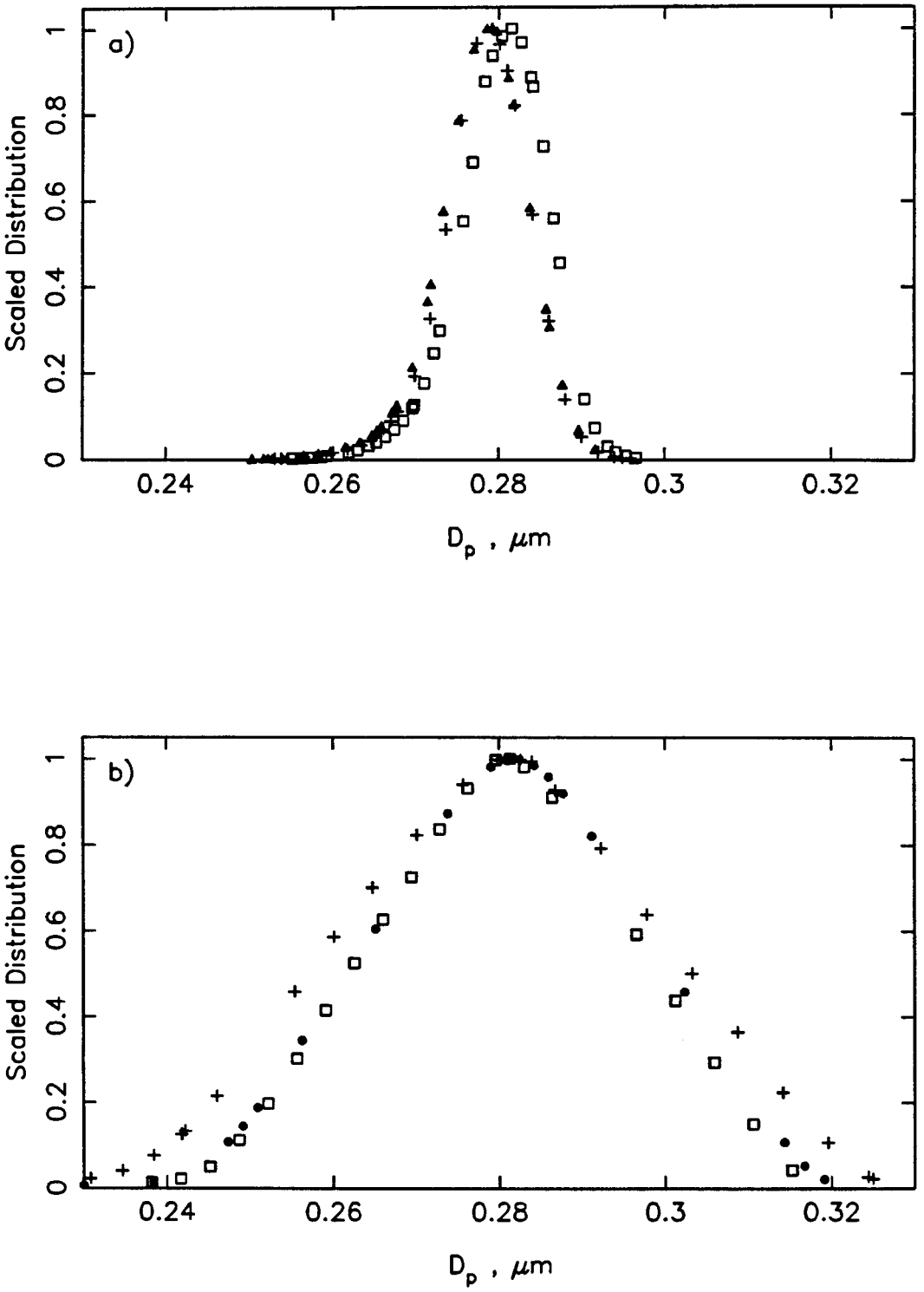

Figure 3.13 Inversion results for 0.27 ± 0.006 μm PSL. Figure a): Q_c= Q_m= 7.0 ℓpm, Q_s= 0.3 ℓpm; EMC1 (□), EMC2(a) (+), EMC2(b) (▲). Figure b): Q_c= Q_m= 10 ℓpm, Q_s= 2 ℓpm; EMC1(a) (□), EMC1(b) (•), EMC2 (+).

Table 3.6

Inversion Results For PSL at Nominal Flowrates
of $Q_c = Q_m = 7$ ℓpm, $Q_s = 0.3$ lpm

PSL (μm)	Classifier	Peak Diameter (μm)	Average Diameter (μm)
$0.14 \pm ?$	EMC1	0.1435	
$0.14 \pm ?$	EMC2(a)	0.1437	0.1435
$0.14 \pm ?$	EMC2(b)	0.1432	
0.198 ± 0.0036	EMC1	0.1929	
0.198 ± 0.0036	EMC2	0.1932	0.1930
0.27 ± 0.006	EMC1	0.2816	
0.27 ± 0.006	EMC2(a)	0.2792	0.2800
0.27 ± 0.006	EMC2(b)	0.2792	

Table 3.7

Inversion Results For PSL at Nominal Flowrates
of $Q_c = Q_m = 10$ ℓpm, $Q_s = 2$ lpm

PSL (μm)	Classifier	Peak Diameter (μm)	Average Diameter (μm)
$0.14 \pm ?$	EMC1(a)	0.1407	
$0.14 \pm ?$	EMC1(b)	0.1419	0.1409
$0.14 \pm ?$	EMC2	0.1401	
0.198 ± 0.0036	EMC1(a)	0.1953	
0.198 ± 0.0036	EMC1(b)	0.1947	0.1944
0.198 ± 0.0036	EMC2	0.1932	
0.27 ± 0.006	EMC1(a)	0.2814	
0.27 ± 0.006	EMC1(b)	0.2813	0.2813
0.27 ± 0.006	EMC2	0.2812	

resulted in a peak diameter of 0.1930 μm, while the 10/10/2 ℓpm data gave 0.1923 μm. The error was 0.09% and 0.3%, respectively.

The three PSL sizes were measured with both classifiers at Q_c= Q_m= 10 ℓpm and Q_s= 2 ℓpm. These results are presented in Figures 3.11, 3.12, 3.13, and Table 3.7. The differences between the diameters determined for these flowrates and those determined for the 7/7/0.3 ℓpm flowrates are 1.8%, 0.7%, and 0.46% for the 0.14, 0.198, and 0.27 μm PSL, respectively. Not surprising was the fact that the largest difference between peak diameters was found for the 0.14 μm PSL. It is a more difficult to assign a "peak" value to a broad distribution than to a sharp distribution. Also, the smaller the particle size, the more likely the distribution is to be affected by the fines associated with the PSL suspension fluid. This could explain why the size distribution for the 0.14 μm PSL was not Gaussian in shape, having a strong tail on the small diameter side, even for the 7/7/0.3 ℓpm distribution.

It is difficult to reach any conclusion given the 0.14 μm (nominal) PSL results. However, the close agreement between peak diameters for the two larger PSL sizes at the two different sets of operating conditions supports the premise that the PSL mean diameter has changed over the years. The size distribution obtained at the 7/7/0.3 ℓpm conditions could be regarded as correct. The PSL sizes were actually 0.193 $\pm$ 0.004 μm and 0.28 $\pm$ 0.005 μm in diameter. More important than the sizing of the PSL, however, is the knowledge that classifiers behave identically under the same operating conditions and the size distribution can be reproduced given a constant aerosol source.

One final check was made on classifier behavior. The reactor experiments would involve measuring shifting size distributions, so the classifier sensitivity to a small peak diameter change had to be determined. To estimate this sensitivity, a $MnSO_4$ aerosol was generated using an atomizer and fed to the first classifier. The voltage on EMC1 was set at 2151 V and the resulting distribution measured with

EMC2. The process was then repeated for EMC1 voltages of 2200 V and 2250 V at the same operating conditions. The voltage scan data were inverted and the results are plotted in Figure 3.14. Given the operating conditions and the voltages 2151, 2200, and 2250 V, the primary peak diameters out of the first classifier were calculated to be 0.1004, 0.1017 and 0.1031 μm, respectively. The corresponding primary peak diameters measured by EMC2 were 0.0993, 0.1014, and 0.1026 μm. While there is surely some error both in the calculated EMC1 diameters and in the inverted EMC2 diameters, the distributions in Figure 3.14 are distinct, recognizable as three different aerosols, and follow the correct trend of increasing size. When comparing aerosol size distributions measured at the same operating conditions, errors in the absolute size will not affect the comparison *between* the distributions, since each distribution experiences the same systematic errors. Although error in the CNC concentrations will be unique to each distribution, the effect on the resulting peak diameter was shown to be minimal. Therefore, the classifier is able to recognize a real peak difference on the order of 0.001 μm.

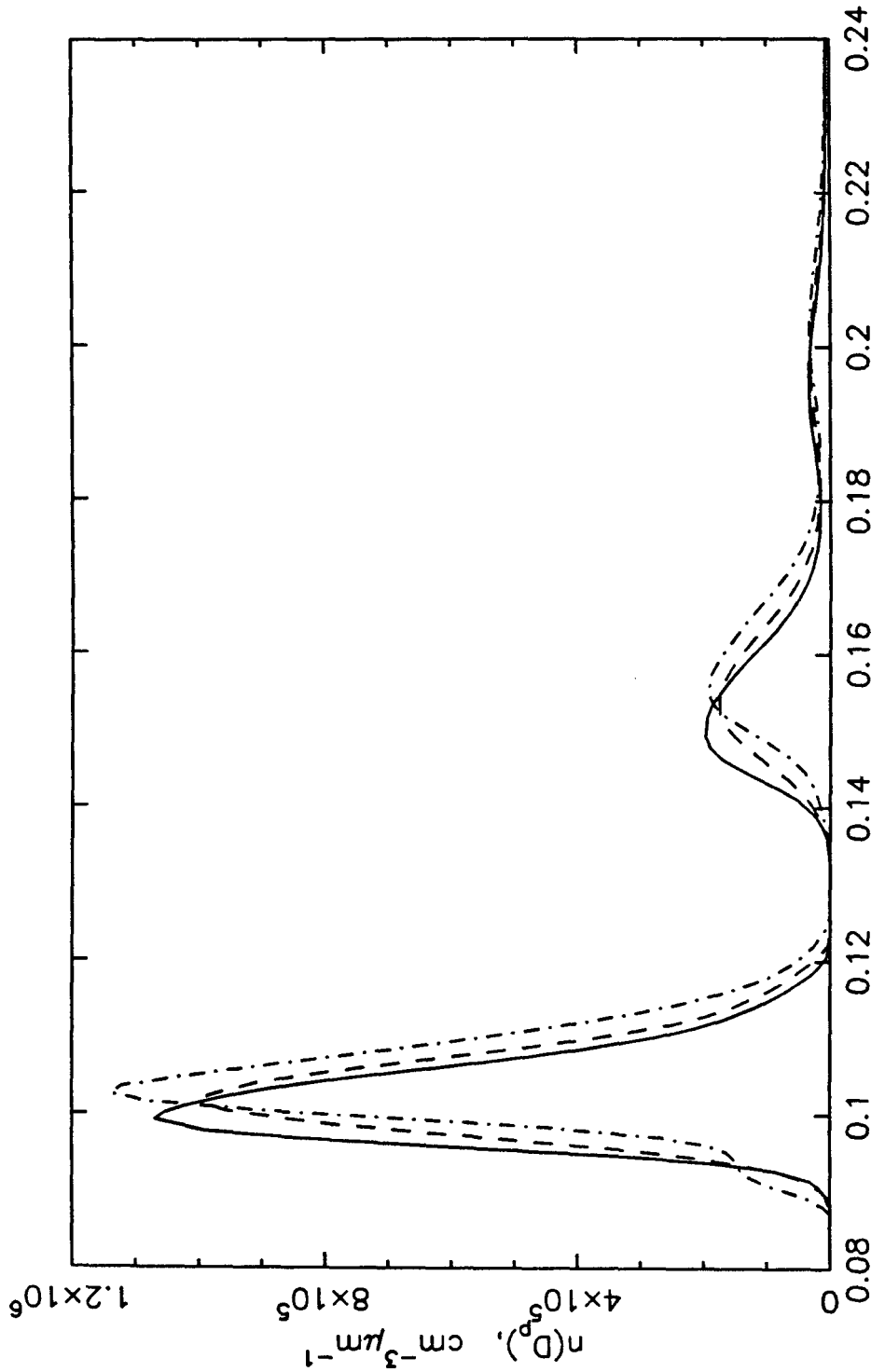

Figure 3.14 Size distribution measured by EMC2 for three EMC1 voltages. $V_1 = 2151$ V (————), $V_2 = 2200$ V (– – – – –), $V_3 = 2250$ V (—·—·—·—).

CHAPTER 4

THE MANGANESE CATALYZED OXIDATION OF S(IV) TO S(VI) IN THE AQUEOUS-PHASE

The various mechanisms by which SO_2 is oxidized in the atmosphere have long been a subject of interest. With the attention that has been focused on the problem of acid rain, the subject continues to be a topic of research. The aqueous-phase metal-catalyzed oxidation of SO_2 by oxygen has been predicted to be a significant contributor to atmospheric sulfate — particularly at night when the gas phase oxidant concentrations fall (Hoffmann and Jacob (1984), Saxena and Seigneur (1987)). Manganese and iron are generally considered the most important of the potential metal catalysts and have been extensively studied. There is still, however, little agreement as to the mechanisms and rate expressions that describe the reactions, or as to the relative importance of iron versus manganese (e.g., Hoffmann and Calvert (1985), Cheng et al. (1971), Clarke and Williams (1983), Nash (1979), and Barrie and Georgii (1976)). This chapter will review critically the literature concerned with manganese-catalyzed S(IV) oxidation by oxygen. In particular, the various methods (bulk phase versus droplet phase) used to study this reaction and the concentration regimes in which they are applicable will be addressed. First, however, a brief discussion concerning the relationship between aerosols and fog/clouds will be presented, since these represent two stages of the atmospheric hydrological cycle to which kinetic rate expressions must be applied.

§4.1 Aerosols Versus Fog/Cloud Droplets

Particles exist in the atmosphere in a wide range of sizes and concentrations. Aerosol particles are considered to be those generally less than a micron in diameter. Ionic strengths of such aqueous particles have been predicted to range

from 1 to 20 M (Stelson and Seinfeld, 1981). Fog droplets, on the other hand, are characterized by diameters of $5 - 10$ μm and ionic strengths from 10^{-3} to 10^{-2} M. The water content of the various phases of aqueous atmospheric particles also varies considerably (Seinfeld, 1986) — aerosols: $10^{-11} - 10^{-10}$ ℓ H_2O/ℓ air; fog: $5 \times 10^{-8} - 5 \times 10^{-7}$ ℓ H_2O/ℓ air; and clouds: $10^{-7} - 10^{-6}$ ℓ H_2O/ℓ air.

The relationship between the aerosol in the atmosphere and fog or clouds is an intimate one. Indeed, Prospero et al. (1983) referred to aerosols as "critical phase change catalysts" because of the significant role they play in vapor-liquid phase changes in the atmosphere. With an increase in the ambient relative humidity, aerosol particles containing soluble species act as condensation nuclei and grow such that thermodynamic equilibrium is maintained between the particle solution and the atmosphere. The growth of a soluble nucleus is described by the Köhler curves, which relate the relative humidity, or saturation ratio, to the droplet diameter given an initial seed aerosol:

$$\ln RH = \frac{4\sigma \overline{v}_w / RT}{D_p} - \frac{6 n_s \overline{v}_w / \pi}{D_p^3}, \tag{1}$$

where σ is the droplet surface tension, $\overline{v}_w$ is the partial molar volume of the water in the droplet, D_p is the droplet diameter, and n_s is the number of moles of solute in the solution. In the above equation it is assumed that the solution is dilute. The value of n_s is determined by the size of the seed aerosol or nucleus. If the solute does not dissociate completely in solution, this must be reflected in the value of n_s used to construct the curves. Figure 4.1 shows the Köhler curves for three different sizes of $MnSO_4$ seed particles assuming either no dissociation or complete dissociation of the salt. Manganese sulfate has an equilibrium association constant of 182 M^{-1}, so the actual Köhler curve would fall somewhere between the two extremes. The humidity corresponding to the maximum point on the curve is known as the critical saturation ratio. When the ambient relative humidity exceeds the critical saturation ratio for a given aerosol particle, the particle will grow indefinitely.

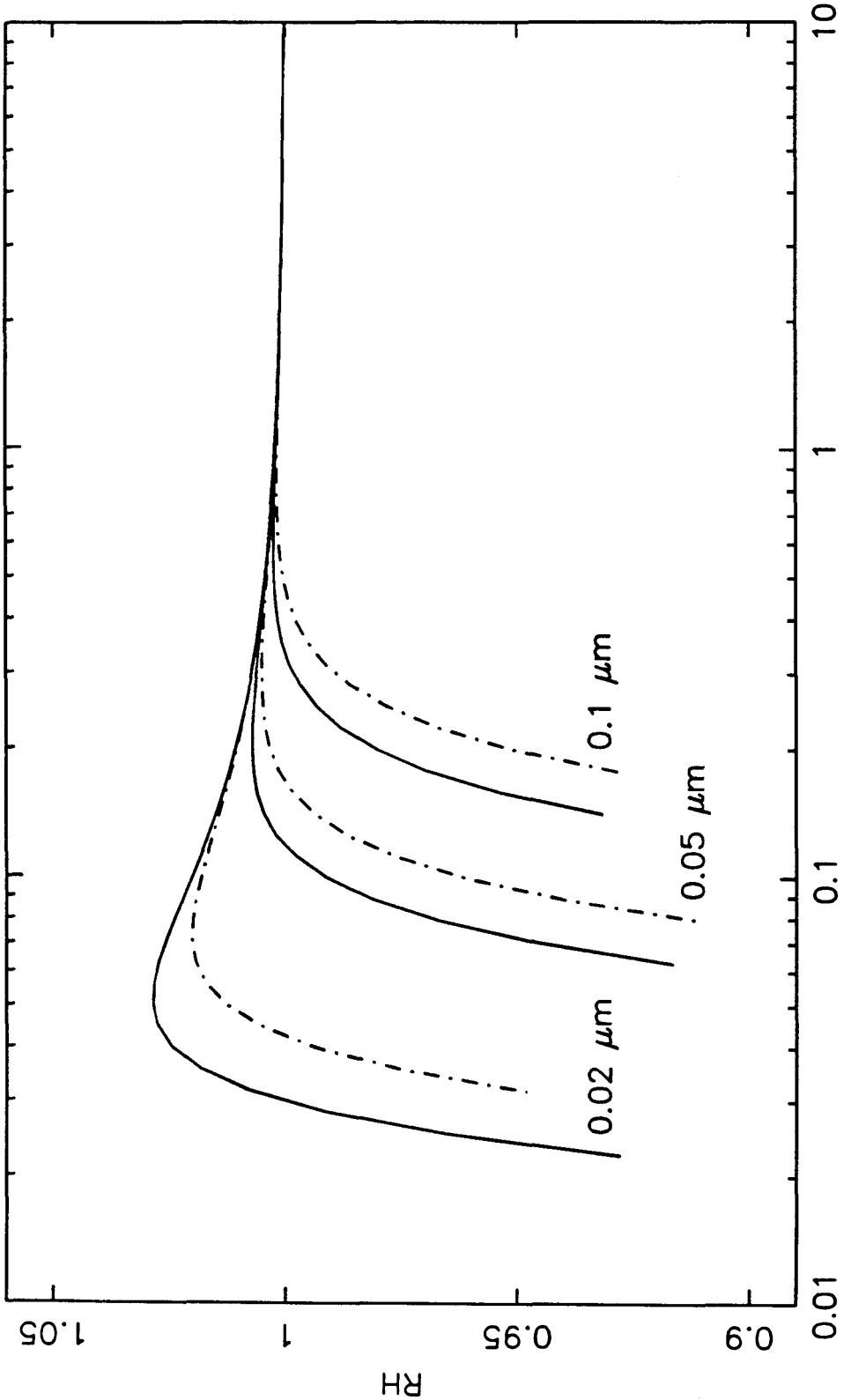

Figure 4.1 Köhler curves for various $MnSO_4$ seed particle diameters at 25°C. No dissociation, $n_s = n_{MnSO_4}$ (————); complete dissociation, $n_s = 2\,n_{MnSO_4}$ (—·—·—·—).

In other words, it is "activated" for growth. It is in this way that atmospheric aerosol gives rise to fog droplets. In a similar manner, when the ambient relative humidity falls below the critical saturation ratio for a particular droplet, the droplet evaporates until it is once again in equilibrium with its surrounding atmosphere.

The relationship between aerosol and fog or clouds is represented schematically in Figure 4.2. This figure is similar to one found in Munger et al. (1983), except that the potential for reaction in the aerosol phase has been included. Note that this figure ignores some of the various methods by which either aerosols or fog/cloud droplets may escape the cycle, e.g., impaction, deposition, or precipitation. Prospero et al. (1983) and Pruppacher (1986) note that an aerosol particle may pass through the fog or cloud phase as many as 10 to 25 times before being deposited as precipitation. The chemical reactions that occur in the dilute fog or cloud droplet will be reflected in the size and composition of the regenerated aerosol particle. In turn, both the aqueous-phase and/or surface reactions that occur in the aerosol, will affect the critical saturation ratio necessary for future fog/cloud events and the resulting fog/cloud droplet chemistry. Cass (1975) noted that coastal morning fogs occurred on the same days as high afternoon aerosol sulfate concentrations. Hough (1987) has modeled cloud formation over hills and found that the composition and concentration of the water-soluble aerosol is critical in determining the chemical composition of the cloud droplets. The species derived from the aerosol also have a substantial effect on the solution ion activity coefficients, which must be calculated to predict the aqueous cloud chemistry.

Thus, given the interrelationship between aerosol and fogs in the atmosphere, the chemistry of fog droplets might depend on the chemistry of aerosol particles. All potentially significant chemical processes must be studied in the concentration regimes representative of both fogs and aerosols. Moreover, it is unlikely that the same mechanism and rate expression that explain observed rates of reaction at ionic strengths of less than 10^{-3} M and concentrations on the order of micromolar

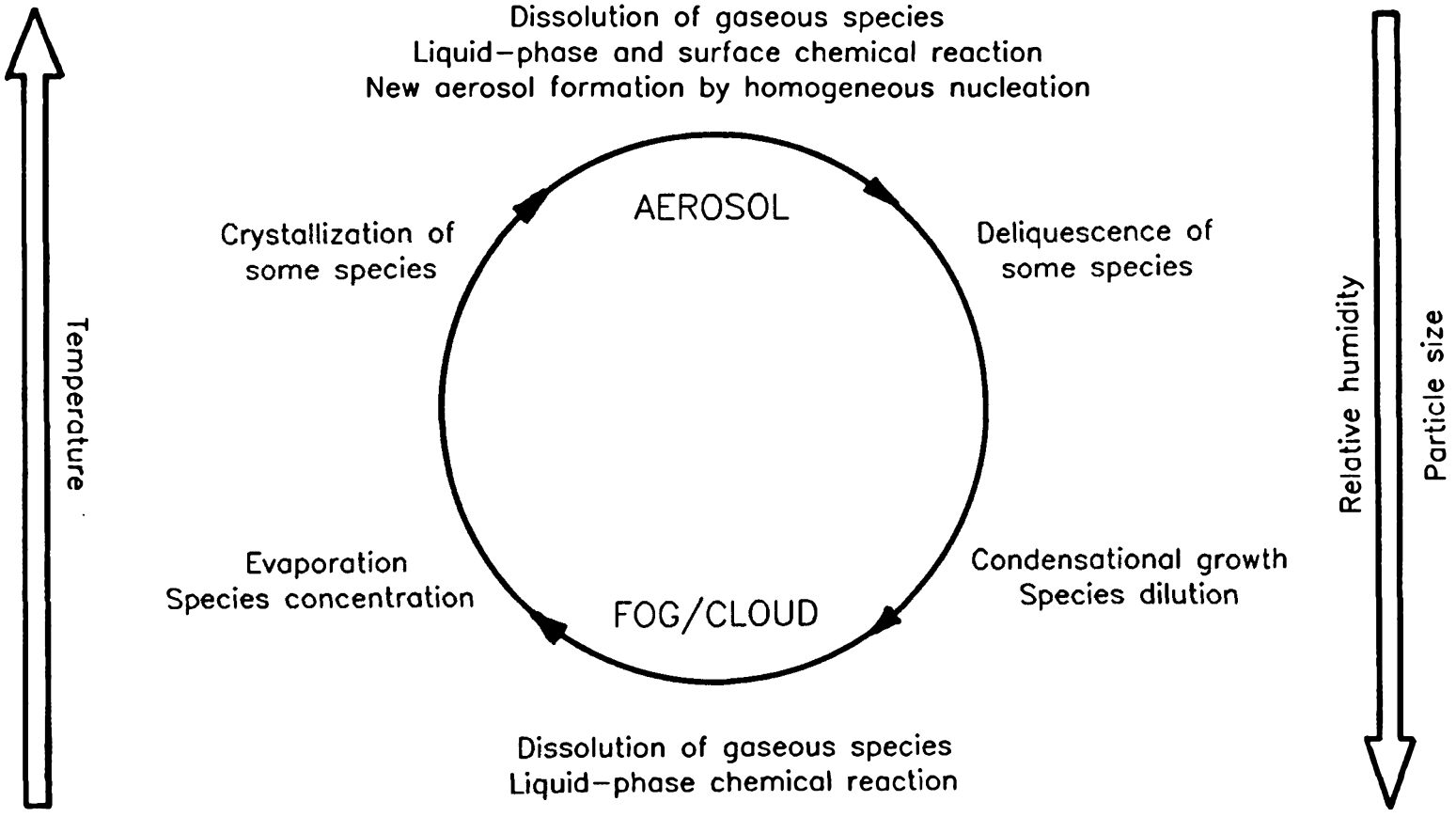

Figure 4.2 The relationship between aerosols and fog or cloud water droplets.

will apply to a situation in which the ionic strength and concentration are both greater than 1 M. The contribution of aerosols as a source in the overall S(VI) budget is likely to be small when compared to that of fog droplets, simply due to the mass difference resulting from the different water contents. However, with the increasing complexity of atmospheric models that attempt to explain fog and cloud formation and because of the importance of aerosols in urban atmospheres and source plumes, knowledge about aerosol chemistry is essential.

§4.2 The Manganese-S(IV) Reaction System

The aqueous-phase manganese-S(IV) reaction system has been studied both in the bulk phase and in the droplet or aerosol phase. Bulk phase studies were done either in batch or flow reactors. In a batch reactor, the rate of reaction was deduced by following the uptake of reactant (S(IV)) or the generation of product (S(VI)). Two types of flow reactors have been used: 1) time resolution of the reactant and/or product concentrations was obtained by sampling along the length of the reactor; or 2) steady-state reactor operation was assumed and the reaction rate was predicted by fitting the reactant and/or product concentrations to the equations describing an ideal continuous stirred tank reactor (CSTR). The concentrations were determined using either a chemical or optical absorption technique. The solution pH was usually monitored.

In aerosol phase studies, the aerosol was generated and passed through a reactor. The initial aerosol manganese concentration is prescribed by thermodynamic equilibrium. The most common method of reaction rate measurement was SO_2 uptake as a function of time. Aerosol size changes were also used as an indication of reaction in several studies. Measurement of the species collected by filtering the reactor effluent resulted in artifact formation and was not a preferred method. Since it was not possible to measure the aerosol solution pH, this was typically estimated.

The results for a number of aqueous-phase manganese-S(IV) system studies are presented in Table 4.1. The phase (bulk or droplet/aerosol), the reactant concentrations, the solution pH, and the predicted reaction rate expressions are given for each study. If a particular value (e.g., pH) was not explicitly stated in the literature, an estimate was made based on those parameters that were given. It has been assumed that SO_2 or S(VI) uptake is equivalent to S(VI) production. This is equivalent to assuming that steady-state conditions exist between the gas phase SO_2 and aerosol phase S(IV) in the aerosol studies.

§4.2.1 Bulk Phase Studies

The results of four bulk phase studies on the S(IV)-manganese system (Coughanowr and Krause (1965), Bronikowski and Pasiuk-Bronikowska (1981), Huss et al. (1982a,b), Lim et al. (1982), Ibusuki and Barnes (1984), and Martin and Hill (1987)) are summarized in Table 4.1. The manganese and S(IV) concentrations at which the experiments were performed are typical of fogwater. The reaction was found to be zero order in oxygen by all investigators except Bronikowski and Pasiuk-Bronikowska (1981). At manganese concentrations greater than 7×10^{-4} M, Bronikowski and Pasiuk-Bronikowska (1981) found first-order dependence on the oxygen concentration. At lower manganese concentrations the oxygen dependence reduced to zero order. Martin and Hill (1987) have identified three regimes of behavior that depend on the S(IV) concentration. The rate of reaction is second order with respect to manganese and zero order in S(IV) for $[S(IV)] \geq 10^{-4}$ M. When $[S(IV)] \leq 10^{-6}$ M, the reaction is first order in both manganese and S(IV). If the initial S(IV) concentration falls between 10^{-6} and 10^{-4} M, the rate is dependent on the initial S(IV) concentration. Whether or not the initial manganese concentration would significantly change the reaction rate in these various regimes was not explored, and the study was typically run with $[Mn^{2+}] < [S(IV)]$. No explicit dependence on the hydrogen ion concentration was observed. There is good agreement between the various researchers as to the order of reaction in the specific

Table 4.1

Reaction Rate Expressions for the
Aqueous-Phase S(IV)-Mn(II) Reaction

Source	Phase	[Mn(II)]*	$[S(IV)]_0^*$ or p_{SO_2}	pH	Rate Expression*	Comments
Coughanowr & Krause (1965)	bulk	2.6(-5) – 6.6(-4)	1.7(-3)	2 – 3†	$R = 456\,[\mathrm{Mn(II)}]^2$	$[O_2]_0 \sim 0.3(-3) - 0.6(-3)$ M, $T = 25°C$. Batch apparatus. $MnSO_4$ used.
	bulk	3.3(-3) – 6.6(-2)	1.9(-3)	3†	$R = 1.791(-3)[\mathrm{Mn(II)}]^{0.1275}$	$[O_2]_0 \sim 0.1(-3) - 0.7(-3)$ M, $T = 25°C$. Flow apparatus. $MnSO_4$ used.
Bronikowski & Pasiuk-Bronikowska (1981)	bulk	9.0(-4) – 6.4(-3)†	7.0(-3) – 1.5(-2)	1†	$R = \frac{[\mathrm{Mn(II)}]^2}{1.6(-2)+0.2[\mathrm{S(VI)}]}$ ($[\mathrm{Mn(II)}] < 7(-4)$ M) $R = \frac{[O_2][\mathrm{Mn(II)}]^2}{1.2[\mathrm{Mn(II)}]^2+0.2[O_2][\mathrm{S(VI)}]}$ ($[\mathrm{Mn(II)}] > 7(-4)$ M)	$T = 20°C$. Batch apparatus, gases bubbled through. $MnSO_4$ used.
Huss et al. (1982a,b) Lim et al. (1982)	bulk	1.0(-5) – 5.0(-4)	1.0(-3) – 1.2(-1)	1 – 4	$R = 10^{2.83-4.07\sqrt{I}/(1+\sqrt{I})}[\mathrm{Mn(II)}]_0^2 + 10^{-0.076-1.01\sqrt{I}/(1+\sqrt{I})}[\mathrm{Mn(II)}][HSO_3^-]$	$[O_2]_0 \sim 1.8(-3) - 0.1$ M, $T = 25°C$. Batch reactor. Strong ionic strength noted independent of acid or salt used ($I = 0.01 - 0.1$ M). No difference in rate of $MnSO_4$ vs. $MnCl_2$. Reaction inhibited by phenolic antioxidants. Lesser inhibition by chelating agents.
Ibusuki & Barnes (1984)	bulk	1.0(-6) – 5.0(-6)	7.0(-6) – 1.3(-5)	3 – 6	$R_{MnSO_4} = 1.67(3)\,[S(IV)][Mn(II)]$ $R_{MnCl_2} = 5.0(3)\,[S(IV)][Mn(II)]$	Solutions saturated in O_2. $T = 23.7°C$. CSTR used. Drop in rate coefficient for pH < 3, pH > 6.

Martin & Hill (1987)	bulk	1.0(-5)	$\geq$ 1.0(-4)	2 - 6	$R = (680)\,10^{-4.07\sqrt{I}/(1+\sqrt{I})}[\mathrm{Mn(II)}]^2$	T = 25°C. Optical cell — batch. $MnCl_2$ used. Ionic strength effect (I = 10^{-3} – 1 M) independent of acid or salt added.
		?	$\leq$ 1.0(-6)	?	$R = (1000)\,10^{-4.07\sqrt{I}/(1+\sqrt{I})}[\mathrm{Mn(II)}][\mathrm{S(IV)}]$	
		?	> 1.0(-6) and < 1.0(-4)	?	$R = f([\mathrm{S(IV)}]_0)$	
Barrie & Georgii (1976)	droplet D_p = 2 mm	1.0(-4)	700 ppb	2 – 3	$R = 940\,[SO_3^{2-}]$ (Mn(II) dependence not determined)	T = 25°C. RH ~ 100%. Droplet suspended at end of pipette. $MnCl_2$ used. 10% droplet volume evaporated /hour. Droplets followed for several hours. Analyzed for composition.
	droplet D_p = 2 mm	1.0(-5)	10 – 1000 ppb	4.5 – 3.5	$R = 1.85(-9)\,[SO_{2,(g)}]^{0.727}$ (p_{SO_2} in ppb, Mn(II) dependence not determined)	Same environmental conditions. 10 – 30 min. absorption time allowed. Mn + Fe synergism observed.
Matteson et al. (1969)	polydisperse aerosol Dry vol. mean dia. = 0.72 μm	0.29 (99.5%)	5 – 140 ppm	?	$R = \frac{0.0037\,p_{SO_2}[\mathrm{Mn(II)}]_0}{53+p_{SO_2}} - \frac{62.7\,[\mathrm{Mn(II)}]_0[\mathrm{S(VI)}]^2}{53+p_{SO_2}}$ (p_{SO_2} in ppm)	T = 25°C. RH = 96%. Tubular reactor. Deliquesced $MnSO_4$ salt. Composition determined by collection on filters. N_{tot} ~ 8(4) particles/cm^3.
Cheng et al. (1971)	polydisperse aerosol supported on teflon beads Dry dia. ~ 0.1 - 3 μm	2.2†	4.5 ppm	?	$R\left(\frac{\mathrm{mol}}{s}\right) = 2.22(-3)\,[SO_{2,(g)}]\,M_{MnSO_4}$ (M_{MnSO_4} = mg $MnSO_4$ in reactor)	T = 23°C. RH = 95%. Packed bed reactor. Deliquesced salts. $MnSO_4$ used. $MnSO_4$ more effective than $MnCl_2$. SO_2 uptake measured. Fractional conversion ↑ with humidity.
Cains & Carabine (1978)	polydisperse aerosol Dry modal dia. = 0.06μm	0.16 (99.7%)	63 ppm	?	$R = \frac{0.0338\,p_{SO_2}[\mathrm{Mn(II)}]_0}{218+p_{SO_2}} - \frac{0.077\,[\mathrm{Mn(II)}]_0[\mathrm{S(VI)}]^2}{218+p_{SO_2}}$ (p_{SO_2} in ppm)	T = 21°C. RH ≥ 96%. Tubular reactor. N_{tot} ~ 10^5 – 10^6 particles/cm^3. $MnSO_4$ used. Size changes measured.

Kaplan et al. (1981)	monodisperse aerosol Dry dia. ~ 5.0 μm	0.06†	0.1 – 1.0 ppm	?	$R = 0.04\,[\mathrm{S(IV)}]$ (Mn(II) dependence not determined)	T = 25°C. RH ~ 90%. Tubular reactor with sheath air. Deliquesced salts. 0.026 moles $MnSO_4$/mole $(NH_4)_2SO_4$. Radioactive sulfur content of aerosols measured. Wet aerosol dia. measured.
Crump et al. (1983a)	polydisperse aerosol Dry dia. ~ 0.1 – 0.5 μm	1 – 2†	10 – 50 ppm	?	$R = 8.3(-5)/[\mathrm{H^+}]$	T ~ 23°C. RH = 90 – 97%. CSTR. Deliquesced $MnSO_4$ salts used. N_{tot} ~ 10^4 particles/cm^3. Wet aerosol diameter measured.
Berresheim & Jaeschke (1986)	polydisperse aerosol Dry dia. ~ 0.01 – 1 μm	2.6 – 5 molal	5 – 120 ppb	~ 2	$R_{MnSO_4} \sim \frac{0.282(-8)\,C_{Mn}^{1.03}[SO_{2,(g)}]}{a(H^+)\,a_\pm(MnSO_4)^{0.64}\,L}$	T = 25°C. RH = 0 – 94%. Plug flow reactor. $N_{tot} = 10^3 - 10^5$ particles/cm^3. Wet aerosol distr. estimated. SO_2 uptake measured. C_{Mn}= 58 – 545 μg/m^3 air.
		1.13 – 3 molal	5 – 120 ppb	3 – 4	$R_{MnCl_2} \sim \frac{0.305(-8)\,C_{Mn}^{0.46}[SO_{2,(g)}]}{a(H^+)\,a_\pm(MnCl_2)^{-0.46}\,L}$	Same aerosol & environmental conditions. C_{Mn}= 73.1 – 881 μg/m^3 air.
		1 – 3 molal	5 – 120 ppb	0.7 – 2	$R_{Mn(NO_3)_2} \sim \frac{141(-8)\,C_{Mn}^{0.64}[SO_{2,(g)}]}{a(H^+)\,a_\pm(Mn(NO_3)_2)^{-0.11}\,L}$ (C_{Mn} is μg Mn(II)/m^3 air, L is ℓ H_2O/ℓ air)	Same aerosol & environmental conditions. C_{Mn}= 26.9 – 256 μg/m^3 air.

* Concentrations are in units of moles/ℓ (M) and rates in moles/(ℓ s) (M s^{-1}) unless otherwise noted.

$X.X(-Y)$ indicates $X.X \times 10^{-Y}$.

(RH%) in [Mn(II)] column indicates the relative humidity corresponding to the stated concentration, neglecting the Kelvin effect: RH = $a_w(conc.)$.

† The value is an estimate.

concentration regimes. For [S(IV)] $\sim$ 0.001 $-$ 0.12 M, Huss et al. (1982a,b) determined that their data were best fit by a two-term rate expression. The second-order manganese term is dominant, while the first-order S(IV) term contributes significantly only at the smallest manganese concentrations ($[Mn^{2+}] \sim 10^{-5}$ M) used in the study. Coughanowr and Krause (1965) studied the reaction up to manganese concentrations of 0.07 M. Above $[Mn^{2+}] = 0.001$ M, the reaction rate became relatively insensitive to changes in the manganese concentration — dropping from second order in manganese to approximately 0.1 in order. The oxidation rate continued to be zero order in S(IV) and O_2. Bassett and Parker (1951) also observed a decrease in the amount of oxidation with increasing manganese concentration, although the transition occurred at 1 M in their study. The rate expression of Bronikowski and Pasiuk-Bronikowska (1981) reduces to zero order in manganese (first order in oxygen) only if the S(VI) concentration is small.

A major breakthrough in understanding the behavior of this system was the recognition that the solution ionic strength* plays a key role in determining the rate coefficient (Huss et al. (1982a,b), Martin and Hill (1987)). At given manganese and S(IV) concentrations, increased ionic strength (10^{-3} M to 1 M) results in a slower reaction rate independent of the specific ions added. Martin and Hill noted that this behavior had previously been incorrectly attributed to a pH dependence (e.g., Martin (1984) and Neytzell de Wilde and Taverner (1958)). A reaction rate dependence on ionic strength is of particular interest as regards atmospheric processes where the ionic strength ranges from $O(10^{-4}$ M) in rain to $O(10^{1}$ M) in deliquesced salt aerosols.

There is some confusion in the literature as to the importance or even existence of an "anion" effect. While the results of Martin and Hill (1987) and Huss

---

* Ionic strength is a function of the ion concentrations (m_i or C_i) and their respective charges (z_i), e.g., $I = \frac{1}{2} \sum_i z_i^2 m_i$. The units assigned to I, either molal (m) or molar (M), will identify which concentration unit was used in the calculation.

et al. (1982a,b) imply that it is the ionic strength, as set by the anion and cation concentrations independent of their nature, which determines the reaction rate, other researchers have noted a reaction rate change in the presence of specific anions. Bassett and Parker (1951) found the sulfate salt of manganese to be a more effective catalyst than the chloride salt. This observation is contrary to the ionic strength dependence mentioned above, since for solutions of equal concentration, the ionic strength of $MnSO_4$ is approximately four-thirds that of $MnCl_2$. Ibusuki and Barnes (1984) found the oxidation of S(IV) to be roughly three times faster if $MnSO_4$ was used instead of $MnCl_2$. They argued that the presence of the manganese salt anion affected the formation of a manganese-S(IV) complex. However, since strong NaOH, HCl, $HClO_4$, and H_2SO_4 solutions were used to adjust the pH, the reaction ionic strength would have been significantly affected. It is therefore difficult to assess the relative importance of ionic strength versus anion effects in the experiments of Ibusuki and Barnes (1984). Huss et al. (1982a,b) tested both $MnSO_4$ and $MnCl_2$ and found no observable difference in the reaction rates. Martin and Hill (1987) used only $MnCl_2$ in their studies.

Clark and Radojevic(1983) observed S(IV) oxidation rates similar to those found in the Mn-S(IV) system, in solutions containing $[Cl^{-1}] > 10^{-3}$ M. *No* manganese catalyst was present. This high oxidation rate was not observed in the presence of sulfate ion or various cations. These results are contrary to those of Martin and Hill (1987) and Huss et al. (1982a), where ion concentrations of $O(10^{-3}$ M) were added to set the solution ionic strength. The S(IV) oxidation rate was not dependent on the nature of the ions added. Clearly, the issue of an "anion," or specifically a chloride ion, effect must be resolved since such an effect would be potentially important in atmospheric waters containing high levels of sea salt.

The manganese-catalyzed S(IV) to S(VI) oxidation by oxygen has been found to be sensitive to inhibition by various organics. Lim et al. (1982) found that a chelating agent such as ethylenediaminetetraacetic acid (EDTA) had a relatively

minor inhibiting effect on the oxidation rate, which could be attributed to increased ionic strength. However, antioxidants such as phenol, resorcinol, pyrocatechol, hydroquinone, and others strongly inhibited the reaction. Martin (1984) reported that 10^{-6} M hydroquinone resulted in a 50% reduction in rate, but the specific reaction conditions were not given. For $[Mn^{2+}] \sim 10^{-4}$ M and $[S(IV)]_0 = 0.015$ M, Lim et al. (1982) found that 10^{-6} M hydroquinone caused a 90% reduction in the oxidation rate. Martin (1984) noted that ethanol, acetone, acetic acid, and formaldehyde had little effect on the reaction. At concentrations of 2×10^{-3} M, toluene and hexene caused a factor of ten reduction in the rate. The greater effect of the antioxidants as opposed to chelating agents was suggested by Lim et al. (1982) as an indication that the S(IV) oxidation occurs via a free radical chain mechanism.

§4.2.2 Droplet/Aerosol Phase Studies

Reaction studies done in the aerosol or droplet phase, while in general suffering from greater uncertainty due to the difficulties of accurately generating, measuring, and collecting the particles, do have an advantage over bulk phase experiments, since mass transfer limitations can be evaluated explicitly. In bulk studies, there is no way to know *a priori* whether or not mass transfer effects are affecting the observed reaction rate. As Kaplan et al. (1981) note, increasing the mixing rate and observing that the reaction rate remains constant merely indicates that mass transfer is maximized. Thus, an intrinsically very fast reaction may still be proceeding only as fast as the reagents can be brought together by mass transfer. A rate expression that was determined under conditions of mass transfer, or diffusion, limitation, is applicable only to the *specific* reaction conditions at which the data were taken *unless* the effect of the diffusion limitation is taken into account. In other words, a rate expression can be used with confidence in future calculations only if mass transfer was not limiting. This is because the reactant concentrations are typically assumed to be those of the bulk phase (e.g.,

$[S(IV)] = H^* p_{SO_2,surface} = H^* p_{SO_2,\infty}$) and the reaction rates are determined accordingly. If significant gas-phase diffusion exists, then $p_{SO_2,surface} < p_{SO_2,\infty}$. Similarly, significant aqueous-phase diffusion would result in an inhomogeneous reactant concentration in the particle, which would in turn affect the measured reaction rate. Therefore, actual reaction conditions are the same as those in the bulk phase only if the experimental system was not mass transfer limited.

Schwartz and Freiberg (1981), Freiberg and Schwartz (1981), and Schwartz (1984) present a method by which droplet phase studies can be checked for mass transfer limitation. The characteristic times for gas-phase diffusion (τ_{dg}), liquid phase diffusion (τ_{da}), and reagent (SO_2) supply to the droplet surface (τ_{reag}) can be compared to the experimental residence time to verify that conditions of steady-state hold in the vapor and liquid phases. In addition, the characteristic times for establishment of the reagent phase equilibrium (τ_{phase}) and liquid phase diffusion (τ_{da}) can be compared to the characteristic time for reaction (τ_{ra}) to determine whether or not the measurements were mass transfer limited. While the smaller diameters associated with aerosol particles as opposed to fog droplets result in smaller diffusion times, the increased concentrations found in deliquesced salt aerosols may produce a countering effect, since the aqueous diffusion coefficient decreases linearly with increasing concentration (Ratcliff and Holdcroft, 1963). The characteristic time analysis was used to determine if the droplet phase manganese-catalyzed S(IV) oxidation studies listed in Table 4.1 (Barrie and Georgii (1976), Matteson et al. (1969), Cheng et al. (1971), Cains and Carabine (1978), Kaplan et al. (1981), Crump et al. (1983a), and Berresheim and Jaeschke (1986)), were diffusion limited. Unless conditions of potential limitation were indicated, it will merely be noted that mass transfer limitation is not expected to have affected the experimental results. Further discussion of the characteristic time analysis can be found in Chapter 5.

The study by Barrie and Georgii (1976) was done using a dilute $MnCl_2$ solu-

tion ([Mn(II)] = $10^{-5} - 10^{-4}$ M). Solution droplets 2 mm (2000 μm) in diameter were suspended from pipettes in an environment of known humidity and SO_2 concentration. Because the droplets were not in thermodynamic equilibrium with their environment, evaporation on the order of 10% volume/hour was observed at 25°C. The rate of sulfate production was found to be proportional to the sulfite ion concentration, and it was postulated that a manganese-sulfite complex was involved in the oxidation mechanism. This work has been criticized recently, in light of the diffusion limitation criteria discussed in the preceding paragraph, as having suffered from mass transfer limitation in both the aqueous and gas phases (Freiberg and Schwartz, 1981). Because of the relatively large droplet size, the characteristic time for aqueous-phase diffusion is estimated to be approximately one minute. Therefore, one would expect aqueous-phase equilibrium to have been established after 1 to 5 minutes of exposure to the atmosphere. If it is assumed that only diffusion transport occurred in the gas phase (possible convective transport is ignored), then deviation of the ratio of the steady-state SO_2 concentration at the droplet surface to the bulk gas-phase concentration ($C_{surface}/C_\infty$) from one is a measure of the extent of gas-phase diffusion limitation. Freiberg and Schwartz (1981) calculated ratios ranging from 0.24 to 0.8 for the various reaction conditions used by Barrie and Georgii. While fans were used to facilitate mixing of the gas phase, it is unknown to what extent the SO_2 transport was affected. The characteristic time for reaction, assuming the reaction was first order in S(IV) ($\tau_{ra} = [\mathrm{S(IV)}]/\overline{R}$, where $\overline{R}$ is the measured reaction rate), ranged from 7 to 180 seconds for the various experimental conditions. Clearly, the criterion for no aqueous-phase diffusion limitation, $\tau_{da} \ll \tau_{ra}$, was not met, casting doubt on the applicability of Barrie and Georgii's reaction rates to atmospheric systems.

Saturation ratios greater than one are needed to maintain droplets at fog/cloud phase $MnSO_4$ concentrations ($O(1\ \mu\mathrm{M})$, see Figure 4.1) if the evaporation problems experienced by Barrie and Georgii (1976) are to be avoided. Because these conditions are extremely difficult to control, the remaining aerosol phase reaction

studies of Table 4.1 have been done using deliquesced manganese salt aerosols at relative humidities less than 96%. Implicit in these experiments is the assumption that equilibrium existed between the aerosol particles and the water vapor in the environment. The composition of the particles is therefore determined by the thermodynamic equilibrium and the physical nature of the particle (Hänel, 1976):

$$a_w(c) = \mathrm{RH} \exp\left(-\frac{4\sigma v_m}{kTD_p}\right), \tag{2}$$

where $a_w(c)$ is the water activity of the particle solution at concentration c, σ is the surface tension of the particle, v_m is the molecular volume of the particle solution, and D_p is the particle diameter. As a rough estimate, the exponential term, or "Kelvin effect," can be set equal to one eliminating the diameter dependency of the equilibrium concentration. The error associated with this assumption will increase with increasing humidity and/or decreasing particle diameter. For the range of particle sizes used in the experiments of Table 4.1, the error is less than $\sim$ 25%. Table 4.2 compares the calculated aerosol equilibrium solution concentrations (RH = $a_w(c)$, SO_2-free atmosphere) with the solution concentrations stated in the aerosol studies of Table 4.1. The concentrations stated by Matteson et al. (1969), Cains and Carabine (1978), and Kaplan et al. (1981) differ considerably from the equilibrium values obtained using RH = $a_w(c)$. How these researchers arrived at the particle solution concentrations stated in their work is unknown, since the concentrations do not represent equilibrium conditions even accounting for the error made in neglecting the Kelvin effect. Matteson et al. (1969) and Cains and Carabine (1978) also mistakenly report the "critical" relative humidity, or deliquescence point, of $MnSO_4$ as 94.3%. The actual values, calculated using solubility data for the various crystalline states of $MnSO_4$ (Washburn, 1926) and the water activity data for $MnSO_4$ solutions (Rard, 1984), range from 82 to 85% relative humidity.

The experiments of Matteson et al. (1969) were performed in a jacketed plexiglas tubular reactor having a residence time ranging from 1 to 15 minutes for

Table 4.2

Aerosol Solution Concentrations at Equilibrium

Source	RH (%)	Concentration (Stated)	Concentration (RH = a_w)*
Matteson et al. (1969)	96	$[MnSO_4] = 0.29$ M	1.89 M
Cheng et al. (1971)	95	—	2.17 M
Cains and Carabine (1978)	96	$[MnSO_4] = 0.16$ M	1.89 M
Kaplan et al. (1981)	90	$[(NH_4)_2SO_4] \sim 5$ M $[MnSO_4] \sim 0.13$ M	2.14 M† 0.055 M
Crump et al. (1983a)	94	—	2.41 M
Berresheim & Jaeschke (1986)	94	$[MnSO_4] = 1.14$ m $[MnCl_2] = 2.69$ m	1.09 m 2.52 m

* $MnSO_4$ and $MnCl_2$ data from Rard (1984) and $(NH_4)_2SO_4$ data from Cohen et al. (1987a)

† Kusik and Meissner (1978) mixing rules used.

flowrates of 40 to 10 ℓpm. The behavior of this reactor regarding the nature of the flowrate, aerosol, and SO_2 profiles developed was not reported. A radially flat temperature, and hence humidity, profile was measured. A nebulizer was used to generate the $MnSO_4$ aerosol and particle number concentrations on the order of 10^5 particles/cm^3 were obtained. The corresponding dry aerosol had a geometric mean diameter of 0.26 μm, a geometric standard deviation of 2.3, and a volume mean diameter of 0.72 μm (this value is mistakenly reported as the "geometric volume mean diameter" by Matteson et al. (1969)). The aerosol was mixed with the humid air prior to entering the reactor. At a solution concentration of 1.89 M (see Table 4.2), the dry volume mean diameter of 0.72 μm would grow to a diameter of approximately 1.55 μm at 96% humidity. Acid (S(VI)) was measured from aerosol samples collected on membrane filters; the SO_2 was not stripped from the gas prior to filtering. Mass transfer limitations should not have affected the measured reaction rates.

The work of Matteson et al. (1969) has been used extensively in the years since its publication (e.g., Cains and Carabine (1978), Wadden et al. (1974)), even though in 1971 Cheng et al. raised the question of artifact formation on the collected filter samples because of the continued exposure to SO_2. Matteson et al. (1969) proposed a reaction mechanism involving the formation of a manganese-S(IV) ion complex and fit their data to the resulting rate expression. It was claimed that the expression for the rate of SO_2 uptake reduced to one second order in manganese, similar to that obtained in the bulk-phase experiments of Coughanowr and Krause (1965). However, Crump et al. (1983a) have shown that an error was made in the calculations and the proposed mechanism results in an SO_2 uptake rate that is instead first order in manganese.

Cheng et al. (1971) adopted quite a different approach in their design of an aerosol reactor. Dry aerosol particles (both submicron and micron in diameter) were deposited on teflon beads, which were then packed into a flow reactor. It was

argued that because of the non-wetting nature of Teflon, the aerosol would deform minimally after deliquescence. The effluent SO_2 concentration, given a constant feed, was measured as a function of time and compared to the effluent from a "dummy," or blank, reactor at the same conditions to give the fractional conversion of SO_2 as a function of time. Approximately 3% deviation from ideal plug flow was expected and roughly compensated for by multiplying the experimentally measured SO_2 conversion by a factor of 1.03. Both $MnSO_4$ and $MnCl_2$ were studied. Again, mass transfer effects are not expected to have influenced the results.

The reaction rates obtained by Cheng et al. (1971) are difficult to compare to those of other researchers because they are a function of the *weight* of $MnSO_4$ in the reactor. This is not the same as determining the rate dependence on the $MnSO_4$ concentration since, regardless of the catalyst loading, at a constant humidity, $[MnSO_4]$ in the drops is fixed by equilibrium (there would be some variation in $[MnSO_4]$ from drop to drop that was due to the Kelvin effect). Cheng et al. determined that $MnSO_4$ was a more effective catalyst than $MnCl_2$ by a factor of 3.5, based on a comparison between a $MnSO_4$ run at 95% humidity and a $MnCl_2$ run at 98% humidity. Because of the differing physical properties of $MnSO_4$ and $MnCl_2$, the same size dry aerosol would lead to aqueous particles of differing concentration ($[MnSO_4] \sim 2.3$ m, $[MnCl_2] \sim 0.42$ m) and ionic strength ($I_{MnSO_4} \sim 9.2$ m, $I_{MnCl_2} \sim 1.3$ m) upon exposure to the same humidity. It is unclear on what basis catalysts used in aerosol phase studies can be "compared" — similar concentrations or ionic strengths (as in the bulk phase studies), or similar environment (as in the atmosphere) — and then what significance can be attached to the results. The two manganese salt experiments compared by Cheng et al. (1971) were not performed at either similar concentrations, similar ionic strengths, or similar humidities. Therefore, the relative catalytic effectiveness of $MnSO_4$ and $MnCl_2$ determined by Cheng et al. (1971) has little meaning beyond this particular study.

Cains and Carabine (1978) used a light scattering technique to observe the

growth of aqueous $MnSO_4$ drops exposed to SO_2. The humidity at which the experiments were run was not stated. It was merely noted that values in excess of 96% were used. A nitrogen sheath was used to contain the aerosol in the measuring device and it is not known if this sheath flow was humidified to the same level as the aerosol-containing gas. As pointed out in Appendix A (Biswas et al., 1987), humidity changes must be avoided when using aerosol sizing instruments if an unbiased distribution is to be measured. The mode diameter of the dry, $MnSO_4 \cdot H_2O$ aerosol distribution was determined to be 0.05 – 0.06 μm, using electron microscopy. The distribution is very polydisperse, having a geometric standard deviation of 2. The characteristic time for coagulation of an aerosol is given by $\tau_{coag} = 2/(\beta N_{tot})$, where the coagulation coefficient β is approximately $10^{-9}\,\mathrm{sec}^{-1}$ for 0.1 – 0.1 μm particle collisions. Given that the total number concentration in this experiment was on the order of 10^6 particles/cm^3, the characteristic time for coagulation was approximately 30 minutes. This time represents a minimum estimate since the distribution was polydisperse and the coagulation coefficient increases for collisions between particles of unlike size. The experimental residence times ranged from 1 to 21 minutes. Cains and Carabine (1978) recognized that the observed particle size changes were due to growth and/or coagulation and that any comparison with theoretical estimates of the particle growth would have to be qualitative, not quantitative.

Distribution mode diameters for the wet aerosol in the absence of SO_2, measured using the light scattering technique, ranged from 0.22 to 0.26 μm for residence times of 2.6 to 21.0 minutes. As a rough estimate, it can be assumed that the dry distribution mode diameter grows into the mode diameter of the wet aerosol distribution. A "dry" 0.06 μm $MnSO_4 \cdot H_2O$ aerosol equilibrates with a 0.29 μm wet particle if a concentration of 0.16 M is assumed. Perhaps this is how Cains and Carabine (1978) arrived at 0.16 M as the aerosol solution concentration value (see Table 4.2). Unfortunately, this concentration corresponds to an experimentally unrealistic relative humidity of greater than 99.9%. Figure 4.3 shows the

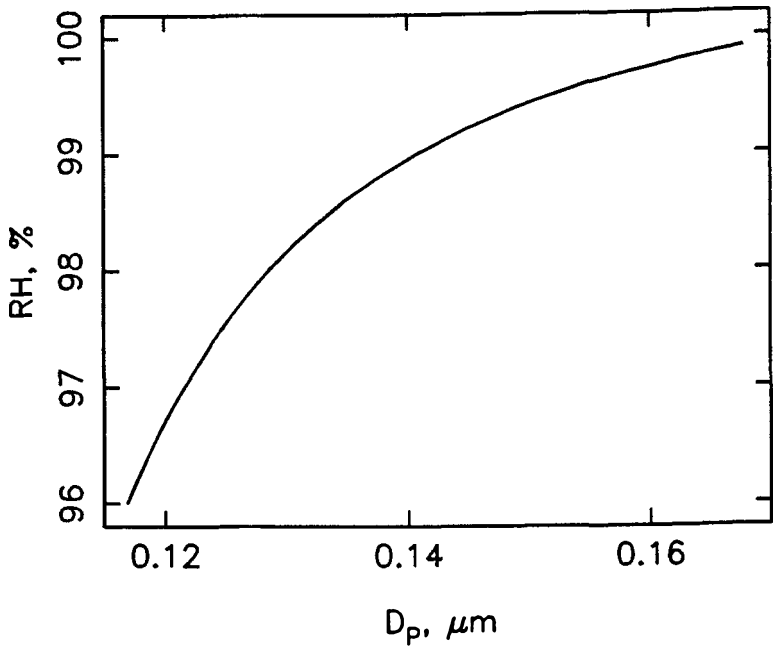

Figure 4.3 Wet aerosol diameter resulting from an 0.06 μm $MnSO_4 \cdot H_2O$ feed particle at 25°C as a function of relative humidity.

equilibrium wet aerosol diameter expected at a range of relative humidities, given the same "dry" 0.06 μm $MnSO_4 \cdot H_2O$ particle. Even at 99% relative humidity the aerosol particle is only 0.14 μm in diameter. The experimental results are not consistent with the results predicted assuming thermodynamic equilibrium. Thus, one can speculate that either significant coagulation had occurred within the first two minutes of residence time, or the sizing measurements were in error. Finally, Cains and Carabine (1978) predicted the particle size as a function of time resulting from the oxidation of S(IV) to S(VI). The second-order rate data of Coughanowr and Krause (1965), fit to the rate expression of Matteson et al. (1969), was used. As mentioned above, Matteson et al.'s expression does not reduce to second-order manganese dependence. Therefore, the value of the theoretical calculations, even allowing for the fact that coagulation was not accounted for, is questionable.

Kaplan et al. (1981) used deliquesced $(NH_4)_2SO_4$ aerosols doped with $MnSO_4$ in an attempt to achieve manganese concentrations less than the equilibrium solution concentration in a droplet of pure manganese salt (see Table 4.2). The overall solution ionic strength remained high, however, on the order of 10 M. Dried aerosol particles of approximately 5 μm were fed into an insulated tubular, laminar flow reactor, where they were contained by a humidified sheath air. The reactor residence time distribution was narrower than that in a laminar flow reactor because the particles were confined to the center portion of the tube. It was assumed that equilibration between the aerosol and the humid sheath air occurred rapidly. Radioactively labeled SO_2 was used. The reactor effluent was fed to an SO_2 stripper where the gas phase SO_2 was removed. In order to maintain equilibrium, the S(IV) desorbed from the particle, quenching the reaction and leaving only S(VI). Finally, the aerosol size was measured using an optical particle counter, after which the particles were collected on a filter and the sulfur radioactivity measured. Even given the larger particle diameters and the higher aerosol solution pH (a result of the buffering nature of the ammonia), calculations show this experiment to be free from mass transfer limitations.

As in the work of Cains and Carabine (1978), the results of Kaplan et al. (1981) are dependent on the wet aerosol size measurement. It is not known how much care was taken with these measurements. Presumably, the S(IV) desorption should have a minimal effect on the aerosol diameter if the relative humidity was maintained constant throughout the process. There is an inconsistency since the dry diameter was stated as being 5 μm and yet the experimental volume-averaged wet aerosol diameters were also approximately 5 μm. A 5 μm dry $(NH_4)_2SO_4$ aerosol particle (neglecting for a moment the small amount of $MnSO_4$) will grow to 9.2 μm in diameter at 90% relative humidity. Analogously, a wet 5 μm particle at 90% humidity results from a 2.5 μm dry $(NH_4)_2SO_4$ particle. Kaplan et al. (1981) assumed all activity coefficients used in the calculations to be 1.0. For solutions having ionic strengths on the order of 10 M, this is not a reasonable

assumption (Cohen, 1987a). The manganese dependence of the rate expression was not determined, since only one relative humidity and one $MnSO_4/(NH_4)_2SO_4$ ratio were used. A first-order dependence of the rate of S(VI) formation on S(IV) was assumed, which resulted in a first order rate constant of approximately 0.04 sec^{-1}. A value of 0.004 sec^{-1} is obtained if a volume-averaged diameter of 9.2 μm is used along with a $MnSO_4$ concentration of 0.055 M (see Table 4.1). A slight increase in the reaction rate with increasing SO_2 concentration (0.1 to 1 ppm) was noted. One particularly interesting observation was that the runs made with manganese-containing aerosols resulted in a S(IV) oxidation rate only 2.5 times faster than that for *pure* $(NH_4)_2SO_4$ aerosols. This is similar to the results of Clarke and Williams (1983), who found only small increases in the S(IV) oxidation rate with the addition of manganese or iron to deliquesced $MgCl_2$, NaCl, and $(NH_4)_2SO_4$ aerosols.

Crump et al. (1983a) used a well-characterized continuous stirred tank reactor (CSTR) to study the growth of $MnSO_4$ aerosols. The high humidities and high SO_2 concentrations used are typical of plume conditions. Low particle number concentrations ($< 10^4$ particles/cm^3) ensured that condensation was the only mechanism by which particle growth occurred. An optical particle counter was used to measure the feed and effluent size distributions. The distributions were then used to predict a rate expression which, given the feed distribution, resulted in the observed effluent distribution. This rate expression was assumed to be zero order in manganese and S(IV), and inversely proportional to the hydrogen ion concentration.

As with the two prior studies discussed here, the work of Crump et al. (1983a) relies heavily on the measured humid aerosol size distribution. It was stated that one-half hour was allowed for the optical particle counter, a Royco Model 226, to equilibrate with the humid stream being measured. However, Biswas et al. (1987) have shown that the Royco Model 226 OPC requires on the order of nine hours

for the humidity to reach a steady state value (e.g., 90%, given a 95% humidity feed). This particularly long adjustment time is due to the hygroscopic nature of the instrument sheath air filters. An attempt was made by Crump et al. (1983a) to compensate for the temperature rise, and subsequent humidity decrease, in the sampling chamber caused by dissipative electronic heating. It was estimated that the humidity within the sizing chamber was 82 to 84% and that the particles being sized were still wet, not dry. The humidity was then theoretically raised back to the level in the CSTR and the equilibrium particle diameter calculated. While this adjustment is not a problem for the pure $MnSO_4$ feed aerosol, the difficulty arises in dealing with the mixed species effluent aerosol where the detailed aqueous phase thermodynamics must be known. Activity coefficients in all of the calculations were assumed to be 1.

The work of Berresheim and Jaeschke (1986) is the most complete reaction kinetics aerosol study done to date. A jacketed tubular, laminar flow reactor with an average reactor residence time of six minutes was used. Characterization studies showed a homogeneous aerosol/gas mixture in the radial direction. No mention was made of the thermal profiles. Sampling ports were located at various points along the reactor length and the SO_2 uptake was measured using a coulometric analyzer with a detection limit of 0.25 ppb. The aerosol was generated using a nebulizer, and number concentrations ranging from 10^3 to 10^5 particles/cm^3 with dry particle sizes ranging from 0.01 to 1 μm were obtained. Coagulation was estimated to be negligible. Dry aerosol, SO_2, and air (humid or dry) were fed through inlets at the top of the reactor. Before an experiment was started, the dry particle size distribution was measured using a TSI Model 3030 Electrical Aerosol Analyzer (EAA). Filter samples of the dry aerosol were also collected to determine the metal mass loading in the air. The reactor humidity was varied from 0 to 94%, or from humidities below the deliquescence level where the particle was solid, to humidities where the particle was liquid.

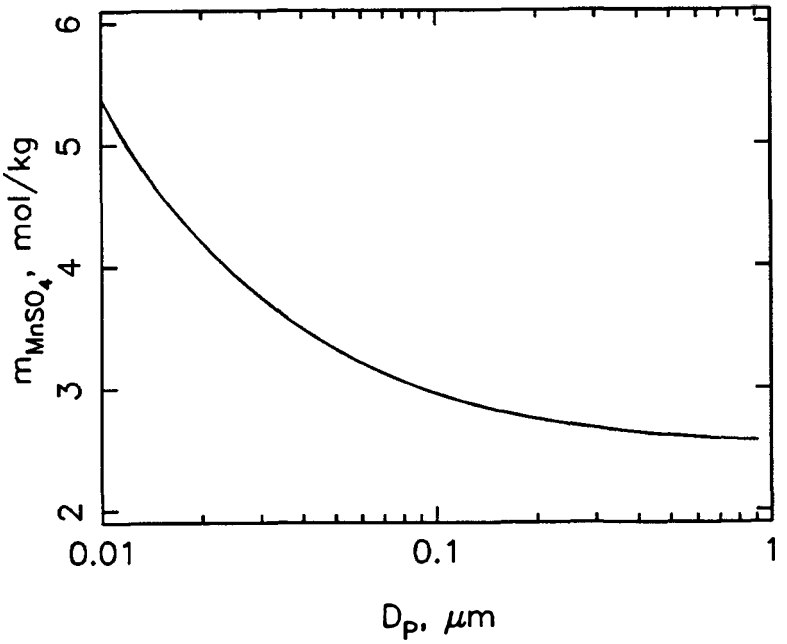

Figure 4.4 $MnSO_4$ concentrations at 94% humidity, 25°C for the diameter range used by Berresheim and Jaeschke (1986).

Expressions for the S(IV) oxidation rates of three salts of manganese — $MnSO_4$, $MnCl_2$, and $MnNO_3$ — were developed. Basically, the reaction rate was assumed to be a function of the metal mass loading (more metal, or aerosol particles, will mean that more SO_2 can be oxidized), the salt activity (aerosol solution concentration), the hydrogen ion activity, and the gas phase SO_2 concentration. An inverse first-order relationship was assumed for the hydrogen ion activity based on the findings of previous dilute, bulk phase studies. Martin and Hill (1987) have since attributed this dependence of the rate of sulfate formation on $[H^+]^{-1}$ to an ionic strength, as opposed to pH, effect.

Given a polydisperse aerosol, particularly one with diameters ranging over several orders of magnitude, every particle will have a different solution concentration. Figure 4.4 shows the range of concentration as a function of diameter that

will exist in a $MnSO_4$ aerosol at 94% humidity. The concentration varies by as much as a factor of two between the maximum and minimum diameters of the size distribution. Berresheim and Jaeschke (1986) used an average salt molality in the fitting of the rate expression — $\langle m \rangle = C_{Me}/(MW_{Me}\, L)$, where C_{Me} is the mass of metal (not salt) per volume of air, L is the water content of the aerosol, and MW_{Me} is the molecular weight of the metal. The aerosol water content was obtained by subtracting the mass of dry aerosol per volume of air from the mass of aerosol at a specified relative humidity per volume of air. Since the wet aerosol size distribution was not actually measured, it had to be inferred using the dry aerosol distribution. In shifting the dry distribution to another humidity, the density of the dry particle was needed, requiring that the the number of waters of hydration be known. Cohen et al. (1987a) found that the "dry" $MnSO_4$ particles studied in their electrodynamic balance actually had an overall stoichiometry of $MnSO_4 \cdot 2.8\, H_2O$ as opposed to an integral number of water molecules. The density of $MnSO_4 \cdot n\, H_2O$ ranges from 3.25 g/cm^3 ($n = 0$) to 2.10 g/cm^3 ($n = 5$). Berresheim and Jaeschke (1986) claimed that $\langle m \rangle$ is equivalent to a number average of the particle salt molality. However, because the calculation of the aerosol water content involved determining the total mass of the aerosol, $\langle m \rangle$ is actually a mass-averaged value. The maximum particle diameter that can be measured using an EAA is 1 μm. The dry size distributions of Berresheim and Jaeschke (1981) indicated that while the majority of particles had diameters less than 0.1 μm, there were still a significant number of particles 1 μm in diameter. A 1 μm diameter particle has $O(10^3)$ times the mass of a 0.1 μm particle, and $O(10^6)$ times the mass of a 0.01 μm particle. Therefore, another aerosol sizing instrument should have been used in conjunction with the EAA to determine the actual number of particles having diameters over 1 μm, since these particles have an exaggerated effect on a mass distribution.

Measurement of the wet aerosol distribution was the weakest link in several of the previous studies, and the absence of this measurement was the weakest link in this study. The uncertainties involved in the assumptions made by Berresheim and

Jaeschke (1986) would have been significantly smaller if a monodisperse aerosol had been used, or if the particle sizes had been limited to those greater than 0.1 μm in diameter, where the magnitude of the Kelvin effect on particle composition is greatly reduced.

Berresheim and Jaeschke (1986) calculated that for a typical atmospheric metal mass loading and relative humidity (55 ng/m^3, 94%), $Mn(NO_3)_2$ is a more effective catalyst than $MnCl_2$, which, in turn, is more effective than $MnSO_4$. However, the percent conversion rates were recalculated at these same conditions using the predicted rate expressions (see Table 4.1), and 2.5%hr^{-1}, 3.5%hr^{-1}, and 0.09%hr^{-1} were obtained instead of 2.5%hr^{-1}, 1.5%hr^{-1}, and 0.09%hr^{-1} (Berresheim and Jaeschke, 1986) for $Mn(NO_3)_2$, $MnCl_2$, and $MnSO_4$, respectively. This would make $MnCl_2$ the most effective catalyst of the three manganese salts. It is interesting that the three salts resulted in different reaction rate expressions indicating some sort of anion effect. At the same relative humidity, $MnCl_2$ and $Mn(NO_3)_2$ result in approximately the same solution molality, and hence, ionic strength. The salt activities are only slightly different. The biggest difference between the two salts is the hydrogen ion activity — $Mn(NO_3)_2$ is considerably more acidic than $MnCl_2$ at the same concentration. Perhaps there are *both* an ionic strength effect ($MnSO_4$, while only slightly more acidic than $MnCl_2$, has a much greater ionic strength for solutions of similar concentration) and a hydrogen ion effect contributing to the S(IV) oxidation rate in concentrated aerosol solutions.

§4.2.3 Proposed Mechanisms

Few reaction mechanisms have been proposed for the aqueous-phase manganese-catalyzed oxidation of SO_2 by oxygen. Of the mechanisms proposed, there are basically two types — free-radical chain mechanisms involving initiation followed by a sequence of electron transfers (e.g., Huss et al. (1982b)) and polar mechanisms involving the formation of an ion complex (e.g., Bassett and Parker

(1951) and Huss et al. (1982b)).

The rate determining step in the mechanism of Bassett and Parker (1951) is one in which the complex $Mn(SO_3)_2O_2^{2-}$ undergoes rearrangement to form Mn^{2+} and SO_4^{2-}. It was argued that the observed dependence of the reaction rate on the anion present was consistent with the existence of a manganese-S(IV) complex. The nature of the anion determines the stability of the manganese-anion complex, which competes with the S(IV) complex (see also Ibusuki and Barnes (1984)). Hoffmann and Boyce (1983) have derived the theoretical rate expression corresponding to Bassett and Parkers's (1951) mechanism. The reaction rate, $R = k\,[Mn^{2+}]^{\alpha}[SO_3^{2-}]^{\beta}[O_2]^{\gamma}$, is either zero, first, or second order in S(IV) ($\beta = 0, 1, 2$), zero or first order in oxygen ($\gamma = 0, 1$), and always first order in manganese ($\alpha = 1$), depending on the reaction conditions (Hoffmann and Boyce, 1983). Second-order S(IV) dependence has not been observed for this system. However, for those conditions where first-order S(IV) and Mn(II) dependence have been found ($[S(IV)] < 10^{-6}$ M, see Martin and Hill (1987)), Bassett and Parker's (1951) mechanism must be considered a possible explanation of the chemistry. Since S(IV) exists primarily as HSO_3^- in the pH range typical of atmospheric aerosols, it is conceivable that bisulfite, not sulfite, complexes with the manganese. Additionally, van Eldik (1986) advises that not enough consideration has been given to O-bonded sulfito species when considering possible Mn-S(IV) complexes. Metal hydroxy species can react rapidly with $SO_{2,aq}$ to form an O-bonded sulfito species, which then undergo electron transfer reactions to form sulfate and reduced metal ions.

In order to explain the two term rate expression describing their data, Huss et al. (1982b) proposed a mechanism that has elements of both the free radical and ion complex type. The "major contribution" chain involves the formation and reaction of the radicals $SO_4^-\cdot$, $SO_3^-\cdot$, $HSO_4^-\cdot$, and $SO_5^-\cdot$. The second-order manganese term results from this portion of the mechanism. The "minor contribution" chain is

actually a polar mechanism involving the ion complexes $MnHSO_3^+$ and $Mn(HSO_3)_2$ and leads to the first-order manganese, first-order S(IV) term in the rate expression. The proposed set of initiation steps is a combination of the formation of two ion complexes, Mn_2^{4+} and $Mn_2(HSO_3)^{3+}$, and free radical formation ($SO_4^-\cdot$, $SO_3^-\cdot$, $OH\cdot$). Free radical reaction with organics has been proposed as the termination step. Because Huss et al. (1982b) worked with pH values ranging from 1 to 4, where the concentration of HSO_3^- dominates that of SO_3^{2-}, the mechanism has been formulated in terms of the oxidation of S(IV) as the bisulfite ion. At the experimental conditions used in the study, the second-order manganese term dominates the reaction rate expression. The mechanism is attractive, however, since it results in both first- and second-order manganese dependence — both of which have been observed by researchers under differing conditions.

§4.2.4 Conclusions

Martin and Hill (1987) were able to reconcile a number of the reported bulk phase reaction rates by plotting $\overline{R}/[\text{Mn(II)}]^2$ as a function of ionic strength ([Mn(II)] indicates the total manganese concentration). Similarly, the observed S(IV) reaction rates divided by [Mn(II)] were plotted as a function of I for the experiments in Table 4.1. Although there is no reason to presume that all the rates are second order in manganese, Figure 4.5 reveals several interesting features. First, at comparable ionic strengths, the value of $\overline{R}/[\text{Mn(II)}]^2$ determined by Martin and Hill (1987) and Huss et al. (1982ab) (the results of these two studies are identical) is several orders of magnitude greater than both the values of Coughanowr and Krause (1965) and the values calculated from the aerosol studies. This is particularly curious since Coughanowr and Krause (1965) performed their experiments in the [S(IV)] and ionic strength regime that Martin and Hill (1987) found resulted in a rate expression second order in manganese. However, the manganese concentration was several orders of magnitude greater than that used by Martin and Hill (1987). This same situation, $[\text{S(IV)}] \leq [\text{Mn(II)}]$, exists in a deliquesced manganese

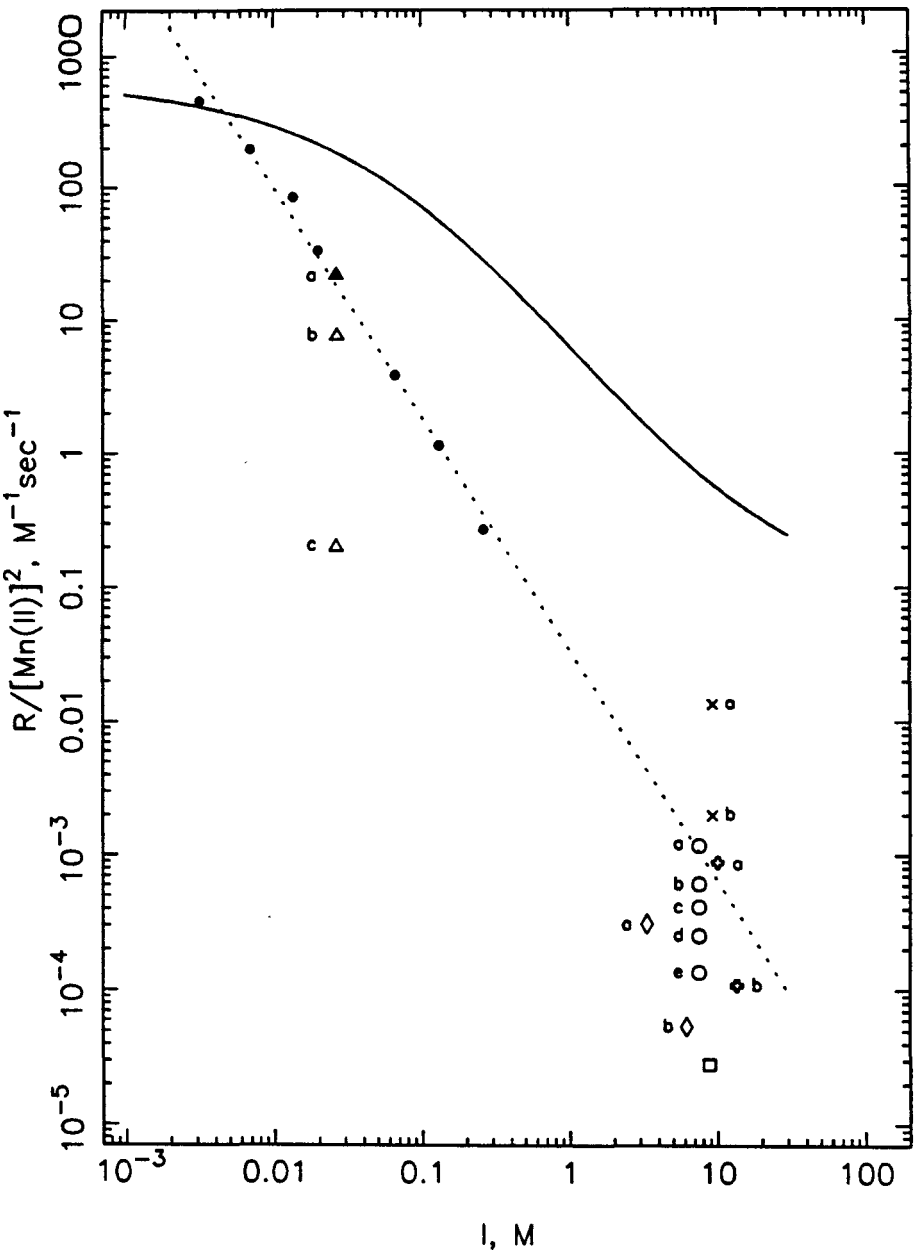

Figure 4.5 Second-order manganese rate constant as a function of ionic strength. Martin and Hill (1987) (————) and Coughanowr and Krause (1965) (•). Matteson et al. (1969) (○) 96% RH and 1.89 M $MnSO_4$: (a) 140 ppm SO_2, (b) 76 ppm SO_2, (c) 21 ppm SO_2, (d) 14 ppm SO_2, (e) 5.6 ppm SO_2. Berresheim and Jaeschke (1986) (◇) $MnCl_2$ at 0.12 ppm SO_2 : (a) 94% RH, (b) 86% RH. Berresheim and Jaeschke (1986) (✪) $MnSO_4$ at 0.12 ppm SO_2 : (a) 94% RH, (b) 89% RH. Kaplan et al. (1981) (×) $MnSO_4$ at 90% RH : (a) Literature rate expression used with [Mn(II)] = 0.055 M, (b) rate expression corrected for 9.2 μm aerosol used with [Mn(II)] = 0.055 M. Cheng et al. (1971) (□) $MnSO_4$ at 4.5 ppm SO_2, 95% SO_2, RH — reaction rate (mol/s) divided by volume of catalyst at [Mn(II)] = 2.2 M. Bronikowski and Pasiuk- Bronikowska (1981) (△) [$MnSO_4$]= 7×10^{-3} M : (a) [O_2]~0.0019 M, (b) [O_2]~ 2.6×10^{-4} M, (c) [O_2]~ 1.4×10^{-4} M.

salt aerosol. Second, the results of Coughanowr and Krause (1965) at high manganese concentrations (and therefore high ionic strengths) can be fit to a straight line: $\overline{R}/[\mathrm{Mn(II)}]^2 = 0.0347\, I^{-1.728}$. Note that if $I \sim 4\,[\mathrm{Mn}^{2+}]$ then $R \sim k'[\mathrm{Mn}^{2+}]^0$, which is to be expected since Coughanowr and Krause found the reaction to be approximately zero order in manganese at high manganese concentrations. If this line is extrapolated, it intersects the cluster of points corresponding to the aerosol studies. And third, given the aerosol study data, it is apparent that the reaction rate is not zero order in S(IV), although it *might* be effectively second order in manganese. Reiterating, although the relationships among the various data in Figure 4.5 are intriguing, there are no firm conclusions that can drawn from the plot — only questions that can be raised.

In spite of the relatively large number of studies that have been performed on the manganese-S(IV) system, a definitive picture of the process is far from apparent. Those conclusions that can be drawn follow primarily from the results of the bulk-phase studies:

(1) For $[\mathrm{S(IV)}] < 10^{-6}$ M, $[\mathrm{Mn(II)}] < 0.1$ M, the reaction rate exhibits first-order S(IV) and first-order Mn(II) dependence,
(2) For $[\mathrm{S(IV)}] > 10^{-4}$ M, the rate is second order in Mn(II) and zero order in S(IV),
(3) The reaction rate decreases with increasing ionic strength for both concentration regimes. This effect had previously been attributed to a pH effect.

The existence of an anion effect is still a matter of debate in the bulk-phase studies. At this time the mechanics of working with aerosols limit the accuracy of reaction rate measurements and the information that can be obtained from aerosol-phase studies. While it is clear that S(IV) to S(VI) oxidation *does* occur in deliquesced manganese salt aerosols, no firm conclusions can be drawn as to the order of the reaction or the existence of an ionic strength effect versus a pH effect. Perhaps the only point of agreement between the various aerosol studies is that the reaction rate increases with relative humidity (decreasing ionic strength and manganese con-

centration). Despite this current inadequacy, aerosol/droplet phase studies must be continued. The technology needed for accurate measurement and sampling of reacting particles will improve. Well-controlled laboratory studies of fogs/clouds are necessary to determine whether or not bulk-phase studies adequately model the chemistry in the complicated chemical-microphysical system that is actually a fog/cloud. Aerosol-phase studies using natural manganese sources such as fly ash are needed. As in the manganese salt studies, the results from fly ash studies are currently ill defined and contradictory. The effect of anions and other possible synergisms needs to be explored further both in dilute and concentrated systems. Finally, an understanding of the actual chemical mechanism is necessary if there is to be any hope of predicting the importance of manganese, as regards the oxidation of SO_2, in the chemically complex atmospheric system.

CHAPTER 5
EXPERIMENTAL PROCEDURE AND RESULTS

The reactor system described in Chapter 2 should be regarded well-defined, well-controlled "atmosphere" rather than a device to generate kinetic data. Proposed rate expressions can be used to predict rates of S(IV) oxidation as they would be in a full atmospheric model — integrally related to and dependent on the thermodynamics and physics of the particle system — and the resulting predicted aerosol growth can then be compared with that measured experimentally. The procedure used to measure the growth of a humid $MnSO_4$ aerosol in the presence of SO_2 under controlled conditions and the observed growth curves are presented in this chapter. The associated theoretical description of the system will be discussed in Chapter 6.

§5.1 Experimental Procedure

The $MnSO_4$ or $MnSO_4/Na_2SO_4$ solutions used in the experiments were made using Milli-Q/R water and reagent grade chemicals. All solutions contained 5 g/ℓ of the salt. For $MnSO_4/Na_2SO_4$ solutions, the desired molar salt ratio was set while maintaining a total concentration of 5 g/ℓ.

The night before an experiment was to be performed, approximately 2 ℓpm humid air were passed through the reactor for a period of approximately 12 hours or until the start of the experiment. The effluent was vented to the waste line through the EG&G 911 bypass (see Figure 2.1). The CSTR pressure was set at typical experimental values using the adjustable valve in the waste line. The SO_2 analyzer and the two heating baths were never turned off.

The distribution of flows in the reactor system was discovered to be very

pressure sensitive and regardless of the flow path at a given time in the experimental procedure, it was necessary to maintain the same pressure profile in the system. Therefore, before an experiment was started, the entire flow system, as it would be configured during the effluent measurements, was turned on and the pressure in the CSTR noted. This pressure would be maintained in the CSTR during the approach to steady state.

At the start of an experiment the syringes were filled with the appropriate salt solution, the syringe pump was started, and air (2.55×10^5 Pa_g = 37 psig) to the atomizer was turned on. The sheath air to EMC1 was started and the inlet pressure set to 5.5×10^4 Pa_g (8 psig). For those experiments in which a pure $MnSO_4$ aerosol was used, the EMC1 voltage was set at 2200 V. A Na_2SO_4 particle in equilibrium with a given relative humidity has a larger diameter than a $MnSO_4$ particle. This is simply a property of the salt. Since approximately the same "wet" feed diameters were desired for each experiment, a smaller initial "dry" particle had to be generated. Hence, a voltage of 1500 V was used if the aerosol was a $MnSO_4$ and Na_2SO_4 mixture.

The SO_2 gas cylinders were opened and the inlet pressure to the SO_2 flowrate capillary set at 3.45×10^4 Pa_g (5 psig). The pressure across this capillary was set so as to provide the desired SO_2 concentration in the CSTR. Downstream of EMC1 the aerosol passed through a neutralizer, over the humidifying bath, into the premix vessel and on to the CSTR. The CSTR effluent was vented to the waste line through the EG&G 911 bypass. Flow to all downstream measuring instruments was turned off and the pressure in the CSTR set to the previously determined value using the adjustable flow valve in the EG&G bypass waste line. An iterative approach was used to set the aerosol flowrate to approximately 2 ℓpm by adjusting the amount of flow vented to the waste line just prior to EMC1 (see Figure 2.1), and to balance the sheath and excess flows of EMC1 at 10 ℓpm — all the while maintaining a constant CSTR pressure.

The system humidity was determined by the room temperature and the humidifier bath temperature. Humidities over 95% were difficult to match in EMC2 and hard on the instrument. If it appeared that the CSTR humidity would exceed 95%, the humidity was lowered by adding dilution air to the CSTR feed.

The system conditions were held stable in this flow configuration for six hours as the reactor approached steady-state operation. After four hours had passed, the SO_2 analyzer was "calibrated" for the day. The teflon filter at the instrument inlet was changed. The voltage readings for zero air and the span gas (either 10 or 100 ppm depending on the SO_2 range being used for this experiment) were checked and set to the values determined during the actual calibration. This ensured that the intermediate concentrations and their corresponding output voltages matched the calibration curve. The sheath air flow to EMC2 was started at this time and the bubbler humidifier temperature controller turned on. The CNC was switched on and allowed to sample filtered room air to assure that steady state temperature conditions had been reached in the CNC before the size distributions were measured.

Approximately five hours after the experiment was started, the CSTR effluent was switched from the EG&G bypass to the measuring instruments. The CNC was hooked up to the EMC2 sample flow. Again, an iterative method was used to balance the sheath and excess flows in EMC2 while adjusting the valve downstream of the EG&G 911 meter to maintain constant pressure in the CSTR. This was done as quickly as possible — within several minutes. Both the EG&G 911 and 880 dew point meters were turned on and balanced. The heating tape on the lines prior to these meters was also turned on to decrease the actual humidity of the air in the sensors. All temperatures, dew points and the SO_2 analyzer were monitored using the PDP-11 computer (see Appendix E, program SAMP.FOR). Sixty readings were taken for each A/D channel at one second intervals and then averaged together. The next set of readings was taken after twenty seconds. This sampling scheme

was used during the all voltage scans.

Because minimal size biasing of the particle size due to humidity changes was desired, the relative humidity in EMC2 was matched to the relative humidity in the CSTR. Any necessary dilution air was added to the classifier sheath air and a pressure of 1.03×10^5 Pa_g (15 psig) maintained at the sheath air capillary inlet.

Once six hours had passed since the start of the experiment and the humidity in EMC2 was set, the effluent voltage scan was measured. Approximately twenty CNC readings were taken for each EMC2 voltage. Since the particle concentration at every voltage was less than 1000 particles/cm^3, the CNC operated in counting mode. The temperatures, dew points, and SO_2 concentration were monitored using the computer and the data saved in a file. The entire scan typically took an hour to complete.

After finishing the effluent scan the dew point meters were rebalanced. The butanol in the CNC was drained and replaced with fresh butanol. The reactor flow was switched to the CSTR bypass. The CSTR bypass valve approximates the pressure drop because of the CSTR and was the *only* valve adjusted in the switch from effluent to feed measurement. A slight redistribution of the flowrates occurred because of the change in the downstream pressure drops when this valve was not used and particle deposition in the lines changed. This resulted in increased line loss during the feed measurement relative to that of the effluent measurement. However, this did not appear to bias the size distributions. When a dry $MnSO_4$ aerosol was measured without the CSTR bypass valve, the feed and effluent distribution peaked at the identical diameters (see Figure 5.1). The CSTR bypass valve was used in all other experiments, eliminating the change in line loss between the scans.

Figure 5.2 shows that some aerosol growth was possible even though the residence time in the lines and premix vessel prior to the CSTR was on the order of 0.5 minutes. In order to determine the aerosol growth resulting from the SO_2

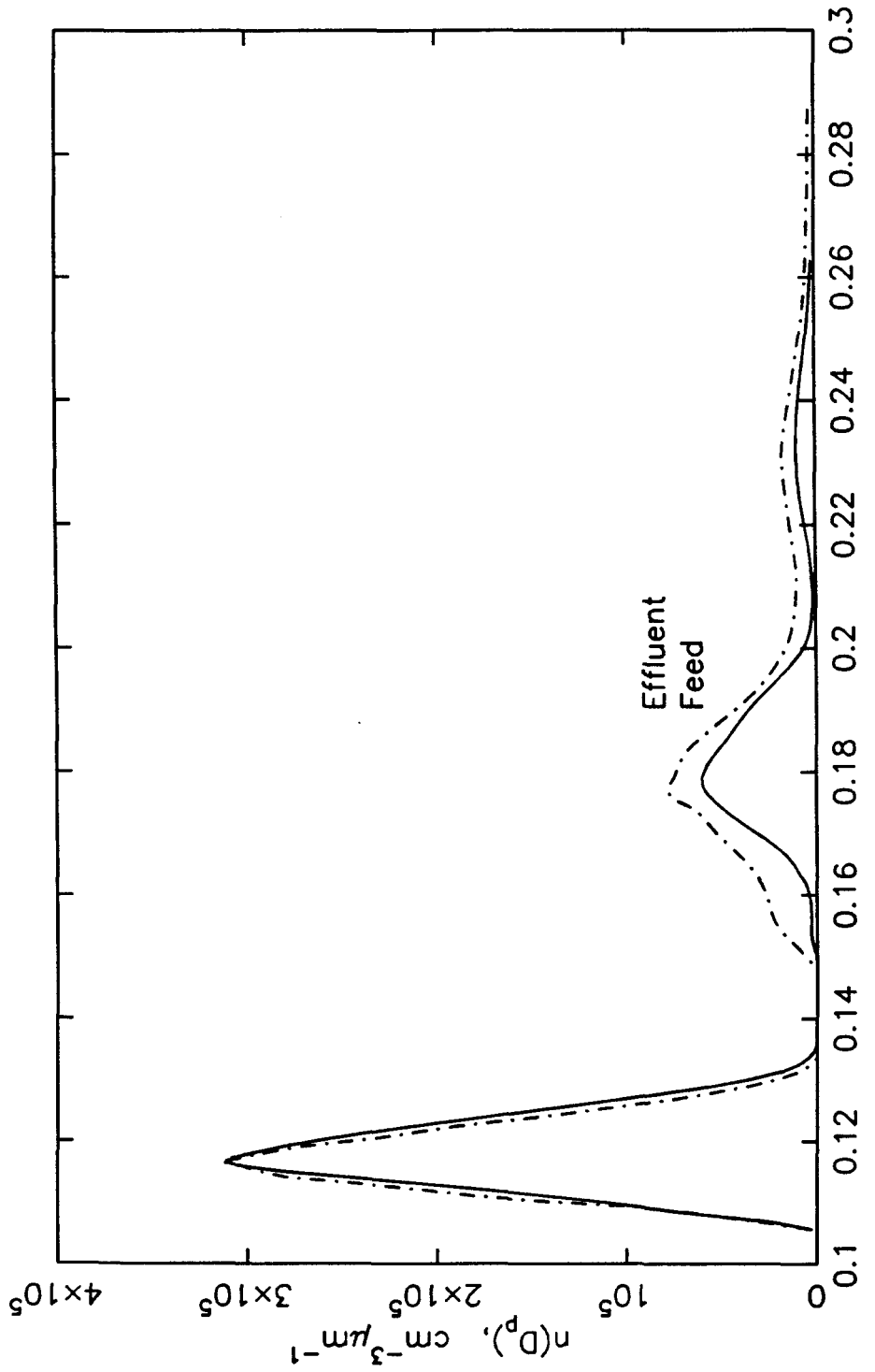

Figure 5.1 Feed and effluent size distributions for dry $MnSO_4$ aerosol measured without the CSTR bypass valve.

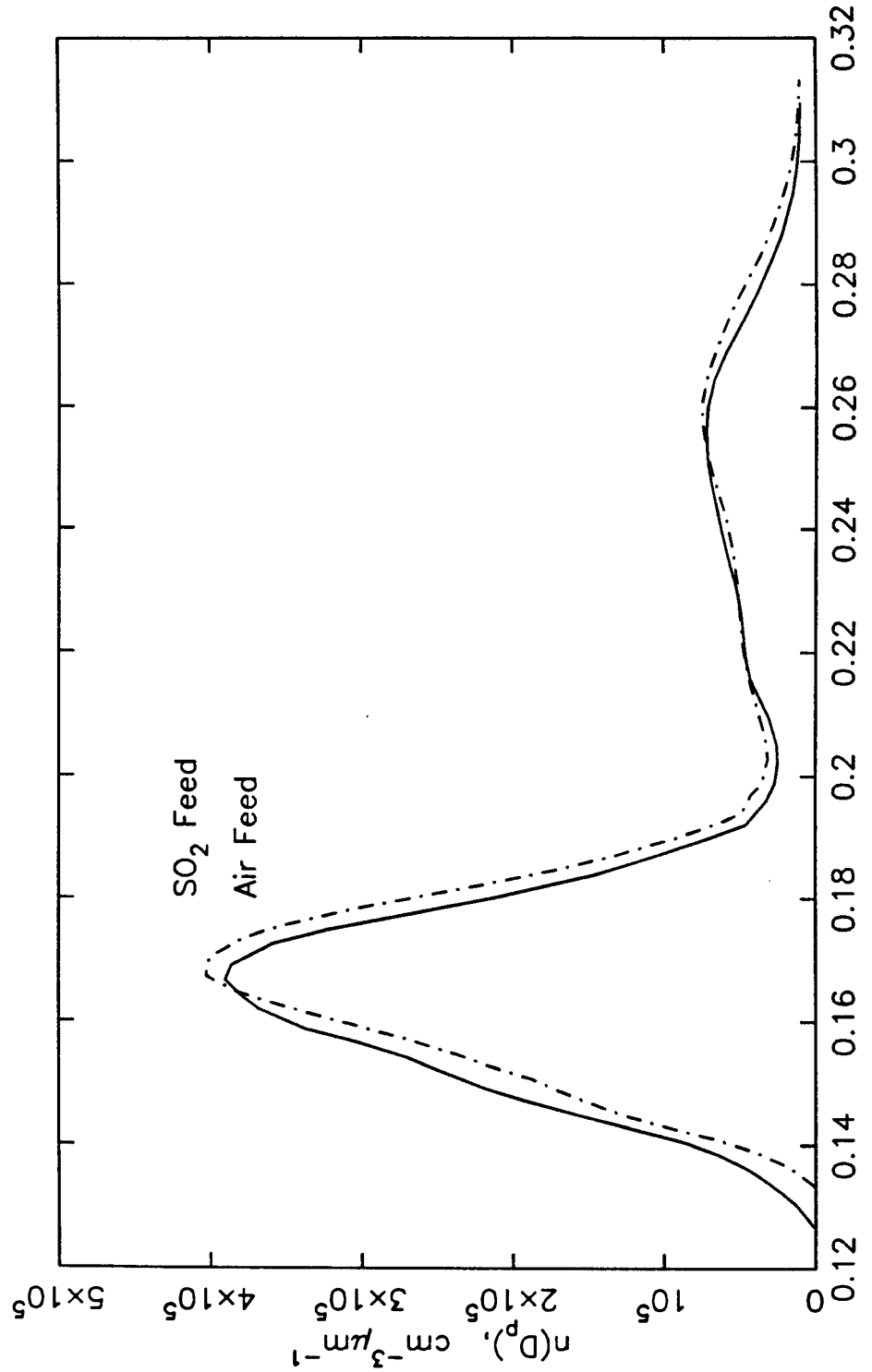

Figure 5.2 Size distributions for air and SO_2 feeds from Experiment 5. Data presented at effluent EMC2 humidity of 92.38%, $T = 23.34°C$, and $[SO_2] = 50.2$ ppm.

oxidation, it was necessary to stop the SO_2 flow for the feed measurements. However, the flow of SO_2, though on the order of tenths of liters per minute, could not simply be stopped, or again the system pressures and flowrates would readjust. The relative humidity would also change since the SO_2 served as a dry, humidity dilution flow. Therefore, ultrapure air was substituted for the SO_2 flow while the feed voltage scan was taken. Temperatures and dew points were monitored by the computer. As with the effluent measurements, the feed scan typically took an hour to complete. Even though feed particle concentrations were higher than those in the effluent, the CNC remained in counting mode.

After finishing the feed voltage scan, the dew point meters were rebalanced, turned off, and the mirrors cleaned. Power to both classifiers was turned off. The CNC was disconnected from the EMC2 sample flow and allowed to sample filtered room air for a half an hour before the butanol was drained and the instrument turned off. The syringe pumps were stopped, the syringes cleaned, and the atomizer waste bottle emptied. All air flow to the system was turned off. Everything except for the heating baths and the SO_2 analyzer was turned off. Those valves through which aerosol passed were dismantled and cleaned after every experiment. The humidifier was disconnected and bypassed. The air flow — this time dry — was started again and fed to the CSTR. The effluent was vented via the EG&G bypass line. In order to dry out EMC2, the bubbler humidifier was bypassed and the sheath air turned back on. Dry air was run through both the reactor and EMC2 for several hours.

Because of the humid, acidic environment the measuring classifier (EMC2) was subjected to, the instrument required constant attention and maintenance. Solid $MnSO_4$ deliquesces at humidities greater than $\sim 83\%$. Therefore, the aerosol deposits on the cylinder, rod, and base of EMC2, which occurred as a natural part of classifier operation, formed a fine liquid layer when the instrument was operated at high humidities. Once classifier EMC2 became "too dirty," it was impossible

to maintain a stable voltage during an experiment and the instrument had to be cleaned. After two experiments, or approximately every 20 hours, the rod, cylinder and base of the classifier were cleaned. All lines and all valves in the instrument were also cleaned. Every other cleaning, the "head" containing the aerosol inlet and the sheath air flow-straightening screens, was disassembled and cleaned. This was not done every time because the screens are delicate and easily damaged. The maintenance requirements of EMC1 were fewer because it was operated dry. The instrument was disassembled and cleaned every 50 – 75 hours of operation.

Each time EMC2 was cleaned, all aerosol lines in the reactor system were also cleaned. If too much time passed between cleanings, the hygroscopic salt deposits in the lines deliquesced under humid conditions and it became increasingly difficult to maintain stable flowrates.

§5.2 Analysis of the Experimental Results

Reactor experiments using a $MnSO_4$ aerosol were performed over a range of humidities (86 - 94%) and SO_2 concentrations (0.1 - 50 ppm). Some variation in the aerosol $MnSO_4$ concentration, other than that resulting from varying the humidity, was achieved using $MnSO_4$ and Na_2SO_4 mixtures. $MnSO_4$ concentrations in the humid aerosol are approximately 0.02 to 3.5 molal in the experiments. The total particle number concentration in the CSTR ranged between 10,000 and 25,000 particles/cm^3. At these number concentrations, the characteristic time for coagulation of 0.1 μm particles is on the order of weeks. Therefore, any particle growth should be the result of condensation in response to chemical reaction in the aerosol phase.

Thermistor and SO_2 concentration data taken during the voltage scans were analyzed using the program ANAL.FOR (see Appendix E). This program corrected the measured dew point temperatures for pressure variations, calculated the relative humidity, and determined time-averaged values for each measured property.

The CNC number concentration data as a function of EMC2 voltage from the feed and effluent scans were fed into a computer. The data were averaged for each voltage and corrected for particle coincidence (see Agarwal and Sem, 1980). The standard deviation of the average number concentration was larger, in general, for low counts and smaller for high counts. However, for every voltage, the deviation was less than 10% of the average concentration. An example feed voltage scan and the accompanying spline fit are shown in Figure 5.3. The size distribution was obtained using Hoppel's inversion routine as discussed in Chapter 3. Table 5.1 (at the end of this chapter) presents the operating conditions for the reactor experiments discussed in this chapter. The actual temperature and SO_2 data taken as a function of time during each experiment are presented graphically in Appendix F. The relative humidity calculated using the dew point temperatures (corrected for pressure) are also included in Appendix F.

§5.2.1 Shifting the Size Distribution

The size distribution of a liquid aerosol is dependent on the humidity of its surrounding atmosphere. Therefore, the distribution resulting from inversion of the feed number concentration data is specific for the humidity at which the measurements were made. This is taken to be the time-averaged classifier humidity for the feed scan. The same is true of the effluent distribution except that the humidity of interest is now the effluent classifier humidity. If the two size distributions are to be compared for signs of aerosol growth, the effluent and feed classifier humidities must be identical. Since this precise requirement was not met experimentally (although the differences in humidity were typically less than 1%, see Table 5.1), the humidities had to be matched theoretically. The diameter of a particle in equilibrium with an atmosphere having humidity RH can be calculated using (Hänel, 1976),

$$a_w(c) = \mathrm{RH} \exp\left(-\frac{4\sigma v_m}{kTD_p}\right), \qquad (1)$$

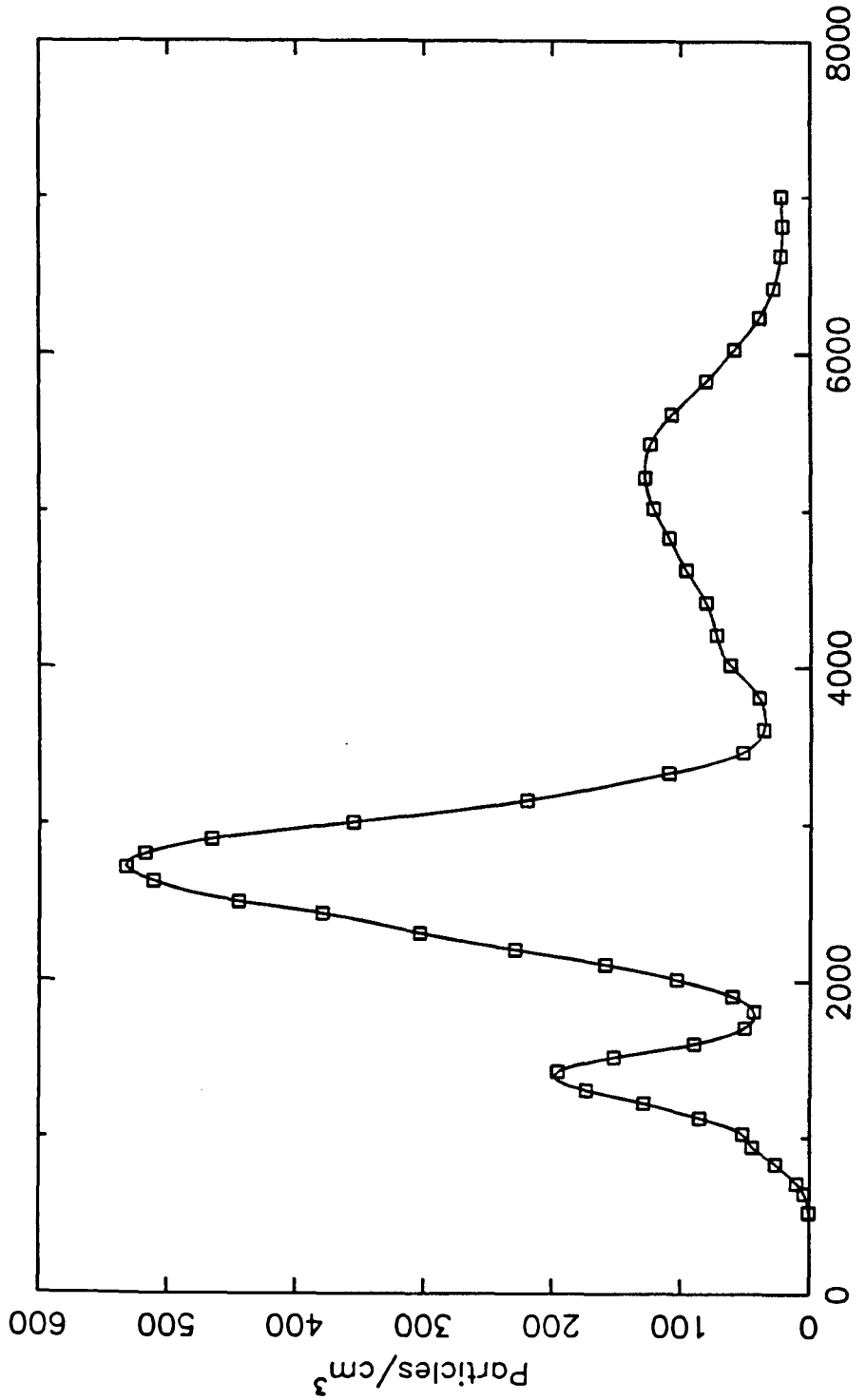

Figure 5.3 Feed voltage scan (□) and spline fit (———) for Experiment 5. Particle concentrations have been corrected for coincidence.

where $a_w(c)$ is the water activity of the particle solution at concentration c, σ is the surface tension of the particle, v_m is the molecular volume of the particle solution, and D_p is the particle diameter. The exponential term accounts for the "Kelvin effect," or the increased vapor pressure over a curved surface. Inasmuch as the surface tension, molecular volume, and water activity are a function of the solute concentration in the particle, they are also a function of particle diameter, and calculating the particle diameter using Equation (1) is an iterative process (unfortunately very little composition dependent surface tension data exists). As particle diameter increases, the Kelvin effect approaches one, and the water activity equals the system relative humidity. The aerosol solution concentration is diameter independent. However, for particle sizes between 0.1 and 0.3 μm, Figure 5.4 shows that including the Kelvin effect makes a considerable difference in the particle water activity and solution concentration. For $MnSO_4$ at 94% relative humidity, neglecting the Kelvin effect would result in a 15% error in the estimation of the particle concentration at 0.1 μm diameter.

Aerosol growth that is due to a change in the ambient relative humidity conserves both solute mass and particle number. Consider a particle having volume v_p at humidity RH, and volume v_p' at humidity RH'. If $\lambda = v_p/v_p'$, then the following is also true,

$$\lambda = c'/c = D_p^3/D_p'^3. \tag{2}$$

The water activity of the particle at RH' is written,

$$a_w(c') = a_w(\lambda c) = \mathrm{RH}' \exp\left(-\frac{4\sigma v_m}{kT(D_p\lambda^{-\frac{1}{3}})}\right). \tag{3}$$

So the procedure for calculating the particle diameter at a new humidity requires first determining the solute concentration at the original humidity and then searching for the value of λ that satisfies Equation (3). Once λ is known, the new particle concentration, volume, and diameter are known. The above equations hold only if the particle remains liquid at the humidity of interest.

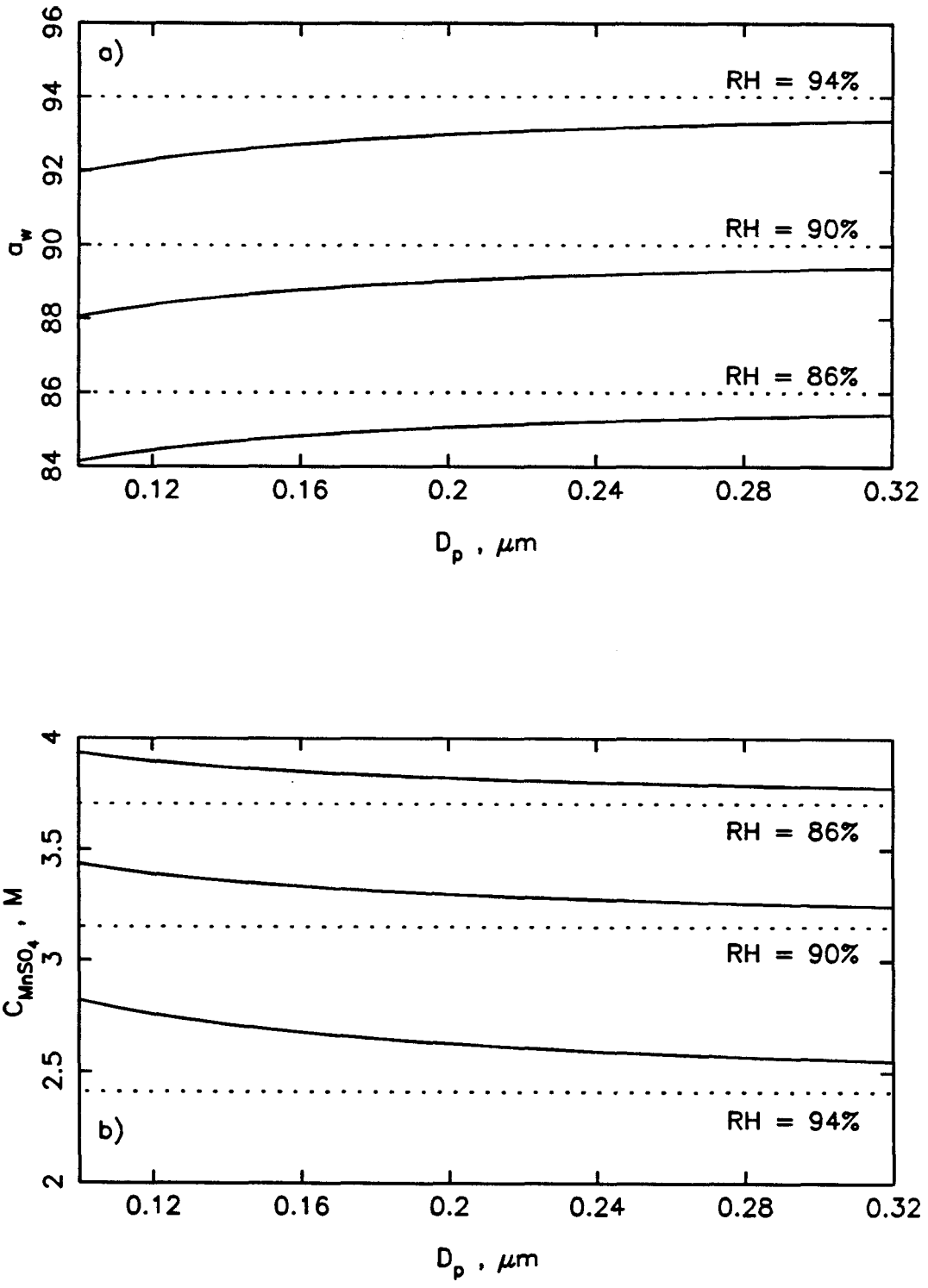

Figure 5.4 Water activity (a) and concentration (b) of a $MnSO_4$ aerosol as a function of diameter, with (————) and without (.....) the the Kelvin effect (T = 23.5 °C).

If the aerosol size distribution, $n(D_p)$, is simply shifted along the diameter axis in response to a humidity change, particle number is not conserved. However, if condensational growth is the only process occurring, particle number *must* be conserved, and

$$dN = n(D_p)\, dD_p = n(D_p')\, dD_p', \tag{4}$$

or,

$$n(D_p') = n(D_p)\, \frac{dD_p}{dD_p'}. \tag{5}$$

The relationship between D_p and D_p' is given by Equation (2). If the Kelvin effect is neglected or negligible and λ is not a function of particle diameter, then

$$n(D_p') = \lambda^{\frac{1}{3}}\, n(D_p). \tag{6}$$

Otherwise, λ is a function of diameter, and

$$n(D_p') = \frac{\lambda^{\frac{1}{3}}}{\left(1 - \dfrac{D_p}{3\lambda}\, \dfrac{d\lambda}{dD_p}\right)}\, n(D_p). \tag{7}$$

In general, if particle sizes shift to larger diameters, a decrease in the magnitude of the distribution is required to conserve particle number. Similarly, a shift in size to smaller diameters requires an increase in the distribution values if particle number is to be conserved.

A decision had to be made as to which size distribution to shift. Should the feed distribution be shifted to effluent classifier conditions, or should the effluent distribution be shifted to feed classifier conditions? If a monodisperse aerosol is fed to a batch reactor, the product will be a monodisperse aerosol since every aerosol particle experiences the same reaction conditions for the same length of time. However, the distribution of residence times that is a property of a continuous stirred tank reactor guarantees that the effluent aerosol distribution from a CSTR will be polydisperse even if the feed was a monodisperse distribution (see Figure 5.5). If

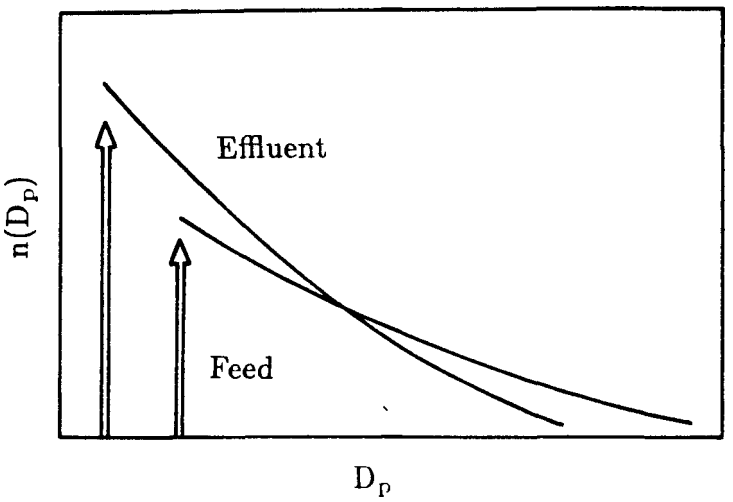

Figure 5.5 CSTR effluent aerosol given a monodisperse feed aerosol.

the reactor feed is polydisperse, the situation is slightly more complicated. Consider a polydisperse feed aerosol in which all particles have the same composition (the Kelvin effect has been neglected). Each feed diameter can be considered a monodisperse feed to the CSTR. It is possible that two particles of different initial diameter will grow to the same final diameter. This is evident in Figure 5.5 and is a result of the particles' having spent different lengths of time in the reactor. These two particles will have differing compositions. The aerosol composition at an initial relative humidity must be known in order to determine the composition and distribution at another humidity. Therefore, the reactor feed distributions should be shifted to the classifier conditions at which the effluent distribution was measured.

The final piece of information needed to shift the size distributions is the water activity as a function of composition for the aerosol salt(s). The water activity data of Rard and Miller (1981) or Rard (1984) were used for those experiments with

pure Na_2SO_4 or pure $MnSO_4$ feed aerosol, respectively. Several experiments were performed using a feed aerosol generated from Na_2SO_4 and $MnSO_4$ mixtures. No water activity data were found for the Na_2SO_4-$MnSO_4$ system so mixing rules were used to generate water activity data as a function of concentration. Cohen et al. (1987b) have studied the success of various mixing rules at predicting water activity when the only information available is the water activity of the individual component salts; i.e., no parameters were used that required knowledge of the mixture behavior *a priori*. Several mixtures were studied, including the $NaCl - (NH)_4SO_4$ system. The success of the mixing rules in predicting the water activity of this particular mixture was of interest in deciding how to treat the Na_2SO_4-$MnSO_4$ system, since sulfate ions are highly associative in solution. Cohen et al. (1987b) found that the ZSR (Zdanovdkii-Stokes-Robinson) and simplified versions of the Pitzer and RWR (Reilly-Wood-Robinson) methods all performed satisfactorily in predicting the water activities of the mixed-electrolyte solutions studied. Any non-ideal behavior, whether due to the high concentrations or to the associative nature of the sulfate ion, was adequately compensated for by the mixing rules.

Kusik and Meissner's (1978) mixing rules were used to predict the water activity of the Na_2SO_4-$MnSO_4$ feed aerosol. This particular method is a special case of the RWR method (Cohen et al., 1987b) and has been used extensively by Stelson et al. (1984) in predicting the behavior of a variety of atmospheric chemical systems. The following equation is generated for the Na_2SO_4-$MnSO_4$ system if total dissociation is assumed,

$$\begin{aligned} \ln a_w^{mix} = {} & \frac{16 m_M}{I^2}(m_M + m_N) \ln a^{\circ}_{w,M}(I) + \frac{9 m_N}{I^2}(m_M + m_N) \ln a^{\circ}_{w,N}(I) \\ & + \frac{MW_{H_2O}}{1000\, I}\left[(8m_M + 9m_N)(m_M + m_N) - I\,(2m_M + 3m_N)\right], \end{aligned} \tag{8}$$

where the subscript M refers to $MnSO_4$ and N refers to Na_2SO_4, m_i is the molality of the ith species in solution, the total ionic strength of the mixture is given by

$I = 3m_N + 4m_M$, $a_{w,i}(I)$ is the water activity of a pure solution of species i having the same total ionic strength as the mixture, and MW_{H_2O} is the molecular weight of water.

As mentioned above, no actual water activity data for the Na_2SO_4- $MnSO_4$ mixture were available, so the results of Equation (8) were compared to the experimental data of Rard and Miller (1981) for an equimolar mixture of Na_2SO_4 and $MgSO_4$. Naturally, comparing a transition metal to an alkali earth metal is not ideal by any means, but at least the charges on the ions are similar (e.g., as opposed to comparing the $Na_2SO_4/MnSO_4$ solution to a Na_2SO_4/NaCl solution). In defense of the comparison, there are several similarities in the behavior of magnesium and manganese — magnesium sulfate has an association constant of the same order of magnitude as manganese sulfate (Smith and Martell, 1982), approximately the same pure component water activity, and neither Mn(II) nor Mg(II) undergoes appreciable hydrolysis below pH = 8 (Baes and Mesmer, 1976). Figure 5.6 shows that the Kusik and Meissner mixing rule successfully predicts the Na_2SO_4-$MgSO_4$ water activity and indeed, predicted Na_2SO_4-$MnSO_4$ water activities of approximately the same value. The effect of ion pairing was not explicitly accounted for in the water activity determination. In subsequent calculations it was assumed that the Na_2SO_4-$MnSO_4$ mixture water activity predicted by Equation (8) was a "reasonable" estimate of the actual, unknown value.

The program that shifts the humid reactor feed distribution to the effluent classifier conditions, SHIFTDP.FOR, is included in Appendix E. This program can be used for either pure manganese sulfate or manganese sulfate/sodium sulfate mixture feed aerosols. The final shifted diameter satisfied both Equation (1) and conserved manganese between the initial and shifted particles. Because the Kelvin effect was included in the calculations, the parameter $\lambda = (D_{p,initial}/D_{p,shifted})^3$ is a function of diameter and Equation (7) should be used to obtain the value of the shifted distribution. However, including the correction $1/\{1 - (D_p/3\lambda)(d\lambda/dD_p)\}$

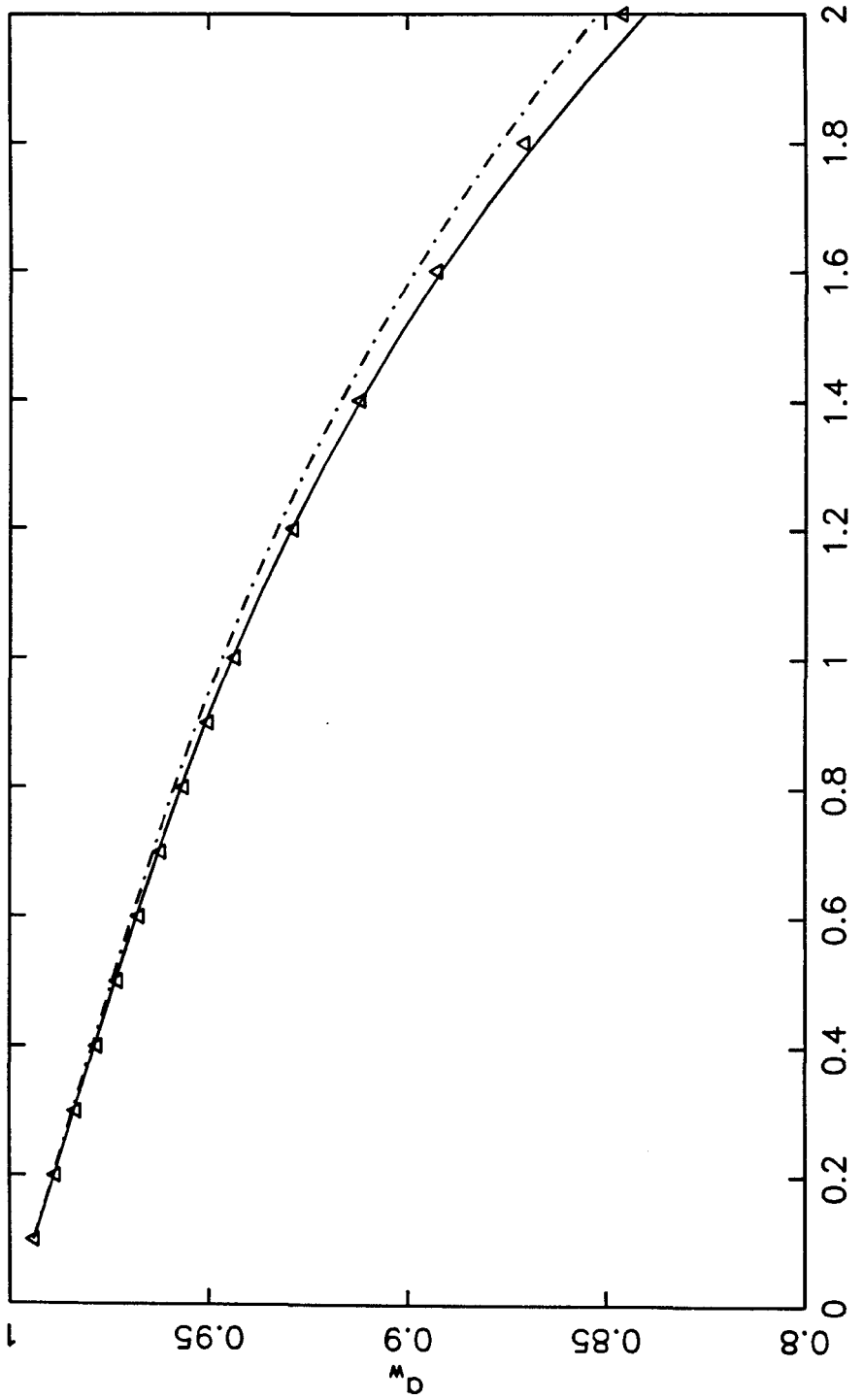

Figure 5.6 Water activities predicted by the Kusik and Meissner (1978) mixing rule for Na_2SO_4- $MnSO_4$ (— · — · —) and and Na_2SO_4-$MgSO_4$ (————) equimolar mixtures compared to the experimental results of Rard and Miller (1981) (△) for Na_2SO_4-$MgSO_4$.

greatly complicates and slows the calculations. Because the relative humidity corrections being made were small, this factor ranged from 0.999285 to 1.003705 for a 0.16 μm particle at the experimental conditions listed in Table 5.1. Less than a 0.4 percent error would be made in the predicted peak distribution value if $\lambda \neq f(D_p)$ were assumed. Therefore, the shifted distribution values were calculated in SHIFTDP.FOR assuming no Kelvin effect (Equation (6)), even though the diameter calculations included the correction. The feed and effluent size distributions at the classifier conditions during the effluent scan are presented in Figures 5.10 through 5.28 at the end of this chapter.

§5.2.2 The Size Distributions

The first two experiments listed in Table 5.1 are "blank" runs and their results indicate what could or could not be regarded as "growth" in the subsequent experiments. In Experiment 1 a humid $MnSO_4$ aerosol was fed to the reactor in the absence of SO_2. The size distribution plot, Figure 5.10, shows no shift between the feed and effluent distributions. This particular run was made before the feed bypass valve was installed (see Chapter 2). Subtle changes in the flow patterns that occurred upon switching to the feed bypass resulted in a larger particle loss for the feed scan. However, the altered deposition pattern did not shift the distribution. From this particular experiment it was concluded that a distribution shift when SO_2 was present could be attributed to reaction of the S(IV) species in the presence of manganese.

In experiment 2 SO_2 was present in the reactor atmosphere, but no manganese was present in the sodium sulfate feed aerosol. Since sodium sulfate was used to decrease the manganese concentration in several of the experiments, it was necessary to show that a shift between the feed and effluent distributions was not due to the sodium ions present in the aerosol. For instance, Clarke and Williams (1983) observed S(IV) oxidation catalyzed by NaCl and $MgCl_2$ solutions several

molar in concentration. Clarke and Radojevic (1983) attributed the catalytic action to the presence of Cl^- and not Na^+ or Mg^{2+}. Nevertheless, the possibility of growth resulting from the presence of sodium had to ruled out in the case of the Na_2SO_4-$MnSO_4$ aerosol. An additional issue that was addressed using the results of this experiment was the fact that the deliquescence point for Na_2SO_4 is commonly taken to be 93% (Washburn, 1926). Since 93% relative humidity was reached in only one of the runs using Na_2SO_4, it was necessary to determine the physical state of the aerosol — liquid or solid.

A solid "deliquesces," or becomes liquid, when the relative humidity of the atmosphere equals the water activity of the saturated salt solution. The feed and effluent for a pure Na_2SO_4 aerosol were measured at approximately 91% relative humidity in Experiment 2. EMC1 was operated at conditions that generated a dry feed aerosol having singly charged particles on the order of 0.091 μm in diameter. The primary peak of the humid feed distribution for this experiment (see Figure 5.11) fell at about 0.152 μm. Clearly, aerosol growth, and therefore deliquescence, had occurred upon humidification to 91%. Indeed, Cohen et al. (1987a) observed deliquescence of a Na_2SO_4 particle at 85 to 86% humidity. The lowest humidity used in a reactor experiment with a Na_2SO_4-$MnSO_4$ feed aerosol was 86.81% (Experiment 15) and the peak diameter of 0.1489 μm would indicate that the aerosol had deliquesced and was liquid.

The size distributions in Figure 5.11 indicate that no growth occurred in Experiment 2. The sodium ion did not catalyze the oxidation of S(IV) to S(VI), which would result in condensational growth. An additional observation can be made from these results — establishment of the S(IV)-SO_2 equilibrium did not result in particle growth. The diameter change resulting from the S(IV)-SO_2 equilibrium was also checked theoretically (see Appendix C for details) and found to be negligible. This was true for both $MnSO_4$ and Na_2SO_4 feed aerosol. For example, if the relative humidity and temperature remained constant at 89.10% and

23.49°C, respectively, the peak feed diameter of 0.1543 μm in Experiment 2 was predicted to grow to 0.15435 μm upon exposure to 14.3 ppm SO_2.

Experiments 3 through 18 in Table 5.1 (Figures 5.12 through 5.27) are actual growth experiments. Some of the runs (13 - 18) were made with a Na_2SO_4-$MnSO_4$ mixture feed in order to decrease the initial concentration of manganese. This did not, however, decrease the total ionic strength of the solution. Figures 5.7a and 5.7b show that while the manganese concentration was lowered by orders of magnitude as δ (moles Na_2SO_4/mole $MnSO_4$) ranged from 0 to 100 in the feed aerosol, the total ionic strength dropped by only ~4 molal. The ionic strength was still several orders of magnitude greater than the ionic strengths of typical of "ideal" solutions (< 0.1 m) or fogwater. Despite the variety of conditions, very little particle growth was observed. The difference in peak diameter between the CSTR feed and effluent ranged 0 (in the case of the blanks) to 7%. There did appear to be a slight increase in the amount of observed growth as the humidity was increased. Results typical of those listed in Table 5.1 were consistently obtained, regardless of the alterations and adjustments made to the reactor system. As mentioned earlier, the possibility that the growth was merely evidence of the aerosol equilibration with S(IV) was considered and rejected. The diameter change resulting from equilibration with the SO_2 would not be resolvable. The possibility that the growth was mass transfer limited was considered next.

§5.2.3 Mass Transfer Considerations

As mentioned at the beginning of this section, any shifts observed in the reactor experiment size distributions can be attributed to condensational growth because the characteristic time of coagulation exceeds the experiment time. However, condensational growth of the aerosol particle occurs as the result of a number of steps — mass transfer and reaction — any one of which could be rate limiting. In kinetic studies it is important that chemical reaction be rate limiting so that the

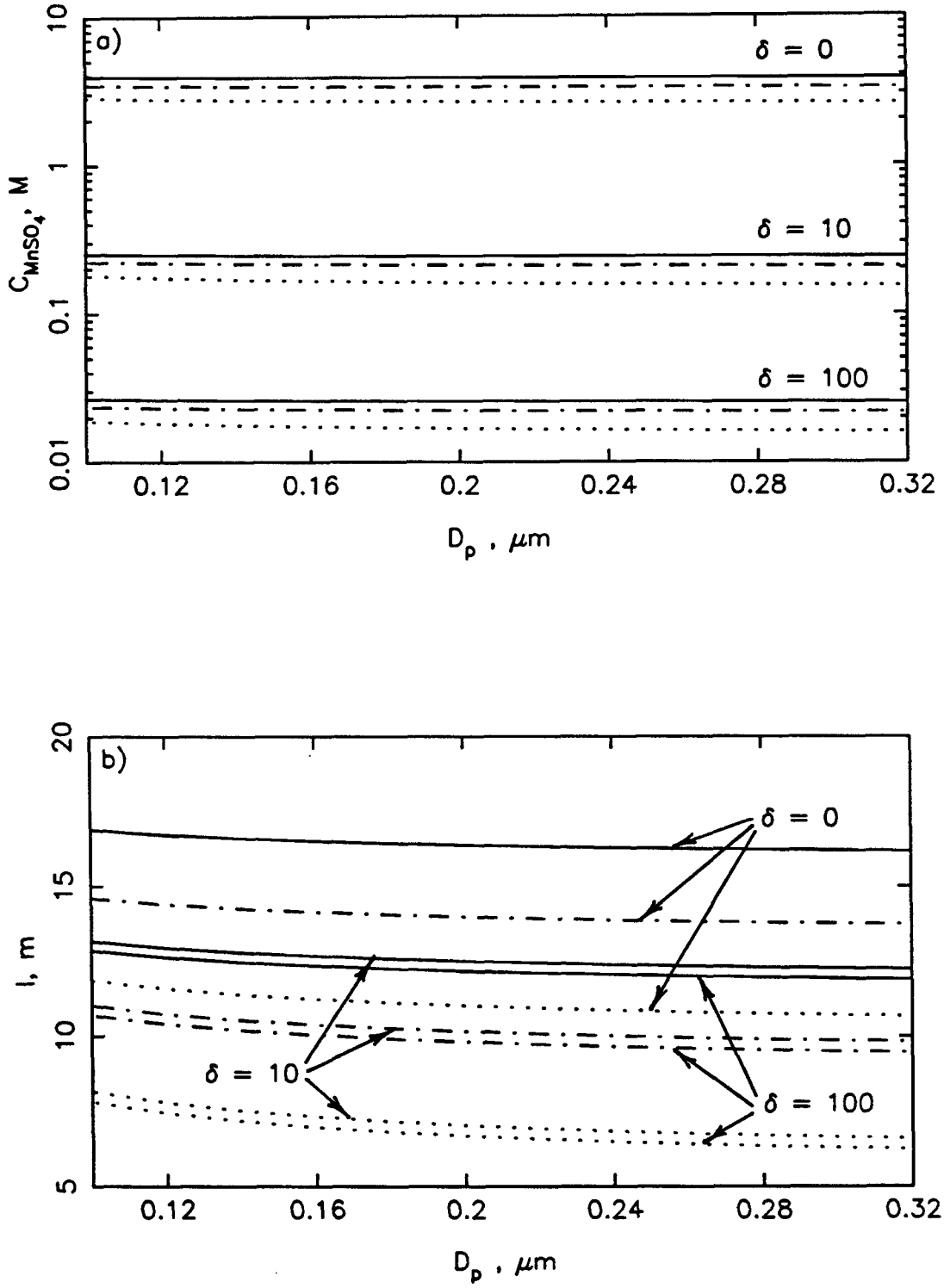

Figure 5.7 $MnSO_4$ concentration (a) and total ionic strength (b) in feed aerosol as a function of diameter and moles Na_2SO_4 /mole $MnSO_4$ (δ). Relative humidity = 86% (·····), 90% (—·—·—·—), or 94% (————).

measured overall rate of reaction is the rate of the intrinsic chemical reaction. This was discussed briefly in Chapter 4 with regard to various studies in the literature. While these reactor experiments are not "kinetic studies" *per se*, if the aerosol system is not mass transfer limited, then the reactor system can be modeled to test the applicability of the various proposed kinetic reaction rates. Growth is a direct, measurable result of the intrinsic reaction rate.

For the reaction of S(IV) to S(VI) to occur in the aqueous-aerosol phase, the following sequence of steps must occur (Schwartz and Freiberg, 1981):

(1) Diffusion of SO_2 from the bulk gas to the surface of the particle.
(2) Transfer of SO_2 across the gas-liquid interface (Henry's law).
(3) Establishment of the equilibrium among the S(IV) species — $SO_2 \cdot H_2O$, HSO_3^-, and SO_3^{2-}.
(4) Diffusion of the various species in the aqueous phase.
(5) Chemical reaction of S(IV) to S(VI).

If step (5) is slowest, the overall rate of conversion of S(IV) will be equal to the intrinsic rate of reaction. By studying the characteristic time required for each step in the sequence, it is possible to determine if the overall rate is mass transfer limited. A reaction system is mass transfer, or diffusion, limited if the gas-phase SO_2 concentration at the particle surface is less than in the bulk-phase and/or the S(IV) concentration in the particle is not homogeneous.

The various characteristic times describing the gas-aerosol system were outlined in Chapter 4 and will be discussed in more detail here (see also Schwartz and Freiberg (1981), Freiberg and Schwartz (1981), and Schwartz (1984)). The characteristic time for diffusion of a species through a bulk gas (step 1 above) describes the establishment of a steady-state gas-phase SO_2 profile, given that diffusion is the only mechanism for transport: $\tau_{dg} = D_p^2/(4\pi^2 D_g)$, where D_g is the gas-phase diffusion coefficient of SO_2 and D_p is the aerosol diameter. Similarly, the charac-

teristic time required to establish a steady-state profile in the aqueous phase S(IV) (step 4) by diffusion is $\tau_{da} = D_p^2/(4\pi^2 D_a)$, where D_a is the diffusion coefficient of the S(IV) species in the aqueous phase. The overall aqueous diffusion coefficient for S(IV) can be written as a weighted mean of the various individual S(IV) species diffusion coefficients (Eriksen, 1969):

$$D_a = \frac{[SO_2 \cdot H_2O]}{[S(IV)]} D_{SO_2} + \frac{[HSO_3^-]}{[S(IV)]} D_{HSO_3^-} + \frac{[SO_3^{2-}]}{[S(IV)]} D_{SO_3^{2-}}, \qquad (9)$$

where $D_{SO_2} = 1.27 \times 10^{-5}\,cm^2/sec$, $D_{HSO_3^-} = 0.75 \times 10^{-5}\,cm^2/sec$, and $D_{SO_3^{2-}} = 0.50 \times 10^{-5}\,cm^2/sec$ at 21°C. Consequently, D_a is a weak function of the solution pH and τ_{da} will increase slightly over the pH range 2 to 8. The diffusivity of S(IV) is also affected by the electrolyte concentration. Given that $D_a = D_a^0(1 - \theta C)$, where D_a^0 is the diffusivity of the species in the pure solvent (e.g., Equation (9) for S(IV)) and C is the electrolyte concentration, Ratcliff and Holdcroft (1963) determined that $\theta = 0.257\,M^{-1}$ for the diffusion of CO_2 in solutions of Na_2SO_4 up to 1 M, and $\theta \sim 0.301\,M^{-1}$ in solutions of $MnSO_4$. If it is assumed that the diffusion of SO_2 is similar to that of CO_2, then for $[MnSO_4] \leq 3$ M, up to an order of magnitude error in the estimate of τ_{da} can be made if the electrolyte effect is ignored.

The time required to establish equilibrium between SO_2 and S(IV) across the gas-liquid interface (step 2) is given by $\tau_{phase} = D_a\{4H^*RT/(\alpha\bar{c})\}^2$, where $\bar{c}$ is the average molecular speed of the SO_2 molecules, α is the sticking coefficient describing the fraction of SO_2 molecules that strike the droplet surface and actually enter the liquid phase, and H^* is the modified Henry's law coefficient, which accounts for the rapid equilibration of the dissolved SO_2 gas with the various S(IV) species (Schwartz and Freiberg, 1981). There is very little agreement between researchers as to the value of α. Reported values for the "self accomodation" coefficient of water range from 0.01 to 1 (Pruppacher and Klett, 1978) with the values for renewed and/or clean surfaces falling at the upper end of the spectrum. A value of 1.0 was

used in estimating the characteristic time for phase equilibrium for these and other laboratory experiments, although $\alpha < 1$ would be expected in the atmosphere. The characteristic time is also a strong function of the solution pH. At low values of the pH, the abundance of hydrogen ion drives the equilibrium towards the gaseous phase so that effectively less SO_2, and thus less time, is required to establish equilibrium at the interface. At high pH values, the high solubility of the S(IV) species requires that more SO_2 be absorbed across the interface, thus increasing the time required to saturate the aqueous phase. Because the characteristic time to establish equilibrium will decrease as SO_2 is absorbed, τ_{phase} calculated at a specific pH is a worst-case estimate.

Two times related to τ_{phase} are the characteristic times for the hydrolysis and subsequent ionization of SO_2 (step 3). The characteristic time for the hydrolysis and ionization of SO_2 to HSO_3^- to occur at 25°C is given by $\tau_{i1}\,(\text{sec}) = [(3.4 \times 10^6) + (2.0 \times 10^8)([H^+]_e + [HSO_3^-]_e)]^{-1}$, if $[SO_2 \cdot H_2O]/(K_1 + [H^+]_e + [HSO_3{}^-]_e) \ll 1$ (Seinfeld, 1986). Similarly, the time for equilibrium to be established between HSO_3^- and SO_3^{2-}, the second ionization of SO_2 is $\tau_{i2}\,(\text{sec}) = [(1.9 \times 10^3) + (3.0 \times 10^{10})([H^+]_e + [SO_3^{2-}]_e)]^{-1}$, if $[HSO_3{}^-]/(K_2 + [H^+]_e + [SO_4{}^{2-}]_e) \ll 1$. For $2 \leq pH \leq 8$ and $p_{SO_2} = 0.1$ to 100 ppm the requisite inequality is satisfied only for the first ionization ($SO_2 \cdot H_2O \rightarrow H^+ + HSO_3^-$). Therefore, at these conditions the assumptions made in obtaining τ_{i2} are not valid. In any event, since the aerosol solution is expected to be acidic, the first ionization equilibrium will dominate the S(IV) speciation. In calculating the characteristic time τ_{i1}, the concentration of HSO_3^- is needed. At equilibrium $[SO_2 \cdot H_2O]$ can be calculated using Henry's law. However, it has not yet been ascertained whether or not sufficient time has been allowed for phase equilibrium to be established, or that gas-phase diffusion limitation is negligible and $p_{SO_2,surface} \sim p_{SO_2,\infty}$. These assumptions are implicit in the calculation of the characteristic time. As a worst-case estimate of $\tau_i 1$, $[HSO_3^-]$ can be assumed to be zero. This corresponds to an infinitely small gas-phase SO_2 concentration.

As mentioned above, more SO_2 is necessary to saturate the aqueous phase as the pH increases. This raises need for an additional characteristic time — one that addresses the ability of gas-phase diffusion (assuming no other form of mixing) to supply a sufficient amount of SO_2 to satisfy the steady-state requirements and saturate the particle. This is independent of the *time* required to establish phase equilibrium, determining only the time required for diffusion to transport the reagent necessary assuming that equilibrium *is* established: $\tau_{reag} = \pi^2 H^* RT \tau_{dg}/3$ (Schwartz and Freiberg, 1981). Again, the strong dependence of H^* on pH results in large values of τ_{reag} as the pH increases.

Figure 5.8 shows the various characteristic times as a function of particle pH for the SO_2-S(IV) system. A particle diameter of 0.1 μm, typical of the reactor experiment aerosol, was used in generating the plot. Three cases have been plotted for the characteristic times of ionization: 1) the "worst" case where $[SO_3^{2-}]$ and $[HSO_3^-]$ are negligible; 2) the S(IV) species are in equilibrium with 0.1 ppm SO_2; and 3) the S(IV) species are in equilibrium with 10 ppm SO_2. For pH > 3.5, τ_{phase} is the controlling characteristic time, increasing from 10^{-6} seconds at pH = 4 to 0.1 seconds at pH = 6. Because the electrolyte concentration was assumed negligible in the generation of Figure 5.8, the actual value of τ_{da} might be up to an order of magnitude greater. This would be important only for pH < 3.5 where aqueous-phase diffusion is the rate determining process.

There are basically two major sets of "time" criteria that must be satisfied by droplet systems if intrinsic reaction rates are to be measured. First, steady-state concentration profiles are achieved in the gas and liquid phases only if the aerosol contact time, or experiment time, is greater than the characteristic times required for establishing these profiles. And second, if the characteristic time of the chemical reaction is greater than the time required to transport the reactant in both phases and the time required to establish phase equilibrium, then the measured rate was not mass transfer limited.

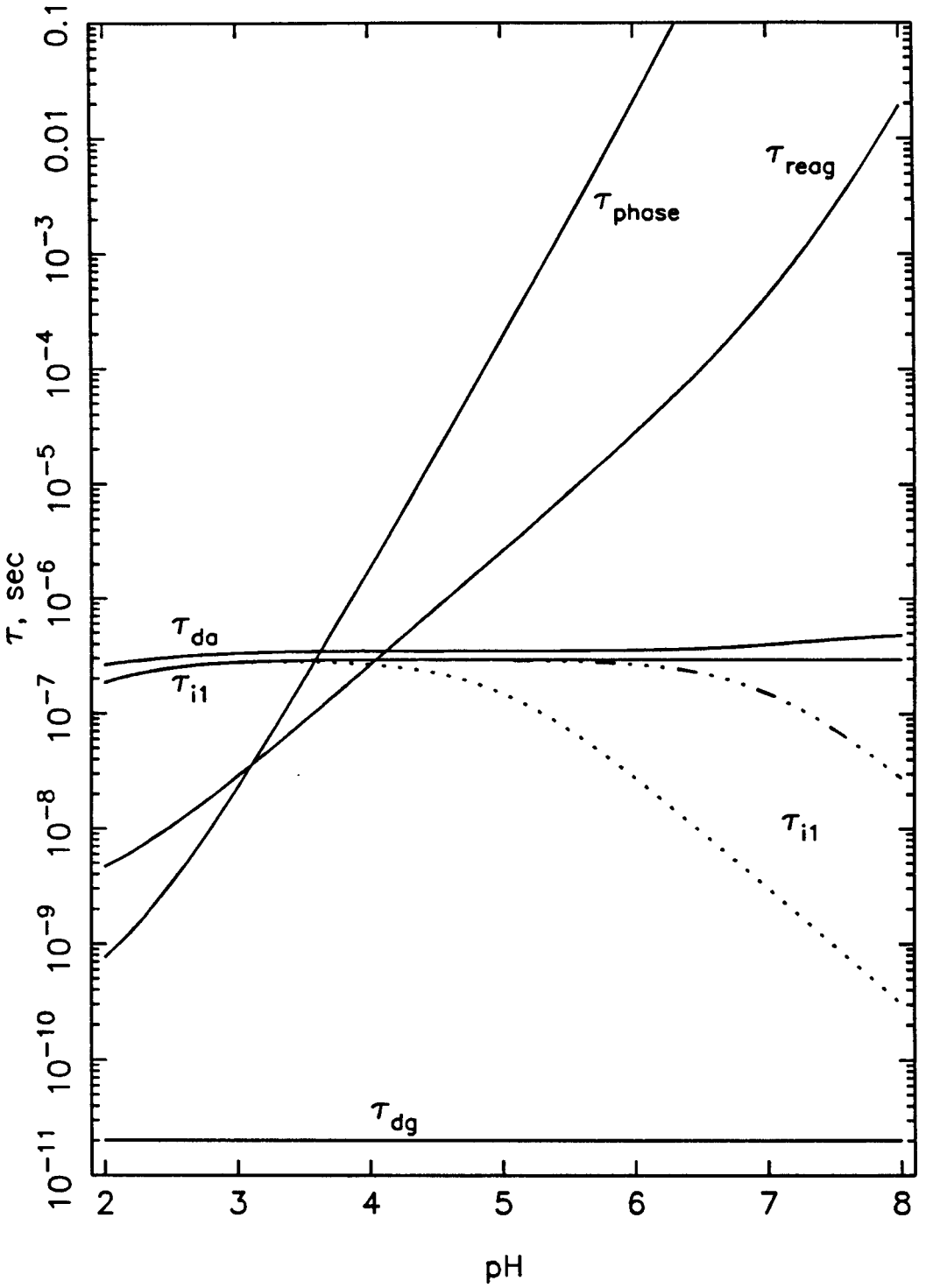

Figure 5.8 Characteristic times associated with establishing steady-state SO_2 and S(IV) concentration profiles in and about a 0.1 μm particle as a function of the particle pH. For τ_{i1}: $p_{SO_2} \sim 0$ ppm (————), $p_{SO_2} = 0.1$ ppm (—··—··—), $p_{SO_2} = 10$ ppm (·····).

In order for gas and liquid phase steady-state concentration profiles to be established, the following criteria must be satisfied,

$$\begin{aligned} \tau_{CSTR} &\gg \tau_{dg}, \\ \tau_{CSTR} &\gg \tau_{reag}, \\ \tau_{CSTR} &\gg \tau_{da}, \end{aligned} \tag{10}$$

where τ_{CSTR} is the aerosol residence time in the CSTR. The mean residence time of the CSTR was approximately one hour. Given the residence time distribution of an ideal CSTR, this means that a fraction 1/e (36.8%) of the aerosol had a reactor residence time greater than τ_{CSTR} and 90% of the particles spent more than 380 seconds in the reactor. From Figure 5.8, it is apparent that for particle pH values less than 7.5, all characteristic times are significantly less than the CSTR residence time, satisfying the criteria in Equation (10). Since the initial pH of a pure $MnSO_4$ solution $O(1\text{ M})$ is 2 to 3 (Berresheim and Jaeschke, 1986), conditions for steady state should have existed in the CSTR.

The second set of characteristic time criteria assures that the measured reaction rate is the intrinsic reaction rate. In other words, the steady-state profiles are not mass transfer limited in either phase. If the droplet is large and additional time is required to transport the reactant, or if the reaction rate is fast and the reactant is quickly consumed, then mass transfer limitations are possible. The criteria that must be satisfied to avoid mass transfer limitation are:

$$\begin{aligned} \tau_{ra} &\gg \tau_{da}, \\ \tau_{ra} &\gg \tau_{phase}, \end{aligned} \tag{11}$$

where τ_{ra} is the characteristic reaction time, assuming first-order S(IV) dependence ($\tau_{ra} = k^{-1} = \frac{1}{[\mathrm{S(IV)}]} \frac{d[\mathrm{S(VI)}]}{dt}$). Even if the experimentally determined rate expressions have a different concentration dependence, an "effective k" can be calculated, describing the rate as if it were first order in S(IV). Figure 5.9a shows the allowable values of k as a function of pH if mass transfer limitations are to be avoided

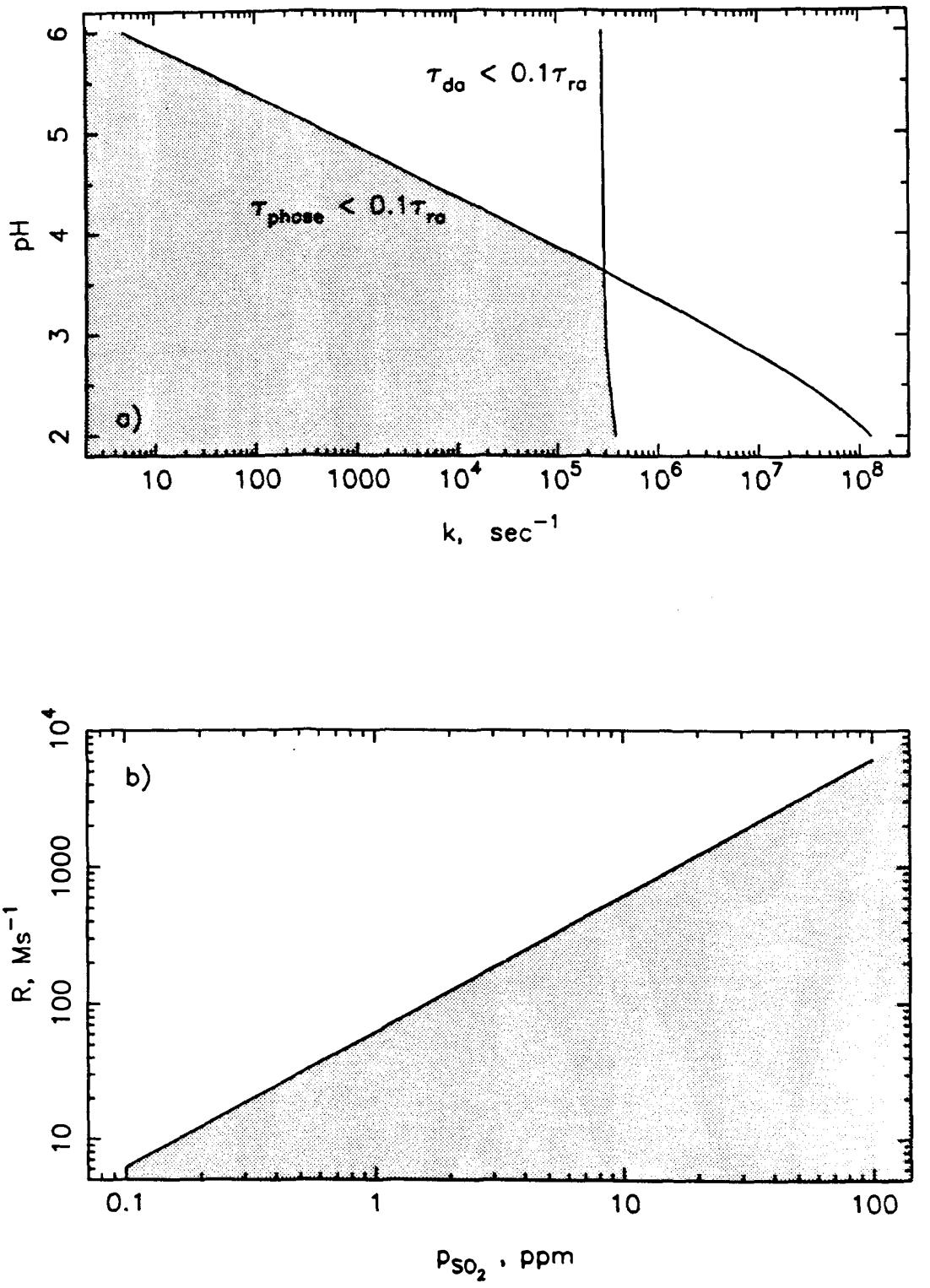

Figure 5.9 Bounds delimiting regions of mass transfer limitation for first-order S(IV) oxidation in an 0.1 μm aerosol particle as a function of the particle pH. Shading indicates region of no mass transfer limitation. a) Region of aqueous and equilibrium-phase limitation, b) Region of gas-phase limitation.

(shaded area). By far the most restricting condition is the establishment of phase equilibrium and the range of k that will not result in mass transfer limitation decreases as pH increases. This is due to the increased solubility of SO_2 at higher pHs. Figure 4.5 shows that in general, the aerosol-phase manganese-S(IV) kinetic studies resulted in a value of $\overline{R}/[\mathrm{Mn(II)}]^2$ ranging from 10^{-4} to $10^{-3}\,(\mathrm{M\,s})^{-1}$. The corresponding range of $\overline{R}$ is 10^{-4} to $10^{-3}\,\mathrm{M\,s^{-1}}$ for $[\mathrm{Mn(II)}] \sim O(1\ \mathrm{M})$. For this range of reaction rates, pH values of 2 to 5 and $p_{SO_2} = 0.1 - 100$ ppm result in first-order reaction rate coefficients k ranging from 6×10^{-4} to $3 \times 10^3\,\mathrm{s^{-1}}$. The lower the pH, the higher the value of k. Again, conditions that were not mass transfer limited should have been achieved.

Mass transfer limitation of the reaction by gas-phase diffusion can be checked by determining the shape of the gas-phase reagent concentration profile. The steady-state equation for diffusion of the reagent species in the gas phase is solved, given that the flux across the droplet surface as a result of gas-phase diffusion equals the reaction rate, and the reagent concentration remains constant in the bulk phase. Only diffusional transport of the species is considered. The following formula describes the reagent concentration profile as a function of distance away from the droplet surface:

$$C(r) = C_\infty - \left(\frac{\overline{R}a^3}{3\,D_g}\right) r^{-1}, \tag{12}$$

where D_g is the gas-phase diffusion coefficient of the reagent species, a is the droplet radius, and $\overline{R}$ is the volume-averaged reaction rate. Existence of a flat species profile in the gas, or $C(a) = C_\infty$ indicates that the droplet reaction rate is not gas-phase diffusion limited. The presence of the droplet does not affect its immediate surroundings and a reactant concentration of C_∞ is "felt" by the droplet. Thus, conditions for no mass transfer limitation due to diffusion of the reactant to the droplet must satisfy the following relation:

$$\frac{\overline{R}a^2}{3\,D_g C_\infty} \ll 1. \tag{13}$$

Note that as the reaction rate increases, the droplet size increases and/or the gas-phase bulk concentration decreases the chances of gas-phase mass transfer limitation increase. It was by rearranging this equation that Schwartz and Freiberg (1981) arrived at the criterion, $\tau_{dg} \ll \tau_{rg}$, where τ_{dg} is the characteristic time for gas-phase diffusion and $\tau_{rg} = \tau_{ra}/(H^*RT) = 1/(kH^*RT)$ is the characteristic time for reaction referenced to the gas-phase reagent concentration. However, it is counterintuitive to use characteristic "times" to describe a result obtained assuming a steady-state gas-phase concentration profile. Therefore, Equation (13) will be used in its present form to determine if mass transfer in the gas-phase limits the rate of reaction. Figure 5.9b shows the region of reaction rates for a 0.1 μm particle as a function of p_{SO_2} that would not be diffusion limited (shaded area). For 0.1 ppm $\leq p_{SO_2} \leq$ 100 ppm, a reaction rate less than 10 Ms^{-1} guarantees a flat gas-phase SO_2 concentration profile. If the volume-averaged reaction rate $\overline{R}$ is again assumed to range from 10^{-4} to 10^{-3} Ms^{-1} for a typical aerosol phase study (see Figure 4.5), then gas-phase diffusion limitation would not appear to be a potential problem.

Throughout the discussion of mass transfer limitation, it was assumed that the temperature of the droplet was uniform and equal to its surroundings. However, the oxidation of S(IV) to S(VI) is an exothermic reaction and the possibility of temperature gradients must be considered. The characteristic times for heat conduction in and about the particle are analogous to those of diffusion. Again, these times are upper bounds since convection is ignored. The thermal diffusivity is defined as $\alpha = k_t/(\rho C_p)$, where k_t is the thermal conductivity, ρ is the density, and C_p is the specific heat of the conducting fluid. For air $\alpha \sim 0.25 cm^2/s$ (Bennett and Myers, 1974) and for a manganese sulfate solution $\alpha \sim 10^{-3} cm^2/s$ (Washburn, 1926). The resulting characteristic times for heat conduction in the particle and in the gas are approximately 10^{-7} and 10^{-11} seconds, respectively. Since the CSTR residence time is orders-of-magnitude greater than either of these two times, the system temperature should be at steady state.

The nature of the steady-state temperature profile, assuming heat transfer occurs via conduction only, can be calculated in a manner analogous to the calculation of the reactant gas-phase concentration profile. Heat generated by reaction (ΔH) equals the conduction rate away from the drop and the bulk gas temperature is T_∞. The condition for a flat temperature profile is given by

$$\frac{\overline{R}a^2(-\Delta H)}{3\,k_{t,air}T_\infty} \ll 1. \tag{14}$$

Penkett (1986) gives ΔH for the reactions of HSO_3^- and SO_3^{2-} with oxygen to form HSO_4^- and SO_4^{2-}, respectively, as approximately -60 kcal/mole. For a particle of 0.1 μm diameter and an air temperature of 25°C, this heat of reaction results in the inequality $\overline{R} \leq 10^3\,\mathrm{M\,s^{-1}}$ if Equation (13) is to be satisfied. Since $\overline{R} \leq 10^{-1}\,\mathrm{M\,s^{-1}}$ is necessary for a flat SO_2 profile, a flat temperature profile will be guaranteed. In addition, the characteristic time for the generation of the heat of reaction is the characteristic time for the reaction itself. Those values of the rate coefficient k that guarantee no mass transfer limitation satisfy the inequality $\tau_{ra} \gg \tau_{da}$. Since τ_{da} is greater than τ_{qa}, the characteristic time for heat conduction in the particle, τ_{ra}, is also greater than τ_{qa}. Therefore, if the reaction rate is free from mass transfer limitations, then $T_{droplet} \sim T_\infty$ is a valid assumption.

Given the prior discussion concerning the characteristic time analysis for mass transfer, every indication is that the CSTR system *should* have been free from mass transfer limitation. Therefore, the small amount of particle growth was evidence of the reaction that had occurred. It was mentioned in Chapter 4 that the manganese catalyzed S(IV) oxidation reaction has been found to be very sensitive to inhibition by a variety of organics. With an experimental setup the size of the CSTR system this is a possibility that cannot be discounted, although care was taken to make the system as clean as possible. In the next chapter the CSTR will be modeled so that any reaction rate expression can be used to predict the effluent distribution given the input feed distribution.

Table 5.1

Operating Conditions for the Reactor System Experiments

Expt	EMC Conditions								Peak	
	T_{feed} (°C)	RH_{feed} (%)	T_{eff} (°C)	RH_{eff} (%)	T_{CSTR} (°C)	RH_{CSTR} (%)	SO_2 (ppm)	$\frac{moles\ Na_2SO_4}{moles\ MnSO_4}$	$D_{p,feed}$ (μm)	$D_{p,eff}$ (μm)
1	23.43	88.83	23.49	89.34	22.70	90.60	0	0	0.1629	0.1629
2	23.46	90.32	23.49	89.10	23.64	91.27	14.3	∞	0.1543	0.1542
3	23.87	89.95	23.54	87.08	23.40	89.40	52.0	0	0.1599	0.1638
4	23.67	91.99	23.18	91.64	23.32	91.66	49.9	0	0.1706	0.1759
5	23.64	93.07	23.34	92.38	23.62	92.78	50.2	0	0.1667	0.1751
6	24.11	89.36	24.04	88.74	24.15	89.97	13.2	0	0.1652	0.1697
7	24.14	91.42	24.08	91.51	24.22	91.99	12.9	0	0.1648	0.1687
8	23.43	93.75	23.20	93.18	23.62	94.39	13.5	0	0.1656	0.1755
9	22.97	88.56	22.91	87.49	23.24	88.73	1.74	0	0.1614	0.1654
10	24.11	92.49	24.01	92.23	23.99	93.79	1.72	0	0.1695	0.1743
11	23.17	89.67	23.38	88.39	23.30	90.10	0.107	0	0.1625	0.1677
12	24.20	92.87	23.89	92.39	23.90	92.90	0.122	0	0.1718	0.1767
13	23.94	92.37	23.60	91.28	23.36	91.72	13.4	9.96	0.1562	0.1600
14	23.60	93.11	23.33	92.68	23.27	94.83	14.4	9.96	0.1540	0.1656
15	23.34	89.35	23.23	90.08	23.21	91.48	14.3	8.84	0.1501	0.1535
16	23.44	86.81	23.16	86.94	22.99	89.47	1.87	8.84	0.1489	0.1526
17	23.34	89.67	23.19	89.69	23.25	91.63	1.85	8.84	0.1471	0.1548
18	23.10	90.26	23.16	89.53	23.36	90.44	13.6	100.	0.1492	0.1577

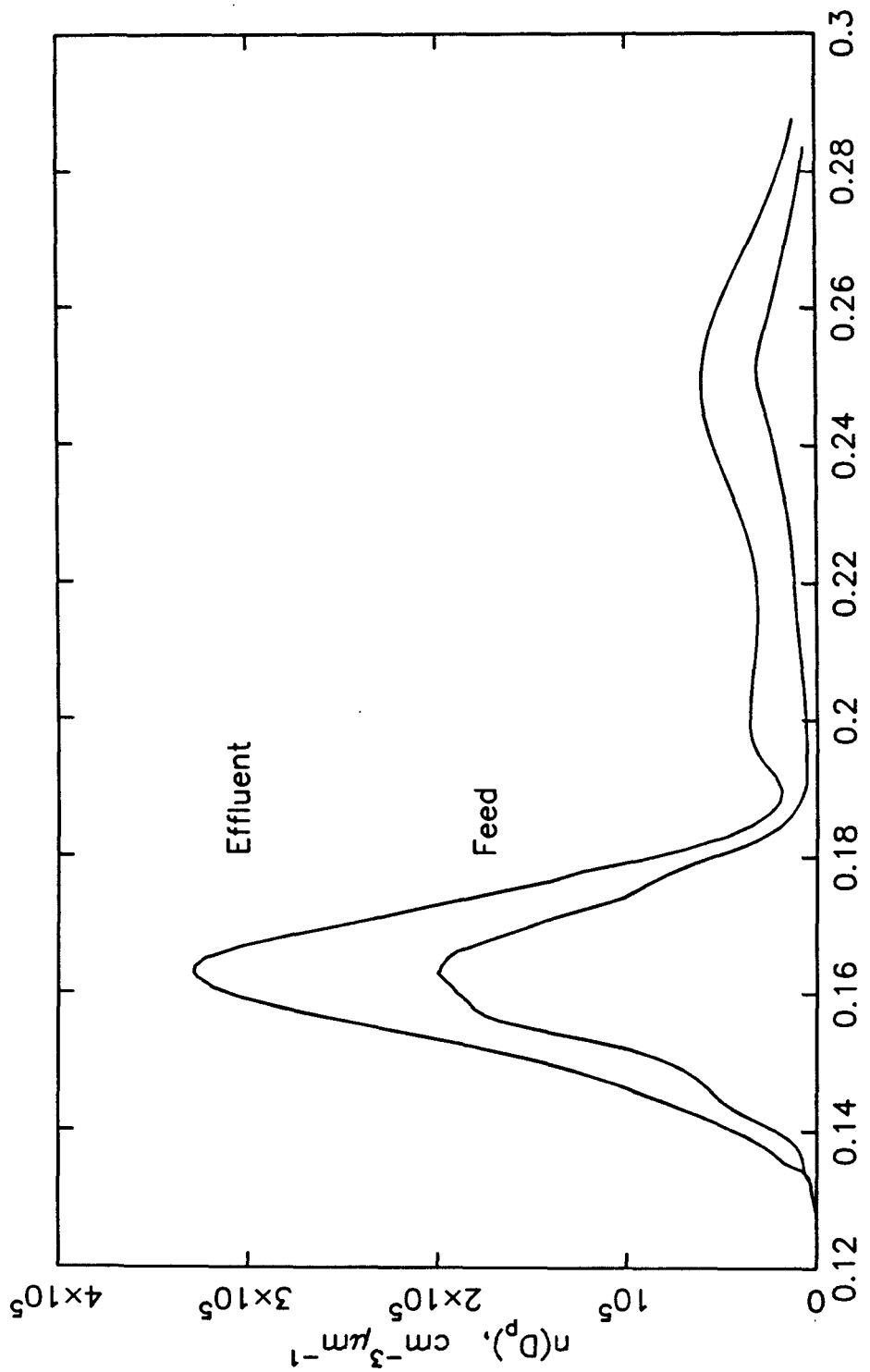

Figure 5.10 Experiment 1: $MnSO_4$ aerosol blank run (0 ppm SO_2) at 23.49°C, 89.34% humidity.

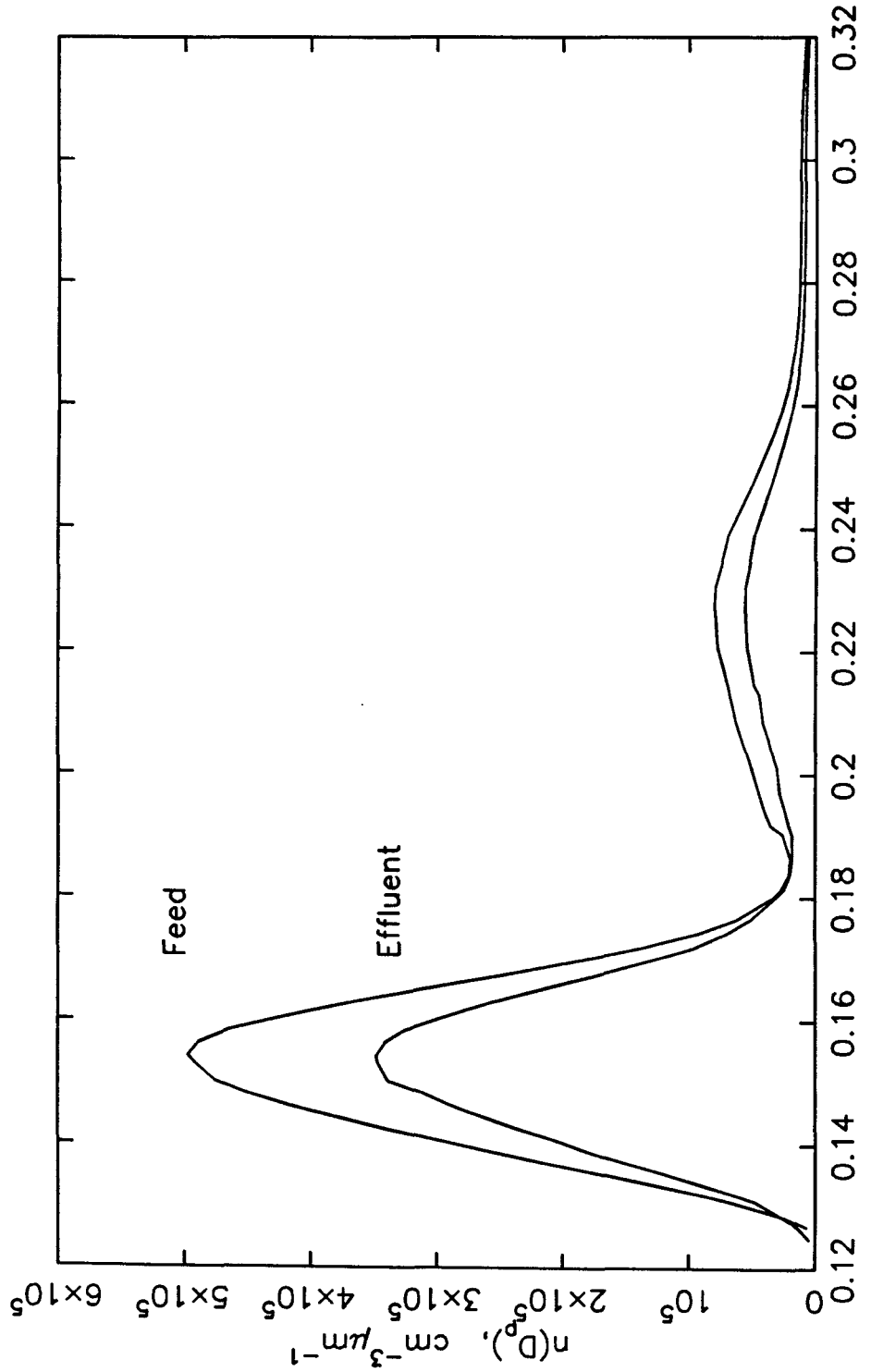

Figure 5.11 Experiment 2: Na_2SO_4 aerosol blank run (no $MnSO_4$) at 14.3 ppm SO_2, 23.49°C, 89.10% humidity.

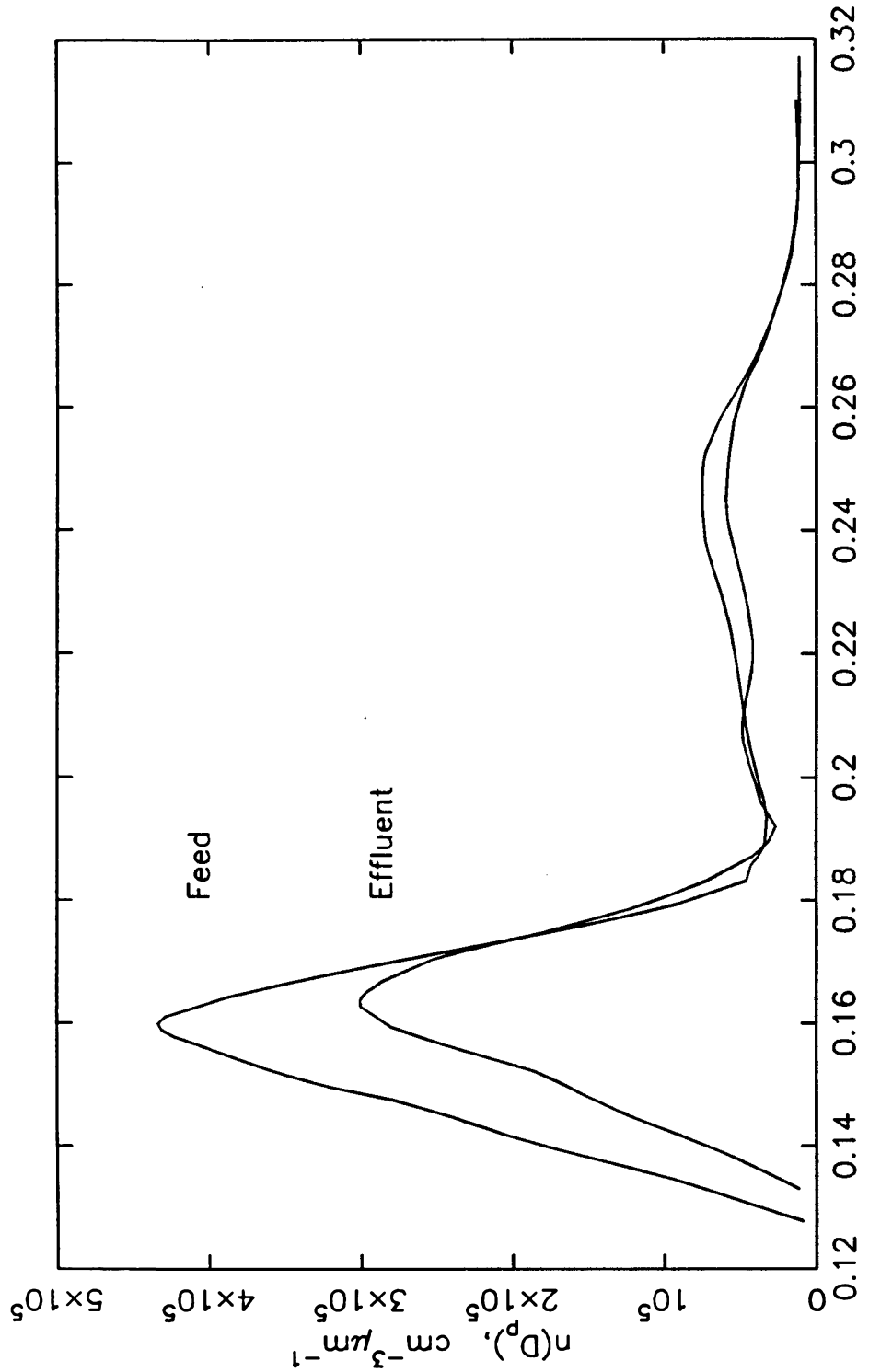

Figure 5.12 Experiment 3: $MnSO_4$ aerosol at 52.0 ppm SO_2, 23.54°C, 87.08% humidity.

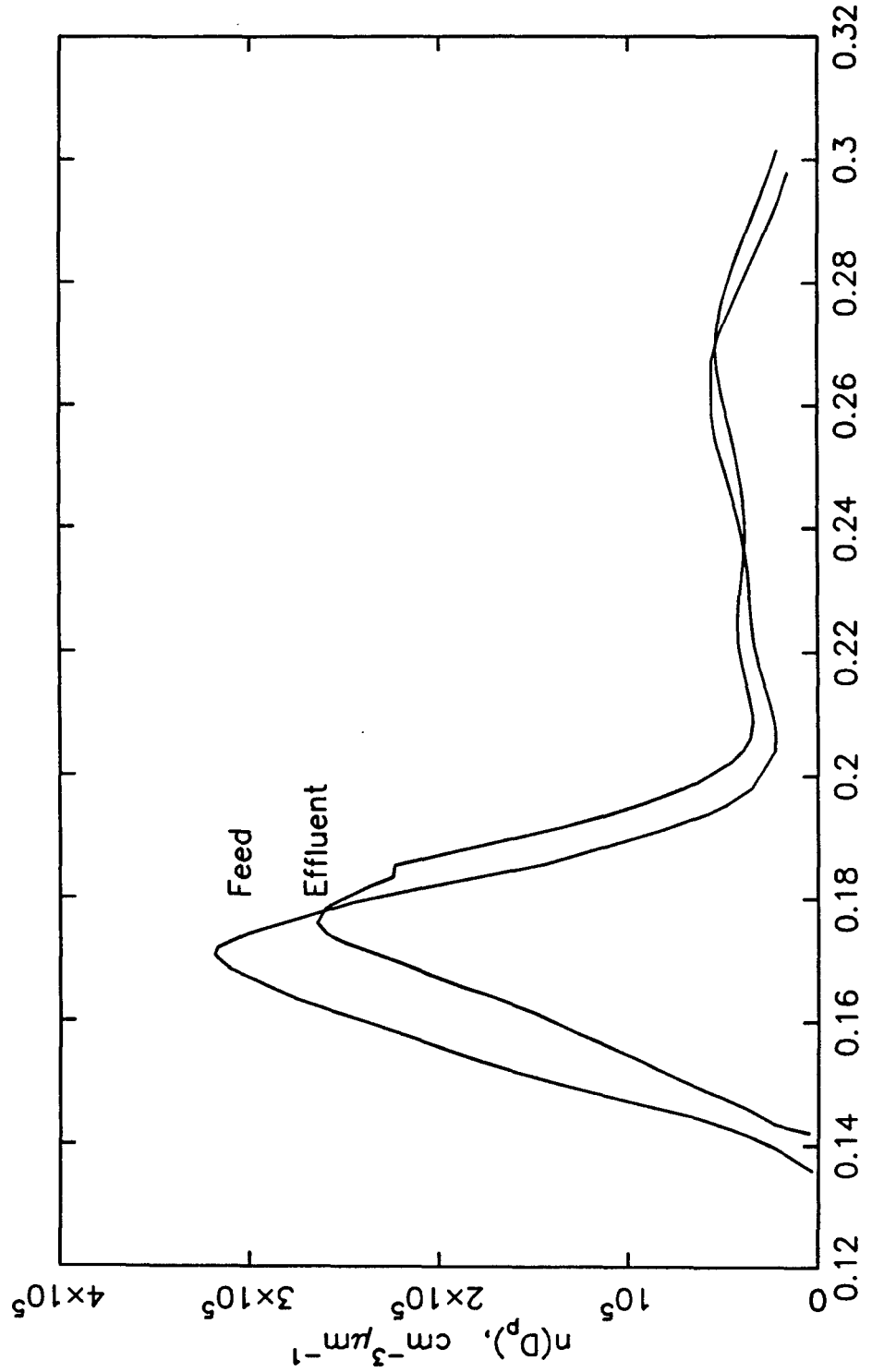

Figure 5.13 Experiment 4: $MnSO_4$ aerosol at 49.9 ppm SO_2, 23.18°C, 91.64% humidity.

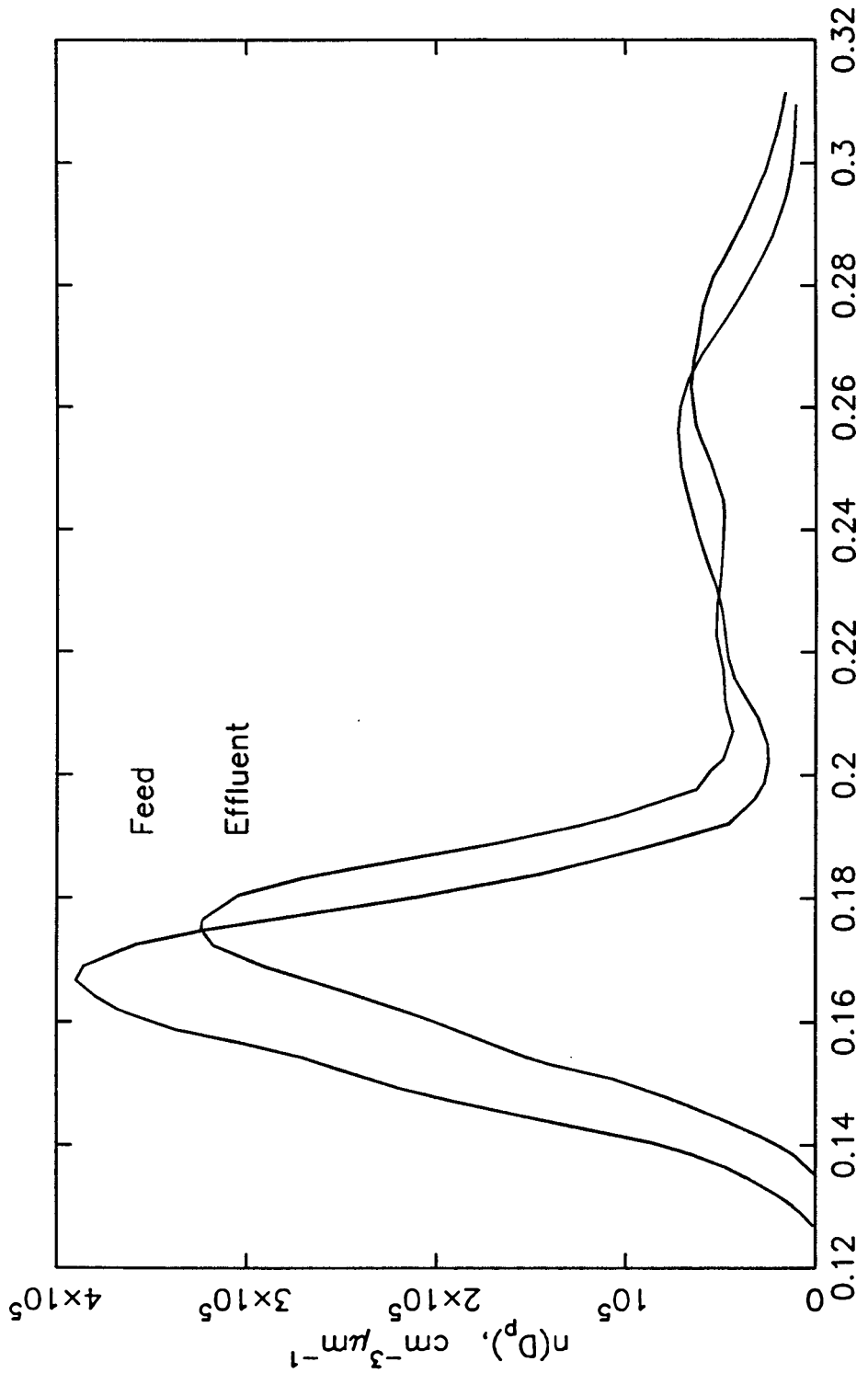

Figure 5.14 Experiment 5: $MnSO_4$ aerosol at 50.2 ppm SO_2, 23.34°C, 92.38% humidity.

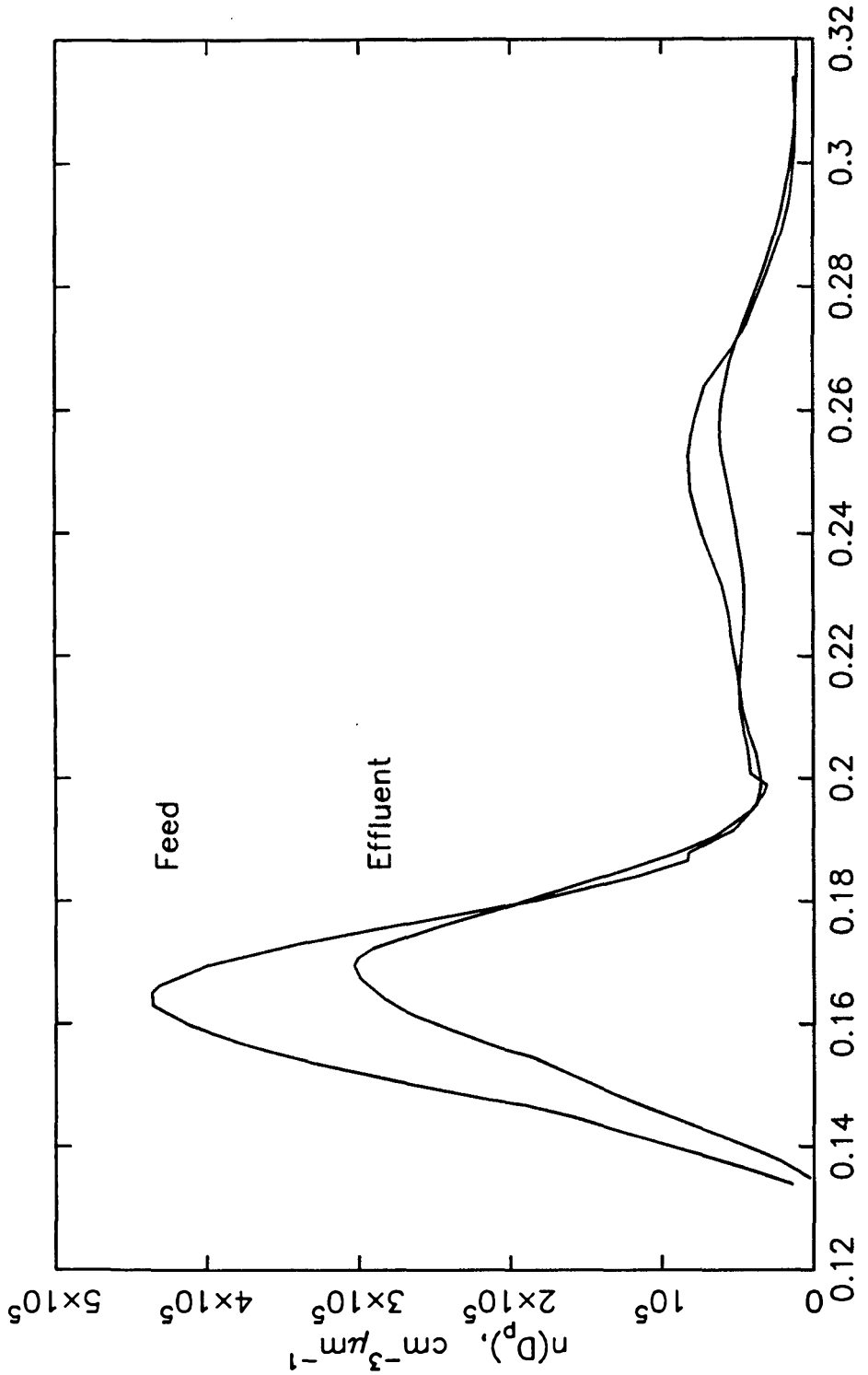

Figure 5.15 Experiment 6: $MnSO_4$ aerosol at 13.2 ppm SO_2, 24.04°C, 88.74% humidity.

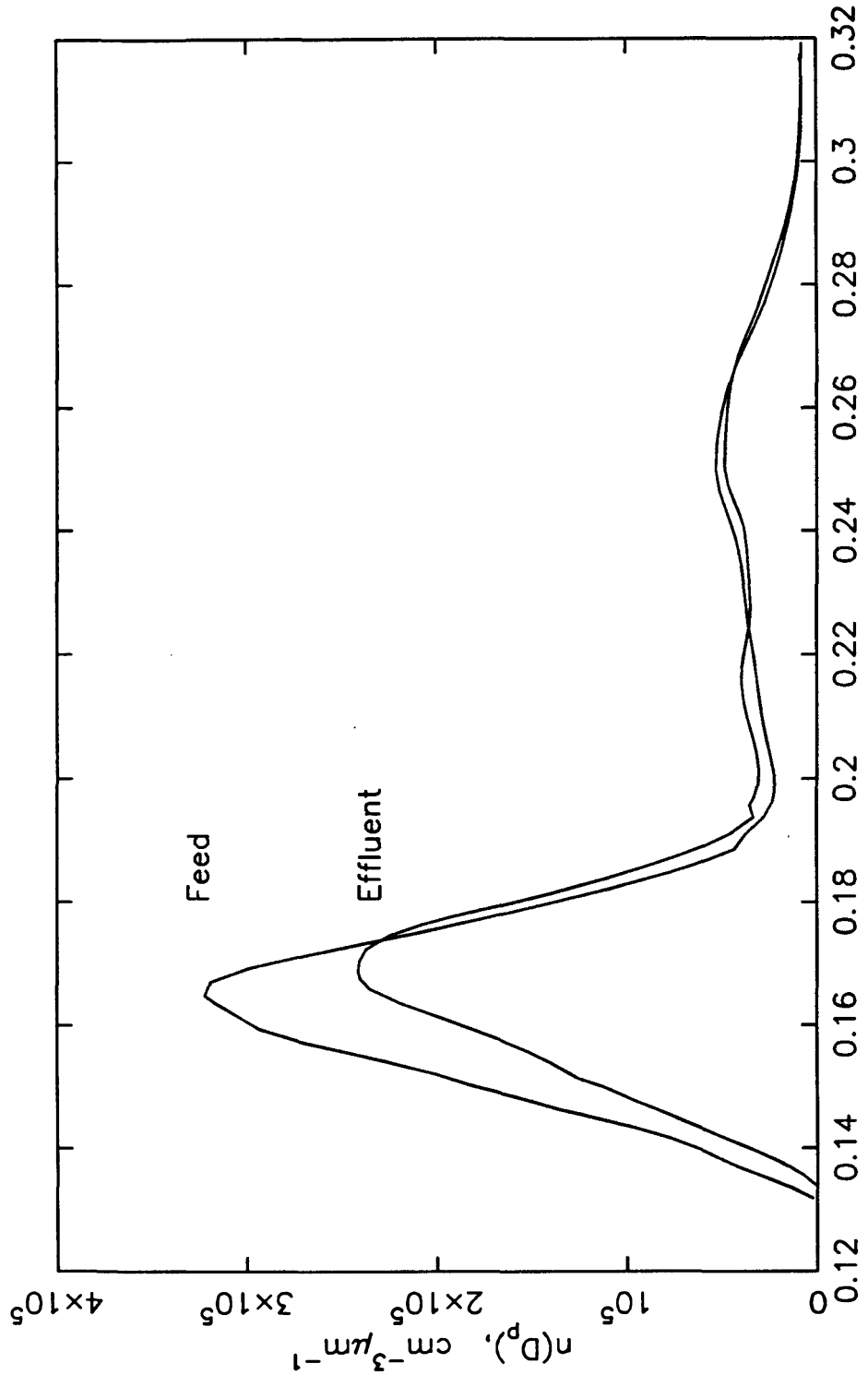

Figure 5.16 Experiment 7: $MnSO_4$ aerosol at 12.9 ppm SO_2, 24.08°C, 91.51% humidity.

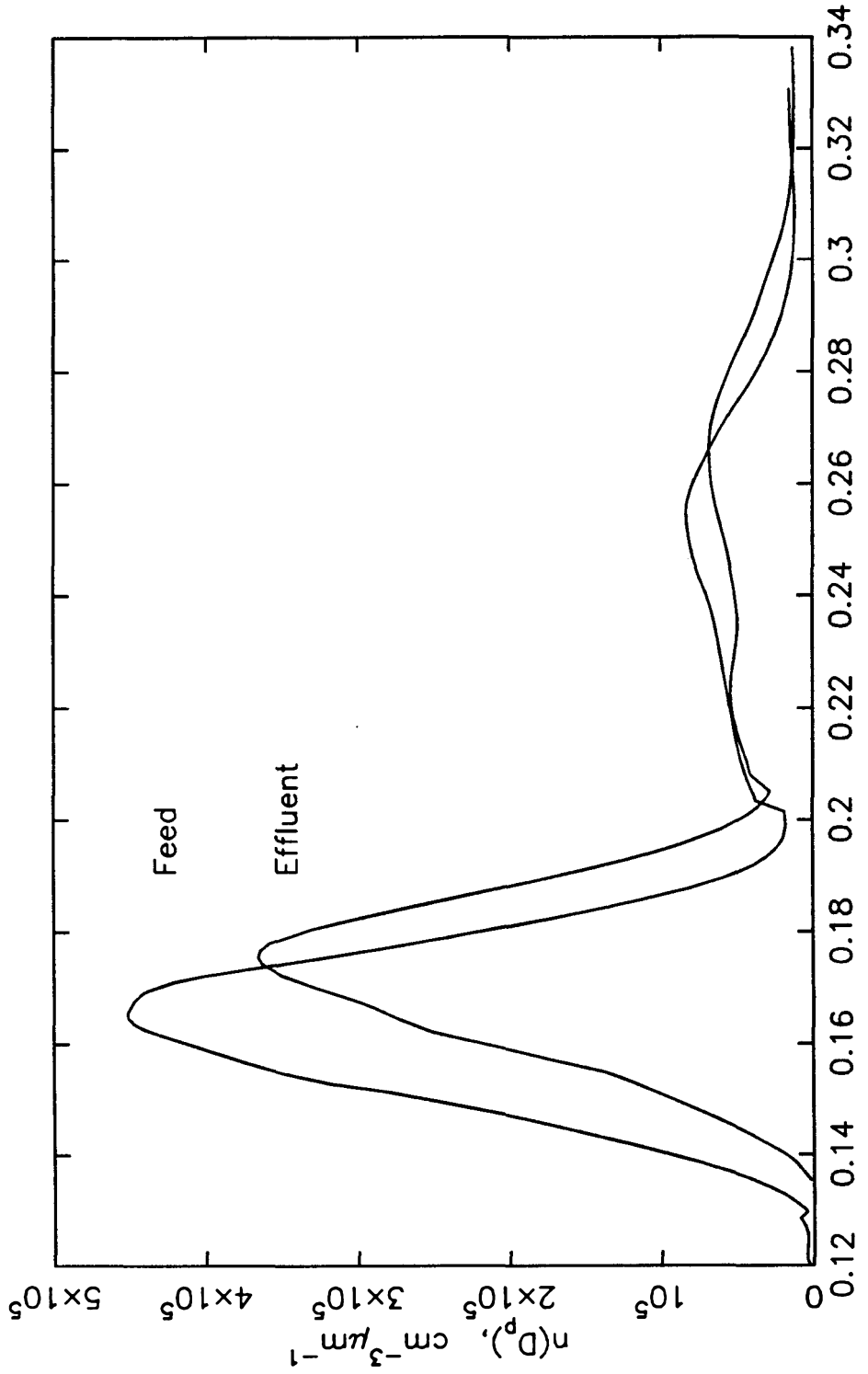

Figure 5.17 Experiment 8: $MnSO_4$ aerosol at 13.5 ppm SO_2, 23.20°C, 93.18% humidity.

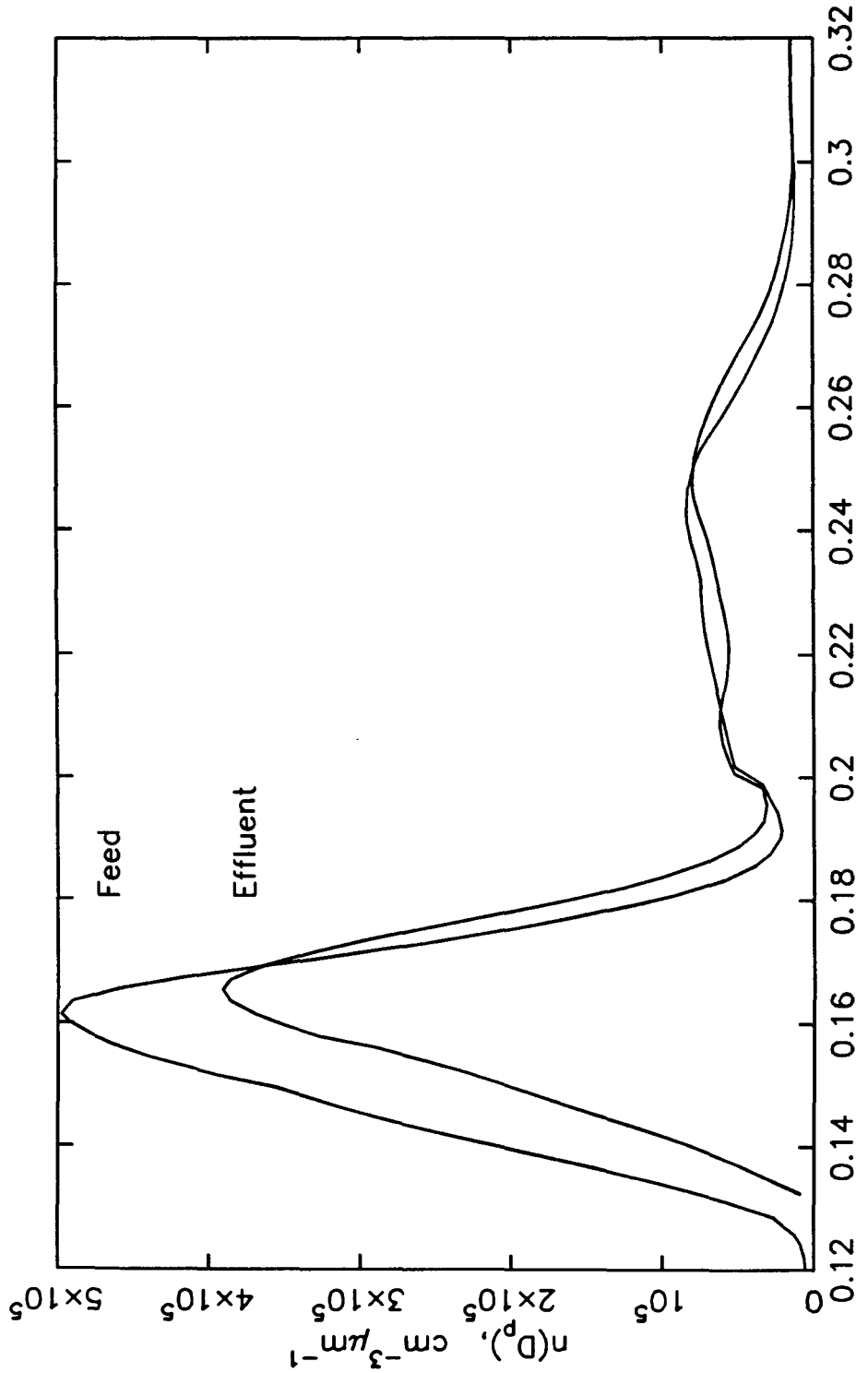

Figure 5.18 Experiment 9: $MnSO_4$ aerosol at 1.74 ppm SO_2, 22.91°C, 87.49% humidity.

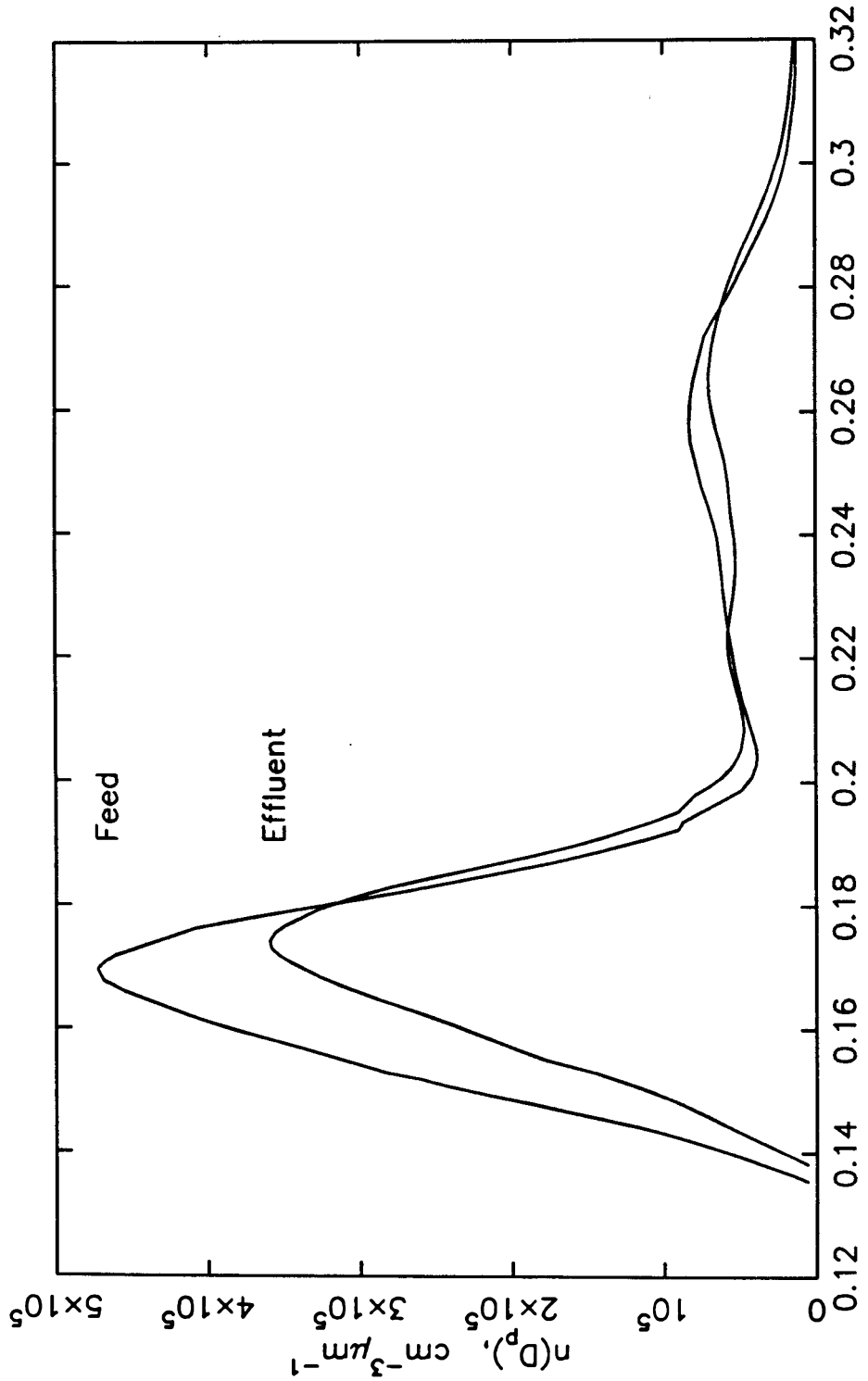

Figure 5.19 Experiment 10: $MnSO_4$ aerosol at 1.72 ppm SO_2, 24.01°C, 92.23% humidity.

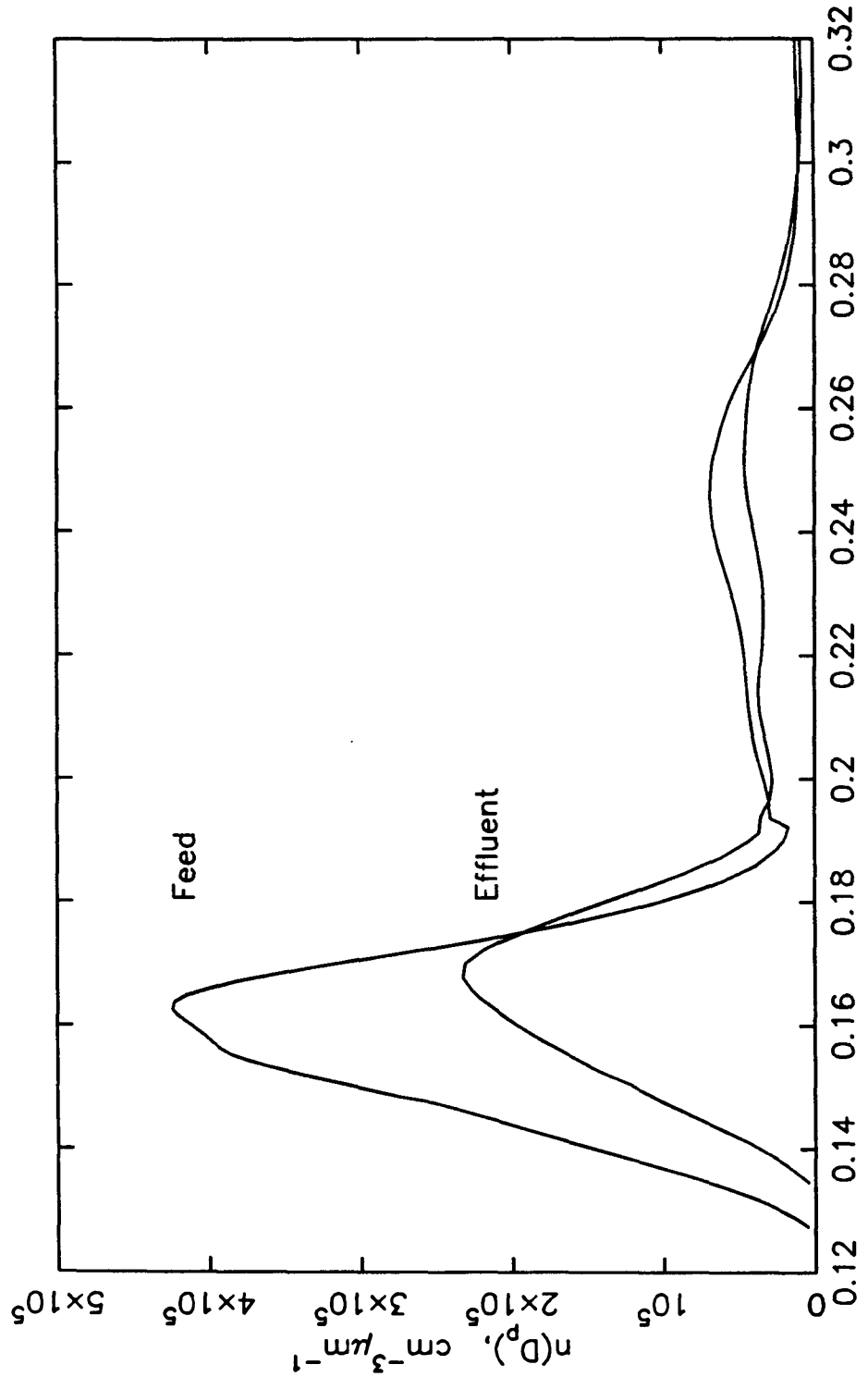

Figure 5.20 Experiment 11: $MnSO_4$ aerosol at 0.107 ppm SO_2, 23.38°C, 88.39% humidity.

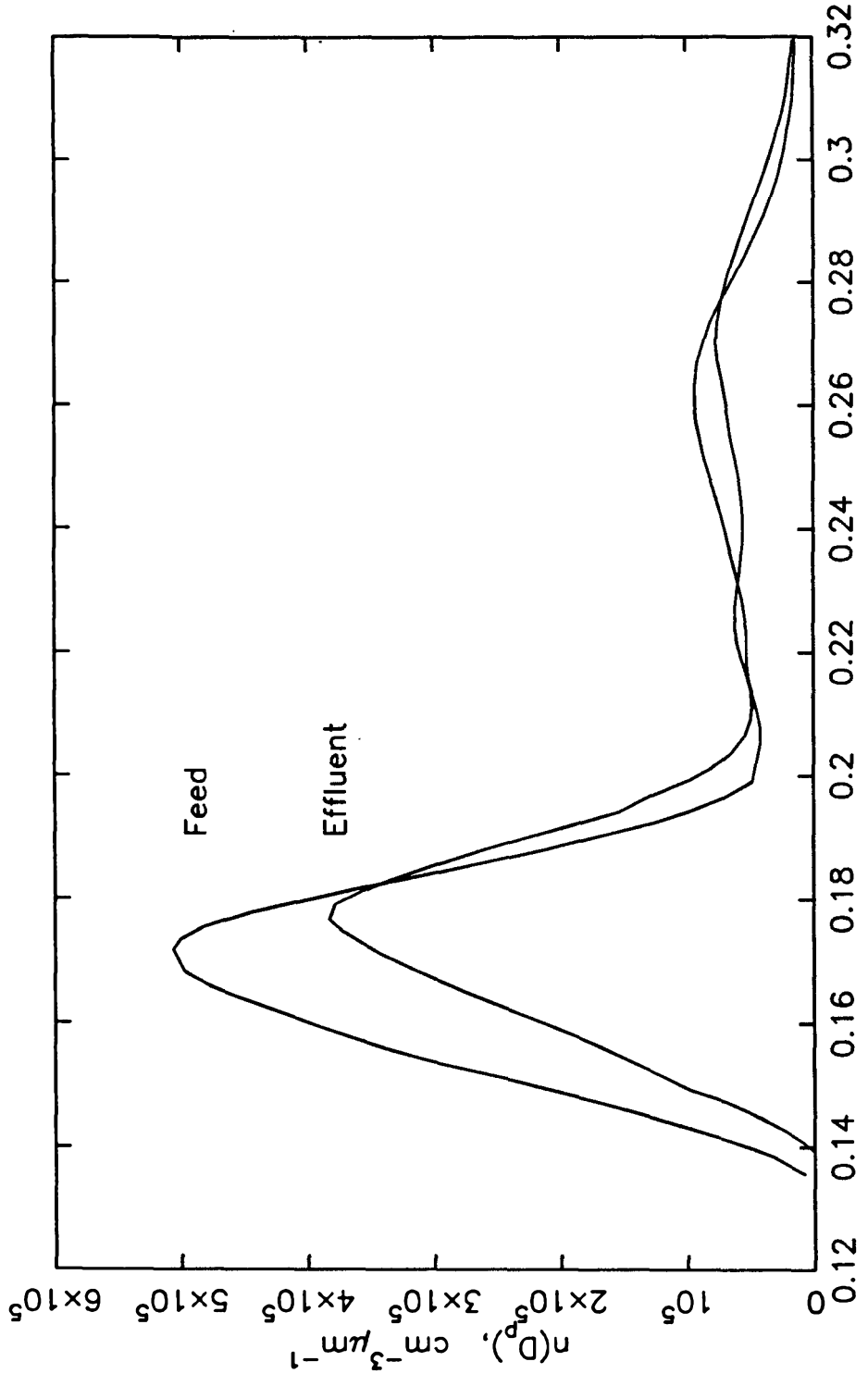

Figure 5.21 Experiment 12: $MnSO_4$ aerosol at 0.122 ppm SO_2, 23.89°C, 92.39% humidity.

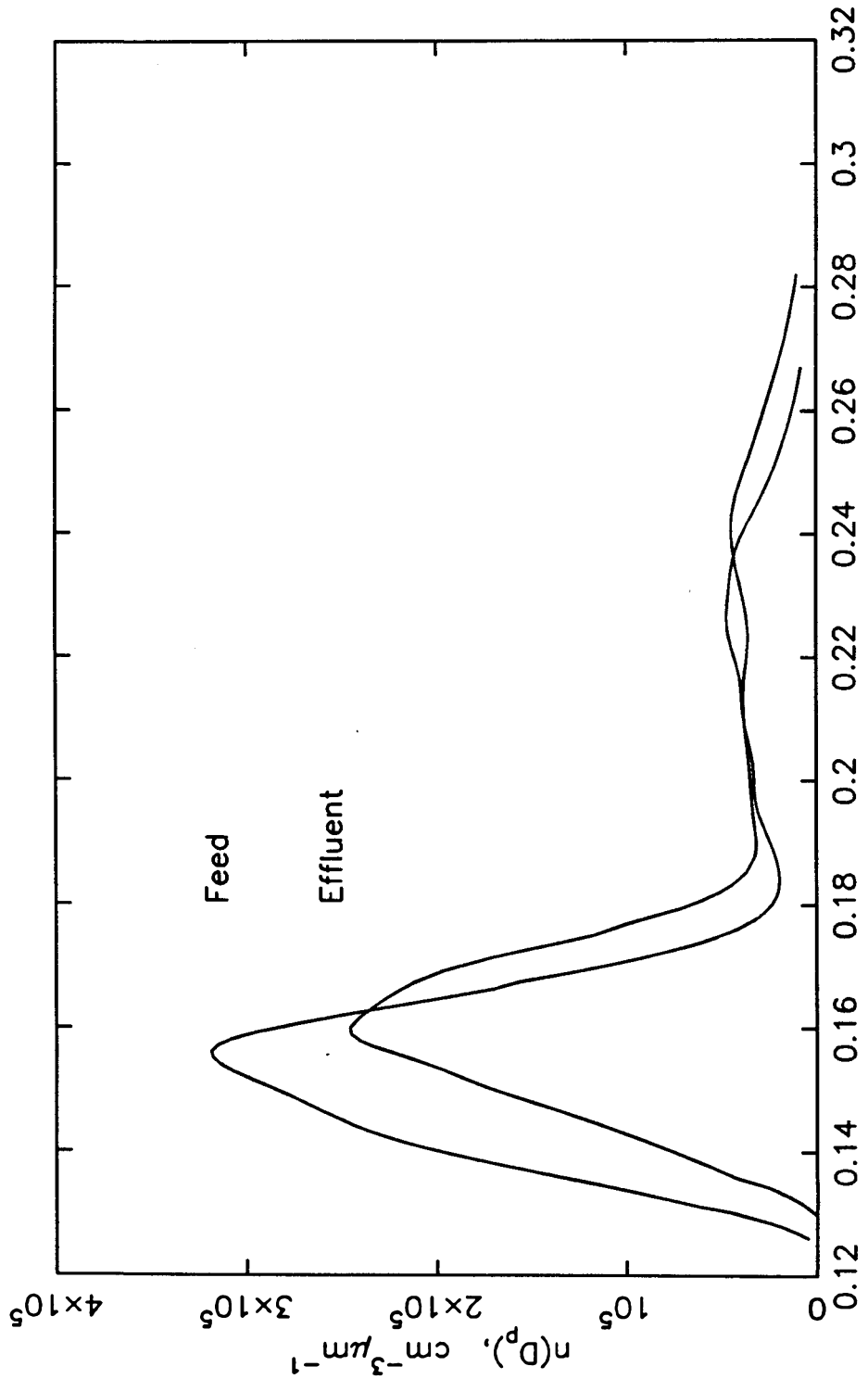

Figure 5.22 Experiment 13: 9.96 moles Na_2SO_4/mole $MnSO_4$ aerosol at 13.4 ppm SO_2, 23.60°C, 91.28% humidity.

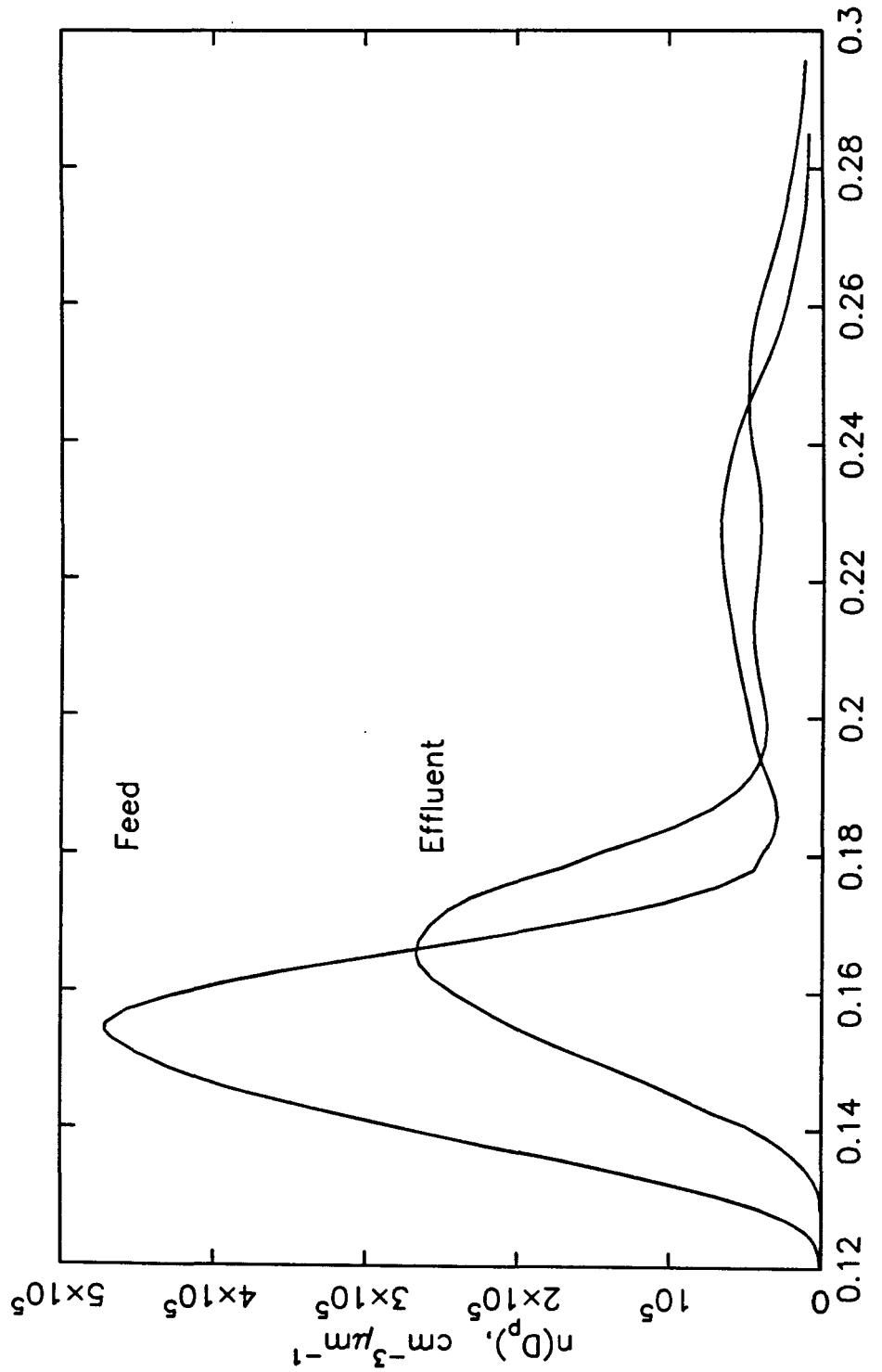

Figure 5.23 Experiment 14: 9.96 moles Na_2SO_4/mole $MnSO_4$ aerosol at 14.4 ppm SO_2, 23.33°C, 92.68% humidity.

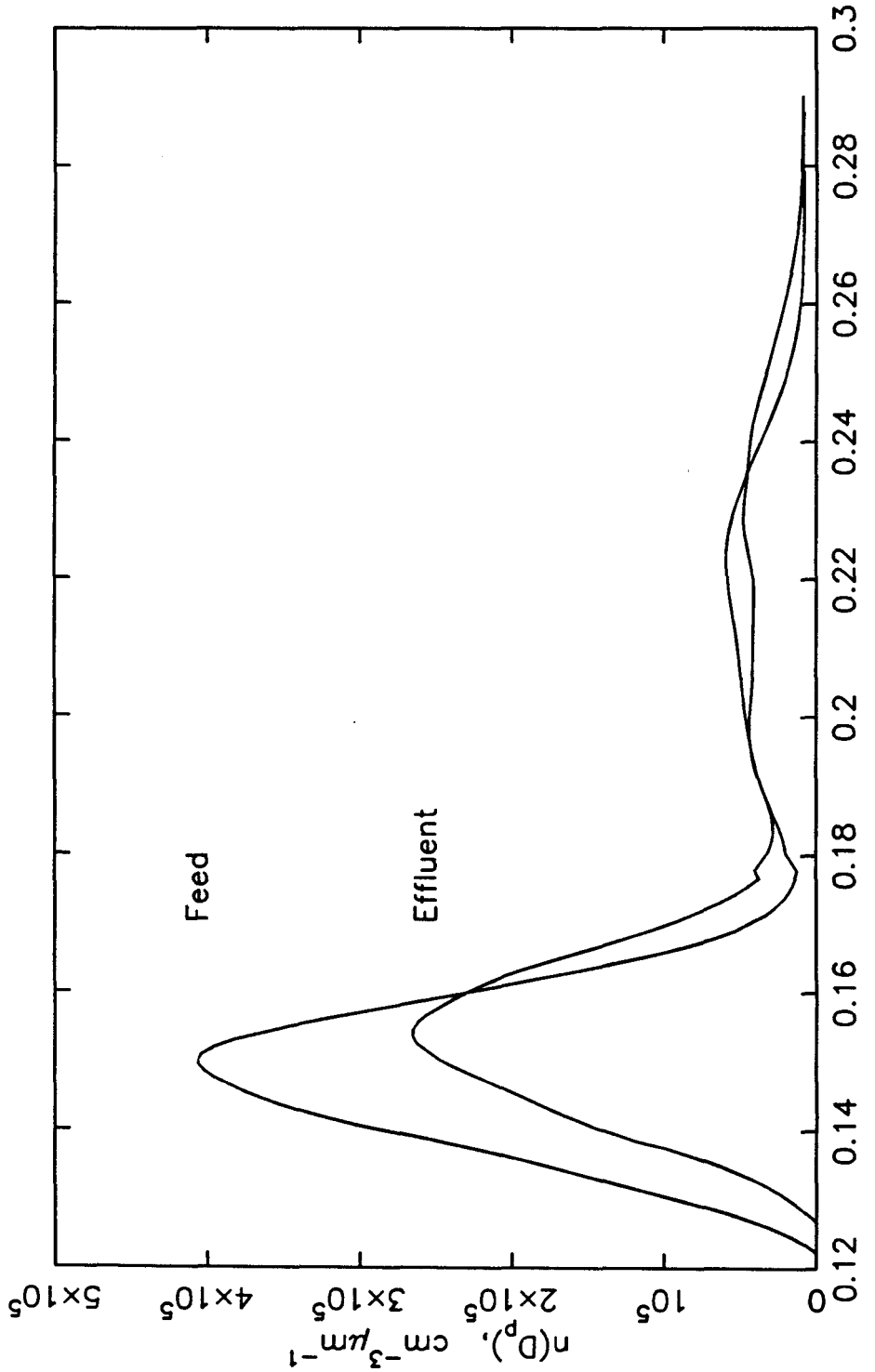

Figure 5.24 Experiment 15: 8.84 moles Na_2SO_4/mole $MnSO_4$ aerosol at 14.3 ppm SO_2, 23.23°C, 90.08% humidity.

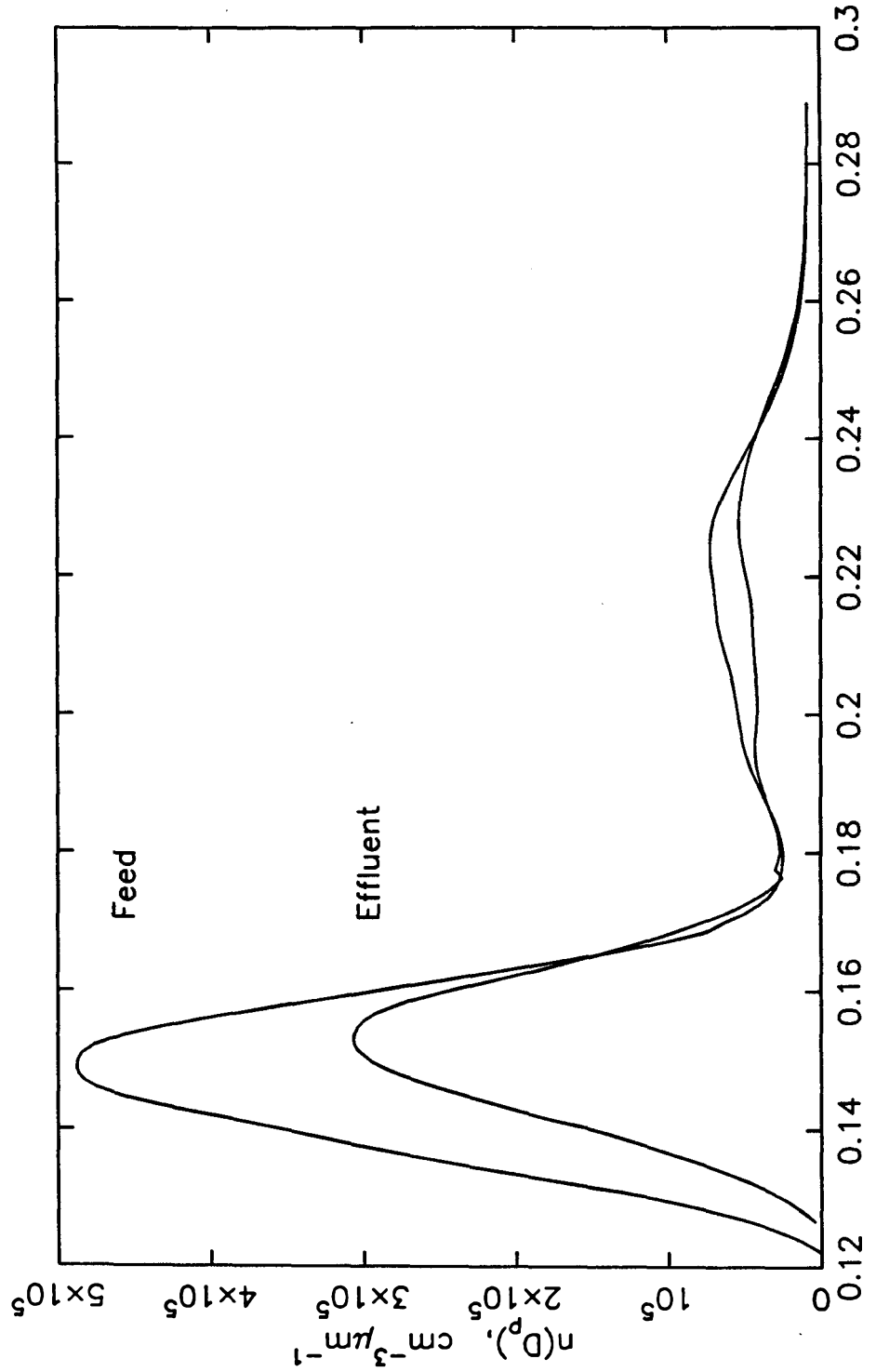

Figure 5.25 Experiment 16: 8.84 moles Na_2SO_4/mole $MnSO_4$ aerosol at 1.87 ppm SO_2, 23.16°C, 86.94% humidity.

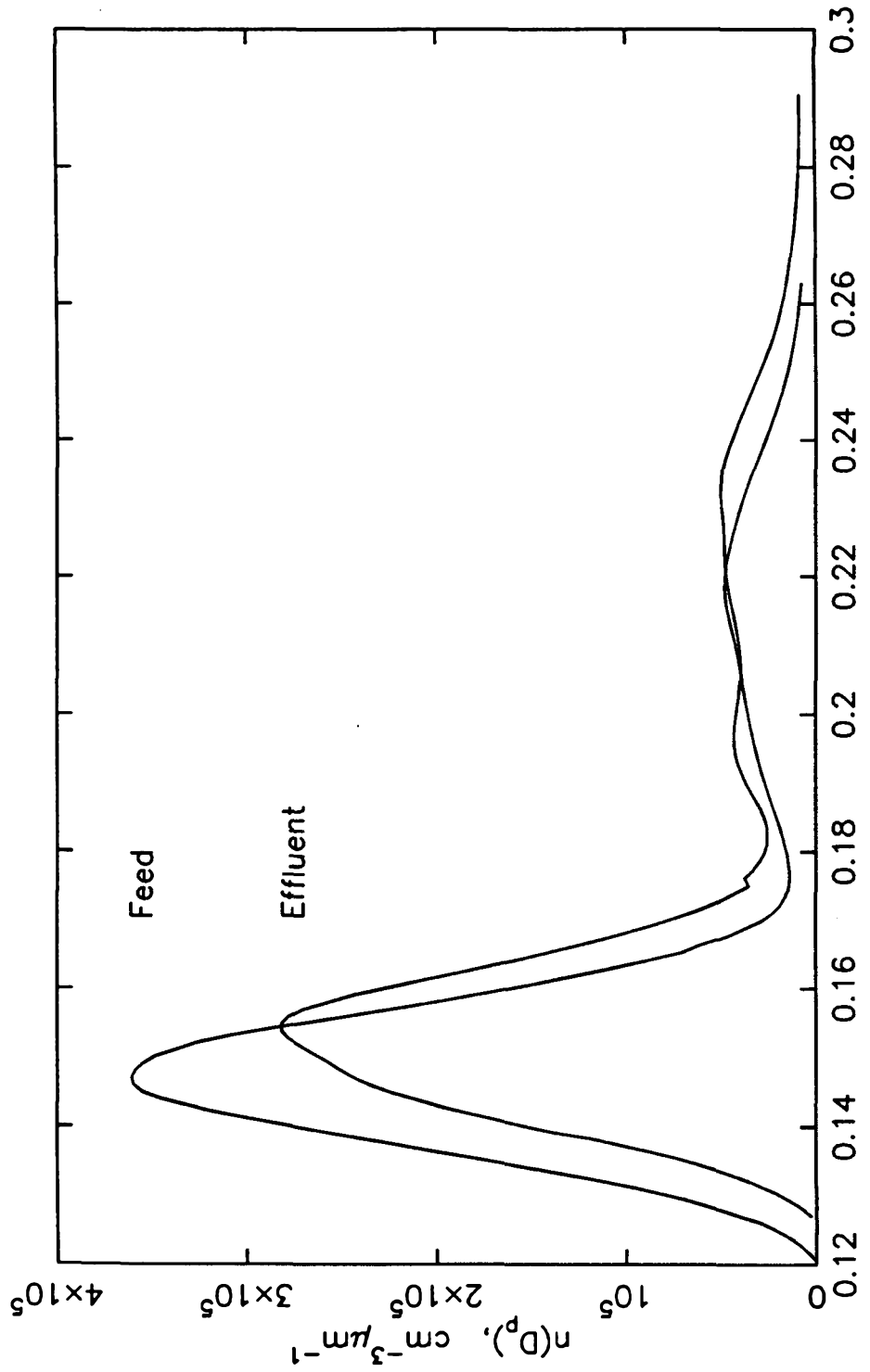

Figure 5.26 Experiment 17: 8.84 moles Na_2SO_4/mole $MnSO_4$ aerosol at 1.85 ppm SO_2, 23.19°C, 89.69% humidity.

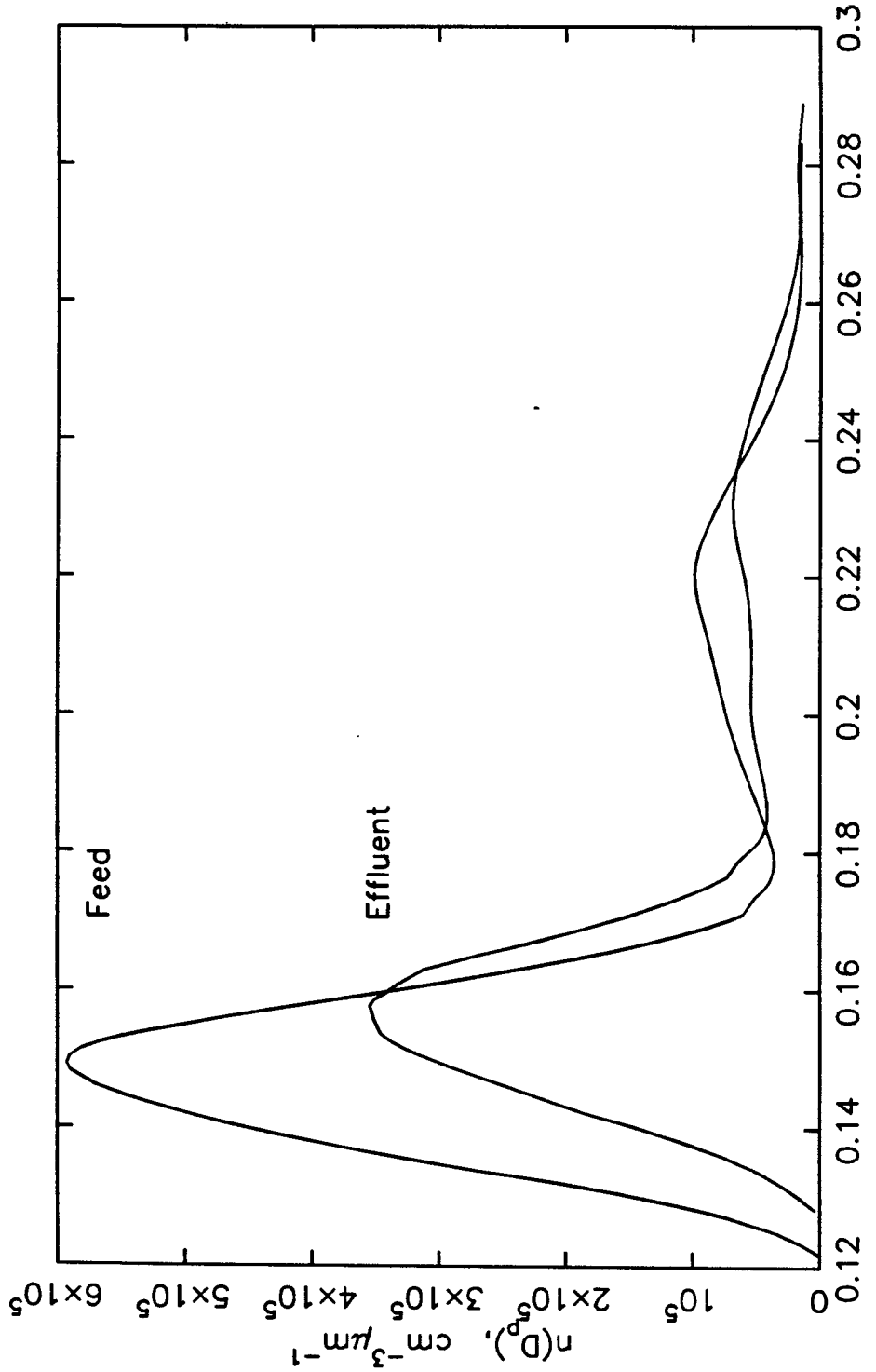

Figure 5.27 Experiment 18: 100. moles Na_2SO_4/mole $MnSO_4$ aerosol at 13.6 ppm SO_2, 23.16°C, 89.53% humidity.

CHAPTER 6
REACTOR SYSTEM MODEL

It is necessary to develop a model to predict the effluent aerosol distribution given the feed distribution and the conditions in the reactor. The predicted effluent distributions corresponding to the various proposed rate expressions discussed in Chapter 4 can then be compared to the actual measured distributions presented in Chapter 5.

§6.1 Description of the CSTR Model

The particle concentration in a given size range can be altered by the processes of condensational growth, deposition, coagulation, and nucleation. In the reactor system used in these studies, only growth and deposition need be considered. As was mentioned in Chapter 5, the particle concentration is too low for coagulation to be a significant mechanism and at relative humidities less than 100% homogeneous nucleation of the water vapor will not occur. The CSTR was shown to be ideally mixed and was operated at steady-state conditions. Therefore, a population balance on particles having size D_p flowing through a CSTR gives

$$\left[\frac{\partial n(D_p)}{\partial t}\right]_{total} = \left[\frac{\partial n(D_p)}{\partial t}\right]_{growth} + \left[\frac{\partial n(D_p)}{\partial t}\right]_{deposition} + \left[\frac{\partial n(D_p)}{\partial t}\right]_{flow} = 0, \quad (1)$$

where $[\partial n(D_p)/\partial t]_{flow}$ represents the net rate at which particles are introduced into the reactor as a result of the feed and effluent flows, and $n(D_p)$ is the size distribution of the reactor aerosol. It is convenient to use the dimensionless size x instead of diameter in defining the various terms in Equation (1), where

$$x = \frac{\ln(D_p/D_{p,min})}{\ln(D_{p,max}/D_{p,min})}. \tag{2}$$

$D_{p,min}$ and $D_{p,max}$ are selected minimum and maximum diameters, respectively. Equation (1) can be rewritten in terms of the dimensionless size merely by replacing D_p with x. In the CSTR model the advantages of using a logarithmically scaled diameter are due less to reducing the range of expected diameters than in simplifying the equations that follow.

The time rate of change of the size distribution that is due to condensational growth can be written,

$$\left[\frac{\partial n(x)}{\partial t}\right]_{growth} = -\frac{\partial(n(x)I(x))}{\partial x}, \tag{3}$$

where $I(x)$ is the particle growth rate dx/dt. $I(x)$ is often referred to as a "growth law," and depends on the physical process that controls the gas-to-particle conversion. This controlling process can be either the diffusion of the vapor to the particle, the surface reaction of an adsorbed molecule on the particle, or the reaction of a dissolved species in the particle volume. Since the aerosol particles studied here were liquid, the possibility of significant surface reaction was ignored. In Chapter 5 it was noted that if mass transfer limitations are absent, then the volume reaction is rate-controlling and particle growth is a measure of the extent of reaction. It was also shown that the probability that reaction rate is indeed controlling is high — the effective reaction rate would have to be unrealistically large for diffusion to become the limiting step.

The particles in the CSTR can be viewed as an aqueous solution consisting of the feed manganese sulfate and the sulfuric acid, or S(VI), generated by reaction. For those experiments run using a Na_2SO_4-$MnSO_4$ feed aerosol, the reactor particles will also include sodium sulfate. Since a pure manganese sulfate feed is just a simple case of the more complicated mixed feed case, all discussion will assume that

a Na_2SO_4-$MnSO_4$ feed aerosol was used. The S(IV) species in equilibrium with the gas-phase SO_2 are present in the particle at concentrations orders of magnitude less than those of the salts and acid. It can be shown that equilibration with SO_2 does not significantly affect the particle size, or in other words, the water activity. Therefore, the S(IV) species will not be considered in the particle water activity calculations and the following relationship can be written:

$$\mathrm{RH} = a_w(C_M, C_N, C_A), \tag{4}$$

where C_M is the concentration of manganese sulfate, C_N is the concentration of sodium sulfate, and C_A is the concentration of sulfuric acid in the particle. The Kelvin effect has been neglected in the CSTR model and the influence of this assumption on the predicted effluent distribution will be discussed later.

Since $I(x)$ is a function of the chemical reaction in the particle volume, it is a function of those factors that determine the reaction rate in the aerosol particle, e.g., temperature, relative humidity, SO_2 concentration, and solution thermodynamics and chemistry. Therefore, the reaction rate is a logical place to start developing an expression for $I(x)$. The exact form of the kinetic expression for the rate of acid formation differs among the various researchers (see Table 4.1), but all satisfy the following relation:

$$R(C_A, C_M) = \frac{1}{v_p}\frac{dN_A}{dt} = \frac{1}{v_p}\frac{d}{dt}(v_p C_A) = \frac{C_A}{v_p}\frac{dv_p}{dt} + \frac{dC_A}{dt}, \tag{5}$$

where N_A is the number of moles of acid produced and v_p is the particle, or reaction, volume. An expression for the time rate-of-change of the acid concentration can be obtained from that for thermodynamic equilibrium. Differentiation of Equation (4) with respect to time gives

$$\frac{\partial a_w}{\partial C_A}\frac{dC_A}{dt} + \frac{\partial a_w}{\partial C_M}\frac{dC_M}{dt} + \frac{\partial a_w}{\partial C_N}\frac{dC_N}{dt} = 0. \tag{6}$$

Since reaction/condensation is the only mechanism by which particle volume changes, the moles of metal are conserved as the particle increases in size. Thus,

$$C_M\, v_p = C_{M,0}\, v_{p,0}, \tag{7}$$

where $C_{M,0}$ and $v_{,0}p$ are the manganese concentration and particle volume of the feed aerosol. Differentiating Equation (7) with respect to time gives

$$\frac{dC_M}{dt} = -\frac{C_{M,0}\, v_{p,0}}{v_p^2}\frac{dv_p}{dt} = -\frac{C_M}{v_p}\frac{dv_p}{dt}. \tag{8}$$

The molar ratio of sodium sulfate to manganese sulfate is fixed by the feed solution composition. Therefore, if $C_N = \delta\, C_M$, then Equation (7) can be written for sodium since it must also be conserved, and the derivative of C_N with respect to time is given by

$$\frac{dC_N}{dt} = \delta\,\frac{dC_M}{dt} = -\delta\,\frac{C_M}{v_p}\frac{dv_p}{dt}. \tag{9}$$

Substituting Equations (8) and (9) into Equation (6) and solving for dC_A/dt gives the expression,

$$\frac{dC_A}{dt} = \left\{ \frac{\dfrac{\partial a_w}{\partial C_M} + \delta\,\dfrac{\partial a_w}{\partial C_N}}{\partial a_w/\partial C_A} \right\} \frac{C_M}{v_p}\frac{dv_p}{dt}. \tag{10}$$

Equation (10) is substituted in Equation (5), which is then rearranged to give the particle volume growth rate in terms of the reaction rate and the solution thermodynamics,

$$\frac{1}{v_p}\frac{dv_p}{dt} = \frac{R(C_A, C_M)}{C_A + C_M \left\{ \dfrac{\dfrac{\partial a_w}{\partial C_M} + \delta\,\dfrac{\partial a_w}{\partial C_N}}{\partial a_w/\partial C_A} \right\}}. \tag{11}$$

The growth rate $I(x) = dx/dt$ can be directly related to Equation (11) using the definition of the dimensionless size and it is now that the advantage of using a logarithmic nondimensionalization becomes apparent:

$$I(x) = \frac{dx}{dt} = \frac{1}{3\ln(D_{p,max}/D_{p,min})} \frac{1}{v_p} \frac{dv_p}{dt}. \tag{12}$$

Equations (11) and (12) can be used to determine the particle growth rate for any reacting aerosol in a humid atmosphere. The growth rate is determined by the reaction kinetics occurring in the particles and the associated thermodynamic equilibrium. Note that expressions for the reaction rate and the particle water activity as a function of composition must be provided.

The second term in Equation (1) accounts for the change in the size distribution resulting from particle deposition. Wall loss in the CSTR depends on the physical properties of the aerosol, the size and shape of the vessel, and the mixing characteristics in the vessel. This functionality is typically expressed in terms of a deposition coefficient β, where

$$\left[\frac{\partial n(x)}{\partial t}\right]_{deposition} = -\beta\, n(x). \tag{13}$$

Crump and Seinfeld (1981) have derived an expression for the deposition coefficient in a turbulently mixed spherical vessel such as the CSTR. Particle deposition was assumed to occur as a result of turbulent diffusion, Brownian diffusion, and gravitational settling in the turbulent boundary layer. The deposition coefficient is given by

$$\beta = \frac{6\sqrt{k_e D}}{\pi R} D_1\left(\frac{\pi v_t}{2\sqrt{k_e D}}\right) + \frac{3v_t}{4R}, \tag{14}$$

where v_t is the particle terminal settling velocity, R is the radius of the vessel, D is the particle diffusivity, k_e is the coefficient of the turbulent eddy diffusivity in the boundary layer ($D_e = k_e y^2$) and D_1 is the Debye function as defined by

$$D_1(x) = \frac{1}{x}\int_0^x \frac{t}{e^t - 1}\, dt. \tag{15}$$

While diameter (D_p) does not appear explicitly in Equation (14), both the particle settling velocity and diffusivity are functions of diameter, resulting in a complicated

dependence of β on D_p. The curve β versus D_p exhibits the "window," or minimum in the size range 0.1 to 1.0 μm, that is also observed in filter efficiency curves. Diffusion has a strong effect on removal of the small particles, while gravitational sedimentation is the controlling mechanism for the larger particles. Between 0.1 and 1.0 μm, neither of these effects has a strong influence on particle behavior and wall loss is at a minimum. Wall loss studies were performed by Crump et al. (1983b) on the present CSTR and the value of k_e was experimentally determined to be $0.00918\,Q^{1.5}$, where Q was expressed in units of liters per minute. The CSTR experiments in the current study were performed at 2 ℓpm. At this flowrate, and using the value of k_e determined by Crump et al. (1983b), the minimum value of β falls at 0.27 μm for particles of density 1 g/cm^3. Particle diameters typical of the aerosol distributions measured in the experiments, 0.1 to 0.3 μm, correspond to β ranging from 1.3×10^{-5} to 2.5×10^{-5} sec^{-1}. Under these conditions the wall loss rate is relatively size independent and one would not expect shifting of the distribution along the diameter range as a result of deposition.

The third and final term in Equation (1) represents the rate at which the size distribution changes with time as a result of flow in and out of the CSTR. This term is given by

$$\left[\frac{\partial n(x)}{\partial t}\right]_{flow} = \frac{n_0(x) - n(x)}{\tau}, \tag{16}$$

where τ is the average reactor residence time and $n_0(x)$ is the value of the feed distribution for particles of dimensionless size x. Equations (3), (13), and (16) are now substituted into Equation (1), to give the full equation describing aerosol behavior in the CSTR at steady state,

$$0 = n_0(x) - n(x) - \tau\,\frac{\partial(n(x)I(x))}{\partial x} - \tau\,\beta(x)\,n(x). \tag{17}$$

An analytical solution of Equation (17) is possible if the feed distribution $n_0(x)$ is monodisperse. In other words,

$$n_0(x) = N_0\,\delta(x - x_0), \tag{18}$$

where N_0 is the number of particles, all of which have diameter x_0. If the feed is monodisperse, all the particles have the same initial concentration (neglecting the Kelvin effect) and as they grow, all particles of size x have the same species concentrations. Consequently, the growth rate $I(x)$ is a unique function of size. For a monodisperse feed aerosol of size x_0, the solution of Equation (17) is then:

$$n(x_0, x) = \frac{N_0}{\tau I(x_0, x)} \exp\left[-\int_{x_0}^{x} \frac{\tau^{-1} + \beta(z)}{I(x_0, z)}\, dz\right] \qquad x \geq x_0. \tag{19}$$

The term $I(x, x_0)$ indicates that the growth rate is for an aerosol particle of size x resulting from a monodisperse feed of size x_0. Because of the distribution of residence times characteristic of a continuous stirred tank reactor, the situation given a polydisperse feed is more complex. Two feed particles of size $x_{0,1}$ and $x_{0,2}$ ($x_{0,1} \neq x_{0,2}$) could spend times t_1 and t_2 ($t_1 \neq t_2$), respectively, in the CSTR and both grow to an effluent size of x. These two particles would, however, have different compositions and therefore, different growth rates. $I(x)$ is no longer a unique function of size if the feed is polydisperse.

Most experimentally generated "monodisperse" aerosols are actually very narrow polydisperse distributions. A perfectly monodisperse CSTR feed aerosol would be extremely difficult to achieve in the laboratory. However, a polydisperse feed aerosol can be considered a linear combination of exactly monodisperse feeds. The composition of the feed aerosol is known, whether or not the distribution is poly- or monodisperse, since it is determined by the relative humidity. Thus, Equation (19) can be solved for each monodisperse feed and the resulting distributions are then added to give the actual CSTR effluent distribution. Once these distributions have been combined, the composition of the effluent is no longer a function of size — each size having, instead, an "average" composition. The dimensionless size distribution can be converted into a dimensional distribution using one of the

following relations,

$$n(x) = \ln\left(\frac{D_{p,max}}{D_{p,min}}\right) n(\ln D_p) = D_p \ln\left(\frac{D_{p,max}}{D_{p,min}}\right) n(D_p). \qquad (20)$$

Therefore, the prediction of the CSTR effluent distribution for any feed aerosol reduces to calculating the particle growth rate. This will be discussed in further detail in the next section.

§6.2 Aerosol Solution Thermodynamics and Chemistry

Perhaps the single most important calculation in the aerosol growth model is the determination of the particle water activity. Particle growth is a result of the absorption of water as reaction products are formed such that the equilibrium relationship RH = a_w is maintained. Experimentally measured water activity data exist for only a few binary mixtures, rarely for a ternary mixture. Therefore, an empirical mixing rule must be used to obtain estimates of the mixture water activity data using the available data for the pure component systems.

The CSTR aerosol was assumed to be a mixture of three species — manganese sulfate, sodium sulfate, and sulfuric acid. As discussed earlier, S(IV) species are present only in trace amounts. As in the distribution shifting calculations discussed in Chapter 5, the Kusik and Meissner (1978) activity coefficient mixing rules were used. Only interactions between ions of opposite charge are considered, and the effect of neutral species is not accounted for by this method. The mixture water activity is derived using the Gibbs-Duhem relation. Pure component water activity data are required for every cation-anion pairing possible in the mixture.

In the CSTR calculations a particle size is selected. Then, knowing the system relative humidity and the feed particle size and composition, the metal concentration is determined by conservation of mass (Equation 7). The only unknown in the equilibrium relation of Equation 4 is the acid concentration and given an expression for the water activity as a function of composition, it can be solved for

iteratively. In order to use Kusik and Meissner's mixing rules the ions in solution must be specified. Five ionic species were considered — 1: H^+, 3: Na^+, 5: Mn^{2+}, 2: SO_4^{2-}, and 4: HSO_4^- — resulting in the following mixing rule for the aerosol water activity:

$$\begin{aligned}
\ln a_w^{mix} = & \frac{(m_{12}+m_{32}+m_{52})}{I^2}\left\{\frac{9}{2}(m_{14}+2m_{12})\ln a^{\circ}_{w,12}(I)\right. \\
& \left.+\frac{9}{2}(m_{34}+2m_{32})\ln a^{\circ}_{w,32}(I)+16(m_{54}+m_{52})\ln a^{\circ}_{w,52}(I)\right\} \\
& +\frac{(m_{14}+m_{34}+2m_{54})}{I^2}\left\{(m_{14}+2m_{12})\ln a^{\circ}_{w,14}(I)\right. \\
& \left.+(m_{34}+2m_{32})\ln a^{\circ}_{w,34}(I)+\frac{9}{2}(m_{54}+m_{52})\ln a^{\circ}_{w,54}(I)\right\} \\
& -\frac{MW_{H_2O}}{1000\,I}\left\{\frac{1}{2}(m_{14}+m_{34})(m_{12}+m_{32}+m_{54})\right. \\
& \left.+(m_{12}+m_{32})(m_{52}+2m_{54})+m_{52}(m_{14}+m_{34}+m_{54})\right\},
\end{aligned} \tag{21}$$

where m_{ij} is the molality of the species formed by ions i and j, $a^{\circ}_{w,ij}$ is the water activity of a binary solution of species ij, and the total ionic strength of the mixture is given by $I = 3(m_{12}+m_{32}+m_{54})+m_{34}+m_{14}+4m_{52}$. The pure component water activity of $Mn(HSO_4)_2$ was approximated by that of $MnCl_2$. $NaHSO_4$ was assumed to have a water activity similar to that of NaCl. The pure component water activity data needed in Equation (21) and their references are given in Table C.1 of Appendix C.

Finally, the concentrations m_M (C_M) and m_N (C_N) determined from the metal mass balance for a given particle size were set equal to m_{52} and m_{12}, respectively. This has several consequences. First, since all the Mn^{2+} and Na^+ were paired with SO_4^{2-}, the concentrations of $Mn(HSO_4)_2$ and $NaHSO_4$ are by necessity equal to zero. And second, while the S(VI) generated by reaction ($m_A = m_{32}+m_{34}$) was allowed to equilibrate between the ions HSO_4^- and SO_4^{2-}, the SO_4^{2-} introduced with the salt was not. Equilibrium calculations show that at low acid concentra-

tions ($m_A < 0.5$ m), the concentration of SO_4^{2-} ions is greater that of the HSO_4^- ions in typical aerosol solutions. As reaction continues and the solution becomes more acidic, the ratio of HSO_4^- ions to SO_4^{2-} ions eventually becomes greater than one. Therefore, the validity of this assumption becomes questionable as the reaction proceeds. However, ionic strength and the manganese and sodium concentrations also decrease as the reaction proceeds. With a lower solution metal concentration, the concentration of S(VI) "belonging" to the salt also decreases, and any error made in assuming $m_{S(VI)} \sim m_{SO_4^{2-}}$ will decrease similarly. Also, as ionic strength falls, the water activity of all species approaches one. The mixing rule is essentially a weighted average of the various pure component water activities at the solution ionic strength. Any error made in assuming only $MnSO_4$ and Na_2SO_4 instead of a $MnSO_4$, Na_2SO_4, $NaHSO_4$, $Mn(HSO_4)_2$ mixture in solution will decrease as the ionic strength declines since the difference between the individual water activity values decreases.

The amount of reaction-generated S(VI) existing as SO_4^{2-} as compared to that existing as HSO_4^- was estimated using Stelson et al.'s (1984) fit of the bisulfate ion dissociation constant,

$$\ln\left[\frac{m_{H^+} m_{SO_4^{2-}}}{m_{HSO_4^-}}\right] = -4.5740 + 4.0071\sqrt{I} - 0.99893\, I + 0.13250\, I^{3/2} - 0.010675\, I^2. \qquad (22)$$

A dissociation constant of the type defined by Equation (22) is often termed a "stoichiometric" equilibrium constant because the solution characteristics are implicit in its value (i.e., $\gamma's \neq 1$). For a given estimate of the acid concentration, an iterative procedure was used to calculate the total ionic strength, and the fraction of acid existing as $H(HSO_4)$ as opposed to H_2SO_4 using Equation (22).

The water activity predicted by Equation (21) is shown in Figure 6.1 for $m_{MnSO_4} = 0 - 3$ molal, $m_{Na_2SO_4} = 0 - 3$ molal, and $m_{acid} = 0$ and 1 molal. The addition of either Na_2SO_4 or acid to pure $MnSO_4$ (top solid curve in Figure 6.1)

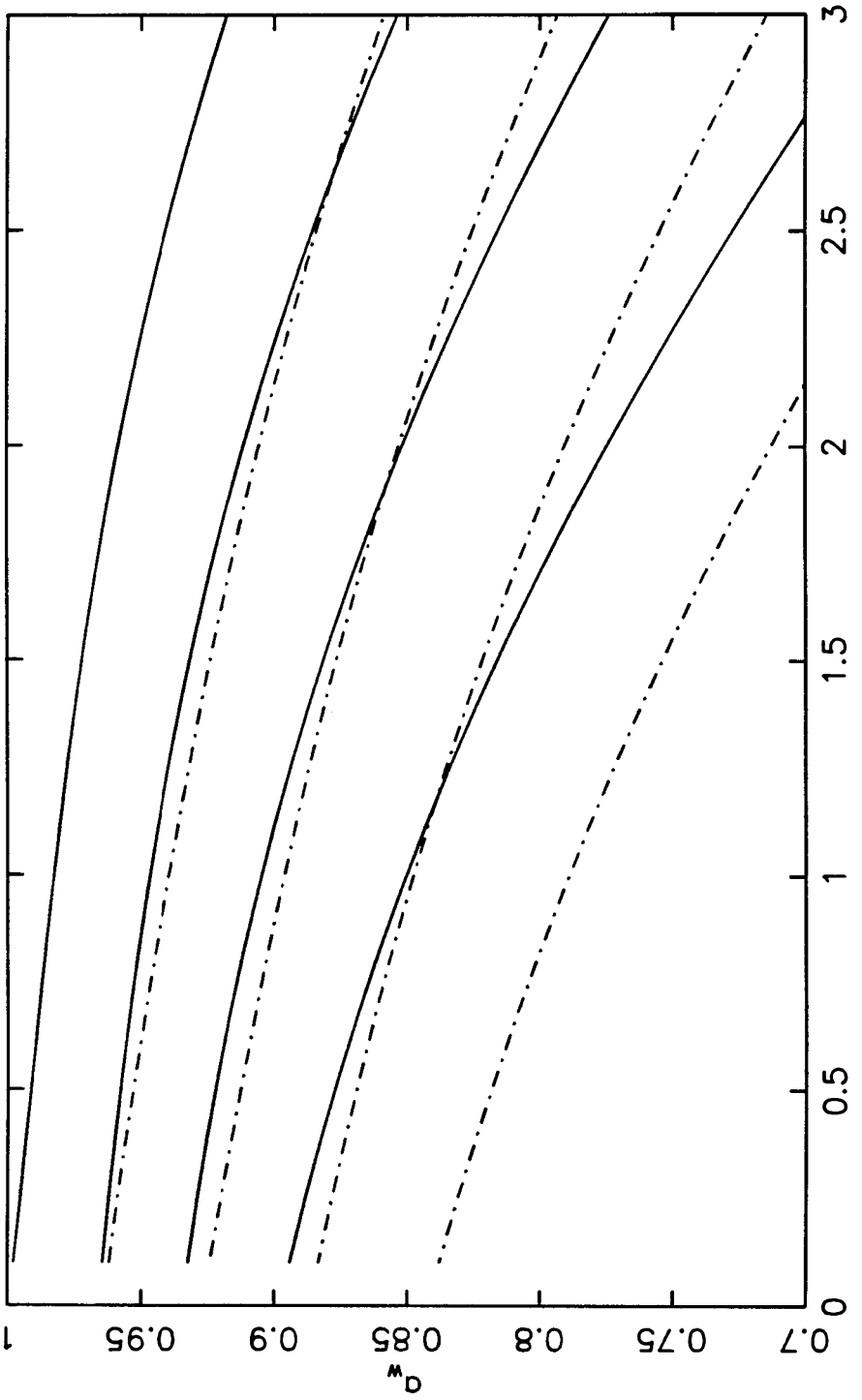

Figure 6.1 Predicted water activity for the $MnSO_4$- Na_2SO_4-H_2SO_4 system. m_A = 0 (————) and m_A = 1 mole/kg (—·—·—·—) for $m_{Na_2SO_4}$ = 0, 1, 2, 3 mole/kg (top to bottom in figure).

causes a decrease in the solution water activity. For all its apparent complexity, the Kusik and Meissner (1978) mixing rule is basically a weighted average of the water activities of the pure components at the solution ionic strength. 1–2 electrolytes such as Na_2SO_4 and $H(HSO_4)$ typically have lower water activities than 2–2 electrolytes such as $MnSO_4$. Figure 6.1 corroborates the intuitive reasoning that as the concentration of acid generated by reaction increases, the salt concentration must decrease in order to maintain a constant water activity. Whether or not the predicted water activities are correct is unknown since actual data do not exist. However, the trends and values are reasonable.

Once the acid concentration has been determined for a given particle size using Equation (21), the reaction rate at these conditions must be determined. Several of the rate expressions listed in Table 4.1 (e.g., Bronikowski and Pasiuk-Bronikowska (1981)) require only the S(VI) and Mn(II) concentrations. These are already known. However, other rate expressions (e.g., Martin and Hill (1987), Crump et al. (1983a), Berresheim and Jaeschke (1986)) require more detailed knowledge of the solution chemistry, for instance, the hydrogen ion and S(IV) concentrations. These values can be obtained from chemical equilibrium calculations. The aerosol solution chemistry was represented by the following set of reactions:

(1) $$SO_2 \rightleftharpoons SO_2 \cdot H_2O,$$

(2) $$SO_2 \cdot H_2O \rightleftharpoons H^+ + HSO_3^-,$$

(3) $$HSO_3^- \rightleftharpoons H^+ + SO_3^{2-},$$

(4) $$HSO_4^- \rightleftharpoons H^+ + SO_4^{2-},$$

(5) $$Mn^{2+} + SO_4^{2-} \rightleftharpoons MnSO_4^0,$$

(6) $$Na^+ + SO_4^{2-} \rightleftharpoons NaSO_4^-.$$

The associated equilibrium expressions are given by

$$K_1 = \frac{m_{SO_2 \cdot H_2O}}{p_{SO_2}} = 1.24 \times 10^{-6} \text{ mol ppm}^{-1} \text{ kg}^{-1}, \tag{23}$$

$$K_2 = \frac{\gamma^2_{H^+,HSO_3^-} m_{H^+} m_{HSO_3^-}}{m_{SO_2 \cdot H_2O}} = 0.0132 \text{ mol kg}^{-1}, \tag{24}$$

$$K_3 = \frac{\gamma^3_{2H^+,SO_3^{2-}} m_{H^+} m_{SO_3^{2-}}}{\gamma^2_{H^+,HSO_3^-} m_{HSO_3^-}} = 6.24 \times 10^{-8} \text{ mol kg}^{-1}, \quad (25)$$

$$K_4 = \frac{\gamma^3_{2H^+,SO_4^{2-}} m_{H^+} m_{SO_4^{2-}}}{\gamma^2_{H^+,HSO_4^-} m_{HSO_4^-}} = 0.012 \text{ mol kg}^{-1}, \quad (26)$$

$$K_5 = \frac{\gamma_{MnSO_4^0} m_{MnSO_4^0}}{\gamma^2_{Mn^{2+},SO_4^{2-}} m_{Mn^{2+}} m_{SO_4^{2-}}} = 190 \text{ mol}^{-1} \text{ kg}, \quad (27)$$

$$K_6 = \frac{\gamma^2_{Na^+,NaSO_4^-} m_{NaSO_4^-}}{\gamma^3_{2Na^+,SO_4^{2-}} m_{Na^+} m_{SO_4^{2-}}} = 6.6 \text{ mol}^{-1} \text{ kg}. \quad (28)$$

Reactions (1) through (3) describe the S(IV) equilibrium and reaction (4) determines the equilibrium between the S(VI) species. These reactions are typical of any S(IV)-S(VI) system. The high concentrations and ionic strengths typical of aqueous aerosols (> 1 M) result in complex solution behavior. All forms of ion-ion interaction increase as the interionic distance decreases and the water "available" for each ion in solution decreases. The interaction between sulfate and sodium and manganese ions was the only ion association considered explicitly (reactions (5) and (6)). It should be recognized that the above reaction scheme is merely an estimate of the chemistry occurring in the aerosol solution. Fortunately, the predicted effluent distribution does not shift along the diameter axis by orders of magnitude with order-of-magnitude changes in the calculated species concentrations.

At thermodynamic equilibrium, the concentration of manganese sulfate in a feed aerosol particle ranges from 2.5 molal at 94% humidity to 3.5 molal at 89% humidity. The assumption of ideal solution behavior is no longer possible at these high concentrations. Once reaction occurs, the manganese sulfate concentration will fall as the acid concentration increases. The total ionic strength (assuming total dissociation of all species) will also fall since sulfuric acid is a mixture of 1−1 and 1−2 electrolytes that have a lower ionic strength than a 2−2 electrolyte at similar concentrations. Nevertheless, solution ionic strengths less than 0.1 M, where simplified formulas for the activity coefficient such as the extended Debye-

Hückel or Güntelberg approximations (Stumm and Morgan, 1981) can be used, are not expected. The activity coefficient mixing rule of Kusik and Meissner (1978) was used to obtain an estimate of the activity coefficients in the aerosol solution:

$$I_{eff} \ln\gamma_{12} = \frac{z_2}{z_1 + z_2} \sum_j m_j \left(\frac{z_1 + z_j}{2}\right)^2 \ln\gamma^{\circ}_{1j}(I_{eff}) + \frac{z_1}{z_1 + z_2} \sum_i m_i \left(\frac{z_i + z_2}{2}\right)^2 \ln\gamma^{\circ}_{i2}(I_{eff}), \quad (29)$$

where i refers to cations and j to anions, z_k is the charge of ion k, I_{eff} is the effective ionic strength of the solution, and γ°_{ij} is the mean activity coefficient of a pure solution containing only ions i and j. The effective ionic strength is defined as $I_{eff} = \frac{1}{2}(\sum_k z_k^2 m_{k,free} + \sum_k z_k^2 m_{k,pair})$ for the various species k in solution. Note that ion-pair $NaSO_4^-$ contributes to solution ionic strength, whereas $MnSO_4^0$ does not. Indeed, the Kusik and Meissner (1978) mixing rule assumes that neutral species have no effect on the activity coefficient of a species in a mixture.

The values of the activity coefficients used in Equations (23) through (28) are given in Table C.1 of Appendix C along with a detailed discussion of the assumptions made in evaluating the activity coefficients. Basically, the lack of data for sulfite species, particularly at high ionic strengths, prompted the assumption that $\gamma_{H^+,HSO_4^-} \sim \gamma_{H^+,HSO_3^-}$ and $\gamma_{2H^+,SO_4^{2-}} \sim \gamma_{2H^+,SO_3^{2-}}$. Data for the hydrogensulfate and -bisulfate species were obtained from Stelson et al.'s (1984) "unmixing" of sulfuric acid water activity data using Kusik and Meissner's (1978) mixing rules. Activity coefficients for the sodium and manganese bisulfate and bisulfite species were approximated by those of sodium chloride and manganese chloride, respectively (Cohen et al., 1987a). Sodium chloride data were also used as an estimate of $\gamma_{Na^+,NaSO_4^-}$. While researchers agree that the activity coefficient of a neutral species such as $MnSO_4^0$ is not likely to equal one for $I > 0$ because of the dipole nature of the pair (Whitfield, 1979), there is little agreement as to the magnitude of the actual value with estimates both greater and less than one being proposed

(Pytkowicz, 1983). In these calculations, $\gamma_{MnSO_4^0} \sim 1$ was assumed for lack of a better estimate at the conditions of interest.

Equations (23) through (27) were solved for a pure manganese sulfate solution in equilibrium with an atmosphere of 1 ppm SO_2. The concentrations of the major species are shown as a function of the total $MnSO_4$ concentration in Figures 6.2a-f for the case of no reaction generated S(VI) ($m_A = 0$). A comparison between the results generated including the activity coefficients calculated using Equation (29) and those obtained assuming a value of one for all activity coefficients, shows that the assumption of ideal solution behavior does not adequately describe the solution. When the activity coefficients are not equal to unity, a revised, or stoichiometric equilibrium constant where $K' = K\,f(\gamma)$, can be thought of as defining the distribution of species. The stoichiometric equilibrium constant may differ considerably from the ideal, or thermodynamic, equilibrium constant. For instance, the concentrations of SO_4^{2-} and H^+ when $\gamma = 1$ are almost an order-of-magnitude lower than if mixture activity coefficients are used. In both cases, the concentration of SO_4^{2-} was greater than that of HSO_4^-. Hydrogen ion concentration, rather than pH, was presented since pH meters actually measure $\text{pH} = \log a_{H+}$. In dilute solutions where $\gamma \sim 1$, the ion activity is approximately equal to the ion concentration. This is no longer true in concentrated solutions, and estimates of the free ion activity coefficient are necessary to calculate the pH. Whitfield (1979) has fit the free hydrogen ion activity coefficients calculated according to the MacInnes convention to the following formula:

$$\log \gamma_{H+} = -0.5108\, I^{1/2} \left[\frac{1 + 0.5 B_D a_D I^{1/2}}{1 + B_D a_D I^{1/2}} \right]^2 + b\, I + c\, I^2, \qquad (30)$$

where I has units of mol kg^{-1}, $B_D a_D = 16.63\ \text{kg}^{1/2}\text{mol}^{-1/2}$, $b = 0.2761\ \text{kg mol}^{-1}$ and $c = 4.9 \times 10^{-4}\ \text{kg}^2\,\text{mol}^{-2}$. Equation (30) is strictly valid up to ionic strengths of 2 molal. In addition, the activity coefficient has not been "mixed" with the other constituents of the aerosol solution. However, if Equation (30) is used to obtain a rough estimate of γ_{H+} at $I = 6$ m, a solution pH of approximately 2.4 is calculated.

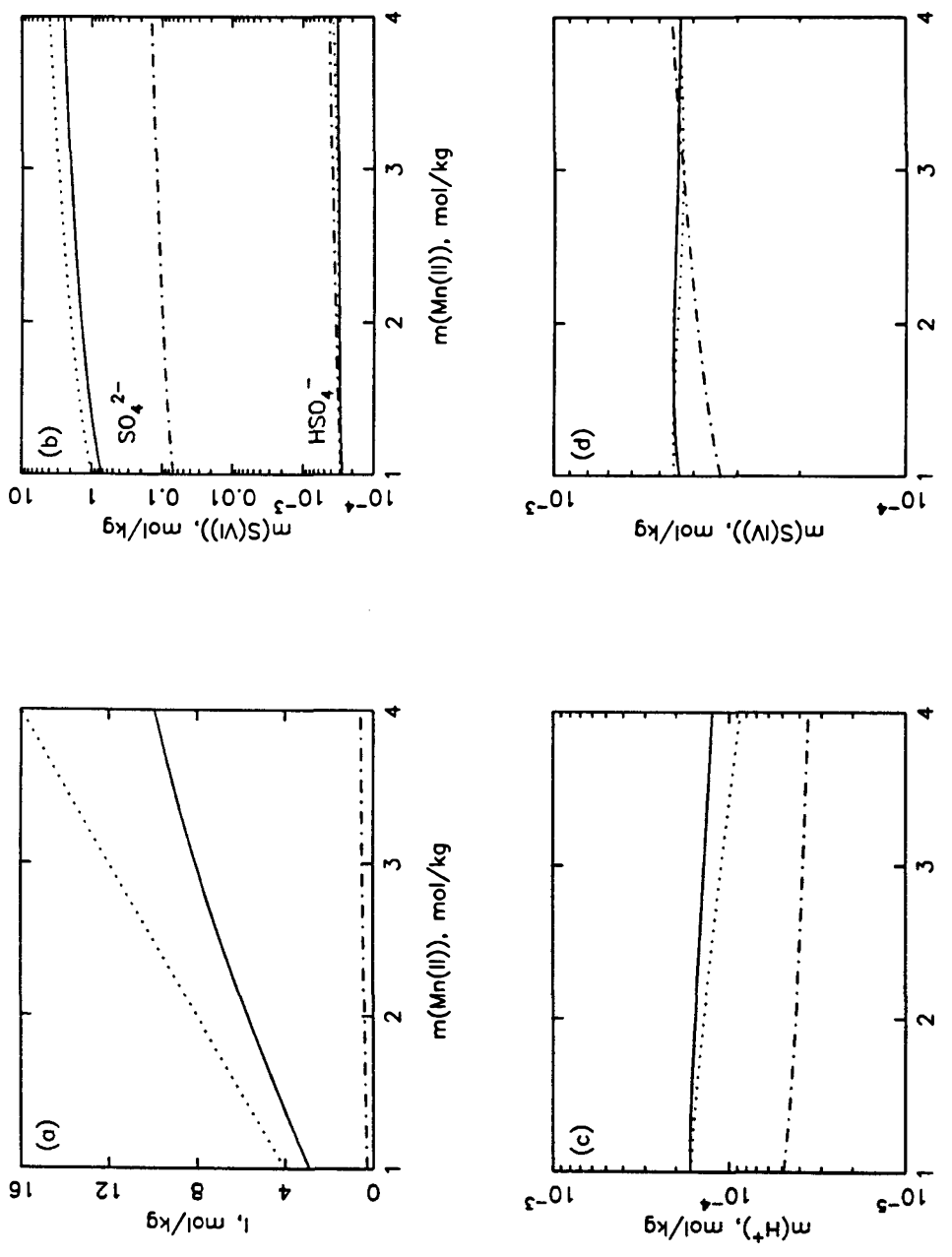

Figure 6.2 Equilibrium concentrations for a pure $MnSO_4$ solution ($m_A = 0$) at $p_{SO_2} = 1$ ppm. $MnSO_4^0$ ion pairs: $\gamma_{ij} = 1$ (—·—·—·—) and $\gamma_{ij} \neq 1$ (————). No ion pairs, $\gamma_{ij} \neq 1$ (……).

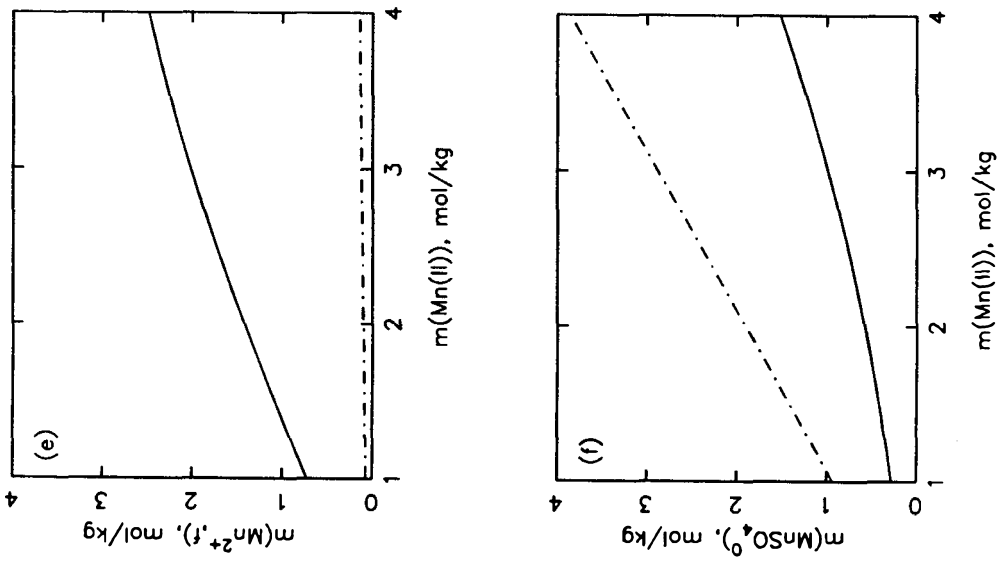

Figure 6.2 (Continued)

This value differs considerably from the value of $-\log m_{H^+} = 3.8$.

The species concentrations obtained assuming that no $MnSO_4^0$ ion pairs are formed are also presented in Figures 6.2a-f. Mixture activity coefficients were used in the calculations. The predicted S(VI), S(IV), and H^+ concentrations are approximately equal to those calculated including the ion pair. The effect on ionic strength is much greater since all of the manganese ion was included in its calculation. Clearly, for the pure $MnSO_4$ case, the use of mixture activity coefficients is more important than the inclusion of the $MnSO_4^0$ ion pair. Figures 6.3a-f show the results of a similar set of calculations ($\gamma = 1$ results are not shown) with $m_A = 1$ molal and 1 ppm SO_2. At these conditions the concentrations of SO_4^{2-} and HSO_4^- are approximately equal. The effective ionic strength has not changed. At the high hydrogen ion concentrations predicted, the total S(IV) concentration is reduced to approximately that of $SO_2 \cdot H_2O$ in equilibrium with the SO_2. The effect of the ion pairs on the species concentrations is more pronounced in this case, particularly regarding the bisulfate ion concentration. Therefore, because including $MnSO_4^0$ ion pairs does have an effect on the solution chemistry as the generated acid concentration increases, Equation (5) was included in the CSTR model chemistry calculations.

Since a number of the CSTR experiments were performed using a $MnSO_4$-Na_2SO_4 feed aerosol, the influence of the sodium on the solution chemistry had to be accounted for in these runs. Three cases were considered: 1) only $NaSO_4^-$ ion pairs (Reaction 6) are formed; 2) only $MnSO_4$ ion pairs (Reaction 5) are formed; and 3) no ion pairs are formed. Figures 6.4a-f show the species concentrations calculated for a $MnSO_4$-Na_2SO_4 solution in equilibrium with 1 ppm SO_2. The molar ratio of $MnSO_4$ to Na_2SO_4 was set at 0.1 and no generated acid was considered present ($m_A = 0$). While allowing only one type of ion pair to form is physically unrealistic, the plots in Figure 6.4 indicate that all three cases give approximately identical results for the H^+, SO_4^{2-}, HSO_4^-, and S(IV)

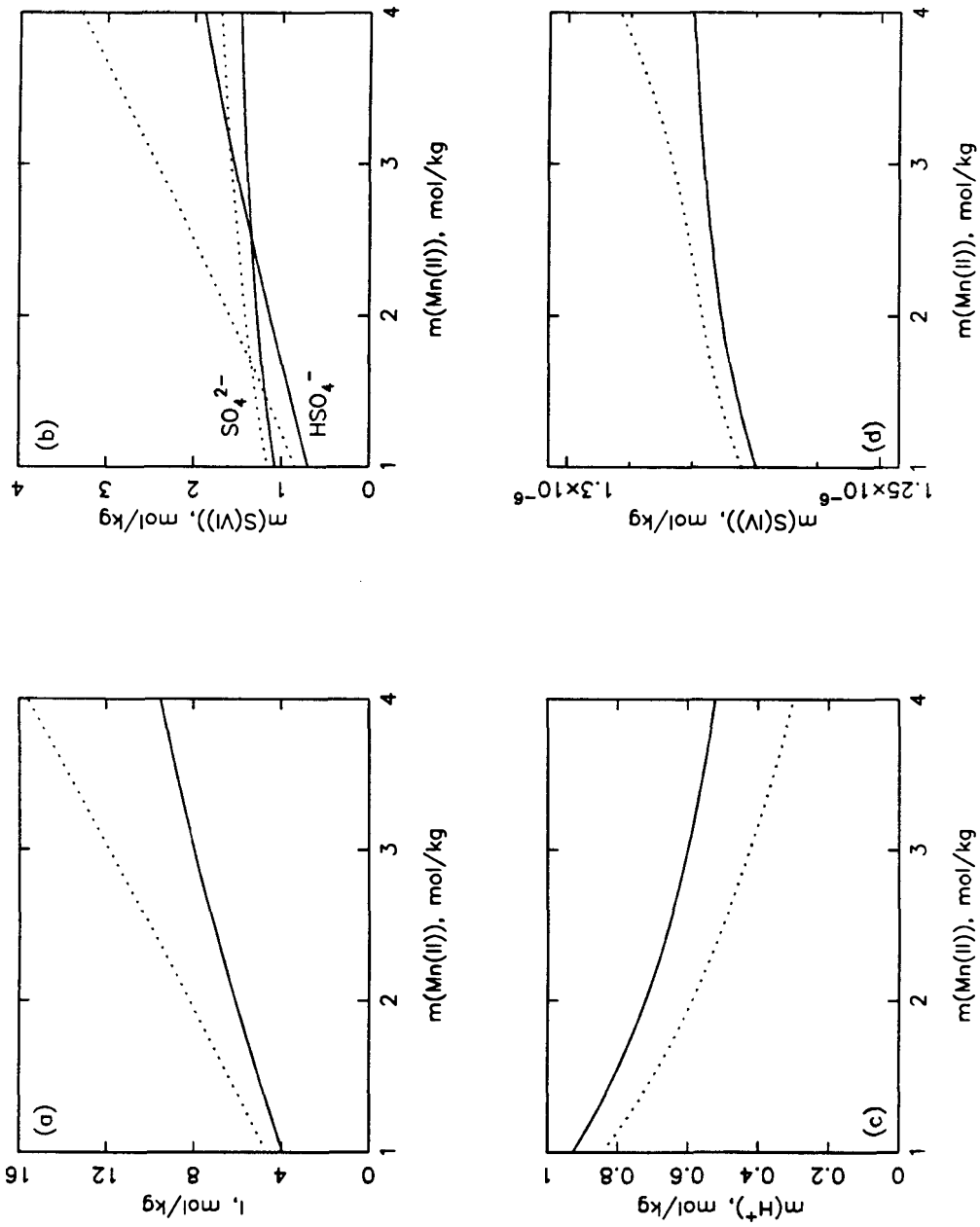

Figure 6.3 Equilibrium concentrations for a pure $MnSO_4$ solution ($m_A = 1$ molal, $\gamma_{ij} \neq 1$) at $p_{SO_2} = 1$ ppm. $MnSO_4^0$ ion pairs (————), no ion pairs (·····).

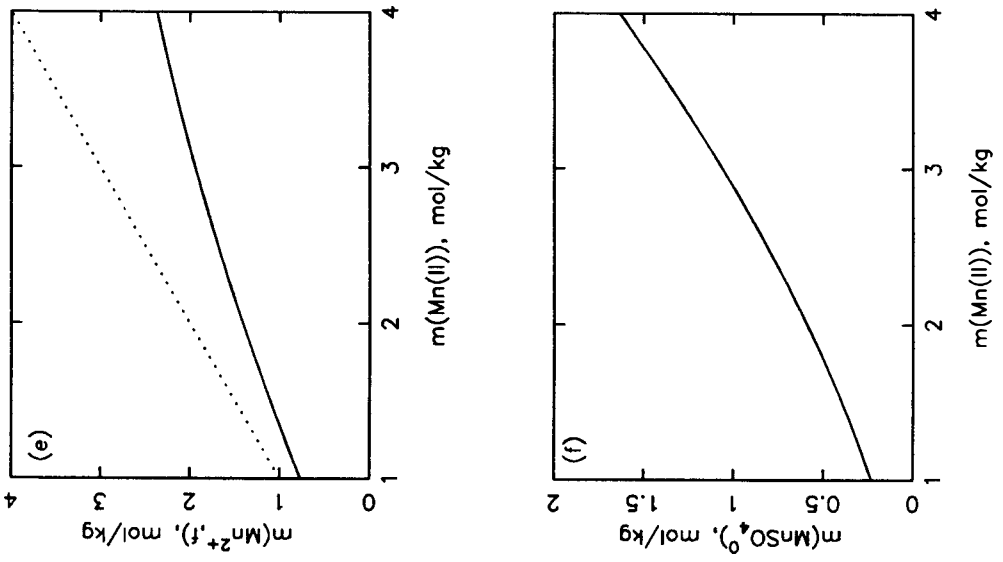

Figure 6.3 (Continued)

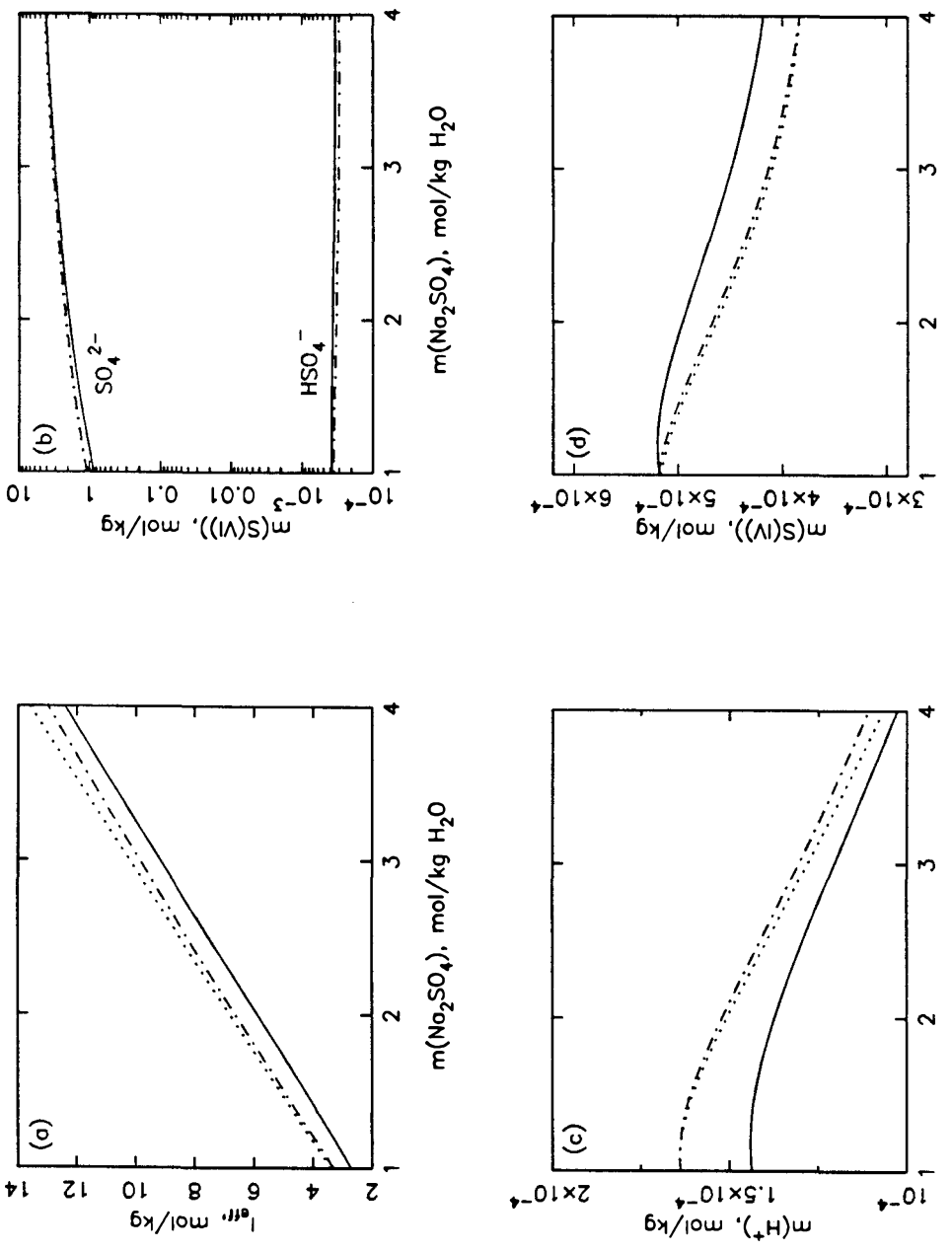

Figure 6.4 Equilibrium concentration for Na_2SO_4- $MnSO_4$ mixture ($m_A = 0$, $\gamma_{ij} \neq 1$) at $p_{SO_2} = 1$ ppm. Molar ratio of $MnSO_4$ to $Na_2SO_4 = 0.1$. $NaSO_4^-$ pairs only (————), $MnSO_4^0$ ion pairs only (– – – –), no ion pairs (.....).

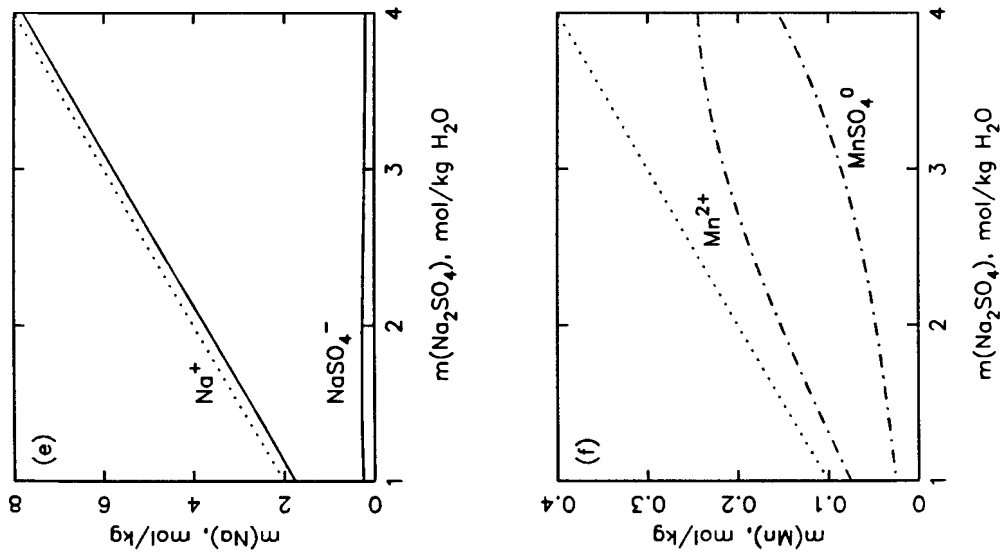

Figure 6.4 (Continued)

concentrations. This is in part due to the reduced tendency of sodium to pair with sulfate ions as compared to manganese and sulfate ions, and in part to the reduced manganese concentration. This behavior did not change significantly as the generated acid concentration was increased and, if anything, the three cases became even more indistinguishable as the molar ratio of $MnSO_4$ to Na_2SO_4 was decreased. Since only minor differences were observed between the three ion-pairing cases considered ($NaSO_4^-$ only, $MnSO_4^0$ only, and no pairs), it is not expected that consideration of both sodium and manganese sulfate ion pairs simultaneously would give significantly different results.

Based upon the equilibrium calculations made at conditions typical of the CSTR experiments, the following decisions were made concerning the chemistry that would be included in the CSTR model calculations. First, reactions (1) through (5) would be used for those experiments having a pure manganese sulfate feed aerosol. Second, for those experiments having a mixed $MnSO_4$-Na_2SO_4 feed aerosol (molar ratios of 0.1 and 0.01 were used), reactions (1) through (4) and (6) were used. Ion pairing of the manganese and sulfate ions was not considered because of the reduced manganese concentration relative to the sodium concentration. And third, mixture activity coefficients determined using Kusik and Meissner's (1978) mixing rule were used for all species, and an activity coefficient of one was assumed for the $MnSO_4^0$ pair. It should be reiterated that highly concentrated, mixed solutions such as those typical of aerosols are very complicated, involving not only ion-solute interaction, but significant ion-ion interactions. A first step in dealing with the nonideality of the solution has been taken by including the activity coefficients and several of the possible ion pairing reactions.

§6.3 Testing the CSTR Model

The CSTR model calculations can be summarized as follows. For a given experiment, the feed distribution ($n_f(D_p)$) is shifted to the measured reactor relative

humidity using the procedure discussed in Chapter 5. The distribution is then converted into a set of diameters and particle concentrations using the trapezoidal rule. In this way the polydisperse feed aerosol is converted into a set of "monodisperse" feed aerosols. Each feed diameter is nondimensionalized using the specified maximum and minimum diameters (Equation (2)) and all future calculations are done on the dimensionless scale. Because of the particular form of nondimensionalization used, and because it was assumed that each feed particle has the same salt concentration, the species concentrations and growth rate for the product aerosol need be calculated only once — for the feed aerosol having size $x = 0$. These results can then be applied to the product aerosol resulting from all feeds having size $0 \leq x \leq 1$. The explanation behind this is presented in Appendix D, but suffice it to say that the number of necessary calculations is greatly decreased.

The integral in Equation (19) is taken over the range of nondimensional particle sizes that have grown from the originally monodisperse feed of size x_0. Therefore, a "set" of N dimensionless particle sizes is generated, $x_{p,j}$, where $1 \leq j \leq N$. The salt concentration in the feed aerosol has been determined using the relation $\mathrm{RH} = a_w(C_M, C_N)$, and since each "effluent" particle of size $x_{p,j}$ has grown from the original feed aerosol, the salt concentration in each is set by the mass balance of Equation (7). Given that $C_M(x_{p,j}) < C_M(x_0)$ and $C_N(x_{p,j}) < C_N(x_0)$, thermodynamic equilibrium is not satisfied for the particle unless additional material is added to the solution. It was assumed that the reaction of S(IV) to S(VI) is the only mechanism by which growth occurs. Therefore, the concentration of reaction-generated acid, C_A, is set using Equations (21) and (22) such that thermodynamic equilibrium is maintained. This data set, the salt and acid concentrations and solution density as a function of the dimensionless size, is a function only of the reactor conditions and the maximum and minimum diameters used in the nondimensionalization. The results at this point are independent of the feed distribution and the reaction rate expression.

Once the concentrations of the major species have been determined for each effluent size in the set, the concentrations of the minor species are determined by chemical equilibrium (Equations (23) through (28)). The rate of reaction is calculated using the specified kinetic expression from the literature and the growth rate $I(x, x_0)$ is obtained using Equations (11) and (12). All the information is now available to calculate the effluent distribution for a given feed size using Equation (19). The composition of each effluent particle is known and the individual effluent distributions are shifted to match the relative humidity of the experimentally measured effluent distribution. The set of effluent distributions corresponding to the set of initial feed diameters is "added" (see Appendix D for details) to give the predicted CSTR effluent distribution. Detailed composition information about the aerosol is no longer available. The CSTR program, using the mechanism of Berresheim and Jaeschke (1986) as an example, is included in Appendix E.

The predicted effluent distribution is a function of many variables, e.g., the CSTR operating conditions (residence time τ, p_{SO_2}, T_{CSTR}, RH_{CSTR}), the particle deposition rate β, and the specified reaction rate expression. If a monodisperse feed is input to the CSTR, the output will be polydisperse because chemical reaction is occurring, and the distribution of residence times characteristic of a CSTR ensures that not all particles experience the same time for growth. Thus, if the *mean* residence time in the CSTR is increased, all particles will experience more time for growth and the effluent distribution should shift to larger sizes on the diameter scale. The converse will be true if the mean residence time is decreased — the limit being zero time spent in the CSTR with the effluent distribution equal to the feed distribution. Figure 6.5 shows the results of this test of the CSTR program. The rate expression of Berresheim and Jaeschke (1986) was used along with the CSTR conditions of Experiment 5 ($T_{CSTR} = 23.62°C$, $p_{SO_2} = 50.2$ ppm, $RH_{CSTR} = 92.8\%$). The predicted effluent distributions were not shifted to another humidity. Wall deposition was neglected in this case and a monodisperse $MnSO_4$ feed of 10^4 particles/cm^3, 0.15 μm in diameter, was used. The mean resi-

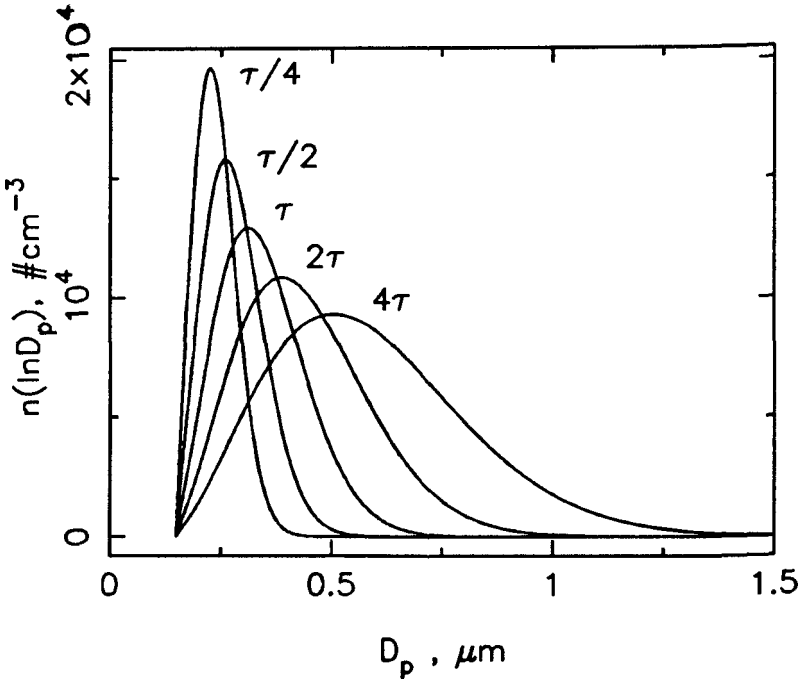

Figure 6.5 Predicted CSTR effluent distributions assuming no wall loss as a function of the residence time, τ = 1 hour. Monodisperse $MnSO_4$ feed: 10^4 particles/cm^3, 0.15 μm in diameter. CSTR conditions of Experiment 5, reaction rate expression of Berresheim and Jaeschke (1986) used.

dence time in the reactor for this particular experiment ($\tau = V/Q$) was one hour. For each of the distributions in Figure 6.5, the total number of particles in the predicted effluent distribution was 10^4 particles/cm^3. This in itself was an important check of the CSTR program — number was conserved in the absence of a particle loss mechanism. The value of τ was varied from 15 minutes to 4 hours and the predicted effluent distributions shifted to larger diameters and broadened as the reactor residence time was increased, as expected. As the residence time was decreased the distribution peak approached the feed diameter and became less polydisperse in nature.

In the absence of reaction, the distribution of residence times has no effect on the aerosol. The input distribution is the same as the effluent distribution. If wall loss is also considered, it is possible, although unlikely, that the distribution

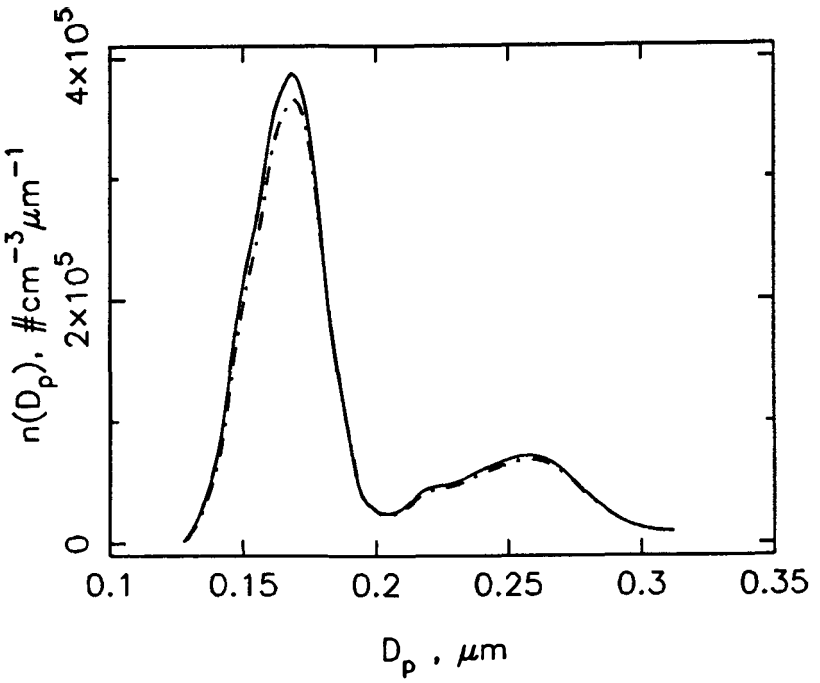

Figure 6.6 Predicted CSTR effluent distribution assuming only deposition and no reaction. (— · — · — ·). Experiment 5 CSTR conditions and feed (————) used.

may shift slightly as a result of the diameter dependent deposition coefficient $\beta(x)$. This situation can be modeled merely by canceling the growth term from Equation (17), and the resulting equation gives the effluent distribution as a fraction of the feed distribution. Figure 6.6 shows the feed distribution for Experiment 5 and the effluent distribution resulting when deposition is the only mechanism affecting the aerosol. The variation in $\beta(x)$ over the diameter range of interest is too small to cause a noticeable distribution shift. The total number of particles in the feed is 18,270 particles/cm^3, while the effluent distribution has only 17,290 particles/cm^3 for a 5.4% difference.

In order to investigate the effect of neglecting the Kelvin effect on the predicted effluent distribution, the growth of a pure $MnSO_4$ monodisperse feed aerosol was considered. Equation (4) was rewritten to include the diameter dependent effect of droplet curvature in determining the thermodynamic equilibrium:

$$\mathrm{RH} = a_w(C_M, C_A)\, e^{f(C_M, C_A)}, \tag{32}$$

where the f is a function of the absolute temperature, surface tension, solution molecular volume, and particle diameter: $f = 4\sigma v_m/(D_p kT)$. If this equation is differentiated with respect to time, the following expression, analogous to Equation (10), is obtained for dC_A/dt,

$$\frac{dC_A}{dt} = \frac{\left\{ e^{f(C_M,C_A)} \frac{\partial a_w}{\partial C_M} + \mathrm{RH} \frac{\partial f}{\partial C_M} \right\}}{\left\{ e^{f(C_M,C_A)} \frac{\partial a_w}{\partial C_A} + \mathrm{RH} \frac{\partial f}{\partial C_A} \right\}} \frac{C_M}{v_p} \frac{dv_p}{dt}. \tag{33}$$

Equations (33) and (5) can then be used to solve for the growth rate $I(x)$ in terms of the reaction rate:

$$I(x) = \left\{ 3 \ln \left(\frac{D_{p,max}}{D_{p,min}} \right) \right\}^{-1} \frac{R(C_A, C_M)}{\dfrac{\left\{ e^{f(C_M,\, C_A)} \frac{\partial a_w}{\partial C_M} + \mathrm{RH} \frac{\partial f}{\partial C_M} \right\}}{\left\{ e^{f(C_M,\, C_A)} \frac{\partial a_w}{\partial C_A} + \mathrm{RH} \frac{\partial f}{\partial C_A} \right\}}}. \tag{34}$$

The partial derivative of function f, assuming the surface tension to be constant, is given by

$$\frac{\partial f}{\partial C_i} = \left(\frac{4\sigma}{kT} \right) \left\{ \frac{1}{D_p} \frac{\partial v_m}{\partial C_i} - \frac{v_m}{D_p^2} \frac{\partial D_p}{\partial C_i} \right\}. \tag{35}$$

The CSTR effluent distribution, given a monodisperse $MnSO_4$ feed aerosol, was calculated using Equations (32) through (35) to determine the growth rate. Berresheim and Jaeschke's (1986) reaction rate expression was used and wall losses were ignored. The CSTR conditions of Experiment 5 were used for a feed aerosol 0.15 μm in diameter having a particle concentration of $10^4/\mathrm{cm}^3$. The results are plotted in Figure 6.7a-b along with the results predicted when the Kelvin effect is neglected. Perhaps the point in the calculations where the effect of neglecting the Kelvin correction is most apparent is in the determination of the initial feed salt concentration. This has been discussed previously (see Figure 5.4) and it was

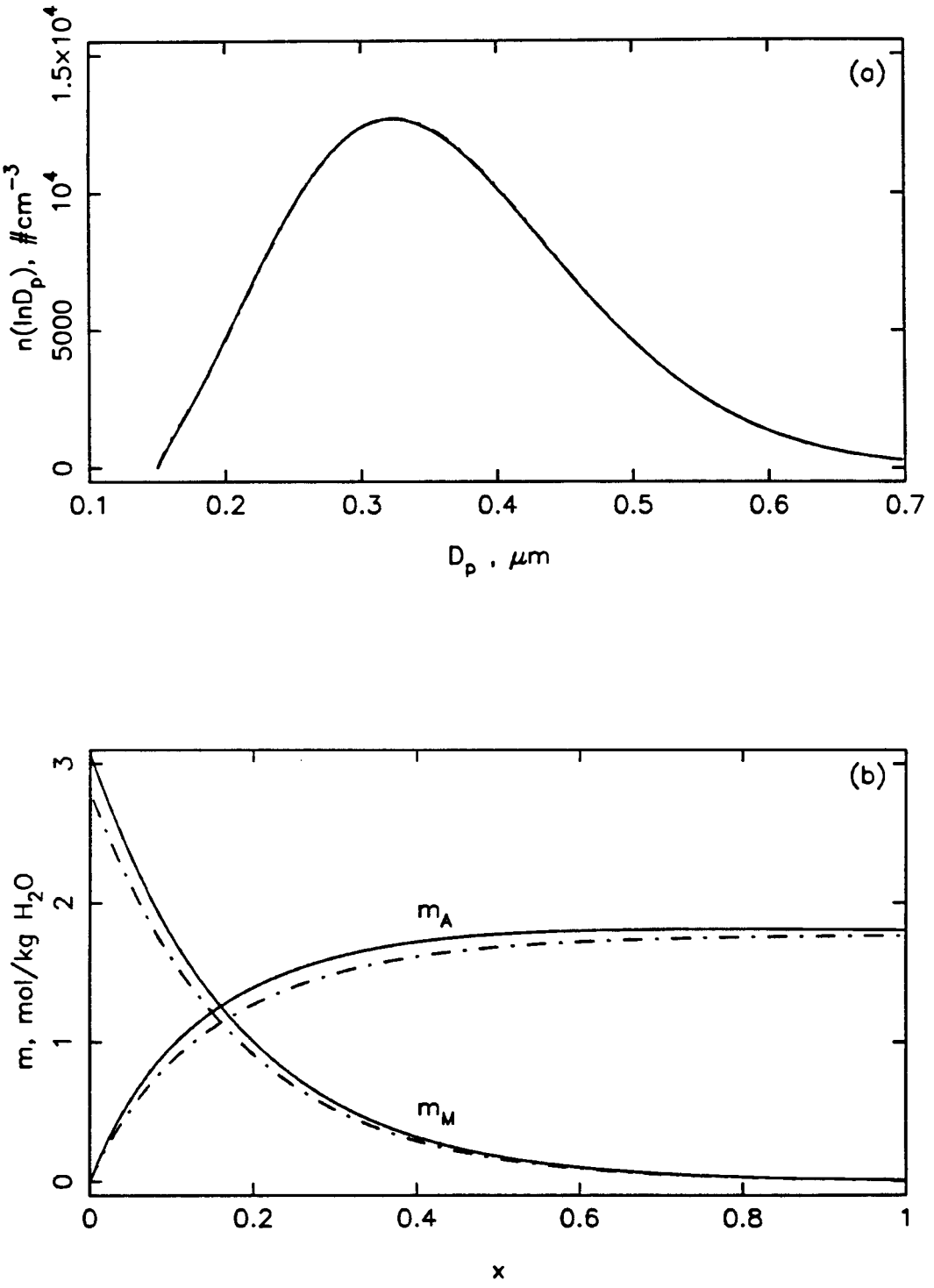

Figure 6.7 Comparison of the predicted CSTR distribution with the Kelvin effect (————) and without (—·—·—). Monodisperse $MnSO_4$ feed: 10^4 particles/cm^3, 0.15 μm in diameter. CSTR conditions of Experiment 5, reaction rate expression of Berresheim and Jaeschke (1986) used. $D_{p,min} = 0.15$ μm and $D_{p,max} = 1.0$ μm.

shown that for particles of approximately 0.1 μm diameter, up to a 15% error in the predicted $MnSO_4$ concentration at 94% relative humidity is possible. Neglecting the Kelvin effect is equivalent to performing the CSTR experiment at a slightly higher humidity. As particle size increases and/or relative humidity is lowered, this error is reduced. Since a low initial feed concentration is predicted without the Kelvin effect, all subsequent salt concentrations determined using the mass balance (Equation 7) are also low. This results in decreased acid concentrations as a function of diameter (see Figure 6.7b). Fortunately, as can be seen in Figure 6.7a, these errors result in an imperceptible shift of the predicted effluent distribution. The peak of the distribution predicted neglecting the Kelvin effect is on the order of 0.002 μm greater than that predicted when the Kelvin effect is included. Naturally, the overall effect of neglecting the Kelvin correction depends on the reaction rate expression used. However, the various expressions used in this study each produced approximately the same effect as seen in Figure 6.7. Therefore, the neglect of the Kelvin effect in the CSTR model calculations was deemed justifiable.

As was shown in Section 6.2, setting the activity coefficients equal to one, as in the case of an ideal, or infinitely dilute solution, resulted in predicted species concentrations that were considerably different than when the mixture activity coefficients were included (see Figure 6.2). All other perturbations of the solution chemistry resulted in changes less severe than this case. Figure 6.8 shows the CSTR effluent distributions, given an 0.15 μm monodisperse feed, predicted when the mixture activity coefficients are used in the equilibrium calculations and when all activity coefficients are assumed to be one. The rate expression of Berresheim and Jaeschke (1986) used in this example is a function of the hydrogen ion concentration, the S(IV) concentration, and the manganese activity, although differences in the predicted rates basically reduce to differences in the hydrogen ion concentration. The predicted distribution for the case $\gamma = 1$ is shifted on the diameter scale by approximately 0.01 μm. Clearly, the effluent distributions have been affected by the choice of the chemistry in this case. It can only be assumed that the actual

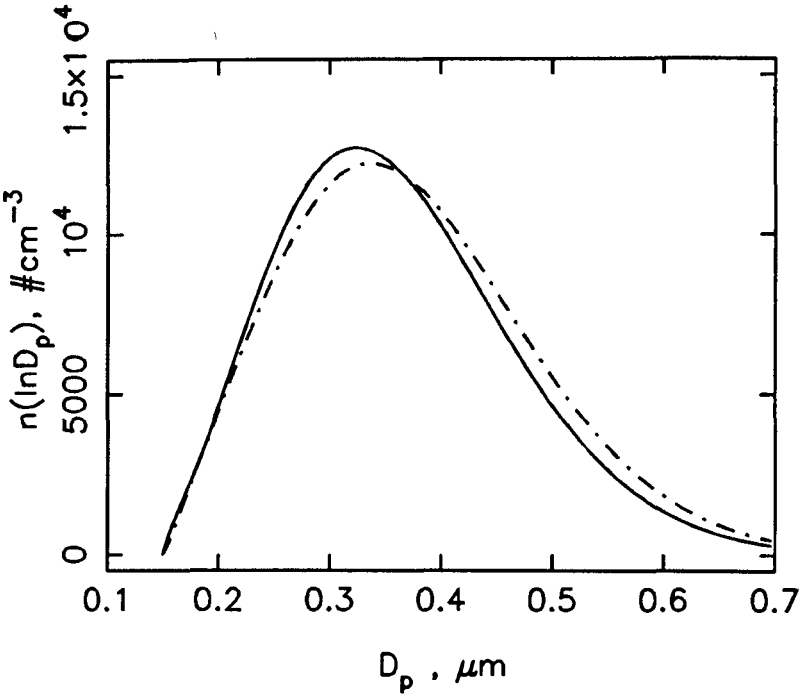

Figure 6.8 Predicted CSTR effluent distributions using $\gamma = 1$ (— · — · — · -) and $\gamma \neq 1$ (————) with Berresheim and Jaeschke's (1986) rate expression. Monodisperse $MnSO_4$ feed: 10^4 particles/cm^3, 0.15 μm in diameter, CSTR conditions of Experiment 5.

solution chemistry is more truly modeled when using the mixture activity coefficients. As to whether or not the reaction scheme being used adequately models the solution is unknown at this time. This example does demonstrate, however, that in a case where the rate expression is dependent on the detailed solution chemistry, orders-of-magnitude differences in the concentrations did not result in an orders-of-magnitude shift of the predicted distribution along the diameter axis. Also, those rate expressions requiring only the total manganese and/or S(VI) concentrations are not affected by the details of the aerosol solution chemistry.

§6.4 Comparison of the Predicted and Experimental CSTR Effluent Distributions

The predicted CSTR effluent distributions for a number of experiments representative of the results presented in Table 5.1 are shown in Figures 6.9 through

6.16. Several of the proposed rate expressions from Table 4.1 were tested for each, in particular, the rate expressions of Berresheim and Jaeschke (1981), Crump et al. (1983a), Bronikowski and Pasiuk-Bronikowska (1981), and Martin and Hill (1987). Also shown in each figure are the predicted reaction rates as a function of the dimensionless diameter x. The variable x can be related to the dimensional effluent diameter D_p resulting from any particular "monodisperse" feed size x_f by the following relation:

$$D_p = D_{p,min} \left(\frac{D_{p,max}}{D_{p,min}} \right)^{x+x_f} . \tag{36}$$

The function $R(C_A, C_M)$ versus x is applicable to all feed diameters, while a plot of R versus D_p would be meaningless. Plots of the manganese, acid, H^+, and S(IV) concentrations and total and effective ionic strength as a function of the dimensionless size x are given in Appendix G for each experiment studied here.

The results presented in this chapter are for Experiments 5, 8, 9, 10, 12, 13, 17, and 18. The first four experiments are runs made with a pure $MnSO_4$ feed and SO_2 concentrations ranging from 0.12 to 50 ppm. The last three experiments listed are mixed $MnSO_4$-Na_2SO_4 feed runs. Molar ratios of $MnSO_4$ to Na_2SO_4 used were 0.1 and 0.01. The data in each figure (6.9 to 6.16) are presented at the effluent EMC humidity, or the humidity at which the effluent aerosol was measured. More complete information on the experimental conditions can be found in Table 5.1.

From scanning through Figures 6.9 to 6.16, several points become obvious. First, the "initial reaction rate," or the reaction rate associated with those particles the size of and only slightly larger than the feed diameter, plays an important role in determining the amount of predicted growth. This is particularly apparent for those runs made with a pure $MnSO_4$ feed. Since the Mn(II) concentration is high, the initial rate will also be high. Also apparent is that unless the rate falls rapidly with increasing size, substantial growth is also predicted. For instance, in Figure 6.14 the reaction rate of Martin and Hill (1987) has a value of approximately 0.02

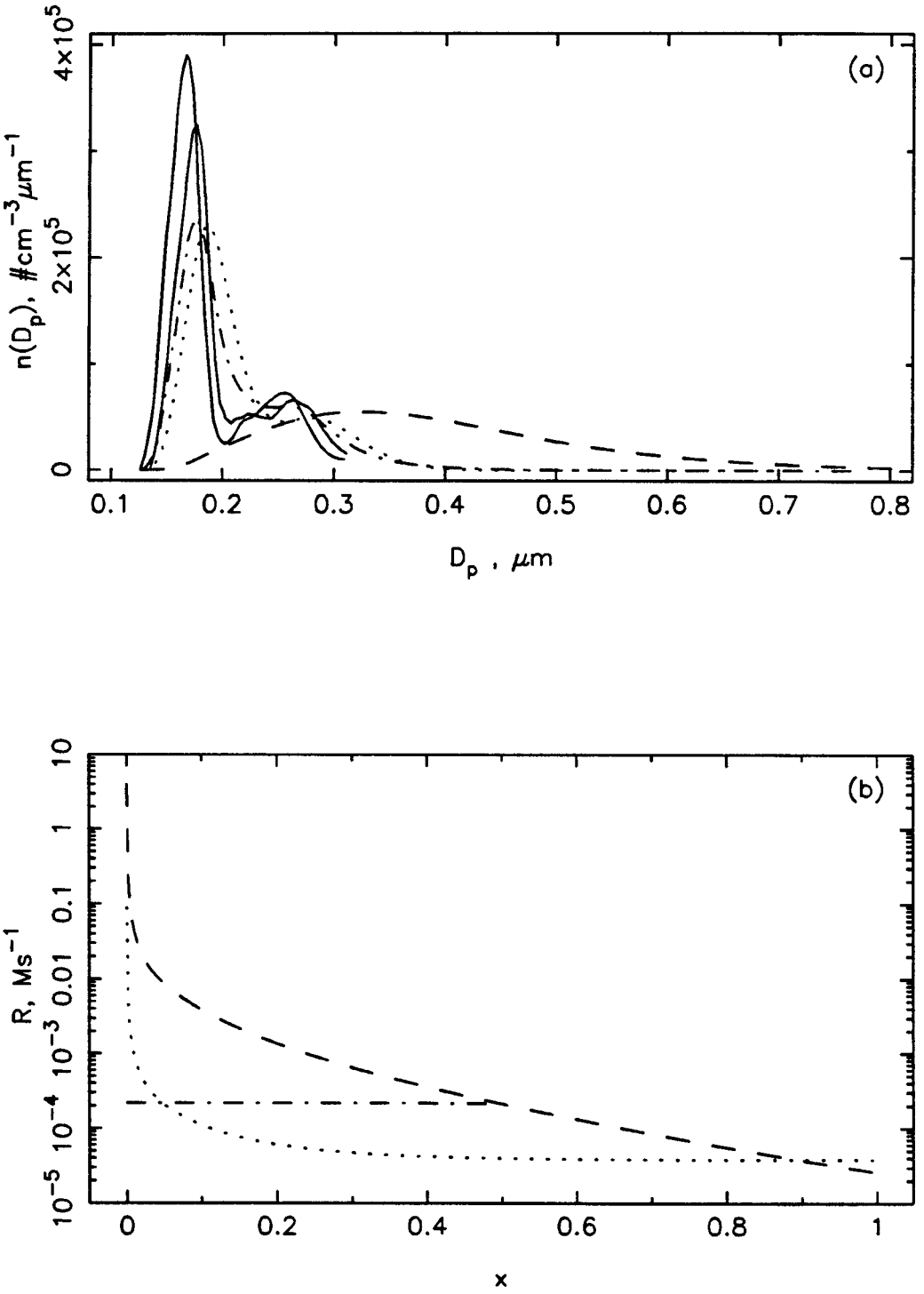

Figure 6.9 Predicted CSTR effluent distributions (a) and reaction rates (b) for Experiment 5 at T = 23.3°C, RH = 92.4%, p_{SO_2} = 50.3 ppm, $D_{p,min}$ = 0.1 μm, $D_{p,max}$ = 1.0 μm. Measured feed and effluent distributions (—————). Berresheim and Jaeschke (1986) (— — — —), Crump et al. (1983a) (· · · · · · · · · ·), Bronikowski and Pasiuk-Bronikowska (1981) (— · — · — ·).

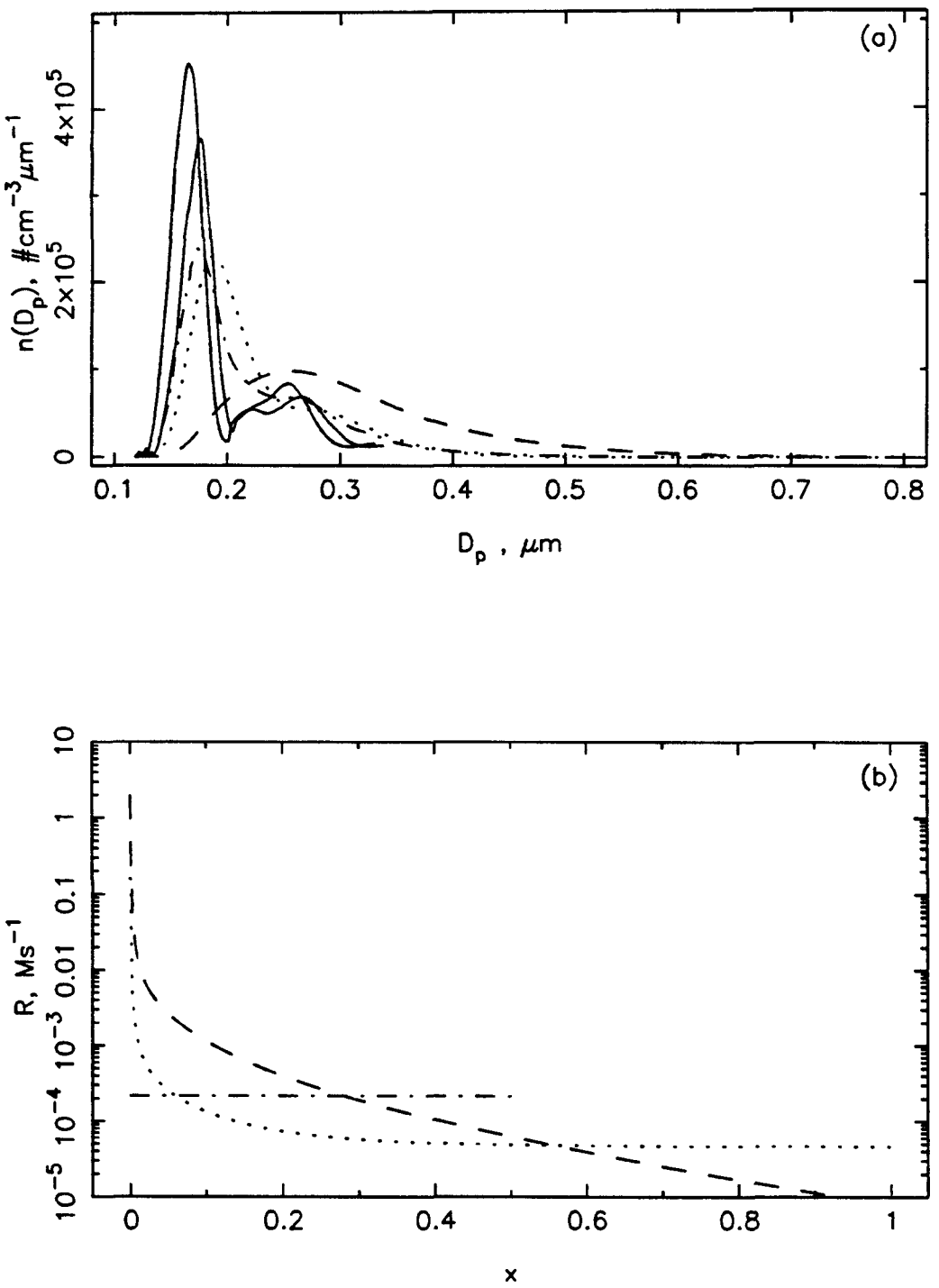

Figure 6.10 Predicted CSTR effluent distributions (a) and reaction rates (b) for Experiment 8 at T = 23.2°C, RH = 93.2%, p_{SO_2} = 13.5 ppm, $D_{p,min}$ = 0.1 μm, $D_{p,max}$ = 1.0 μm. Measured feed and effluent distributions (————). Berresheim and Jaeschke (1986) (— — — —), Crump et al. (1983a) (· · · · · · · · · ·), Bronikowski and Pasiuk-Bronikowska (1981) (— · — · — ·).

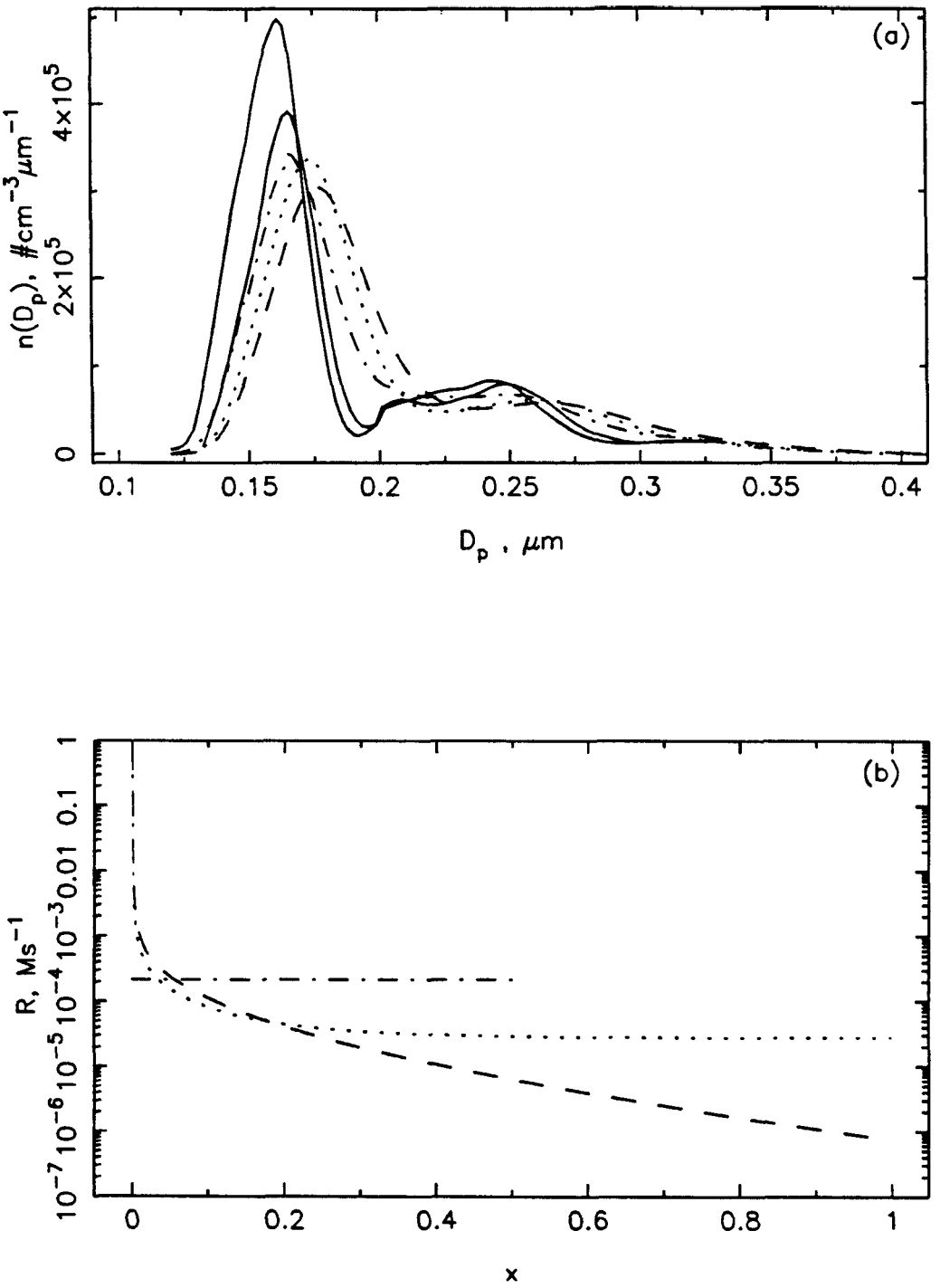

Figure 6.11 Predicted CSTR effluent distributions (a) and reaction rates (b) for Experiment 9 at T = 22.9°C, RH = 87.5%, p_{SO_2} = 1.74 ppm, $D_{p,min}$ = 0.1 μm, $D_{p,max}$ = 1.0 μm. Measured feed and effluent distributions (————). Berresheim and Jaeschke (1986) (— — — —), Crump et al. (1983a) (·····), Bronikowski and Pasiuk-Bronikowska (1981) (—·—·—·—).

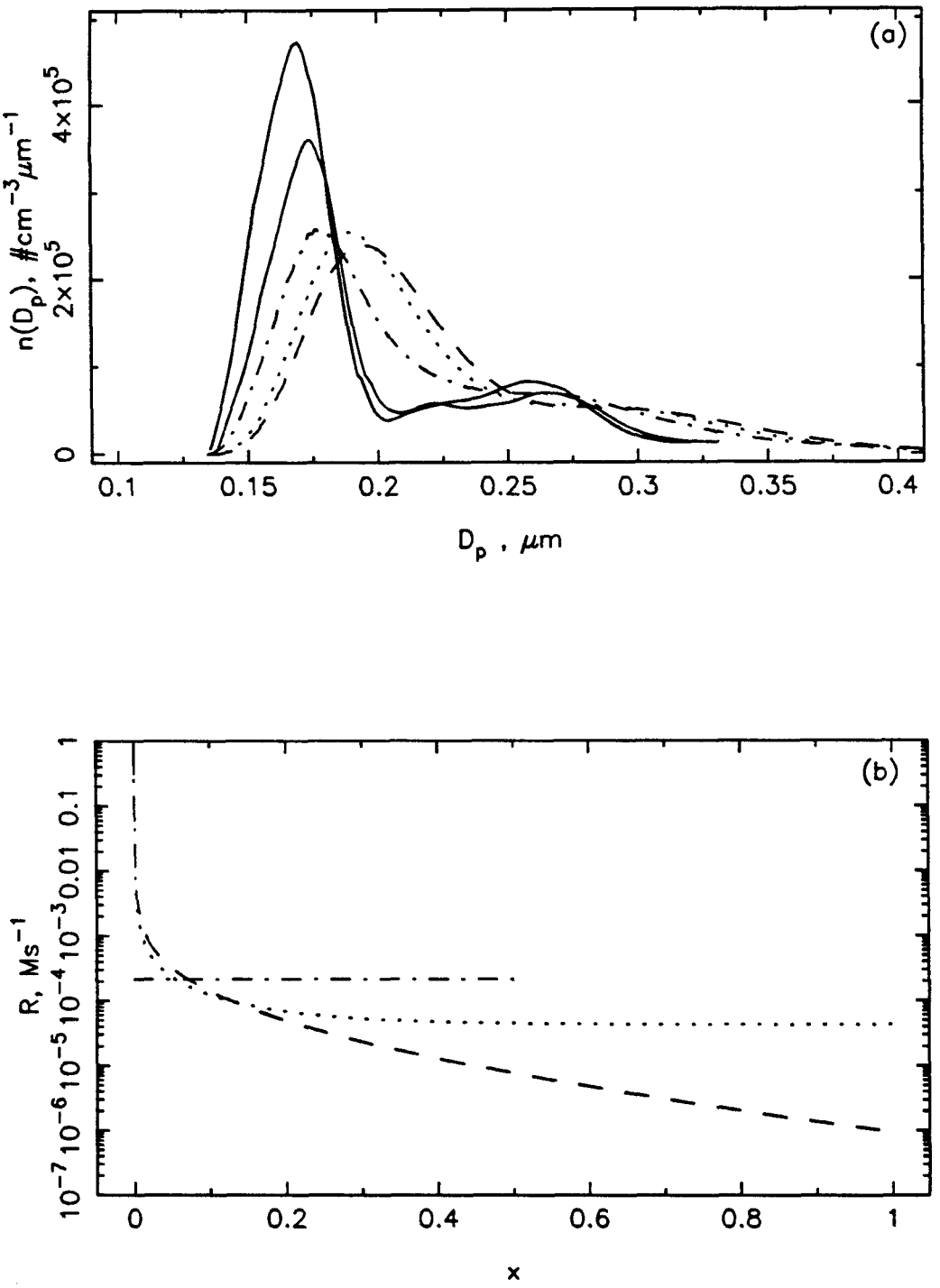

Figure 6.12 Predicted CSTR effluent distributions (a) and reaction rates (b) for Experiment 10 at T = 24.0°C, RH = 92.2%, p_{SO_2} = 1.72 ppm, $D_{p,min}$ = 0.1 μm, $D_{p,max}$ = 1.0 μm. Measured feed and effluent distributions (————). Berresheim and Jaeschke (1986) (— — — —), Crump et al. (1983a) (·····), Bronikowski and Pasiuk-Bronikowska (1981) (— · — · —).

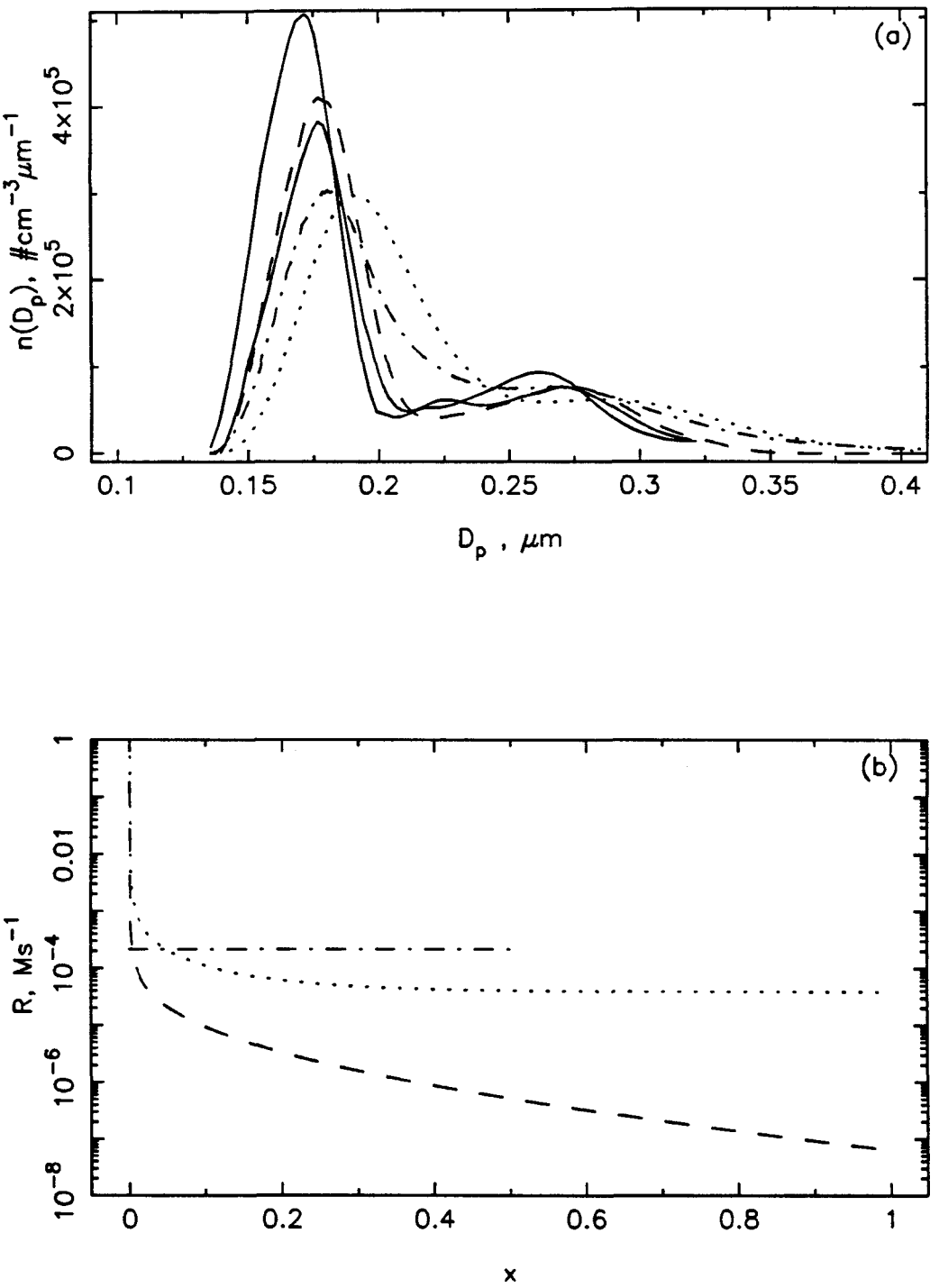

Figure 6.13 Predicted CSTR effluent distributions (a) and reaction rates (b) for Experiment 12 at T = 23.9°C, RH = 92.4%, p_{SO_2} = 0.12 ppm, $D_{p,min}$ = 0.1 μm, $D_{p,max}$ = 1.0 μm. Measured feed and effluent distributions (—————). Berresheim and Jaeschke (1986) (— — — — —), Crump et al. (1983a) (·····), Bronikowski and Pasiuk-Bronikowska (1981) (—·—·—·—).

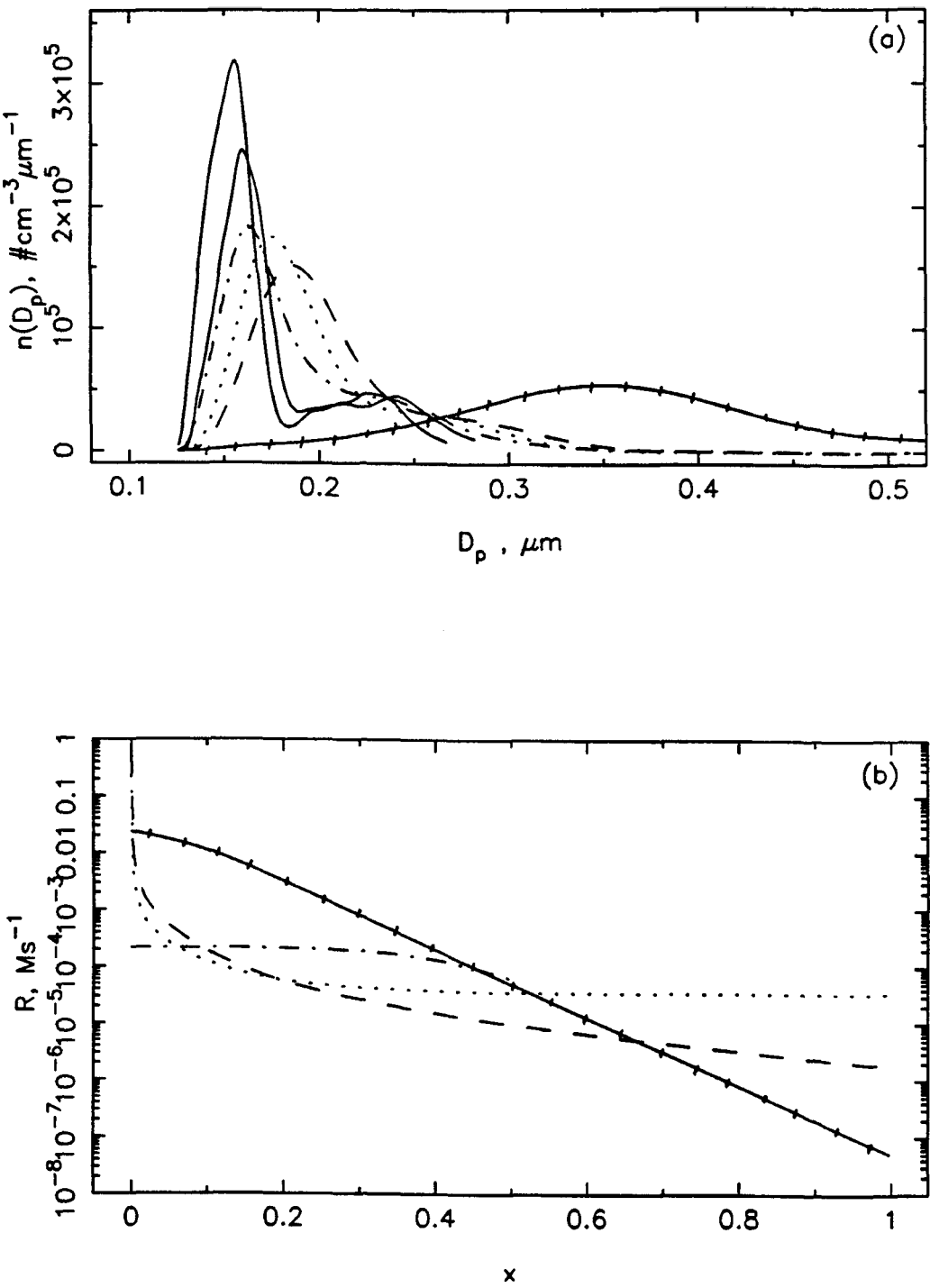

Figure 6.14 Predicted CSTR effluent distributions (a) and reaction rates (b) for Experiment 13 at T = 23.6°C, RH = 91.3%, p_{SO_2} = 13.4 ppm, 0.1 moles $MnSO_4$/ mole Na_2SO_4, $D_{p,min}$ = 0.1 μm, $D_{p,max}$ = 1.0 μm. Measured feed and effluent distributions (————). Berresheim and Jaeschke (1986) (— — — — —), Crump et al. (1983a) (·····), Bronikowski and Pasiuk-Bronikowska (1981) (—·—·—·), Martin and Hill (1987) (—·—·—·—).

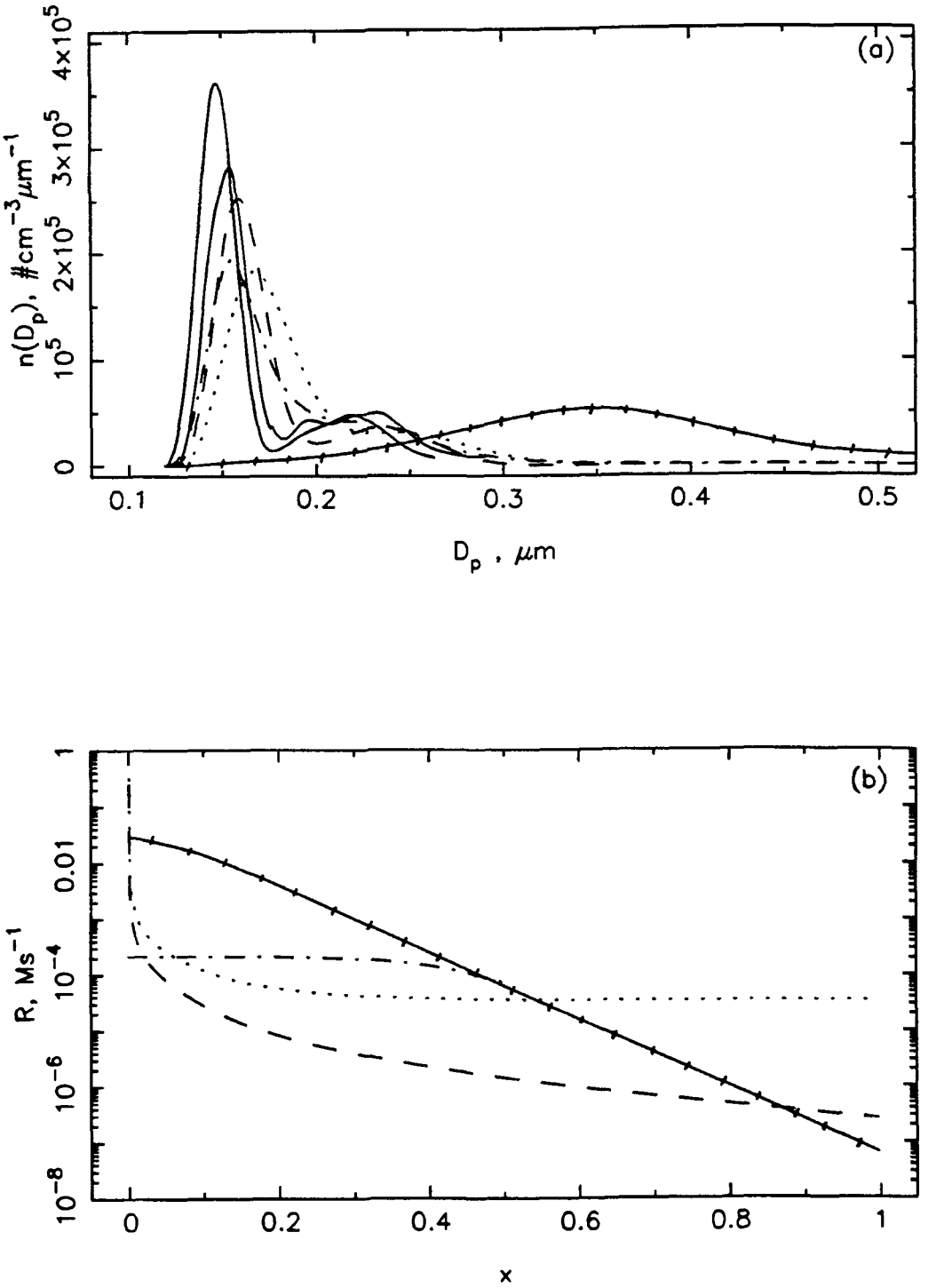

Figure 6.15 Predicted CSTR effluent distributions (a) and reaction rates (b) for Experiment 17 at T = 23.2°C, RH = 89.7%, p_{SO_2} = 1.85 ppm, 0.11 moles $MnSO_4$/ mole Na_2SO_4, $D_{p,min}$ = 0.1 μm, $D_{p,max}$ = 1.0 μm. Measured feed and effluent distributions (————). Berresheim and Jaeschke (1986) (— — — — —), Crump et al. (1983a) (· · · · · · · · · · · ·), Bronikowski and Pasiuk-Bronikowska (1981) (— · — · —), Martin and Hill (1987) (—+—+—+—).

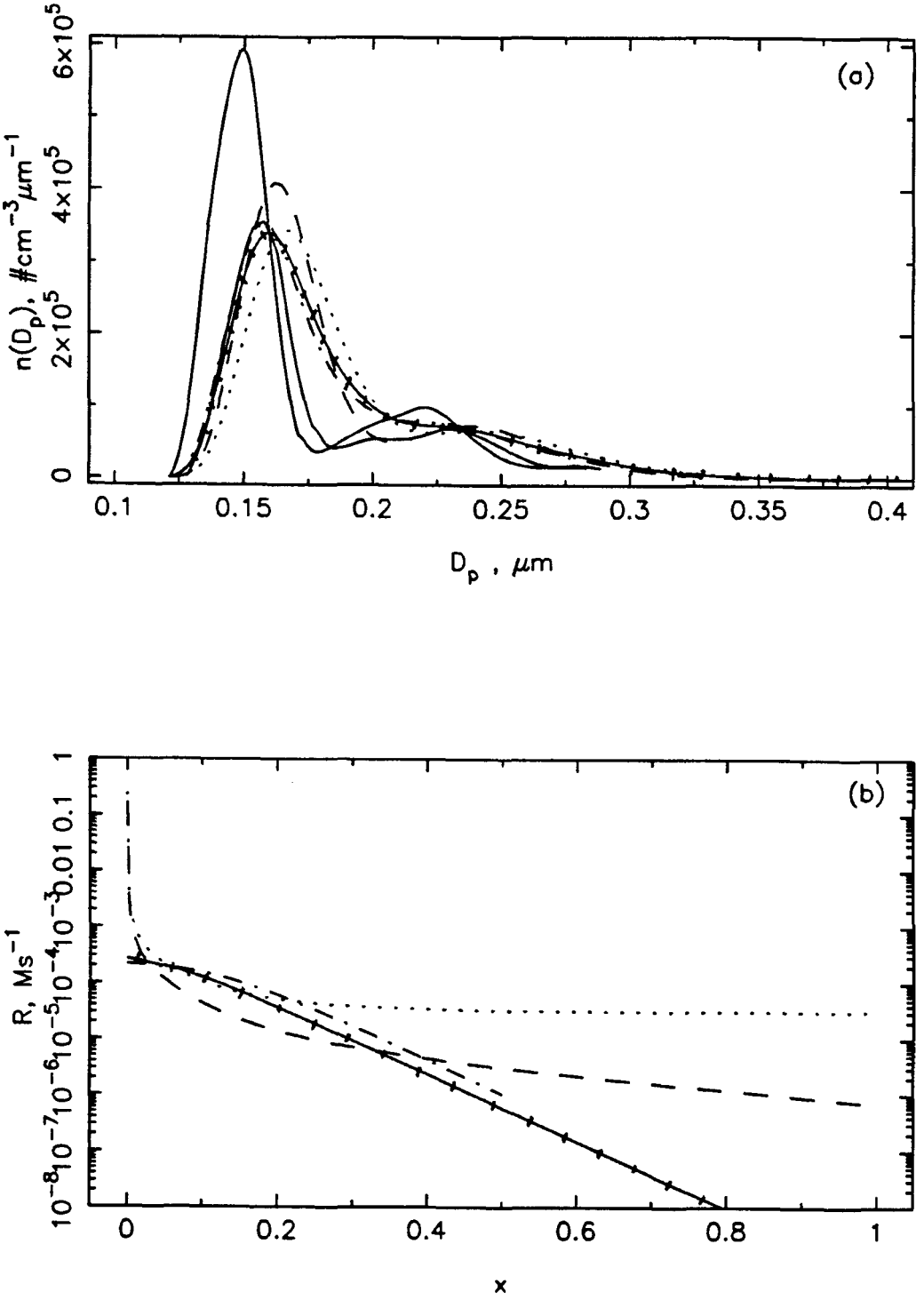

Figure 6.16 Predicted CSTR effluent distributions (a) and reaction rates (b) for Experiment 18 at T = 23.2°C, RH = 89.5%, p_{SO_2} = 13.6 ppm, 0.01 moles $MnSO_4$/ mole Na_2SO_4, $D_{p,min}$ = 0.1 μm, $D_{p,max}$ = 1.0 μm. Measured feed and effluent distributions (————). Berresheim and Jaeschke (1986) (— — — —), Crump et al. (1983a) (.....), Bronikowski and Pasiuk-Bronikowska (1981) (— · — · —), Martin and Hill (1987) (—+—+—).

$M\,s^{-1}$ at $x = 0$, lower than that of Berresheim and Jaeschke (1986) ($\sim 1.0\,M\,s^{-1}$) and Crump et al. (1983a) ($\sim 0.1 M\,s^{-1}$), and yet predicts a size distribution peak at $\sim$0.35 μm. Martin and Hill's (1987) reaction rate falls less rapidly as a function of x than do the other proposed rates. A well-defined relationship between the initial reaction rate, the rate of change of the reaction rate with x, and the amount of predicted growth, is not possible; however, it can be loosely stated that the initial reaction rate "places" the distribution along the diameter axis, and the behavior of dR/dx determines the spread and peak of the distribution.

The reaction rate expression proposed by Bronikowski and Pasiuk-Bronikowska (1981) for manganese concentrations greater than 7×10^{-4} M is a function of the manganese, S(VI), and O_2 concentrations. It was assumed that the aqueous-phase oxygen concentration was in equilibrium with the gas-phase air oxygen since diffusion limitation should not affect the oxygen transfer. For those experiments in which a pure $MnSO_4$ feed was used, the reaction rate is approximately constant — $R \sim [O_2]/1.2$ — since the S(VI) term in the denominator is multiplied by the oxygen concentration and becomes negligible relative to the square of the manganese. When a mixed $MnSO_4$-Na_2SO_4 feed with a molar ratio of 0.1 was used, the reaction rate was still approximately constant. However, a mixed feed having a molar ratio of 0.01 (Figure 6.16, Experiment 18) results in the reaction rate falling slowly as the dimensionless size x increased. This is because the significantly lower manganese concentration, which continued to fall as the size increased (see Figure G.8), allowed the S(VI) term to play a role in determining the overall rate. Only the reaction-generated acid, C_A, was attributed to the S(VI) term in the rate expression. No difference resulted in the predicted effluent distribution when S(VI) $= C_A + C_M + C_N$ was used because of the large influence of the second order manganese terms and the small O_2 concentration.

The second-order manganese rate expression of Martin and Hill (1987) was used in these predictions (see Table 4.1). It is claimed that this expression is valid

when [S(IV)] > 10^{-4} molal (note that for dilute solutions molar ~ molal). The plots in Appendix G indicate that the S(IV) concentration typically ranged from 10^{-6} to 10^{-4} molal as a result of the high H^+ concentration. Unfortunately, this is precisely the range of S(IV) concentrations for which Martin and Hill (1987) have not specified a rate expression and in fact, they claim that the reaction rate constant is dependent on the initial sulfur concentration even though the rate is zero order in S(IV). Therefore, when considering the results of Martin and Hill (1987), it should be remembered that the rate expression was used in a concentration regime for which it was not intended. This is often the case in aerosol studies, however, since the available kinetic rate expressions are frequently determined at concentrations typical of cloud and fogwater.

The total number concentrations of the experimentally measured feed and effluent aerosol and the total effluent number concentration predicted by each of the rate expressions are shown in Table 6.1. The predicted total number agrees to within 3% among the various rate expressions. This is not surprising since only wall deposition is being considered and the range of particle sizes, even for the poorest match of predicted and experimental distribution, is narrow enough that the deposition coefficient does not change significantly. The agreement between the experimentally measured and theoretically predicted number concentration varies from approximately 2% for Experiment 17 to 37% for Experiment 18. In general, the difference between measured and predicted total number was about 10% and the predicted number was greater than the measured concentration. There is little correlation between the accuracy of the total number and peak diameter predictions. Some of the difference in the total number concentrations can be attributed to the teflon lines carrying the aerosol from the feed bypass to the reactor and back again (see Figure 2.1). This is the only difference between the feed and effluent aerosol flow paths. Line loss due to convectional diffusion is negligible. Pui (1987) has studied the deposition of charged aerosol in teflon lines and found the phenomenon to be quite complicated — the losses depending not only on particle

Table 6.1

Experimental and Predicted Particle Total Number

Expt	Measured Feed	Measured Effluent	Berresheim & Jaeschke (1986)	Bronikowski & Pasiuk-Bronikowska (1981)	Crump et al. (1983a)	Martin & Hill (1987)
5	18270	16450	16940	17060	17090	—
8	20720	17570	19400	18860	19090	—
9	21620	17860	19900	19830	19750	—
10	22330	18180	20480	20120	20350	—
12	24450	19510	21820	22780	22790	—
13	12080	10570	11450	11410	11420	11320
17	11590	10960	10660	10700	10840	10820
18	21650	14760	20220	20240	20330	20260

diameter and flowrate, but also on time and the amount of bending the tubing has undergone, which affected the electric field associated with the tubing. In any event, as was shown in the "blank" runs, Experiments 1 and 2, the feed and effluent distributions are not affected to the extent that a shift in the distribution is observed.

The predicted effluent distributions exhibited in Figures 6.9 through 6.16 show that Bronikowski and Pasiuk-Bronikowska's (1981) rate expression consistently predicted the correct peak diameter, although the predicted size distributions display more broadening due to the CSTR residence time distribution than was observed experimentally. For all intents and purposes, the SO_2 oxidation rate of Bronikowski reduces to a constant on the order of 2×10^{-4} $M s^{-1}$ for the experimental conditions used here. Comparison between the predicted size distributions using the rate expression of Berresheim and Jaeschke (1986) and those observed improved as the SO_2 concentration was decreased. In the case of Experiment 12 (Figure 6.13), the measured distribution was predicted exactly. Particularly noteworthy is the fact that the SO_2 concentration used in Experiment 12 was 0.122 ppm, the highest concentration that Berresheim and Jaeschke (1986) used in fitting their rate expression. This could mean one of several things. The amount of growth/reaction at higher SO_2 concentrations (> 1 ppm) does not continue at the same rate as for lower concentrations. Or, an inhibitor in the experimental CSTR system prevented the observation of the expected growth at the higher SO_2 concentrations. Unfortunately, it was not possible to run experiments at SO_2 concentrations less than 0.1 ppm to determine whether or not the distribution predicted by Berresheim and Jaeschke's (1986) rate expression continued to match the measured distribution in the SO_2 concentration regime at which their study was conducted.

The experiments carried out made with a mixed Na_2SO_4-$MnSO_4$ feed did not result in effluent distributions significantly different from those obtained using a pure $MnSO_4$ feed. This observation was confirmed by the results calculated

using Bronikowski and Pasiuk-Bronikowska's (1986) rate expression. With the significantly lower manganese concentration of Experiment 18 ([Mn(II)] $< 10^{-2}$ molal), the rate expression of Martin and Hill (1987) gave a reasonable prediction of the effluent distribution, although the manganese concentrations of Experiments 13 and 17 ([Mn(II)] < 0.2 molal) were still sufficiently high that growth was grossly overpredicted.

The nature of the aerosol distribution out of the CSTR given a particular rate expression is more easily observed if a monodisperse feed is used. Figure 6.17 presents the resulting effluent distributions obtained for Experiments 5, 9, 12, 13, and 18, if a feed of 10^4 particles/cm^3 having diameter 0.15 μm is used. The strong sensitivity of Berresheim and Jaeschke's (1986) rate expression to the SO_2 concentration is apparent from the results of Experiments 5 and 12. The relative humidity was approximately equal for the two runs, but p_{SO_2} was 50 and 0.122 ppm for Experiments 5 and 12, respectively. The predicted effluent distribution peak shifts from $\sim$ 0.25 μm to 0.16 μm as the SO_2 concentration decreases. Decreasing the manganese concentration while maintaining a constant SO_2 concentration had less of an effect on the predicted effluent distribution. Basically, Berresheim and Jaeschke's (1986) rate expression (see Table 4.1) reduces to $R \sim \alpha p_{SO_2}$ at high H^+ concentrations. Martin and Hill's (1987) rate expression, on the other hand, is a strong function of the manganese concentration — second order. As the manganese concentration is dropped by a factor of 100 in Experiment 18, the reaction rate decreases to the extent that a significant fraction of the feed particles experience negligible growth and the effluent distribution resembles an exponential decay curve. For those experiments in which a pure manganese feed was used, Martin and Hill's (1987) rate expression resulted in unreasonable shifts of the effluent distribution along the diameter axis. As mentioned earlier, the rate expression of Bronikowski and Pasiuk-Bronikowska (1981) results in an approximately constant rate value. The reaction rate was slow enough that a large fraction of the feed particles experienced negligible growth. The effluent distribution is approximately

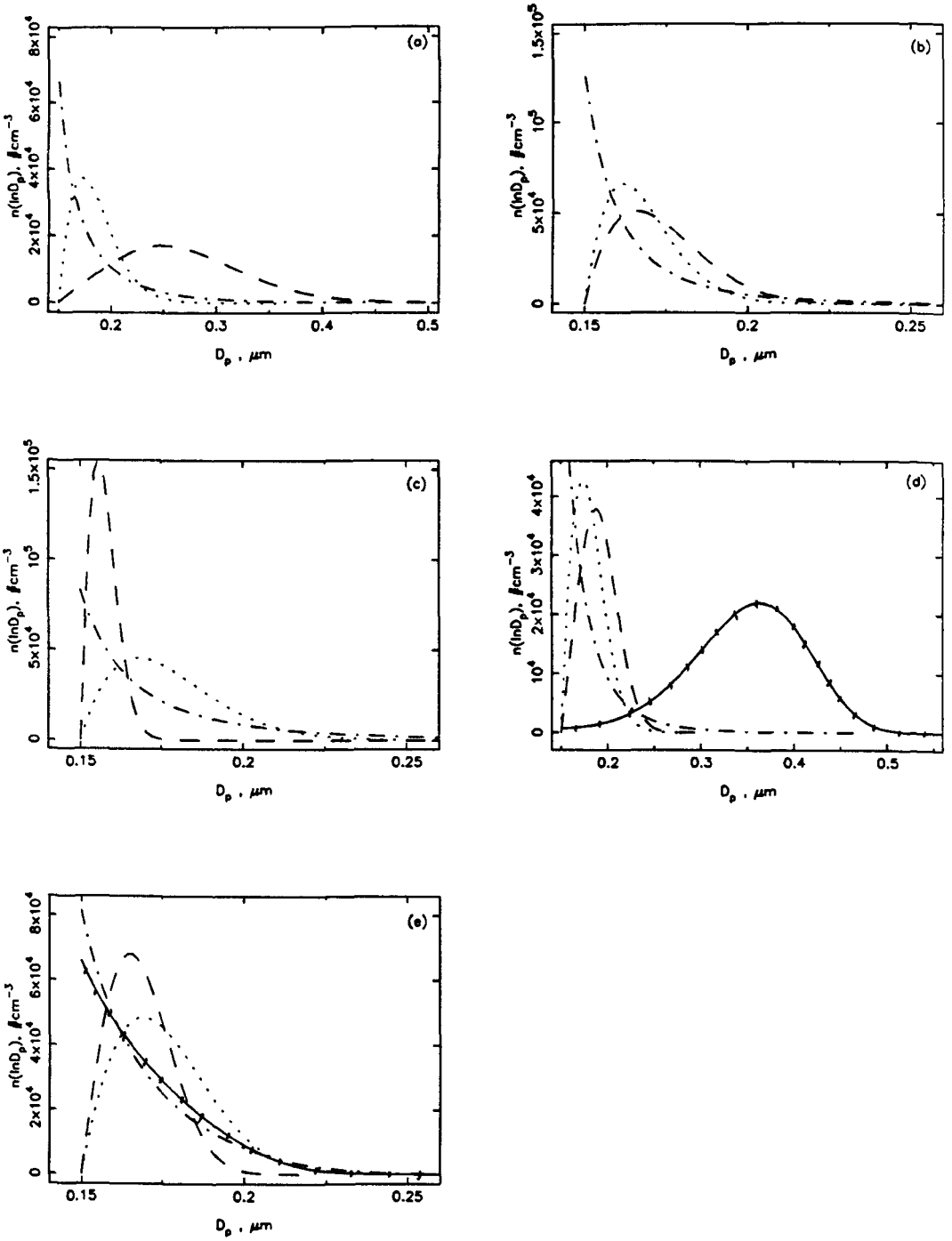

Figure 6.17 Predicted effluent distributions given a monodisperse feed of 0.15 μm, 10^4 particles/cm^3. $D_{p,min}$ = 0.1 μm and $D_{p,max}$ = 1 μm. Rate expressions of Berresheim and Jaeschke (1986) (— — — —), Crump et al. (1983a) (·····), Bronikowski and Pasiuk-Bronikowska (1981) (—·—·—·), and Martin and Hill (1987) (—•—•—•—). CSTR conditions: (a) Expt. 5, (b) Expt. 9, (c) Expt. 12, (d) Expt. 13, and (e) Expt. 18.

constant regardless of the reaction conditions used in this study.

In Chapter 4, Figure 4.5, the value of $R/[\mathrm{Mn(II)}]^2$ was shown for the aerosol studies presented in Table 4.1. The data fell in a region significantly below the values predicted by Martin and Hill's (1987) rate constant expression — 10^{-5} $\mathrm{M^{-1}s^{-1}} < R/[\mathrm{Mn(II)}]^2 < 10^{-2}$ $\mathrm{M^{-1}s^{-1}}$ as opposed to approximately 1 $\mathrm{M^{-1}s^{-1}}$ at $I \sim 10$ M. Given the reaction rate of Bronikowski and Pasiuk-Bronikowska (1986), the values of $R/[\mathrm{Mn(II)}]^2$ were plotted for the initial conditions ([Mn(II)] at $x = 0$) for each of the experiments discussed in this chapter (see Figure 6.18). For Experiments 5, 8, 9, 10 and 12 (pure manganese feed), the values range from 2 to 3 $\times 10^{-5}\mathrm{M^{-1}s^{-1}}$, while for Experiments 13 and 17 (0.1 moles $MnSO_4$/mole Na_2SO_4), the values are approximately 5 to 7 $\times 10^{-3}$ $\mathrm{M^{-1}s^{-1}}$. The value of $R/[\mathrm{Mn(II)}]^2$ for Experiment 18 (0.01 moles $MnSO_4$/mole Na_2SO_4) is 0.5 $\mathrm{M^{-1}s^{-1}}$. Since a constant value of R is being assumed, the value of $R/[\mathrm{Mn(II)}]^2$ will increase with increasing x. This also corresponds to a decreasing value of I. However, it was argued earlier that the initial rate and smaller dimensionless sizes have the greatest impact on the resulting distribution, so only those values are plotted in Figure 6.18. Naturally, the location of the "experimental" points on this graph depends strongly on the reaction rate used in the calculation. Since the reaction rate of Bronikowski and Pasiuk-Bronikowska (1981) was the lowest at $x = 0$ of those rate expressions tested, the value of $R/[\mathrm{Mn(II)}]^2$ would only increase, were one of the other possible initial rates used. Given this initial reaction rate, which does reasonably well at predicting the observed CSTR effluent distribution, those experiments in which a pure $MnSO_4$ feed was used fall into the same region of the plot as do previous aerosol studies — if any inhibition was present, it did not reduce the reaction rate to the extent that the data were completely dissimilar from that of other researchers. As the manganese concentration was decreased, the values $R/[\mathrm{Mn(II)}]^2$ approached those determined by Martin and Hill (1987) in a bulk-phase study using dilute $MnCl_2$ solutions.

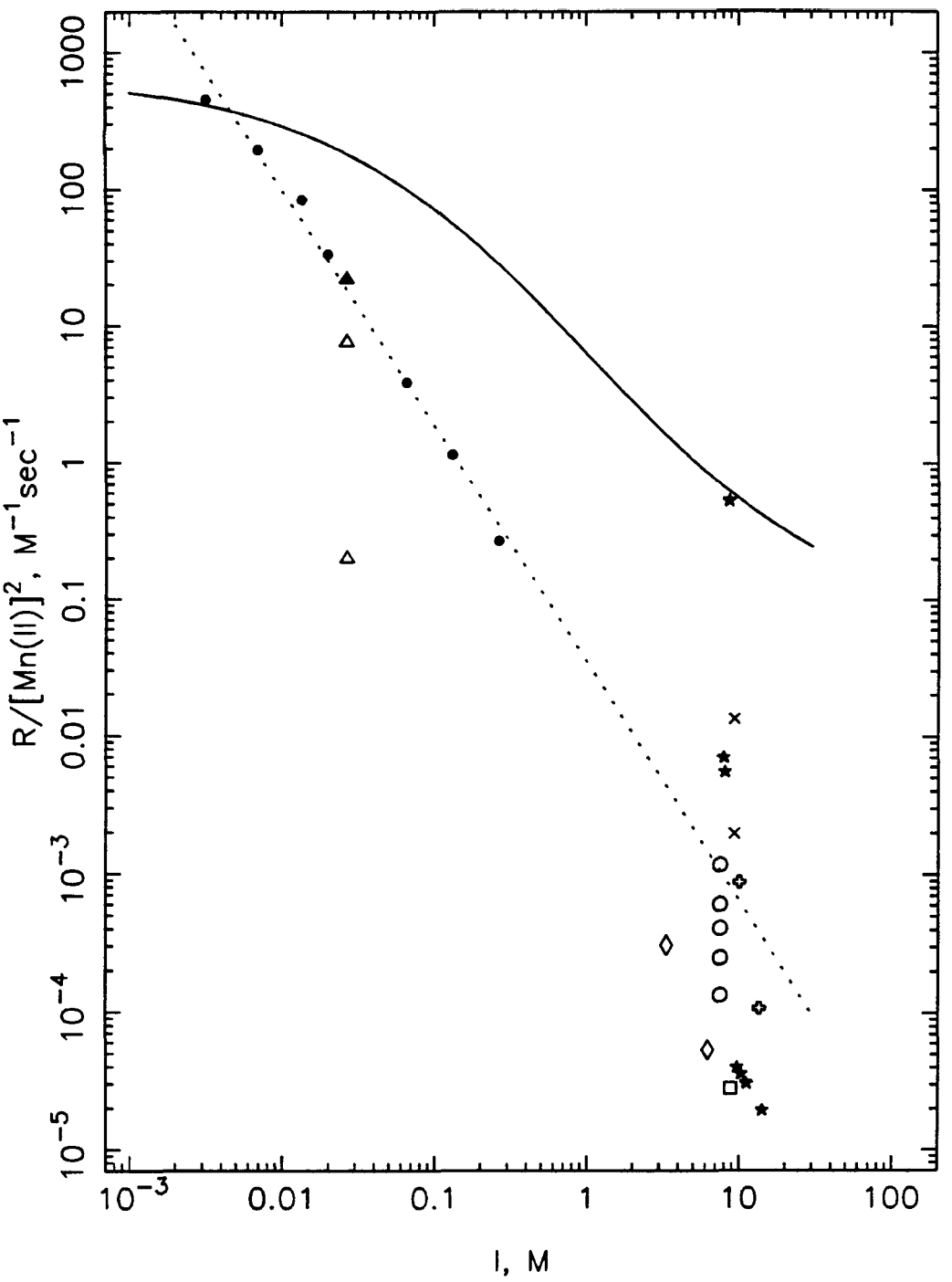

Figure 6.18 Second-order manganese rate constant as a function of ionic strength. Martin and Hill (1987) (————) and Coughanowr and Krause (1965) (•). Reaction rate of 2×10^4 $M^{-1}s^{-1}$ and [Mn(II)] at $x = 0$ for Experiments 5, 8, 9, 10, 12, 13, 17, and 18 ($\star$). See caption of Figure 4.5 for description of additional symbols.

§6.5 Atmospheric Conversion Rate of SO_2

The experiments described in this work were performed at conditions intended to replicate those of a polluted urban atmosphere or plume. Indeed, SO_2 concentrations ranging from 0.1 to 5 ppm have been measured in power plant plumes (Johnson et al., 1979) and SO_2 concentrations in an urban environment range from 1 to 100 ppb (e.g., Appel (1978), McMurry and Wilson (1983)). The average liquid water content in the experiments reported here was approximately 100 μg H_2O/m^3 air. This value is typical of aerosols, where $L = 10^{-11} - 10^{-10}$ or $10 - 100$ μg H_2O/m^3 air (Seinfeld, 1986). The mass loading of manganese in the reactor feed aerosol ranged from 10 to 30 $\mu g/m^3$ air for the pure manganese sulfate aerosol and from 0.1 to 0.3 $\mu g/m^3$ for the case of 0.01 moles $MnSO_4$/mole Na_2SO_4. The global atmospheric manganese mass loading ranges from 0.02 to 0.17 $\mu g/m^3$ (Lee and von Lehmden, 1973). Although the concentration of manganese in fog (e.g., $\sim$ 10 μM, Munger et al. (1983)) and rain (e.g., $\sim$ 0.4 μM, Penkett et al. (1979)) water exist, measurements of the concentration of manganese in aqueous atmospheric aerosols do not. The soluble fraction of atmospheric manganese has been estimated to range from 20 (Barrie and Georgii, 1976) to 90% (Beilke and Gravenhorst, 1978) of the total manganese. Since 100% of the manganese in the CSTR experiment was soluble, the manganese levels were approximately 100 times those expected in the ambient aerosols. On the other hand, the ionic strength of ambient aerosol is estimated to be on the order of 10 molal (Stelson and Seinfeld, 1981) — equivalent to those of deliquescent pure salts. If a soluble manganese mass loading of 0.055 $\mu g/m^3$ is assumed, then the concentration of manganese in solution is of the order 0.01 molal given a water content of 0.1 mg/m^3. Only those CSTR experiments in which a $MnSO_4$-Na_2SO_4 molar ratio of 0.01 was used have initial manganese concentrations of this magnitude. Therefore, while the experiments using a pure $MnSO_4$ aerosol are "representative" of atmospheric aerosol, those experiments in which a $MnSO_4$-Na_2SO_4 aerosol was used actually approach atmospheric conditions.

The percent conversion of SO_2 can be written as,

$$\%\,\mathrm{hr}^{-1} = 3.6 \times 10^5\, R\, \frac{L\, R_{gas}\, T}{p_{SO_2}}, \tag{36}$$

where L is the aerosol water content ($\ell\, H_2O/\ell$ air) and R is the reaction rate ($M\,s^{-1}$). If an average reaction rate of 2×10^{-4} $M\,s^{-1}$ is assumed, the percent conversion ranges from 1.76%/hr to 0.02%/hr for SO_2 concentrations of 0.1 ppm to 10 ppm, respectively, and an atmospheric water content of 10^{-10} $\ell H_2O/\ell$air (0.1 mg H_2O/m^3 air). If the same conditions ($L = 10^{-10}$ and p_{SO_2} = 0.1 to 10 ppm) are assumed along with a manganese concentration of 55 ng/m^3 ($m_{MnSO_4} \sim 0.01$ molal), Martin and Hill's (1987) rate expression gives percent conversions of 5.5 to 0.055%/hr and 0.5 to 0.005%/hr for ionic strengths of 1 and 10 M, respectively. At these same conditions, Berresheim and Jaeschke's (1986) expression results in a conversion rate of 1.8%/hr at a pH of 3. Since Berresheim and Jaeschke's (1986) reaction rate holds for low SO_2 concentrations, this value might not be expected to be correct at 10 ppm. Clearly, the basic trends (decreasing conversion with increasing SO_2) and values of the rate of conversion are similar. Measured rates of overall atmospheric SO_2 conversion range from 0 to 10%/hr (see Table 5.1 in Seinfeld, 1986) and the relative importance of the oxidation of SO_2 by O_2, catalyzed by dissolved manganese in aerosols versus aqueous SO_2 oxidation by H_2O_2 or O_3, for example, depends on the atmospheric conditions (e.g., Hoffmann and Jacob (1984), Hoffmann and Calvert (1985), Saxena and Seigneur (1987)). The formation of S(VI) via reaction affects the subsequent behavior of the aerosol and its role in the atmosphere.

CHAPTER 7

CONCLUSIONS AND RECOMMENDATIONS FOR FUTURE WORK

The current studies were carried out not to determine a fundamental reaction rate expression for the manganese system, but rather to investigate whether or not, in a model typical of the type used in atmospheric studies involving both aerosol thermodynamics and kinetics, aerosol growth could be adequately predicted by the existing reaction rate expressions. Particle growth is a parameter often used in field or smog chamber studies to track the extent of reaction. Since many of the previous aerosol-phase investigations suffer from errors made in the measurement of the humid aerosol size, care was taken to ensure that minimal biasing of the size distribution occurred within the electrostatic mobility classifier being used for the measurements. The experimental studies were performed at relative humidities ranging from 86 to 94% and SO_2 concentrations of 0.1 to 50 ppm in an ideal continuous stirred tank reactor. Either a pure $MnSO_4$ or mixed Na_2SO_4-$MnSO_4$ feed aerosol was used, resulting in initial manganese concentrations of approximately 0.02 to 3.5 molal.

A slow, approximately constant reaction rate (Bronikowski and Pasiuk-Bronikowska, 1981) was found to best predict the observed growth over the entire range of conditions used in this study. However, as the CSTR operating conditions approach those used by Berresheim and Jaeschke (1986) (low p_{SO_2}) in the determination of the rate expression, their rate expression correctly predicts the CSTR effluent distribution. Similarly, at the lowest manganese concentrations used in these experiments (0.01 moles $MnSO_4$/mole Na_2SO_4), the rate expression of Martin and Hill (1987), which was measured in bulk-phase experiments at low concentrations of $MnCl_2$, correctly predicts the effluent growth.

The results of the CSTR model indicate that the various proposed rate expressions for the oxidation of SO_2 as catalyzed by manganese differ considerably. Atmospheric models that include this pathway for SO_2 oxidation will be strongly affected by the particular rate expression chosen. In addition, the results discussed in the previous paragraph lead towards the conclusion that extending the use of rate expressions beyond the range of conditions for which they were determined could result in erroneous predictions. If this is indeed so, the case for performing aerosol chemistry studies in both the droplet and bulk phase still stands — rate expressions determined in typical dilute solution, bulk-phase experiments will not adequately represent a concentrated deliquesced salt aerosol. Table 7.1 presents a general comparison of the advantages and disadvantages of the bulk- and droplet-phase experiments used to study aerosol chemistry. Quite clearly, the disadvantages, or potential problems, associated with a droplet-phase study exceed those associated with a bulk-phase study. These problems are typically instrumental, not fundamental, in nature. However, a bulk-phase experiment will never be fully able to model a particulate system since the behavior and properties of a droplet (e.g., surface tension, diffusion of the gaseous species *to* the droplet, etc.) are not included.

Basically, then, the state of aerosol chemistry is such that bulk-phase studies are inadequate because of their neglect of the effect of particle microphysics and the low concentrations typically used, and droplet-phase studies produce results that are generally inferior and incomplete when compared to similar bulk-phase studies because of the instrumentation and control problems associated with such an experiment. It appears that a new method is needed to study aerosol growth and reaction — one that uses droplets instead of bulk solution, but also eliminates the array of aerosol generating equipment, measuring instruments, flow lines, etc., that are currently required for droplet-phase studies. It is suggested that the electrodynamic balance, or quadrupole, could be used in this capacity. In an electrodynamic balance, a single particle is suspended in an electric field in a small, confined cham-

Table 7.1

Comparison of Methods Used to
Study Aerosol Chemistry

	Typical Measurements	Advantages	Disadvantages
Droplet-Phase Studies	Diameter growth SO_2 uptake filter samples	Interaction of physics and chemistry typical of atmosphere. Mass transfer limitation unlikely.	Large experimental apparatus — difficult to define and control. Chemical composition of individual particles unknown. Indirect measurements of reaction used. Sample biasing (filters or equipment) difficult to control.
Bulk-Phase Studies	S(VI) production S(IV) production pH	Well-defined reaction system. Direct measurement of product and feed composition.	Chemical and physical behavior separated. Potential mass transfer problems.

ber. This device offers the benefits of studying an actual aerosol particle, but avoids much of the handling and apparatus needed to generate and maintain an aerosol flow. The balance could simply be used to measure growth (mass changes) as a function of time and (much) later, perhaps, to spectroscopically follow the progress of reaction. One might anticipate that ensuring a sufficient supply of the reacting gas without significantly perturbing the droplet would involve some care.

As this study progressed, it became apparent that there is a serious deficit of water activity and activity coefficient data for atmospherically relevant systems. This is particularly true for mixtures. The fields of aqueous-phase atmospheric chemistry and modeling rest, then, upon a foundation of mixing rules. Since a mixing rule is basically just an empirical formula, the assumption that they adequately model complicated atmospheric solutions is unverified. The electrodynamic balance has been used to obtain water activity and activity coefficient data for several salts and salt mixtures. While the data are not as accurate as those obtained from isopiestic studies, they can be generated more readily, and results at ionic strengths typical of aerosols are obtained. It is recommended that the generation of thermodynamic data using the electrodynamic balance be continued. Studies of sulfuric acid-salt mixtures should be done, if possible, since these systems are particularly relevant in the atmosphere.

REFERENCES

AGARWAL, J. K. and SEM, G. J. (1980) Continuous flow, single-particle-counting condensation nucleus counter. *J. Aerosol Sci.*, **11**:343-357.

APPEL, B. R., KOTHNY, E. L., HOFFER, E. M., HIDY, G. M. and WESOLOWSKI, J. J. (1978) Sulfate and nitrate data from the California Aerosol Characterization Experiment (ACHEX). *Environ. Sci. & Tech.*, **12**:418-425.

BAES, C. F. and MESMER, R. E. (1976) *The Hydrolysis of Cations.* John Wiley & Sons, New York.

BARRIE, L. A. and GEORGII, H. W. (1976) An experimental investigation of the absorption of sulfur dioxide by water drops containing heavy metal ions. *Atmos. Environ.*, **10**:743-749.

BASSETT, H. and PARKER, W. G. (1951) The oxidation of sulfurous acid. *J. Chem. Soc.*, **1951**:1540-1560.

BENNETT, C. O. and MYERS, J. E. (1974) *Momentum, Heat, and Mass Transfer (2nd ed.).* McGraw-Hill Book Co., New York.

BERRESHEIM, H. and JAESCHKE, W. (1986) Study of metal aerosol systems as a sink for atmospheric SO_2. *J. Atmos. Chem.*, **4**:311-334.

BIELKE, S. and GRAVENHORST, G. (1978) Heterogeneous SO_2-oxidation in the droplet phase. *Atmos. Environ.*, **12**:231-239.

BISWAS, P., JONES, C. L. and FLAGAN, R. C. (1987) Distortion of size distributions by condensation and evaporation in aerosol instruments. Accepted for publication in *Aerosol Sci. Tech.*.

BRADFORD, E. B. and VANDERHOFF, J. W. (1955) Electron microscopy of monodisperse latexes. *J. Applied Phys.*, **26**:864-871.

BRONIKOWSKI, T. and PASIUK-BRONIKOWSKA, W. (1981) The rate for SO_2 autoxidation in aqueous $MnSO_4$ solutions containing H_2SO_4. *Chem. Engr. Sci.*, **32**:215-219.

CAINS, P. W. and CARABINE, M. D. (1978) Oxidation of sulfur dioxide in aerosol droplets, catalyzed by manganous sulfate. *J. Chem. Soc. Faraday I*, **74**:2689-2702.

CASS, G. R. (1975) *Dimensions of the Los Angeles* SO_2*/sulfate problem.* Memo **15**, Environ. Quality Lab., California Inst. of Tech., Pasadena, California.

CHENG, R. T., CORN, M. and FROHLIGER, J. O. (1971) Contribution to the reaction kinetics of water soluble aerosols and SO_2 in air at ppm concentrations.

Atmos. Environ., **5**:987-1008.

CLARKE, A. G. and RADOJEVIC, M. (1983) Chloride ion effects on the aqueous oxidation of SO_2. *Atmos. Environ.*, **3**:617-624.

CLARKE, A. G. and WILLIAMS, P. T. (1983) The oxidation of sulfur dioxide in electrolyte droplets. *Atmos. Environ.*, **3**:607-615.

COHEN, M. D., FLAGAN, R. C. and SEINFELD, J. H. (1987a) Studies of concentrated electrolyte solutions using the electrodynamic balance. I. Water activities for single-electrolyte solutions. *J. Phys. Chem.*, in press.

COHEN, M. D., FLAGAN, R. C. and SEINFELD, J. H. (1987b) Studies of concentrated electrolyte solutions using the electrodynamic balance. II. Water activities for mixed-electrolyte solutions. *J. Phys. Chem.*, in press.

COUGHANOWR, D. R. and KRAUSE, F. E. (1965) The reaction of SO_2 and O_2 in aqueous solutions of $MnSO_4$. *Ind. Engr. Chem. Fund.*, **4**:61-66.

CRUMP, J. G. (1983) *Aerosol deposition, growth, and dynamics in the continuous stirred tank reactor.* Ph.D. Thesis, Chem. Engr. Dept., California Inst. of Tech., Pasadena, California.

CRUMP, J. G. and SEINFELD, J. H. (1981) Turbulent deposition and gravitational sedimentation of an aerosol in a vessel of arbitrary shape. *J. Aerosol Sci.*, **12**:405-415.

CRUMP, J. G., FLAGAN, R. C. and SEINFELD, J. H. (1983a) An experimental study of the oxidation of sulfur dioxide in aqueous manganese sulfate aerosols. *Atmos. Environ.*, **17**:1277-1289.

CRUMP, J. G., FLAGAN, R. C. and SEINFELD, J. H. (1983b) Particle wall loss rates in vessels. *Aerosol Sci. Tech.*, **2**:303-309.

ERIKSEN, T. E. (1969) Diffusion studies in aqueous solutions of sulfur dioxide. *Chem. Engr. Sci.*, **24**:273-278.

FREIBERG, J. E. and SCHWARTZ, S. E. (1981) Oxidation of SO_2 in aqueous droplets: Mass-transport limitation in laboratory studies and the ambient atmosphere. *Atmos. Environ.*, **15**:1145-1154.

HAGEN, D. E. and ALOFS, D. J. (1983) Linear inversion method to obtain aerosol size distributions from measurements with a differential mobility analyzer. *Aerosol Sci. Tech.*, **2**:465-475.

HÄNEL, G. (1976) The properties of atmospheric aerosol particles as functions of the relative humidity at thermodynamic equilibrium with the surrounding moist air. *Adv. in Geophysics*, **19**:73-188.

HIDY, G. M. (1982) Evidence for heterogeneous reactions in the atmosphere,

in *Heterogeneous Atmospheric Chemistry* (D. R. Schryer, ed.). American Geophysical Union, Washington, D.C., 204-214.

HIRSCHFELDER, J. O., CURTISS, C. F. and BIRD, R. B. (1964) *Molecular Theory of Gases and Liquids.* John Wiley & Sons, New York.

HOFFMANN, M. R. and BOYCE, S. D. (1983) Catalytic autoxidation of aqueous sulfur dioxide in relationship to atmospheric systems, in *Trace Atmospheric Constituents* (S. E. Schwartz, ed.). John Wiley & Sons, New York, pp. 147-190.

HOFFMANN, M. R. and CALVERT, J. G. (1985) *Chemical transformation modules for eulerian acid deposition models. Volume II: The aqueous-phase chemistry.* Acid Deposition Modeling Project, NCAR.

HOFFMANN, M. R. and JACOB, D. J. (1984) Kinetics and mechanisms of the catalytic oxidation of dissolved sulfur dioxide in aqueous solution: An application to nighttime fog water chemistry, in SO_2, NO *and* NO_2 *Oxidation Mechanisms: Atmospheric Considerations* (J. G. Calvert, ed.). Butterworth Publishers, Boston, pp. 101-172.

HOPPEL, W. A. (1978) Determination of the aerosol size distribution from the mobility distribution of the charged fraction of aerosols. *J. Aerosol Sci.*, **9**:41-54.

HOPPEL, W. A. and FRICK, G. M. (1986) Ion-aerosol attachment coefficients and the steady-state charge distribution on aerosols in a bipolar ion environment. *Aerosol Sci. Tech*, **5**:1-21.

HOUGH, A. M. (1987) A computer modeling study of the chemistry occurring during cloud formation over hills. *Atmos. Environ.*, **21**:1073-1095.

HUSS, JR., A., LIM, P. K. and ECKERT, C. A. (1982a) Oxidation of aqueous sulfur dioxide. 1. Homogeneous manganese(II) and iron(III) catalysis at low pH. *J. Phys. Chem.*, **86**:4224-4228.

HUSS, JR., A., LIM, P. K. and ECKERT, C. A. (1982b) Oxidation of aqueous sulfur dioxide. 2. High-pressure studies and proposed reaction mechanisms. *J. Phys. Chem.*, **86**:4229-4233.

IBUSUKI, T. and BARNES, H. M. (1984) Manganese(II) catalyzed sulfur dioxide oxidation in aqueous solution at environmental concentrations. *Atmos. Environ.*, **18**:145-151.

JAESCHKE, W. (1986) Multiphase atmospheric chemistry, in *Chemistry of Multiphase Atmospheric Systems* (W. Jaeschke, ed.). Springer-Verlag, New York, pp. 3-40.

JOHNSON, F. G., CONOLLY, J. L., EVANS, R. B. and ZELLER, T. M. (1979) *Airborne measurements of power plant plumes in West Virginia.* EPA-600/4-79-043.

KAPLAN, D. J., HIMMELBLAU, D. M. and KANAOKA, C. (1981) Oxidation of sulfur dioxide in aqueous ammonium sulfate aerosols containing manganese as a catalyst. *Atmos. Environ.*, **15**:763-773.

KNUTSON, E. O. and WHITBY, K. T. (1975) Aerosol classification by electrical mobility: apparatus, theory, and applications. *J. Aerosol Sci.*, **6**:443-451.

KOUSAKA, Y., OKUYAMA, K. and ENDO, Y. (1981) Calibration of differential mobility analyser by visual method. *J. Aerosol Sci.*, **12**:339-348.

KOUSAKA, Y., ADACHI, M., OKUYAMA, K., KITADA, N. and MOTOUCHI, T. (1983) Bipolar charging of ultrafine aerosol particles. *Aerosol Sci. Tech*, **2**:421-427.

KOUSAKA, Y., OKUYAMA, K. and ADACHI, M. (1985) Determination of particle size distribution of ultra-fine aerosols using a differential mobility analyzer. *Aerosol Sci. Tech.*, **4**:209-225.

KUSIK, C. L. and MEISSNER, H. P. (1978) Electrolyte activity coefficients in inorganic processing. *Amer. Inst. Chem. Engr. Symp. Ser.*, **74(173)**:14-20.

LEE, R. E. and VON LEHMDEN, D. J. (1973) Trace metal pollution in the environment. *J. Air Poll. Control Assoc.*, **23**:853-857.

LIM, P. K., HUSS, JR., A. and ECKERT, C. A. (1982) Oxidation of aqueous sulfur dioxide. 3. The effects of chelating agents and phenolic antioxidants. *J. Phys. Chem.*, **86**:4234-4237.

LIU, B. Y. H. and LEE, K. W. (1975) An aerosol generator of high stability. *Amer. Ind. Hygiene Assoc. J.*, **36**:861-865.

LIU, B. Y. H. and PUI, D. Y. H. (1974a) Equilibrium bipolar charge distribution of aerosols. *J. Colloid Interface Sci.*, **2**:305-312.

LIU, B. Y. H. and PUI, D. Y. H. (1974b) Electrical neutralization of aerosols. *J. Aerosol Sci.*, **5**:465-472.

LIU, B. Y. H., PUI, D. Y. H., WHITBY, K. T., KITTELSON, D. B., KOUSAKA, Y. and MCKENZIE, R. L. (1978) The aerosol mobility chromatograph: a new detector for sulfuric acid aerosols. *Atmos. Environ.*, **12**:99-104.

LIU, B. Y. H., PUI, D. Y. H., RUBOW, K. L. and SZYMANSKI, W. W. (1985) Electrostatic effects in aerosol sampling and filtration. *Amer. Ind. Hygiene Assoc. J.*, **29**:251-269.

MARTIN, L. R. and HILL, M. W. (1987) The manganese catalyzed oxidation of sulfur: Ionic strength and the literature rates. Submitted to *Atmos. Environ.*.

MARTIN, L. R. (1984) Kinetic studies of sulfite oxidation in aqueous studies, in SO_2, NO *and* NO_2 *Oxidation Mechanisms: Atmospheric Considerations*

(J. G. Calvert, ed.). Butterworth Publishers, Boston, pp. 63-100.

MATTESON, M. J., STÖBER, W. and LUTHER, H. (1969) Kinetics of the oxidation of sulfur dioxide by aerosols of manganese sulfate. *Ind. Engr. Chem. Fund.*, **8**:677-687.

MCMURRY, P. H. and WILSON, J. C. (1983) Droplet phase (heterogeneous) and gas phase (homogeneous) contributions to secondary ambient aerosol formation as functions of relative humidity. *J. Geophys. Res.*, **88**:5101-5108.

MIDDLETON, P., KIANG, C. S. and MOHNEN, V. A. (1982) The relative importance of various urban sulfate aerosol production mechanisms — A theoretical comparison, in *Heterogeneous Atmospheric Chemistry* (D. R. Schryer, ed.). American Geophysical Union, Washington, D.C., pp. 221-230.

MUNGER, J. W., JACOB, D. J., WALDMAN, J. M. and HOFFMANN, M. R. (1983) Fogwater chemistry in an urban atmosphere. *J. Geophys. Res.*, **88**:5109-5121.

NASH, T. (1979) The effect of nitrogen dioxide and of some transition metals on the oxidation of dilute bisulfite solutions. *Atmos. Environ.*, **13**:1149-1154.

NEYTZELL DE WILDE, F. G. and TAVERNER, L. (1958) Experiments relating to the possible production of an oxidizing acid leach liquor by auto-oxidation for the extraction of uranium. *2nd. UN Internatl. Conf. on the Peaceful Uses of Atomic Energy Proc.*, **3**:303-317.

PENKETT, S. A., JONES ,B. M. R. and EGGLETON, A. E. J. (1979) A study of SO_2 oxidation in stored rainwater samples. *Atmos. Environ.*, **13**:139-147.

PENKETT, S. A. (1986) Laboratory studies of the multiphase S^{IV} — S^{VI} conversion rate, in *Chemistry of Multiphase Atmospheric Systems* (W. Jaeschke, ed.). Springer-Verlag, New York, pp. 507-540.

PILINIS, C. and SEINFELD, J. H. (1987) Continues development of a general equilibrium model for inorganic multicomponent atmospheric aerosols. *Atmos. Environ.*, in press.

PRESS, W. H., FLANNERY, B. P., TEUKOLSKY, S. A. and VETTERLING, W. T. (1986) *Numerical Recipes: The Art of Scientific Computing.* Cambridge University Press, New York.

PROSPERO, J. M., CHARLSON, R. J., MOHNEN, V., JAENICKE, R., DELANY, A. C., MOYERS, J., ZOLLER, W. and RAHN, K. (1983) The atmospheric aerosol system: an overview. *Rev. Geophys. and Space Phys.*, **21**:1607-1629.

PRUPPACHER, H. R. (1986) The role of cloudphysics in atmospheric multiphase systems: Ten basic statements, in *Chemistry of Multiphase Atmospheric*

Systems (W. Jaeschke, ed.). Springer-Verlag, New York, pp. 133-190.

PRUPPACHER, H. R. and KLETT, J. D. (1978) *Microphysics of Clouds and Precipitation.* D. Reidel Publishing Co., Boston.

PUI, D.Y. H. (1987) *personal communication.*

PYTKOWICZ, R. M. (1983) *Equilibria, Nonequilibria, and Natural Waters.* Volume I. John Wiley & Sons, New York.

RADER, D. J. and MCMURRY, P. H. (1986) Application of the tandem differential mobility analyzer to studies of droplet growth or evaporation. *J. Aerosol Sci.*, **17**:771-787.

RARD, J. A. (1984) Isopiestic determination of the osmotic and activity coefficients of aqueous $MnCl_2$, $MnSO_4$, and $RbCl_2$ at 25 °C. *J. Chem. Eng. Data* , **29**:443-450.

RARD, J. A. and MILLER, D. G. (1981) Isopiestic determination of the osmotic coefficients of aqueous Na_2SO_4, $MgSO_4$ and $Na_2SO_4 - MgSO_4$ at 25 °C. *J. Chem. Eng. Data* , **26**:33-38.

RATCLIFF, G. A. and HOLDCROFT, J. G. (1963) Diffusivities of gases in aqueous electrolyte solutions. *Trans. Inst. Chem. Engrs.*, **41**:315-319.

SAXENA, P. and SEIGNEUR, C. (1987) On the oxidation of SO_2 to sulfate in atmospheric aerosols. *Atmos. Environ.*, **21**:807-812.

SCHWARTZ, S. E. (1984) Gas-aqueous reactions of sulfur and nitrogen oxides in liquid-water clouds, in SO_2, NO *and* NO_2 *Oxidation Mechanisms: Atmospheric Considerations* (J. G. Calvert, ed.). Butterworth Publishers, Boston, pp. 173-208.

SCHWARTZ, S. E. and FREIBERG, J. E. (1981) Mass-transport limitation to the rate of reaction of gases in liquid droplets: Application to oxidation of SO_2 in aqueous solutions. *Atmos. Environ.*, **15**:1129-1144.

SEINFELD, J. H. (1986) *Atmospheric Chemistry and Physics of Air Pollution.* John Wiley & Sons, New York.

SMITH, A. E. and MARTELL, R. M. (1982) *Critical Stability Constants. Volume 5: First Supplement.* Plenum Press, New York.

STELSON, A. W., BASSETT, M. E. and SEINFELD, J. H. (1984) Thermodynamic equilibrium properties of aqueous solutions of nitrate, sulfate and ammonium, in *Chemistry of Particles, Fogs and Rain* (J. L. Durham, ed.). Butterworth Publishers, Boston, pp. 1-51.

STELSON, A. W. and SEINFELD, J. H. (1981) Chemical mass accounting of urban aerosol. *Environ. Sci. Tech.*, **15**:671-679.

STOLZENBURG, M. R. and MCMURRY, P. H. (1985) Diffusion effects in electrostatic classification of ultrafine aerosols. Presented at the *AAAR Conference*, November 18-22, Albuquerque, NM.

TEN BRINK, H. M., PLOMP, A., SPOELSTRA, H. and VAN DE VATE, J. F. (1983) A high-resolution electrical mobility aerosol spectrometer (MAS). *J. Aerosol Sci.*, **14**:589-597.

VAN ELDIK, R. (1986) Transition metal as potential catalysts in atmospheric oxidation processes, in *Chemistry of Multiphase Atmospheric Systems* (W. Jaeschke, ed.). Springer-Verlag, New York, pp. 541-566.

WADDEN, R. A., QUON, J. E. and HULBERT, H. M. (1974) A model of a growing, coagulating aerosol. *Atmos. Environ.*, **8**:1009-1028.

WASHBURN, E. W. (ed.) (1926) *International Critical Tables.* McGraw-Hill, New York.

WHITFIELD, M. (1979) Activity coefficients in natural waters, in *Activity Coefficients in Electrolyte Solutions*, Volume II (R. M. Pytkowicz, ed.). CRC Press, Inc., Boca Raton, Florida, pp. 153-300.

APPENDIX A

DISTORTION OF SIZE DISTRIBUTIONS BY CONDENSATION AND EVAPORATION IN AEROSOL INSTRUMENTS

by

+Pratim Biswas
Department of Mechanical Engineering

Carol L. Jones
Department of Chemical Engineering

*Richard C. Flagan
Department of Environmental Engineering

California Institute of Technology
Pasadena, CA 91125.

accepted for publication in

Aerosol Science and Technology

* To whom correspondence should be addressed.
+ At present: Department of Environ. Engr.
University of Cincinnati
Cincinnati, OH 45221-0071

ABSTRACT

Aerosols which contain volatile species or condensable vapors may be altered by changes in temperature, pressure, and vapor concentration. When such changes occur within aerosol sampling instruments, the measured size distribution can be distorted significantly. The distortion of particle size distributions in a number of commonly used aerosol instruments, including cascade impactors, both conventional and low pressure instruments, and optical particle counters, is explored both theoretically and experimentally in this paper. Ammonium sulfate aerosols in humid atmospheres have been used to test the instruments. In a low pressure impactor in which the pressure is intentionally reduced to facilitate the collection of small particles, a water containing particle may shrink due to evaporation as the pressure is reduced. However, if the sample flow is also accelerated to high velocities, aerodynamic cooling can lead to condensation of water vapor and particle growth. Either of these competing effects may lead to erroneous estimates of the particle size distribution. Optical particle counters generally use a recirculated sheath air flow. Pumps and electrical dissipation heat this air, leading to a temperature increase that shifts the vapor equilibrium, causing a decrease in particle size due to evaporation. Modifications have been made to avoid this distortion in measured size distributions.

1. Introduction

Most aerosol sizing instruments are calibrated with dry, non-volatile particles in the absence of any condensible vapors. These intruments are then routinely used to sample atmospheric or combustion exhaust aerosols at high humidities. Extreme conditions, approaching or exceeding 100% relative humidity, are occasionally encountered, e.g., in sampling fog. Pressure or temperature changes within the instruments may disturb the vapor equilibrium and result in biased size distribution measurements. Roeber (1957) reported that particle adhesion in impactors improved at high jet velocities due to the formation of a thin layer of water around the particles. Hochrainer and Zebel (1981) looked at this problem for the impactor built by Mercer et al. (1970). With non-hygroscopic aerosols no condensation was observed unless the inlet aerosol was highly supersaturated. Hygroscopic aerosols showed condensation only if the inlet humidity was above the deliquescent point. The growth of a 2 micron particle in the last stage of the Mercer (1970) impactor was shown to be negligible for an inlet humidity of 12.7%. However, impactors are routinely operated at higher humidities, so size changes may become significant.

This work explores the distortion of particle size distributions, both theoretically and experimentally, in a number of commonly used instruments: (i) a low pressure impactor with high velocity stages (Hering et al., 1978); (ii) a conventional six stage impactor, operated in the incompressible flow regime; and (iii) a laser optical particle counter.

Ammonium sulfate aerosols under humid conditions were used as a test case for this study. Ammonium sulfate was chosen because it is an important component of atmospheric aerosols, activity data are readily available (Robinson and Stokes, 1959; Wishaw and Stokes, 1954; Washburn, 1928) and it forms chemically stable droplets, facilitating data interpretation. Droplet growth within the instrument was predicted for different initial particle sizes and relative humidities. Experiments performed to corroborate the predictions uncovered additional aerosol measurement problems. We begin with a discussion of the basic problem and then will address specific instruments.

2. Theory

2.1 Relative Humidity Relations

The amount of vapor in a gas is expressed in terms of its partial pressure. If the vapor is water, the more commonly used term is humidity. The relative humidity, RH, is defined as the ratio of the water vapor pressure to the saturation vapor pressure at the local temperature. A similar definition could be used for vapors other than water. In this paper, relative humidity is used in this broader sense.

If the amount of vapor condensing or evaporating in the instrument is negligible relative to the total amount present, the relative humidity, $(RH)_1$, at a temperature T_1, and pressure P_1, can be expressed as:

$$(RH)_1 = (RH)_o \left(\frac{p_{sat}(T_o)}{p_{sat}(T_1)}\right)\left(\frac{P_1}{P_o}\right) \qquad (1)$$

where p_{sat} is the saturation vapor pressure, and P is the total pressure. Both temperature and pressure variations lead to changes in the relative humidity. These two effects are illustrated in Figure 1 for water vapor in air. When both temperature and pressure vary, the value of $(RH)_1/(RH)_0$ can be obtained by multiplying the individual ratios obtained from Figure 1. In the case of an adiabatic, isentropic flow ($T \alpha P^{\frac{\gamma-1}{\gamma}}$) the temperature decrease associated with expansion of the gas results in an increase in relative humidity as indicated by the dashed line in Figure 1.

2.2 Particle Growth

Consider an isolated droplet of diameter d in the presence of a vapor. When p_d, the vapor pressure at the droplet surface, equals the ambient vapor pressure p_{vap}, there is a vapor equilibrium and no net transport of vapor. However, a change in the ambient relative humidity leads to vapor transport until a new equilibrium state is attained. The equation for vapor transport can be written as (Friedlander, 1977)

$$\frac{dv}{dt} = \frac{2\pi D d v_m}{kT}(p_{vap}-p_d)F(Kn) \qquad (2)$$

where F(Kn) is a correction factor to account for vapor transport in the transition and non-continuum regime. The modified Fuchs-Sutugin expression (Fuchs and Sutugin, 1971) is reasonably accurate over the entire range of Knudsen numbers and

was used to calculate F(Kn) in the present calculations.

Expressing the local vapor pressure, p_{vap}, in terms of the relative humidity, i.e.,

$$p_{vap} = (RH)\ p_{sat} \tag{3}$$

the vapor pressure at the droplet surface,

$$p_d = a_w(m)\exp\left(\frac{4\sigma v_m}{dkT}\right)p_{sat}(T)$$

becomes

$$p_d = RH_d p_{sat}(T) \tag{4}$$

where $a_w(m)$, the water activity of the droplet solution, is a function of the molality, m, of the droplet solution. The exponential term describes the increase in vapor pressure at the surface due to curvature, or Kelvin effect, and is approximately 1.0 for aqueous particles having diameters greater than 0.1 micron. For simplicity, the product of this term and the activity is called RH_d, the equilibrium relative humidity at the droplet surface.

With Eqns. (3) and (4), Eqn. (2) can be rewritten in terms of the particle diameter,

$$\frac{d(d)}{dt} = \frac{4Dv_m}{dkT}\ p_{sat}(RH-RH_d)F(Kn)\ . \tag{5}$$

Given the ambient conditions, initial size and composition of the droplet, and activity data, Eqn. (4) can be integrated to describe the instantaneous rate of particle growth or evaporation. The time scale which is a characteristic of the time required to reach equilibrium, i.e., the characteristic time for droplet

growth, is

$$\tau = \frac{d^2 k T}{4 D v_m p_{sat} (RH - RH_d) F(Kn)} \quad . \qquad (6)$$

The variation of the characteristic time with particle size is shown in Figure 2. A few microseconds are required for an ammonium sulfate droplet 0.1 micron in diameter to re-equilibrate given a relative humidity change of about 20%.* We can use Eqn. (5) to follow a particle's size as it passes through an instrument.

Inorganic salts, such as ammonium sulfate, do not form liquid droplets until the relative humidity exceeds a certain value, called the "deliquescent point" (RHD). When the relative humidity is reduced from above the deliquescent point, the transition to a dry state does not occur at RHD, but at a lower "crystallization humidity" or RHC. This lower humidity for crystallization results from the supersaturation of the salt solution that is required to nucleate the solid phase. For ammonium sulfate, RHD is 81% and RHC is typically 36-40% (Tang, 1980; Orr et al., 1958).

---

* As written, Eqns. (2) and (5) assume the droplet to be in thermal equilibrium with its surroundings. This assumption is valid since the characteristic time for thermal equilibrium is significantly smaller than both the characteristic time for growth and the typical residence time in an instrument. If, as a worst-case study, heat conduction is considered to be the only method of heat transfer, $\tau_{thermal} \sim 0.25\mu$sec for an 0.1 micron diameter particle and $\tau_{thermal} \sim 0.07\mu$sec for an 0.05 micron particle.

3. The Low Pressure Impactor

Particles larger than a few tenths of a micron in diameter are readily classified in atmospheric pressure cascade impactors. To collect smaller particles it is necessary to reduce the pressure so that the particle begins to slip relative to the surrounding gas or to use very small jets. An extreme example of the former approach is the low pressure impactor developed by Hering et al. (1978). A size cut of 0.05 μm is achieved in the final stage. To accomplish this in a compact instrument with a single jet on each stage, the last two stages are operated at both low pressures and sonic jet velocities (Mach number, $M = u/a = 1$). The high velocities lead to considerable aerodynamic cooling. Table 1 lists the stagnation pressure and calculated temperature at the throat of each impactor stage and of the critical flow orifice that is used to reduce the pressure.

A simple model of the flow in the reactor can capture the essential features of the environment through which the particles must pass. The flow is subdivided into four regions as illustrated in Figure 3, i.e., (1) the entrance to the throat; (2) a parallel flow region in the throat and the region near the jet outlet; (3) a stagnation flow region where the influence of the impaction plate is felt; and (4) the region immediately downstream of the impaction plate. The parallel flow region typically extends to halfway between the jet outlet and the impaction plate (Mercer et al., 1970; Marple, 1970; Flagan, 1982). The flow in the stagnation region can be modeled with the

Hiemenz flow that includes viscous boundary layer effects (Schlichting, 1962). Region 1 was modeled as a conical converging flow. Boundary layer effects were neglected in both the entrance and throat regions.

Table 1 shows that the relative humidity changes significantly from stage to stage in the impactor. The increase in humidity due to aerodynamic cooling competes with the decrease due to a pressure reduction to reduce the relative humidity in stages 5, 6, and 8, and to increase humidity in the other stages.

3.2 Growth Calculations

The growth equation (Eqn. 5) was integrated numerically for particles entering on different streamlines to follow the changes in particle size as the aerosol flows through the impactor. These size changes bias the apparent size distribution as deduced from the particulate mass collected on the various impactor stages. This bias is clearly illustrated in Figure 4 by plots of the calculated fraction of particles collected on each stage as a function of the aerodynamic diameter the particles had at the inlet to the impactor. Three inlet relative humidities are examined here: the "dry" aerosol conditions used in the instrument calibration (RH = 0%, Hering et al., 1978), a humidity slightly below the deliquescent point (RHD = 81% for ammonium sulfate) and finally, a high humidity such that the aerosol particles enter the impactor as liquid droplets (RH=95%).

Consider, for example, stage 3 operating dry (RH = 0%). Figure 4 indicates that fifty percent of the 2 μm particles

entering the impactor are collected upstream of stage 3, with the remaining 50% being collected on stage 3. Approximately 50% of the 1 μm particles are also collected on stage 3 under dry conditions, with the other 50% proceeding to subsequent stages for collection. At an inlet humidity of 80%, the particles grow in stage 3 due to the increased relative humidity caused by aerodynamic cooling. The effective 50% cutoff diameter (initial size of particles collected with 50% efficiency) for the stage decreases to approximately 0.75 microns. The large decrease is primarily due to the deliquescence of the particles at 81% relative humidity. At an inlet humidity of 95%, the particles are wet when they enter the impactor, and the collection of small particles does not increase markedly (d_{50} =0.9 μm). The change in small particle collection is similar on stage 4. The fraction of larger particles collected on this stage decreases somewhat at high relative humidities because of the increased collection on stage 3 due to the growth occurring there.

The increased collection on the upper stages at high relative humidites reduces the number of large particles entering stage 5 and, hence, their collection on that stage. The fraction of wet particles collected on stage 5 decreases substantially due to the considerable drop in relative humidity and corresponding decrease in particle size. Some of the particles that bypass stage 5 are collected on stage 6, increasing the collection of wet particles. Again, the efficiency of collection of small wet particles is reduced somewhat. The most dramatic changes occur

on stage 7 due to the large increase in relative humidity. Even inlet humidities as low as 25% lead to substantial particle growth and size distribution distortion. The amount collected on stage 8 is greatly reduced at elevated humidities because of the increased collection efficiency of the particles on stage 7.

These results clearly indicate the severity of measurement biases at high humidities in this instrument. The nature of the distortion is very much dependent on the kind of aerosol particle (thermodynamic properties) and the inlet conditions (pressure, temperature, relative humidity). For dry ammonium sulfate particles at inlet relative humidities greater than about 25% but less than 70%, size changes occur only in stages 7 and 8 and the size distribution tends to shift towards the larger diameters. Particles entering at relative humidities between 70 and 81% (dry at the inlet) become wet in the upper stages, increasing the fraction collected there and decreasing collection on the subsequent stages. However, large size increases lead to increased collection efficiency occurring on stage 7. This complicated shift could cause a unimodal size distribution to appear multimodal. For inlet relative humidities greater than the deliquescent point, the general trend is a slight increase in the fraction collected on the upper stages, a considerable decrease in stages 5 and 6, followed by a large increase in stage 7, and again a decrease in stage 8. Much of the data obtained with this instrument show a more pronounced minimum on stages 5 and 6 that has not generally been observed with other instruments (Ouimette and Flagan, 1982); this is quite possibly the result of

these sampling biases.

3.3 Experimental Verification

Tests were carried out using monodisperse ammonium sulfate aerosol particles with inlet relative humidities both below the deliquescent point (dry particles), and above the deliquescent point (wet particles). Because of the crystallization hysteresis described in section 2.2, the two aerosol generation systems illustrated in Fig. 5 were used. An approximately monodisperse inlet aerosol was generated by classifying the dry particles and the inlet size was calculated assuming equilibrium at the inlet relative humidity. The modified ROYCO optical particle counter (described in section 5) was used to confirm the inlet sizes of the particles. Temperature and relative humidity were monitored using an EG&G Model 911 Digital Dew Point Hygrometer. Thin stainless steel strips, pretreated in a furnace at 900 ^{o}C, were coated with vaseline and used as impaction substrates. The quantity of ammonium sulfate collected on each stage was determined by a flash vaporization/flame photometric detection technique (Roberts and Friedlander, 1976) using a Meloy 285 Sulfur analyzer.

The results for high inlet relative humidities are plotted in Fig. 6. The calibration data predicts that dry particles with an aerodynamic diameter of 0.2 μm at the inlet would be collected on stages 5 and 6 (see dotted line). At 90% RH (Figure 6a) the particles were, in fact, primarily extracted on stage 7 corroborating the predictions of the droplet growth

model. Similarly, dry 0.05 micron particles would be collected by stage 8 or the backup filter, but the growth of the humid aerosol (Figure 6b) in stage 7 leads to the particles being collected there instead. The results in Figure 6c experimentally show that even small, initially dry particles (0.024 μm, initial RH = 63%) are actually collected several stages prior to the collection stage predicted for a totally dry aerosol. Results for aerosols at other inlet humidities and initial sizes can be found in Biswas, (1985).

4. Conventional Cascade Impactor

We have seen the particle size distributions measured by impactors operated at low pressures and high velocities can be severely distorted. Shifts were predicted for stages operated with no intentional upstream pressure drops and with Mach numbers well below 0.3, the nominal limit of incompressible flow. Thus, some size bias may occur even in conventional impactors operated strictly within the accepted guidelines of incompressible flow.

Sierra's Model 266 multistage impactor has been well characterized by numerous studies. It has cylindrical nozzles and was designed for operation in the incompressible flow regime, i.e., the pressure drop across each stage is normally small so the jet Mach number is kept below 0.3. Table 2 lists the conditions for each of the stages when the impactor is operated with a Mach number of 0.27 for the last stage. The increase in relative humidity in

the first four stages is minimal, but is followed by a 4% and 19% increase in stages 5 and 6, respectively.

Growth calculations, analogous to those described above, were carried out for this impactor. It was found that for humidities above 67% at the inlet, particle growth would occur in stage 6 (see Fig. 7). At 80% relative humidity both the fifth and sixth stages were affected. For an inlet humidity greater than 84%, the relative humidity at stage 6 exceeds 100% and considerable growth of small particles can be expected.

The behavior of ammonium sulfate aerosols in this impactor was also examined experimentally using the aforementioned aerosol generation systems. The mass collected on each greased stage was determined by first extracting the ammonium sulfate from the slide, and then using ion chromatography to determine the amount of NH_4^+ in the extract solution (Stainton et al., 1977).

The experimental results are shown in Fig. 8. While the deviation from dry conditions is not as great as for the low pressure impactor, significantly more aerosol is collected on stage 6 than is predicted using dry aerosol calibration data, even for a humidity less than the deliquescent point. Thus, we see that, while operating impactors at Mach numbers less than the incompressible flow limit of 0.3 may be acceptable from a momentum point of view, it may still lead to biased size distributions. The jet Mach numbers of impactors used to sample aerosol at high relative humidities should be limited to much

lower values to avoid such biases. These results suggest that jet Mach numbers as low as 0.1 can lead to severe biases at high relative humidity, but that the biases are small at humidities in excess of 90 percent for jet Mach numbers below 0.05. It is important to remember, however, that Mach number alone does not determine the size biasing. The type of aerosol, the inlet conditions, the temperature and pressure ratios, and the impactor geometry (throat length, jet-to-plate spacing, etc.) for each stage must be examined to evaluate the extent of the distortion in a particular impactor and aerosol.

5. Optical Particle Counter

Single particle optical counters measure the intensity of light scattered from individual particles as they pass through an illuminated volume. To focus the aerosol flow within the view volume of the optics and to minimize depsition on the optics, it is common practice to introduce a sheath flow of clean air coaxially with the aerosol flow. Flow metering is facilitated by recirculating part of the aerosol flow after filtering, as illustrated by the pneumatic system of the Hiac/Royco Model 226 Laser Aerosol Counter shown in Fig. 9. With this recirculation system, the exhaust flow is equal to the inlet flow rate and independent of the sheath flow.

Crump et al. (1983) encountered difficulties in measuring manganese sulfate aerosols at high relative humidities due to the heating of the sheath air by dissipation in the pump

and instrument electronics. To examine the extent of heating, temperature and dewpoint probes of an EG&G dewpoint hydrometer have been installed in the recirculation loop. Temperature increases of 2 to 3 ^{o}C were observed, as shown in Fig. 10a. Moreover, the temperature increased slowly over about 4 hours.

An additional problem was detected as the temperature and humidity were monitored. For an inlet humidity of 95%, the measured sheath air humidity only reached 90% after a period of 9 hours (Fig. 10b). This slow reponse was traced to the hygroscopic nature of the cartridge filters supplied by the manufacturer. These factors, the temperature increase and the filter water uptake, clearly indicate the possibility of instrumentation biases in size distribution measurements depending on the previous history of the instrument. The temperature of the sheath air is controlled by addition of a counterflow heat exchanger. The two cartridge filters in the flow path were replaced by a single 47 mm Teflon membrane filter. The filter is replaced at the beginning of each run to avoid the problem of loading by hydroscopic particles. These modifications are shown in Figure 11. The sheath air humidity was monitored and found to reach a steady value in less than an hour. The variations of the sheath air temperature and relative humidity for the modified instrument are shown in Fig. 10. The possibility of biases in the sizes of small particles due to the aerodynamics of the aerosol jet remains, however, as indicated in Table III.

6. Conclusions

Aerosol instruments are generally designed to achieve sharp size resolution, and this performance is verified by calibration with dry aerosols. High relative humidities are frequently encountered in the sampling of ambient aerosols. Pressure and temperature variations within aerosol instruments can lead to changes in particle size at relative humidities as low as 25-70 percent depending upon the specific instrument and aerosol. In this paper we have demonstrated such size shifts both theoretically and experimentally. In the optical particle counter, simple instrument modifications were identified to ameliorate the biases.

These results indicate the need for caution in interpreting aerosol size distribution measurements. Low pressure impactors can lead to severe sampling biases. Even in impactors designed for operation at ambient pressure, biases can be significant at high relative humidities, even if jet Mach numbers are below the nominal limit for incompressible flow of 0.3. Dissipation of heat can lead to sampling biases in optical particle counters and, possibly, in other instruments. The large data base obtained with suspect instruments must be carefully evaluated to avoid erroneous data interpretation. Temperature and relative humidity data are, unfortunately, not always reported with aerosol measurements, precluding corrections for such biases. In future applications of suspect instruments, the measurement and reporting of these parameters could greatly

enhance the value of the data obtained.

There is a need for instruments that minimize sampling biases. In the design and evaluation of such instruments, it is not sufficient that good size resolution be obtained with the traditional calibration aerosols, i.e., polystyrene latices, dry fluorescein particles, or droplets of low volatility organics. The properties of the aerosols that will actually be sampled must be taken into account, and the most extreme operating conditions likely to be encountered should be examined.

Acknowledgement

This research was supported by Environmental Protection Agency grants Nos. R-809191 and 810857. The conclusions represent the views of the authors and do not necessarily represent the opinion, policies, or recommendation of the U.S. Environmental Protection Agency.

NOMENCLATURE

a_w : Water activity

d : Droplet diameter

D : Diffusion coefficient

k : Boltzmann's constant

Kn : Knudsen number

p : Partial pressure of the vapor

P : Total pressure

RH : Relative humidity

RH_d : Product of Kelvin correction term and water activity

RHC : Crystallization Humidity

RHD : Deliquescent point

t : Time

T : Temperature (K)

v : Volume of droplet

v_m : Molecular volume

Greek

σ : Surface tension

γ : Ratio of specific heats, C_p/C_v

τ : Residence time

Subscripts

d : Surface of droplet

sat : Saturated state

vap : vapor property

REFERENCES

Biswas, P. (1985) Impactors for aerosol measurements: developments and sampling biases. Ph.D. Thesis, Mech. Eng. Dept., California Inst. of Tech., Pasadena, California.

Biswas, P., and Flagan, R.C. (1984) High velocity inertial impactor. Environ. Sci. Tech. 18:611-616.

Crump, J.G., Flagan, R.C., and Seinfeld, J.H. (1983) An experimental study of the oxidation of sulfur dioxide in aqueous manganese sulfate aerosols. Atmos. Environ. 17(7):1277-1289.

Flagan, R.C. (1982) Compressible flow inertial impactors. J. Colloid Interface Sci. 87:291-299.

Friedlander, S.K. (1977) Smoke, Dust and Haze. Wiley-Interscience, New York.

Fuchs, N.A., and Sutugin, A.G. (1971) High-dispersed aerosols. In Topics in Current Aerosol Research. G.M. Hidy and J.R. Brock, eds., Pergamon, Oxford, vol. 2, p.34.

Hering, S.V., Flagan, R.C., and Friedlander, S.K. (1978) Design and evaluation of new low-pressure impactor. I. Environ. Sci. Tech. 12:667-673.

Hochrainer, D., and Zebel, G. (1981) The influence of the expansion humidity on the deposition of particles in impactors. J. Aerosol Sci. 12:49-53.

Marple, V.A. (1970) Fundamental study of inertial impactors. Ph.D. Thesis, Mech. Eng. Dept., U. of Minnesota, Minneapolis, Minnesota.

Mercer, T.T., Tillery, M.I., and Newton, G.J. (1970) A multistage, low flow rate cascade impactor. J. Aerosol Sci. 1:9-15.

Orr, C. Jr., Hurd, F.K., and Corbett, W.J. (1958) Aerosol size and relative humidity. J. Colloid Sci. 13:472-482.

Ouimette, J.R., and Flagan, R.C. (1982) The extinction coefficient of multicomponent aerosol. Atmos. Environ. 16:2405-2419.

Roberts, P.S., and Friedlander, S.K. (1976) Analysis of sulfur in deposited aerosol particles by vaporization and flame photometric detection. Atmos. Environ. 10:403-408.

Robinson, R.A., and Stokes, R.H. (1959) Electrolyte Solutions, Butterworths, London.

Roeber, R. (1957) Staub 50:418-420.

Stainton, M.P., Capel, M.S., and Armstrong, F.A.J., (1977) The Chemical Analysis of Fresh Water, pp. 69-71, Freshwater Institute, Winnepeg.

Tang, I.N. (1980) Deliquescence properties and particle size change in hygroscopic aerosol. In Generation of Aerosols and Facilities for Exposure Experiments. K. Willeke, ed., Ann Arbor Sciences, Ann Arbor, pp. 153-167.

Washburn, E.W., ed. (1928) International Critical Tables, McGraw-Hill, New York, vol. 3, p. 363.

Wishaw, B.F., and Stokes, R.H. (1954) Activities of aqueous ammonium sulphate solutions. Trans. Faraday Soc. 50:952-954.

Table I: OPERATING CONDITIONS FOR THE LOW PRESSURE IMPACTOR

Conditions at throat for a 1 lpm flow rate
Inlet Pressure = 745 mmHg
Inlet Temperature = 298 K

Stage	Velocity (m/s)	Pressure (mmHg)	Temperature (K)	Residence Time (microsec)	$\frac{(RH)_{jet}}{(RH)_{inlet}}$
I	3.5	744	297.9	1635	1.005
II	11.0	743	297.9	544	1.004
III	22.0	740	297.7	272	1.015
IV	54.0	720	295.7	111	1.111
Orifice	300.0	150	248.4	20	9.750
V	93.0	140	292.2	65	0.268
VI	150.0	106	275.3	40	0.627
VII	300.0	56	248.4	20	3.254
VIII	300.0	29	248.4	20	0.521

TABLE II: OPERATING CONDITIONS FOR THE SIERRA IMPACTOR, MODEL 266

Conditions at 4 lpm
Inlet Pressure = 760 mmHg
Inlet Temperature = 298 K

STAGE	MACH NUMBER	T (K)	P (mmHg)	RESIDENCE TIME (ms)	$\frac{(RH)_{jet}}{(RH)_{inlet}}$
I	0.004	298.0	760.0	6.32	1.000
II	0.008	298.0	760.0	2.32	1.000
III	0.017	297.9	759.9	2.51	1.003
IV	0.044	297.9	759.2	0.836	1.004
V	0.122	297.3	753.7	0.259	1.035
VI	0.273	294.4	728.5	0.118	1.190

TABLE 3: ROYCO OPTICAL PARTICLE COUNTER, MODEL 226

Sample Flow Rate	:	5 cc/s
Sheath Flow Rate	:	30 cc/s
U (Jet Velocity)	:	103 m/s
Mach Number	:	0.3
Pressure Ratio (Measuring Region to Inlet)	:	0.94
$\frac{(RH)\text{measuring region}}{(RH)\text{inlet}}$	:	1.3
Residence Time	:	39 microseconds

FIGURE CAPTIONS

Figure 1 Variation of relative humidiy with temperature (a) and pressure (b) (T =298K, p =1 atmosphere). Solid curves indicate variation with temperature at constant pressure, and with pressure at constant temperature. Broken line shows variation with pressure for adiabatic expansion.

Figure 2 Characteristic time for droplet growth at an initial relative humidity of 95%. (1) Δ RH=10%, P=1 atmos; (2) Δ RH-20%, P=1 atmos; (3) Δ RH=10%, P=0.1 atmos.

Figure 3 Illustration of an impactor stage showing the four regions into which the flow was divided for model calculations.

Figure 4 Calculated collection efficiences for ammonium sulfate aerosol on the stages of the low pressure impactor of Hering et al. (1979) showing the influence of relative humidity. (____) dry particles RH=0%; (__ __ __) RH_{inlet}=95%; (__·__) RH_{inlet}=80%; (__x__) RH_{inlet}=70%; (_·_·_·) RH_{inlet}=25%.

Figure 5 Schematic diagrams of the aerosol generation used in the experimental examination of sampling biases. (a) system for production of dry particles; (b) system for production of wet particles.

Figure 6 Mass distributions of ammonium sulfate aerosol collected with the low pressure impactor of Hering et al. (1979). (____) experimental data; (__ _ __) predicted taking particle growth into account; (_ _ _) predicted assuming constant particle size. (a) d_0=0.2μm, RH_0=90%; (b) d_0=0.05μm, RH_0=92.5%; (c) d_0=0.024μm, RH_0=63%.

Figure 7 Predicted collection efficiences for Sierra impactor operated with a Mach number of 0.27 on Stage 6. Ammonium sulfate aerosol. (____) dry aerosol; (_ _ _) RH_0=75%; (__ . __) RH_0=80%.

Figure 8 Mass distributions of an ammonium sulfate aerosol collected with the Sierra impactor. (____) experimental data; (__ . __) predicted taking particle growth into account; (_ _ _) predicted assuming constant particle size. (a) d_0= 0.19μm, RH_0=70%; (b) d_0=0.28μm, RH_0=91.5%.

Figure 9 Schematic of the flow system in the Hiac/Royco Model 226 Laser Optical Particle Counter.

Figure 10 Variation in temperature (a) and relative humidity (b) of the sheath air in the Hiac/Royco optical Particle counter. ■: inlet air; ●: sheath air; ▲: sheat air of modified instrument.

Figure 11 Schematic of flow system of the modified Hiac/Royco optical particle counter.

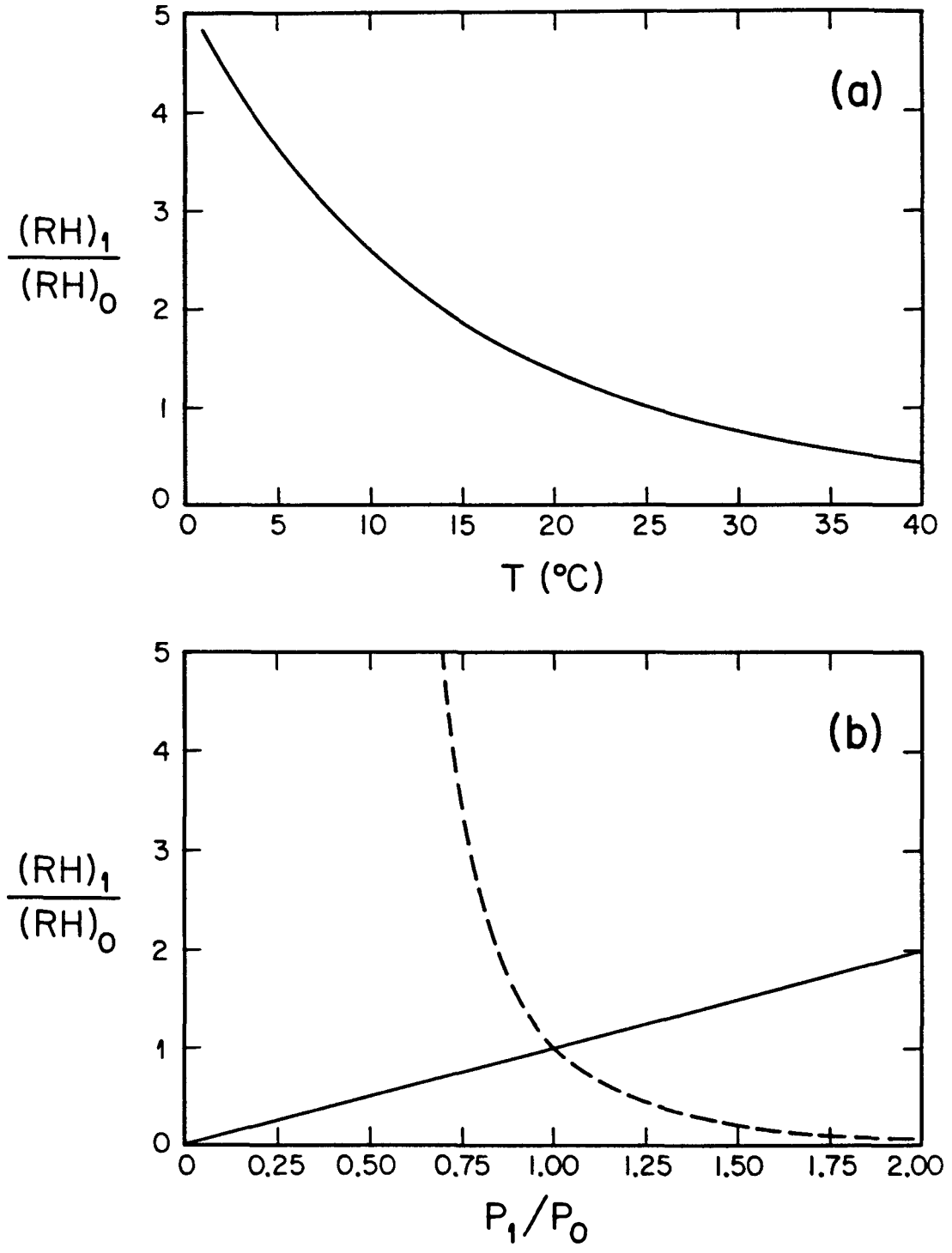
(a)
$\frac{(RH)_1}{(RH)_0}$
0
1
2
3
4
5
0
5
10
15
20
25
30
35
40
T (°C)
(b)
$\frac{(RH)_1}{(RH)_0}$
0
1
2
3
4
5
0
0.25
0.50
0.75
1.00
1.25
1.50
1.75
2.00
P_1/P_0

Figure 1

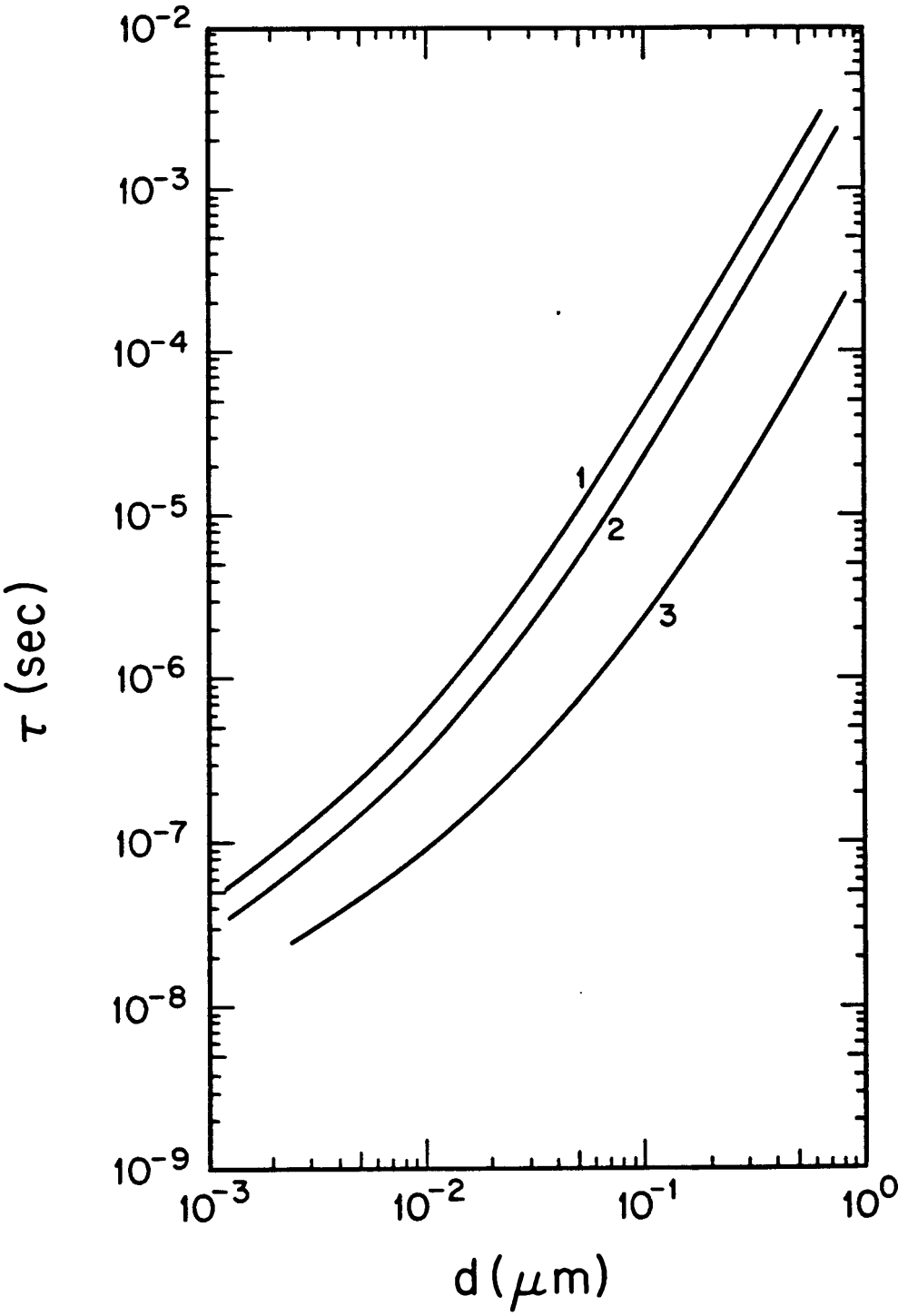

Figure 2

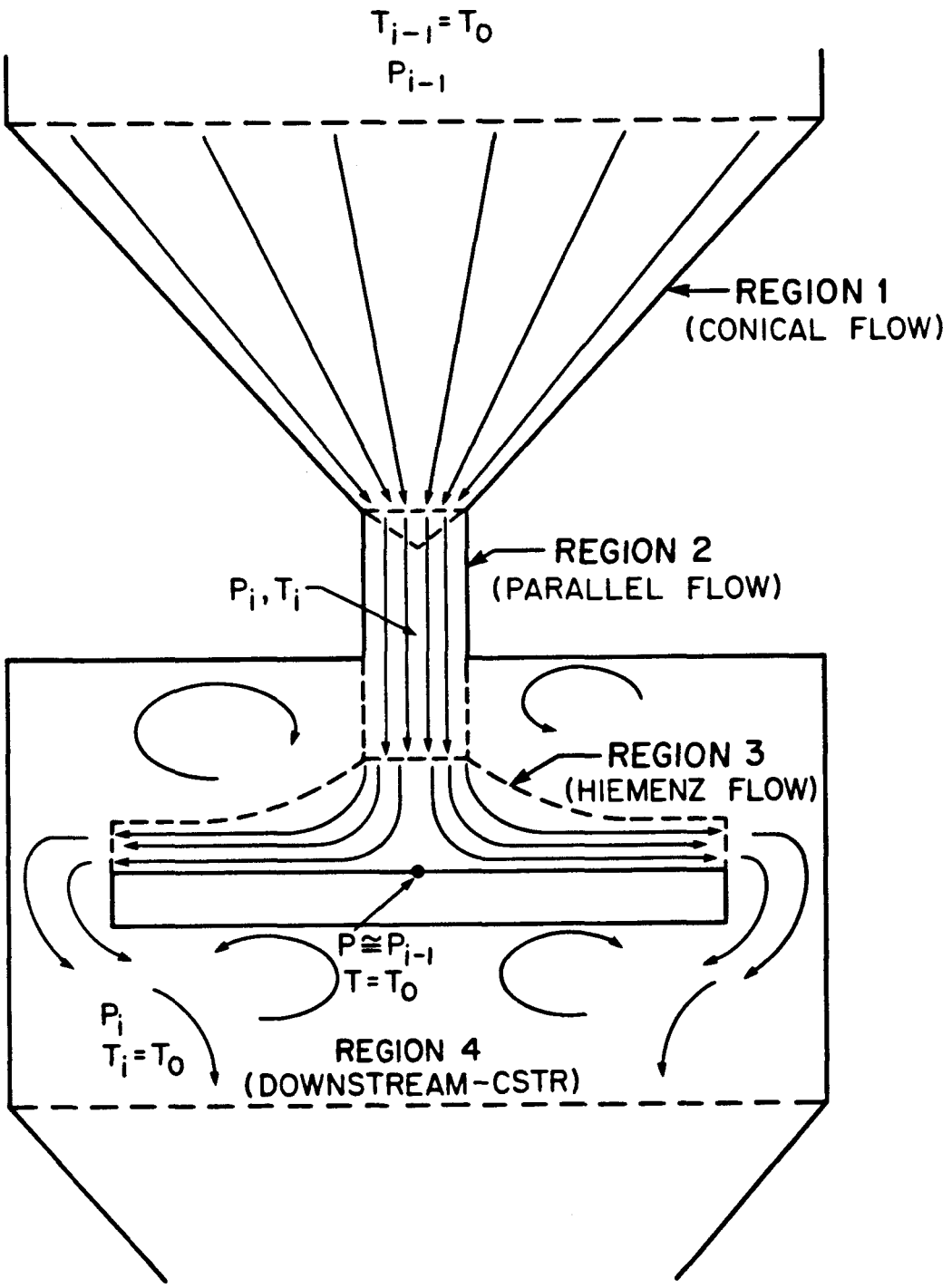
$T_{i-1} = T_0$
P_{i-1}
REGION 1
(CONICAL FLOW)
REGION 2
(PARALLEL FLOW)
P_i, T_i
REGION 3
(HIEMENZ FLOW)
$P \cong P_{i-1}$
$T = T_0$
P_i
$T_i = T_0$
REGION 4
(DOWNSTREAM-CSTR)

Figure 3

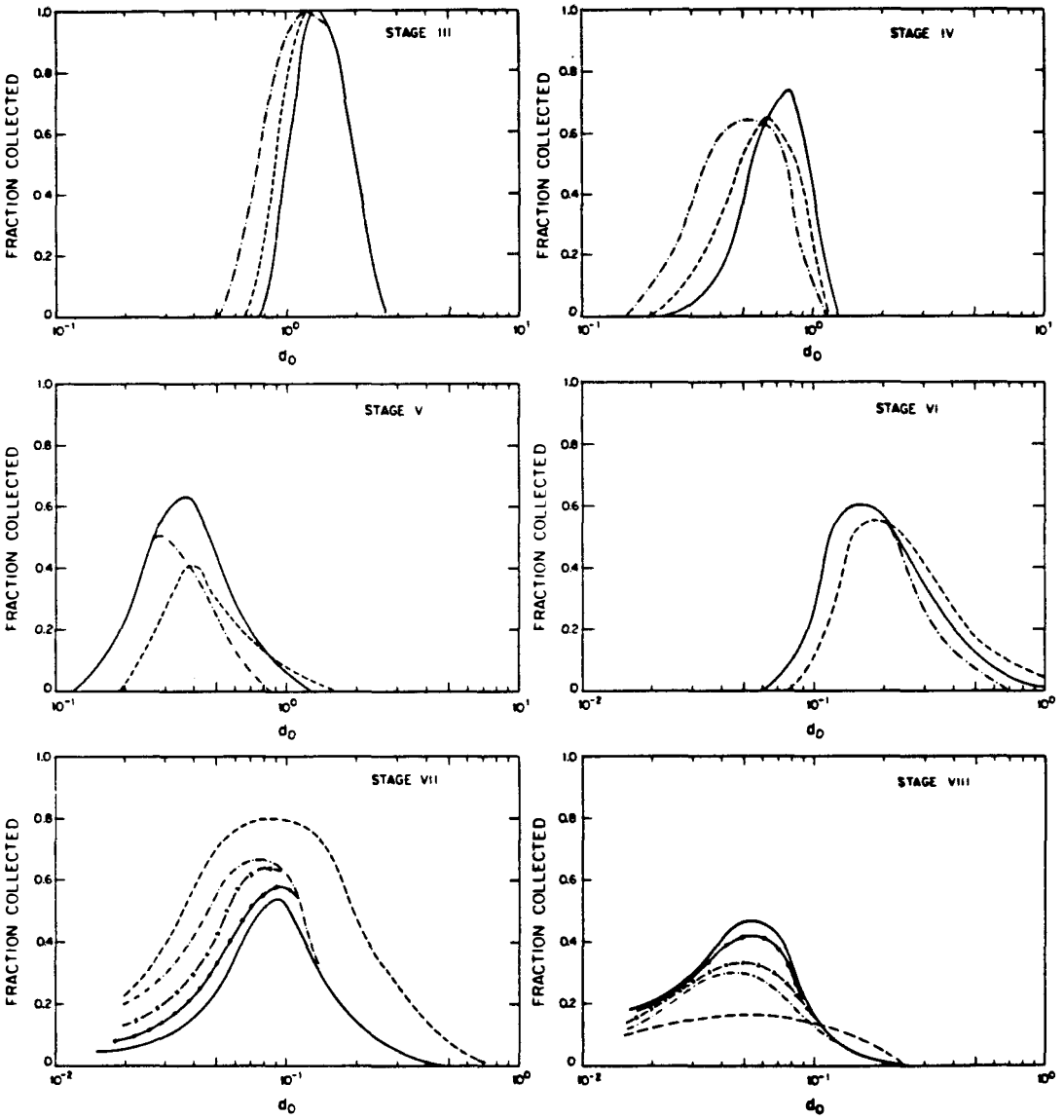
STAGE III
STAGE IV
STAGE V
STAGE VI
STAGE VII
STAGE VIII
FRACTION COLLECTED
d_0

Figure 4

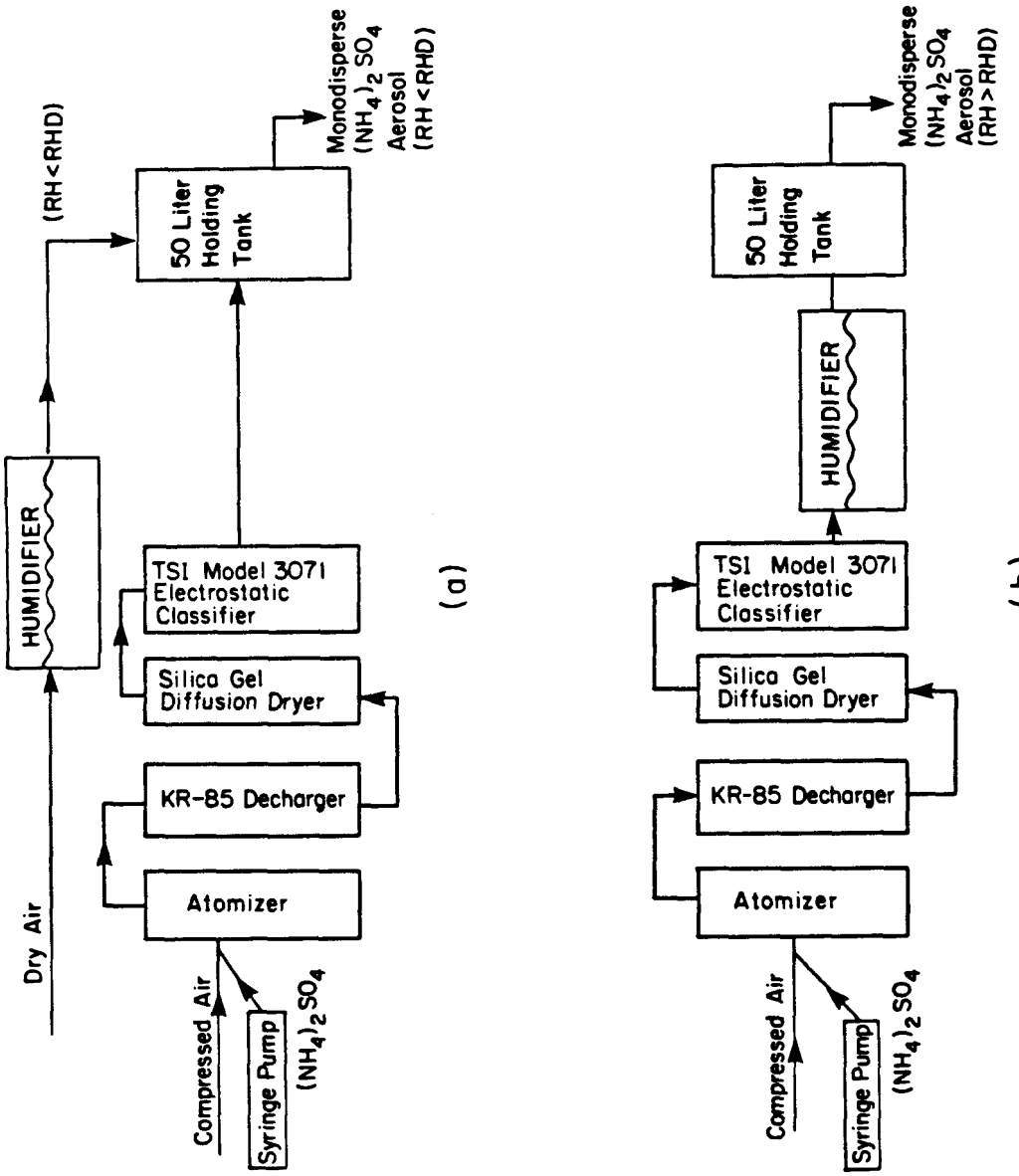
Monodisperse
$(NH_4)_2SO_4$
Aerosol
(RH < RHD)
50 Liter
Holding
Tank
(RH < RHD)
HUMIDIFIER
TSI Model 3071
Electrostatic
Classifier
Silica Gel
Diffusion Dryer
KR-85 Decharger
Atomizer
Dry Air
Compressed Air
Syringe Pump
$(NH_4)_2SO_4$
(a)
Monodisperse
$(NH_4)_2SO_4$
Aerosol
(RH > RHD)
50 Liter
Holding
Tank
HUMIDIFIER
TSI Model 3071
Electrostatic
Classifier
Silica Gel
Diffusion Dryer
KR-85 Decharger
Atomizer
Compressed Air
Syringe Pump
$(NH_4)_2SO_4$
(b)

Figure 5

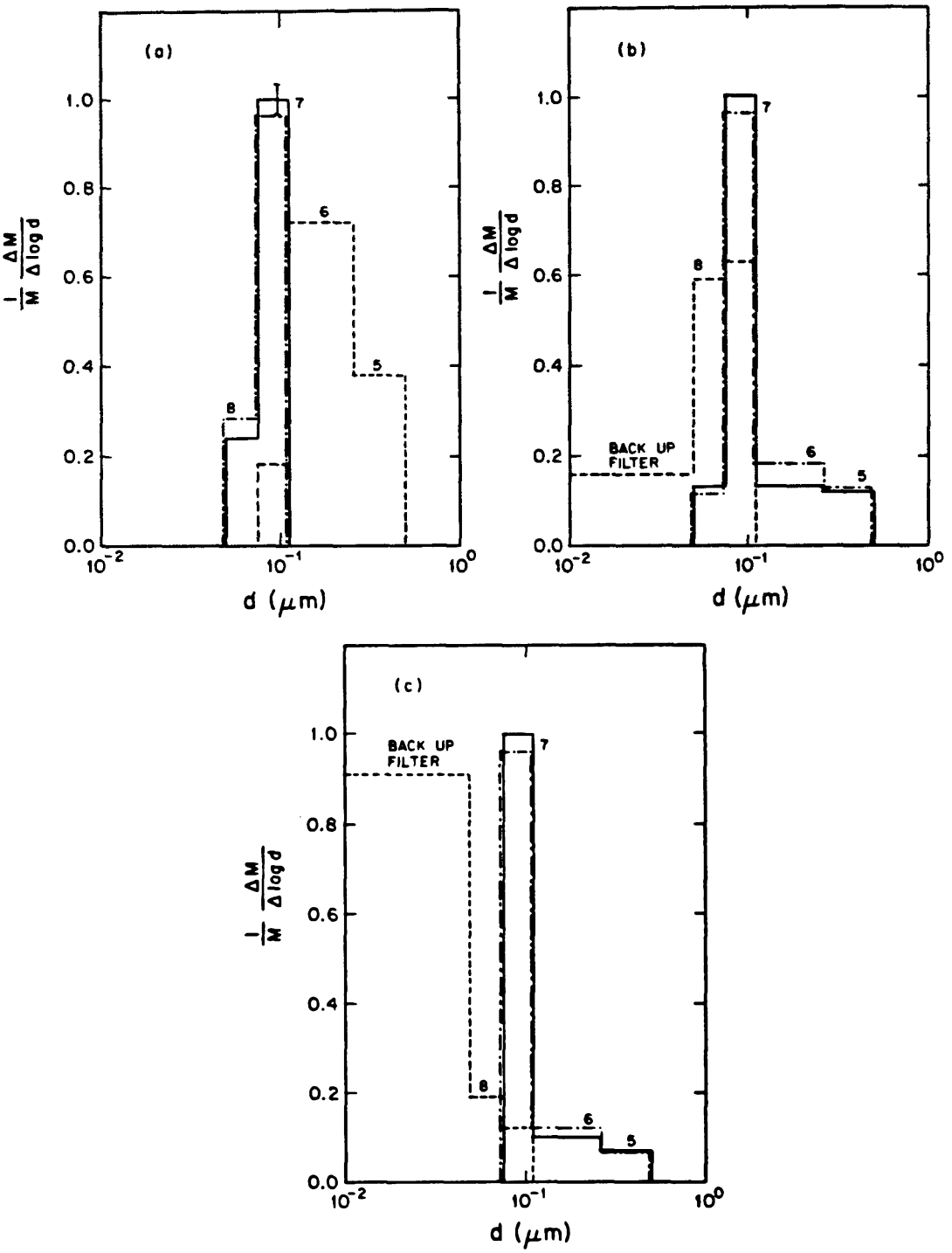
(a)
(b)
(c)
1.0
0.8
0.6
0.4
0.2
0.0
$\frac{1}{M}\frac{\Delta M}{\Delta \log d}$
10^{-2}
10^{-1}
10^{0}
d (μm)
7
6
5
8
BACK UP FILTER

Figure 6

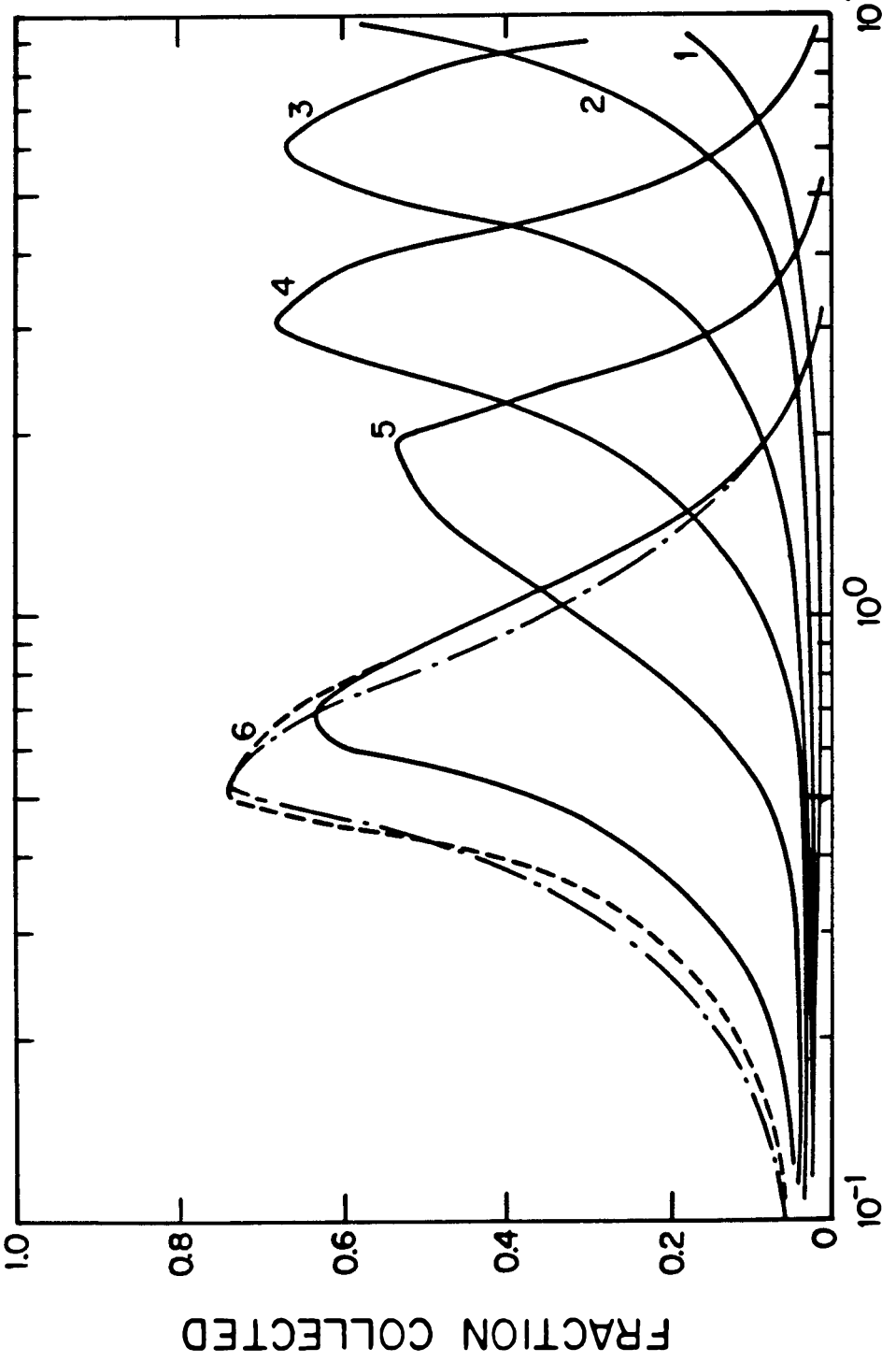

Figure 7

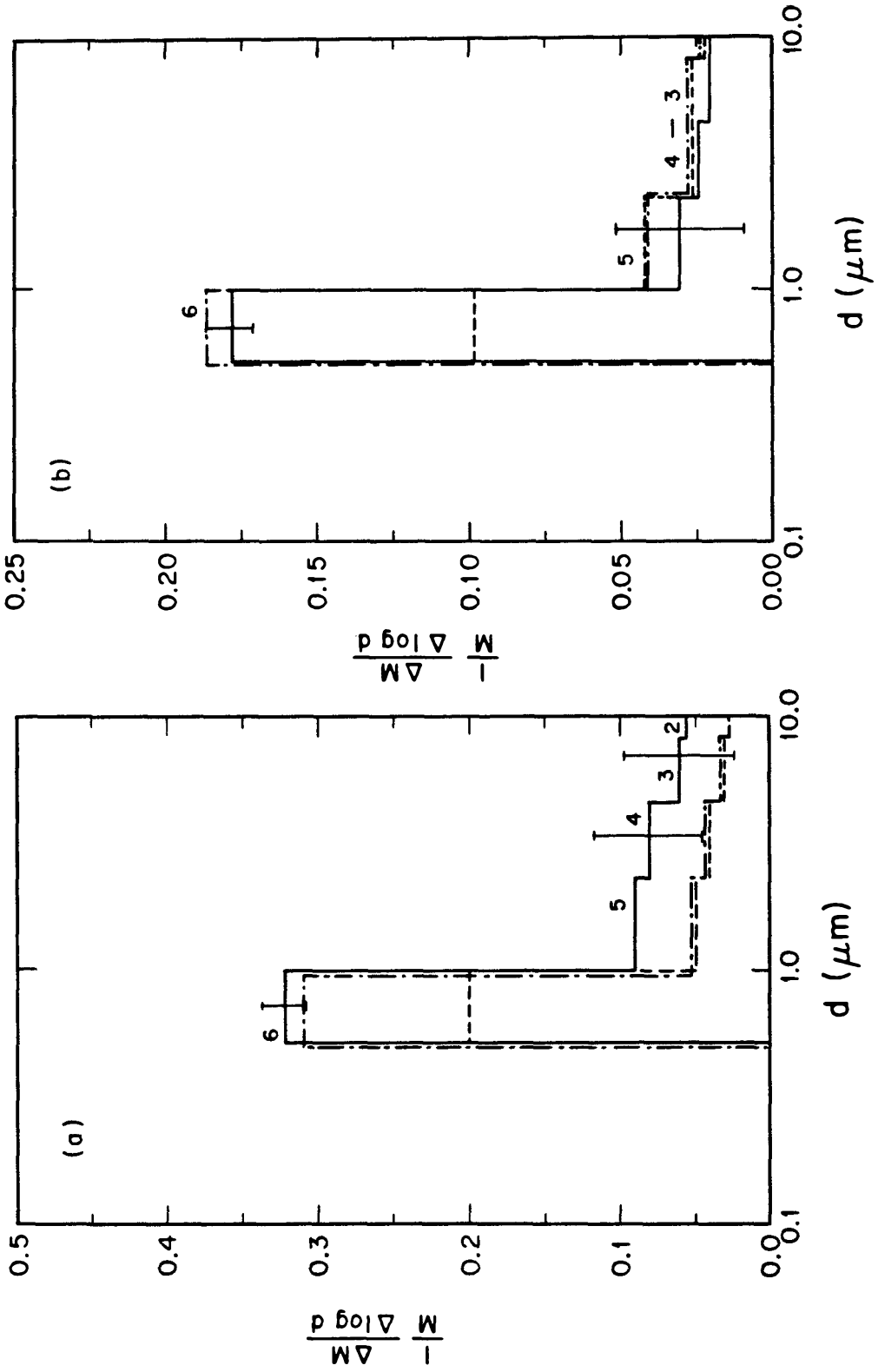

Figure 8

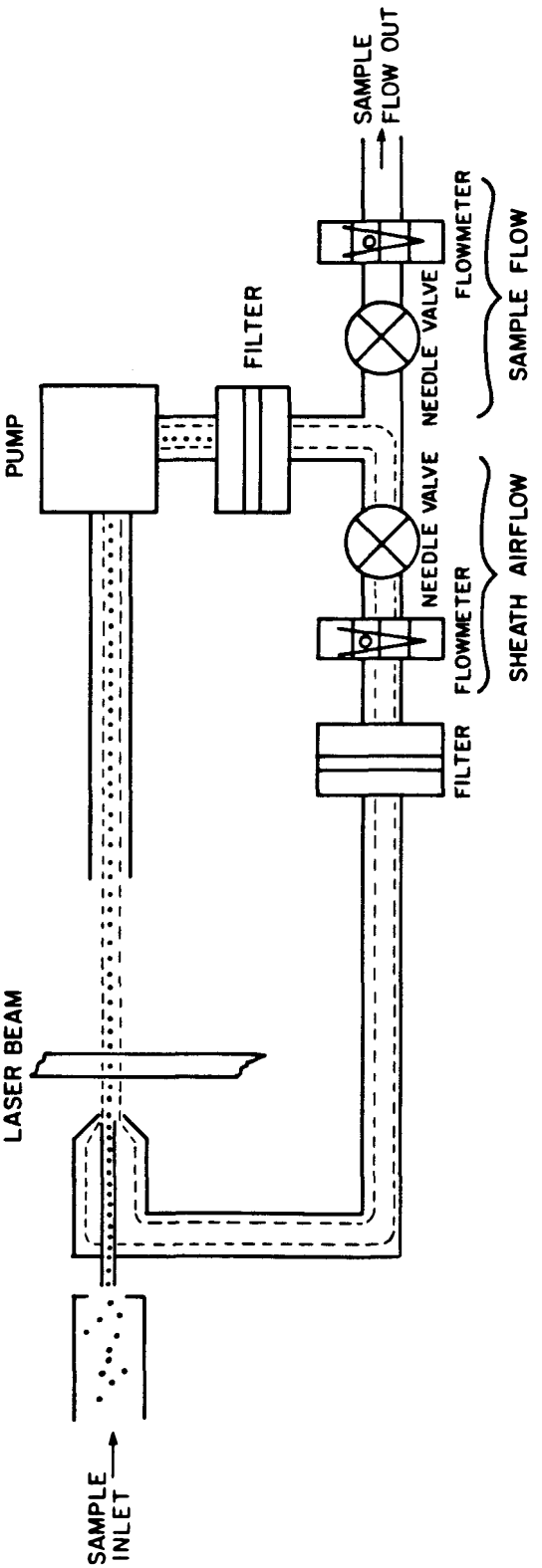
SAMPLE FLOW OUT
FLOWMETER
SAMPLE FLOW
NEEDLE VALVE
FILTER
PUMP
NEEDLE VALVE
FLOWMETER
SHEATH AIRFLOW
FILTER
LASER BEAM
SAMPLE INLET

Figure 9

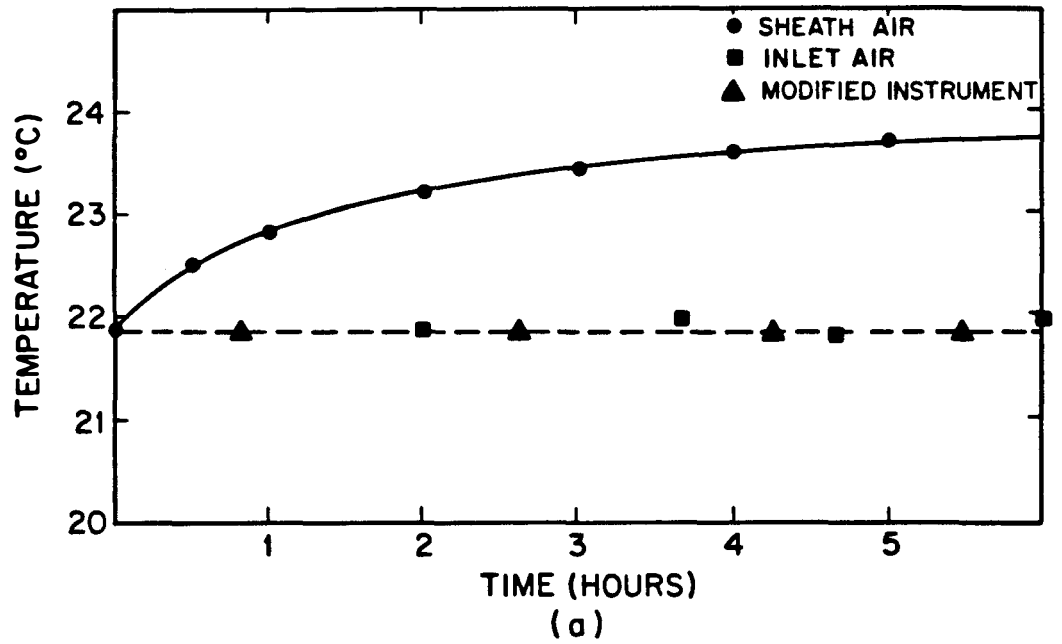
SHEATH AIR
INLET AIR
MODIFIED INSTRUMENT
TEMPERATURE (°C)
24
23
22
21
20
1
2
3
4
5
TIME (HOURS)
(a)

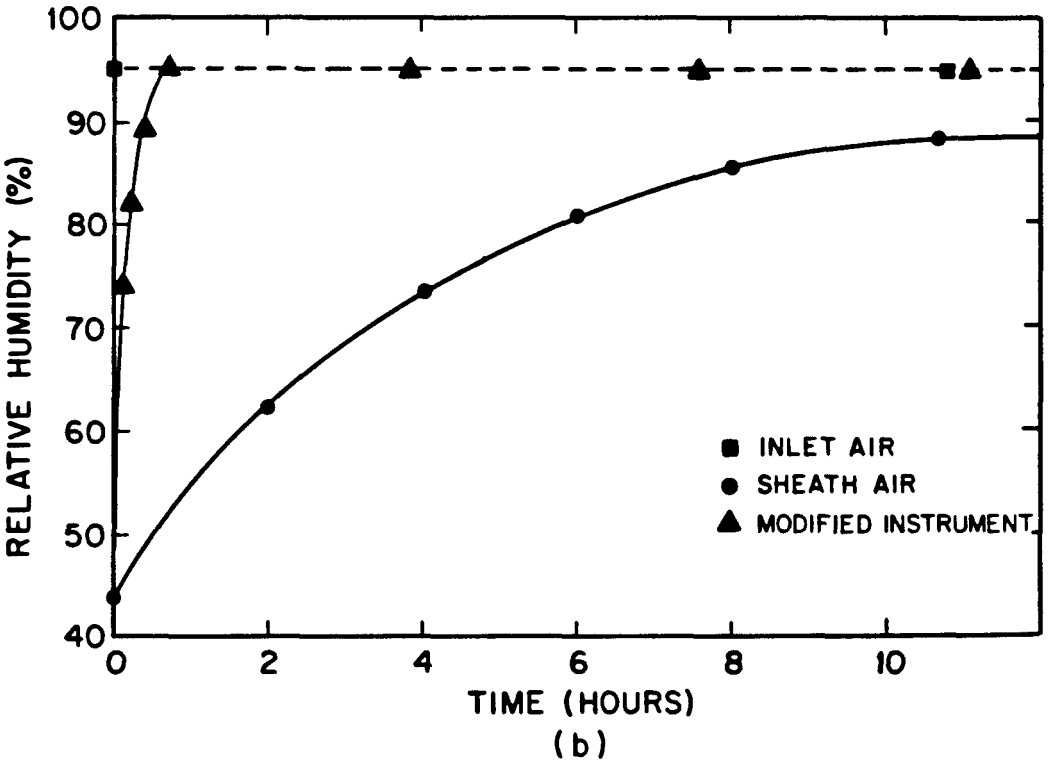
RELATIVE HUMIDITY (%)
100
90
80
70
60
50
40
0
2
4
6
8
10
TIME (HOURS)
INLET AIR
SHEATH AIR
MODIFIED INSTRUMENT
(b)

Figure 10

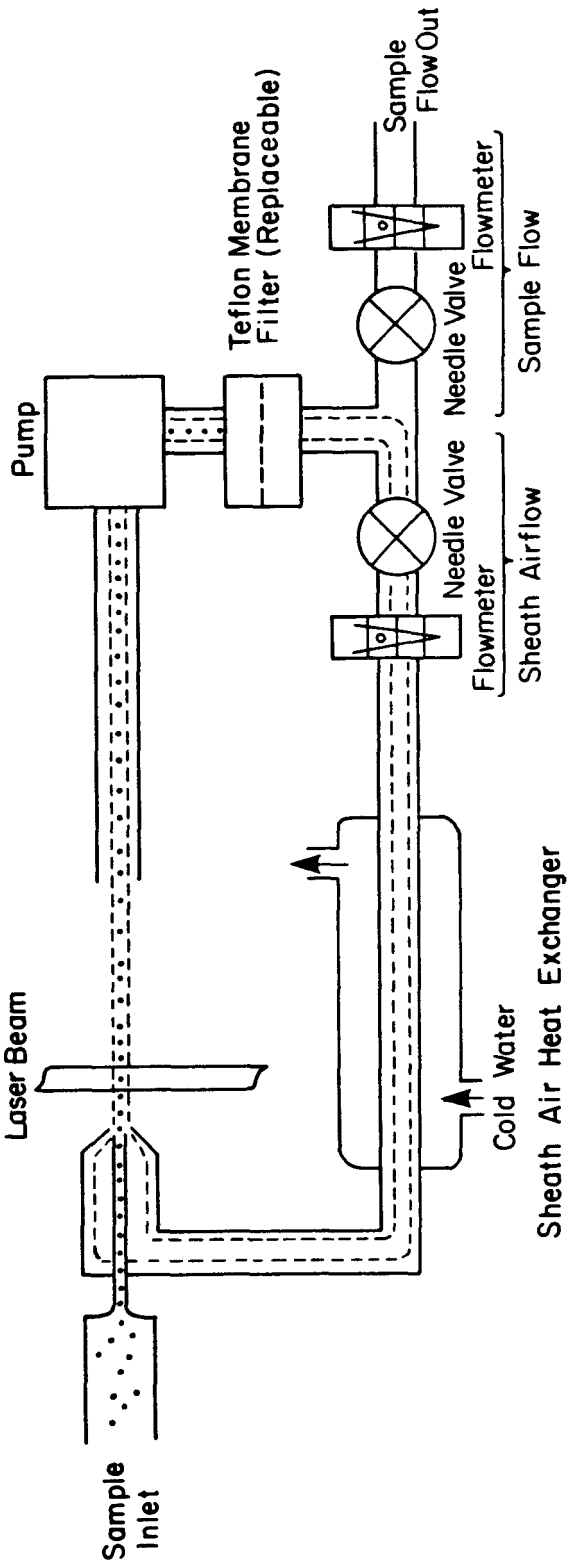
Sample Inlet
Laser Beam
Pump
Teflon Membrane Filter (Replaceable)
Sample Flow Out
Flowmeter
Needle Valve
Sample Flow
Needle Valve
Flowmeter
Sheath Airflow
Cold Water
Sheath Air Heat Exchanger

Figure 11.

APPENDIX B

ESTIMATION OF DEW POINT METER SENSOR CONTAMINATION

Since diameter changes are being studied in this work, it is important that every effort be made to understand the error inherent in their determination. The diameter of a liquid particle is extremely sensitive to the relative humidity of its environment. Relative humidity is a function of the air temperature and the moisture content, as measured by the dew point temperature. The possibility of soluble contaminants affecting the dew point measurement must be considered.

When the relative humidity is usually calculated, the following relation applies:

$$\mathrm{RH}_1 = \frac{P_{\mathrm{H_2O}}(T)}{P^{sat}_{\mathrm{H_2O}}(T)} = \frac{P^{sat}_{\mathrm{H_2O}}(T_{DP_1})}{P^{sat}_{\mathrm{H_2O}}(T)}. \tag{1}$$

It should be noted that this equation assumes first, that the solution is ideal, and second, that the solution is pure water. If the solution is a mixture of some solute and water, the decreased water concentration must be taken into account. Once again the solution is considered ideal.

$$\mathrm{RH}_2 = \frac{x_{\mathrm{H_2O}}\, P^{sat}_{\mathrm{H_2O}}(T_{DP_2})}{P^{sat}_{\mathrm{H_2O}}(T)} \tag{2}$$

How does T_{DP_1}, the dew point temperature that would have been measured had there been no contamination, compare to T_{DP_2}, the dew point actually measured with contamination? Fitting the saturated water vapor pressure data from 18 to 26°C with Antoine's equation

$$\ln P^{sat}_{\mathrm{H_2O}}(T) = \frac{-5313.88}{T} + 20.988 \quad (\mathrm{mmHg}), \tag{3}$$

and setting $\mathrm{RH}_1 = \mathrm{RH}_2$, gives

$$\ln x_{\mathrm{H_2O}} = 5313.88 \left(\frac{1}{T_{DP_2}} - \frac{1}{T_{DP_1}} \right). \tag{4}$$

Figure B.1 shows the relationship between the dew point temperatures as described by Equation (4). Clearly, increasing contamination has a dramatic effect on the dew point temperature — shifting the temperature upwards by more than one degree for a 10% drop in the water fraction.

If a dew point measurement is taken using a contaminated sensor, but the dew point correction of Equation (4) is not applied, how much error will result in the relative humidity? Equation (2) can be rewritten, $RH_2 = x_{H_2O} RH_0$, and the relative humidity RH_0 corrected for the effect of contaminated sensor.

The first source of contamination that will be considered is the equilibrium

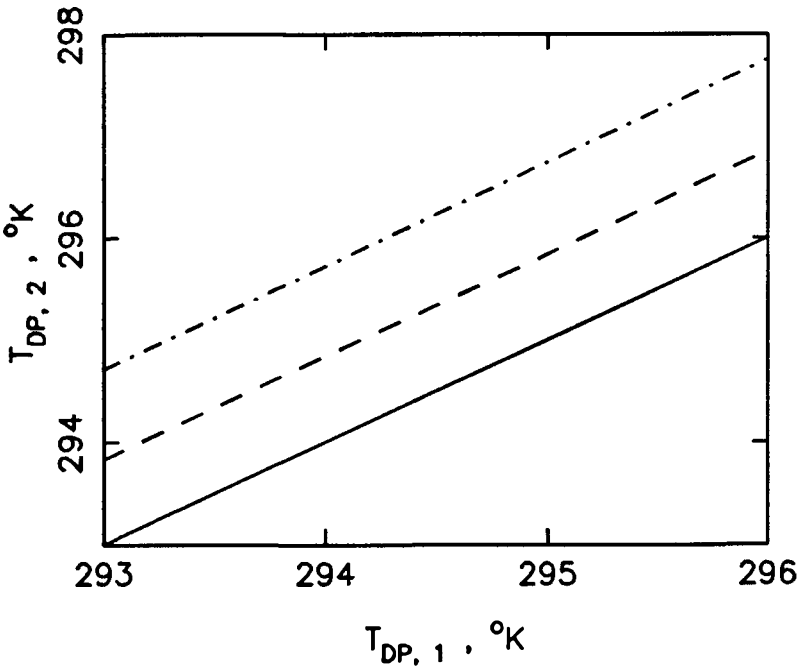

Figure B.1 The effect of contamination on the dew point temperature. $x_{H_2O} = 1.0$ (————), $x_{H_2O} = 0.95$ (— — — —), $x_{H_2O} = 0.90$ (— · — · — · —).

between the condensate and the gas-phase SO_2 . Consider the reactions

$$SO_2 \rightleftharpoons SO_2 \cdot H_2O, \tag{5}$$

$$SO_2 \cdot H_2O \rightleftharpoons H^+ + HSO_3^-, \tag{6}$$

$$HSO_3^- \rightleftharpoons H^+ + SO_3^{2-}, \tag{7}$$

$$H_2O \rightleftharpoons H^+ + OH^-. \tag{8}$$

The equilibrium constants at 25°C are

$$K_5 = 1.24 \times 10^{-6}\ \text{ppm}^{-1}\,\text{M},$$
$$K_6 = 0.0132\,\text{M},$$
$$K_7 = 6.24 \times 10^{-8}\,\text{M},$$
$$K_8 = 10^{-14}\,\text{M}^2.$$

Given the SO_2 gas-phase concentration, a charge balance can be performed on the reaction system ((5) – (8)) and the component concentrations obtained. If it is assumed that the solution density is 1 g/cm^3, or 55.56 mol/ℓ, then the water mole fraction is simply

$$x_{H_2O} = \frac{55.56 - \sum_i c_i}{55.56}, \tag{9}$$

where c_i is the molar concentration of the ith component. For $[SO_2]$ = 10 to 100 ppm, $x_{H_2O} = 0.999$. Thus, contamination due to the SO_2 - [S(IV)] equilibrium has a negligible effect on dew point temperature and relative humidity.

The second source of possible sensor contamination is aerosol deposition. The aerosol is not filtered from the air flow before the dew point meter. Approximately 1.14 ℓpm of air and SO_2, containing 10000 particles/cm^3, flow through the sensor housing. Because of the complex geometry of the annular space between the housing and the sensor, it is simply assumed that all of the 1.14 ℓpm flows across the mirror. This results in a velocity of 16.6 cm/s and a Reynold's number of 53 for the air flow in the mirror "channel" (see Figure B.2 for a schematic of the mirror channel).

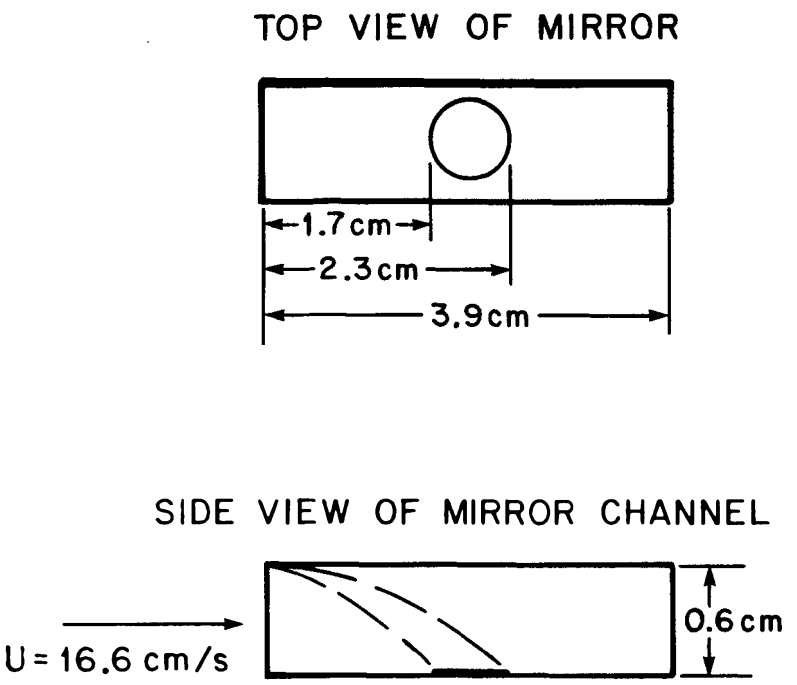

Figure B.2 Schematic of the dew point meter mirror channel.

An estimate of the particle deposition on the mirror is obtained using the fraction, f, of particles removed by gravitational settling in an infinitely wide channel of height $2H$ and length L, for laminar flow with velocity U,

$$f^2(3-2f) = \frac{Lv_t}{2UH}, \tag{10}$$

where v_t is the terminal velocity of the particles. If the fraction is first calculated for L equal to the distance to the mirror's leading edge, and then again for L equal to the mirror's opposite edge; the difference between the two fractions is an estimate of the fractional deposition on the mirror. See Figure B.2 for the values of L that were used in these calculations. For 0.1 μm particles having a density of 1 g/cm^3, the terminal settling velocity v_t is 3.0×10^{-6} cm/s. The fraction of particles that deposit on the mirror is approximately 6.7×10^{-5}. A typical

particle concentration of 10,000 particles/cm^3 flowing over the mirror will result in a particle deposition rate of 46,000 particles/hr. In order to make a rough estimate of the contamination level this represents, it was assumed that each particle has a solute concentration of 1 M. The solute depositing on the mirror amounts to 2.4×10^{-14} mol/hr. Finally, it is estimated that there are 0.05 moles of condensate (water) on the mirror, assuming a 0.001 inch thick layer. Given these parameters, a five-hour run will deposit $O(10^{-13})$ moles of solute into the condensate, resulting in no change of the water concentration.

Thus, it can be concluded that neither the gas phase SO_2 nor the aerosol particles will significantly contaminate the dew point sensor over the course of a typical experiment.

APPENDIX C

ESTIMATION OF THE AEROSOL GROWTH RESULTING FROM THE SO_2 - S(IV) EQUILIBRIUM

Because the goal of the reactor experiments was to observe the aerosol growth that was due to the manganese catalyzed S(IV) to S(VI) oxidation, it was necessary to determine how much growth, if any, is attributable to the SO_2 - S(IV) equilibrium. The $MnSO_4$ feed aerosol can be considered to consist of three ions in equilibrium — Mn^{2+}, SO_4^{2-}, and HSO_4^-. The initial $MnSO_4$ concentration is determined by the equilibrium between the drop and the humid atmosphere (see Chapter 5),

$$a_w = \mathrm{RH} \exp\left(-\frac{4\sigma v_m}{kTD_p}\right). \tag{0}$$

Upon exposure to SO_2, the equilibrium between the S(IV) species and SO_2 is established within microseconds and is described by the following reaction system:

$$SO_2 \rightleftharpoons SO_2 \cdot H_2O, \tag{1}$$

$$SO_2 \cdot H_2O \rightleftharpoons H^+ + HSO_3^-, \tag{2}$$

$$HSO_3^- \rightleftharpoons H^+ + SO_3^{2-}, \tag{3}$$

$$HSO_4^- \rightleftharpoons H^+ + SO_4^{2-}. \tag{4}$$

Because the solution will be acidic, pH values less than 5 are expected, the concentration of OH^- ions was neglected. Pure $MnSO_4$ at 90% humidity has an equilibrium concentration on the order of 3 m (molal), or 2.8 M (molar), and a corresponding ionic strength of 12 m. The assumption of unity activity coefficients, or ideal solution behavior, is not possible and the following equilibrium equations must be used:*

$$K_1 = \frac{m_{SO_2 \cdot H_2O}}{p_{SO_2}} = 1.24 \times 10^{-6} \,\mathrm{mol\,ppm^{-1}\,kg^{-1}}, \tag{5}$$

* m_i is used to indicate the molality of species i.

$$K_2 = \frac{\gamma^2_{H^+,HSO_3^-}\, m_{H^+} m_{HSO_3^-}}{m_{SO_2 \cdot H_2O}} = 0.0132 \text{ mol kg}^{-1}, \tag{6}$$

$$K_3 = \frac{\gamma^3_{2H^+,SO_3^{2-}}\, m_{H^+} m_{SO_3^{2-}}}{\gamma^2_{H^+,HSO_3^-}\, m_{HSO_3^-}} = 6.24 \times 10^{-8} \text{ mol kg}^{-1}, \tag{7}$$

$$K_4 = \frac{\gamma^3_{2H^+,SO_4^{2-}}\, m_{H^+} m_{SO_4^{2-}}}{\gamma^2_{H^+,HSO_4^-}\, m_{HSO_4^-}} = 0.012 \text{ mol kg}^{-1}. \tag{8}$$

The activity coefficients in the above equations are for the specified ions in the aerosol solution mixture. Activity coefficients presented in the literature are typically for a pure binary solution. Therefore, a mixing rule must be used to obtain the necessary mixture coefficients given the pure component data. As with the water activity calculated in Chapter 5, the Kusik and Meissner (1978) mixing rule was used. This can be expressed as follows:

$$\begin{aligned} I \ln\gamma_{12} = {} & \frac{z_2}{z_1 + z_2} \sum_j m_j \left(\frac{z_1 + z_j}{2} \right)^2 \ln\gamma^\circ_{1j}(I) \\ & + \frac{z_1}{z_1 + z_2} \sum_i m_i \left(\frac{z_i + z_2}{2} \right)^2 \ln\gamma^\circ_{i2}(I), \end{aligned} \tag{9}$$

where I is the solution ionic strength, the i and j subscripts refer to cations and anions, respectively, and γ°_{12} is the mean activity coefficient for a binary solution containing only ions i and j. The neutral species $SO_2 \cdot H_2O$ is assumed to have no effect on the coefficient.

The primary difficulty in using any mixing rule is obtaining the necessary data. In order to use the above mixing rule, "pure" component activity coefficient data are needed for the species $MnSO_4$, $Mn(HSO_4)_2$, $MnSO_3$, $Mn(HSO_3)_2$, $H_2(SO_4)$, $H(HSO_4)$, $H_2(SO_3)$, and $H(HSO_3)$. The assumptions made in gathering the activity coefficient data are discussed in the following paragraphs and the data used in the calculations are presented in Table C.1.

Any solution containing bisulfate ions will also contain sulfate ions formed by

dissociation equilibrium (4). The measured water activity of sulfuric acid (Rard et al. (1976), Rard (1983)) is actually data for the ternary system H^+, HSO_4^-, and SO_4^{2-}. However, the activity coefficient mixing rule above requires pure component data for the hypothetical solutions containing *only* sulfate or bisulfate anions. Stelson et al. (1984) has used the mixing rules of Kusik and Meissner (1978) to "unmix" the sulfuric acid data and obtain "pure" component activity coefficients for the systems H^+,HSO_4^- and $2H^+$,SO_4^{2-}. Since mixing rules are basically empirical formulations, the resulting activity coefficients are a function of the mixing rule used to generate them. However, $\gamma^\circ_{2H^+,SO_4^{2-}}$ is the same order of magnitude as the measured $\gamma^\circ_{2Na^+,SO_4^{2-}}$ and the behavior of $\gamma^\circ_{H^+,HSO_4^-}$ is similar to that of other univalent acids (Stelson et al. (1984)). The "unmixed" activity coefficients of sulfuric acid exhibit reasonable behavior.

There are very little data for manganese salts — possibly because manganese is not an important component of seawater. The data of Rard (1984) was used to calculate $\gamma^\circ_{Mn^{2+},SO_4^{2-}}$. No $Mn(HSO_4)_2$ data were found. Since this is a 1 - 2 electrolyte, it will behave differently from the 2 - 2 $MnSO_4$ electrolyte. The Pitzer coefficients for $MnCl_2$ determined by Cohen et al. (1987) for the concentration range 0.1 to 12 m were used to estimate $\gamma^\circ_{Mn^{2+},2HSO_4^-}$.

Rosenblatt (1981), recognizing the lack of sulfite data, has estimated the Pitzer parameters for sodium, potassium, calcium, and magnesium sulfite and bisulfite salts. The estimated error in the activity coefficient accuracy is ±25%. Goldberg (1981) has collected data from a variety of sources and presents the "best" sodium sulfite data along with a fit of the data. The maximum molality of 2 corresponds to a solution ionic strength of 6 molal. Huss and Eckert (1977) determined the activity coefficient of the hydrogen-bisulfite ion pair for ionic strengths less than 0.06 M. The ionic strength expected in the aerosol will be several hundred times this limit. Given the lack of data for the various sulfite and bisulfite compounds in the appropriate ionic strength range, sulfate data were used to approximate

the sulfite activity coefficients, and bisulfate data was used to approximate the bisulfite coefficients for both the manganese and hydrogen ion pairs. Some error is introduced in making this assumption, although no more than would be introduced by extending the available data orders of magnitude past current experimental limits. In addition, the concentrations of sulfite, bisulfite, and bisulfate will be several orders of magnitude less than the sulfate concentration that will minimize the overall error in the mixed coefficients that is due to these estimates.

A charge balance on the reaction system (1) – (4) gives:

$$2\,m_{Mn^{2+}} + m_{H+} = 2\,m_{SO_4^{2-}} + m_{HSO4-} + 2\,m_{SO_3^{2-}} + m_{HSO_3^-}. \qquad (10)$$

The equilibrium Equations (5) – (8) and the fact that $m_{Mn^{2+}} = m_{HSO_4^-} + m_{SO_4^{2-}}$ (this calculation will determine the droplet size at the instant after equilibrium is established and before the S(IV) to S(VI) reaction begins) can be combined to give an equation that can be solved iteratively for the hydrogen ion concentration given the manganese concentration,

$$m_{H+}^2 - m_{H+}m_{Mn^{2+}} \left\{ \frac{\left(1 + \dfrac{2K_4\gamma^2_{H+,HSO_4^-}}{m_{H+}\gamma^3_{2H+,SO_4^{2-}}}\right)}{\left(1 + \dfrac{K_4\gamma^2_{H+,HSO_4^-}}{m_{H+}\gamma^3_{2H+,SO_4^{2-}}}\right)} - 2 \right\}$$

$$- \left\{ K_1K_2p_{SO_2}\left[\frac{1}{\gamma^2_{H+,HSO_3^-}} + \frac{2K_3}{\gamma^3_{2H+,SO_3^{2-}}\,m_{H+}}\right]\right\} = 0. \qquad (11)$$

The final piece of information needed is the water activity, since the particle must be in equilibrium with its humid surroundings at all times. The Kusik and Meissner (1978) water activity mixing rule requires that the concentration of the individual salts that can be formed from every possible combination of the cations and anions be known. However, the charge balance and equilibrium equations give only ion concentrations. Fortunately, the choice of the set of salts formed from a

group of ions that satisfy the charge balance is not unique. For example, given ion concentrations of $m_{Mn^{2+}} = 2.5$, $m_{Na^+} = 0.5$, $m_{Cl^-} = 1.0$, and $m_{SO_4^{2-}} = 2.25$, the species sets $m_{MnSO_4} = 2.25$, $m_{MnCl_2} = 0.25$, and $m_{NaCl} = 0.5$, or $m_{MnSO_4} = 2.0$, $m_{MnCl_2} = 0.5$, and $m_{Na_2SO_4} = 0.25$, both result in a mixture water activity of 0.908. The following hierarchy was used in "creating" the ion-pair species: $MnSO_4 > Mn(HSO_4)_2 > MnSO_3 > Mn(HSO_3)_2 > H_2(SO_4) > H(HSO_4) > H_2(SO_3) > H(HSO_3)$. The predominant ionic species in the aerosol solution was Mn^{2+} and because good $MnSO_4$ water activity exists, as much Mn^{2+} as possible was attributed to the electrolyte $MnSO_4$. In a typical solution, there was usually just enough bisulfite ion left to combine with the hydrogen ion after all the manganese species were formed.

The Kusik and Meissner (1978) mixing rules result in the following equation to describe the aerosol solution containing 3: H^+, 5: Mn^{2+}, 2: SO_4^{2-}, 4: HSO_4^-, 6: SO_4^{2-}, and 8: HSO_3^- ions:

$$
\begin{aligned}
\ln a_w^{mix} = \frac{(2m_{32} + m_{34} + 2m_{36} + m_{38})}{I^2} \Bigg\{ & \frac{9}{2}(m_{32} + m_{52}) \ln a^{\circ}_{w,32}(I) \\
& + (m_{34} + 2m_{54}) \ln a^{\circ}_{w,34}(I) + \frac{9}{2}(m_{36} + m_{56}) \ln a^{\circ}_{w,36}(I) \\
& + (m_{38} + 2m_{58}) ln\, a^{\circ}_{w,38}(I) \Bigg\} \\
& + \frac{(m_{52} + m_{54} + m_{56} + m_{58})}{I^2} \Bigg\{ 16(m_{32} + m_{52}) \ln a^{\circ}_{w,52}(I) \\
& + \frac{9}{2}(m_{34} + 2m_{54}) \ln a^{\circ}_{w,54}(I) + 16(m_{36} + m_{56}) \ln a^{\circ}_{w,36}(I) \\
& + \frac{9}{2}(m_{38} + 2m_{58}) \ln a^{\circ}_{w,58}(I) \Bigg\} \\
& - \frac{MW_{H_2O}}{1000\, I} \Bigg\{ \frac{1}{2}(m_{34} + m_{38})(m_{32} + m_{36} + m_{54} + m_{58}) \\
& + 2(m_{32} + m_{36})(m_{54} + m_{58}) \\
& + (m_{52} + m_{56})(m_{54} + m_{58} + m_{32} + m_{36} + m_{34} + m_{38}) \Bigg\},
\end{aligned}
\tag{12}
$$

where m_{ij} is the molality of the species formed by ions i and j, I is the ionic

strength of the mixture, and $a^{\circ}_{w,ij}$ is the water activity of a binary solution of species ij. The same assumptions made in determining the activity coefficients were made in calculating the individual binary water activities.

Finally, the procedure for shifting a size distribution after SO_2 equilibration can be summarized as follows. A constant system atmosphere — relative humidity, temperature, pressure, and SO_2 concentration — was assumed. The initial manganese concentration was calculated for each particle size. Because the Kelvin effect was taken into account, the concentration decreased slightly with increasing particle diameter. The initial manganese concentration was used as a starting guess for the determination of the equilibrium concentration. Given a manganese concentration, the hydrogen ion concentration was calculated. Because the activity coefficients are also a function of the hydrogen ion concentration, this had to be done iteratively. The "species" were formed and the water activity calculated. This value was compared to the water activity calculated using the water activity and an initial particle diameter guess. The manganese concentration was adjusted until these two values agreed. However, because these calculations depended on the particle diameter guess, the validity of this guess was now checked. The moles of manganese from the feed particle (a conserved quantity) and the just calculated solution total concentration were used to calculate a new particle diameter. If the correct diameter was used in the equilibrium calculations, it and the new diameter would be identical. If, however, the particle diameter guess was incorrect, the average of the two diameters was used as a initial guess and the equilibrium calculations were repeated. This iterative process continued until the particle diameter guess and the calculated diameter agreed to within some specified tolerance. Because of the number of iterations necessary to arrive at the final diameter, the program was slow, taking on the order of $3\frac{1}{2}$ hours to shift a distribution of 56 diameters ($\sim$ 4 minutes/feed diameter). The program listing, SO2EQM.FOR, is given in Appendix E.

It was found that the SO_2 equilibrium resulted in an insignificant change in the particle diameter. For instance, at constant operating conditions of 23°C and 93% relative humidity, an 0.16 μm diameter $MnSO_4$ aerosol particle grew to 0.16006 μm when placed in a 15 ppm SO_2 atmosphere. This amount of growth is not detectable using the electrical mobility classifier as a sizing device. Figure C.1 shows the distribution resulting from the equilibration of the feed aerosol for Experiment 5 when equilibrated with 50.2 ppm SO_2.

Several of the reactor experiments were run with a feed aerosol that consisted of a sodium sulfate and manganese sulfate mixture. The molar ratio was either 10 or 100 moles Na_2SO_4 per mole $MnSO_4$. Since Na_2SO_4 and $MnSO_4$ have considerably different water activities, the growth of a sodium sulfate particle when it is equilibrated with an SO_2 atmosphere was calculated. The mixing rules for activity coefficients and water activities had to be rederived since the sodium ion is singly charged, whereas the manganese ion was doubly charged. The solution charge balance was also changed, resulting in a new formula for the hydrogen ion. Because the moles of sodium sulfate did not equal moles of sodium ions, special care had to be taken in converting species to ions and ions to species. Assumptions similar to those made for the $MnSO_4$ system were made when calculating the activity coefficients and water activities, i.e., sulfites $\rightarrow$ sulfates and $NaHSO_4 \rightarrow$ NaCl (see Table C.1). As in the case of manganese sulfate, an insignificant, unobservable amount of growth occurred upon equilibration with sulfur dioxide for pure sodium sulfate particles. Therefore, the Na_2SO_4-$MnSO_4$ feed aerosol will also undergo a negligible amount of growth when placed in a sulfur dioxide atmosphere.

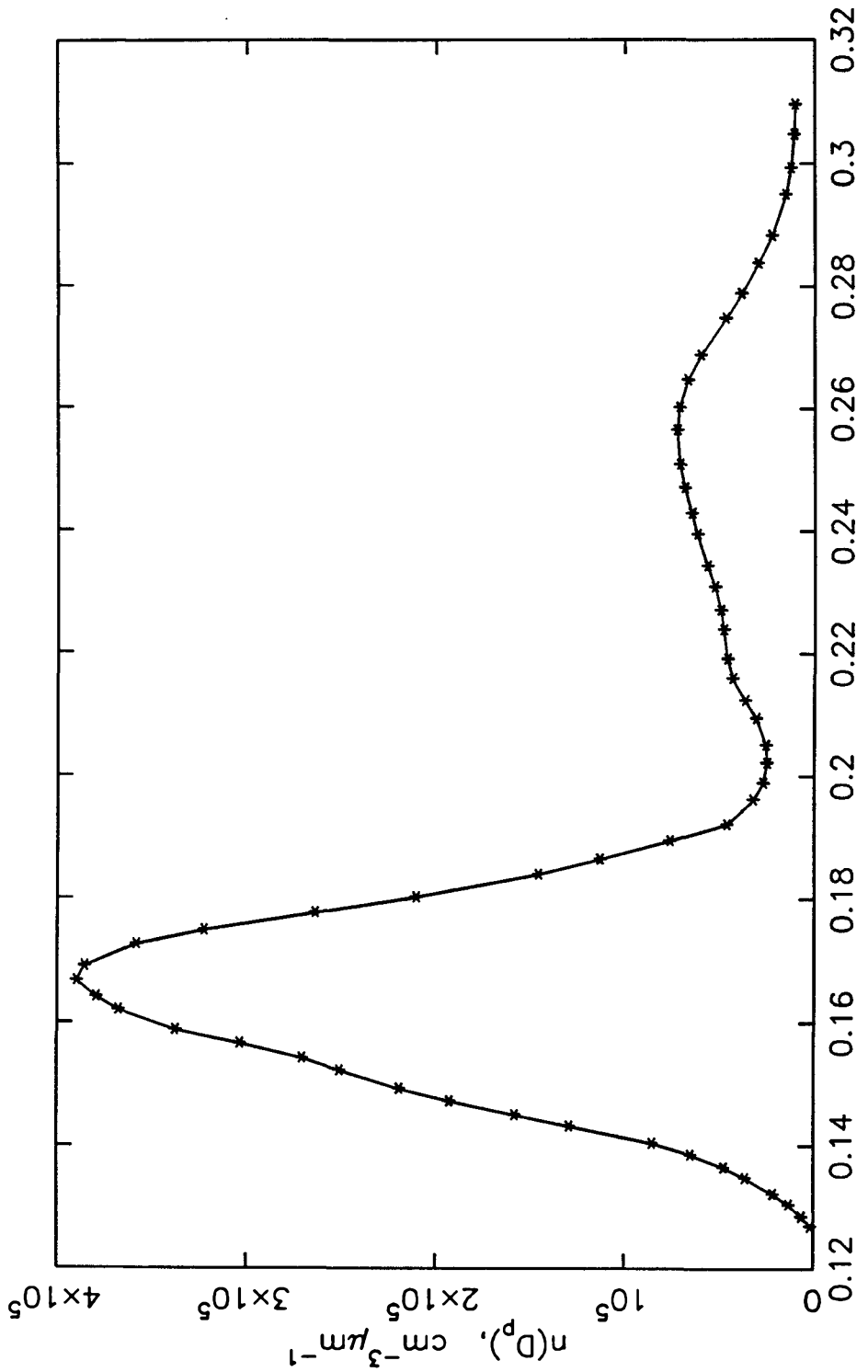

Figure C.1 $MnSO_4$ feed distribution (_____) and distribution shifted due to equilibration with 50.2 ppm SO_2 (*). $T = 23.34°C$, RH = 92.38% (Experiment 5).

Table C.1

Activity Coefficient and Water Activity Data

Species	Formula	Source
$MnSO_4$	$\ln \gamma^{\circ}_{Mn^{2+},SO_4^{2-}} = -9.4097\, m^{0.5} - 49.9297\, m^{0.75} + 319.5924\, m - 766.8403\, m^{1.25} + 1018.469\, m^{1.5} - 807.7082\, m^{1.75} + 378.8511\, m^2 - 96.1819\, m^{2.25} + 10.0539\, m^{2.5}$	Rard (1984)
	$a^{\circ}_{w,MnSO_4} = 0.999382 - 0.162799 \times 10^{1}\, m + 0.916004 \times 10^{-3}\, m^2 - 0.119784 \times 10^{-2}\, m^3 - 0.245205 \times 10^{-3}\, m^4 + 0.465363 \times 10^{-4}\, m^5$	
$Mn(HSO_4)_2$	$\ln \gamma^{\circ}_{Mn^{2+},2HSO_4^{-}} \sim \ln \gamma^{\circ}_{Mn^{2+},2Cl^{-}}$	Cohen et al. (1987)
	Pitzer's coefficients for $MnCl_2$: $\beta^{(0)}_{MX} = 0.25811$, $\beta^{(1)}_{MX} = 2.31108$, $C^{\phi}_{MX} = -0.010540$, $\alpha = 2.0$	
	$a^{\circ}_{w,Mn(HSO_4)_2} \sim a^{\circ}_{w,MnCl_2} = 0.9989 - 3.639 \times 10^{-2}\, m - 2.049 \times 10^{-2}\, m^2 + 4.286 \times 10^{-3}\, m^3 - 4.137 \times 10^{-4}\, m^4 + 1.960 \times 10^{-5}\, m^5 - 3.417 \times 10^{-7}\, m^6$	
H_2SO_4	$\ln \gamma^{\circ}_{2H^+,SO_4^{2-}} = 0.0244133 - 1.7997\, I^{0.5} + 0.263197\, I + 0.152819\, I^{1.5} - 0.512581 \times 10^{-1}\, I^2 + 0.431276 \times 10^{-2}\, I^{2.5}$	Stelson et al. (1984)
	$a^{\circ}_{w,H_2SO_4} = \exp\left(-\left\{I \ln \gamma^{\circ}_{2H^+,SO_4^{2-}} - \int_0^I \ln \gamma^{\circ}_{2H^+,SO_4^{2-}} dI + I\right\}/n_{H_2O}\right)$	

$H(HSO_4)$	$\ln \gamma^{\circ}_{H^+,HSO_4^-} = 0.371591 \times 10^{-2} - 0.908027\, I^{0.5} + 1.25847\, I - 0.547089\, I^{1.5} + 0.217464\, I^2 - 0.426523 \times 10^{-1}\, I^{2.5} + 0.292312 \times 10^{-2}\, I^3$ $a^{\circ}_{w,H(HSO_4)} = \exp\left(-2\left\{I \ln \gamma^{\circ}_{H^+,HSO_4^-} - \int_0^I \ln \gamma^{\circ}_{H^+,HSO_4^-} dI + I\right\}/n_{H_2O}\right)$	Stelson et al. (1984)
Na_2SO_4	$\ln \gamma^{\circ}_{2Na^+,SO_4^{2-}} = -4.0744\, m^{0.5} + 9.7222\, m - 7.03886\, m^{1.25} - 9.94097\, m^{1.5} + 17.27803\, m^{1.75} - 9.31217\, m^2 + 1.77454\, m^{2.25}$ $a^{\circ}_{w,Na_2SO_4} = 0.998754 - 0.0358089\, m + 0.406391 \times 10^{-2}\, m^2 - 0.111982 \times 10^{-2}\, m^3$	Rard & Miller (1981)
$NaHSO_4$	$\ln \gamma^{\circ}_{Na^+,HSO_4^-} \sim \ln \gamma^{\circ}_{Na^+,Cl^-}$ Pitzer's coefficients for NaCl: $\beta^{(0)}_{MX} = 0.10820,\ \beta^{(1)}_{MX} = 0.03127$ $C^{\phi}_{MX} = -0.002469,\ \alpha = 2.0$ $a^{\circ}_{w,NaHSO_4} \sim a^{\circ}_{w,NaCl} = 1.0084 - 4.939 \times 10^{-2}\, m + 8.888 \times 10^{-3}\, m^2 - 2.157 \times 10^{-3}\, m^3 + 1.617 \times 10^{-4}\, m^4 - 1.990 \times 10^{-6}\, m^5 - 1.142 \times 10^{-7}\, m^6$	Cohen et al. (1987)

REFERENCES

COHEN, M. D., FLAGAN, R. C. and SEINFELD, J. H. (1987) Studies of concentrated electrolyte solutions using the electrodynamic balance. I. Water activities for single-electrolyte solutions. *J. Phys. Chem.*, in press.

GOLDBERG, R. N. (1981) Evaluated activity and osmotic coefficients for aqueous solutions: Thirty-six uni-bivalent electrolytes. *J. Phys. Chem. Ref. Data*, **10**:671-764.

HUSS, JR., A. and ECKERT, C. A. (1977) Equilibria and ion activities in aqueous sulfur dioxide solutions. *J. Phys. Chem.*, **81**:2268-2270.

KUSIK, C. L. and MEISSNER, H. P. (1978) Electrolyte activity coefficients in inorganic processing. *Amr. Inst. Chem. Engr. Symp. Ser.*, **74(173)**:14-20.

RARD, J. A. (1983) Isopiestic determination of the osmotic coefficients of aqueous H_2SO_4. *J. Chem. Eng. Data* , **28**:384-387.

RARD, J. A. (1984) Isopiestic determination of the osmotic and activity coefficients of aqueous $MnCl_2$, $MnSO_4$, and $RbCl_2$ at 25 °C. *J. Chem. Eng. Data* , **29**:443-450.

RARD, J. A., HABENSCHUSS, A. and SPEDDING, F. H. (1976) A review of the osmotic coefficients of aqueous H_2SO_4 at 25°C. *J. Chem. Eng. Data* , **21**:374-379.

RARD, J. A. and MILLER, D. G. (1981) Isopiestic determination of the osmotic coefficients of aqueous Na_2SO_4, $MgSO_4$ and $Na_2SO_4 - MgSO_4$ at 25 °C. *J. Chem. Eng. Data* , **26**:33-38.

ROSENBLATT, G. M. (1981) Estimation of activity coefficients in concentrated sulfite-sulfate solutions. *AIChE J.*, **27**:619 626.

STELSON, A. W., BASSETT, M. E. and SEINFELD, J. H. (1984) Thermodynamic equilibrium properties of aqueous solutions of nitrate, sulfate and ammonium, in *Chemistry of Particles, Fogs and Rain* (J. L. Durham, ed.). Butterworth Publishers, Boston, pp. 1-51.

APPENDIX D

COMMENTS CONCERNING THE CSTR MODEL CALCULATIONS

As shown in Chapter 6, the CSTR effluent size distribution can be predicted given a known feed size distribution. A polydisperse feed distribution can be considered to be simply linear combination of monodisperse feeds. Consequently, the CSTR model actually entails calculating the effluent distribution for each of a specified number of feed diameters. As the number of feed sizes increases, so does the required computer time. "Shortcuts" and methods used in the model computations, along with some of the physical property data required, will be discussed in this appendix.

First, however, a brief description of the CSTR calculations is necessary to understand the details described later (see Chapter 6, §6.3). For each feed diameter, a set of sizes is generated representing the effluent distribution resulting from the original feed distribution. The dimensionless size range 0 to 1 (or any fraction thereof, i.e., if the reaction rate is slow, one needs to use only $0 < x < 0.5$) is divided evenly into a specified number of divisions. Since the salt concentration in the "parent" particle is known, the salt concentration for this particle after it has grown to a specified size is also known. This concentration, along with the system relative humidity, is used to infer the acid concentration necessary such that RH $= a_w(salt, acid)$ is true. Given the salt and acid concentrations, the solution chemistry (see Chapter 6, Equations (23) through (28)) for the droplet is used to determine the concentrations of H^+ and S(IV), and the reaction rate calculated. This information, for each of the sizes in the set corresponding to the feed diameter, is then used to calculate the integral in Equation (19), Chapter 6. The resulting distribution represents the CSTR effluent, given a monodisperse feed. A similar distribution is generated, using each size in the set of feed diameter versus total number describing the feed distribution. The set of effluent distributions are

then "added," giving the effluent distribution predicted by the thermodynamics, chemistry, and kinetics assumed. The feed aerosol is treated as a histogram. Thus, each monodisperse "size" actually has a finite width associated with it. If the reaction rate is fast, or the effluent distribution for a monodisperse feed is rather smooth and "flat," the finite width has little effect when the effluent distribution set is added, since little change occurs over this width. However, if the reaction rate is slow and the effluent distributions resemble exponential decay curves, the initial rapid change in the size distribution results is apparent in the final distribution. The distribution appears to oscillate. In this case it is necessary to use a larger number of feed diameters when constructing the initial histogram.

The Kelvin effect was neglected in the model calculations. Therefore, every feed particle, regardless of size, has the same initial salt concentration. Since the salt does not evaporate, salt mass is conserved. If particle diameter growth is due only to condensation, then the salt concentration can be calculated at any subsequent diameter. For instance, a particle initially having diameter $D_{p,0}$ and manganese concentration $C_{m,0}$ will have a manganese concentration of

$$C_{m,f} = C_{m,0} \left(\frac{D_{p,0}}{D_{p,f}} \right)^3 , \tag{1}$$

at a final diameter of $D_{p,f}$. This relation is true whether or not reaction is occurring in the particle.

Because of the distribution of residence times associated with a CSTR, a monodisperse feed aerosol will result in a polydisperse effluent aerosol. Consequently, the point was made in Chapter 5 that given a polydisperse feed aerosol, aerosol particles of the same diameter in the CSTR effluent will have a differing composition since they could have resulted from *any* feed particle of smaller size. The salt and acid concentrations at thermodynamic equilibrium must be calculated for the particles "grown" from *each* particular feed size. However, because the Kelvin effect is being ignored and the calculations are being done on the nondimensional scale $x = 0$ to 1, where

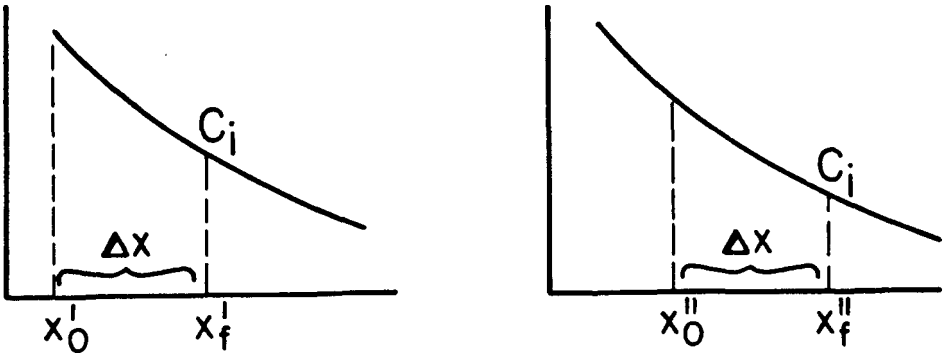

Figure D.1 CSTR effluent particles have the same concentration, regardless of the initial feed size, Δx along the dimensionless size axis.

$$x = \frac{\ln(D_p/D_{p,min})}{\ln(D_{p,max}/D_{p,min})}, \tag{2}$$

the growth of only one feed size need be considered. If Equation (1) is written for two feed particles of different size (the initial concentration is identical),

$$C^I_{m,f} = C_{m,0}\left(\frac{D^I_{p,0}}{D^I_{p,f}}\right)^3 \qquad \text{and} \qquad C^{II}_{m,f} = C_{m,0}\left(\frac{D^{II}_{p,0}}{D^{II}_{p,f}}\right)^3, \tag{3}$$

and the case is considered where $C^I_{m,f} = C^{II}_{m,f}$, then

$$\frac{D^I_{p,0}}{D^I_{p,f}} = \frac{D^{II}_{p,0}}{D^{II}_{p,f}}. \tag{4}$$

Equation (2) can be used to nondimensionalize these diameters, giving

$$x^I_f - x^I_0 = x^{II}_f - x^{II}_0 = \Delta x,$$

or

$$x^I_f = x^I_0 + \Delta x. \tag{5}$$

Thus, working on the nondimensional size range, the particle composition and kinetics have to be determined for only one set of x_f. These values can then be used to determine the composition for any new x_f at corresponding Δx values (see Figure D.1).

Once the individual effluent distributions have been generated for the "monodisperse" feeds, they must be combined into the overall effluent distribution resulting from the polydisperse feed. If the distributions all corresponded to the same set of diameters, obtaining the effluent distribution would merely involve adding the distribution values for a given diameter. However, since the diameters of the feed distribution are not necessarily evenly spaced (the sharper the peak, the more diameters used in that region of the diameter range during the data inversion) and a spline fit was not used to calculate a set of evenly spaced values (too many diameters would be necessary to adequately describe both the peak and the entire feed distribution), simple addition of effluent distributions was not possible. To begin, calculated distribution values less than a set value of 10^{-5} were neglected to save computer time. A working diameter range was obtained by searching for the minimum and maximum diameter in the distributions resulting from the minimum and maximum feed diameters, respectively. This range was then divided into a set of equally spaced diameters. For each of the individual effluent distributions, the distribution value was obtained at the diameters in the generated set. Logarithmic interpolation was used. The new set of distributions was then added ($n(\ln D_{p,j})_{tot} = \sum_{i=1}^{N} n_i(\ln D_{p,j})$) to obtain the final effluent distribution. Because the diameter was nondimensionalized on the natural log scale, the calculated distributions are actually $n(\ln D_p)$:

$$n(x) = \ln\left(\frac{D_{p,max}}{D_{p,min}}\right) n(\ln D_p) = D_p \ln\left(\frac{D_{p,max}}{D_{p,min}}\right) n(D_p). \tag{6}$$

The final $n(\ln D_p)$ distribution was converted to $n(D_p)$ so that it could be compared to the experimental result. An example of the distribution addition is given in Figure D.2, where three lognormal distributions (different diameter sets for each) were combined. The total number of the three source distributions was defined to be 8×10^4 particles/cm^3. The area under the final distribution gave a total number count of 7.997×10^4 particles/cm^3 for a percent difference of 0.04.

Finally, the calculation of the deposition coefficient $\beta(D_p)$ requires the viscos-

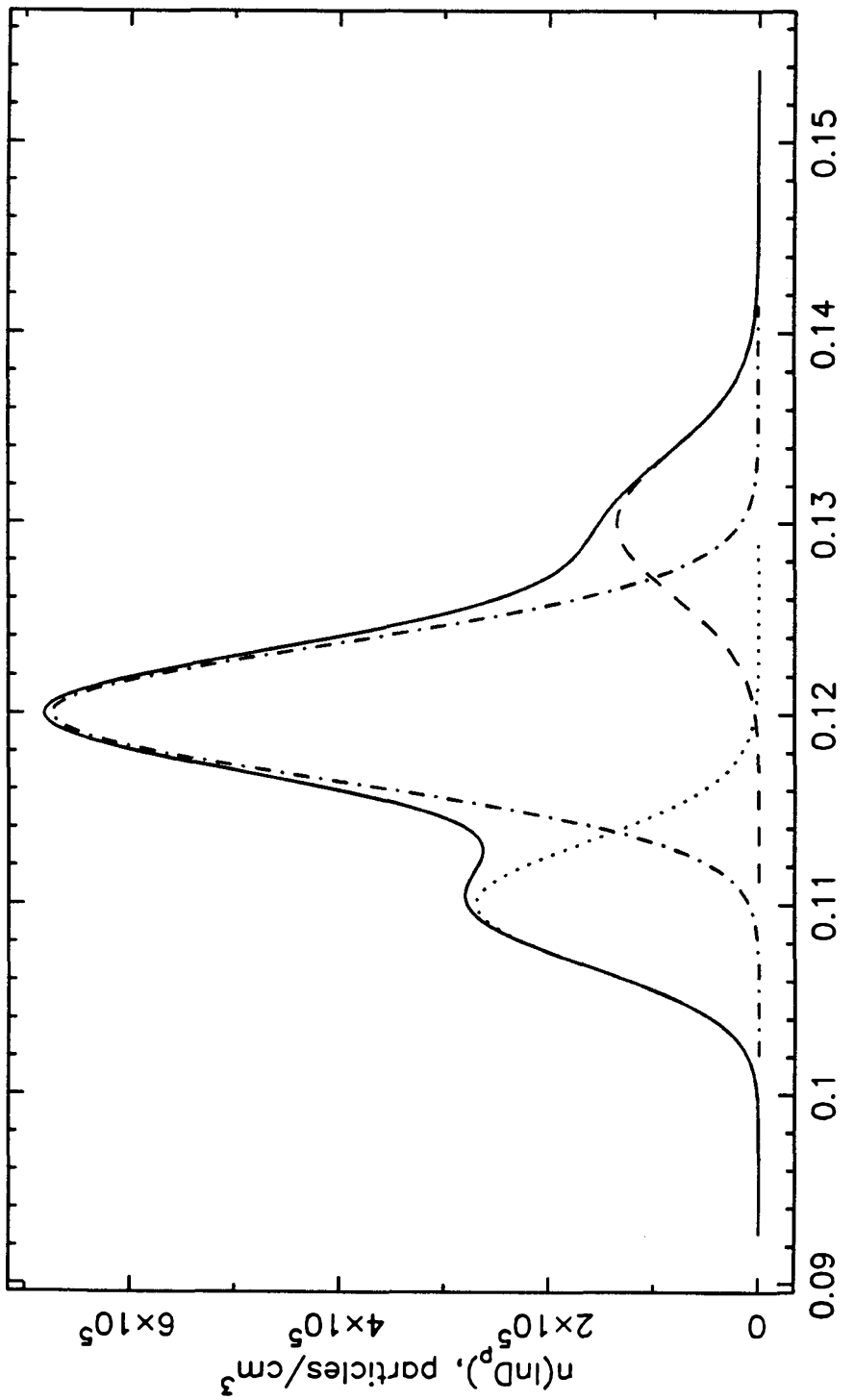

Figure D.2 Example of the distribution addition algorithm. Distribution 1: $D_{p,g} = 0.11$ μm, $\sigma = 1.03$, $N_{tot} = 2 \times 10^4$ particles/cm^3 (.....). Distribution 2: $D_{p,g} = 0.12$ μm, $\sigma = 1.03$, $N_{tot} = 5 \times 10^4$ particles/cm^3 (-·-·-·-·-). Distribution 2: $D_{p,g} = 0.13$ μm, $\sigma = 1.03$, $N_{tot} = 1 \times 10^4$ particles/cm^3 (– – – – –). Final distribution generated by the algorithm (————).

ity and density of the humid air. Hirschfelder et al. (1964) have calculated that the viscosity of saturated air is less than 1% different from that of dry air. Therefore, a viscosity of 0.0001833 poise (dry air at $\sim$ 23°C (Weast, 1979)) was used. The density of humid air was obtained from the correlation given by Weast (1979):

$$\rho = 1.2929 \left(\frac{273.13}{T} \right) \left(\frac{P_{atm} - 0.3783\,\mathrm{RH}\,P_{sat}(T)}{760} \right), \tag{7}$$

where the units of ρ are g/ℓ, temperature is in degrees Kelvin, and the pressures have units of millimeters of mercury. The Debye function is also needed to calculate the deposition coefficient. The series expansion used was obtained from Abramowitz and Stegun (1972):

$$\frac{1}{x}\int_0^{\infty} \frac{t}{e^t - 1}\,dt = \frac{\pi^2}{6x} - \frac{1}{x}\sum_{k=1}^{\infty} \frac{e^{-kx}}{k}\left(x + \frac{1}{k}\right) \qquad x > 0. \tag{8}$$

Solution density data for $MnSO_4$, Na_2SO_4, and H_2SO_4 from Washburn (1926) were used. The water activity and activity coefficient data listed in Table C.1 were used in the CSTR model calculations.

REFERENCES

ABRAMOWITZ, M. and STEGUN, I. A. (eds.) (1972) *Handbook of Mathematical Functions.* Dover Publications, Inc., New York.

HIRSCHFELDER, J. O., CURTISS, C. F. and BIRD, R. B. (1964) *Molecular Theory of Gases and Liquids.* John Wiley & Sons, New York.

WASHBURN, E. W. (ed.) (1926) *International Critical Tables.* McGraw-Hill, New York.

WEAST, R. C. (ed.) (1979) *Handbook of Chemistry and Physics.* 60th edition, CRC Press, Inc., Boca Raton, Florida.

APPENDIX E

COMPUTER PROGRAMS

```
      PROGRAM SAMP
C
C WRITTEN FOR PDP-11. RT-11 OPERATING SYSTEM.
C This program takes A/D readings over a given time and averages the
C readings, then repeats the sequence a specified time later.  Any
C number of A/D channels may be sampled "at the same time". The
C A/D read program was written by Dale Warren (in ASSEMBLY). A value
C is returned that must be multiplied by (10./4096.) to give the
C voltage. The calibration results are used to turn the voltages
C into temperatures or concentrations.
C
      DIMENSION SUMV(16), SUMV2(16), ICHAN(16), AVER(16), STDEV(16)
      INTEGER FILE(20), DAT(5), TIMEST(4), TIMEFN(4), IDENT(16)
      BYTE ASK1, ASK2, ASK3, ASK4, ASK5, ASK6
C
C Assign the logical numbers 5 and 6 to this terminal.
C
      CALL ASSIGN(5,'TT:')
      CALL ASSIGN(6,'TT:')
C
      CALL DATE(DAT)
C
      KRUN = 1
C
C Set the array ICHAN initially to 0 (all channels off).
C
  171     DO 201 I = 1,16
  201     ICHAN(I) = 0
C
      WRITE(6,10)
   10     FORMAT(/1X,'**************************************************'
     1    /1X,'HOW MANY A/D CHANNELS TO BE SAMPLED: ',$)
      READ(5,*)  NOCHAN
C
C We will now find out what channels will be sampled and turn them
C "on". In other words, we will set ICHAN(I)=1 for an "on" channel.
C Note that for channel 0, ICHAN(1) is used, for channel 1, ICHAN(2)
C is used, etc. At this time we will also associate a given channel
C with a given instrument so that the correct calibration results can
C be used.
C
      WRITE(6,900)
  900     FORMAT(/1X,'THE FOLLOWING IDENTIFICATION NOS. ARE TO BE USED.'
     1    /5X,'0.......DEW POINT'
     1    /5X,'2.......CSTR TEMP'
     1    /5X,'3.......EGG880'
     1    /5X,'4.......THERMISTOR #4, ROOM TEMP'
     1    /5X,'5.......THERMISTOR #5, EMC INLET'
     1    /5X,'6.......THEMRISTOR #6, EMC OUTLET'
```

```
     1    /5X,'7.......SO2 METER'
     1    /5X,'8.......VOLTAGE ONLY')
C
          DO 11 J = 1, NOCHAN
          WRITE(6,12)
   12         FORMAT(/1X,'ENTER A/D CHANNEL (0-15) AND IDENT NO.: ',$)
          READ(5,*) I, IDENT(I+1)
   11     ICHAN(I+1) = 1
C
C If the SO2 meter is being used, check which range.
C
          DO 549 J = 1, 16
          IF(IDENT(J).NE.7) GO TO 549
          WRITE(6,548)
  548         FORMAT(/1X,'ENTER L FOR LOW, H FOR HIGH SO2 RANGE: ',$)
          READ(5,70) ASK6
  549     CONTINUE
C
C So now we know the channels. Need the sample times. These will be the
C same---we have "simultaneous" sampling of the channels.
C
      IF(KRUN.EQ.1) GO TO 16
   15 IF(ASK4.NE.'Y') GO TO 155
C
   16 WRITE(6,20)
   20     FORMAT(/1X,'NUMBER OF READINGS AVERAGED TOGETHER (DEFAULT=60):
     1 ',$)
      READ(5,21) NAVG
   21    FORMAT(I3)
      IF(NAVG.EQ.0) NAVG = 60
C
      WRITE(6,30)
   30     FORMAT(/1X,'HOW MANY SAMPLES DO YOU WANT TO TAKE: ',$)
      READ(5,*)  NSAMP
C
      IF(KRUN.EQ.1) GO TO 17
  155 IF(ASK5.NE.'Y') GO TO 55
C
   17 WRITE(6,40)
   40     FORMAT(/1X,'***NOTE ALL TIMES ENTERED ARE THE SAME FOR EACH CH
     1ANNEL***'//1X,'FOR A GIVEN "SAMPLE", WHAT TIME DO YOU WANT BETWEEN
     1'/1X'READINGS (DEFAULT IS THE 00:00:01:00): ',$)
      READ(5,50)  JHR, JMIN, JSEC, JTIC
   50     FORMAT(I2,1X,I2,1X,I2,1X,I2)
      IF(JHR.EQ.0.AND.JMIN.EQ.0.AND.JSEC.EQ.0.AND.JTIC.EQ.0) JSEC = 1
      TIME1 = FLOAT(JHR)*3600. + FLOAT(JMIN)*60. + FLOAT(JSEC)
     1          + FLOAT(JTIC)/60.
C
      IF(NSAMP.EQ.1) GO TO 55
      WRITE(6,45)
   45     FORMAT(/1X,'ENTER THE TIME BETWEEN SAMPLES (DEFAULT IS 00:00:2
     10:00): ',$)
      READ(5,50) IHR, IMIN, ISEC, ITIC
      IF(IHR.EQ.0.AND.IMIN.EQ.0.AND.ISEC.EQ.0.AND.ITIC.EQ.0) ISEC = 20
```

```
      TIME2 = FLOAT(IHR*60) + FLOAT(IMIN) + FLOAT(ISEC)/60. +
     1        FLOAT(ITIC)/3600.
C
C So TIME2 is the time between sample end and sample beginning. To get th
e
C time between sample starts, need to add the sample duration time.
C
      TIME2 = TIME2 + (NAVG*TIME1)/60.
C
   55 WRITE(6,60)
   60     FORMAT(/1X,'SAVE DATA ON DISK: ',$)
      READ(5,70)  ASK1
   70     FORMAT(A)
      IF(ASK1.NE.'Y') GO TO 100
   75 WRITE(6,80)
   80     FORMAT(/1X,'$FILENAME: ',$)
      READ(5,90) FILE
   90     FORMAT(20A2)
C
C This hopping around prevents one from opening an already existing file
C and writing the current data OVER stored data. Idiot proof.
C
      OPEN(UNIT=3, NAME=FILE, TYPE='OLD', ERR=1000)
      WRITE(6,95)
   95     FORMAT(/1X,'***DATA FILE BY THAT NAME ALREADY EXISTS. RENAME**
     1*')
      CLOSE(UNIT=3)
      GO TO 75
 1000 OPEN(UNIT=3, NAME=FILE, TYPE='NEW')
C
C Ready the data file and screen for printing.
C
      WRITE(3,110) (DAT(J), J = 1,5)
  100 WRITE(6,110) (DAT(J), J = 1,5)
  110     FORMAT(//1X,'*******************************************'
     1    /1X,'SAMPLING SESSION.................',5A2)
      IF(ASK1.NE.'Y') GO TO 156
      WRITE(3,157) FILE
      WRITE(6,157) FILE
  157     FORMAT(1X,'DATA FILENAME.....................',20A2/)
C
  156    DO 101 JJ = 1, 16
         IF(ICHAN(JJ).EQ.0) GO TO 101
         ICH = JJ - 1
         IF(ASK1.NE.'Y') GO TO 102
         WRITE(3,103) ICH, NSAMP
  102    WRITE(6,103) ICH, NSAMP
  103        FORMAT(1X,'A/D CHANNEL ',I2,' WILL BE SAMPLED ',I2,
     1       ' TIMES')
  101    CONTINUE
      IF(ASK1.NE.'Y') GO TO 104
      WRITE(3,200) TIME2, NAVG, TIME1
  104 WRITE(6,200) TIME2, NAVG, TIME1
  200     FORMAT(1X,'THE TIME BETWEEN SAMPLE STARTS IS ',F7.3,' MINUTES'
```

```
     1    /1X,I3,' READINGS, ',F4.2,' SECOND(S) APART, WILL BE AVERAGED.
     1    '///46X,'AVERAGE',3X,'STD.'/1X,'SAMPLE',2X,'CHANNEL',3X,
     1    'TIME START',3X,'TIME FINISH',3X,'T OR PPM',2X,'DEV.'/)
C
C We are going to have to scan through the A/D channels but let's not
C waste any more time than necessary. Find the min and max of the
C channels we have to scan.
C
      ICHMIN = 16
      ICHMAX = 1
          DO 111 K = 1, 16
          IF(ICHAN(K).EQ.1.AND.K.LE.ICHMIN) ICHMIN = K
          IF(ICHAN(K).EQ.1.AND.K.GE.ICHMAX) ICHMAX = K
  111     CONTINUE
C
C Start the sampling loop. The time of day clock will be used for
C all timing since we will not need times less than a second.
C
        DO 140 K = 1, NSAMP
C
C Take the time of day at the beginning of a sample, take a sample,
C take time of day at end of sample, then delay. This is done for
C each channel being sampled.
C
            DO 141 J = ICHMIN, ICHMAX
            SUMV2(J) = 0.
  141       SUMV(J) = 0.
        CALL TIME(TIMEST)
C
            DO 120 KK = 1, NAVG
                DO 121 JJ = ICHMIN, ICHMAX
                IF(ICHAN(JJ).EQ.0) GO TO 121
                ICH = JJ - 1
                CALL ADREAD(ICH, IVAL)
                VOLT = FLOAT(IVAL)*(10./4096.)
C
C Turn the voltage into temperature. These are the calibration values.
C
                IF(IDENT(JJ).EQ.0) TEMP = 10.2065*VOLT - 40.5446
                IF(IDENT(JJ).EQ.2) TEMP = 9.99373*VOLT - 39.5549
                IF(IDENT(JJ).EQ.3) TEMP = 16.4088*VOLT - 42.8378
                IF(IDENT(JJ).EQ.4) TEMP = 9.93568*VOLT + 0.14367
                IF(IDENT(JJ).EQ.5) TEMP = 9.91262*VOLT + 0.12189
                IF(IDENT(JJ).EQ.6) TEMP = 9.87885*VOLT + 0.15949
                IF(IDENT(JJ).EQ.7.AND.ASK6.EQ.'H') TEMP =
     1              0.0391477 + 10.041*VOLT - 0.0734104*
     1              (VOLT**2) + 0.00658533*(VOLT**3)
                IF(IDENT(JJ).EQ.7.AND.ASK6.EQ.'L') TEMP =
     1              -0.0529 + 0.29412*VOLT
C
C If the ident no. is 8, we want only the voltage--not some conversion.
C
                IF(IDENT(JJ).EQ.8) TEMP = VOLT
C
```

```
                SUMV2(JJ) = SUMV2(JJ) + TEMP**2
                SUMV(JJ) = SUMV(JJ) + TEMP
  121           CONTINUE
              IF(KK.EQ.NAVG) GO TO 120
              CALL ISLEEP(JHR, JMIN, JSEC, JTIC)
  120         CONTINUE
C
          CALL TIME(TIMEFN)
C
C Now get the average value and std. deviation and print it out. Note
C that the std. deviation is of the VALUE, not the voltage.
C
          AVGN = FLOAT(NAVG)
              DO 122 JJ = ICHMIN, ICHMAX
              IF(ICHAN(JJ).EQ.0) GO TO 122
              AVER(JJ) = SUMV(JJ)/AVGN
              SM = AVGN*SUMV2(JJ) - SUMV(JJ)**2
              STDEV(JJ) = SQRT(SM/(AVGN*(AVGN-1.)))
  122         CONTINUE
C
              DO 126 JJ = ICHMIN, ICHMAX
              IF(ICHAN(JJ).EQ.0) GO TO 126
              ICH = JJ - 1
              IF(ASK1.NE.'Y') GO TO 125
              WRITE(3,130) K, ICH, (TIMEST(J),J=1,4), (TIMEFN(J),J=1,4),
     1                     AVER(JJ), STDEV(JJ)
  125         WRITE(6,130) K, ICH, (TIMEST(J),J=1,4), (TIMEFN(J),J=1,4),
     1                     AVER(JJ), STDEV(JJ)
  130            FORMAT(2X,I2,7X,I2,7X,4A2,5X,4A2,5X,F7.4,2X,F7.4)
  126         CONTINUE
C
C Now have the program "sleep" between samples.
C
          IF(K.EQ.NSAMP) GO TO 140
          CALL ISLEEP(IHR, IMIN, ISEC, ITIC)
  140     CONTINUE
C
       IF(ASK1.NE.'Y') GO TO 145
       WRITE(3,150)
       CLOSE(UNIT=3)
C
C Want to run again? Give various options for changing sampling
C conditions.
C
  145 WRITE(6,150)
  150     FORMAT(/1X,'*******************************************')
      WRITE(6,160)
  160     FORMAT(///1X,'DO YOU WANT TO RUN THE WHOLE THING OVER? ',$)
      READ(5,70)  ASK2
      IF(ASK2.NE.'Y') STOP
      KRUN = KRUN + 1
      WRITE(6,170)
  170     FORMAT(/1X,'DO YOU WANT TO (DEFAULT=NO FOR ALL QUESTIONS):'
     1           /10X,'1) TO CHANGE CHANNELS? ',$)
```

```
      READ(5,70) ASK3
      WRITE(6,271)
  271     FORMAT(10X,'2) TO CHANGE NUMBER OF READINGS AND SAMPLES? ',$)
      READ(5,70) ASK4
      WRITE(6,272)
  272     FORMAT(10X,'3) TO CHANGE THE TIMING? ',$)
      READ(5,70)  ASK5
      IF(ASK3.EQ.'Y')  GO TO 171
      GO TO 15
C
      END
```

```
      PROGRAM ANAL
C
C WRITTEN FOR PDP-11. RT-11 OPERATING SYSTEM.
C This program analyzes the data taken using X A/D channels during a
C growth experiment and puts it in a file for further use.
C Either the feed or effluent results can be analyzed. Dew point
C temperatures are corrected for pressure.
C NOTE: ALL TIMES ARE CONSECUTIVE AND IT IS ASSUMED THAT ALL TIMES
C       ARE EITHER BEFORE OR AFTER MIDNIGHT!!!!!!!
C
C
      DIMENSION VALUE(130,7), TIME1(130), TIME2(130), TIME(130),
     1          AVG(7), AVGDEV(7), DEVAVG(7), EMCAVG(130)
      INTEGER FILE(20), NULL(120), HR1, SEC1, HR2, SEC2
      BYTE TYPE
      COMMON/PRESS/PATM, P880, P911, PEMC, PCSTR
C
C Assign units 5 and 6 to the terminal.
C
      CALL ASSIGN(5,'TT:')
      CALL ASSIGN(6,'TT:')
C
C Now we have to get the file information.
C
      WRITE(6,10)
   10     FORMAT(/1X,'***NOTE THAT THIS PROGRAM ASSUMES ALL DATA TAKEN'
     1    /1X,'EITHER BEFORE OR AFTER MIDNIGHT.')
      WRITE(6,20)
   20     FORMAT(/1X,'WHAT IS THE NAME OF THE DATA FILE TO BE READ? ',$)
      READ(5,30) FILE
   30     FORMAT(20A2)
      OPEN(UNIT=3, NAME=FILE, TYPE='OLD')
C
C Is this a feed or effluent file.?
C
      WRITE(6,40)
   40     FORMAT(/1X,'AN EFFLUENT OR FEED DATA FILE (E OR F)? ',$)
      READ(5,50) TYPE
   50     FORMAT(A)
      IF(TYPE.EQ.'F') GO TO 70
      WRITE(6,60)
   60     FORMAT(/1X,'WAS SO2 DATA TAKEN? ',$)
      READ(5,50) SO2
C
C User must input the number of lines in the data file prior to the data.
C
   70 WRITE(6,80)
   80     FORMAT(/1X,'HOW MANY LINES ARE THERE BEFORE THE DATA? ',$)
      READ(5,*) NUM
```

```
C
      DO 100 I = 1, NUM
          READ(3,90) (NULL(J), J = 1, 60)
   90         FORMAT(60A2)
  100 CONTINUE
C
C If this is effluent data, 7 channels are used. If this is feed data,
C 6 channels are used.
C
      NCHAN = 7
      IF(TYPE.EQ.'F') NCHAN = 6
      IF(TYPE.EQ.'E'.AND.SO2.EQ.'N') NCHAN = 6
C
      WRITE(6,110)
  110     FORMAT(/1X,'HOW MANY DATA POINTS PER CHANNEL? ',$)
      READ(5,*) NPTS
C
      IF(NPTS.LE.130) GO TO 130
      WRITE(6,120)
  120     FORMAT(/1X,'NO. POINTS EXCEEDS PROGRAMMED ARRAY DIMENSIONS.')
      STOP
C
C Zero the averaging and std. deviation variables.
C
  130     DO 140 J = 1, 7
          DEVAVG(J) = 0.
          AVGDEV(J) = 0.
  140     AVG(J) = 0.
C
C Read in the data.
C
      MAX = NCHAN
          DO 170 I = 1, NPTS
              DO 160 J = 1, NCHAN
              READ(3,150) ICH, HR1, MIN1, SEC1, HR2, MIN2, SEC2,
     1                    A, B
  150            FORMAT(10X,I2,7X,I2,1X,I2,1X,I2,5X,I2,1X,I2,1X,I2,
     1                 5X,F7.4,2X,F7.4)
              IF(ICH.EQ.0) K = 1
              IF(ICH.EQ.1) K = 2
              IF(ICH.EQ.2) K = 3
              IF(ICH.EQ.3) K = 4
              IF(ICH.EQ.4) K = 5
              IF(ICH.EQ.5) K = 6
              IF(ICH.EQ.6) K = 7
              IF(K.GT.MAX) MAX = K
              VALUE(I,K) = A
              AVG(K) = AVG(K) + A
              AVGDEV(K) = AVGDEV(K) + B
              TIME1(I) = FLOAT(HR1)+FLOAT(MIN1)/60.+FLOAT(SEC1)/3600.
              TIME2(I) = FLOAT(HR2)+FLOAT(MIN2)/60.+FLOAT(SEC2)/3600.
  160         CONTINUE
  170     CONTINUE
C
```

```
C Since I am now using the same no. of channels, but the corresponding
C channels numbers may or may not be consecutive, set the maximum K
C value equal to NCHAN since we want to scan thru to this number.
C
      NCHAN = MAX
C
      CLOSE(UNIT=3)
C
C Now I have everything I need. I can start to analyze the data. Start
C by getting the time in terms of "elapsed time". Then let the "time"
C be the average, or midpoint, of the initial and final times for each
C sample.
C
      START = TIME1(1)
         DO 180 I = 1, NPTS
         TIME1(I) = TIME1(I) - START
         TIME2(I) = TIME2(I) - START
         TIME(I) = (TIME1(I) + TIME2(I))/2.
  180    CONTINUE
C
C Input the atmospheric pressure and the delP at each measuring condition
.
C The dewpoint at pressure A is different from at pressure B even though
C they may have the same water content. I'll have to correct for this.
C
      WRITE(6,190)
  190     FORMAT(/1X,'PATM(mmHg)? ',$)
      READ(5,*) PATM
      WRITE(6,200)
  200     FORMAT(/1X,'DP880(cmH20), DP911, DPEMC, AND DPCSTR(inH20)? ',
     1,$)
      READ(5,*) DP880, DP911, DPEMC, DPCSTR
C
C Convert PATM to inH20. Calculate the absolute pressure at each point.
C
      PFACT = 406.8/760.
      PATM = PATM * PFACT
      P911 = PATM + DP911
      P880 = PATM + (DP880/2.54)
      PEMC = PATM + DPEMC
      PCSTR = PATM + DPCSTR
C
C Given constant water content and P1.ne.P2, then we have to adjust
C the dewpoint (taken at P1), to what the value would be at P2.
C i.e. we use the value TDP911, taken at P911, and adjust it to TDPCSTR
C at PCSTR---this dewpoint is then used to calculate RH in the CSTR.
C
         DO 210 I = 1, NPTS
         CALL DEWPT(VALUE(I,1), PCSTR, P911, VALUE(I,1))
         CALL DEWPT(VALUE(I,2), PEMC, P880, VALUE(I,2))
  210    CONTINUE
C
C Calculate the average values (AVG), the standard dev. of the average
C (DEVAVG), and the average of the std. dev. of the readings (AVGDEV).
```

```
C
          DO 230 J = 1, NCHAN
          AVGDEV(J) = AVGDEV(J)/NPTS
          AVG(J) = AVG(J)/NPTS
              DO 220 I = 1, NPTS
              DEVAVG(J) = DEVAVG(J) + (VALUE(I,J)-AVG(J))**2
  220         CONTINUE
          DEVAVG(J) = SQRT(DEVAVG(J)/FLOAT(NPTS-1))
  230     CONTINUE
C
C Write into 2 files, one with headings, one without (for plotting).
C The format depends on whether this is a feed or effluent file.
C ***** Do the effluent type files first. *****
C
      SUM1 = 0.
      SUM2 = 0.
      SUM3 = 0.
      SUM21 = 0.
      SUM22 = 0.
      SUM23 = 0.
C
      IF(TYPE.EQ.'F') GO TO 370
C
      IF(SO2.EQ.'Y') WRITE(52,240) FILE
  240     FORMAT(1X,'************************************'
     1    /1X,'EFFLUENT RESULTS FOR ',20A2
     1    /1X,'************************************'/////
     1    1X,'TEMPERATURES'//
     1    1X,'TIME       DEWPOINT     ROOM    CSTR',13X,'EMC2',
     1    15X,'SO2'/
     1    1X,'          911     880                ',4X,'INLET   OUTLET',
     1    3X,'AVERAGE'/
     1    1X,'         (@PCSTR)(@PEMC)'/
     1    1X,'-------------------------------------------------------------
----
     1-------------'/
     1    1X,' hrs    deg C   deg C   deg C   deg C',3X,'deg C    deg C',
     1    4X,'deg C',5X,'ppm'/
     1    1X,'-------------------------------------------------------------
----
     1-------------'//)
C
      IF(SO2.EQ.'N') WRITE(52,250) FILE
  250     FORMAT(1X,'************************************'
     1    /1X,'EFFLUENT RESULTS FOR ',20A2
     1    /1X,'************************************'/////
     1    1X,'TEMPERATURES'//
     1    1X,'TIME       DEWPOINT     ROOM    CSTR',13X,'EMC2'/
     1    1X,'          911     880                ',4X,'INLET   OUTLET',
     1    3X,'AVERAGE'/
     1    1X,'         (@PCSTR)(@PEMC)'/
     1    1X,'-------------------------------------------------------------
----
     1-------'/
```

```
     1    1X,' hrs    deg C   deg C   deg C   deg C',3X,'deg C    deg C',
     1    4X,'deg C',/
     1    1X,'-------------------------------------------------------------
----
     1-------'//)
C
          DO 300 I = 1, NPTS
C
C Calculate the classifier RHs at the average (in/out) EMC temp.
C
          EMCAVG(I) = (VALUE(I,7)+VALUE(I,6))/2.
C
          IF(SO2.EQ.'N') GO TO 270
          WRITE(51,260) TIME(I), VALUE(I,1), VALUE(I,2), VALUE(I,4),
     1                  VALUE(I,3), VALUE(I,6), VALUE(I,7),
     1                  EMCAVG(I), VALUE(I,5)
          WRITE(52,260) TIME(I), VALUE(I,1), VALUE(I,2), VALUE(I,4),
     1                  VALUE(I,3), VALUE(I,6), VALUE(I,7),
     1                  EMCAVG(I), VALUE(I,5)
  260         FORMAT(1X,F5.3,3X,F6.3,2X,F6.3,2X,F6.3,2X,F6.3,
     1                2X,F6.3,3X,F6.3,3X,F6.3,3X,F6.3)
          GO TO 290
  270     WRITE(51,280) TIME(I), VALUE(I,1), VALUE(I,2), VALUE(I,4),
     1                  VALUE(I,3), VALUE(I,6), VALUE(I,7), EMCAVG(I)
          WRITE(52,280) TIME(I), VALUE(I,1), VALUE(I,2), VALUE(I,4),
     1                  VALUE(I,3), VALUE(I,6), VALUE(I,7), EMCAVG(I)
  280         FORMAT(1X,F5.3,3X,F6.3,2X,F6.3,2X,F6.3,2X,F6.3,
     1                2X,F6.3,3X,F6.3,3X,F6.3,3X,F6.3)
C
C Get the sum and sum squared of the calculated temps.
C
  290     SUM1 = SUM1 + EMCAVG(I)
          SUM21 = SUM21 + EMCAVG(I)**2
C
  300     CONTINUE
C
C Calculate the average temp value.
C
       EMCDEV = SQRT((NPTS*SUM21 - SUM1**2)/FLOAT(NPTS*(NPTS-1)))
       EMCA   = SUM1/NPTS
C
C Write out the average values.
C
       WRITE(52,310) AVG(1), DEVAVG(1), AVGDEV(1),
     1               AVG(2), DEVAVG(2), AVGDEV(2),
     1               AVG(3), DEVAVG(3), AVGDEV(3),
     1               AVG(4), DEVAVG(4), AVGDEV(4),
     1               AVG(6), DEVAVG(6), AVGDEV(6),
     1               AVG(7), DEVAVG(7), AVGDEV(7),
     1               EMCA, EMCDEV
  310     FORMAT(/1X,'-------------------------------------------------
-----
     1----------------------'/
     1    ///1X,'AVG 911 DEW TEMP   = ',F6.3,' +/- ',F6.4,
```

```
     1    ' deg C,  AVG DEV. IN A/D READING = ',F6.4,
     1    /1X,'AVG 880 DEW TEMP   = ',F6.3,' +/- ',F6.4,
     1    ' deg C,  AVG DEV. IN A/D READING = ',F6.4,
     1    /1X,'AVG CSTR TEMP      = ',F6.3,' +/- ',F6.4,
     1    ' deg C,  AVG DEV. IN A/D READING = ',F6.4,
     1    /1X,'AVG ROOM TEMP      = ',F6.3,' +/- ',F6.4,
     1    ' deg C,  AVG DEV. IN A/D READING = ',F6.4,
     1    /1X,'AVG EMCIN TEMP     = ',F6.3,' +/- ',F6.4,
     1    ' deg C,  AVG DEV. IN A/D READING = ',F6.4,
     1    /1X,'AVG EMCOUT TEMP    = ',F6.3,' +/- ',F6.4,
     1    ' deg C,  AVG DEV. IN A/D READING = ',F6.4,
     1    /1X,'AVG EMC TEMP       = ',F6.3,' +/- ',F6.4,
     1    ' deg C')
C
      IF(SO2.EQ.'Y') WRITE(52,320) AVG(5), DEVAVG(5), AVGDEV(5)
  320     FORMAT(1X,'AVG SO2 CONC.       = ',F6.3,' +/- ',F6.4,
     1    ' ppm,  AVG DEV. IN A/D READING = ',F6.4)
C
      WRITE(52,330)
  330     FORMAT(///1X,'RELATIVE HUMIDITY'//
     1    1X,'TIME',2X,'CSTR RH',2X,'EMC2 RH'/
     1    1X,'----------------------'/
     1    1X,' hrs',2X,'   %   ',2X,'   %   '/
     1    1X,'----------------------'//)
C
C Now we have to calculate the relative humidities and correct for
C the fact that the pressure and temp varies slightly throughout the
C system.
C
          DO 350 I = 1, NPTS
          CALL RHE(VALUE(I,1), VALUE(I,2), VALUE(I,3), EMCAVG(I),
     1             RH1, RH2)
          RH1 = RH1*100.
          RH2 = RH2*100.
          WRITE(53,340) TIME(I), RH1, RH2
          WRITE(52,340) TIME(I), RH1, RH2
  340         FORMAT(1X,F5.3,3X,F6.2,2X,F6.2)
C
          SUM2 = SUM2 + RH1
          SUM3 = SUM3 + RH2
          SUM22 = SUM22 + RH1**2
          SUM23 = SUM23 + RH2**2
C
  350     CONTINUE
C
      RH1DEV = SQRT((NPTS*SUM22 - SUM2**2)/FLOAT(NPTS*(NPTS-1)))
      RH1AVG = SUM2/NPTS
      RH2DEV = SQRT((NPTS*SUM23 - SUM3**2)/FLOAT(NPTS*(NPTS-1)))
      RH2AVG = SUM3/NPTS
C
      WRITE(52,360) RH1AVG, RH1DEV, RH2AVG, RH2DEV
  360     FORMAT(/1X,'----------------------'
     1    ///1X,'AVG CSTR RH   = ',F6.2,' +/- ',F5.3,'%'
     1    /1X,'AVG EMC RH    = ',F6.2,' +/- ',F5.3,'%')
```

```
C
      CLOSE(UNIT=51)
      CLOSE(UNIT=52)
      CLOSE(UNIT=53)
C
      STOP
C
C ***** Now for the feed files. *****
C
  370 WRITE(52,380) FILE
  380     FORMAT(1X,'************************************'
     1    /1X,'FEED RESULTS FOR ',20A2
     1    /1X,'************************************'/////
     1    1X,'TEMPERATURES'//
     1    1X,'TIME        DEWPOINT     ROOM    ',12X,'EMC2'/
     1    1X,'          911     880            ',3X,'INLET   OUTLET',
     1    3X,'AVERAGE'/
     1    1X,'         (@PCSTR)(@PEMC)'/
     1    1X,'-------------------------------------------------------
     1-'/
     1    1X,' hrs    deg C   deg C   deg C  ',3X,'deg C    deg C',
     1    4X,'deg C',/
     1    1X,'-------------------------------------------------------
     1-'//)
C
          DO 400 I = 1, NPTS
C
C Calculate the classifier RHs at the average (in/out) EMC temp.
C
          EMCAVG(I) = (VALUE(I,7)+VALUE(I,6))/2.
C
          WRITE(51,390) TIME(I), VALUE(I,1), VALUE(I,2), VALUE(I,4),
     1                  VALUE(I,6), VALUE(I,7), EMCAVG(I)
          WRITE(52,390) TIME(I), VALUE(I,1), VALUE(I,2), VALUE(I,4),
     1                  VALUE(I,6), VALUE(I,7), EMCAVG(I)
  390         FORMAT(1X,F5.3,3X,F6.3,2X,F6.3,2X,F6.3,4X,F6.3,3X,
     1               F6.3,3X,F6.3)
C
C Get the sum and sum squared of the calculated temp.
C
          SUM1 = SUM1 + EMCAVG(I)
          SUM21 = SUM21 + EMCAVG(I)**2
C
  400     CONTINUE
C
C Calculate the average temp value.
C
      EMCDEV = SQRT((NPTS*SUM21 - SUM1**2)/FLOAT(NPTS*(NPTS-1)))
      EMCA   = SUM1/NPTS
C
C Write out the average values.
C
      WRITE(52,410) AVG(1), DEVAVG(1), AVGDEV(1),
     1              AVG(2), DEVAVG(2), AVGDEV(2),
```

```
     1              AVG(4), DEVAVG(4), AVGDEV(4),
     1              AVG(6), DEVAVG(6), AVGDEV(6),
     1              AVG(7), DEVAVG(7), AVGDEV(7),
     1              EMCA, EMCDEV
  410     FORMAT(/1X,'-------------------------------------------------
-----
     1---------'/
     1    ///1X,'AVG DEW 911 TEMP   = ',F6.3,' +/- ',F6.4,
     1    ' deg C, AVG DEV. IN A/D READING = ',F6.4,
     1    /1X,'AVG DEW 880 TEMP   = ',F6.3,' +/- ',F6.4,
     1    ' deg C, AVG DEV. IN A/D READING = ',F6.4,
     1    /1X,'AVG ROOM TEMP      = ',F6.3,' +/- ',F6.4,
     1    ' deg C, AVG DEV. IN A/D READING = ',F6.4,
     1    /1X,'AVG EMCIN TEMP     = ',F6.3,' +/- ',F6.4,
     1    ' deg C, AVG DEV. IN A/D READING = ',F6.4,
     1    /1X,'AVG EMCOUT TEMP    = ',F6.3,' +/- ',F6.4,
     1    ' deg C, AVG DEV. IN A/D READING = ',F6.4,
     1    /1X,'AVG EMC TEMP       = ',F6.3,' +/- ',F6.4,' deg C')
C
C Now we have to calculate the relative humidities and correct for
C the fact that the pressure and temp varies slightly throughout the
C system.
C
      WRITE(52,420)
  420     FORMAT(///1X,'RELATIVE HUMIDITY'//
     1    1X,'TIME',4X,'FEED RH*',3X,'EMC RH'/
     1    1X,'-------------------------'/
     1    1X,' hrs',4X,'   %    ',3X,'   %   '/
     1    1X,'-------------------------'//)
C
C We'll calculate the RH of the feed at PCSTR and average
C CSTR temp (calculated in effluen analysis).
C
          WRITE(6,430)
  430         FORMAT(/1X,'"CSTR" TEMP TO CALC. FEED RH AT? ',$)
          READ(5,*) TCSTR
C
          DO 450 I = 1, NPTS
          CALL RHF(VALUE(I,1), VALUE(I,2), TCSTR, EMCAVG(I), RH1, RH2)
          RH1 = RH1*100.
          RH2 = RH2*100.
          WRITE(53,440) TIME(I), RH1, RH2
          WRITE(52,440) TIME(I), RH1, RH2
  440         FORMAT(1X,F5.3,3X,F6.2,4X,F6.2)
C
          SUM2 = SUM2 + RH1
          SUM3 = SUM3 + RH2
          SUM22 = SUM22 + RH1**2
          SUM23 = SUM23 + RH2**2
C
  450     CONTINUE
C
      RH1DEV = SQRT((NPTS*SUM22 - SUM2**2)/FLOAT(NPTS*(NPTS-1)))
      RH1AVG = SUM2/NPTS
```

```
      RH2DEV = SQRT((NPTS*SUM23 - SUM3**2)/FLOAT(NPTS*(NPTS-1)))
      RH2AVG = SUM3/NPTS
C
      WRITE(52,460) TCSTR, RH1AVG, RH1DEV, RH2AVG, RH2DEV
  460     FORMAT(/1X,'--------------------------'
     1    /1X,'* FEED RH CALCULATED AT TCSTR = ',F6.3,' deg C'
     1    ///1X,'AVG FEED RH  = ',F6.2,' +/- ',F5.3,'%'
     1    /1X,'AVG EMC RH   = ',F6.2,' +/- ',F5.3,'%')
C
      CLOSE(UNIT=51)
      CLOSE(UNIT=52)
      CLOSE(UNIT=53)
C
      STOP
      END
C
C
C ---------------------------------------------------------------
      SUBROUTINE RHE(TDP911, TDP880, TCSTR, TEMC, RHCSTR, RHEMC)
C
      COMMON/PRESS/PATM, P880, P911, PEMC, PCSTR
C
C This program calculates the relative humidity of the system
C given the ambient temperature and the dew point--EFFLUENT FILES.
C Call the subroutine which calculates the saturation vapor
C pressure.
C
      CALL PSAT(TCSTR, PSATCS)
      CALL PSAT(TEMC, PSATE)
      CALL PSAT(TDP911, PSAT9)
      CALL PSAT(TDP880, PSAT8)
C
C Calculate the relative humidity.
C
      RHCSTR = PSAT9/PSATCS
      RHEMC = PSAT8/PSATE
C
      RETURN
      END
C
C
C ---------------------------------------------------------------
      SUBROUTINE RHF(TDP911, TDP880, TCSTR, TEMC, RHFEED, RHEMC)
C
      COMMON/PRESS/PATM, P911, P880, PEMC, PCSTR
C
C This program calculates the relative humidity of the system
C given the ambient temperature and the dew point--FEED FILES.
C Call the subroutine which calculates the saturation vapor
C pressure.
C
      CALL PSAT(TCSTR, PSATCS)
      CALL PSAT(TEMC, PSATE)
      CALL PSAT(TDP911, PSAT9)
```

```
      CALL PSAT(TDP880, PSAT8)
C
C Calculate the relative humidity.
C
      RHFEED = PSAT9/PSATCS
      RHEMC = PSAT8/PSATE
C
      RETURN
      END
C
C
C-----------------------------------------------------------------
C This subroutine calculates the dewpoint at P2, given the dewpoint
C at P1.
C
      SUBROUTINE DEWPT(T1, P2, P1, T2)
C
      TT = T1 + 273.15
      T2 = 1./((1./TT)+(1./5313.88)*ALOG(P1/P2))
      T2 = T2 - 273.15
C
      RETURN
      END
C
C
C-----------------------------------------------------------------
C This subroutine calculates the water vapor pressure given the
C temperature in degrees Centigrade (1/29/86 FIT USED).
C
      SUBROUTINE PSAT(T,P)
C
      TT = T + 273.15
      P = EXP(20.9878 - (5313.88/TT))
C
      RETURN
      END
```

```
      PROGRAM SHIFTDP
C
C This program calculates the new size distribution at RH2 given a
C feed distribution measured at RH1. This is for a MnSO4+Na2SO4 mix
C where the ratio of MnSO4 to Na2SO4 is known. Also can be used for
C pure MnSO4 particles.
C
      IMPLICIT DOUBLE PRECISION(A-H,L,M,O-Z)
      DOUBLE PRECISION ITOT1, ITOT2
      CHARACTER*20 FILE3, FILE4, FILE5, FILE7, FILE8
      CHARACTER*5 NAME
      DIMENSION DP1(500), DIST1(500), DP2(500), DIST2(500)
      COMMON/ONE/MWMN, MWNA, MWH2O, MWSOLN, VM, MMN, MNA,
     1           RHOSOL, AVAG, DELTA, CMN, CNA, TOL
      COMMON/TWO/MOLMN, MOLNA, CMN1, CNA1
      COMMON/THREE/FACTOR2, ITER, RH2, LAMDA
C
C Input the initial particle diameter, the initial relative humidity,
C the initial temperature. The final diameter and humidity.
C Input the molar ratio of MnSO4 to Na2SO4.
C
      WRITE(*,10)
   10     FORMAT(/1X,'Enter date of the experiment [mm,dd] => '\)
      READ(*,*) IMON, IDAY
      WRITE(*,20)
   20     FORMAT(/1X,'Enter initial temp (C) and RH (%) => '\)
      READ(*,*) TEMP1, RH1
      WRITE(*,30)
   30     FORMAT(/1X,'Enter final temp (C) and RH (%)   => '\)
      READ(*,*) TEMP2, RH2
      WRITE(*,40)
   40     FORMAT(/1X,'Enter moles MnSO4/moles Na2SO4.'
     1           /1X,'If have pure MnSO4, enter 1.d10. => '\)
      READ(*,*) DELTA1
      WRITE(*,50)
   50     FORMAT(/1X,'Input no. of particle diameters => '\)
      READ(*,*) NUM
      IF(IMON.EQ.10) IMON = 0
      WRITE(FILE3,60) IMON, IDAY
   60     FORMAT('DISTFA.',I1,I2)
      OPEN(3, FILE=FILE3, STATUS='OLD')
          DO 70 I = 1, NUM
          READ(3,*) DP1(I), DISTLN, DIST1(I)
   70     CONTINUE
      CLOSE(3)
      WRITE(*,80)
   80     FORMAT(/1X,'Enter name of output file (NNNNN) => '\)
      READ(*,90) NAME
   90     FORMAT(A)
```

```
C
C System constants. The surface tension is assumed to be constant
C at average of that for MnSO4 and Na2SO4 for lack of better data
C (if we have a mixture).
C
      BOLTZK = 1.3804D-16
      AVAG   = 6.023D23
      MWH2O  = 18.01D0
      MWMN   = 151.0D0
      MWNA   = 142.0D0
      PI     = 3.14159D0
      DELTA = 1.D0/DELTA1
      IF(DELTA1.EQ.1.D10) DELTA = 0.D0
      IF(DELTA.NE.0.D0) SIGMA = 74.93D0
      IF(DELTA.EQ.0.D0) SIGMA = 75.15D0
C
C Write information in the data files.
C
      WRITE(FILE4,100) NAME,4,IMON,IDAY
      WRITE(FILE7,100) NAME,7,IMON,IDAY
      WRITE(FILE8,100) NAME,8,IMON,IDAY
  100     FORMAT(A,I1,'.',I1,I2)
      OPEN(4, FILE=FILE4, STATUS='NEW')
      OPEN(7, FILE=FILE7, STATUS='NEW')
      OPEN(8, FILE=FILE8, STATUS='NEW')
C
      IF(IMON.EQ.0) IMON = 10
      WRITE(4,110) IMON,IDAY
      WRITE(7,110) IMON,IDAY
      WRITE(8,110) IMON,IDAY
  110 FORMAT(/1X,'AIR FEED SHIFTED.  ',I2,'/',I2,'/86')
C
      WRITE(4,140) TEMP1, RH1, TEMP2, RH2, DELTA
  140 FORMAT(1X,'-------------------------------------------',
     1       /1X,'The initial temperature is (C)        = ',F6.3,
     1       /1X,'The initial relative humidity is (%)  = ',F6.3,
     1       /1X,'The final temperature is (C)          = ',F6.3,
     1       /1X,'The final relative humidity is (%)    = ',F6.3,
     1       /1X,'Moles Na2SO4/moles MnSO4              = ',F7.3,
     1       /1X,'-------------------------------------------'
     1      //3X,'DPOLD',6X,'DISTOLD',7X,'DPNEW',6X,'DISTNEW')
      WRITE(7,150) TEMP1, RH1, DELTA
  150 FORMAT(1X,'---------------------------------------',
     1       /1X,'The temperature is (C)        = ',F6.3,
     1       /1X,'The relative humidity is (%)  = ',F6.3,
     1       /1X,'Moles Na2SO4/moles MnSO4      = ',F7.3,
     1       /1X,'---------------------------------------'
     1       //3X,'DP1',6X,'MMN1',4X,'MNA1',6X,'CMN1',5X,
     1           'CNA1',5X,'ITOT1',5X,'AW1')
      WRITE(8,160) TEMP2, RH2, DELTA
  160 FORMAT(1X,'---------------------------------------',
     1       /1X,'The temperature is (C)        = ',F6.3,
     1       /1X,'The relative humidity is (%)  = ',F6.3,
     1       /1X,'Moles Na2SO4/moles MnSO4      = ',F7.3,
```

```
     1       /1X,'----------------------------------------'
     1       //3X,'DP2',6X,'MMN2',4X,'MNA2',6X,'CMN2',5X,
     1           'CNA2',5X,'ITOT2',5X,'AW2')
C
C Convert the temperature to degrees Kelvin and the diameter into
C centimeters. We are working in the cgs system. Remove percent from RH.
C
      RH1 = RH1/100.D0
      T1 = TEMP1 + 273.15D0
      RH2 = RH2/100.D0
      T2 = TEMP2 + 273.15D0
      FACTOR1 = 4.D0 * SIGMA/(BOLTZK * T1)
      FACTOR2 = 4.D0 * SIGMA/(BOLTZK * T2)
      TOL = 1.D-06
C
C Start to iterate on diameters.
C
          DO 240 I = 1, NUM
          DP1(I) = DP1(I) * 1.D-04
C
C Begin to iterate. Solve for CMN knowing that CNA=DELTA*CMN. Calculate
C AW1 by first assuming that VM=VMH2O. Set initial molalities of 0.
C
          ITER = 0
          VM = MWH2O/AVAG
          MMNOLD = 0.D0
          MNAOLD = 0.D0
C
C In this case we're going to work on the molality scale.
C Calculate the water activity using the assumed values.
C
  170     AW1 = RH1 * DEXP(-FACTOR1 * VM/DP1(I))
          IF(AW1.GT.1.0D0) AW1 = 1.0D0
C
C The function MOLAL calculates the molalities in the solution
C so that Kusik-Meisner's mixing rule gives a water activity of AW1.
C
          CALL MOLAL(AW1)
C
C We have MMN and MNA for this AW1, calculated using VM. Check to see
C if these current values (both) are within a tolerance value of
C the previous values. If so, go on. If not, recalculate AW1 using
C the new VM and repeat.
C
          ITER = ITER + 1
          IF(ITER.GT.100) THEN
              WRITE(*,180)
  180             FORMAT(/1X,'TOO MANY ITERATIONS FOR AW1.')
              STOP
          ELSE
          ENDIF
          IF(DABS(MMN-MMNOLD).LT.TOL.AND.DABS(MNA-MNAOLD).LT.TOL)
     1        GO TO 190
          MMNOLD = MMN
```

```
          MNAOLD = MNA
          GO TO 170
C
C Now we have the true conc in the drop at RH1 and T1. If only
C relative humidity and temperature changes are affecting the
C size of the drop, the moles of Na2SO4 and MnSO4 in this
C particular drop are constant.
C
  190     MMN1 = MMN
          MNA1 = MNA
          CMN1 = CMN
          CNA1 = CNA
          ITOT1 = 3.D0*MNA1 + 4.D0*MMN1
          RHO1 = RHOSOL
          MWDP1 = MWSOLN
          MOLMN = (CMN1/1000.D0)*(PI*DP1(I)**3/6.D0)
          MOLNA= (CNA1/1000.D0)*(PI*DP1(I)**3/6.D0)
C
C Now we need the conditions at RH2, T2. Search lamda space until
C RH2 = ACTIV(LAMDA*CMN1)*KELVIN. LAMDA is the ratio between the new
C and the old particle volume. Also, LAMDA = CNA2/CNA1 = CMN2/CMN1.
C Since DELTA = MNA1/MMN1 = CNA1/CMN1 = MNA2/MMN2 = CNA2/CMN2,
C we need only pass LAMDA*CMN1=CMN2 and from this CNA2 can be found.
C It is important to remember that LAMDA is a "volume" ratio and
C molarity must be used. We will convert to molality in the
C subroutine.
C
          ITER = 0
          DP20 = DP1(I)
          LAMDA = 0.01D0
C
C Find the LAMDA value for this DP20.
C
  200     CALL LAMDAA(DP20)
C
C So, presumably we have found the correct lamda value. But we were
C using DP20 in the kelvin correction. This will not be the correct
C diameter. Need to iterate so that we're using the correct diameter
C when we do the correction. What is the diameter that corresponds to
C the concentration conditions we just determined?
C
          CNA2 = LAMDA * CNA1
          CMN2 = LAMDA * CMN1
          MMN2 = MMN
          MNA2 = MNA
          ITOT2 = 3.D0*MNA2 + 4.D0*MMN2
          VOLSOL = (MOLMN/CMN2) * 1000.D0
          DP21 = (6.D0 * VOLSOL/PI)**(1./3.)
C
C Calculate the water activity using the above molarities. Then
C calculate the particle diameter using the latest constants.
C
          AW2 = ACTIVC(LAMDA)
          IF(AW2.GT.1.0D0) AW = 1.0D0
```

```
          DP22 = (FACTOR2 * VM/DLOG(RH2/AW2))
C
C See if convergence criterion is met.
C
          IF((DABS(DP21-DP22)*1.D04).LE.TOL) GO TO 210
          DP20 = (DP21 + DP22)/2.0D0
          GO TO 200
C
C So now we have the final value of DP2 and can calculate LAMDA and
C the size distribution. DIST(x')=LAMDA**(1/3)*DIST(x) where
C x'=x/LAMDA**(1/3). Note that the diameter dependence of LAMDA is
C being ignored here. Makes less than 0.5% difference in distribution
C value.
C
  210     DP1(I) = DP1(I) * 1.D04
          DP2(I) = DP21 * 1.D04
          LAMDA = (DP1(I)/DP2(I))**3.D0
          DIST2(I) = LAMDA**(1./3.) * DIST1(I)
C
          WRITE(4,220) DP1(I), DIST1(I), DP2(I), DIST2(I)
  220         FORMAT(1X,F8.6,2X,1PE12.6,3X,0PF8.6,2X,1PE12.6)
          WRITE(7,230) DP1(I), MMN1, MNA1, CMN1, CNA1, ITOT1, AW1
          WRITE(8,230) DP2(I), MMN2, MNA2, CMN2, CNA2, ITOT2, AW2
  230         FORMAT(1X,5(F7.5,2X),F7.3,2X,F7.5)
          WRITE(*,*) I
  240     CONTINUE
      CLOSE(7)
      CLOSE(8)
C
C Integrate the old and new distributions.
C
      IF(NUM.EQ.1) GO TO 270
      SUM1 = 0.D0
      SUM2 = 0.D0
          DO 250 I = 1, NUM-1
          SUM1 = SUM1 + 0.5*(DP1(I+1)-DP1(I))*(DIST1(I)+DIST1(I+1))
          SUM2 = SUM2 + 0.5*(DP2(I+1)-DP2(I))*(DIST2(I)+DIST2(I+1))
  250     CONTINUE
      DIFF = DABS(SUM1-SUM2)*100.D0/SUM2
C
      WRITE(4,260) SUM1, SUM2, DIFF
  260     FORMAT(/1X,'TOTAL FROM SHIFTED dN/dDp CURVE  = ',1PE15.7,
     1           /1X,'TOTAL FROM ORIGINAL dN/dDp CURVE = ',1PE15.7,
     1           /1X,'PERCENT DIFFERENCE               = ',0PF7.4)
C
  270 CLOSE(4)
C
      STOP
      END
C
C
C ---------------------------------------------------------------
      SUBROUTINE MOLAL(AW)
C
```

```
      IMPLICIT DOUBLE PRECISION(A-H,L,M,O-Z)
      DOUBLE PRECISION ITOT
      COMMON/ONE/MWMN, MWNA, MWH2O, MWSOLN, VM, MMN, MNA,
     1           RHOSOL, AVAG, DELTA, CMN, CNA, TOL
C
C From the main program we know AW1. If DELTA*MMN is substituted into
C the Kusik-Meisner rules, we get ln(AW)=f(MMN). MMN can be solved
C for by searching for MMN such that ln(AW)-f(MMN) = 0.
C Use similar triangle iteration.
C
      MMIN = 0.0D0
      IF(DELTA.EQ.0.D0) THEN
           MMAX = 4.95D0
      ELSE
           MMAX = 3.D0*3.81D0/(3.D0*DELTA+4.D0)
      ENDIF
   10 FMIN = AW - ACTIVM(MMIN)
      FMAX = AW - ACTIVM(MMAX)
      MNEW = MMAX - (MMAX-MMIN)*FMAX/(FMAX-FMIN)
      FNEW = AW - ACTIVM(MNEW)
      IF(DABS(MMIN-MNEW).LE.TOL.OR.DABS(MMAX-MNEW).LE.TOL) GO TO 20
      IF(FNEW.LT.0.D0) MMIN = MNEW
      IF(FNEW.GT.0.D0) MMAX = MNEW
      GO TO 10
C
C Now we have the value of MMN which results in a value of AW using
C Kusik-Meisner's mixing rules. Knowing DELTA and MMN, calculate MNA.
C
   20 MMN = MNEW
      MNA = DELTA * MMN
C
C The concentration is needed to calculate the solution density
C and the density is needed to get the concentration from the molalities.
C Iterate, initially assuming density of water.
C
      VBARM = 0.113661D0
      VBARN = 0.989754D0
      RHO0 = 1.0D0
   30 CMN = MMN*RHO0/(1.D0 + MMN*MWMN/1000. + MNA*MWNA/1000.)
      CNA = MNA*RHO0/(1.D0 + MMN*MWMN/1000. + MNA*MWNA/1000.)
      RHOSOL = 1. + (1.-VBARM)*MWMN*CMN/1000. + (1.-VBARN)*MWNA
     1         *CNA/1000.
      IF(DABS(RHOSOL-RHO0).LT.TOL) GO TO 40
      RHO0 = RHOSOL
      GO TO 30
C
C Calculate the solution molecular volume.
C
   40 XMN = MMN/(MMN + MNA + 1000./MWH2O)
      XNA = MNA/(MMN + MNA + 1000./MWH2O)
      MWSOLN = XMN*MWMN + XNA*MWNA + (1.-XMN-XNA)*MWH2O
      VM = MWSOLN/(RHOSOL * AVAG)
C
C Return to the main program with new estimates of MMN, MNA, VM.
```

```
C
      RETURN
      END
C
C
C -------------------------------------------------------------
      FUNCTION ACTIVM(M)
C
      IMPLICIT DOUBLE PRECISION(A-H,L,M,O-Z)
      DOUBLE PRECISION ITOT
      COMMON/ONE/MWMN, MWNA, MWH2O, MWSOLN, VM, MMN, MNA,
     1           RHOSOL, AVAG, DELTA, CMN, CNA, TOL
C
C This function calculates the water activity of the Na2SO4-MnSO4
C mixture using Kusik-Meisner's mixing rules, given the Mn molality.
C
      SUM = 3.DO*DELTA + 4.DO
      ITOT = SUM * M
      IF(DELTA.EQ.O.DO) THEN
          AWN = O.DO
      ELSE
          AWN = DLOG(AWNO(ITOT))
      ENDIF
      AWM = DLOG(AWMO(ITOT))
      AW = (DELTA+1.DO)*(9.DO*DELTA*AWN + 16.DO*AWM)/
     1          SUM**2 - (MWH2O*DELTA*M)/(1OOO.DO*SUM)
      ACTIVM = DEXP(AW)
C
      RETURN
      END
C
C
C -------------------------------------------------------------
      FUNCTION AWNO(ITOT)
C
      IMPLICIT DOUBLE PRECISION(A-H,L,M,O-Z)
      DOUBLE PRECISION ITOT
C
C Find the pure Na2SO4 molality which results in a pure solution
C ionic strength equal to the solution ionic strength.
C
      M = ITOT/3.ODO
      IF(M.GT.3.814DO) THEN
            WRITE(*,10)
   10           FORMAT(/1X,'Na2SO4 MOLALITY TOO GREAT.')
            STOP
      ELSE
      ENDIF
      AWNO = 0.998754DO - 0.358089D-01*M + 0.406391D-02*M*M
     1       - 0.111982D-02*M**3
C
      RETURN
      END
C
```

```
C
C -------------------------------------------------------------
      FUNCTION AWM0(ITOT)
C
      IMPLICIT DOUBLE PRECISION(A-H,L,M,O-Z)
      DOUBLE PRECISION ITOT
C
C Find the pure MnSO4 molality which results in a pure solution
C ionic strength equal to the solution ionic strength.
C
      M = ITOT/4.0D0
      IF(M.GT.4.9664D0) THEN
            WRITE(*,10)
   10           FORMAT(/1X,'MnSO4 MOLALITY TOO GREAT.')
            STOP
      ELSE
      ENDIF
      AWM0 = 0.999382D0 - 0.162799D-01*M + 0.916004D-03*M*M
     1       - 0.119784D-02*M**3 - 0.245205D-03*M**4
     1       + 0.465363D-04*M**5
C
      RETURN
      END
C
C
C -------------------------------------------------------------
      SUBROUTINE LAMDAA(DP)
C
      IMPLICIT DOUBLE PRECISION(A-H,L,M,O-Z)
      DOUBLE PRECISION ITOT
      COMMON/ONE/MWMN, MWNA, MWH2O, MWSOLN, VM, MMN, MNA,
     1           RHOSOL, AVAG, DELTA, CMN, CNA, TOL
      COMMON/TWO/MOLMN, MOLNA, CMN1, CNA1
      COMMON/THREE/FACTOR2, ITER, RH2, LAMDA
C
C Find the value of LAMDA which gives AW2. LAMDA=CMN2/CMN1.
C If this is the first time at finding LAMDA, need to get in
C the ballpark before we start taking small steps. If this
C subroutine is being called for a recheck after adjustment of
C AW2, then use the LAMDA found on the previous call as the
C starting point.
C
      IF(ITER.NE.0) GO TO 20
      KOUNT = 0
   10 AW0 = ACTIVC(LAMDA)
      LAMDA0 = LAMDA
C
C We're going to recalculate AW2=RH2*KELVIN every time because
C VM is constantly being updated in ACTIVC function and this
C should speed convergence.
C
      IF(AW0.LE.RH2*DEXP(-FACTOR2*VM/DP)) GO TO 20
      LAMDA = LAMDA + 0.01D0
      KOUNT = KOUNT + 1
```

```
      IF(KOUNT.GT.200) GO TO 90
      GO TO 10
   20 STEP = 1.D-06
      EPS = 1.D-06
          DO 30 J = 1, 10
          AW0 = ACTIVC(LAMDA0)
          DAW = (ACTIVC(LAMDA0+STEP) - AW0)/STEP
          IF(DAW.EQ.0.) GO TO 40
          LAMDA = LAMDA0 - (AW0 - RH2*DEXP(-FACTOR2*VM/DP))/DAW
          IF(DABS(LAMDA-LAMDA0).LT.EPS) GO TO 110
          IF(LAMDA.EQ.0.D0.OR.LAMDA.GT.8.D0) GO TO 40
          LAMDA0 = LAMDA
   30     CONTINUE
   40 LAMDA = LAMDA0
      H = 0.005D0
   50 IF(ACTIVC(LAMDA).LE.RH2*DEXP(-FACTOR2*VM/DP)) GO TO 60
      LAMDA = LAMDA + H
      GO TO 50
   60 H = H/2.D0
      IF(H.LE.5.D-06) GO TO 110
   70 IF(ACTIVC(LAMDA).GT.RH2*DEXP(-FACTOR2*VM/DP)) GO TO 80
      LAMDA = LAMDA - H
      GO TO 70
   80 H = H/2.D0
      IF(H.LE.5.D-06) GO TO 110
      GO TO 50
C
   90 WRITE(*,100)
  100     FORMAT(/1X,'CANNOT FIND APPROPRIATE LAMDA.')
      STOP
C
C Now we have LAMDA given DP.
C
  110 RETURN
      END
C
C
C -------------------------------------------------------------
      FUNCTION ACTIVC(LAMDA)
C
      IMPLICIT DOUBLE PRECISION(A-H,L,M,O-Z)
      DOUBLE PRECISION ITOT, LAMDA
      COMMON/ONE/MWMN, MWNA, MWH2O, MWSOLN, VM, MMN, MNA,
     1           RHOSOL, AVAG, DELTA, CMN, CNA, TOL
      COMMON/TWO/MOLMN, MOLNA, CMN1, CNA1
C
C This function calculates the water activity of the Na2SO4-MnSO4
C mixture using Kusik-Meisner's mixing rules, given LAMDA.
C First we have to calculate CMN2 and CNA2 knowing LAMDA,
C CMN1 and CNA1.
C
      CMN = LAMDA * CMN1
      CNA = LAMDA * CNA1
C
```

```
C Now convert these to molalities.
C
      VBARM = 0.113661D0
      VBARN = 0.989754D0
      RHOSOL = 1.D0 + (1.D0-VBARN)*MWNA*CNA/1000.D0 +
     1         (1.D0-VBARM)*MWMN*CMN/1000.D0
      MMN = CMN/(RHOSOL - CNA*MWNA/1000.D0 - CMN*MWMN/1000.D0)
      MNA = CNA/(RHOSOL - CNA*MWNA/1000.D0 - CMN*MWMN/1000.D0)
      XNA = MNA/(MNA + MMN + 1000.D0/MWH2O)
      XMN = MMN/(MNA + MMN + 1000.D0/MWH2O)
      MWSOLN = XNA*MWNA + XMN*MWMN + (1.D0-XNA-XMN)*MWH2O
      VM = MWSOLN/(RHOSOL * AVAG)
C
C Now calculate the water activity at these molalities using Kusik &
C Meisner's mixing rule
C
      ITOT = 3.D0*MNA + 4.D0*MMN
      SUM = MMN + MNA
      IF(DELTA.EQ.0.D0) THEN
          AWN = 0.D0
      ELSE
          AWN = DLOG(AWN0(ITOT))
      ENDIF
      AWM = DLOG(AWM0(ITOT))
      AW = SUM*(9.D0*MNA*AWN + 16.D0*MMN*AWM)/ITOT**2
     1      - (MWH2O/(1000.D0*ITOT))*((9.D0*MNA+8.D0*MMN)*SUM -
     1      ITOT*(3.D0*MNA+2.D0*MMN))
      ACTIVC = DEXP(AW)
C
      RETURN
      END
```

```
      PROGRAM SO2EQM
C
C THIS PROGRAM CALCULATES THE GROWTH EXPECTED GIVEN EQUILIBRATION OF A
C MnSO4 PARTICLE WITH AN SO2 ATMOSPHERE.
C
      IMPLICIT DOUBLE PRECISION(A-H,L,M,O-Z)
      DIMENSION DPO(100), DIST(100)
      COMMON/OP/T, RH, PSO2, MMNO, CMNO, MOLMN
C
C INPUT ALL THE OPERATING CONDITIONS AND NO. OF DIAMETERS IN TOP
C TWO LINES OF THE DIA,DIST DATA FILE.
C
      WRITE(*,10)
   10     FORMAT(/1X,'ENTER NAME OF DATA FILE WITH:'
     1           /10X,'T(C), RH(%), pSO2 (ppm)'
     1           /10X,'NO. DIAMETERS'
     1           /10X,'DIA(1) (um), DIST(1), ... ETC.'/)
      READ(3,*) T, RH, PSO2
      RH = RH/100.D0
      T = T + 273.15D0
C
C ENTER THE DPO FILE.
C
      READ(3,*) NUM
          DO 30 I = 1, NUM
          READ(3,*) DPO(I), DIST(I)
          DPO(I) = DPO(I)*1.D-04
   30     CONTINUE
      CLOSE(3)
C
          DO 40 I = 1, NUM
C
C CALCULATE THE INITIAL MANGANESE SULFATE CONCENTRATION -- BEFORE
C EXPOSURE TO THE SO2 (MMNO, CMNO).
C
          CALL INITIAL(DPO(I))
C
C NOW WE NEED TO CALCULATE THE NEW DIAMETER AFTER EQUILIBRATION
C WITH THE SO2. THIS WILL INVOLVE CALCULATING THE EQUILIBRIUM
C CONDITIONS AT A GIVEN PSO2 AND MnSO4 CONCENTRATION (START
C WITH THE FEED VALUE MMNO), THEN CALCULATING THE NEW WATER ACTIVITY
C AND SEEING IF AW=RH*(KELVIN).
C
          CALL EQUIB(DPO(I), CMNF, LAMDA, DPF)
          DIST(I) = DIST(I)*LAMDA**(1./3.)
          WRITE(4,50) DPF, DIST(I), LAMDA, DPO(I)*1.D04
   50         FORMAT(1X,F7.5,2X,E12.5,2X,F7.5,2X,F7.5)
          WRITE(*,*) I
   40     CONTINUE
```

```
      CLOSE(4)
C
      STOP
      END
C
C
C -------------------------------------------------------------
      SUBROUTINE INITIAL(DP)
C
      IMPLICIT DOUBLE PRECISION(A-H,M,O-Z)
      COMMON/OP/T, RH, PSO2, MMNO, CMNO, MOLMN
C
C THIS SUBROUTINE CALCULATES THE INITIAL CONDITION OF THE PARTICLE.
C SYSTEM CONSTANTS.
C
      BOLTZK = 1.3804D-16
      AVAG = 6.023D23
      MWH2O = 18.0D0
      MWMN = 151.D0
      PI = 3.141594D0
      SIGMA = 75.15D0
      VBARM = 0.113661D0
      MOLH2O = 1000.D0/MWH2O
C
C WE'RE GOING TO ACCOUNT FOR THE KELVIN EFFECT.
C
      FACTOR = 4.D0 * SIGMA/(BOLTZK * T * DP)
C
C WILL SOLVE FOR CMN BY COMPUTING AW - RH*(KELVIN FACTOR) = 0.
C INITIALIZE THE MOLECULAR VOLUME OF THE SOLUTION TO THAT OF H2O.
C
      MMNOLD = 0.D0
      VM = MWH2O/AVAG
   10 AW = RH * DEXP(-FACTOR*VM)
      IF(AW.GT.1.D0) AW = 1.D0
C
C USE SIMILAR TRIAGNLE ITERATION TO GET MOLALITY AT THIS WATER ACTIVITY.
C
      MMIN = 0.D0
      MMAX = 4.5D0
   20 FMIN = AW - DEXP(AW520(4.D0*MMIN)/MOLH2O)
      FMAX = AW - DEXP(AW520(4.D0*MMAX)/MOLH2O)
      MNEW = MMAX - (MMAX-MMIN)*FMAX/(FMAX-FMIN)
      FNEW = AW - DEXP(AW520(4.D0*MNEW)/MOLH2O)
      IF(DABS(MMIN-MNEW).LE.1.D-06.OR.DABS(MMAX-MNEW).LE.1.D-06)
     1      GO TO 30
      IF(FNEW.LT.0.D0) MMIN = MNEW
      IF(FNEW.GT.0.D0) MMAX = MNEW
      GO TO 20
C
C OK, WE HAVE THE MOLALITY GIVEN THIS ESTIMATE OF THE WATER ACTIVITY.
C IS THIS THE RIGHT ONE?
C
   30 IF(DABS(MMNOLD-MNEW).LT.1.D-07) GO TO 60
```

```
      MMNOLD = MNEW
C
C NOW LET'S CALCULATE THE MOLECULAR VOLUME USING THIS NEW MOLALITY
C AND REDO THE CALCULATON. FIRST NEED TO TURN THE MOLALITY INTO A
C MOLARITY. WILL HAVE TO ITERATE.
C
      RHOO = 1.DO
   40 CMNOLD = MMNOLD*RHOO/(1.DO + MMNOLD*MWMN/1000.DO)
      RHOSOL = 1.DO + (1.DO-VBARM)*MWMN*CMNOLD/1000.DO
      IF(DABS(RHOSOL-RHOO).LT.1.D-06) GO TO 50
      RHOO = RHOSOL
      GO TO 40
   50 XMN = MMNOLD/(MMNOLD + 1000.DO/MWH2O)
      MWSOLN = XMN*MWMN + (1.DO-XMN)*MWH2O
      VM = MWSOLN/(RHOSOL*AVAG)
      GO TO 10
C
C WE'VE FOUND THE VALUES WHICH SOLVE THE KELVIN EQUATION.
C
   60 MMNO = MMNOLD
      CMNO = CMNOLD
      MOLMN = (CMNO/1000.DO)*(PI*DP**3/6.DO)
C
      RETURN
      END
C
C
C -------------------------------------------------------------
      SUBROUTINE EQUIB(DPO, CMNF, LAMDA, DPF)
C
      IMPLICIT DOUBLE PRECISION(A-H,L,M,O-Z)
      COMMON/OP/T, RH, PSO2, MMNO, CMNO, MOLMN
      COMMON/CURRENT/CMN, CA, RHOSOL, VM
C
C THIS SUBROUTINE CALCULATES THE CONCENTRATION OF MANGANESE IN THE
C DROPLET AFTER EQUILIBRATION WITH SO2. THE KELVIN EFFECT IS
C ACCOUNTED FOR.
C CONSTANTS NEEDED.
C
      BOLTZK = 1.3804D-16
      SIGMA = 75.15DO
      FACTOR = 4.DO * SIGMA/(BOLTZK * T)
C
C LAMDA = CMNEW/CMNOLD. SEARCH LAMDA SPACE UNTIL RH = AW(LAMDA*CMNO).
C IT IS IMPORTANT TO REMEMBER THAT LAMDA IS A "VOLUME" RATIO.
C EVERYTIME SET LAMDA, NEED TO CONVERT CONC. TO MOLALITY, DO EQUIL.
C CALCULATION, THEN AW CALCULATION. SET DPF INITIALLY TO DPO. FIND
C LAMDA FOR THIS VALUE, THEN CHANGE DP AND CONTINUE.
C
      DPFO = DPO
C
C FIND LAMDA FOR THE SET DIAMETER.
C
      LAMDAO = 1.DO
```

```
   10 STEP = 1.D-07
      EPS = 1.D-07
          DO 20 J = 1, 15
          AWO = ACTIV(LAMDAO)
          L = LAMDAO+STEP
          DAW = (ACTIV(L) - AWO)/STEP
          LAMDA = LAMDAO - (AWO-RH*DEXP(-FACTOR*VM/DPFO))/DAW
          IF(DABS(LAMDA-LAMDAO).LT.EPS) GO TO 30
          LAMDAO = LAMDA
   20     CONTINUE
   30 LAMDA = LAMDAO
      CMNF = LAMDA*CMNO
C
C NOW WE HAVE LAMDA FOR THIS DIAMETER. IS THIS THE RIGHT DIAMETER?
C WHAT DIAMETER DOES THE ACTIVITY PREDICT? IF THIS IS NOT THE
C CORRECT DIAMETER, AVERAGE THE INITIAL GUESS AND THE ACTIVITY
C PREDICTED VALUE AND USE AS THE NEW GUESS FOR ANOTHER ITERATION.

      VOLSOL = (MOLMN/CMNF)*1000.DO
      DPF1 = (6.DO*VOLSOL/3.141594DO)**(1./3.)
      DPF2 = (FACTOR*VM/DLOG(RH/AWO))
      DPFO = (DPF1+DPF2)/2.DO
      IF((DABS(DPF1-DPF2)*1.DO4).LE.5.D-06) GO TO 40
      GO TO 10
C
   40 DPF = DPFO*1.DO4
C
      RETURN
      END
C
C
C -------------------------------------------------------------
      FUNCTION ACTIV(LAMDA)
C
      IMPLICIT DOUBLE PRECISION(A-H,L,M,O-Z)
      COMMON/EQION/MMN, MHSO4, MSO4, MHSO3, MSO3, MH
      COMMON/OP/T, RH, PSO2, MMNO, CMNO, MOLMN
      COMMON/CURRENT/CMN, CA, RHOSOL, VM
C
      IF(LAMDA.EQ.1.DO) THEN
C
C THIS IS THE FIRST RUN THROUGH. SIMPLY LET MMN = MMNO.
C THEN CONVERT THE MOLALITIES (THE ACID IN PARTICULAR) TO MOLARITIES.
C MH WILL => CA. PROVIDE AN INITIAL ESTIMATE OF RHOSOL.
C
          MMN = MMNO
          RHOSOL = 1.DO
          CALL REAC
          CALL AW(AWMIX)
          CALL MTOC
          ACTIV = AWMIX
          RETURN
C
      ELSE
```

```
C
C NOW LAMDA IS BEING VARIED IN THE SEARCH. HAVE PREVIOUS ESTIMATES
C OF ACID CONCENTRATIONS SO CAN TURN THE NEW CMN INTO MMN FOR THE
C EQUILIBRIUM AND ACTIVITY CALCULATIONS. DO EQUILIBRIUM, GET ACTIVITY,
C AND THEN TURN THE CURRENT MOLALITIES (PARTICULARLY MH) INTO
C CONCENTRATIONS FOR THE NEXT ITERATION.
C
          CMN = LAMDA*CMNO
          CALL CTOM
          CALL REAC
          CALL AW(AWMIX)
          CALL MTOC
          ACTIV = AWMIX
          RETURN
      ENDIF
C
      END

C -------------------------------------------------------------
      SUBROUTINE REAC
C
      IMPLICIT DOUBLE PRECISION(A-H,M,O-Z)
      DOUBLE PRECISION ITOT
      COMMON/EQION/MMN, MHSO4, MSO4, MHSO3, MSO3, MH
      COMMON/COEF/GAM32, GAM34, GAM36, GAM38, ITOT
      COMMON/CONST/RK1, RK2, RK3, RK4
      COMMON/OP/T, RH, PSO2, MMNO, CMNO, MOLMN
C
C THIS SUBROUTINE CALCULATES THE CONCENTRATIONS GIVEN A MANGANESE CONC.
C AND AN SO2 ATMOSPHERE. THE RELATIVE HUMIDITY IS CONSTANT AND THIS
C IS BEFORE ANY REACTION TAKES PLACE SO MMN = MHSO4 + MSO4 = MSVI.
C SET OF REACTIONS AS FOLLOWS:
C
C                 SO2(g)        = SO2.H2O(1)         1)
C                 SO2.H2O(1)    = H(+) + HSO3(-)     2)
C                 HSO3(-)       = H(+) + SO3(2-)     3)
C                 HSO4(-)       = H(+) + SO4(2-)     4)
C
C CA = S(VI) = HSO4(-) + SO4(2-).  ALL EQUILIBRIUM CONSTANTS
C ARE AT 25C.
C
      RK1 = 1.24D-06
      RK2 = 0.0132D0
      RK3 = 6.24D-08
      RK4 = 1.2D-02
C
C SOLVE FOR H(+) ITERATIVELY, AFTER DOING A CHARGE BALANCE.
C ACCOUNT FOR ACTIVITY COEFFICIENTS (Gij(MH)). ALL CONC. CAN
C BE EXPRESSED IN TERMS OF m(H+) AND THEIR GAMMAS. SINCE THIS
C IS AN ITERATIVE PROCESS, SIMPLY KEEP UPDATING THE GAMMAS NEEDED
C FOR THE CONCENTRATION CALCULATIONS, BUT CONSIDER THEM 1 INITIALLY.
C
      MHSTART = 1.D-6
      MHEND = 1.0D0
```

```
      GAM38 = 1.D0
      GAM36 = 1.D0
      GAM34 = 1.D0
      GAM32 = 1.D0
      CC = RK1*RK2*PSO2
      MH = MHSTART
      CALL GAMMA(MH, MMN)
      AA = -CC * (1.D0/(GAM38**2) + 2.D0*RK3/((GAM36**3)*MH))
      BB = -MMN * ((1.D0 + 2.D0*RK4*(GAM34**2)/(MH*(GAM32**3)))/
     1       (1.D0+RK4*(GAM34**2)/(MH*(GAM32**3))) - 2.D0)
      F = MH**2 + BB*MH + AA
   10 MHNEW = 10.D0* MH
      CALL GAMMA(MHNEW, MMN)
      AANEW = -CC * (1.D0/(GAM38**2) + 2.D0*RK3/((GAM36**3)*MHNEW))
      BBNEW = -MMN * ((1.D0 + 2.D0*RK4*(GAM34**2)/(MHNEW*(GAM32**3)
     1          ))/(1.D0+RK4*(GAM34**2)/(MHNEW*(GAM32**3))) - 2.D0)
      FNEW = MHNEW**2 + BBNEW*MHNEW + AANEW
      IF((F/FNEW).GT.0.D0) THEN
            MH = MHNEW
            BB = BBNEW
            F = FNEW
            GO TO 10
      ELSE
      ENDIF
C
C NOW WE ARE STRADDLING THE F=0 LINE. TAKE THE LOG AVG. OF THE MH'S
C AND SEE WHAT F WE GET.
C
      I = 1
   20 MHAVG = 10**((DLOG10(MH) + DLOG10(MHNEW))/2.)
      CALL GAMMA(MHAVG, MMN)
      AAAVG = -CC * (1.D0/(GAM38**2) + 2.D0*RK3/((GAM36**3)*MHAVG))
      BBAVG = -MMN * ((1.D0 + 2.D0*RK4*(GAM34**2)/(MHAVG*(GAM32**3)
     1          ))/(1.D0+RK4*(GAM34**2)/(MHAVG*(GAM32**3))) - 2.D0)
      FAVG = MHAVG**2 + BBAVG*MHAVG + AAAVG
C
C CHECK WHETHER WE SHOULD KEEP MH OR MHNEW.
C
      IF((FAVG/F).GT.0.D0) THEN
            F = FAVG
            BB = BBAVG
            MH = MHAVG
      ELSE
            FNEW = FAVG
            BBNEW = BBAVG
            MHNEW = MHAVG
      ENDIF
C
C SEE IF CONVERGENCE TOLERANCE IS MET.
C
      IF((ABS(MH-MHNEW)/MH).GT.1.D-08) THEN
            IF(I.GT.1000) GO TO 30
            I = I + 1
            GO TO 20
```

```
      ELSE
      ENDIF
C
C SUCCESSFUL ITERATION. WE NOW HAVE MH(+). CALCULATE OTHER CONC.
C
      MHSO3 = RK1*RK2*PSO2/(MH*(GAM38**2))
      MSO3 = RK1*RK2*RK3*PSO2/((GAM36**3)*MH**2)
      MHSO4 = MMN/(1.D0+RK4*(GAM34**2)/(MH*(GAM32**3)))
      MSO4 = RK4*MHSO4*(GAM34**2)/(MH*(GAM32**3))
      RETURN
C
   30 WRITE(*,40) MH, MH1
   40     FORMAT(/1X,'CALCULATION OF H+ FAILED AFTER 1000 ITERATIONS.'
     1    /1X,'MH = ',E15.8,5X,'MH1 = ',E15.8)
   50 STOP
C
      END
C
C
C ---------------------------------------------------------------
      SUBROUTINE GAMMA(M3, M5)
C
      IMPLICIT DOUBLE PRECISION(A-H,M,O-Z)
      DOUBLE PRECISION ITOT
      COMMON/COEF/GAM32, GAM34, GAM36, GAM38, ITOT
      COMMON/CONST/RK1, RK2, RK3, RK4
      COMMON/OP/T, RH, PSO2, MMNO, CMNO, MOLMN
C
C WE HAVE MH(+) AND INITIAL ESTIMATES OF THE MIXTURE GAMMAS. CALCULATE
C THE CONCENTRATIONS NEEDED FOR THE MIXTURE CALCULATION.
C 3:H+, 5:Mn2+, 2:SO42-, 4:HSO4-, 6:SO32-, 8:HSO3-
C
   10 M8 = RK1*RK2*PSO2/(M3*(GAM38**2))
      M6 = RK1*RK2*RK3*PSO2/((GAM36**3)*M3**2)
      M4 = M5/(1.D0+RK4*(GAM34**2)/(M3*(GAM32**3)))
      M2 = RK4*M4*(GAM34**2)/(M3*(GAM32**3))
C
C NEED TO HAVE THE IONIC STRENGTH SINCE THE PURE COMPONENT GAMMAS
C WILL BE MATCHED TO THIS VALUE.
C
      ITOT = 0.5D0*(M3 + M4 + M8 + 4.D0*(M5 + M2 + M6))
C
C CALCULATE THE PURE COMPONENT ln(gamma)'S NEEDED. FOR LACK OF
C BETTER DATA, SET SULFITE VALUES EQUAL TO SULFATE VALUES.
C
      G32 = G320(ITOT)
      G34 = G340(ITOT)
      G36 = G32
      G38 = G34
      G52 = G520(ITOT)
      G54 = G540(ITOT)
      G56 = G52
      G58 = G54
C
```

```
      X = 9.D0/4.D0
      Y = 4.D0
C
C THE MIXING RULES OF KUSIK AND MEISSNER ARE USED TO GET THE
C MIXED ACTIVITY COEFFICIENTS.
C
      GAM320 = DEXP(((2.D0/3.D0)*(X*M2*G32 + M4*G34 + X*M6*G36 +
     1         M8*G38) + (1.D0/3.D0)*(X*M3*G32 + Y*M5*G52))/ITOT)
      GAM340 = DEXP(((1.D0/2.D0)*(X*M2*G32 + M4*G34 + X*M6*G36 +
     1         M8*G38) + (1.D0/2.D0)*(M3*G34 + X*M5*G54))/ITOT)
      GAM360 = GAM320
      GAM380 = GAM340
C
C THESE GAMMAS WERE CALCULATED USING CONCENTRATIONS THAT WERE BASED
C ON INITIAL GUESSES OF THE GAMMAS. WANT TO ITERATE UNTIL THE
C CALCULATED GAMMAS EQUAL THE GAMMAS USED IN THE CONC. CALCULATIONS.
C
      IF(DABS(GAM32-GAM320).GT.1.D-04.OR.DABS(GAM34-GAM340).GT.
     1   1.D-04.OR.DABS(GAM36-GAM360).GT.1.D-04.OR.DABS(GAM38-
     1   GAM380).GT.1.D-04) THEN
         GAM32 = (GAM320+GAM32)/2.D0
         GAM34 = (GAM340+GAM34)/2.D0
         GAM36 = (GAM360+GAM36)/2.D0
         GAM38 = (GAM380+GAM38)/2.D0
         GO TO 10
      ELSE
      ENDIF
C
      RETURN
      END
C
C
C -------------------------------------------------------------
      SUBROUTINE AW(AWMIX)
C
      IMPLICIT DOUBLE PRECISION(A-H,M,O-Z)
      DOUBLE PRECISION ITOT
      COMMON/EQION/MMN, MHSO4, MSO4, MHSO3, MSO3, MH
C
C THIS SUBROUTINE CALCULATES THE WATER ACTIVITY ASSOCIATED WITH THIS
C SOLUTION. THE KUSIK-MEISSNER MIXING RULES ARE USED. THE POSSIBLE
C SPECIES ARE H+,HSO3-; H+,HSO4-; Mn2+,SO42-; Mn2+,2 HSO4-; Mn2+,2 HSO3-;
C 2H+,SO42-; 2H+,SO32-; MN2+,SO32-. GIVEN THE ION CONCENTRATIONS,
C GENERATE THE "SPECIES." COMBINE AS MUCH OF THE Mn2+ WITH SO42- AS
C POSSIBLE.
C
      M5 = MMN
      M3 = MH
      M2 = MSO4
      M4 = MHSO4
      M6 = MSO3
      M8 = MHSO3
      IF(M5.GT.M2) THEN
           M52 = M2
```

```
            M5 = M5 - M2
            M2 = 0.D0
            M32 = 0.D0
      ELSE
            M52 = M5
            M2 = M2 - M5
            M5 = 0.D0
            M54 = 0.D0
            M56 = 0.D0
            M58 = 0.D0
      ENDIF
C
C IF THERE IS Mn2+ LEFT, HSO4- CAN BE COMBINED WITH IT. IF THERE IS
C NO Mn2+, THEN JUST MAKE ACIDS.
C
      IF(M5.NE.0.D0) THEN
            IF((M4/2.D0).LT.M5) THEN
               M54 = M4/2.D0
               M5 = M5 - M54
               M4 = 0.D0
               M34 = 0.D0
            ELSE
               M54 = M5
               M4 = M4 - 2.D0*M54
               M5 = 0.D0
               M56 = 0.D0
               M58 = 0.D0
            ENDIF
      ELSE
            M32 = M2
            M34 = M4
            M36 = M6
            M38 = M8
            GO TO 10
      ENDIF
C
C IF THERE IS Mn2+ LEFT, SO32- CAN BE COMBINED WITH IT. IF THERE
C IS NO Mn2+, THEN JUST MAKE REMAINING ACIDS.
C
      IF(M5.NE.0.D0) THEN
            IF(M6.LT.M5) THEN
               M56 = M6
               M5 = M5 - M56
               M6 = 0.D0
               M36 = 0.D0
            ELSE
               M56 = M5
               M6 = M6 - M56
               M5 = 0.D0
               M58 = 0.D0
            ENDIF
      ELSE
            M32 = M2
            M34 = M4
```

```
            M36 = M6
            M38 = M8
            GO TO 10
      ENDIF
C
C IF THERE IS Mn2+ LEFT, HSO3- CAN BE COMBINED WITH IT. IF THERE
C IS NO Mn2+, THEN JUST MAKE REMAINING ACIDS.
C
      IF(M5.NE.0.D0) THEN
            M58 = M5
            M8 = M8 - 2.D0*M58
            M5 = 0.D0
      ELSE
            M32 = M2
            M34 = M4
            M36 = M6
            M38 = M8
      ENDIF
C
C ALL Mn2+ MUST BE GONE NOW. SIMPLY TAKE REMAINING NONZERO ANIONS
C AND MAKE ACIDS. THIS WILL USE UP H+.
C
      M32 = M2
      M34 = M4
      M36 = M6
      M38 = M8
C
C KUSIK-MEISSNER MIXING RULES HAVE BEEN USED FOR A 6 ION SYSTEM ---
C 3: H+, 5: Mn2+, 2: SO42-, 4: HSO4-, 6: SO32-, 8: HSO3-.
C
   10 ITOT = 3.D0*(M32 + M36 + M58 + M54) + M34 + M38 + 4.D0*
     1        (M52 + M56)
C
C GET nw*ln(aw) FOR EACH COMPONENT. THE SULFITE WATER ACTIVITIES
C HAVE BEEN SET TO THE SULFATE VALUES SINCE NO GOOD DATA FOR HIGH
C IONIC STRENGTHS EXISTS FOR THE SULFITES.
C
      AW32 = AW320(ITOT)
      AW34 = AW340(ITOT)
      AW36 = AW32
      AW38 = AW34
      AW52 = AW520(ITOT)
      AW54 = AW540(ITOT)
      AW56 = AW52
      AW58 = AW54
C
C OK, CALCULATE nw*ln(awmix) USING THE KM MIXING RULES.
C
      MOLH2O = 1000.D0/18.D0
      SUM3 = 2.D0*M32 + M34 + 2.D0*M36 + M38
      SUM5 = M52 + M54 + M56 + M58
      SUM2 = M32 + M52
      SUM4 = M34 + 2.D0*M54
      SUM6 = M36 + M56
```

```
      SUM8 = M38 + 2.D0*M58
      AWMIX = SUM3*((9.D0/2.D0)*SUM2*AW32 + SUM4*AW34 + (9.D0/2.D0)
     1         *SUM6*AW36 + SUM8*AW38)/ITOT**2 + SUM5*(16.D0*SUM2
     1         *AW52 + (9.D0/2.D0)*SUM4*AW54 + 16.D0*SUM6*AW56
     1         + (9.D0/2.D0)*SUM8*AW58)/ITOT**2 - (0.5D0*(M34+M38)
     1         *(M32+M36+M54+M58) + 2.D0*(M32+M36)*(M54+M58) +
     1         (M52+M56)*(M54+M58+M32+M36+M34+M38))/ITOT
C
      AWMIX = DEXP(AWMIX/MOLH2O)
C
      RETURN
      END
C
C
C -------------------------------------------------------------
      SUBROUTINE MTOC
C
      IMPLICIT DOUBLE PRECISION(A-H,L,M,O-Z)
      COMMON/EQION/MMN, MHSO4, MSO4, MHSO3, MSO3, MH
      COMMON/CURRENT/CMN, CA, RHOSOL, VM
C
C TAKE THE EQUILIBRIUM RESULTS AND TURN THEM INTO MOLARITIES. NEED
C TO DO THIS SINCE LAMDA IS A VOLUME BASED PARAMETER. ALL THE
C MANGANESE WILL BE CONSIDERED TO BE MnSO4 AND ALL THE HYDROGEN
C WILL BE SULFURIC ACID.
C
      VBARM = 0.113661D0
      VBARA = 0.429195D0
      AVAG = 6.023D23
      MWMN = 151.D0
      MWA = 98.D0
      MWH2O = 18.0D0
C
C HAVE TO ITERATE.
C
      RHO0 = RHOSOL
   10 CMN = MMN*RHO0/(1.D0 + MMN*MWMN/1000.D0 + MH*MWA/1000.D0)
      CA = MH*RHO0/(1.D0 + MMN*MWMN/1000.D0 + MH*MWA/1000.D0)
      RHOSOL = 1.D0 + (1.D0-VBARM)*MWMN*CMN/1000.D0 + (1.D0-
     1          VBARA)*MWA*CA/1000.D0
      IF(DABS(RHOSOL-RHO0).LT.1.D-06) GO TO 20
      RHO0 = RHOSOL
      GO TO 10
C
C GET THE NEW MOLECULAR VOLUME SO WE CAN DO THE KELVIN CALCULATION.
C
   20 XMN = MMN/(MMN + MH + 1000.D0/MWH2O)
      XA = MH/(MMN + MH + 1000.D0/MWH2O)
      MWSOLN = XA*MWA + XMN*MWMN + (1.D0-XMN-XA)*MWH2O
      VM = MWSOLN/(RHOSOL*AVAG)
C
C SO WE HAVE THE CONCENTRATION OF TOTAL MANGANESE. SINCE THE MAJORITY
C IS MNSO4, ABOVE ASSUMPTION WASN'T TOO BAD.
C
```

```
      RETURN
      END
C
C
C -------------------------------------------------------------
      SUBROUTINE CTOM
C
      IMPLICIT DOUBLE PRECISION(A-H,L,M,O-Z)
      COMMON/EQION/MMN, MHSO4, MSO4, MHSO3, MSO3, MH
      COMMON/CURRENT/CMN, CA, RHOSOL, VM
C
C A NEW LAMDA HAS BEEN GUESSED AND THE CONCENTRATION OF MANGANESE.
C HAS TO BE TURNED INTO A MOLALITY FOR THE SUBSEQUENT CALCULATIONS.
C THE CURRENT VALUE OF CA (PREVIOUS ITERATION) WILL BE USED. THIS
C WILL ALL BE SMOOTHED OVER SINCE THIS IS AN ITERATIVE METHOD.
C NEW RHOSOL HAS TO BE CALCULATED. MACID IS UNIMPORTANT. ALL THE
C MANGANESE WILL BE CONSIDERED TO BE MnSO4 AND ALL THE ACID WILL
C BE SULFURIC ACID.
C
      VBARM = 0.113661D0
      VBARA = 0.429195D0
      MWMN = 151.D0
      MWA = 98.D0
      MWH2O = 18.0D0
C
      RHOSOL = 1.D0 + (1.D0-VBARM)*MWMN*CMN/1000.D0 + (1.D0-
     1          VBARA)*MWA*CA/1000.D0
      MMN = CMN/(RHOSOL - CMN*MWMN/1000.D0 - CA*MWA/1000.D0)
C
C SO WE HAVE THE CONCENTRATION OF TOTAL MANGANESE. SINCE THE MAJORITY
C IS MNSO4, ABOVE ASSUMPTION WASN'T TOO BAD.
C
      RETURN
      END
C
C
C -------------------------------------------------------------
      FUNCTION AW520(ITOT)
C
      IMPLICIT DOUBLE PRECISION(A-H,M,O-Z)
      DOUBLE PRECISION ITOT
C
C The water activity data of Rard (1984) was fit with a polynomial.
C Find the pure MnSO4 molality which results in a pure solution
C ionic strength equal to the solution ionic strength.
C
      M = ITOT/4.D0
      AW52 = 0.999382D0 - 0.162799D-01*M + 0.916004D-03*M*M
     1       - 0.119784D-02*M**3 - 0.245205D-03*M**4
     1       + 0.465363D-04*M**5
C
C Calculate nw*ln(aw).
C
      AW520 = (1000.D0/18.D0)*DLOG(AW52)
```

```
C
      RETURN
      END
C
C
C -------------------------------------------------------------
      FUNCTION AW340(ITOT)
C
C This function calculates nw*ln(aw(H,HSO4)) using Rard's (1976) data,
C "unmixed" by the Kusik-Meissner rules (Stelson, 1984).
C
      IMPLICIT DOUBLE PRECISION(A-H,M,O-Z)
      DOUBLE PRECISION ITOT
C
C These coefficients fit to curves on p.30 of Stelson.
C
      A0 = 0.371591D-02
      A1 = -0.908027D0
      A2 = 1.25847D0
      A3 = -0.547089D0
      A4 = 0.217464D0
      A5 = -0.426523D-01
      A6 = 0.292312D-02
      SQI = DSQRT(ITOT)
C
C ln GAMMA(H,HSO4)
C
      GHSO4 = A0 + A1*SQI + A2*SQI**2 + A3*SQI**3 + A4*SQI**4
     1          + A5*SQI**5 + A6*SQI**6
C
C Integral from 0 to ITOT of lnGAMMA(H,HSO4)dI
C
      GHSO4I = A0*SQI**2 + A1*(2.D0/3.D0)*SQI**3 +
     1          A2*(1.D0/2.D0)*SQI**4 + A3*(2.D0/5.D0)*SQI**5 +
     1          A4*(1.D0/3.D0)*SQI**6 + A5*(2.D0/7.D0)*SQI**7 +
     1          A6*(1.D0/4.D0)*SQI**8
C
C Now calculate nw*ln(aw).
C
      AW340 = -2.D0*(ITOT*GHSO4 - GHSO4I + ITOT)
C
      RETURN
      END
C
C
C -------------------------------------------------------------
      FUNCTION AW320(ITOT)
C
C This function calculates nw*ln(aw(2H,SO4)) using Rard's (1976) data,
C "unmixed" by the Kusik-Meissner rules (Stelson, 1984).
C
      IMPLICIT DOUBLE PRECISION(A-H,M,O-Z)
      DOUBLE PRECISION ITOT
C
```

```
C These coefficients fit to curves on p.30 of Stelson.
C
      A0 = 0.244133D-01
      A1 = -1.7997D0
      A2 = 0.263197D0
      A3 = 0.152819D0
      A4 = -0.512581D-01
      A5 = 0.431276D-02
      SQI = DSQRT(ITOT)
C
C ln GAMMA(2H,SO4)
C
      GSO4 = A0 + A1*SQI + A2*SQI**2 + A3*SQI**3 + A4*SQI**4
     1          + A5*SQI**5
C
C Integral from 0 to ITOT of lnGAMMA(2H,SO4)dI
C
      GSO4I = A0*SQI**2 + A1*(2.D0/3.D0)*SQI**3 +
     1         A2*(1.D0/2.D0)*SQI**4 + A3*(2.D0/5.D0)*SQI**5 +
     1         A4*(1.D0/3.D0)*SQI**6 + A5*(2.D0/7.D0)*SQI**7
C
C Now calculate nw*ln(aw).
C
      AW320 = -(ITOT*GSO4 - GSO4I + ITOT)
C
      RETURN
      END
C
C
C ---------------------------------------------------------------
      FUNCTION AW540(ITOT)
C
C This function calculates the "pure" MnCl2 water activity. This
C is being used to approximate the activity of Mn(HSO4)2 and Mn(HSO3)2.
C Mark Cohen's (1987) data fit is used.
C
      IMPLICIT DOUBLE PRECISION(A-H,M,O-Z)
      DOUBLE PRECISION ITOT
C
C Want the activity at that molality that corresponds to the
C mixture total ionic strength.
C
      MM = ITOT/3.D0
C
      AW54 = 0.9989D0 - 3.639D-02*MM - 2.049D-02*MM**2
     1          + 4.286D-03*MM**3 - 4.137D-04*MM**4
     1          + 1.960D-05*MM**5 - 3.417D-07*MM**6
C
C Calculate nw*ln(aw).
C
      AW540 = (1000.D0/18.D0)*DLOG(AW54)
C
      RETURN
      END
```

```
C
C
C ---------------------------------------------------------------
      FUNCTION G340(ITOT)
C
C This function calculates ln(gamma(H,HSO4)) using Rard's (1976) data,
C "unmixed" by the Kusik-Meissner rules (Stelson, 1984).
C
      IMPLICIT DOUBLE PRECISION(A-H,M,O-Z)
      DOUBLE PRECISION ITOT
C
C These coefficients fit to curves on p.30 of Stelson.
C
      A0 = 0.371591D-02
      A1 = -0.908027D0
      A2 = 1.25847D0
      A3 = -0.547089D0
      A4 = 0.217464D0
      A5 = -0.426523D-01
      A6 = 0.292312D-02
      SQI = DSQRT(ITOT)
C
C ln GAMMA(H,HSO4)
C
      G340 = A0 + A1*SQI + A2*SQI**2 + A3*SQI**3 + A4*SQI**4
     1       + A5*SQI**5 + A6*SQI**6
C
      RETURN
      END
C
C
C ---------------------------------------------------------------
      FUNCTION G320(ITOT)
C
C This function calculates ln(gamma(2H,SO4)) using Rard's (1976) data,
C "unmixed" by the Kusik-Meissner rules (Stelson, 1984).
C
      IMPLICIT DOUBLE PRECISION(A-H,M,O-Z)
      DOUBLE PRECISION ITOT
C
C These coefficients fit to curves on p.30 of Stelson.
C
      A0 = 0.244133D-01
      A1 = -1.7997D0
      A2 = 0.263197D0
      A3 = 0.152819D0
      A4 = -0.512581D-01
      A5 = 0.431276D-02
      SQI = DSQRT(ITOT)
C
C ln GAMMA(2H,SO4)
C
      G320 = A0 + A1*SQI + A2*SQI**2 + A3*SQI**3 + A4*SQI**4
     1         + A5*SQI**5
```

```
C
      RETURN
      END
C
C
C -----------------------------------------------------------------
      FUNCTION G520(ITOT)
C
C This function calculates ln(gamma(Mn,SO4)) using Rard's (1984)
C data fit.
C
      IMPLICIT DOUBLE PRECISION(A-H,M,O-Z)
      DIMENSION RR(8), A(8)
      DOUBLE PRECISION ITOT
      DATA RR/0.75D0,1.D0,1.25D0,1.5D0,1.75D0,2.D0,2.25D0,2.5D0/
      DATA A/-21.39843D0,159.7962D0,-426.0224D0,611.08138D0,
     1       -513.9961D0,252.5674D0,-66.58744D0,7.181363D0/
C
C Calculate molality of MnSO4 solution that has same ionic strength
C as mixture.
C
      M = ITOT/4.D0
C
C ln GAMMA(Mn,SO4)
C
      SUM = 0.D0
          DO 10 I = 1, 8
          SUM = SUM + A(I)*((RR(I)+1.D0)/RR(I))*(M**RR(I))
   10     CONTINUE
      G520 = -9.4097D0*DSQRT(M) + SUM
C
      RETURN
      END
C
C
C -----------------------------------------------------------------
      FUNCTION G540(ITOT)
C
C This function calculates ln(gamma(Mn,2HSO4)) using Mark Cohen's
C (1987) improved Pitzer coefficients for MnCl2 as an estimate.
C
      IMPLICIT DOUBLE PRECISION(A-H,M,O-Z)
      DOUBLE PRECISION ITOT
C
C Pitzer's coefficients.
C
      BMX0 = 0.25811D0
      BMX1 = 2.31108D0
      CPHI = -0.010540D0
      A1 = 2.0D0
      SQI = DSQRT(ITOT)
C
      SUM = 1.D0 + 1.2*SQI
      FG = -0.392D0*(SQI/SUM + (2.D0/1.2D0)*DLOG(SUM))
```

```
      BMX = 2.D0*BMX0 + 2.D0*BMX1*(1.D0 - DEXP(-SQI*A1**2)*(1.D0
     1       + A1*SQI - 0.5D0*ITOT*A1**2))/(ITOT*A1**2)
      CG = 1.5D0*CPHI
C
C Calculate molality of Mn(HSO4)2 solution that has same ionic strength
C as mixture.
C
      M = ITOT/3.D0
C
C ln GAMMA(Mn,2HSO4)
C
      G540 = 2.D0*FG + (4.D0/3.D0)*M*BMX + (2.D0/3.D0)*(2**1.5)*
     1       (M**2)*CG
C
      RETURN
      END
```

```
      PROGRAM CSTR
C
C ***************************************************************************
C THIS PROGRAM CALCULATES WHAT THE EFFLUENT FROM THE CSTR WILL BE IF
C I HAVE A GIVEN FEED DISTRIBUTION AND ATMOSPHERE.
C ***************************************************************************
C
      IMPLICIT REAL(A-H,M,O-Z)
      CHARACTER*20 FILE
C
C ******* THIS MAY NEED TO BE CHANGED FOR INDIVIDUAL RUNS ***********
C *                                                                 *
C * THE DIMENSIONS NEED TO BE CHANGED CORRESPONDING TO THE NUMBER   *
C * OF FEED DIAMETERS (ARRAYS: DP,DISTLN,XF,DPF,DISTF,XINT), AND TO *
C * THE NONDIMENSIONAL DIAMETER (X) SCALE. IDIV1=2*IDIV2-1. (ARRAYS *
C * (IDIV1): DP,DISTLN) (ARRAYS (IDIV2): XP, CAOUT,CMOUT,CNOUT,GROW,*
C * RHO, DAWDCA, DAWDCM, DAWDCN).                                   *
C *                                                                 *
C ***************************************************************************
C
      DOUBLE PRECISION DPMIN, DRATIO, TEMPO, PO, Q, RHO, DELTA, MN,
     1                 DELTA1, PSO2, TO, RH1, DPMAX, DP(56,251), MA,
     1                 DISTLN(56,251), D(400), DIST(56,400), RXN, MH,
     1                 MSIV, RHOL, ITOT, IEFF, MM
      COMMON/HOME/ XP(501), CAOUT(501), XF(56), DPF(56), DISTF(56),
     1             CMOUT(501), GROW(501), RHO(501), XINT(56,251),
     1             DAWDCA(501), DAWDCM(501), DAWDCN(501),
     1             CNOUT(501)
C
      COMMON/TWO/ DPMIN, DRATIO, TEMPO, PO, Q, RHO, DELTA, PSO2
      COMMON/TEN/ RXN, MH, MSIV, MN, MM, MA, RHOL, IEFF
C
C
C ENTER THE OPERATING AND ATMOSPHERIC CONDITIONS.
C
      WRITE(*,10)
   10     FORMAT(/1X,'ENTER CSTR TEMP(C), PRESS(mmHg) => '$)
      READ(*,*) TO, PO
      WRITE(*,20)
   20     FORMAT(/1X,'ENTER CSTR SO2 CONCENTRATION (PPM) => '$)
      READ(*,*) PSO2
      WRITE(*,30)
   30     FORMAT(/1X,'ENTER CSTR FLOWRATE (LPM) => '$)
      READ(*,*) Q
      WRITE(*,40)
   40     FORMAT(/1X,'ENTER CSTR RH AND EMC RH (%) => '$)
      READ(*,*) RHO, RH1
      WRITE(*,50)
   50     FORMAT(/1X,'ENTER MOL MnSO4/MOL Na2SO4.'
```

```
     1           /1X,'IF HAVE PURE Na2SO4, EXIT PROGRAM'
     1           /1X,'IF HAVE PURE MnSO4, ENTER 1.D10. => '$)
      READ(*,*) DELTA1
      WRITE(*,60)
   60     FORMAT(/1X,'ENTER THE FRACTION (BLANKET) LOSS'
     1           /1X,'OF PARTICLES IN THE TEFLON LINES => '$)
      READ(*,*) XLOSS
C
      RHO = RHO/100.0
      TEMPO = TO + 273.15D0
      RH1 = RH1/100.0
      DELTA = 1.D0/DELTA1
      IF(DELTA1.EQ.1.D10) DELTA = 0.D0
      XLOSS = 1.0 - XLOSS
C
C WORK ON A NONDIMENSIONAL DIAMETER RANGE--X=ln(Dp/Dp1)/ln(Dp2/Dp1).
C WE NEED TO DIVIDE THE DIAMETER RANGE OVER WHICH WE'RE GOING
C TO CALCULATE THE EFFLUENT DISTRIBUTION (I.E. THE EFFLUENT DISTR
C IS GOING TO HAVE LARGER DIAMETERS THAT THE FEED SO YOU CAN'T
C SIMPLY USE THE FEED DIAMETERS). ENTER THE UPPER LIMIT AND THE
C NO. OF DIVISIONS TO BE USED. WE'RE GOING TO LET "ONE" FEED SIZE
C "GROW" OVER THIS ENTIRE RANGE.
C
      WRITE(*,70)
   70     FORMAT(/1X,'ENTER MIN,MAX DIAMETERS EXPECTED (uM) => '$)
      READ(*,*) DPMIN, DPMAX
C
C NOW READ IN THE FEED DISTRIBUTION WHICH HAS BEEN SHIFTED TO CSTR RH.
C
      WRITE(*,80)
   80     FORMAT(/1X,'ENTER FEED DISTR FILE NAME => '$)
      READ(*,90) FILE
   90     FORMAT(A)
      OPEN(UNIT=11, FILE=FILE, STATUS='OLD', CARRIAGECONTROL='LIST')
      WRITE(*,100)
  100     FORMAT(/1X,'ENTER NO. OF FEED DIAMETERS => '$)
      READ(*,*) NUM
          DO 110 I = 1, NUM
          READ(11,*) DPF(I), DISTF(I)
  110     CONTINUE
      CLOSE(UNIT=11)
C
C FOR THE CALCULATIONS WE NEED A TOTAL NO., NOT n(Dp). CALCULATE
C THE TOTAL NO. OF PARTICLES BETWEEN DPF(J) AND DPF(J+1). THIS
C IS delN(J). THEN ASSIGN THIS NO. TO THE AVERAGE DIAMETER
C (DPF(J)+DPF(J+1))/2. NOW THE NO. OF FEED POINTS IS NUM-1
C IF THERE IS A LOSS (SIZE INDEPENDENT) TO BE ACCOUNTED FOR
C DO SO HERE. IT IS SIMPLY ASSUMED TO BE A FRACTIONAL LOSS
C FOR ALL SIZES---IF THERE IS NO LINE LOSS, XLOSS=1.
C
          DO 120 J = 1, NUM-1
          TOTN = (DISTF(J)+DISTF(J+1))*(DPF(J+1)-DPF(J))/2.0
          DD = (DPF(J+1) + DPF(J))/2.0
          DISTF(J) = XLOSS * TOTN
```

```
          DPF(J) = DD
  120     CONTINUE
      NUM = NUM - 1
C
C MAKE THE FEED DISTRIBUTION DIAMETERS NONDIMENSIONAL.
C
      DRATIO = DPMAX/DPMIN
          DO 130 I = 1, NUM
          XF(I) = DLOG(DPF(I)/DPMIN)/DLOG(DRATIO)
  130     CONTINUE
C
C IDIV1 IS A FINER SCALE THAN IDIV2. WE'LL SAVE DATA ON THE
C IDIV2 SCALE, BUT INTEGRATE ON THE IDIV1 SCALE. IDIV1=2*IDIV2-1.
C
      IDIV1 = 501
      IDIV2 = 251
C
C THE DATA FILES MAY ALREADY HAVE BEEN GENERATED ON A PREVIOUS
C RUN THROUGH. THESE FILES ARE DEPENDENT ON THE DPMIN,DPMAX,IDIV1,IDIV2,
C VAL USED; THE ENVIRONMENTAL CONDITIONS; AND THE KINETICS USED. THEY
C ARE INDEPENDENT OF THE PARTICULAR FEED DISTRIBUTION.
C
      WRITE(*,140)
  140     FORMAT(/1X,'TO READ IN CHEMISTRY DATA FILES (SAME'
     1     /1X,'OPERATING CONDITIONS), ENTER 1. OTHERWISE 0. => '$)
      READ(*,*) ICALC
      IF(ICALC.EQ.1) THEN
          WRITE(*,150)
  150         FORMAT(/1X,'ENTER CHEMISTRY FILE NAME => '$)
          READ(*,90) FILE
          OPEN(UNIT=8, FILE=FILE, STATUS='OLD', CARRIAGECONTROL='LIST')
          WRITE(*,160)
  160         FORMAT(/1X,'ENTER DERIVATIVE FILE NAME => '$)
          READ(*,90) FILE
          OPEN(UNIT=9, FILE=FILE, STATUS='OLD', CARRIAGECONTROL='LIST')
              DO 170 I = 1, IDIV1
              READ(8,200) XP(I),CNOUT(I),CAOUT(I),CMOUT(I),RHO(I)
              READ(9,210) DAWDCA(I), DAWDCM(I), DAWDCN(I)
  170         CONTINUE
          CLOSE(UNIT=8)
          CLOSE(UNIT=9)
      ELSE
          GO TO 185
      ENDIF
C
C IF WANT TO RUN DIFFERENT KINETICS WITH SAME OP CONDITIONS AND DPMIN,
C DPMAX, ETC., DON'T ENTER GROWTH FILES. CALCULATE NEW ONES.
C
      WRITE(*,180)
  180     FORMAT(/1X,'TO READ IN GROWTH DATA FILE (SAME'
     1     /1X,'OPERATING CONDITIONS), ENTER 1. OTHERWISE 0. => '$)
      READ(*,*) ICALC
      IF(ICALC.EQ.1) THEN
          WRITE(*,182)
```

```
  182         FORMAT(/1X,'ENTER GROWTH FILE NAME => '$)
          READ(*,90) FILE
          OPEN(UNIT=10, FILE=FILE, STATUS='OLD', CARRIAGECONTROL='LIST')
              DO 181 I = 1, IDIV1
              READ(10,210) XP(I), GROW(I), RXN
  181         CONTINUE
          CLOSE(UNIT=10)
          GO TO 260
      ELSE
          GO TO 230
      ENDIF
C
C SINCE WE DON'T HAVE THE CHEMISTRY DATA FILE ALREADY CALCULATED,
C NEED TO DO THAT. CALCULATE THE XP(I). WE'LL LOOK AT PRODUCT
C DIAMETERS RANGING FROM XF TO XF+(IDIV1-1)/VAL. THIS ASSUMES
C THE INTEGRAL OF THE DISTRIBUTION PROPERTY FROM XF+(IDIV-1)/VAL
C TO INFINITY EQUALS ZERO.
C
  185 WRITE(*,186) IDIV1
  186     FORMAT(/1X,'ENTER VAL (> IDIV1=',I3,') => '$)
      READ(*,*) VAL
          DO 190 I = 1, IDIV1
          XP(I) = FLOAT(I-1)/VAL
  190     CONTINUE
C
C START THE PROGRAM. FOR FEED SIZE = 0, DETERMINE CONC. AND AEROSOL
C CURRENT FOR A GIVEN PRODUCT SIZE.  I DON'T NEED TO DO THIS FOR ALL
C FEED/PRODUCT SIZE COMBINATIONS BECAUSE FOR FEED SIZE XF,2 AND PRODUCT
C SIZE XP,2, THE CONCENTRATIONS ARE THE SAME AS FOR FEED SIZE XF,1 = 0
C AND PRODUCT SIZE XP,1=XP,2-XF,2. THIS IS ALL BECAUSE OF THE LN
C SIZE SCALE. IN OTHER WORDS, AT A GIVEN DELTA DOWN THE X SCALE, THE
C PRODUCT CONCENTRATION IS THE SAME IF YOU HAD XF,1 OR XF,2. SO CALC
C XP,1 FOR INITIAL SIZE OF ZERO. THIS THEN EQUALS DELTA AND CAN BE
C ADDED TO ARBITRARY FEED SIZES TO GET THE CONCENTRATIONS.
C ---------------------------------------------------------------
C THE DATA GENERATED BY SUBROUTINE CONC IS INDEPENDENT OF THE KINETICS
C THAT WILL BE USED AND INDEPENDENT OF THE FEED DISTRIBUTION. IT IS
C DEPENDENT ONLY ON THE ENVIRONMENTAL CSTR CONDITIONS.
C ---------------------------------------------------------------
C
      WRITE(*,150)
      READ(*,90) FILE
      OPEN(UNIT=8, FILE=FILE, STATUS='NEW', CARRIAGECONTROL='LIST')
      WRITE(*,160)
      READ(*,90) FILE
      OPEN(UNIT=9, FILE=FILE, STATUS='NEW', CARRIAGECONTROL='LIST')
      WRITE(*,150)
      READ(*,90) FILE
      OPEN(UNIT=10, FILE=FILE, STATUS='NEW', CARRIAGECONTROL='LIST')
          DO 220 I = 1, IDIV1
          CALL CONC(I,XP(I),CNOUT(I),CAOUT(I),CMOUT(I),RHO(I),
     1              DAWDCA(I), DAWDCM(I), DAWDCN(I), ITOT)
          WRITE(*,*) I
          WRITE(8,200) XP(I),CNOUT(I),CAOUT(I),CMOUT(I),RHO(I)
```

```
          WRITE(9,210) DAWDCA(I), DAWDCM(I), DAWDCN(I)
          WRITE(10,215) XP(I), ITOT
  200         FORMAT(1X,5(F10.7,2X))
  210         FORMAT(1X,3(1P(E15.7),2X))
  215         FORMAT(1X,2(F10.7,2X))
  220     CONTINUE
      CLOSE(UNIT=8)
      CLOSE(UNIT=9)
      CLOSE(UNIT=10)
C
C NOW WE HAVE THE COMPOSITION DATA, WE NEED TO CALCULATE THE
C AEROSOL CURRENT, WHICH IS A FUNCTION OF THE KINETICS. SAVE THE
C GROWTH PARAMETER IN A DATAFILE. THE DATA FROM CURRENT IS INDEPENDENT
C OF THE FEED DISTRIBUTION SINCE IT WAS CALCULATED ON A NONDIMENSIONAL
C SCALE. IT IS DEPENDENT ON THE MIN/MAX DIAMETERS USED TO NONDIMEN-
C SIONALIZE THE SCALE. SAVE THE MOLALITY RESULTS OF THE SPECIES.
C
  230 WRITE(*,182)
      READ(*,90) FILE
      OPEN(UNIT=9, FILE=FILE, STATUS='NEW', CARRIAGECONTROL='LIST')
      WRITE(*,182)
      READ(*,90) FILE
      OPEN(UNIT=10, FILE=FILE, STATUS='NEW', CARRIAGECONTROL='LIST')
      WRITE(*,182)
      READ(*,90) FILE
      OPEN(UNIT=11, FILE=FILE, STATUS='NEW', CARRIAGECONTROL='LIST')
          DO 250 I = 1, IDIV1
          RHOL = RHO(I)
          GROW(I) = CURRENT(CAOUT(I), CMOUT(I), CNOUT(I), DAWDCA(I),
     1                DAWDCM(I), DAWDCN(I))
          WRITE(9,210) XP(I), GROW(I), RXN
          WRITE(10,240) XP(I), MH, MSIV, MM, MA, MN
          WRITE(11,215) XP(I), IEFF
  240         FORMAT(1X,6(1P(E12.5),1X))
  250     CONTINUE
      CLOSE(UNIT=9)
      CLOSE(UNIT=10)
      CLOSE(UNIT=11)
C
C FROM HERE ON THE RESULT IS DEPENDENT ON THE FEED DISTRIBUTION.
C ZERO THE INTEGRAL VARIABLES. XINT(I,J) IS THE INTEGRAL FROM 0 TO
C XP(2J-1) ON THE IDIV1 SCALE (J IS ON THE IDIV2 SCALE) FOR FEED SIZE I.
C
  260     DO 280 I = 1, NUM
              DO 270 J = 1, IDIV2
              XINT(I,J) = 0.0
  270         CONTINUE
  280     CONTINUE
C
C CALCULATE THE CSTR RESIDENCE TIME IN SEC.
C
      TAU = 118.*60./Q
      TINV = 1.0/TAU
      H = XP(2)
```

```
C
C INTEGRATE FROM XF TO XP. WE'RE INTEGRATING ON THE IDIV1 SCALE,
C BUT SAVING ONLY THE VALUES ON THE IDIV2 SCALE. REMEMBER,
C IDIV2 = (IDIV1 + 1)/2.
C
          DO 300 I = 1, NUM
              DO 290 J = 2, IDIV2
              T1 = (TINV+BETA(XF(I)+XP(2*J-3),RHO(2*J-3)))/GROW(2*J-3)
              T2 = (TINV+BETA(XF(I)+XP(2*J-2),RHO(2*J-2)))/GROW(2*J-2)
              T3 = (TINV+BETA(XF(I)+XP(2*J-1),RHO(2*J-1)))/GROW(2*J-1)
              XINT(I,J) = XINT(I,J-1) + (H/3.)*(T1 + 4.*T2 + T3)
  290         CONTINUE
  300     CONTINUE
C
C NOW CALCULATE THE DISTRIBUTIONS (dN/dlnDp) GIVEN EACH "MONODISPERSE"
C FEED DISTRIBUTION.
C
      DENOM = DLOG(DRATIO)
          DO 320 I = 1, NUM
              DO 310 J = 1, IDIV2
              DISTX = DISTF(I)*EXP(-XINT(I,J))/(TAU*GROW(2*J-1))
              DP(I,J) = DPMIN * DRATIO**(XF(I)+XP(2*J-1))
              DISTLN(I,J) = DISTX/DENOM
  310         CONTINUE
  320     CONTINUE
C
C THESE DISTRIBUTIONS ARE FOR THE CSTR RH. NOW SHIFT THEM BACK TO
C THE EMC EFFLUENT RH SO THE FINAL DISTRIBUTION CAN BE COMPARED TO
C THE EMC DISTRIBUTION DIRECTLY. THIS MUST BE DONE BEFORE THE FEED
C DISTRIBUTIONS ARE COMBINED BECAUSE WE STILL KNOW THE COMPOSITION
C OF A GIVEN PARTICLE (A PARTICLE OF SIZE XF(1)+XP(10) HAS SAME
C COMPOSITION AS ONE OF SIZE XF(2)+XP(10)). FOR J>1, USE PREVIOUS
C LAMDA VALUE AS INITIAL GUESS.
C
      IF(RH1.EQ.RH0) GO TO 350
           DO 340 I = 1, NUM
               DO 330 J = 1, IDIV2
               K = 2*J - 1
               CALL SHIFT(J,RH1,CAOUT(K),CMOUT(K),CNOUT(K),DP(I,J))
  330          CONTINUE
           WRITE(*,*) I
  340      CONTINUE
C
C ****** THIS SECTION NEEDS TO BE DONE IN DOUBLE PRECISION  ******
C ****** OR THE ROUND-OFF ERROR CAUSES PROBLEMS.             ******
C FIND THE MAXIMUM DIAMETER HAVING A SIGNIFICANT DISTRIBUTION VALUE.
C SEARCH THE DISTRIBUTION CORRESPONDING TO THE MAXIMUM FEED DIAMETER.
C
  350     DO 360 J = 1, IDIV2
          K = IDIV2 - (J - 1)
          IF(DISTLN(NUM,K).LT.1.D-5) THEN
              GO TO 360
          ELSE
              DPMAX = DP(NUM,K)
```

```
            GO TO 370
          ENDIF
  360     CONTINUE
C
C SIMILARLY, FIND THE MINIMUM DIAMETER HAVING A SIGNIFICANT DIS-
C TRIBUTION VALUE. SEARCH THE DISTRIBUTION OF THE SMALLEST FEED DIA.
C
  370     DO 380 J = 1, IDIV2
          IF(DISTLN(1,J).LT.1.D-5) THEN
            GO TO 380
          ELSE
            DPMIN = DP(1,J)
            GO TO 390
          ENDIF
  380     CONTINUE
C
  390 WRITE(*,*) DPMIN, DPMAX
C
C THIS DIAMETER RANGE IS GOING TO BE DIVIDED INTO 400 DIAMETERS.
C
      JDIV = 399
C
C DETERMINE THE DISTRIBUTION VALUE AT EACH OF THE DIAMETERS.  LINEARLY
C INTERPOLATE IF NECESSARY.
C
  400 DELD = (DPMAX-DPMIN)/FLOAT(JDIV)
          DO 440 J = 1, JDIV+1
            D(J) = DPMIN + DELD*(J-1)
C
            DO 430 I = 1, NUM
C
C TAKE CARE OF THE CONDITIONS THAT WOULD CAUSE US PROBLEMS--------
C IF THE LARGEST VALUE OF THE DISTR IS LESS THAN D, WE DON'T NEED
C TO LOOK AT THIS DISTR.
C
            IF(DP(I,IDIV2).LT.D(J)) THEN
              DIST(I,J) = 0.D0
              GO TO 430
            ELSE
            ENDIF
C
C IF THE SMALLEST VALUE OF THE DISTR IS GREATER THAN D, WE DON'T NEED
C TO LOOK AT THIS DISTR.
c
            IF(DP(I,1).GT.D(J)) THEN
              DIST(I,J) = 0.D0
              GO TO 430
            ELSE
            ENDIF
C
C NOW FIND THE DIAMETERS WHICH BOUND D(J) AND INTERPOLATE.
C IF THE DISTRIBUTION VALUE AT THIS POINT IS < 1.D-05, PASS.
C
              DO 410 K = 2, IDIV2
```

```
                IF(DP(I,K).LT.D(J)) GO TO 410
                IF(DISTLN(I,K).LT.1.D-5.AND.DISTLN(I,K-1).LT.
     1                1.D-5) THEN
                      DIST(I,J) = 0.D0
                      GO TO 430
                ELSE
                ENDIF
C
C OTHERWISE, LET'S DO LOG INTERPOLATION TO GET DISTLN(I,D).
C
                KLOW = K - 1
                KHIGH = K
                GO TO 420
  410           CONTINUE
  420         DIST(I,J) = DEXP(DLOG(DISTLN(I,KLOW)) + DLOG(DISTLN(I,
     1                KHIGH)/DISTLN(I,KLOW))*DLOG(D(J)/DP(I,KLOW))/
     1                DLOG(DP(I,KHIGH)/DP(I,KLOW)))
  430         CONTINUE
            WRITE(*,*) J
  440       CONTINUE
C
C NOW COMPUTE THE SIZE DISTR n(Dp) GIVEN THE VALUES FOR ALL THE
C DISTRIBUTIONS AT D(J). DIST(I,J) IS STILL n(lnDp) AND IS DIVIDED
C BY DIAMETER TO TURN IT INTO n(Dp). INTEGRATE IT ALSO.
C
        WRITE(*,450)
  450     FORMAT(/1X,'ENTER OUTPUT DISTR FILE NAME => '$)
        READ(*,90) FILE
        OPEN(UNIT=60, FILE=FILE, STATUS='NEW', CARRIAGECONTROL='LIST')
        SUM = 0.D0
            DO 480 J = 1, JDIV+1
            DSTR = 0.D0
                DO 460 I = 1, NUM
                DSTR = DSTR + DIST(I,J)
  460           CONTINUE
            DSTR = DSTR/D(J)
            WRITE(60,470) D(J), DSTR
  470           FORMAT(1X,F8.6,2X,D15.8)
            IF(J.EQ.1) THEN
                DSTR0 = DSTR
                GO TO 480
            ELSE
                SUM = SUM + 0.5D0*(D(J)-D(J-1))*(DSTR+DSTR0)
                DSTR0 = DSTR
            ENDIF
  480       CONTINUE
        WRITE(60,*) SUM
        CLOSE(60)
C
        WRITE(*,490)
  490       FORMAT(/1X,'*********************************'
     1             /1X,' HOORAY!!! THE RUN IS FINISHED. '
     1             /1X,'*********************************')
C
```

```
      STOP
      END
C
C
C -------------------------------------------------------------
      SUBROUTINE CONC(I, X, CNA, CSVI, CMN, RHO, DAWDCA,
     1                DAWDCM, DAWDCN, ISTR)
C
      IMPLICIT DOUBLE PRECISION(A-H,M,O-Z)
      DOUBLE PRECISION ITOT, ISTR
      REAL X, CNA, CSVI, CMN, RHO, DAWDCA, DAWDCM, DAWDCN
      COMMON/TWO/ DPMIN, DRATIO, TEMP, P, Q, RH, DELTA, PSO2
      COMMON/THREE/ MWSOLN, RHOSOL
      COMMON/NINE/ CMNEW
      COMMON/STRGTH/ITOT
C
C ****************************************************************
C  ******* THIS SUBROUTINE AND ALL SUBSEQUENT FUNCTIONS **********
C ******** ARE DONE IN DOUBLE PRECISION SO THAT DESIRED **********
C ******** TOLERANCES CAN BE REACHED.                  **********
C ****************************************************************
C
C THIS SUBROUTINE CALCULATES THE AEROSOL COMPOSITION.
C FIRST CALCULATE HOW MANY MOLES OF Mn AND Na THERE ARE IN THE FEED.
C NEED THE WATER ACTIVITY CORRESPONDING TO THIS RH AND 0 MOLES ACID.
C WE'RE NOT ACCOUNTING FOR THE KELVIN EFFECT---TOO COMPLICATING.
C
      TOL = 1.D-06
      XF = 0.0D0
      XP = X
C
C SINCE CM0 IS THE SAME FOR EVERY FEED PARTICLE, ONLY CALCULATE IT THE
C FIRST TIME. THIS WILL SAVE SOME TIME. USE A SUBROUTINE THAT IS ONLY
C FOR ACID-FREE SOLN. SETTING MA=0 CAUSES SOME PROBLEMS IN THE FULL
C KM FORMULAS. TOO FUSSY FOR NEWTON'S METHOD, USE SIMILAR TRIANGLES.
C
      IF(I.NE.1) GO TO 20
      CM0 = 0.01D0
      CN0 = 0.01D0
      IF(DELTA.EQ.0.D0) THEN
          CMMAX = 5.0D0
      ELSE
          CMMAX = (3.0D0*3.810D0)/(3.0D0*DELTA+4.0D0)
      ENDIF
      CNMAX = DELTA*CMMAX
   10 FMIN = RH - ACTIVC(0.D0,CM0,CN0)
      FMAX = RH - ACTIVC(0.D0,CMMAX,CNMAX)
      CMNEW = CMMAX - (CMMAX-CM0)*FMAX/(FMAX-FMIN)
      CNNEW = CMNEW * DELTA
      FNEW = RH - ACTIVC(0.D0,CMNEW,CNNEW)
      IF(DABS(CM0-CMNEW)/CMNEW.LE.TOL.OR.DABS(CMMAX-CMNEW)/CMNEW
     1       .LE.TOL) GO TO 20
      IF(FNEW.LT.0.0D0) CM0 = CMNEW
      IF(FNEW.GT.0.0D0) CMMAX = CMNEW
```

```
      CNO = DELTA * CMO
      CNMAX = CMMAX * DELTA
      GO TO 10
C
C NOW WE KNOW THE CONCENTRATION OF Mn AND Na IN THE FEED. FIND THE NO.
C MOLES AND THEN THE CONCENTRATION IN PARTICLE SIZE X.
C
   20 DPF = DPMIN * DRATIO**XF
      DP =  DPMIN * DRATIO**XP
      CM = CMNEW * (DPF/DP)**3
      CN = CM * DELTA
C
C NOW, AT THIS NEW Mn CONCENTRATION, FIND CA SUCH THAT THE DROP IS IN
C THERMODYNAMIC EQUILIBRIUM AT RH. IF DP=DPF (X=XF) THEN CM=CMNEW
C BECAUSE THE DROPLET HASN'T CHANGED IN SIZE. THEREFORE, IN THIS CASE
C CA=0.
C
      IF(DPF.EQ.DP) THEN
           CA = 0.D0
           GO TO 40
      ELSE
      ENDIF
      CA0 = 0.0D0
      CAMAX = 2.0D0
   30 FMIN = RH - ACTIVC(CA0,CM,CN)
      FMAX = RH - ACTIVC(CAMAX,CM,CN)
      CA = CAMAX - (CAMAX-CA0)*FMAX/(FMAX-FMIN)
      FNEW = RH - ACTIVC(CA,CM,CN)
      IF(DABS(CA0-CA)/CA.LE.TOL.OR.DABS(CAMAX-CA)/CA.LE.TOL)
     1       GO TO 40
      IF(FNEW.LT.0.D0) CA0 = CA
      IF(FNEW.GT.0.D0) CAMAX = CA
      GO TO 30
C
   40 RHO = RHOSOL
      AW = ACTIVC(CA,CM,CN)
C
C THE DERIVATIVE OF AW WRT THE VARIOUS COMPONENTS APPEARS TO BE
C RELATIVELY INSENSITIVE TO THE VALUE OF STEP.
C
      STEP = 1.D-05
      DAWDCM = (ACTIVC(CA,CM+STEP,CN) - AW)/STEP
      DAWDCN = (ACTIVC(CA,CM,CN+STEP) - AW)/STEP
      DAWDCA = (ACTIVC(CA+STEP,CM,CN) - AW)/STEP
      CNA = CN
      CMN = CM
      CSVI = CA
      ISTR = ITOT
C
      RETURN
      END
C
C
C -------------------------------------------------------------
```

```
      FUNCTION ACTIVC(CA, CM, CN)
C
      IMPLICIT DOUBLE PRECISION(A-H,M,O-Z)
      DOUBLE PRECISION ITOT, ITOT2
      COMMON/TWO/ DPMIN, DRATIO, TEMP, P, Q, RH, DELTA, PSO2
      COMMON/THREE/ MWSOLN, RHOSOL
      COMMON/STRGTH/ITOT
C
C THIS FUNCTION CALCULATES THE WATER ACTIVITY OF THE Na2SO4-MnSO4-
C H2SO4 MIXTURE USING KUSIK-MEISSNER'S MIXING RULES.
C CONVERT MOLARITIES TO MOLALITIES. IT IS ASSUMED THAT THE MAJOR
C SPECIES MnSO4, Na2SO4 AND H2SO4 WILL DETERMINE THE WATER ACTIVITY.
C THE MINOR S(IV) SPECIES ARE IGNORED FOR NOW.
C
      MWH2O  = 18.0D0
      MWM    = 151.0D0
      MWN    = 142.0D0
      MWA     = 98.0D0
      MOLH2O = 1000.0D0/18.D0
      VBARM = 0.113661D0
      VBARN = 0.989754D0
      VBARA = 0.429195D0
      RHOSOL = 1.D0 + (1.D0-VBARN)*MWN*CN/1000.D0 + (1.D0-VBARM)
     1          *MWM*CM/1000.D0 + (1.D0-VBARA)*MWA*CA/1000.D0
      MM = CM/(RHOSOL - CN*MWN/1000.D0 - CM*MWM/1000.D0
     1       - CA*MWA/1000.D0)
      MN = CN/(RHOSOL - CN*MWN/1000.D0 - CM*MWM/1000.D0
     1       - CA*MWA/1000.D0)
      MA = CA/(RHOSOL - CN*MWN/1000.D0 - CM*MWM/1000.D0
     1       - CA*MWA/1000.D0)
      XN = MN/(MA + MN + MM + 1000.D0/MWH2O)
      XM = MM/(MA + MN + MM + 1000.D0/MWH2O)
      XA  = MA/(MA + MN + MM + 1000.D0/MWH2O)
      MWSOLN = XN*MWN + XM*MWM + XA*MWA + (1.D0-XN-XM-XA)*MWH2O
C
C THE SPECIES IN SOLUTION ARE ASSUMED TO BE MnSO4, Na2SO4, HHSO4,
C 2H(SO4). NEED TO GET THE RATIO OF H,HSO4 TO 2H,SO4 AT THIS TOTAL
C ACID CONCENTRATION. RATIO IS CALCULATED USING THE FUNCTION WHICH
C DESCRIBES THE DISSOCIATION OF "PURE" H2SO4 AT A SPECIFIC IONIC
C STRENGTH (A STOICHIOMETRIC EQUILIBRIUM CONSTANT). 1: Na+, 3: H+,
C 5: Mn2+, 2:SO42-, 4: HSO4-
C
      M52 = MM
      M12 = MN
      TOL = 1.D-06
      STEP = 1.D-01
C
C IF MA=0, THEN THERE IS NO POINT IN FINDING M32 AND M34.
C Q IS THE EQUILIBRIUM CONSTANT FOR HSO4(-) = H(+) + SO4(2-).
C
      IF(MA.NE.0.D0) GO TO 10
      M32 = 0.0D0
      GO TO 50
C
```

```
C STEP IS SET. HOWEVER, IF MA=0.1D0, WE WILL HAVE A PROBLEM IN
C CALCULATING Q2. SO CHECK TO SEE THAT STEP<MA AND RESET IF IT
C ISN'T.
C
   10 IF(STEP.GE.MA) THEN
          STEP = STEP/10.D0
          GO TO 10
      ELSE
      ENDIF
C
C FIND M32 BY STEPPING THROUGH MOLALITY UNTIL Q1=f(ITOT)=Q2=f(M).
C Q1 VS. ITOT IS A VERY FLAT CURVE---HENCE THE VERY SMALL TOLERANCE.
C M32 < MA.
C
      M32 = 0.0D0
   20 ITOT = (3.0D0*M12 + 4.0D0*M52 + MA) + 2.0D0*M32
      Q1 = -4.5740D0 + 4.0071D0*DSQRT(ITOT) - 0.99893D0*ITOT
     1    + 0.13250D0*(DSQRT(ITOT)**3) - 0.010675D0*ITOT**2
      Q1 = DEXP(Q1)
      Q2 = 2.D0*M32*(M12+M32+M52)/(MA-M32)
      IF(Q2.LT.Q1) THEN
          M32 = M32 + STEP
          GO TO 20
      ELSE
          IF(DABS(Q2-Q1).LT.TOL) GO TO 50
          IF(M32.GT.MA) GO TO 30
          M32 = M32 - STEP
          STEP = STEP/10.D0
          M32 = M32 + STEP
          GO TO 20
      ENDIF
   30 WRITE(*,40)
   40     FORMAT(/1X,'COULD NOT FIND M32.')
      STOP
C
C KNOWING M32 AND MA, CALCULATE M34.
C
   50 M34 = MA - M32
      ITOT = 3.D0*M12 + 4.D0*M52 + 3.D0*M32 + M34
C
C CALCULATE THE MIXTURE WATER ACTIVITY. THE WATER ACTIVITY OF
C (2H,SO4), (H,HSO4), Na2SO4(PURE) AND MnSO4(PURE) AT THE IONIC
C STRENGTH OF THE MIXTURE WILL BE NEEDED.
C THE WATER ACTIVITIES ARE USED IN THE FORM nw*ln(aw) TO HELP
C ELIMINATE SOME OF THE POSSIBLE COMPUTATIONAL ERROR.
C
      IF(DELTA.EQ.0) THEN
          AW12 = 0.D0
          AW14 = 0.D0
      ELSE
          AW12 = MOLH2O*DLOG(AWNO(ITOT))
          AW14 = MOLH2O*DLOG(AWNACL(ITOT))
      ENDIF
      IF(MA.EQ.0) THEN
```

```
          AW32 = 0.D0
          AW34 = 0.D0
        ELSE
          AW32 = AWSO4(ITOT)
          AW34 = AWHSO4(ITOT)
        ENDIF
        AW52 = MOLH2O*DLOG(AWMO(ITOT))
        AW54 = MOLH2O*DLOG(AWMNCL2(ITOT))
C
        SUM1 = M52 + M12 + M32
        SUM2 = M34 + 2.D0*M32
        ITOT2 = ITOT**2.D0
        AW = SUM1*(9.D0*M12*AW12 + (9.D0/2.D0)*SUM2*AW32 +
       1     16.D0*M52*AW52)/ITOT2 + M34*(2.D0*M12*AW14 +
       1     SUM2*AW34 + (9.D0/2.D0)*M52*AW54)/ITOT2 -
       1     ((M34/2.0D0+M52)*(M12+M32) + M52*M34)/ITOT
        ACTIVC = DEXP(AW/MOLH2O)
C
        RETURN
        END
C
C
C ---------------------------------------------------------------
        FUNCTION CURRENT(CSVI, CMN, CNA, DAWDCA, DAWDCM, DAWDCN)
C
        IMPLICIT DOUBLE PRECISION(A-H,M,O-Z)
        DOUBLE PRECISION IEFF
        REAL CNA, CSVI, CMN, CURRENT, DAWDCA, DAWDCM, DAWDCN
        COMMON/TWO/ DPMIN, DRATIO, TEMP, P, Q, RH, DELTA, PSO2
        COMMON/TEN/ RXN, MH, MSIV, MN, MM, MA, RHOL, IEFF
C
C THIS SUBROUTINE CALCULATES THE AEROSOL CURRENT, I = (1/vp)dvp/dt,
C USING THE S(VI) RATE EXPRESSION.
C
        CA = CSVI
        CM = CMN
        CN = CNA
        DCA = DAWDCA
        DCM = DAWDCM
        DCN = DAWDCN
        RXN = R(CA, CM, CN)
        RATE = RXN/((CM*DCM + CN*DCN)/DCA + CA)
        CURRENT = RATE/(3.D0*DLOG(DRATIO))
C
        RETURN
        END
C
C
C ---------------------------------------------------------------
        REAL FUNCTION BETA(X, RHO)
C
        IMPLICIT REAL(A-H,M,O-Z)
        DOUBLE PRECISION DPMIN, DRATIO, TEMP, P, Q, RH, DELTA, PSO2
        COMMON/TWO/ DPMIN, DRATIO, TEMP, P, Q, RH, DELTA, PSO2
```

```
C
C THIS FUNCTION CALCULATES THE WALL DEPOSITION RATE. SEE CRUMP'S THESIS
C CALCULATE THE EDDY DIFFUSION COEFFICIENT. RESULTS OF CRUMP AND
C SEINFELD ARE USED. DIFFKE = 0.00918*Q**(3/2). (1/SEC)
C
      DIFFKE = 0.009180 * (Q**1.5)
C
C CALCULATE THE DIMENSIONAL SIZE, CUNNINGHAM CORRECTION FACTOR,
C
      DP = DPMIN * (DRATIO)**X
      XLAMDA = 6.53E-02 * (TEMP/296.2) * (760.0/P)
      S = XLAMDA/DP
      CUNN = 1.D0 + 2.492*S + 0.84*S*EXP(-0.55/S)
C
C NEED THE DENSITY AND VISCOSITY OF MOIST AIR. HCB CALCULATE THAT
C VISCOSITY OF MOIST AIR CHANGES <1% FOR SATURATED AIR.  THEREFORE
C USE DRY AIR VISCOSITY. DENSITY FOR CRC.
C
      E = RH * PSAT(TEMP)
      RHOAIR = 1.2929E-03 * (273.2/TEMP) * ((P - 0.3783*E)/760.0)
C
C DIFFUSIVITY (EINSTEIN-STOKES), AND TERMINAL SETTLING VELOCITY.
C
      PI = 3.14159
      G = 980.0
      BOLTK = 1.38038E-16
      VISC = 0.0001833
      DIFF = (BOLTK * TEMP * CUNN * 1.E04)/(3.0 * PI * VISC * DP)
      VS = (RHO * G * DP**2 * CUNN * 1.E-08) * (1.0-RHOAIR/RHO)/
     1     (18.0 * VISC)
C
C CALCULATE THE DEBYE INTEGRAL.
C
      Y = PI * VS/(2.0 * SQRT(DIFFKE * DIFF))
      IF(Y.LE.1.0) THEN
             DEBYE = 1.0 - (Y/4.0) + (Y**2/36.0) - (Y**4/3600.0)
     1               + (Y**6/211680.0) - (Y**8/1088640.0) +
     1               (Y**10/34508800.0)
      ELSE
             SUM = 0.0
                DO 10 I = 1, 10
                SUM = SUM + EXP(-Y*I)*(1.D0/FLOAT(I)+Y)/FLOAT(I)
   10           CONTINUE
             DEBYE = PI**2/(6.0*Y) - SUM/Y
      ENDIF
C
C ENTER THE CSTR RADIUS (CM). CALCULATE BETA.
C
      RADIUS = 33.33610
      BETA = 6.0*SQRT(DIFFKE*DIFF)*DEBYE/(PI*RADIUS) + VS*3.0/
     1       (4.0*RADIUS)
C
      RETURN
      END
```

```
C
C ------------------------------------------------------------
C FUNCTION PSAT CALCULATES THE SATURATED VAPOR PRESSURE OF AIR AT T.
C
      FUNCTION PSAT(T)
      DOUBLE PRECISION T
C
      PSAT = EXP(-5313.88/T + 20.9878)
C
      RETURN
      END
C
C
C ------------------------------------------------------------------
      SUBROUTINE SHIFT(J, RH1, CA, CMN, CNA, DP1)
C
      IMPLICIT DOUBLE PRECISION(A-H,L,M,O-Z)
      REAL CA, CMN, CNA
      COMMON/FOUR/ LAMDA
C
C THIS SUBROUTINE SHIFTS THE PARTICLE FROM ONE HUMIDITY TO ANOTHER.
C CALCULATE THE NO. OF MOLES OF MATERIAL IN THE INITIAL PARTICLE.
C THIS WILL REMAIN CONSTANT.
C
      CA1 = CA
      CMN1 = CMN
      CNA1 = CNA
      DP1 = DP1 * 1.D-04
      PI = 3.141594D0
      MOLMN = (CMN1/1000.D0)*(PI*DP1**3/6.D0)
C
C NOW WE NEED THE CONDITIONS AT RH2, T2. SEARCH LAMDA SPACE UNTIL
C RH2 = ACTIV(LAMDA*CMN1). LAMDA IS THE RATIO BETWEEN THE NEW
C AND THE OLD PARTICLE VOLUME. ALSO, LAMDA = CNA2/CNA1 = CMN2/CMN1.
C SINCE DELTA = MNA1/MMN1 = CNA1/CMN1 = MNA2/MMN2 = CNA2/CMN2,
C WE NEED ONLY PASS LAMDA*CMN1=CMN2 AND FROM THIS CNA2 CAN BE FOUND.
C IT IS IMPORTANT TO REMEMBER THAT LAMDA IS A "VOLUME" RATIO.
C THE KELVIN EFFECT WILL NOT BE ACCOUNTED FOR HERE SINCE IT WAS
C IGNORED IN THE PREVIOUS COMPUTATIONS.
C
      CALL LAMDAA(J, RH1, CA1, CMN1, CNA1)
C
C SO, PRESUMABLY WE HAVE FOUND THE CORRECT LAMDA VALUE FOR THIS RH.
C
      CMN2 = LAMDA * CMN1
      VOLSOL = (MOLMN/CMN2) * 1000.D0
      DP2 = (6.D0 * VOLSOL/PI)**(1./3.)
C
C SINCE WE'RE WORKING WITH n(lnDp) THERE IS NO CORRECTION TO BE
C MADE TO THE MAGNITUDE OF THE DISTRIBUTION. IT'S A STRAIGHT FORWARD
C DIAMETER SHIFT.
C
      DP1 = DP2 * 1.D04
C
```

```
      RETURN
      END
C
C
C -------------------------------------------------------------------
      SUBROUTINE LAMDAA(IDO, RH1, CA1, CMN1, CNA1)
C
      IMPLICIT DOUBLE PRECISION(A-H,L,M,O-Z)
      COMMON/TWO/ DPMIN, DRATIO, TEMP, P, Q, RH, DELTA, PSO2
      COMMON/FOUR/ LAMDA
C
C FIND THE VALUE OF LAMDA WHICH GIVES AW2. LAMDA=CMN2/CMN1.
C
      IF(IDO.NE.1) GO TO 20
      KOUNT = 0
      LAMDA = 0.01D0
   10 AWO = ACTIVC(LAMDA*CA1,LAMDA*CMN1,LAMDA*CNA1)
      LAMDAO = LAMDA
      IF(AWO.LE.RH1) GO TO 20
      LAMDA = LAMDA + 0.10D0
      KOUNT = KOUNT + 1
      IF(KOUNT.GT.200) GO TO 90
      GO TO 10
   20 STEP = 1.D-06
      EPS = 1.D-06
          DO 30 J = 1, 10
          AWO = ACTIVC(LAMDAO*CA1,LAMDAO*CMN1,LAMDAO*CNA1)
          L = LAMDAO+STEP
          DAW = (ACTIVC(L*CA1,L*CMN1,L*CNA1)- AWO)/STEP
          IF(DAW.EQ.0.) GO TO 40
          LAMDA = LAMDAO - (AWO-RH1)/DAW
          IF(DABS(LAMDA-LAMDAO).LT.EPS) GO TO 110
          IF(LAMDA.EQ.0.D0.OR.LAMDA.GT.8.D0) GO TO 40
          LAMDAO = LAMDA
   30     CONTINUE
   40 LAMDA = LAMDAO
      H = 0.005D0
   50 IF(ACTIVC(LAMDA*CA1,LAMDA*CMN1,LAMDA*CNA1).LE.RH1) GO TO 60
      LAMDA = LAMDA + H
      GO TO 50
   60 H = H/2.D0
      IF(H.LE.5.D-06) GO TO 110
   70 IF(ACTIVC(LAMDA*CA1,LAMDA*CMN1,LAMDA*CNA1).GT.RH1) GO TO 80
      LAMDA = LAMDA - H
      GO TO 70
   80 H = H/2.D0
      IF(H.LE.5.D-06) GO TO 110
      GO TO 50
C
   90 WRITE(*,100)
  100     FORMAT(/1X,'CANNOT FIND APPROPRIATE LAMDA.')
      STOP
C
C NOW WE HAVE LAMDA. THIS IS INDEPENDENT OF DP SINCE WE'RE IGNORING
```

```
C THE KELVIN EFFECT.
C
  110 RETURN
      END
C
C
C -------------------------------------------------------------
      FUNCTION R(CA, CM, CN)
C
      IMPLICIT DOUBLE PRECISION(A-H,M,O-Z)
      DOUBLE PRECISION IEFF
      COMMON/TWO/ DPMIN, DRATIO, TEMP, P, Q, RH, DELTA, PSO2
      COMMON/TEN/ RXN, MH, MSIV, MN, MM, MA, RHOL, IEFF
      COMMON/COEF/GAM32, GAM34, GAM36, GAM38, GAM52, GAM52P
      COMMON/CONST/RK1, RK2, RK3, RK4, RK5
C
C KINETIC RATE EXPRESSION USED IS FROM BERRESHEIM AND JAESCHKE (1986).
C THIS FUNCTION CALCULATES THE POSTULATED REACTION RATE d(S(VI))/dt.
C SET OF REACTIONS AS FOLLOWS:
C
C                  SO2(g) + H2O = SO2.H2O(1)         1)
C                  SO2.H2O(1)   = H(+) + HSO3(-)     2)
C                  HSO3(-)      = H(+) + SO3(2-)     3)
C                  HSO4(-)      = H(+) + SO4(2-)     4)
C                  Mn(2+) + SO4(2-) = MnSO4(0)       5)
C
C S(VI) = HSO4(-) + SO4(2-).  MA IS ACID GENERATED DUE TO RXN.
C ALL EQUILIBRIUM CONSTANTS ARE AT 25C.
C
      RK1 = 1.24D-06
      RK2 = 0.0132D0
      RK3 = 6.24D-08
      RK4 = 1.2D-02
      RK5 = 190.D0
C
C CONVERT MOLARITIES TO MOLALITIES.
C
      MWH2O  = 18.0D0
      MWM    = 151.0D0
      MWN    = 142.0D0
      MWA     = 98.0D0
      MOLH2O = 1000.0D0/18.D0
      VBARM = 0.113661D0
      VBARN = 0.989754D0
      VBARA = 0.429195D0
      MM = CM/(RHOL - CN*MWN/1000.D0 - CM*MWM/1000.D0
     1       - CA*MWA/1000.D0)
      MN = CN/(RHOL - CN*MWN/1000.D0 - CM*MWM/1000.D0
     1       - CA*MWA/1000.D0)
      MA = CA/(RHOL - CN*MWN/1000.D0 - CM*MWM/1000.D0
     1       - CA*MWA/1000.D0)
C
C SOLVE FOR H(+) ITERATIVELY, AFTER DOING A CHARGE BALANCE.
C ACCOUNT FOR ACTIVITY COEFFICIENTS (Gij(MH)). ALL CONC. CAN
```

```
C BE EXPRESSED IN TERMS OF m(H+) AND THEIR GAMMAS. SINCE THIS
C IS AN ITERATIVE PROCESS, SIMPLY KEEP UPDATING THE GAMMAS NEEDED
C FOR THE CONCENTRATION CALCULATIONS, BUT CONSIDER THEM 1 INITIALLY.
C
      MHSTART = 1.D-6
      MHEND = 10.0D0
      GAM38 = 1.D0
      GAM36 = 1.D0
      GAM34 = 1.D0
      GAM32 = 1.D0
      GAM52 = 1.D0
      GAM52P = 1.D0
      CC = RK1*RK2*PSO2
      MH = MHSTART
      CALL GAMMA(MH, MM, MN, MA, IEFF)
      AA = -CC*(1.D0/(GAM38**2) + 2.D0*RK3/((GAM36**3)*MH))
      DD = 1.D0 + MH*(GAM32**3)/(RK4*(GAM34**2))
      BB =         DD - (MA+MN)*RK5*(GAM52**2)/GAM52P
      XX = (-BB + DSQRT(BB**2 + 4.D0*(MA+MM+MN)*DD*RK5*(GAM52**2)/
     1      GAM52P))/(2.D0*DD*RK5*(GAM52**2)/GAM52P)
      F = (1.D0+(XX*(GAM32**3)/(RK4*(GAM34**2))))*MH**2
     1    - 2.D0*MA*MH + AA
   10 MHNEW = 10.D0* MH
      CALL GAMMA(MHNEW, MM, MN, MA, IEFF)
      AANEW = -CC*(1.D0/(GAM38**2) + 2.D0*RK3/((GAM36**3)*MHNEW))
      DDNEW = 1.D0 + MHNEW*(GAM32**3)/(RK4*(GAM34**2))
      BBNEW =         DDNEW - (MA+MN)*RK5*(GAM52**2)/GAM52P
      XXNEW = (-BBNEW + DSQRT(BBNEW**2 + 4.D0*(MA+MM+MN)*DDNEW*RK5
     1      *(GAM52**2)/GAM52P))/(2.D0*DDNEW*RK5*(GAM52**2)/GAM52P)
      FNEW = (1.D0+(XXNEW*(GAM32**3)/(RK4*(GAM34**2))))*MHNEW**2
     1    - 2.D0*MA*MHNEW + AANEW
      IF((F/FNEW).GT.0.D0) THEN
            MH = MHNEW
            BB = BBNEW
            AA = AANEW
            DD = DDNEW
            XX = XXNEW
            F = FNEW
            GO TO 10
      ELSE
      ENDIF
C
C NOW WE ARE STRADDLING THE F=0 LINE. TAKE THE LOG AVG. OF THE MH'S
C AND SEE WHAT F WE GET.
C
      I = 1
   20 MHAVG = 10**((DLOG10(MH) + DLOG10(MHNEW))/2.)
      CALL GAMMA(MHAVG, MM, MN, MA, IEFF)
      AAAVG = -CC*(1.D0/(GAM38**2) + 2.D0*RK3/((GAM36**3)*MHAVG))
      DDAVG = 1.D0 + MHAVG*(GAM32**3)/(RK4*(GAM34**2))
      BBAVG =         DDAVG - (MA+MN)*RK5*(GAM52**2)/GAM52P
      XXAVG = (-BBAVG + DSQRT(BBAVG**2 + 4.D0*(MA+MM+MN)*DDAVG*RK5
     1      *(GAM52**2)/GAM52P))/(2.D0*DDAVG*RK5*(GAM52**2)/GAM52P)
      FAVG = (1.D0+(XXAVG*(GAM32**3)/(RK4*(GAM34**2))))*MHAVG**2
```

```
     1    - 2.D0*MA*MHAVG + AAAVG
C
C CHECK WHETHER WE SHOULD KEEP MH OR MHNEW.
C
      IF((FAVG/F).GT.0.D0) THEN
            F = FAVG
            BB = BBAVG
            AA = AAAVG
            DD = DDAVG
            XX = XXAVG
            MH = MHAVG
      ELSE
            FNEW = FAVG
            BBNEW = BBAVG
            AANEW = AAAVG
            DDNEW = DDAVG
            XXNEW = XXAVG
            MHNEW = MHAVG
      ENDIF
C
C SEE IF CONVERGENCE TOLERANCE IS MET.
C
      IF((ABS(MH-MHNEW)/MH).GT.1.D-04) THEN
            IF(I.GT.1000) GO TO 30
            I = I + 1
            GO TO 20
      ELSE
      ENDIF
C
C SUCCESSFUL ITERATION. WE NOW HAVE H(+) MOLALITY. CALCULATE THE
C THE S(IV) CONCENTRATION.
C
      MSIV = RK1*PSO2 + RK1*RK2*PSO2/((GAM38**2)*MH) +
     1        RK1*RK2*RK3*PSO2/((GAM36**3)*MH**2)
C
C CONVERT TO MOLARITIES SINCE MOST RATE EQUATIONS WRITTEN IN TERMS OF
C MOLARITIES. ASSUME THAT SOLUTION DENSITY PRIMARILY SET BY MA,MM,MN.
C H+ AND S(IV) ARE MINOR SPECIES.
C
      CH = MH*RHOL/(1.D0 + MN*MWN/1000.D0 + MM*MWM/1000.D0
     1       + MA*MWA/1000.D0)
      CSIV = MSIV*RHOL/(1.D0 + MN*MWN/1000.D0 + MM*MWM/1000.D0
     1       + MA*MWA/1000.D0)
C
C USING COHEN ET AL'S (1987A) PITZER CORRELATION FOR MnSO4 ACTIVITY
C COEFFICIENT. ASSUME THAT (CME**1.03)/L IS APPROXIMATELY CME/L WHICH IS
C MM*MWMe(METAL MW). AT MOST, A 10% ERROR. NOTE THAT "ALL" METAL, NOT
C JUST Mn(2+) IS BEING USED IN THIS CALCULATION.
C
      HSTAR = CSIV*1.D06/PSO2
      RGAS = 0.08205D0
      AMNSO4 = MM*DEXP(G520(4.D0*MM))
      CMEL = MM * 54.938D0
      R = 0.282D+01*CMEL*CSIV/((AMNSO4**0.64D0)*HSTAR*RGAS*TEMP*CH)
```

```
      RETURN
C
   30 WRITE(*,40) MH, MH1
   40     FORMAT(/1X,'CALCULATION OF H+ FAILED AFTER 1000 ITERATIONS.'
     1    /1X,'MH = ',E15.8,5X,'MH1 = ',E15.8)
      STOP
C
      END
C
C
C ---------------------------------------------------------------
      SUBROUTINE GAMMA(M3, MM, MN, MA, IEFF)
C
      IMPLICIT DOUBLE PRECISION(A-H,M,O-Z)
      DOUBLE PRECISION IEFF
      COMMON/TWO/ DPMIN, DRATIO, TEMP, P, Q, RH, DELTA, PSO2
      COMMON/COEF/GAM32, GAM34, GAM36, GAM38, GAM52, GAM52P
      COMMON/CONST/RK1, RK2, RK3, RK4, RK5
C
C WE HAVE MH(+) AND INITIAL ESTIMATES OF THE MIXTURE GAMMAS. CALCULATE
C THE CONCENTRATIONS NEEDED FOR THE MIXTURE CALCULATION.
C 1:Na+, 3:H+, 5:Mn2+, 2:SO42-, 4:HSO4-, 6:SO32-, 8:HSO3-
C
   10 DD = 1.D0 + M3*(GAM32**3)/(RK4*(GAM34**2))
      BB =         DD - (MA+MN)*RK5*(GAM52**2)/GAM52P
      M2 = (-BB + DSQRT(BB**2 + 4.D0*(MA+MM+MN)*DD*RK5*(GAM52**2)/
     1     GAM52P))/(2.D0*DD*RK5*(GAM52**2)/GAM52P)
      M4 = M2*M3*(GAM32**3)/(RK4*(GAM34**2))
      M8 = RK1*RK2*PSO2/(M3*(GAM38**2))
      M6 = RK1*RK2*RK3*PSO2/((GAM36**3)*M3**2)
      M5 = M2*DD - (MA+MN)
      M1 = 2.D0*MN
C
C NEED TO HAVE THE IONIC STRENGTH SINCE THE PURE COMPONENT GAMMAS
C WILL BE MATCHED TO THIS VALUE. SINCE THE FREE MN(II) IONS ONLY
C ARE USED IN THE CALCULATION, THIS IS EFFECTIVE IONIC STRENGTH.
C
      IEFF = 0.5D0*(M1 + M3 + M4 + M8 + 4.D0*(M5 + M2 + M6))
C
C CALCULATE THE PURE COMPONENT ln(gamma)'S NEEDED. FOR LACK OF
C BETTER DATA, SET SULFITE VALUES EQUAL TO SULFATE VALUES.
C ION-PAIRING IS NOT ACCOUNTED FOR IN THE PURE GAMMAS.
C THE SODIUM SULFATE IS ASSUMED TO DISSOCIATE COMPLETELY.
C
      G32 = G320(IEFF)
      G34 = G340(IEFF)
      G36 = G32
      G38 = G34
      G52 = G520(IEFF)
      G54 = G540(IEFF)
      G56 = G52
      G58 = G54
      G12 = G120(IEFF)
      G14 = G140(IEFF)
```

```
C
      X = 9.D0/4.D0
      Y = 4.D0
C
C THE MIXING RULES OF KUSIK AND MEISSNER ARE USED TO GET THE
C MIXED ACTIVITY COEFFICIENTS.
C
      GAM320 = DEXP(((2.D0/3.D0)*(X*M2*G32 + M4*G34 + X*M6*G36 +
     1          M8*G38) + (1.D0/3.D0)*(X*M3*G32 + Y*M5*G52
     1          + X*M1*G12))/IEFF)
      GAM340 = DEXP(((1.D0/2.D0)*(X*M2*G32 + M4*G34 + X*M6*G36 +
     1          M8*G38) + (1.D0/2.D0)*(M3*G34 + X*M5*G54
     1          + M1*G14))/IEFF)
      GAM520 = DEXP(((Y*M2*G52 + X*M4*G54 + Y*M6*G56 + X*M8*G58)
     1          + (X*M3*G32 + Y*M5*G52 + X*M1*G12))/(2.D0*IEFF))
      GAM360 = GAM320
      GAM380 = GAM340
C
C THESE GAMMAS WERE CALCULATED USING CONCENTRATIONS THAT WERE BASED
C ON INITIAL GUESSES OF THE GAMMAS. WANT TO ITERATE UNTIL THE
C CALCULATED GAMMAS EQUAL THE GAMMAS USED IN THE CONC. CALCULATIONS.
C
      IF(DABS(GAM32-GAM320).GT.1.D-04.OR.DABS(GAM34-GAM340).GT.
     1    1.D-04.OR.DABS(GAM36-GAM360).GT.1.D-04.OR.DABS(GAM38-
     1    GAM380).GT.1.D-04.OR.DABS(GAM52-GAM520).GT.1.D-04) THEN
         GAM32 = (GAM320+GAM32)/2.D0
         GAM34 = (GAM340+GAM34)/2.D0
         GAM36 = (GAM360+GAM36)/2.D0
         GAM38 = (GAM380+GAM38)/2.D0
         GAM52 = (GAM520+GAM52)/2.D0
         GO TO 10
      ELSE
      ENDIF
C
      RETURN
      END
C
C
C ---------------------------------------------------------------
      FUNCTION G340(IEFF)
C
C THIS FUNCTION CALCULATES ln(gamma(H,HSO4)) USING RARD'S (1976) DATA,
C "UNMIXED" BY THE KUSIK-MEISSNER RULES (STELSON, 1984).
C
      IMPLICIT DOUBLE PRECISION(A-H,M,O-Z)
      DOUBLE PRECISION IEFF
C
C THESE COEFFICIENTS FIT TO CURVES ON P.30 OF STELSON ET AL.
C
      A0 = 0.371591D-02
      A1 = -0.908027D0
      A2 = 1.25847D0
      A3 = -0.547089D0
      A4 = 0.217464D0
```

```
      A5 = -0.426523D-01
      A6 = 0.292312D-02
      SQI = DSQRT(IEFF)
C
C ln GAMMA(H,HSO4)
C
      G340 = A0 + A1*SQI + A2*SQI**2 + A3*SQI**3 + A4*SQI**4
     1       + A5*SQI**5 + A6*SQI**6
C
      RETURN
      END
C
C
C -------------------------------------------------------------
      FUNCTION G320(IEFF)
C
C THIS FUNCTION CALCULATES ln(gamma(2H,SO4)) USING RARD'S (1976) DATA,
C "UNMIXED" BY THE KUSIK-MEISSNER RULES (STELSON, 1984).
C
      IMPLICIT DOUBLE PRECISION(A-H,M,O-Z)
      DOUBLE PRECISION IEFF
C
C THESE COEFFICIENTS FIT TO CURVES ON P.30 OF STELSON ET AL.
C
      A0 = 0.244133D-01
      A1 = -1.7997D0
      A2 = 0.263197D0
      A3 = 0.152819D0
      A4 = -0.512581D-01
      A5 = 0.431276D-02
      SQI = DSQRT(IEFF)
C
C ln GAMMA(2H,SO4)
C
      G320 = A0 + A1*SQI + A2*SQI**2 + A3*SQI**3 + A4*SQI**4
     1         + A5*SQI**5
C
      RETURN
      END
C
C
C -------------------------------------------------------------
      FUNCTION G120(IEFF)
C
C THIS FUNCTION CALCULATES ln(gamma(2Na,SO4)) USING RARD AND
C MILLER'S (1981) DATA FIT.
C
      IMPLICIT DOUBLE PRECISION(A-H,M,O-Z)
      DIMENSION RR(6), A(6)
      DOUBLE PRECISION IEFF
      DATA RR/1.D0,1.25D0,1.5D0,1.75D0,2.D0,2.25D0/
      DATA A/4.861114D0,-3.910475D0,-5.96458D0,10.99511D0,
     1      -6.20811D0,1.228528D0/
C
```

```
C CALCULATE MOLALITY OF Na2SO4 SOLUTION THAT HAS SAME IONIC STRENGTH
C AS MIXTURE.
C
      M = IEFF/3.D0
C
C ln GAMMA(2Na,SO4)
C
      SUM = 0.D0
          DO 10 I = 1, 6
          SUM = SUM + A(I)*((RR(I)+1.D0)/RR(I))*(M**RR(I))
   10     CONTINUE
      G120 = -4.0744D0*DSQRT(M) + SUM
C
      RETURN
      END
C
C
C ---------------------------------------------------------------
      FUNCTION G140(IEFF)
C
C THIS FUNCTION CALCULATES ln(gamma(Na,HSO4)) USING MARK COHEN'S
C (1987A) IMPROVED PITZER COEFFICIENTS FOR NaCl AS AN ESTIMATE.
C
      IMPLICIT DOUBLE PRECISION(A-H,M,O-Z)
      DOUBLE PRECISION IEFF
C
C PITZER'S COEFFICIENTS.
C
      BMX0 = 0.10820D0
      BMX1 = 0.03127D0
      CPHI = -0.002469D0
      A1 = 2.0D0
      SQI = DSQRT(IEFF)
C
      SUM = 1.D0 + 1.2*SQI
      FG = -0.392D0*(SQI/SUM + (2.D0/1.2D0)*DLOG(SUM))
      BMX = 2.D0*BMX0 + 2.D0*BMX1*(1.D0 - DEXP(-SQI*A1**2)*(1.D0
     1      + A1*SQI - 0.5D0*IEFF*A1**2))/(IEFF*A1**2)
      CG = 1.5D0*CPHI
C
C CALCULATE MOLALITY OF NaHSO4 SOLUTION THAT HAS SAME IONIC STRENGTH
C AS MIXTURE.
C
      M = IEFF
C
C ln GAMMA(Na,HSO4)
C
      G140 = FG + M*BMX + (M**2)*CG
C
      RETURN
      END
C
C
C ---------------------------------------------------------------
```

```
      FUNCTION G520(IEFF)
C
C THIS FUNCTION CALCULATES ln(gamma(Mn,SO4)) USING RARD'S (1984)
C DATA FIT.
C
      IMPLICIT DOUBLE PRECISION(A-H,M,O-Z)
      DIMENSION RR(8), A(8)
      DOUBLE PRECISION IEFF
      DATA RR/0.75D0,1.D0,1.25D0,1.5D0,1.75D0,2.D0,2.25D0,2.5D0/
      DATA A/-21.39843D0,159.7962D0,-426.0224D0,611.08138D0,
     1       -513.9961D0,252.5674D0,-66.58744D0,7.181363D0/
C
C CALCULATE MOLALITY OF MnSO4 SOLUTION THAT HAS SAME IONIC STRENGTH
C AS MIXTURE.
C
      M = IEFF/4.D0
C
C ln GAMMA(Mn,SO4)
C
      SUM = 0.D0
          DO 10 I = 1, 8
          SUM = SUM + A(I)*((RR(I)+1.D0)/RR(I))*(M**RR(I))
   10     CONTINUE
      G520 = -9.4097D0*DSQRT(M) + SUM
C
      RETURN
      END
C
C
C ---------------------------------------------------------------
      FUNCTION G540(IEFF)
C
C THIS FUNCTION CALCULATES ln(gamma(Mn,2HSO4)) USING MARK COHEN'S
C (1987A) IMPROVED PITZER COEFFICIENTS FOR MnCl2 AS AN ESTIMATE.
C
      IMPLICIT DOUBLE PRECISION(A-H,M,O-Z)
      DOUBLE PRECISION IEFF
C
C PITZER'S COEFFICIENTS.
C
      BMX0 = 0.25811D0
      BMX1 = 2.31108D0
      CPHI = -0.010540D0
      A1 = 2.0D0
      SQI = DSQRT(IEFF)
C
      SUM = 1.D0 + 1.2*SQI
      FG = -0.392D0*(SQI/SUM + (2.D0/1.2D0)*DLOG(SUM))
      BMX = 2.D0*BMX0 + 2.D0*BMX1*(1.D0 - DEXP(-SQI*A1**2)*(1.D0
     1      + A1*SQI - 0.5D0*IEFF*A1**2))/(IEFF*A1**2)
      CG = 1.5D0*CPHI
C
C CALCULATE MOLALITY OF Mn(HSO4)2 SOLUTION THAT HAS SAME IONIC STRENGTH
C AS MIXTURE.
```

```
C
      M = IEFF/3.D0
C
C ln GAMMA(Mn,2HSO4)
C
      G540 = 2.D0*FG + (4.D0/3.D0)*M*BMX + (2.D0/3.D0)*(2**1.5)*
     1       (M**2)*CG
C
      RETURN
      END
C
C
C ---------------------------------------------------------------
      FUNCTION AWNO(ITOT)
C
      IMPLICIT DOUBLE PRECISION(A-H,M,O-Z)
      DOUBLE PRECISION ITOT
C
C WATER ACTIVITY DATA OF RARD AND MILLER (1981) FIT WITH POLYNOMIAL.
C FIND THE PURE Na2SO4 MOLALITY WHICH RESULTS IN A PURE SOLUTION
C IONIC STRENGTH EQUAL TO THE SOLUTION IONIC STRENGTH.
C
      M = ITOT/3.D0
C
      AWNO = 0.998754D0 - 0.358089D-01*M + 0.406391D-02*M*M
     1       - 0.111982D-02*M**3
C
      RETURN
      END
C
C
C ---------------------------------------------------------------
      FUNCTION AWMO(ITOT)
C
      IMPLICIT DOUBLE PRECISION(A-H,M,O-Z)
      DOUBLE PRECISION ITOT
C
C WATER ACTIVITY DATA OF RARD (1984) WAS FIT WITH A POLYNOMIAL.
C FIND THE PURE MnSO4 MOLALITY WHICH RESULTS IN A PURE SOLUTION
C IONIC STRENGTH EQUAL TO THE SOLUTION IONIC STRENGTH.
C
      M = ITOT/4.D0
C
      AWMO = 0.999382D0 - 0.162799D-01*M + 0.916004D-03*M*M
     1       - 0.119784D-02*M**3 - 0.245205D-03*M**4
     1       + 0.465363D-04*M**5
C
      RETURN
      END
C
C
C ---------------------------------------------------------------
      FUNCTION AWHSO4(ITOT)
C
```

```
C THIS FUNCTION CALCULATES nw*ln(aw(H,HSO4)) USING RARD'S (1976) DATA,
C "UNMIXED" BY THE KUSIK-MEISSNER RULES (STELSON ET AL., 1984).
C
      IMPLICIT DOUBLE PRECISION(A-H,M,O-Z)
      DOUBLE PRECISION ITOT
C
C THESE COEFFICIENTS FIT TO CURVES ON P.30 OF STELSON ET AL.
C
      A0 = 0.371591D-02
      A1 = -0.908027D0
      A2 = 1.25847D0
      A3 = -0.547089D0
      A4 = 0.217464D0
      A5 = -0.426523D-01
      A6 = 0.292312D-02
      SQI = DSQRT(ITOT)
C
C ln GAMMA(H,HSO4)
C
      GHSO4 = A0 + A1*SQI + A2*SQI**2 + A3*SQI**3 + A4*SQI**4
     1          + A5*SQI**5 + A6*SQI**6
C
C INTEGRAL FROM 0 TO ITOT OF lnGAMMA(H,HSO4)dI
C
      GHSO4I = A0*SQI**2 + A1*(2.D0/3.D0)*SQI**3 +
     1          A2*(1.D0/2.D0)*SQI**4 + A3*(2.D0/5.D0)*SQI**5 +
     1          A4*(1.D0/3.D0)*SQI**6 + A5*(2.D0/7.D0)*SQI**7 +
     1          A6*(1.D0/4.D0)*SQI**8
C
C NOW CALCULATE nw*ln(aw).
C
      AWHSO4 = -2.D0*(ITOT*GHSO4 - GHSO4I + ITOT)
C
      RETURN
      END
C
C
C -------------------------------------------------------------
      FUNCTION AWSO4(ITOT)
C
C THIS FUNCTION CALCULATES nw*ln(aw(2H,SO4)) USING RARD'S (1976) DATA,
C "UNMIXED" BY THE KUSIK-MEISSNER RULES (STELSON ET AL., 1984).
C
      IMPLICIT DOUBLE PRECISION(A-H,M,O-Z)
      DOUBLE PRECISION ITOT
C
C THESE COEFFICIENTS FIT TO CURVES ON P.30 OF STELSON ET AL.
C
      A0 = 0.244133D-01
      A1 = -1.7997D0
      A2 = 0.263197D0
      A3 = 0.152819D0
      A4 = -0.512581D-01
      A5 = 0.431276D-02
```

```
      SQI = DSQRT(ITOT)
C
C ln GAMMA(2H,SO4)
C
      GSO4 = A0 + A1*SQI + A2*SQI**2 + A3*SQI**3 + A4*SQI**4
     1          + A5*SQI**5
C
C INTEGRAL FROM 0 TO ITOT OF lnGAMMA(2H,SO4)dI
C
      GSO4I = A0*SQI**2 + A1*(2.D0/3.D0)*SQI**3 +
     1         A2*(1.D0/2.D0)*SQI**4 + A3*(2.D0/5.D0)*SQI**5 +
     1         A4*(1.D0/3.D0)*SQI**6 + A5*(2.D0/7.D0)*SQI**7
C
C NOW CALCULATE nw*ln(aw).
C
      AWSO4 = -(ITOT*GSO4 - GSO4I + ITOT)
C
      RETURN
      END
C
C
C ---------------------------------------------------------------
      FUNCTION AWMNCL2(ITOT)
C
C THIS FUNCTION CALCULATES THE "PURE" MnCl2 WATER ACTIVITY GIVEN
C THE SOLUTION IONIC STRENGTH. USED TO APPROXIMATE THE ACTIVITY OF
C Mn(HSO4)2. (COHEN ET AL. (1987A)).
C
      IMPLICIT DOUBLE PRECISION(A-H,M,O-Z)
      DOUBLE PRECISION ITOT
C
C WANT THE ACTIVITY AT THAT MOLALITY THAT CORRESPONDS TO THE
C MIXTURE TOTAL IONIC STRENGTH.
C
      MM = ITOT/3.D0
C
      AWMNCL2 = 0.9989D0 - 3.639D-02*MM - 2.049D-02*MM**2
     1           + 4.286D-03*MM**3 - 4.137D-04*MM**4
     1           + 1.960D-05*MM**5 - 3.417D-07*MM**6
C
      RETURN
      END
C
C
C ---------------------------------------------------------------
      FUNCTION AWNACL(ITOT)
C
C THIS FUNCTION CALCULATES THE "PURE" NaCl WATER ACTIVITY GIVEN THE
C SOLUTION IONIC STRENGTH. DATA OF COHEN ET AL. (1987A) USED TO
C APPROXIMATE Na(HSO4).
C
      IMPLICIT DOUBLE PRECISION(A-H,M,O-Z)
      DOUBLE PRECISION ITOT
C
```

```
C WANT THE ACTIVITY AT THAT MOLALITY THAT CORRESPONDS TO THE
C MIXTURE TOTAL IONIC STRENGTH.
C
      MN = ITOT
C
      AWNACL = 0.989065D0 - 0.101740D-01*MN - 0.894629D-02*MN**2
     1          + 0.817718D-03*MN**3 - 0.289621D-04*MN**4
     1          + 0.365706D-06*MN**5
C
      RETURN
      END
```

APPENDIX F

EXPERIMENTAL TEMPERATURE, HUMIDITY, AND SO_2 DATA

The figures in Appendix F present graphically the temperature, humidity, and SO_2 data as a function of time for each $MnSO_4/SO_2$ reactor experiment. Data were collected during both the feed and effluent size distribution scans. The calibration formulas presented in Table 3.1 were used to convert the instrument voltages into the desired physical quantities. While the relative humidity was not measured directly, the values calculated using the appropriate dew points (corrected for pressure) and temperatures are presented as a matter of interest. Table 5.1 presents a summary of the data presented here.

Eight plots are presented for each experiment: a) the EMC2 aerosol inlet (○) and sample outlet (▫) temperatures measured during the effluent scan; b) the EMC2 (△) and CSTR (+) dew point temperatures measured during the effluent scan; c) the CSTR temperature measured during the effluent scan (*); d) the SO_2 concentration measured during the effluent scan (◇); e) the EMC2 aerosol inlet (●) and sample outlet (▪) temperatures measured during the feed scan; f) the EMC2 dew point temperature measured during the feed scan (▲); g) the relative humidity in the CSTR (+) and in EMC2 (△) during the effluent scan; and h) the EMC2 relative humidity during the feed scan (▲). The solid lines represent the time-averaged value for the given measurement.

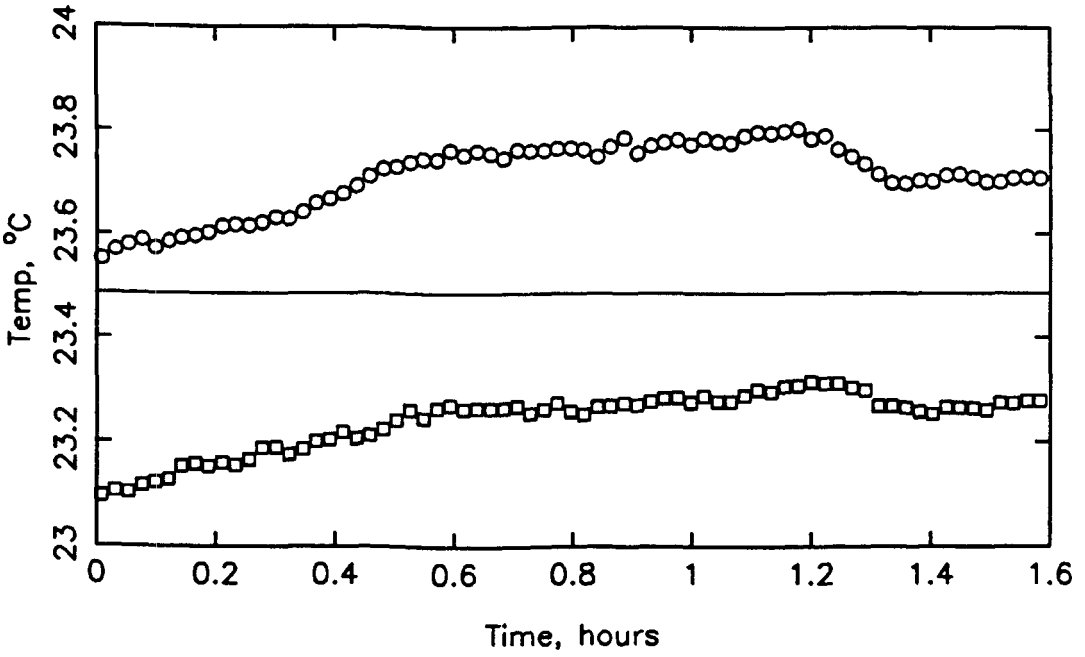

Figure F.1a Experiment 1: Effluent EMC2 inlet and outlet temperatures.

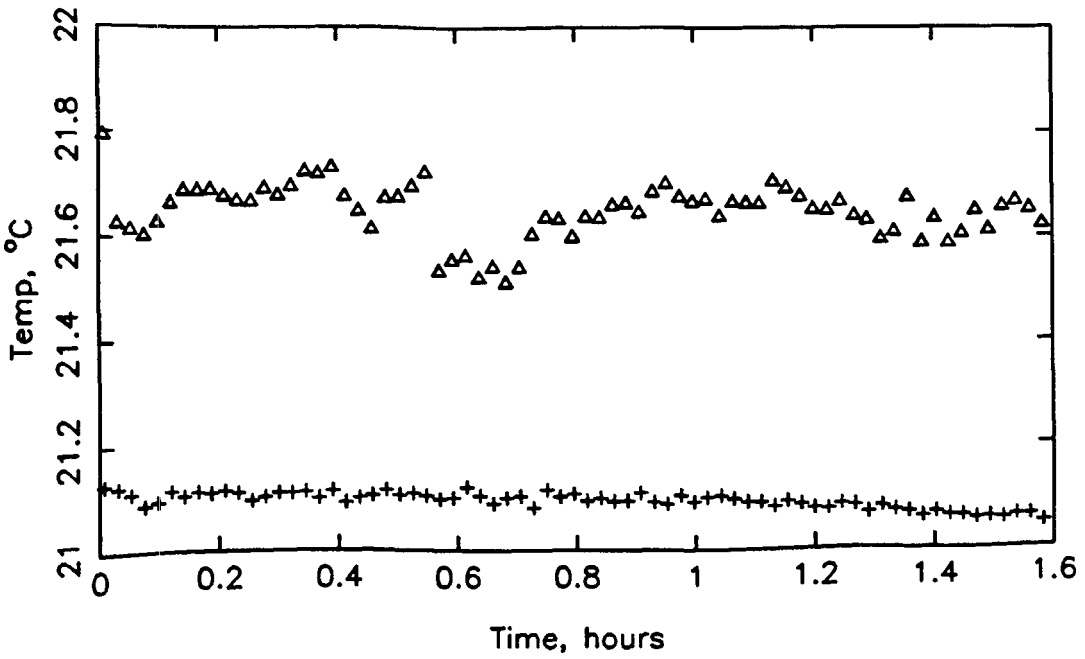

Figure F.1b Experiment 1: Effluent EMC2 and CSTR dew point temperatures.

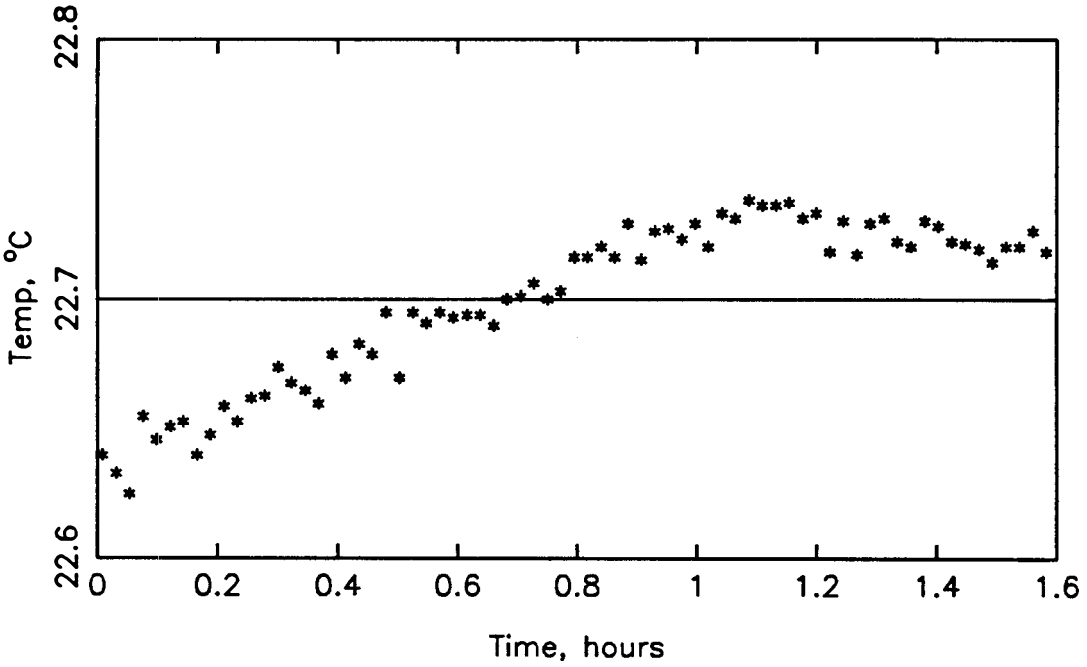

Figure F.1c Experiment 1: Effluent CSTR temperature.

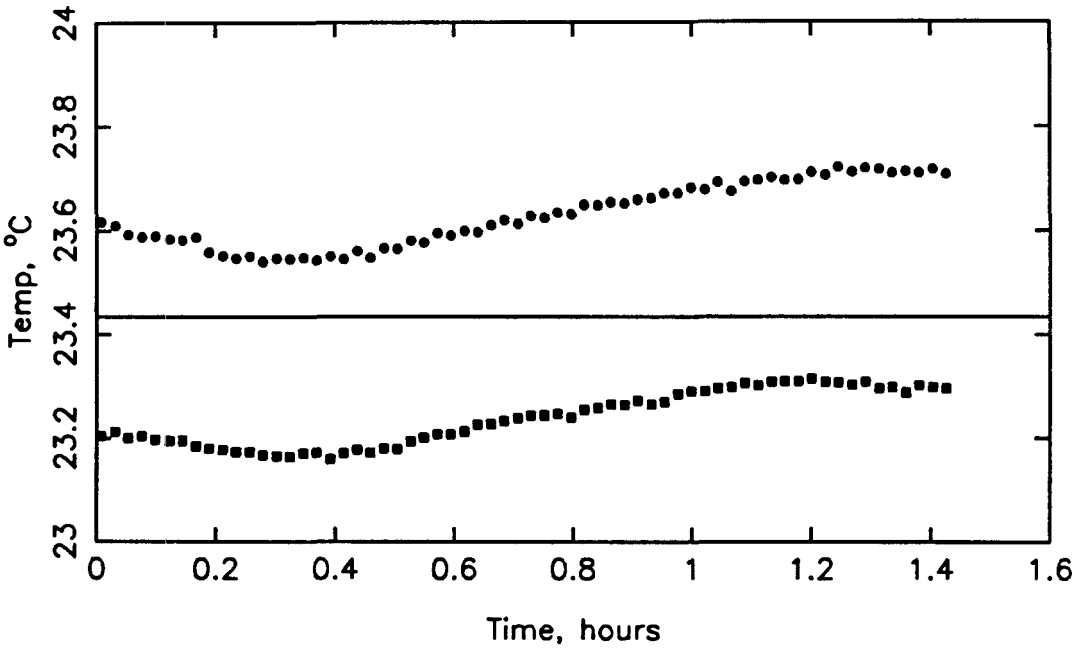

Figure F.1e Experiment 1: Feed EMC2 inlet and outlet temperatures.

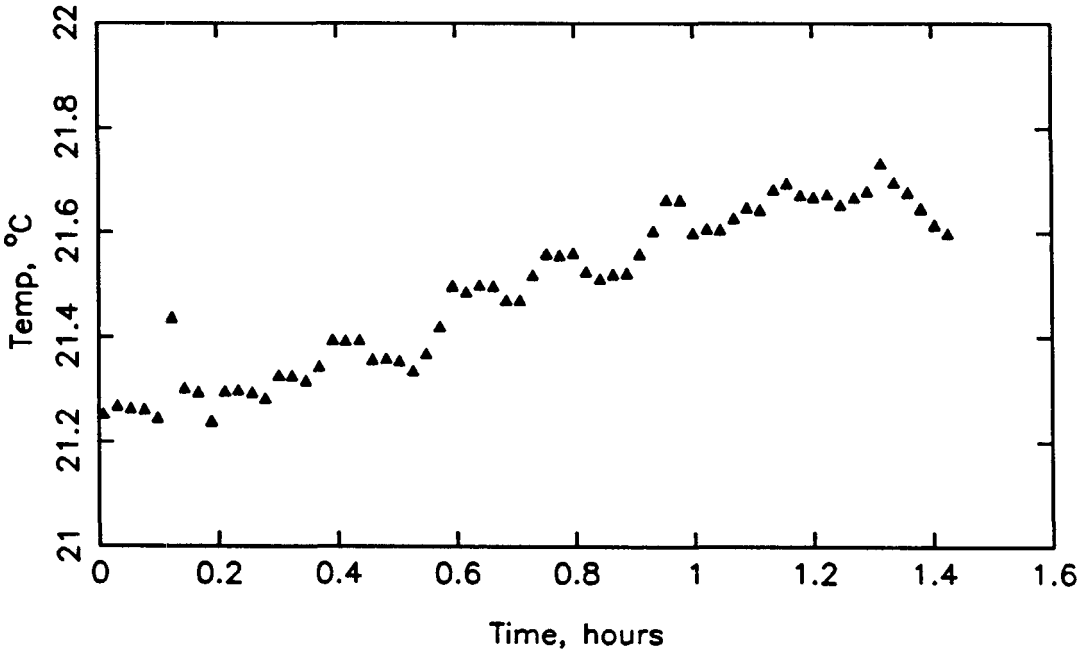

Figure F.1f Experiment 1: Feed EMC2 dew point temperatures.

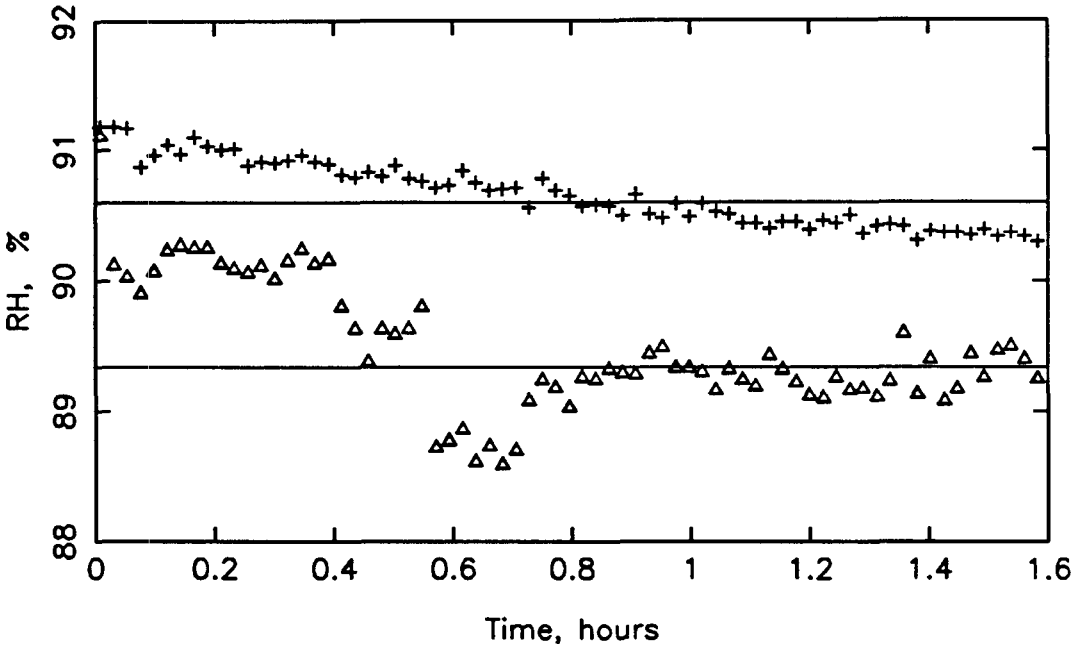

Figure F.1g Experiment 1: Effluent EMC2 and CSTR relative humidity.

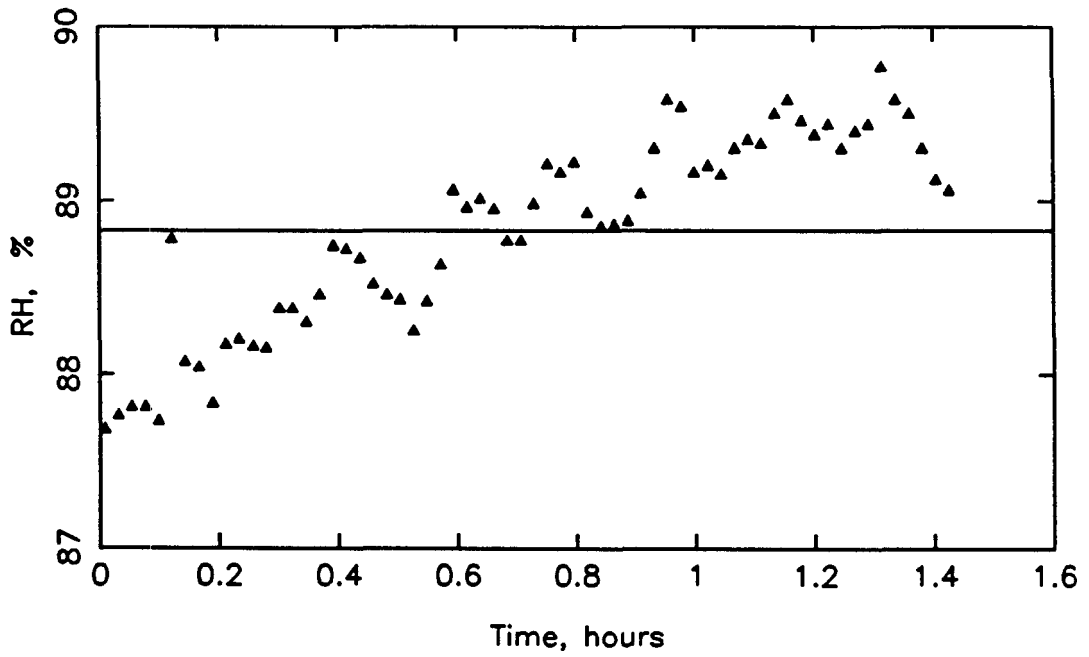

Figure F.1h Experiment 1: Feed EMC2 relative humidity.

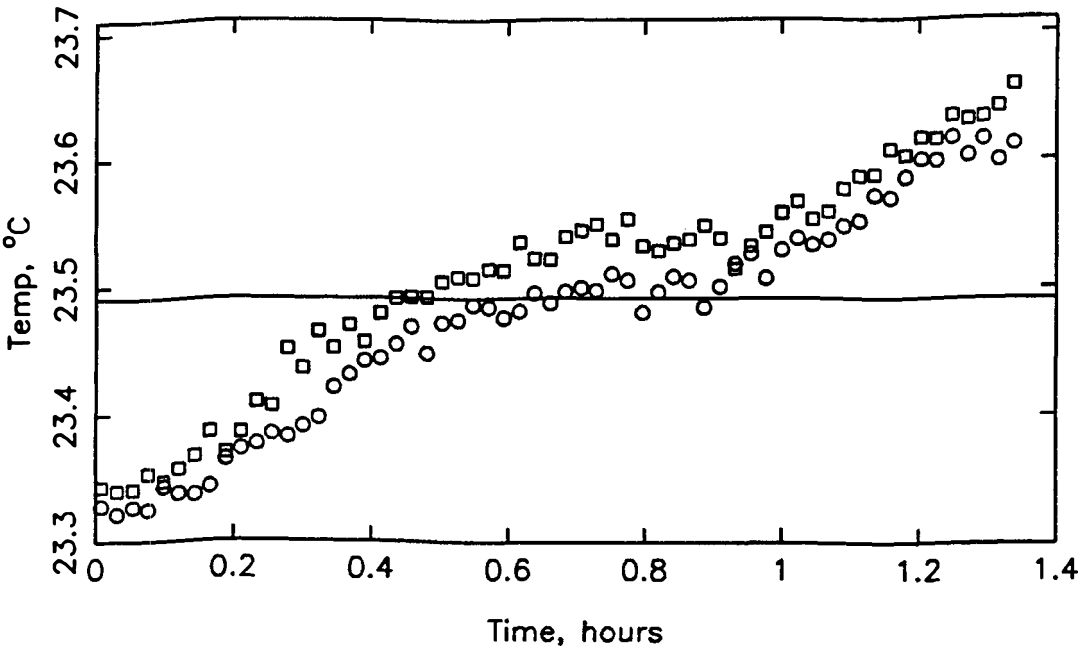

Figure F.2a Experiment 2: Effluent EMC2 inlet and outlet temperatures.

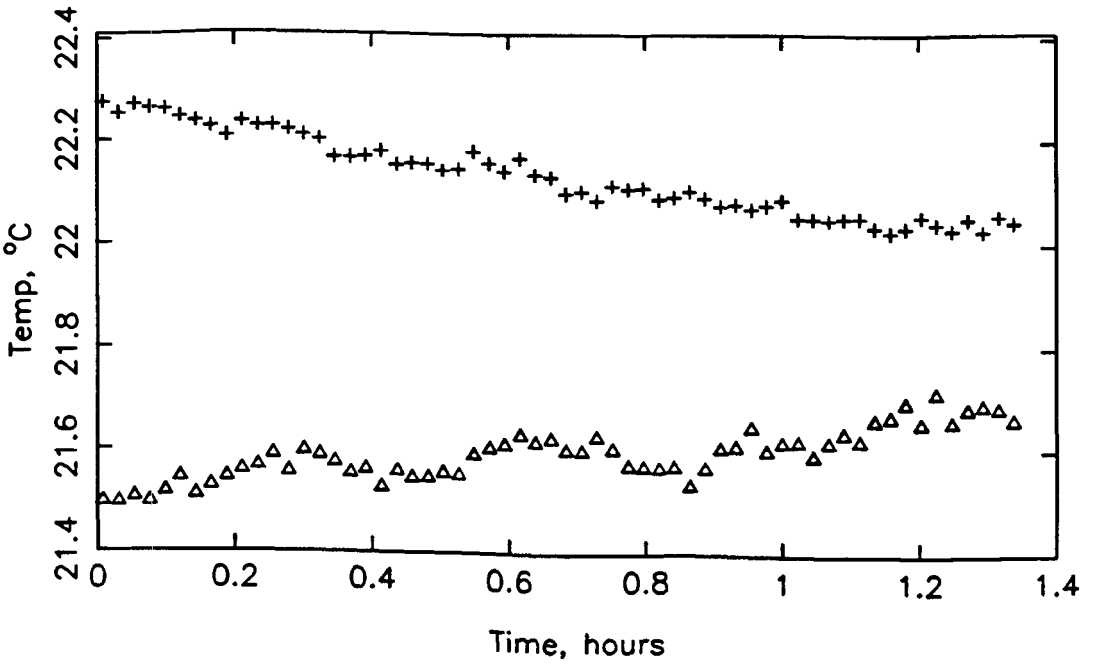

Figure F.2b Experiment 2: Effluent EMC2 and CSTR dew point temperatures.

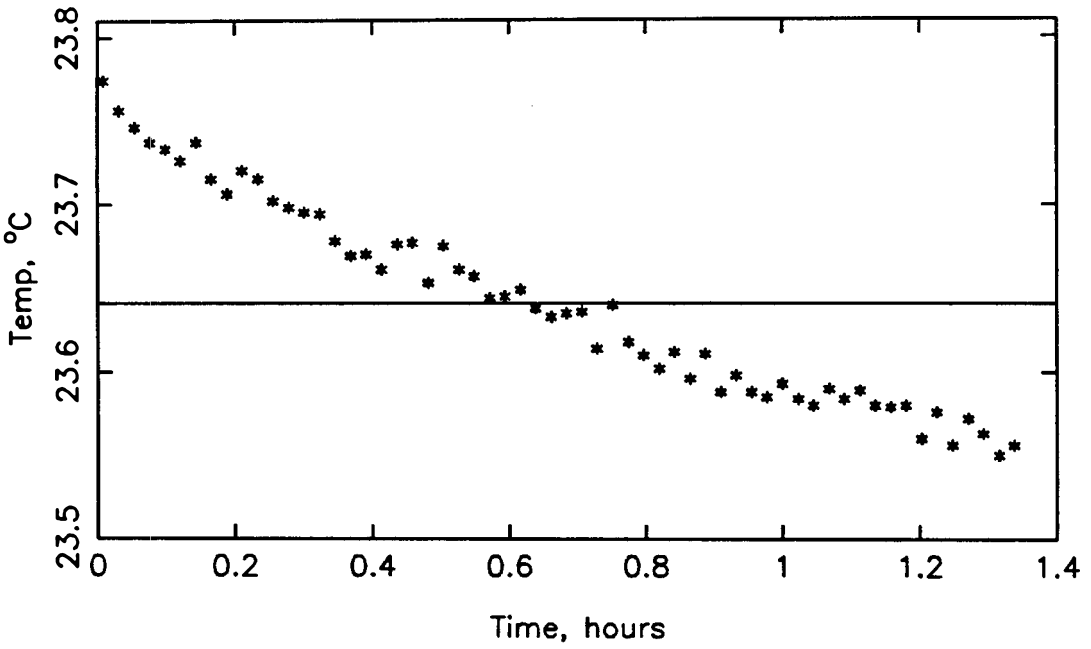

Figure F.2c Experiment 2: Effluent CSTR temperature.

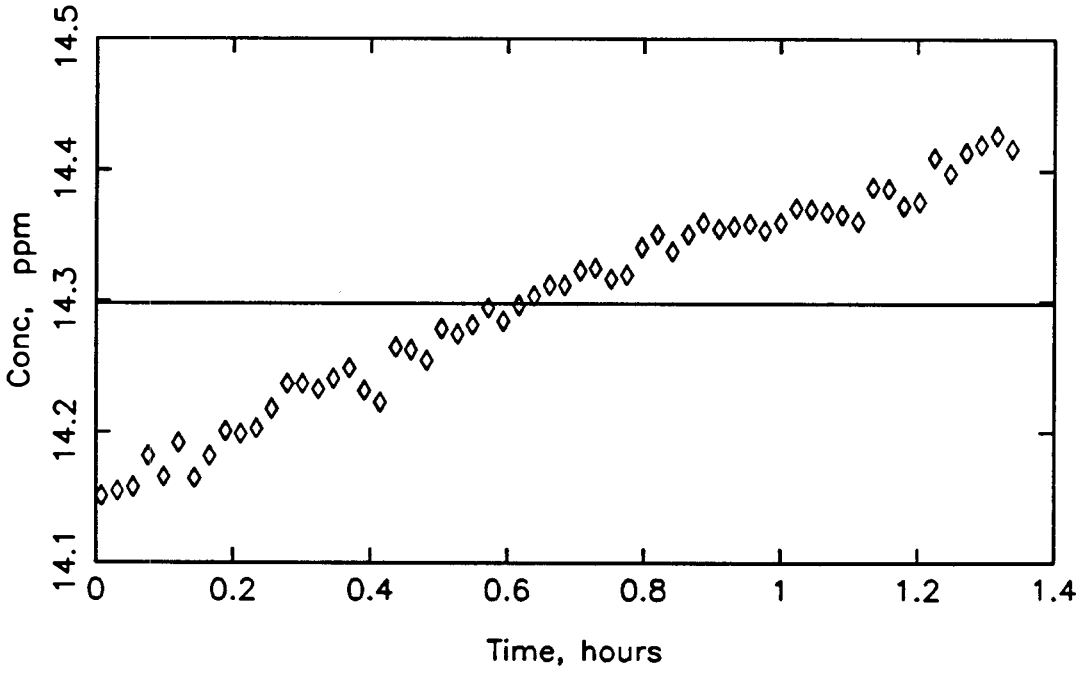

Figure F.2d Experiment 2: Effluent SO_2 concentration.

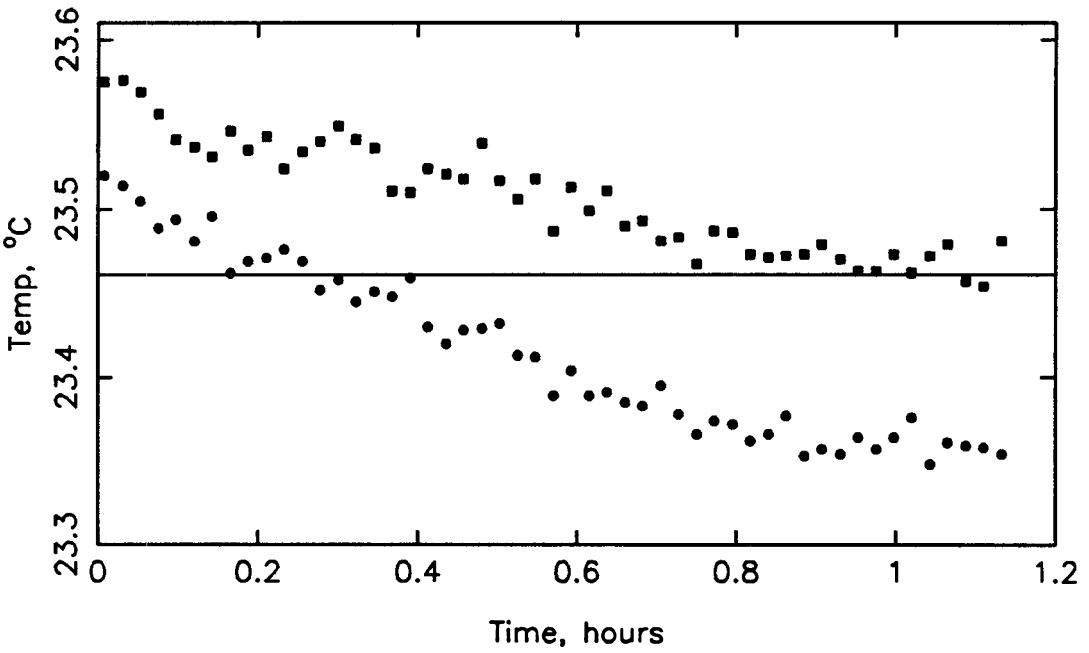

Figure F.2e Experiment 2: Feed EMC2 inlet and outlet temperatures.

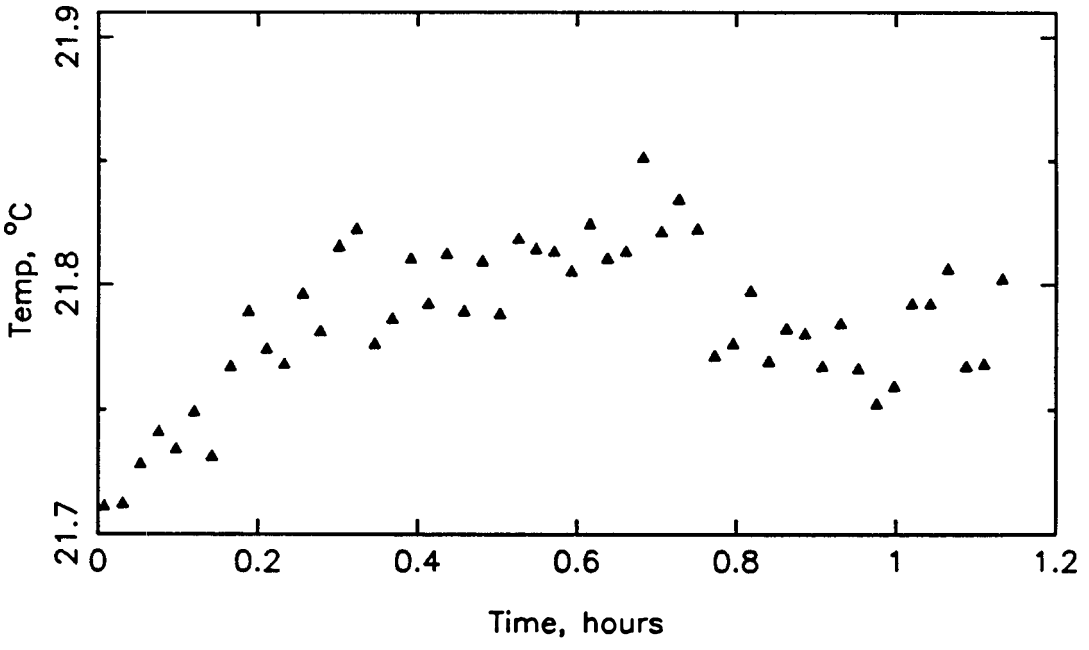

Figure F.2f Experiment 2: Feed EMC2 dew point temperature.

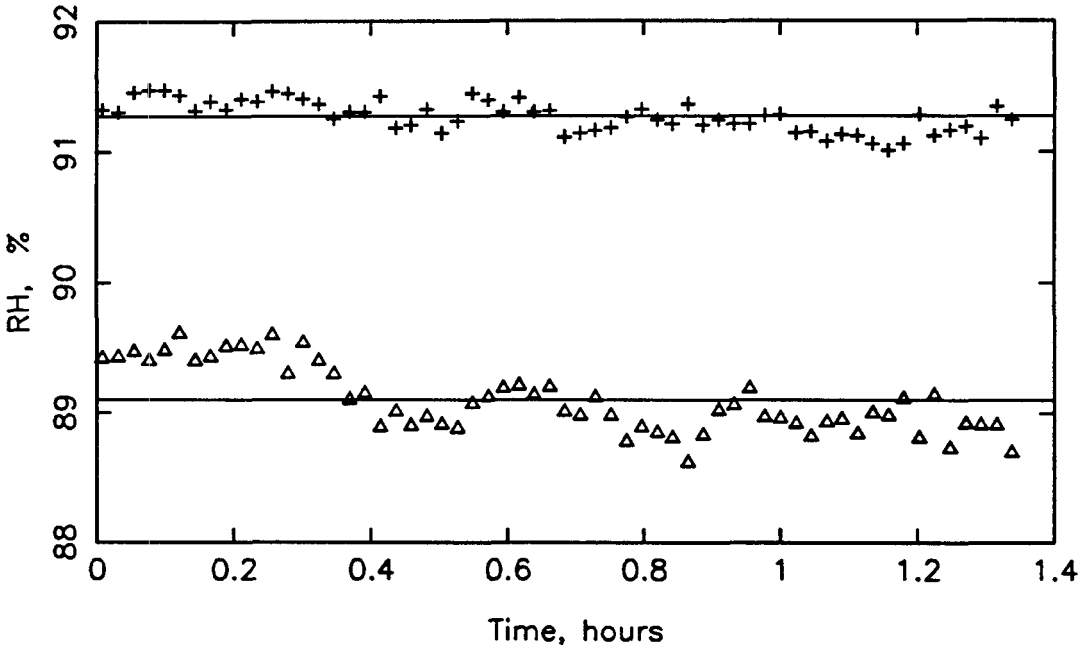

Figure F.2g Experiment 2: Effluent EMC2 and CSTR relative humidity.

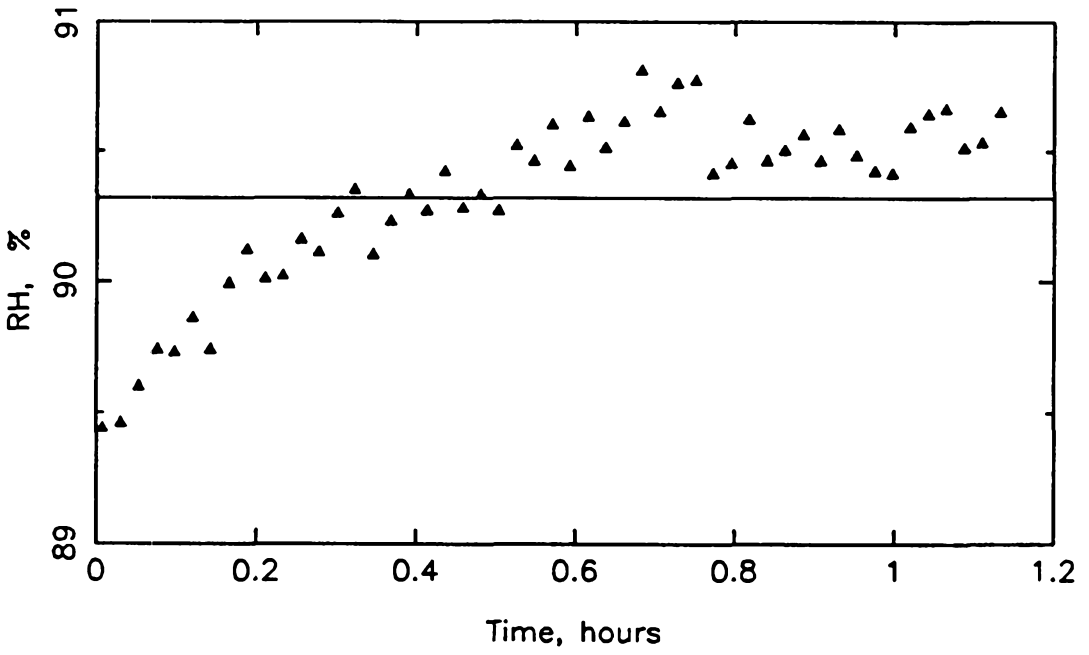

Figure F.2h Experiment 2: Feed EMC2 relative humidity.

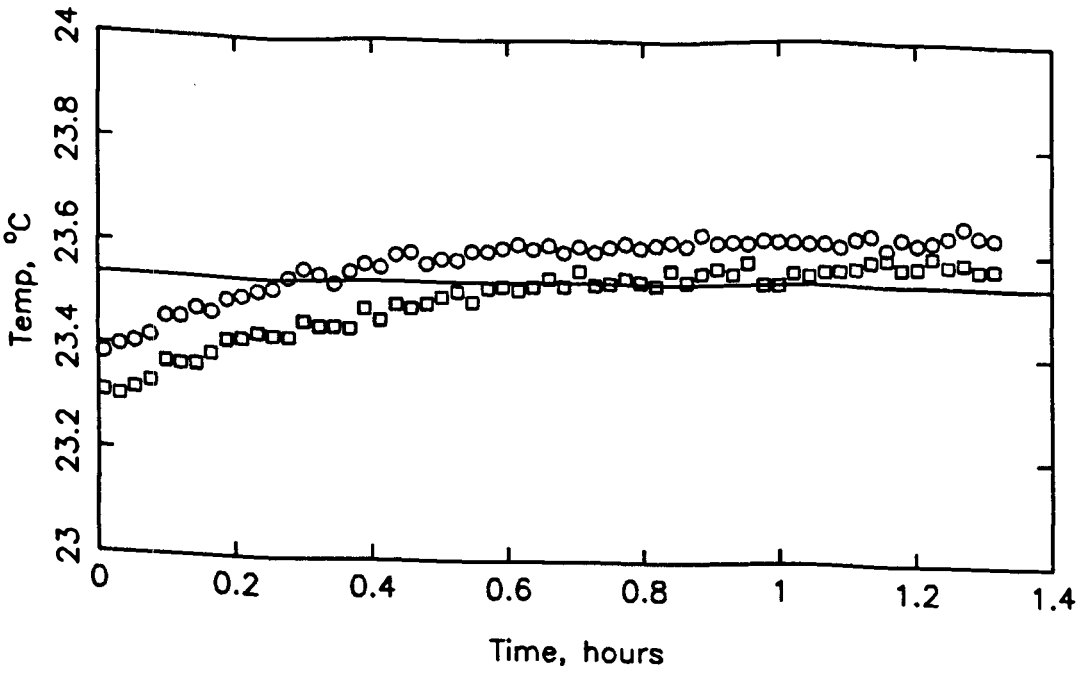

Figure F.3a Experiment 3: Effluent EMC2 inlet and outlet temperatures.

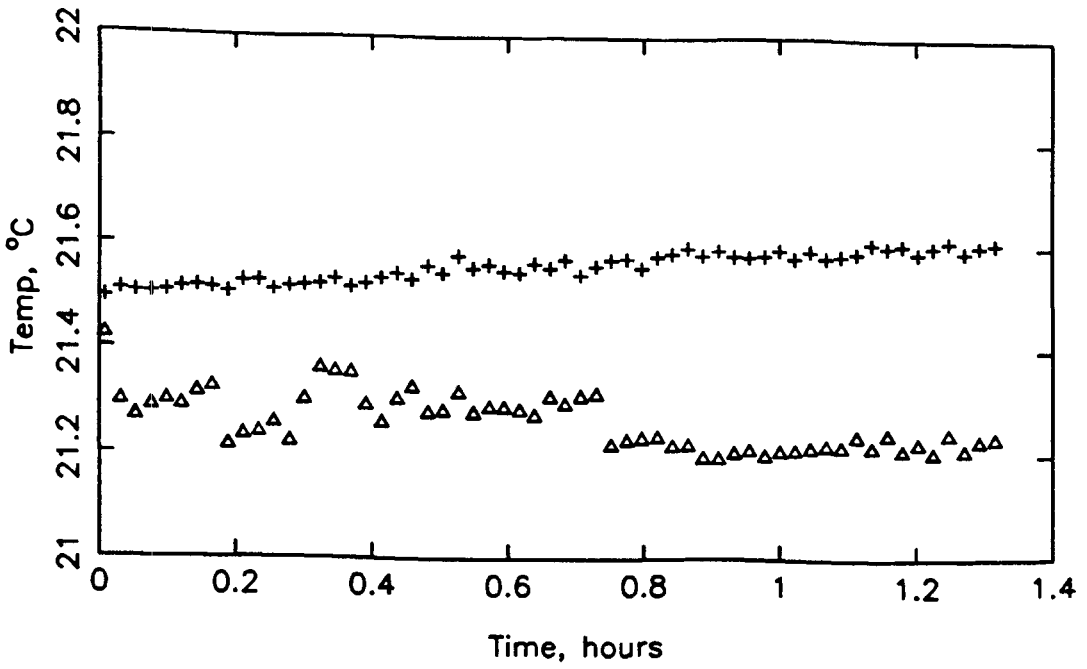

Figure F.3b Experiment 3: Effluent EMC2 and CSTR dew point temperatures.

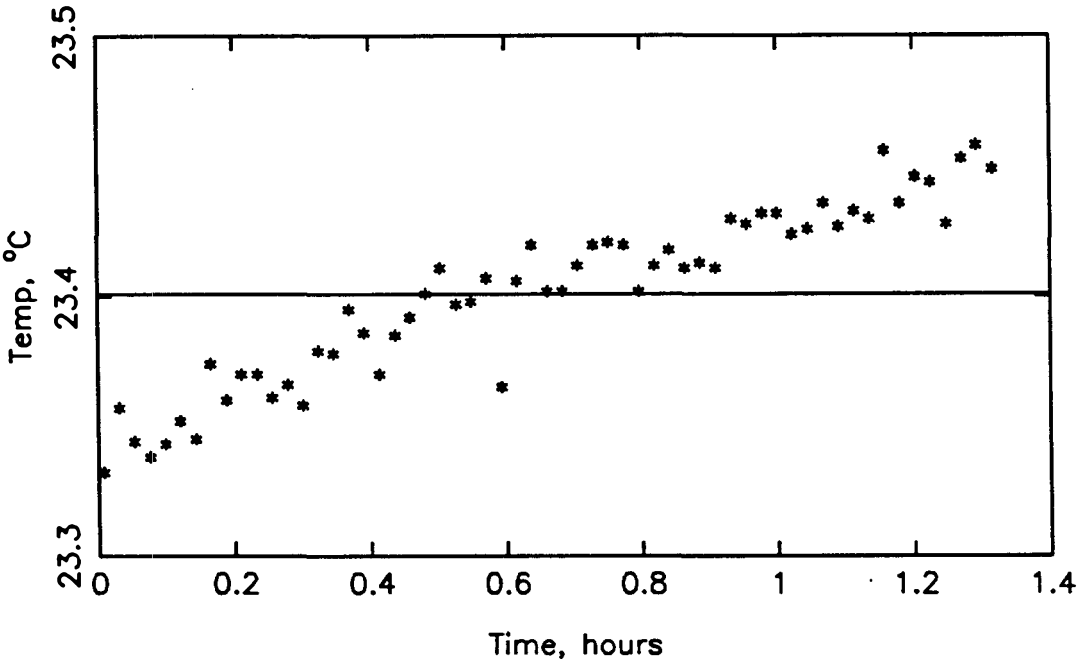

Figure F.3c Experiment 3: Effluent CSTR temperature.

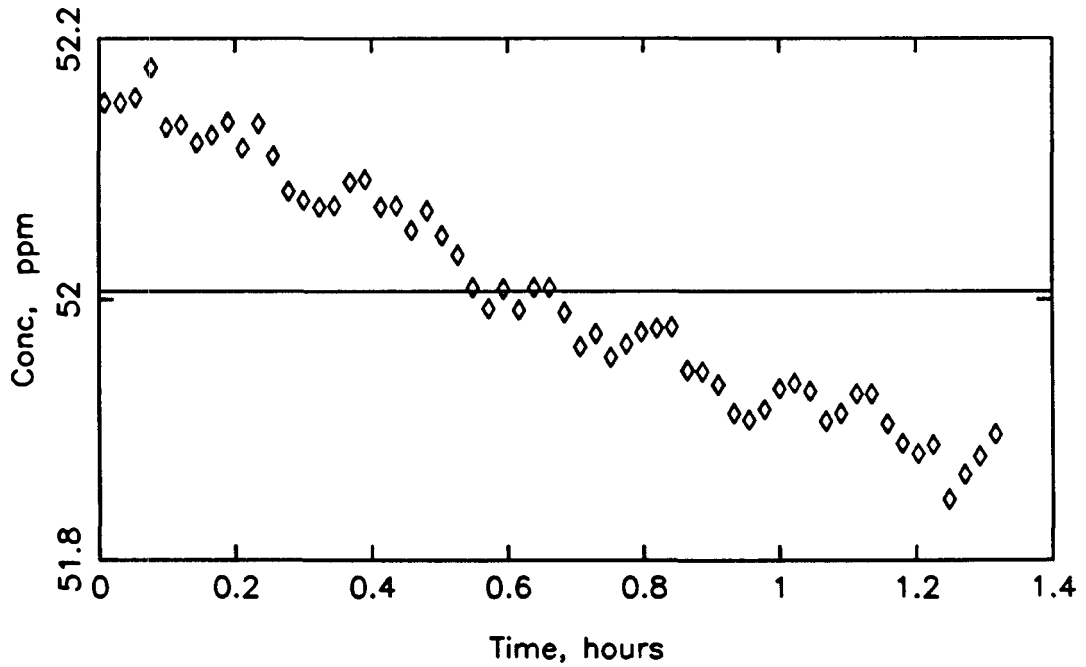

Figure F.3d Experiment 3: Effluent SO_2 concentration.

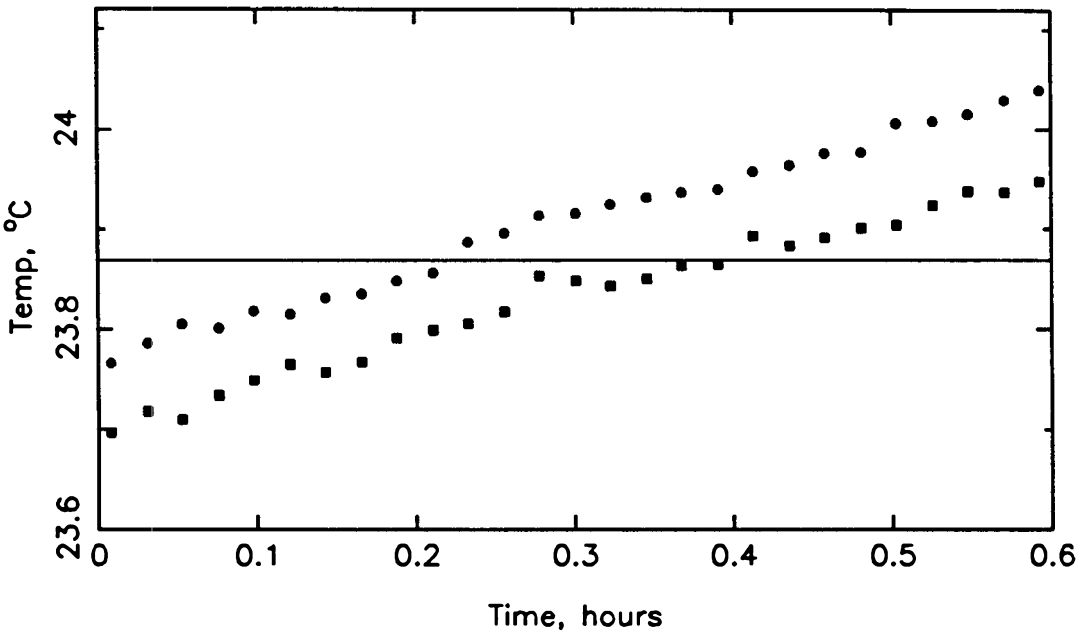

Figure F.3e Experiment 3: Feed EMC2 inlet and outlet temperatures.

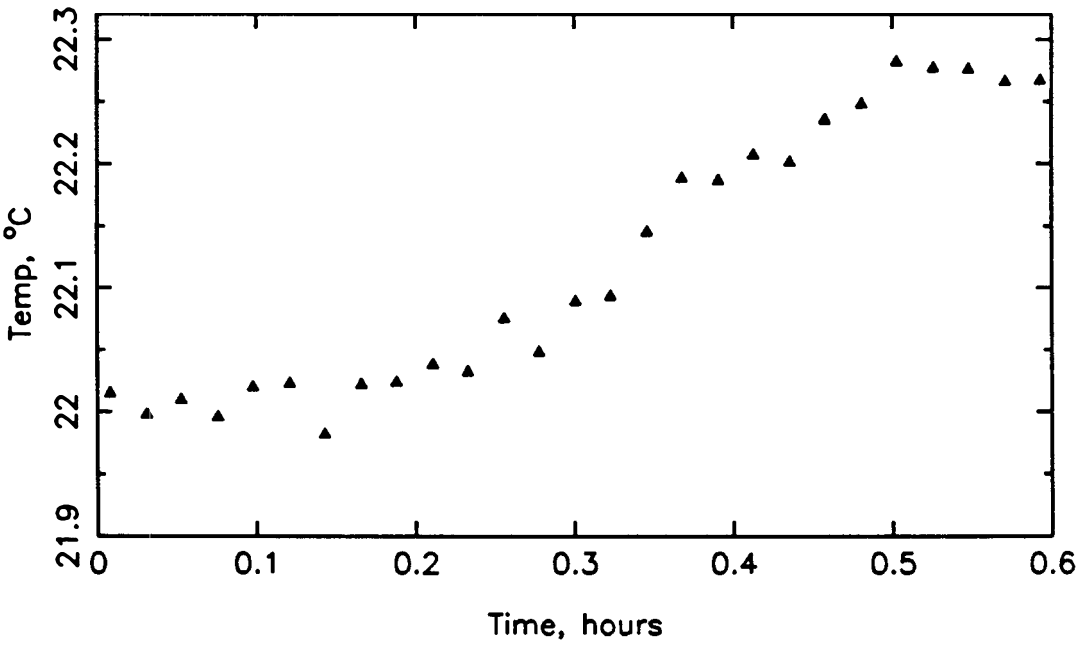

Figure F.3f Experiment 3: Feed EMC2 dew point temperature.

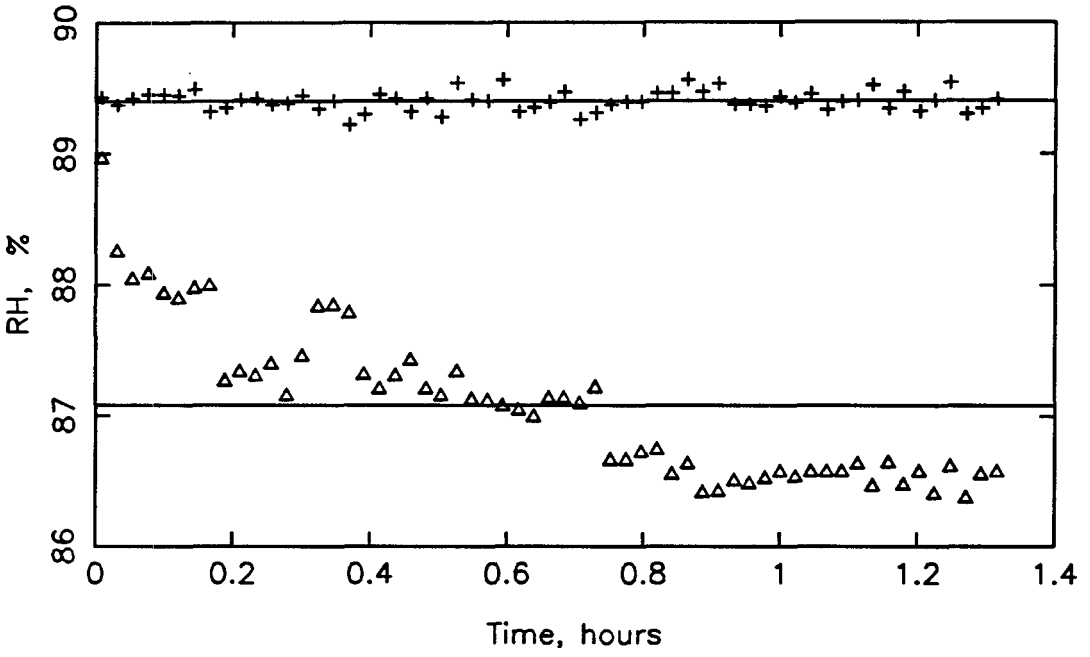

Figure F.3g Experiment 3: Effluent EMC2 and CSTR relative humidity.

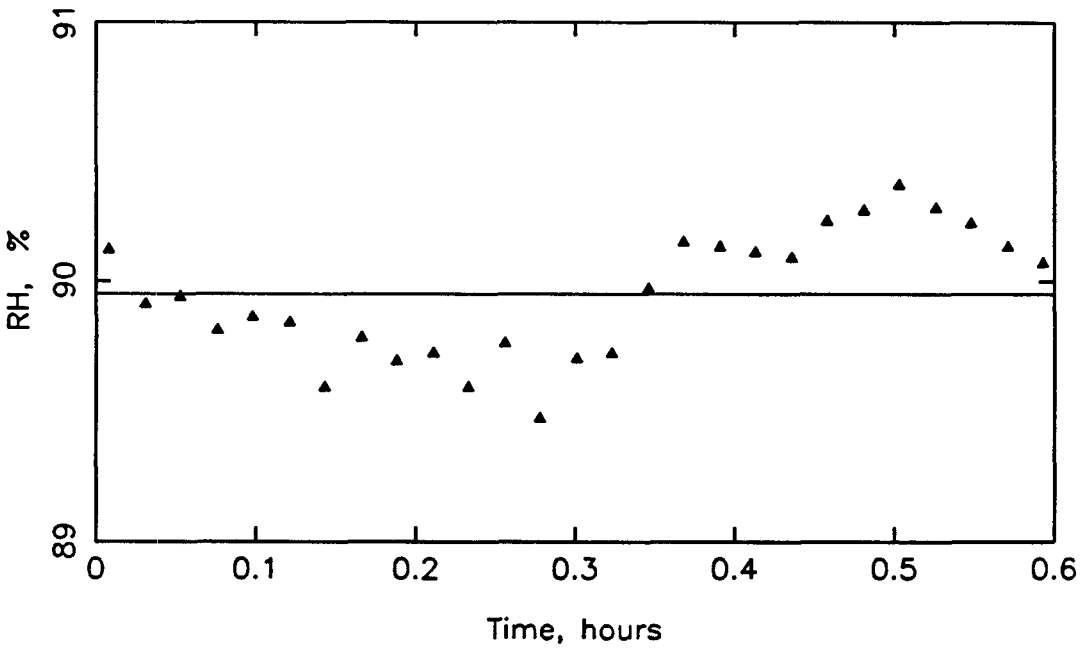

Figure F.3h Experiment 3: Feed EMC2 relative humidity.

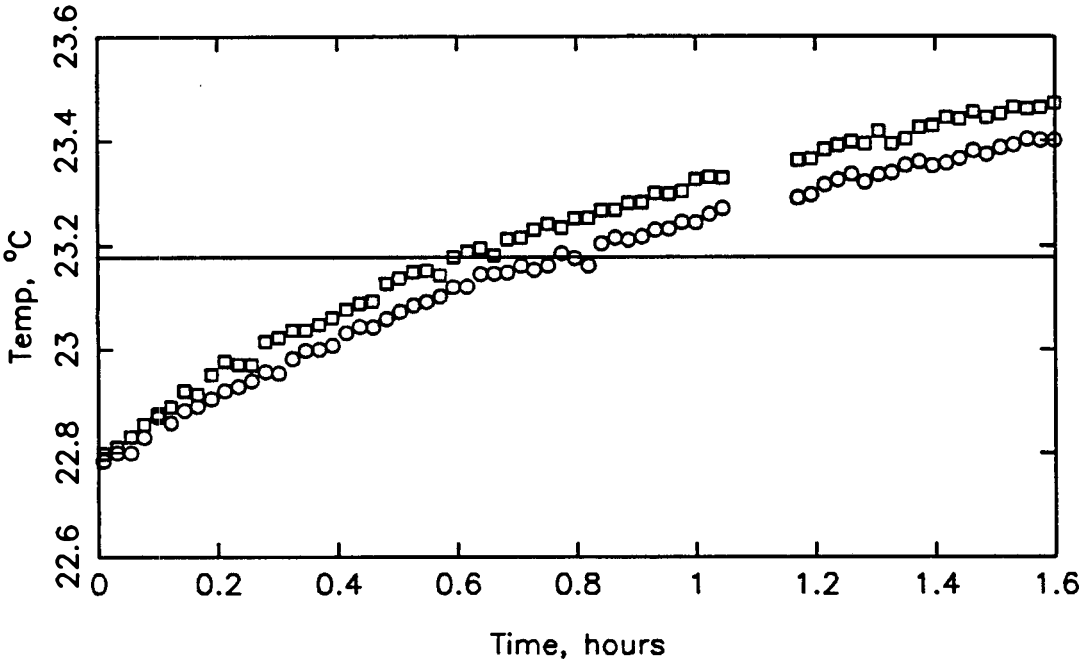

Figure F.4a Experiment 4: Effluent EMC2 inlet and outlet temperatures.

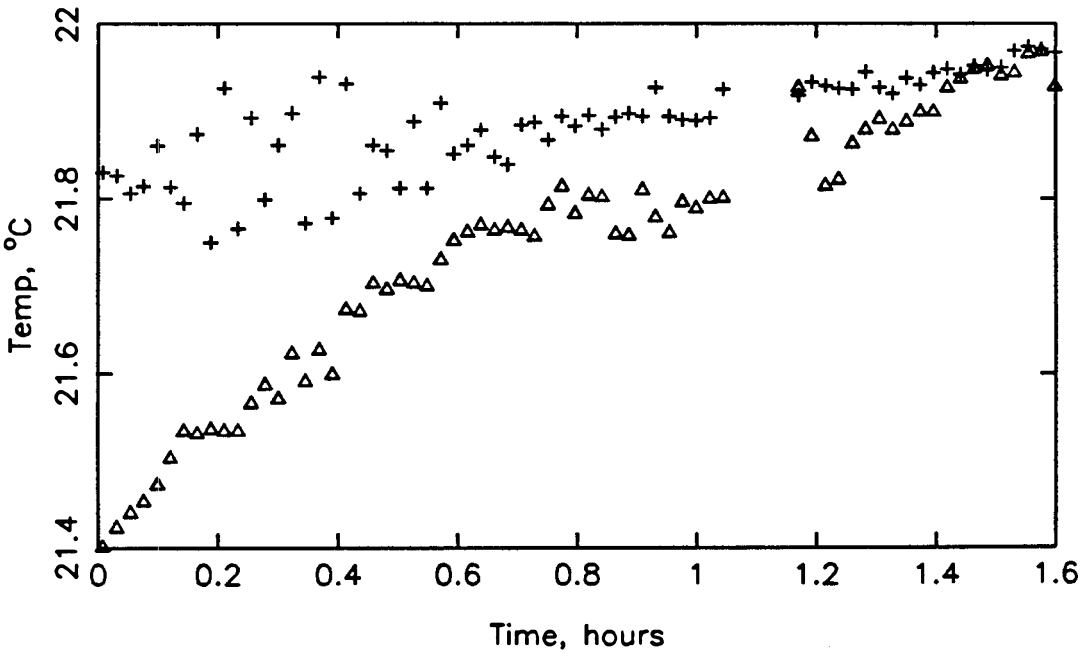

Figure F.4b Experiment 4: Effluent EMC2 and CSTR dew point temperatures.

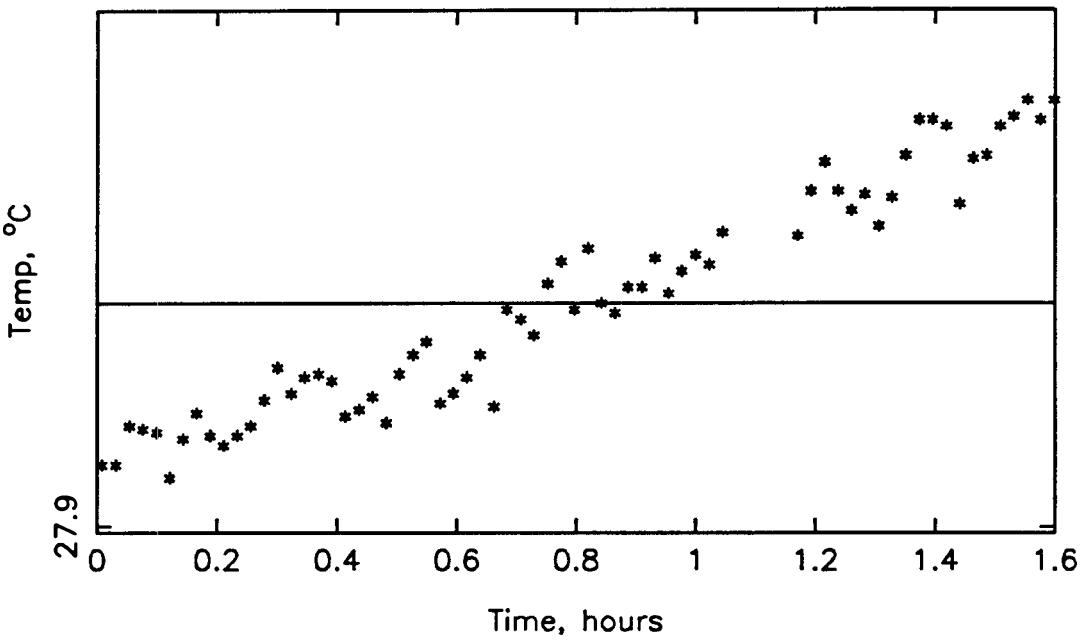

Figure F.4c Experiment 4: Effluent CSTR temperature.

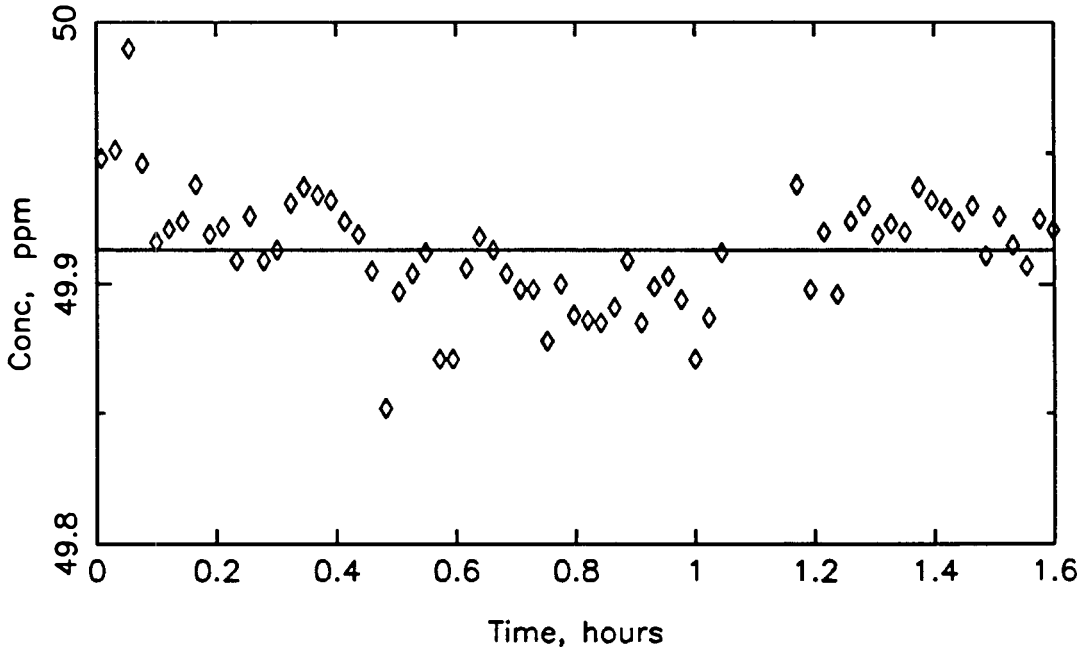

Figure F.4d Experiment 4: Effluent SO_2 concentration.

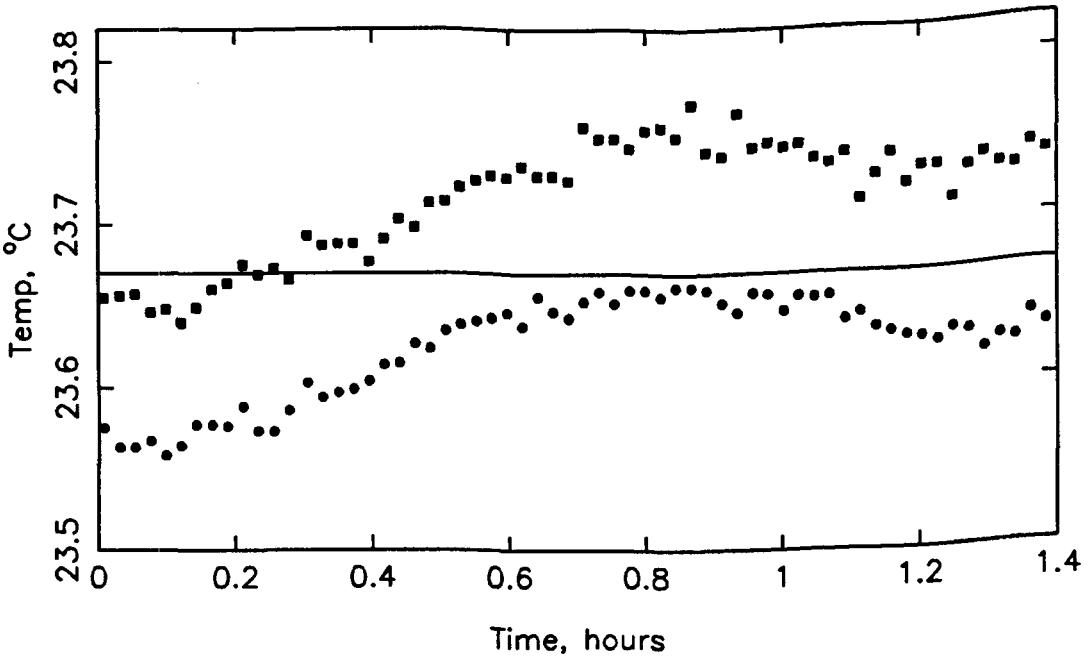

Figure F.4e Experiment 4: Feed EMC2 inlet and outlet temperatures.

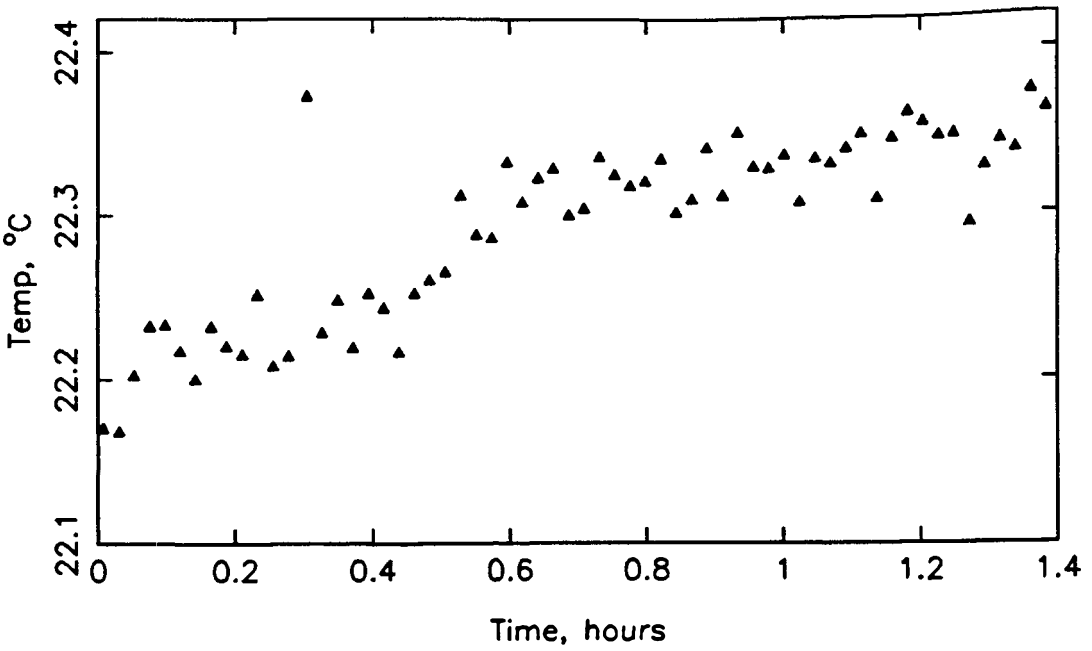

Figure F.4f Experiment 4: Feed EMC2 dew point temperature.

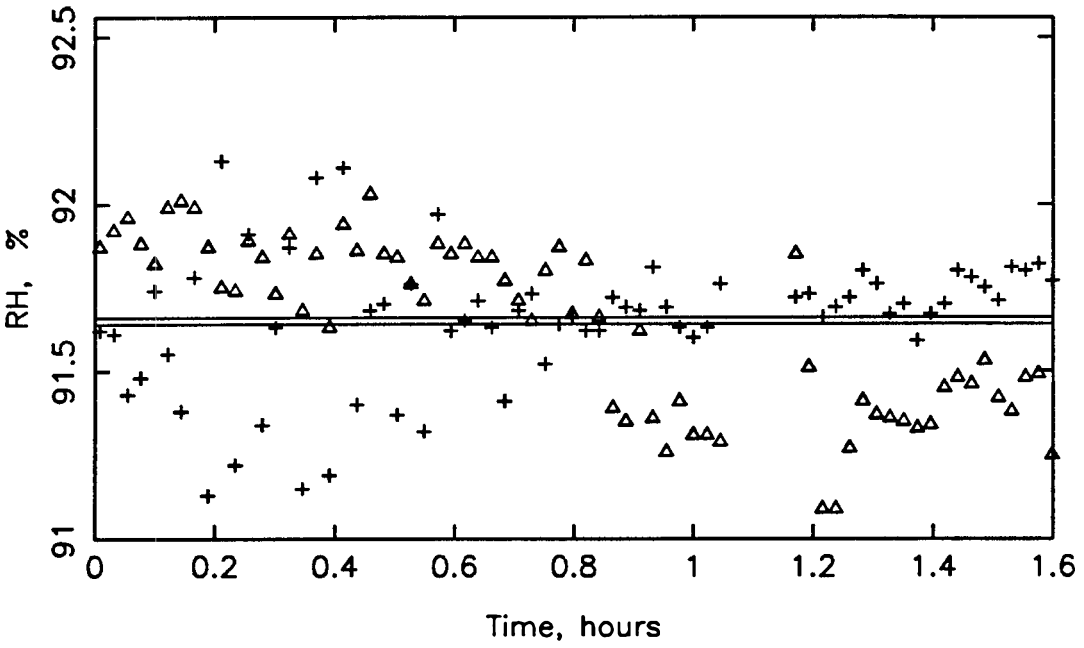

Figure F.4g Experiment 4: Effluent EMC2 and CSTR relative humidity.

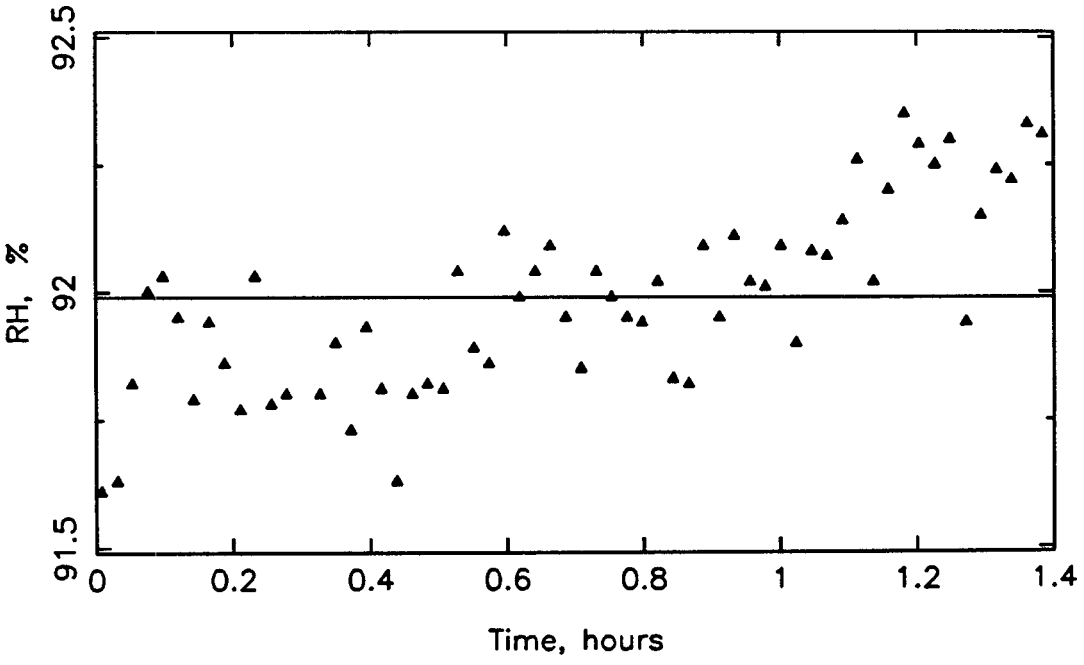

Figure F.4h Experiment 4: Feed EMC2 relative humidity.

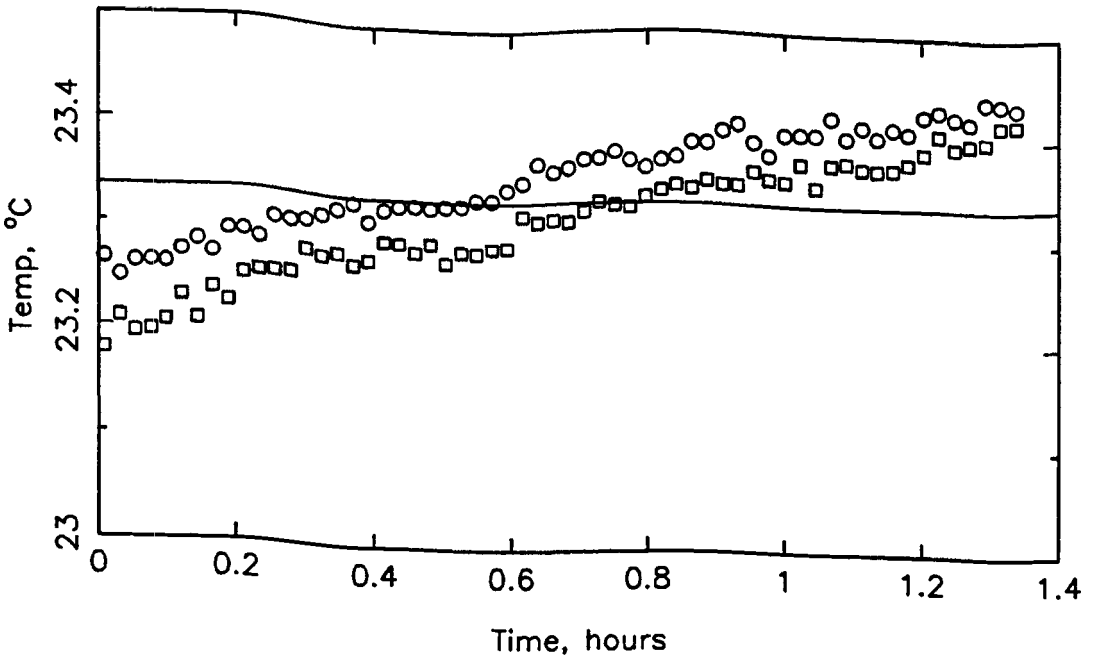

Figure F.5a Experiment 5: Effluent EMC2 inlet and outlet temperatures.

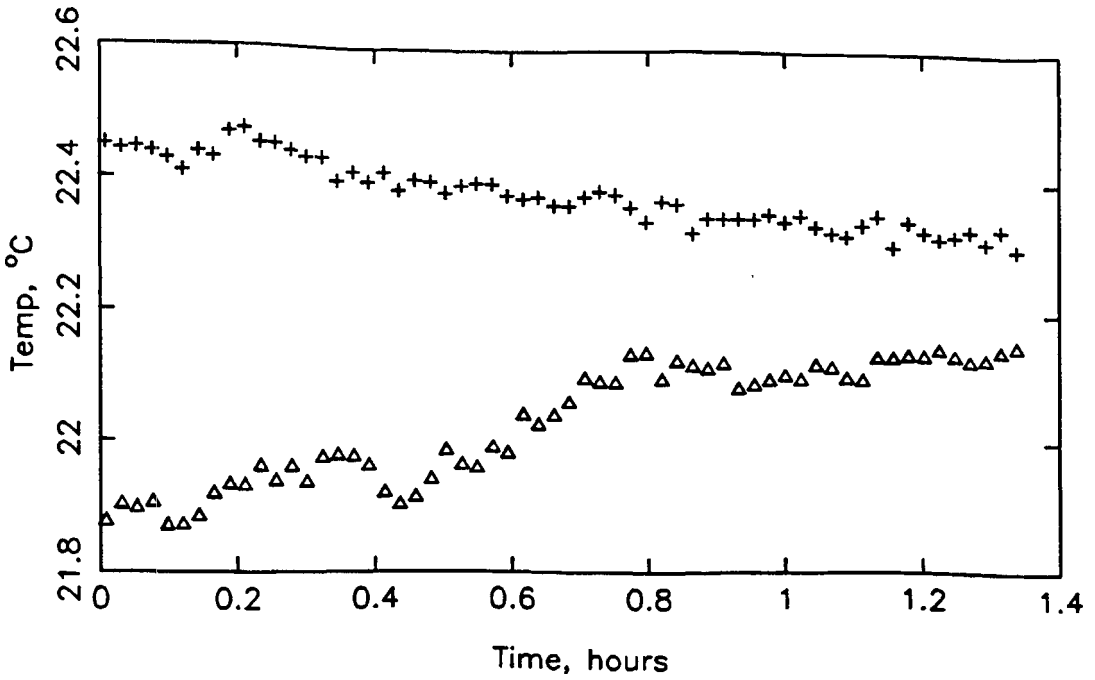

Figure F.5b Experiment 5: Effluent EMC2 and CSTR dew point temperatures.

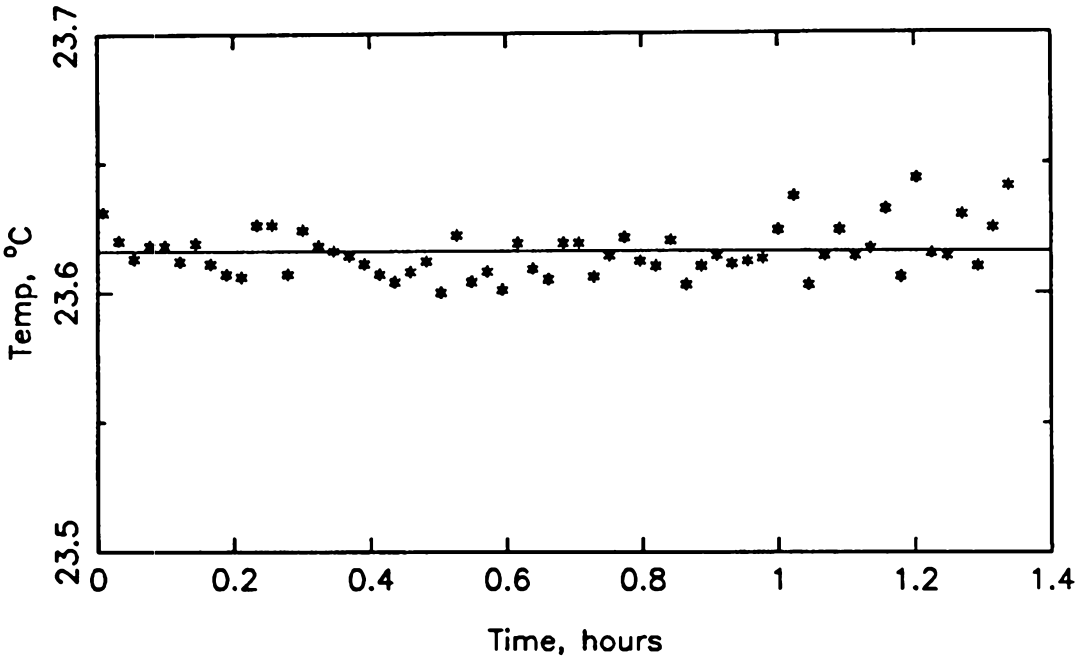

Figure F.5c Experiment 5: Effluent CSTR temperature.

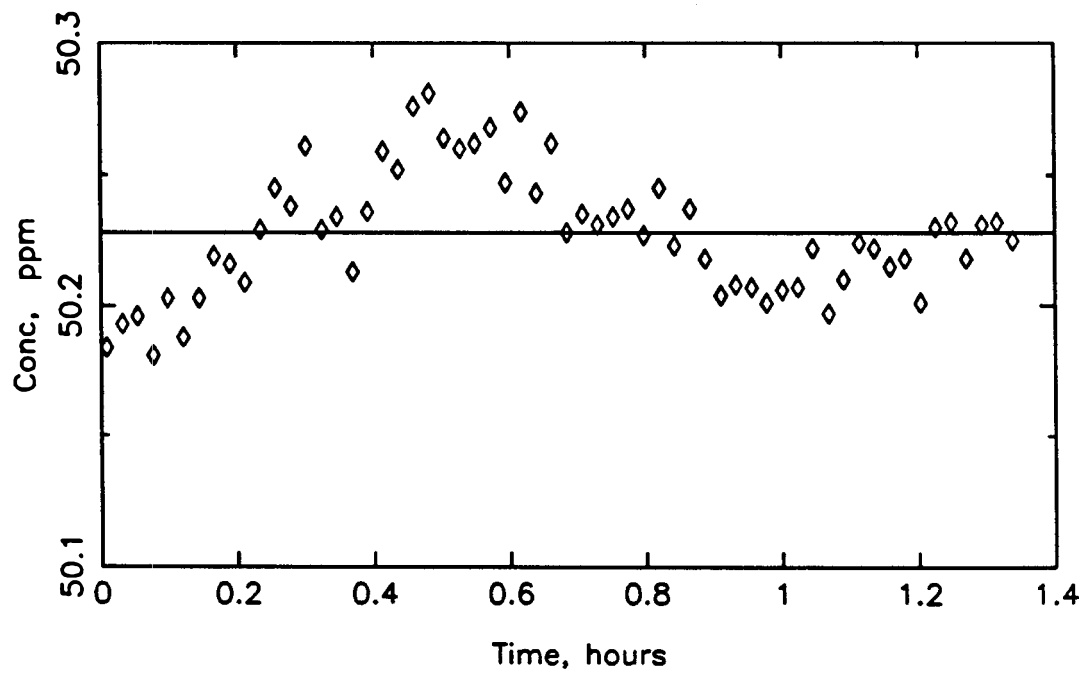

Figure F.5d Experiment 5: Effluent SO_2 concentration.

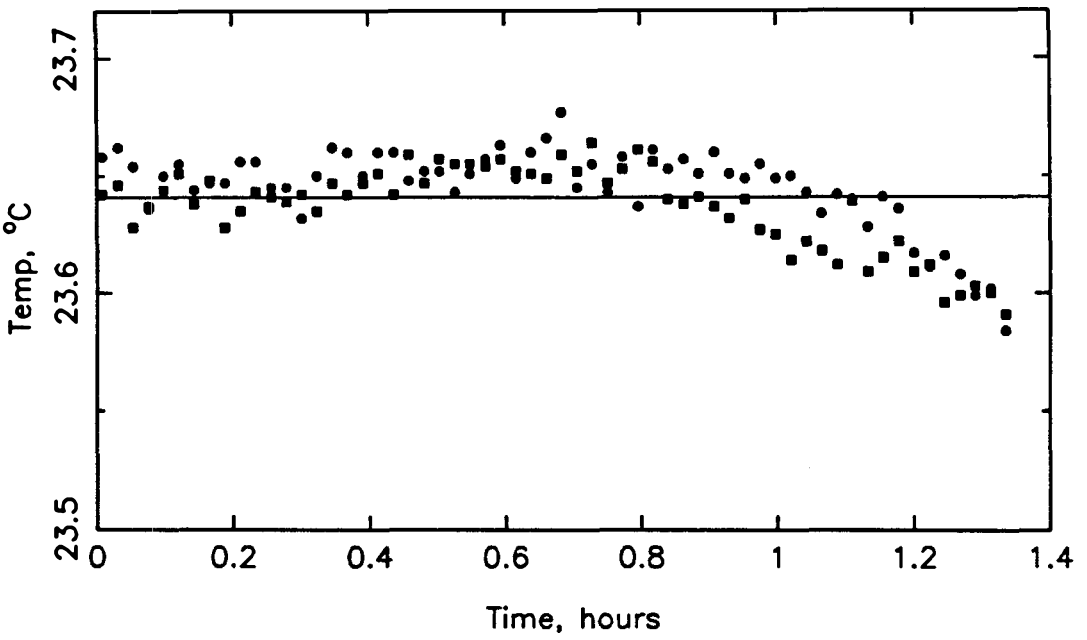

Figure F.5e Experiment 5: Feed EMC2 inlet and outlet temperatures.

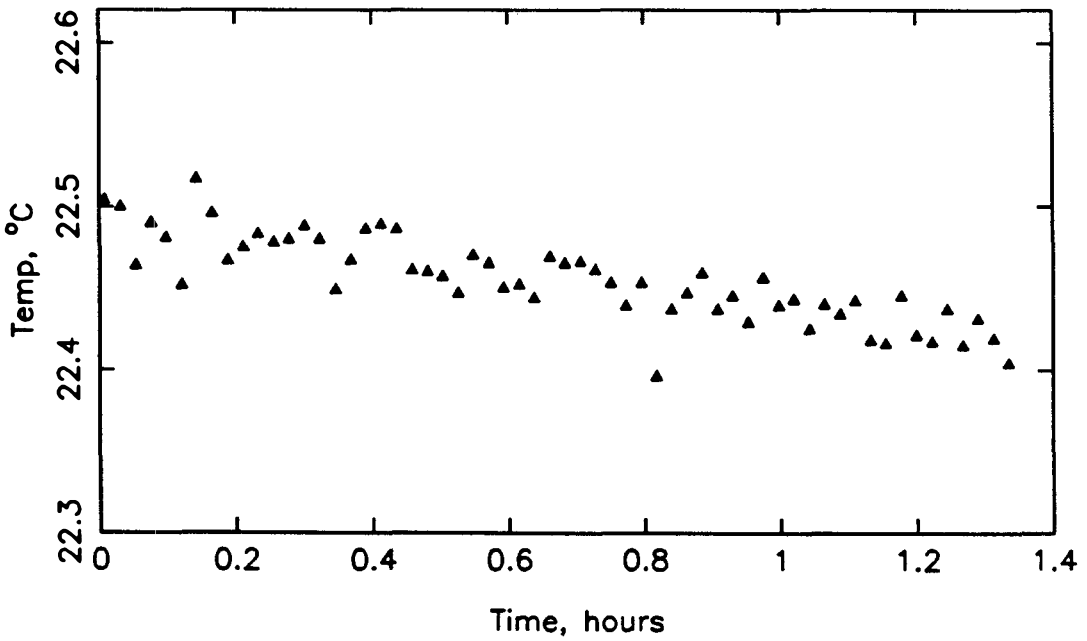

Figure F.5f Experiment 5: Feed EMC2 dew point temperature.

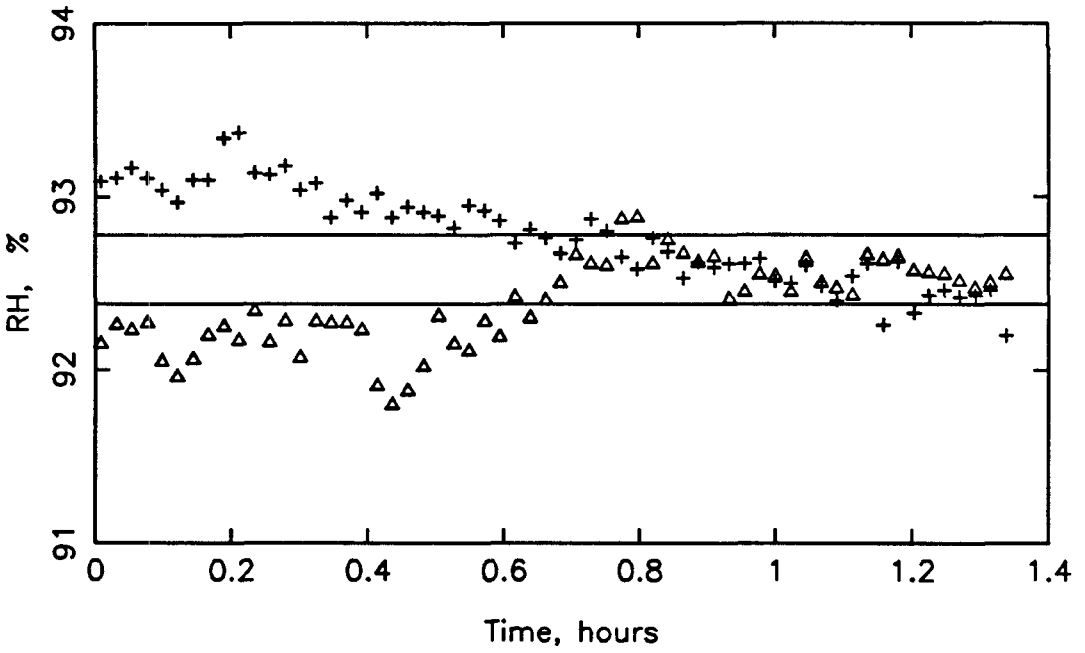

Figure F.5g Experiment 5: Effluent EMC2 and CSTR relative humidity.

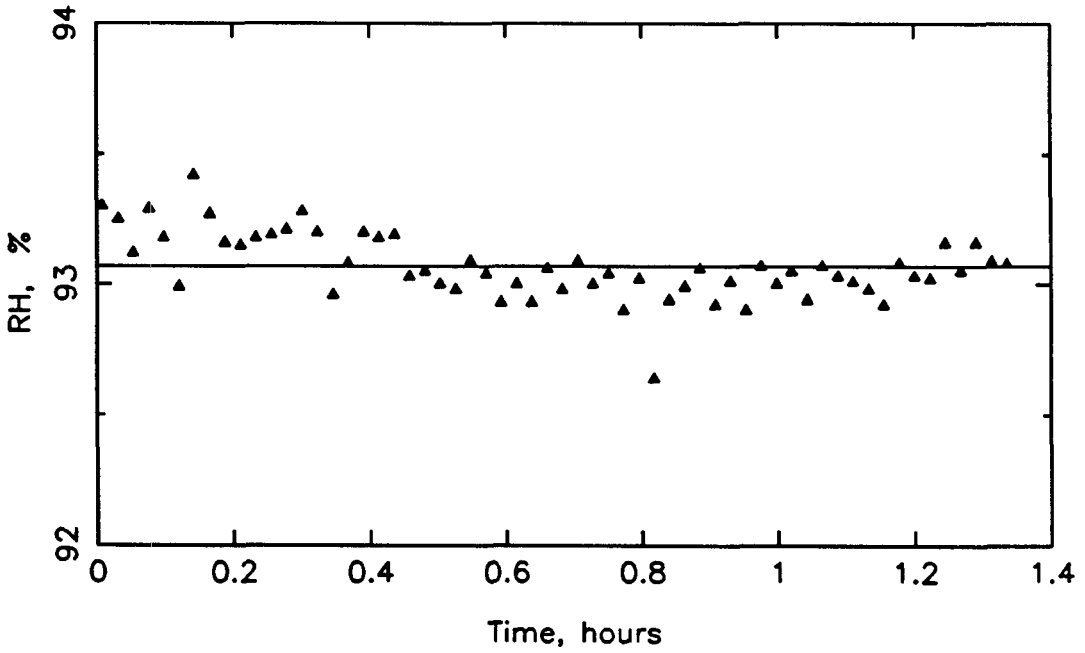

Figure F.5h Experiment 5: Feed EMC2 relative humidity.

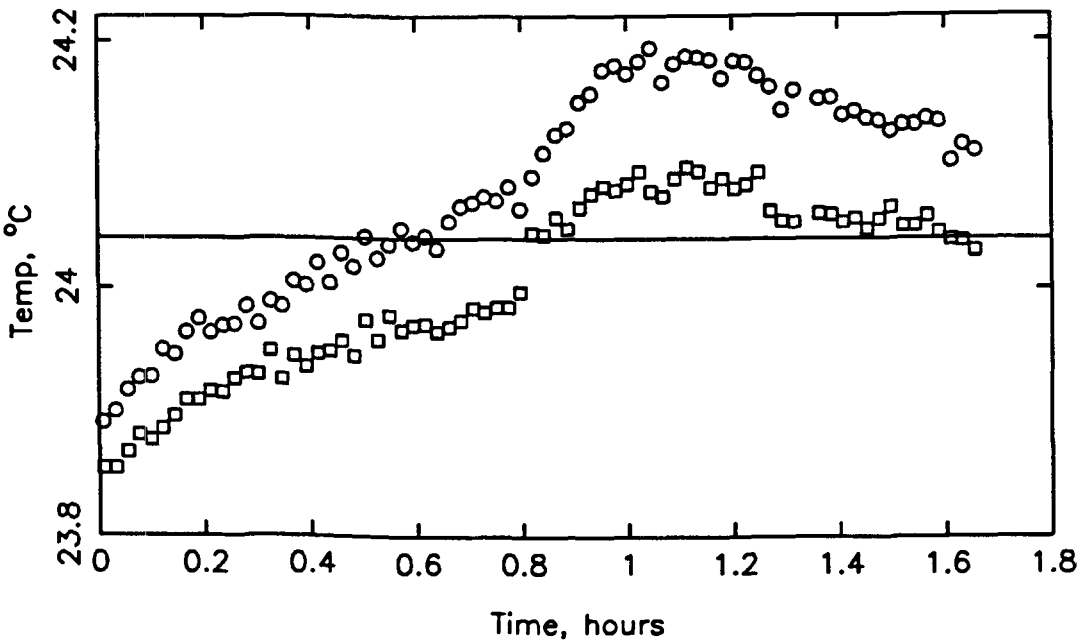

Figure F.6a Experiment 6: Effluent EMC2 inlet and outlet temperatures.

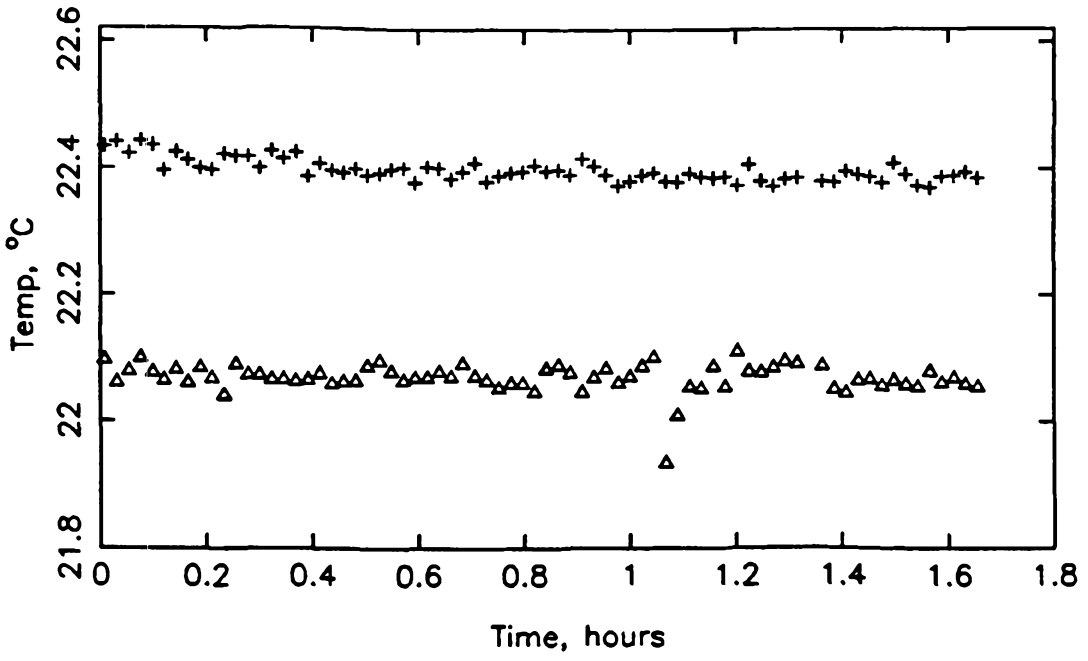

Figure F.6b Experiment 6: Effluent EMC2 and CSTR dew point temperatures.

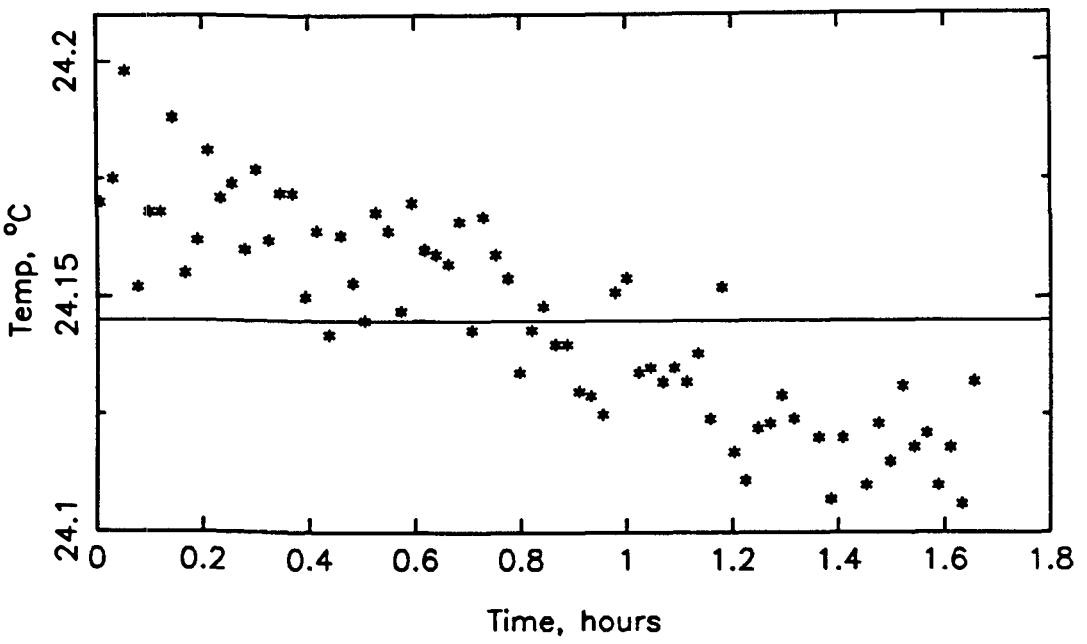

Figure F.6c Experiment 6: Effluent CSTR temperature.

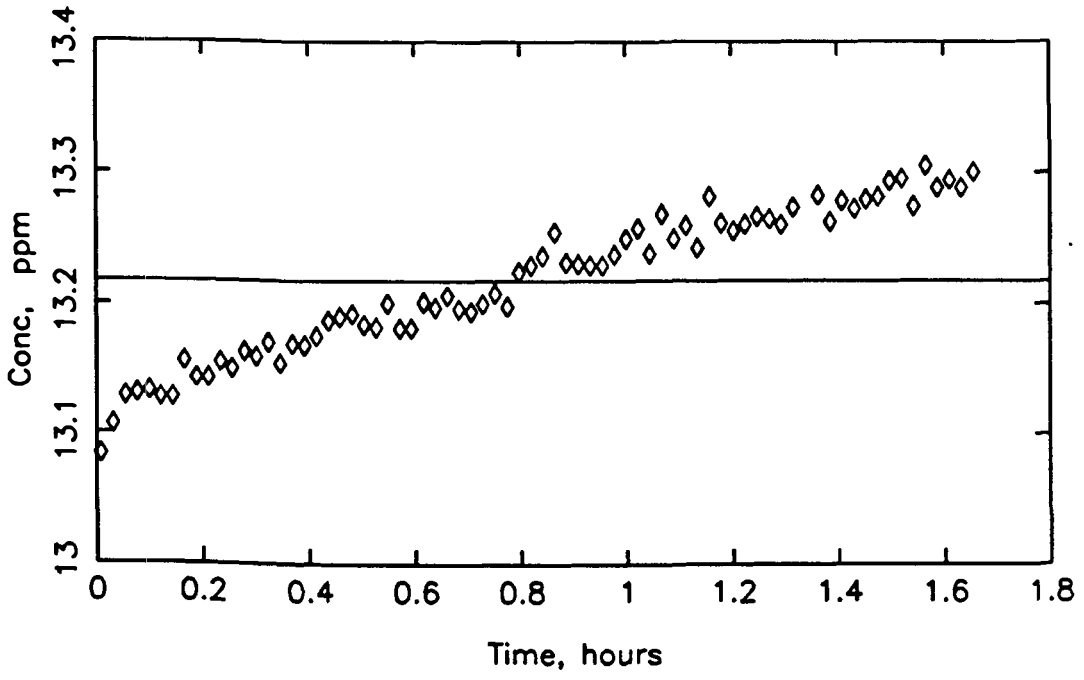

Figure F.6d Experiment 6: Effluent SO_2 concentration.

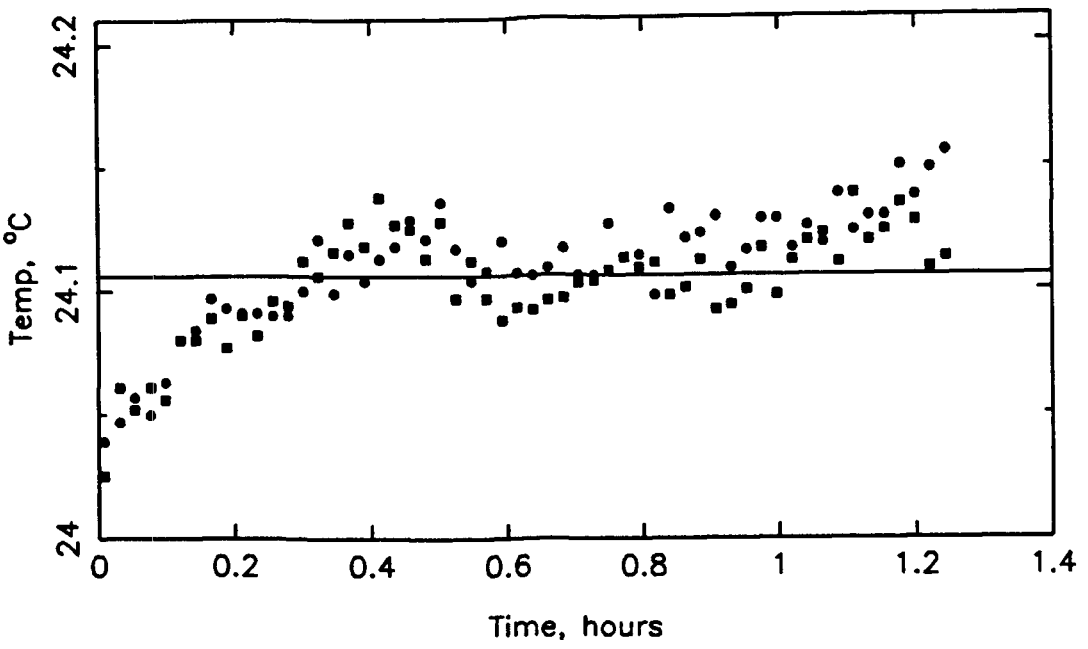

Figure F.6e Experiment 6: Feed EMC2 inlet and outlet temperatures.

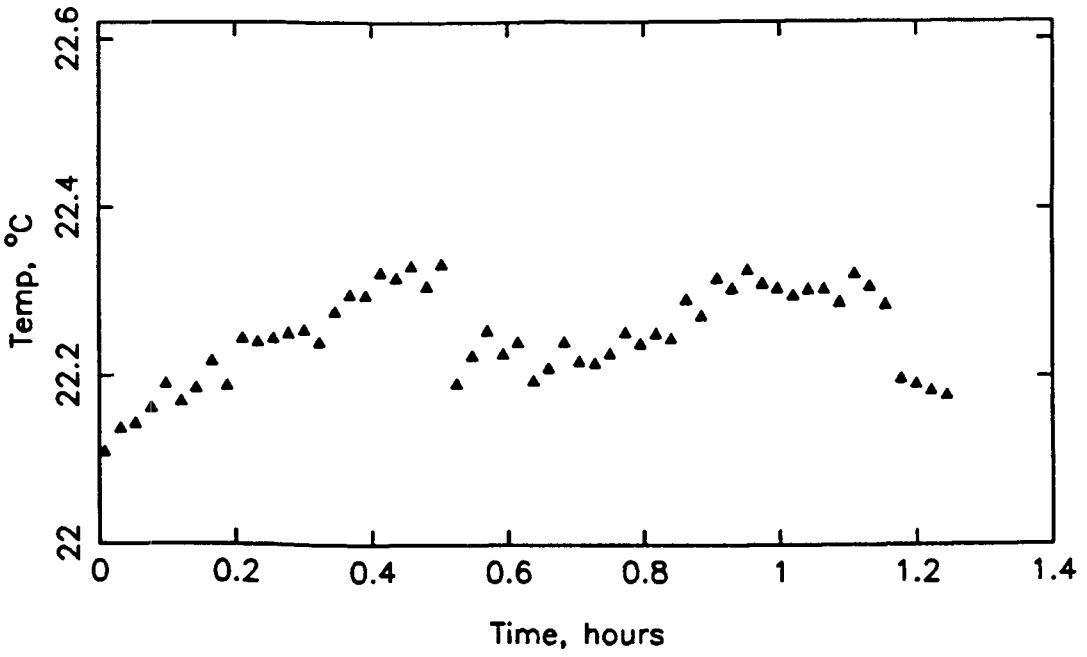

Figure F.6f Experiment 6: Feed EMC2 dew point temperature.

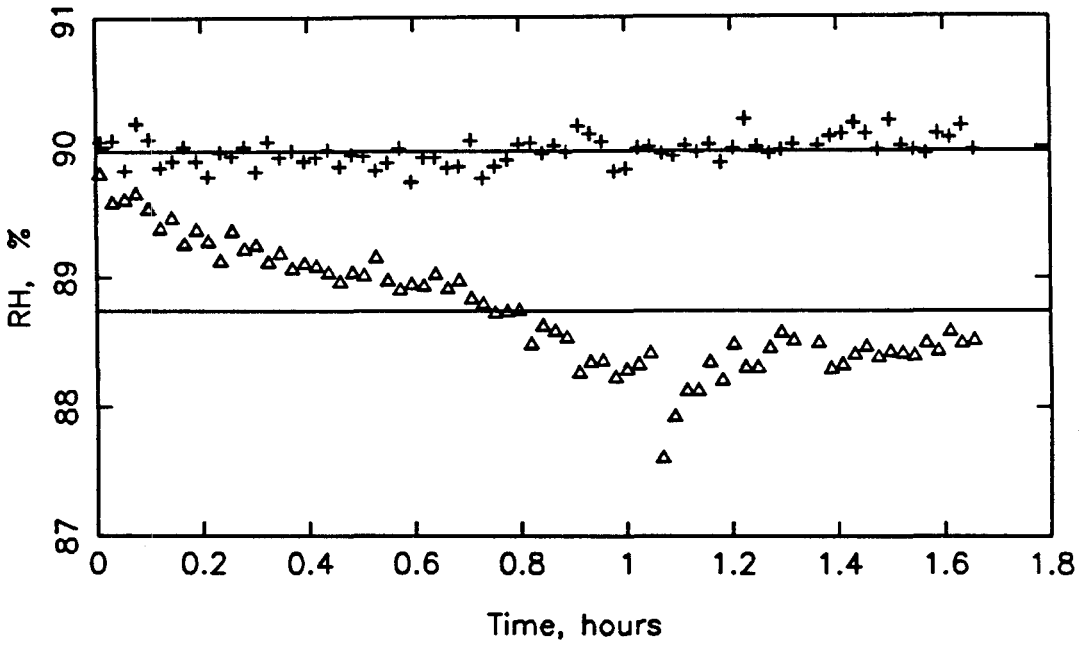

Figure F.6g Experiment 6: Effluent EMC2 and CSTR relative humidity.

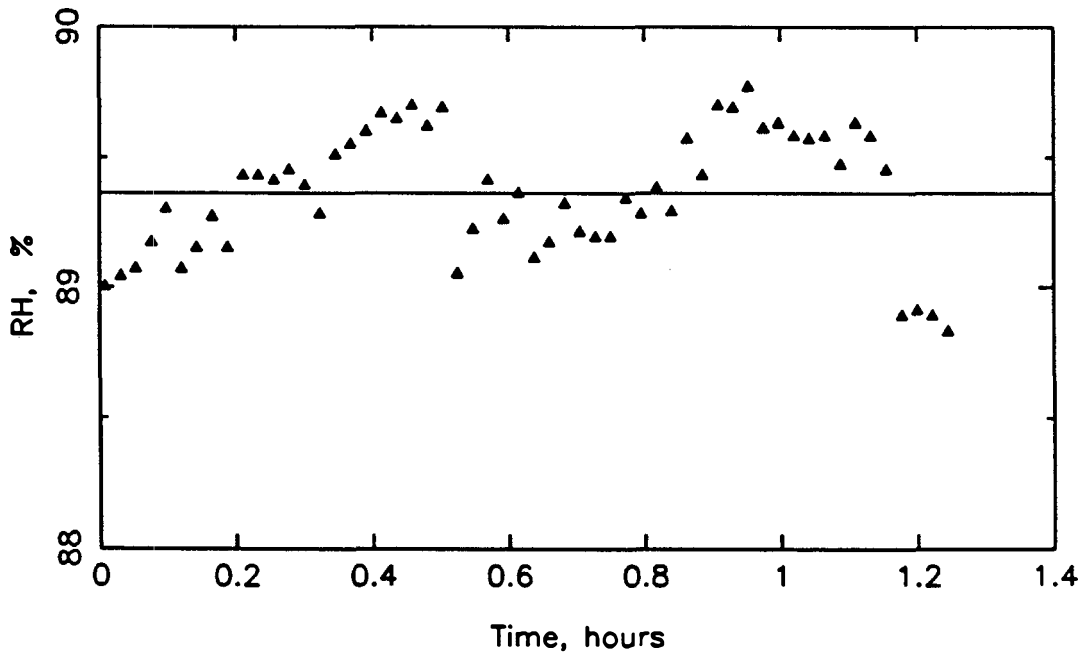

Figure F.6h Experiment 6: Feed EMC2 relative humidity.

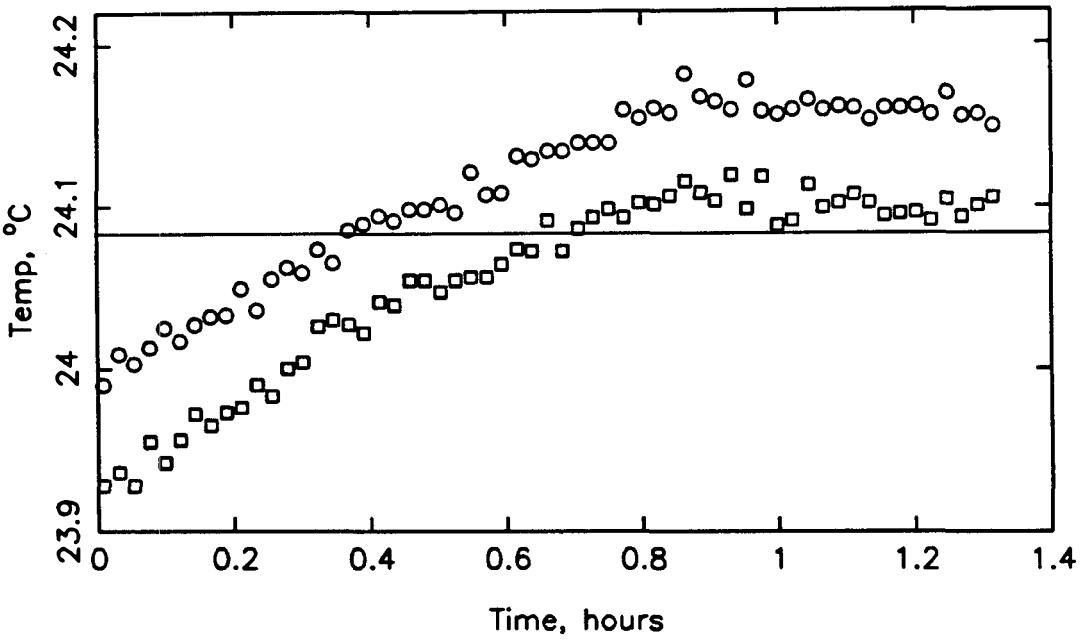

Figure F.7a Experiment 7: Effluent EMC2 inlet and outlet temperatures.

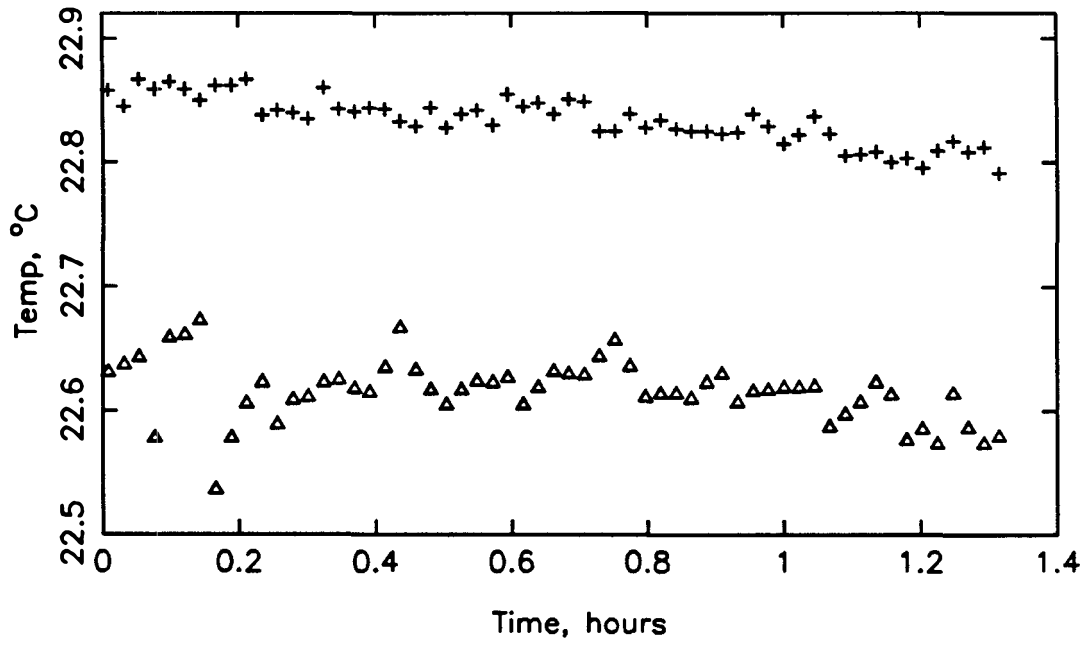

Figure F.7b Experiment 7: Effluent EMC2 and CSTR dew point temperatures.

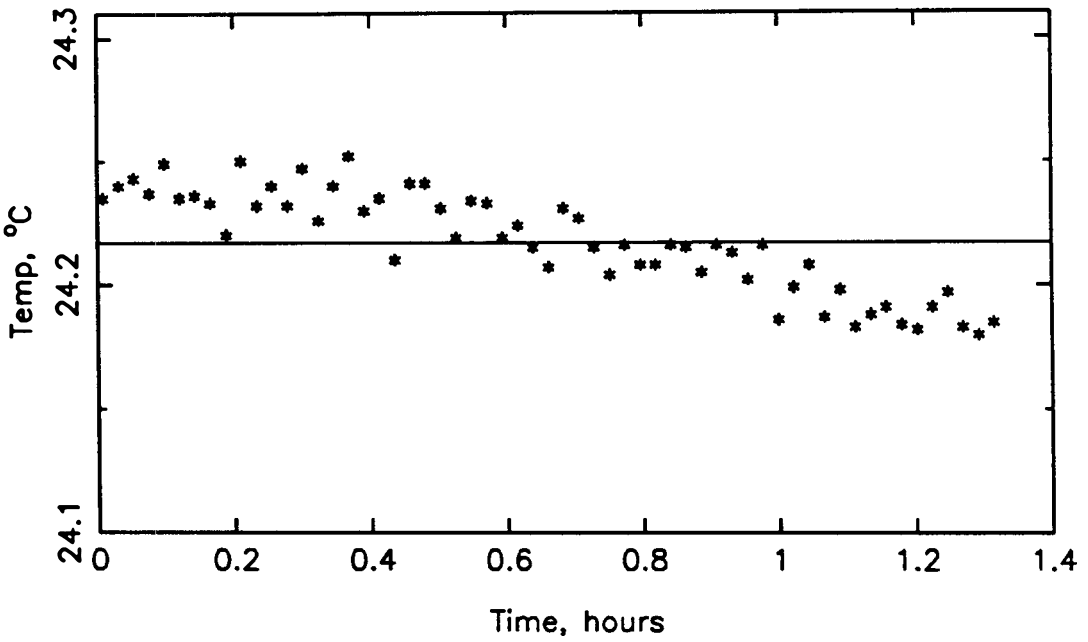

Figure F.7c Experiment 7: Effluent CSTR temperature.

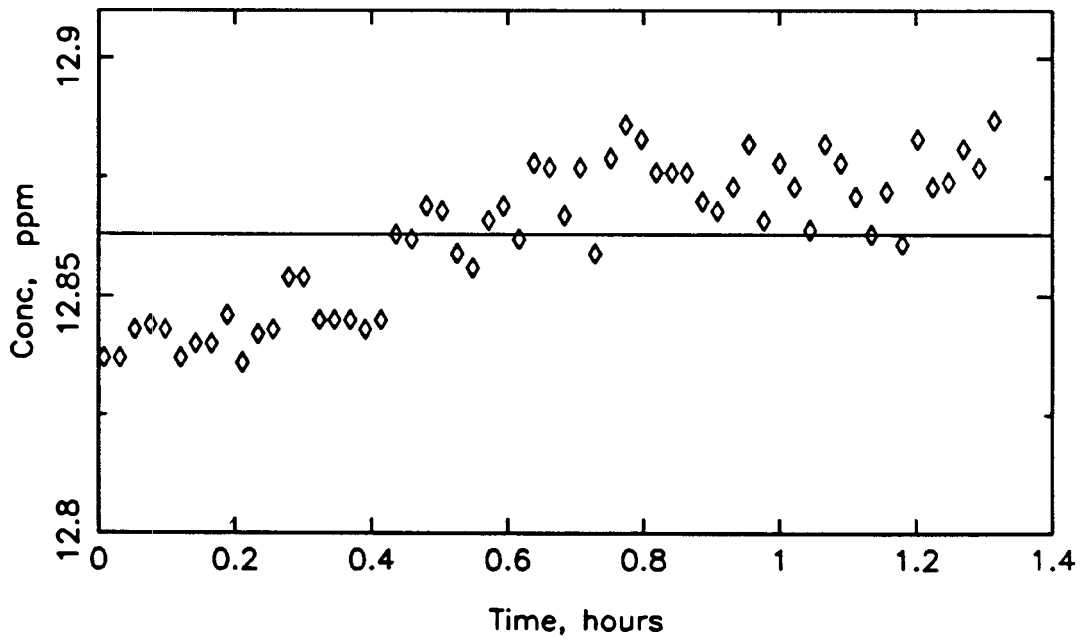

Figure F.7d Experiment 7: Effluent SO_2 concentration.

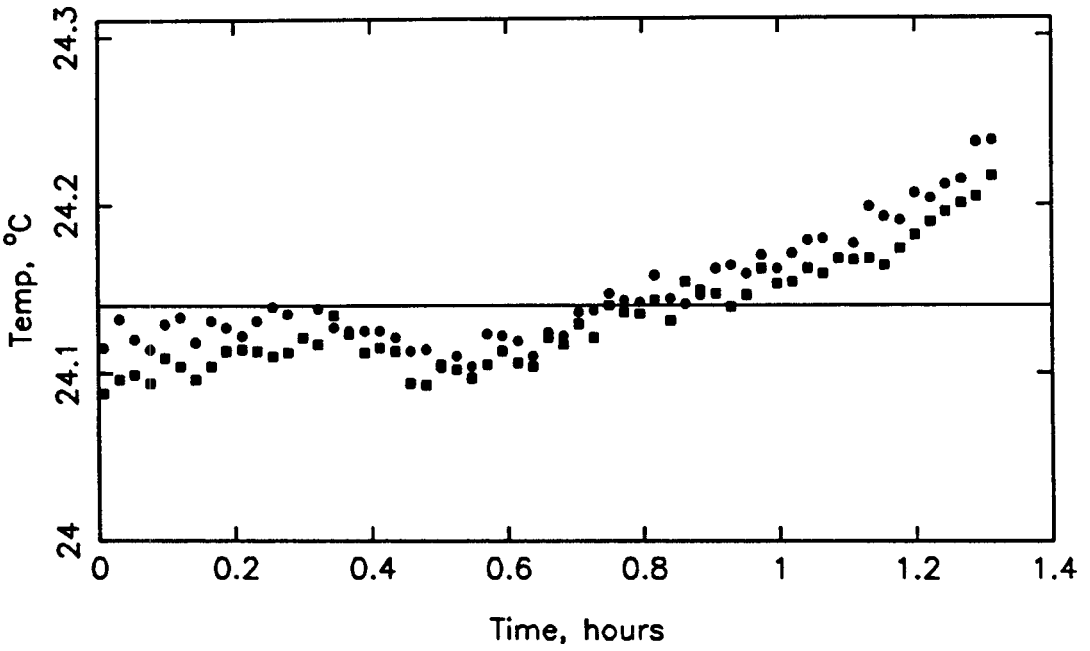

Figure F.7e Experiment 7: Feed EMC2 inlet and outlet temperatures.

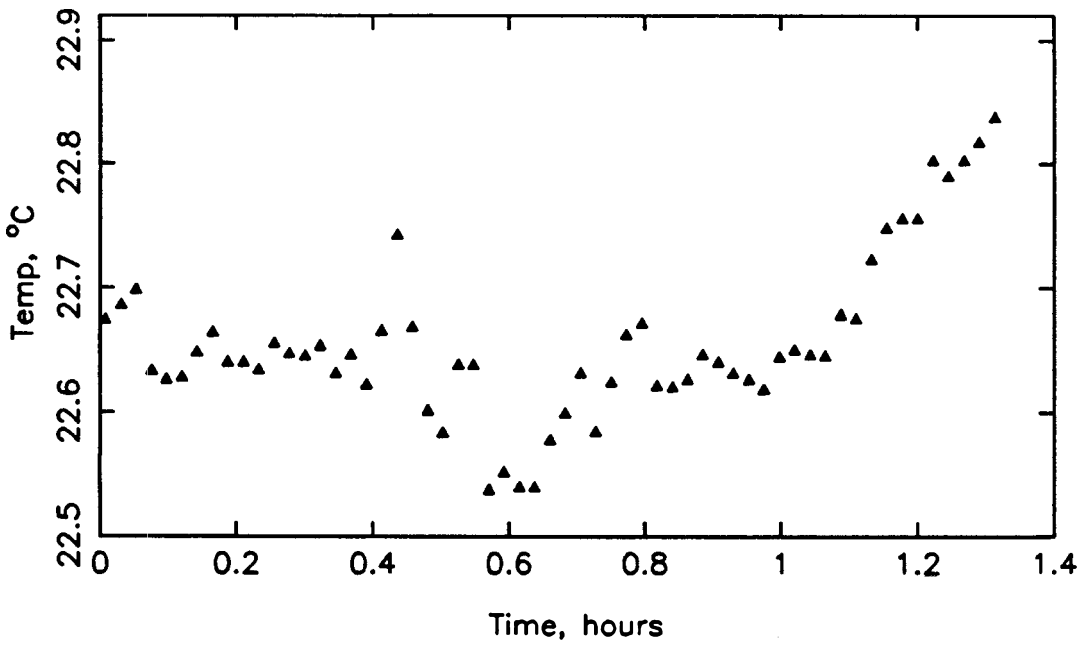

Figure F.7f Experiment 7: Feed EMC2 dew point temperature.

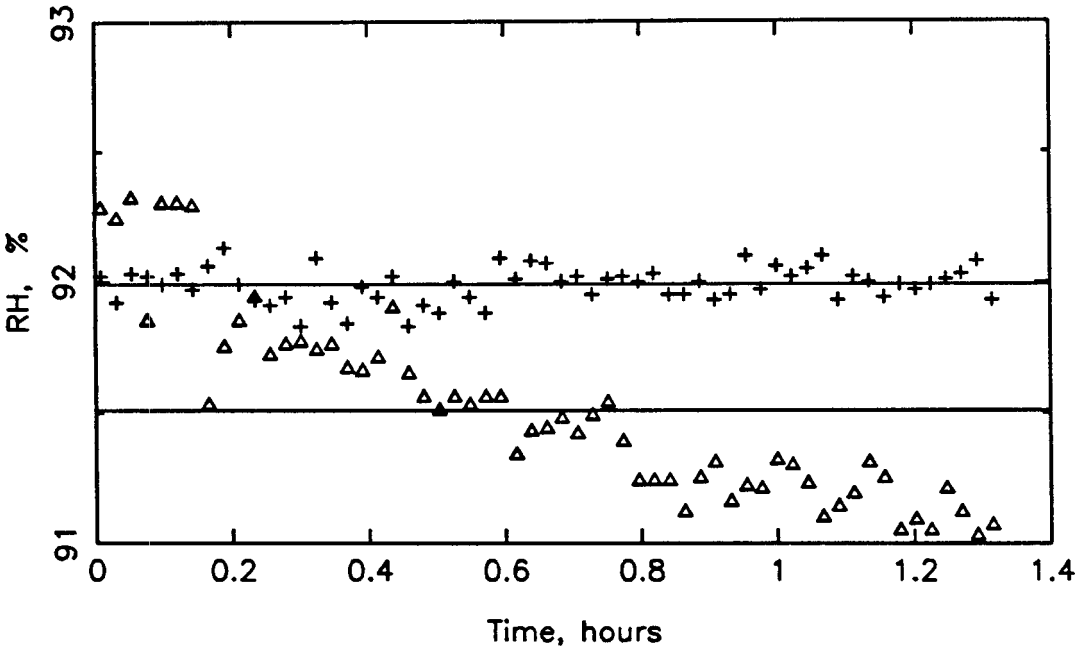

Figure F.7g Experiment 7: Effluent EMC2 and CSTR relative humidity.

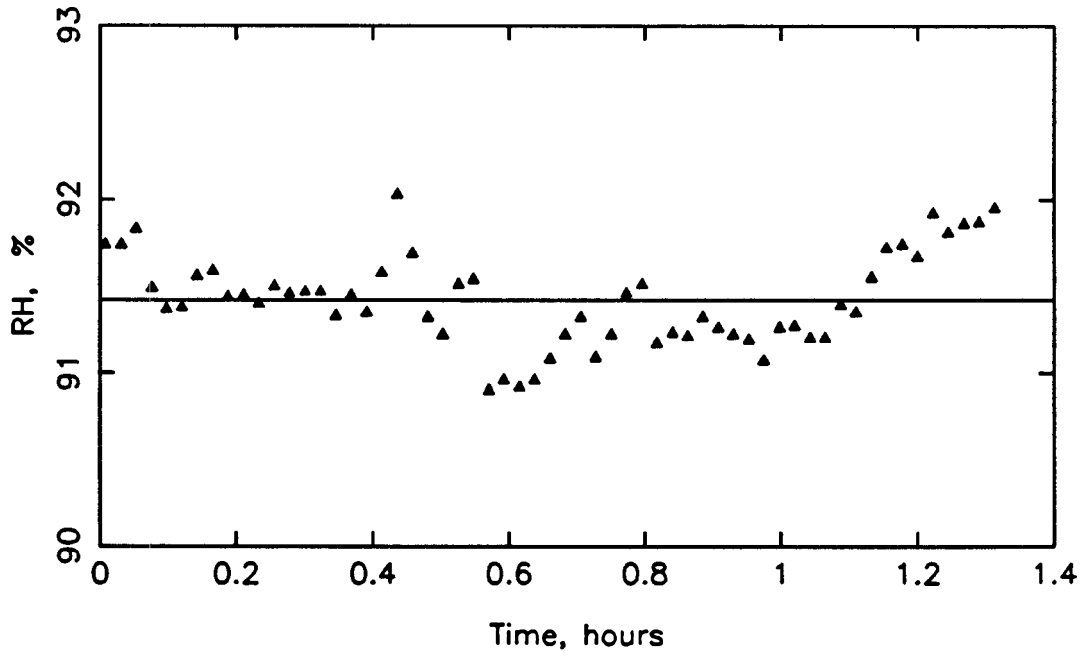

Figure F.7h Experiment 7: Feed EMC2 relative humidity.

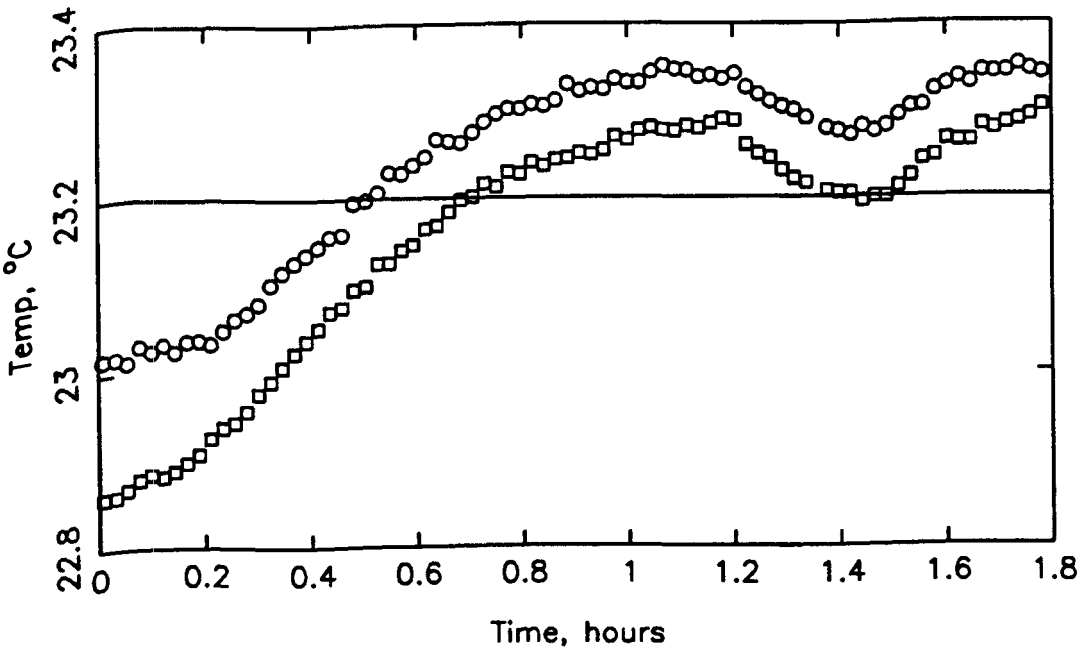

Figure F.8a Experiment 8: Effluent EMC2 inlet and outlet temperatures.

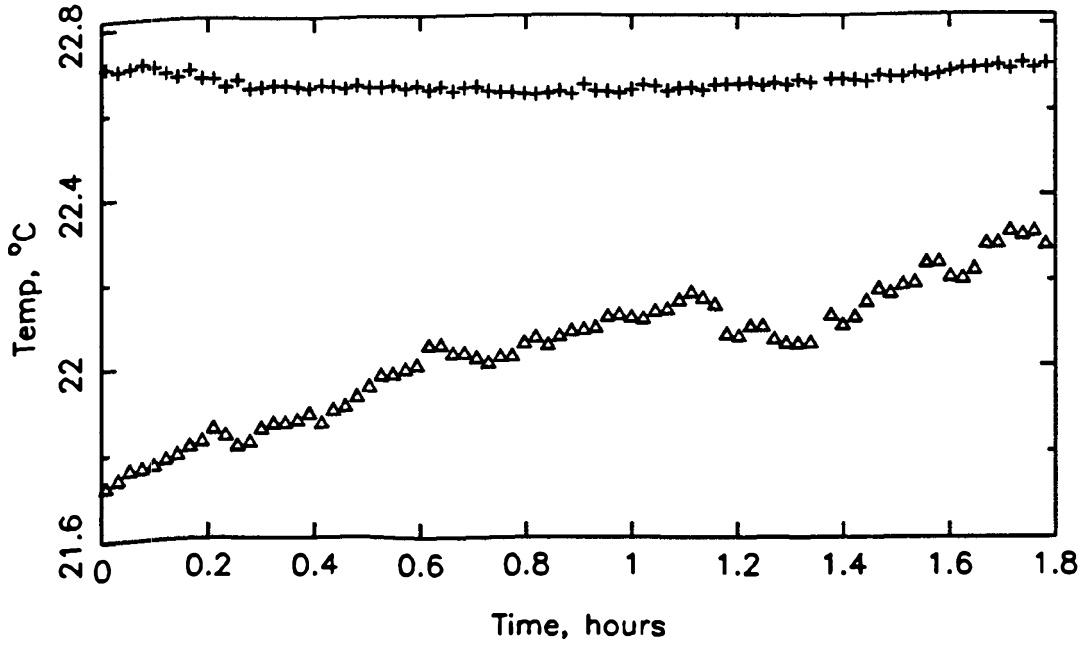

Figure F.8b Experiment 8: Effluent EMC2 and CSTR dew point temperatures.

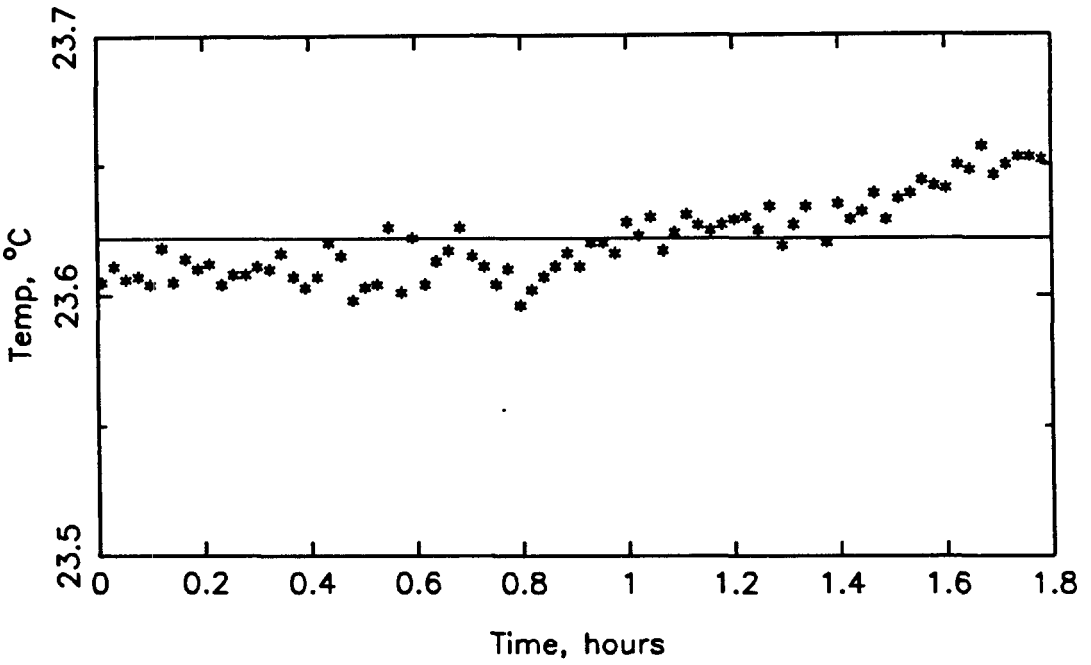

Figure F.8c Experiment 8: Effluent CSTR temperature.

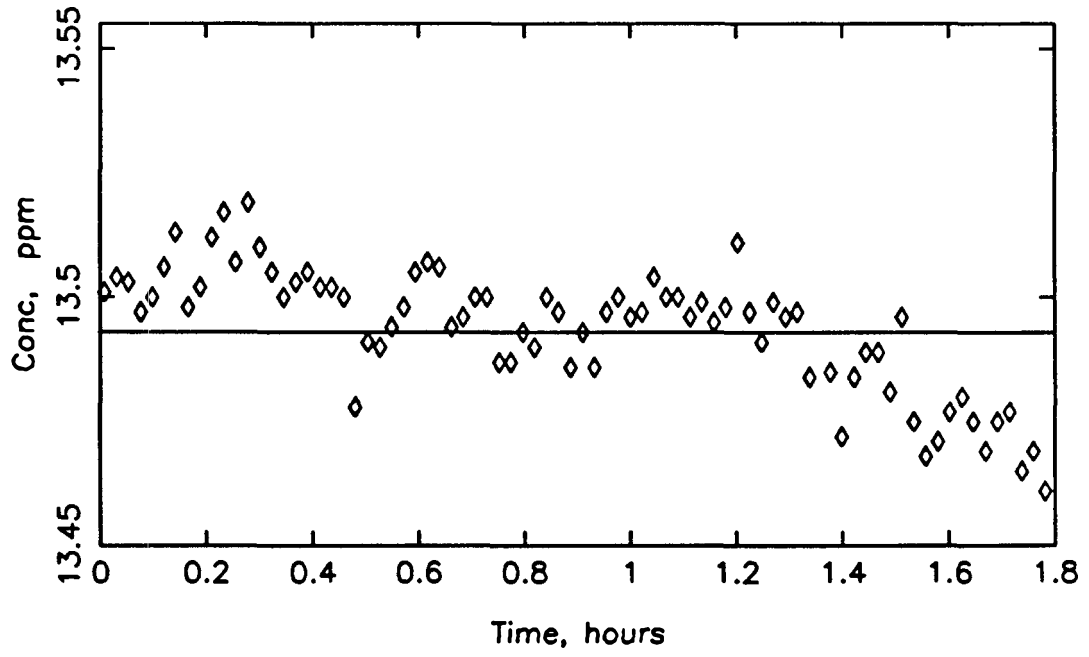

Figure F.8d Experiment 8: Effluent SO_2 concentration.

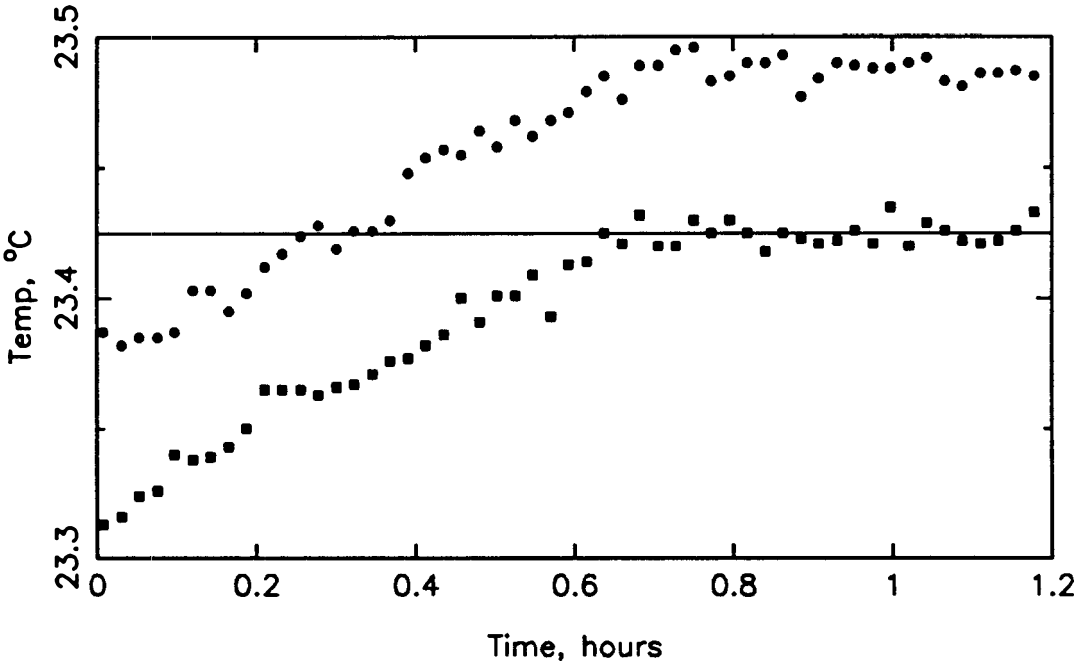

Figure F.8e Experiment 8: Feed EMC2 inlet and outlet temperatures.

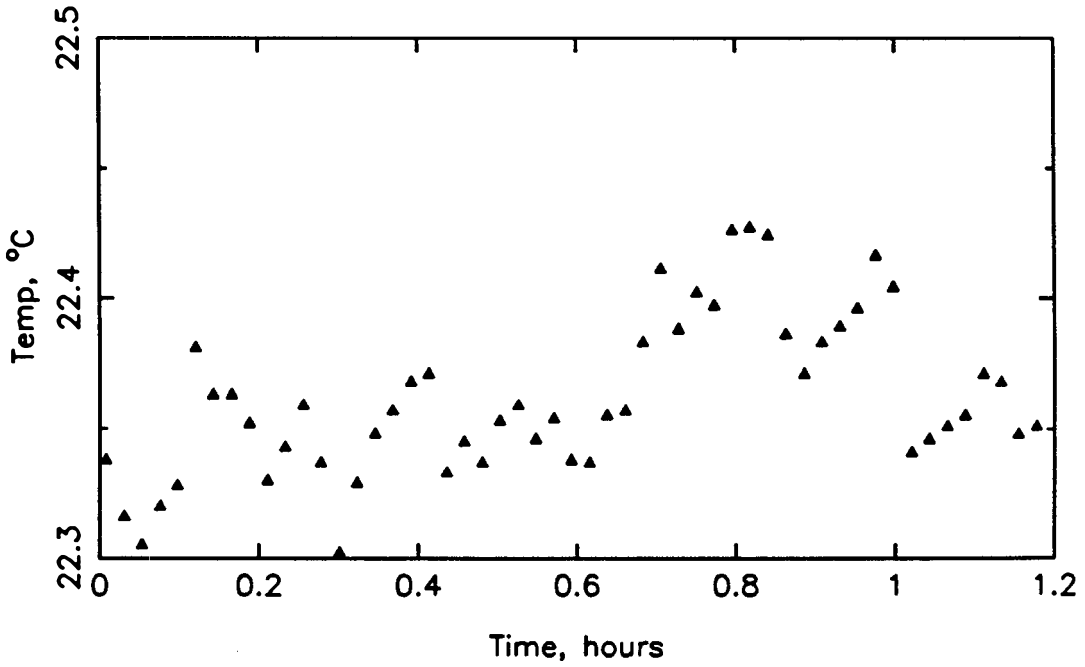

Figure F.8f Experiment 8: Feed EMC2 dew point temperature.

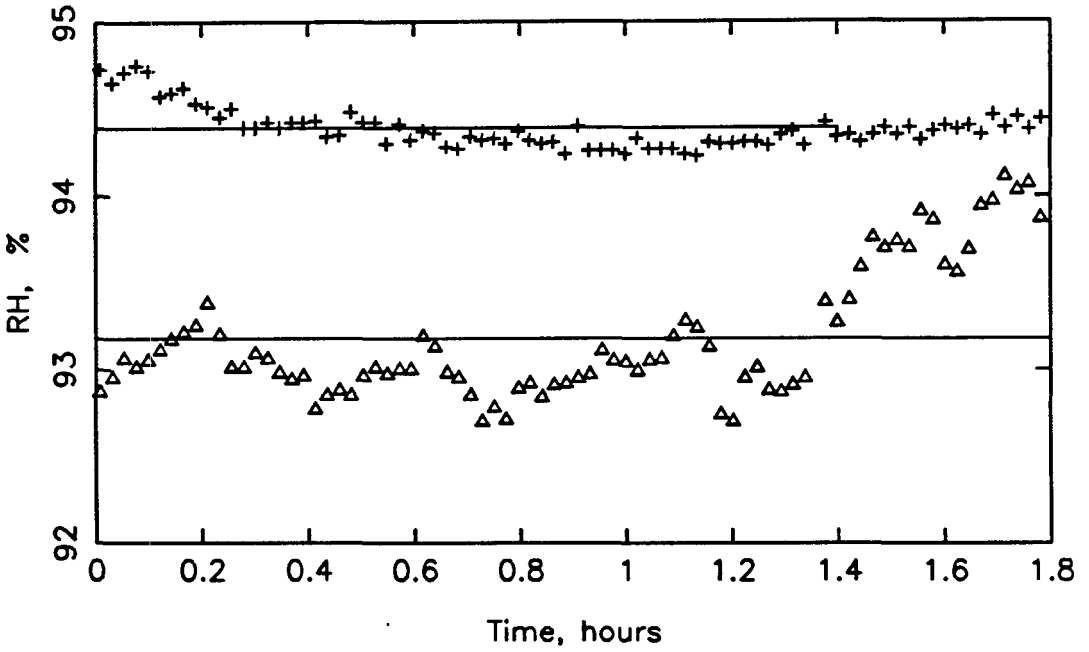

Figure F.8g Experiment 8: Effluent EMC2 and CSTR relative humidity.

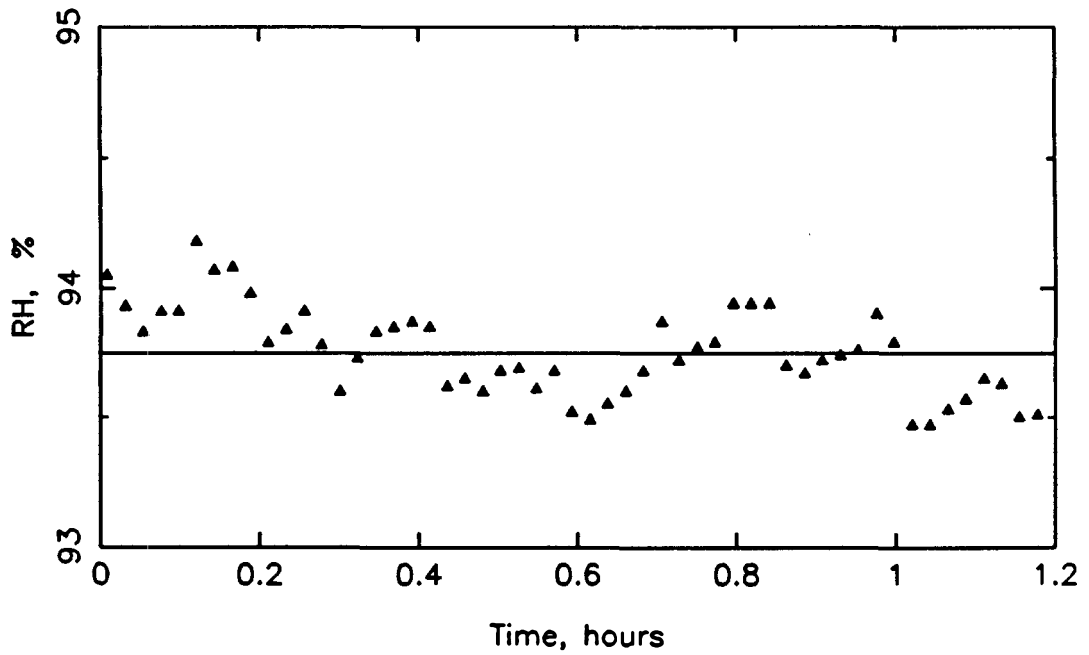

Figure F.8h Experiment 8: Feed EMC2 relative humidity.

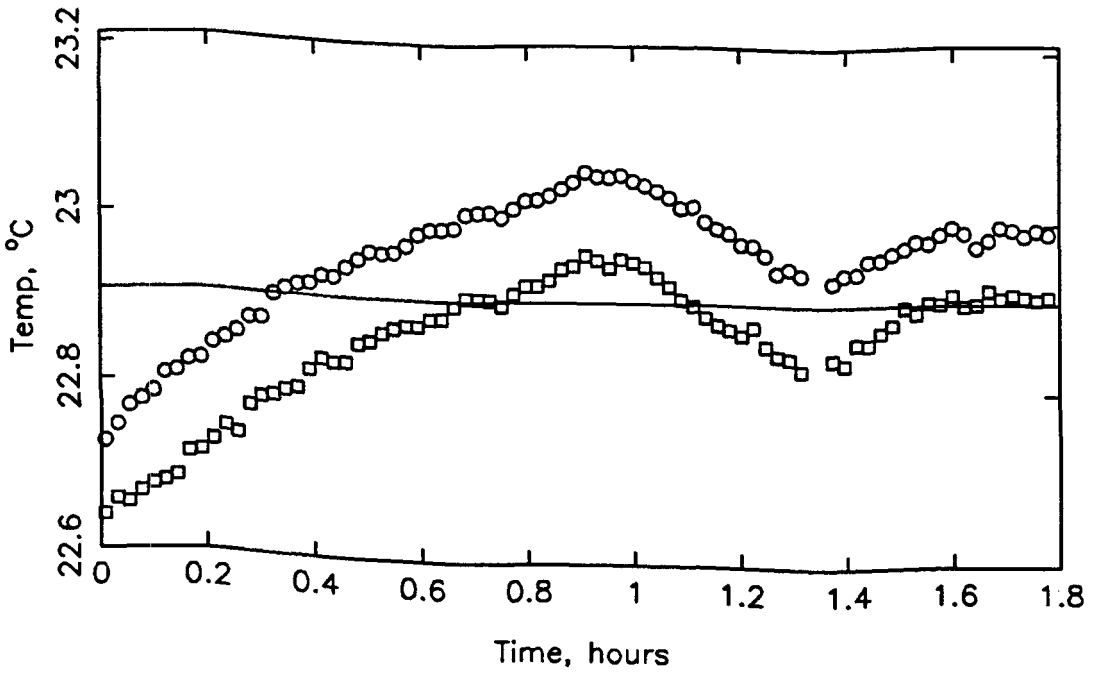

Figure F.9a Experiment 9: Effluent EMC2 inlet and outlet temperatures.

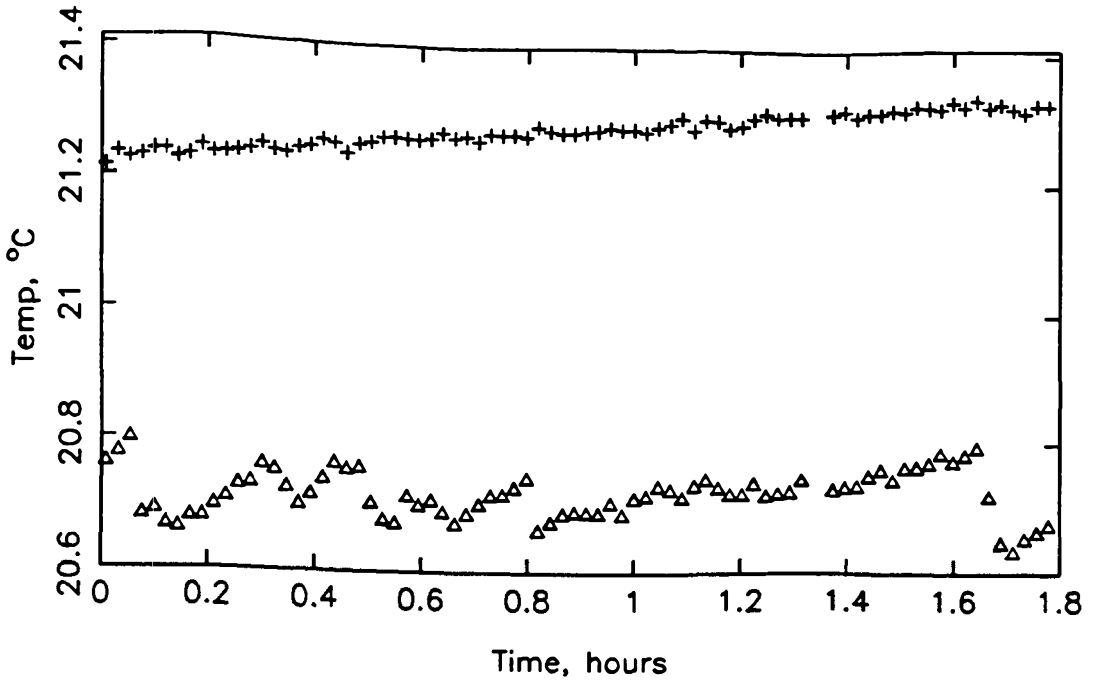

Figure F.9b Experiment 9: Effluent EMC2 and CSTR dew point temperatures.

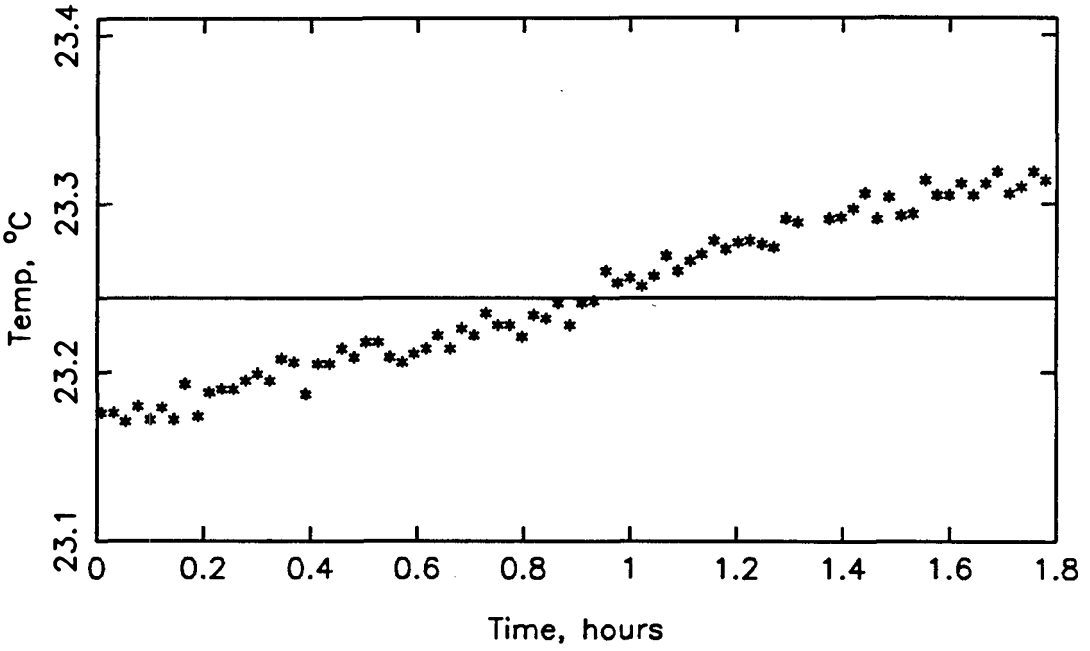

Figure F.9c Experiment 9: Effluent CSTR temperature.

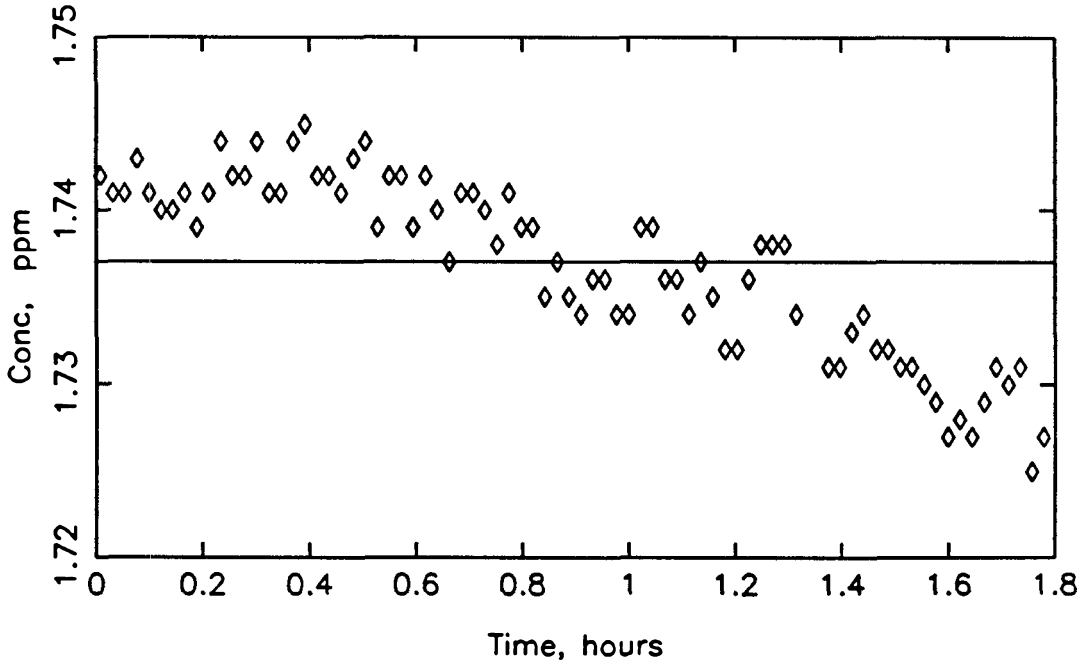

Figure F.9d Experiment 9: Effluent SO_2 concentration.

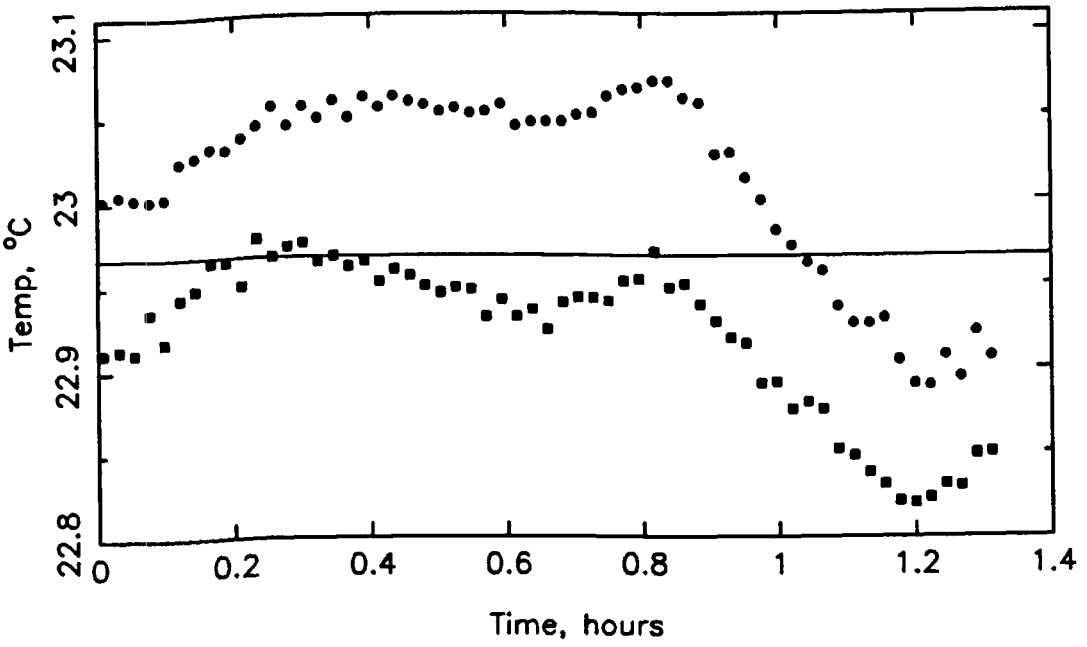

Figure F.9e Experiment 9: Feed EMC2 inlet and outlet temperatures.

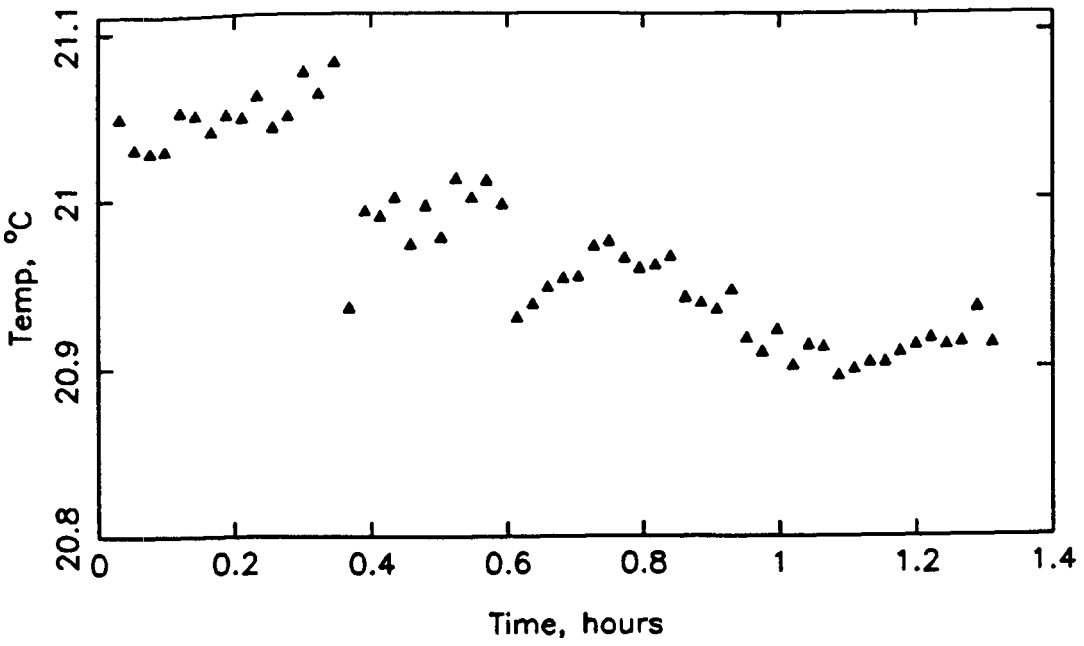

Figure F.9f Experiment 9: Feed EMC2 dew point temperature.

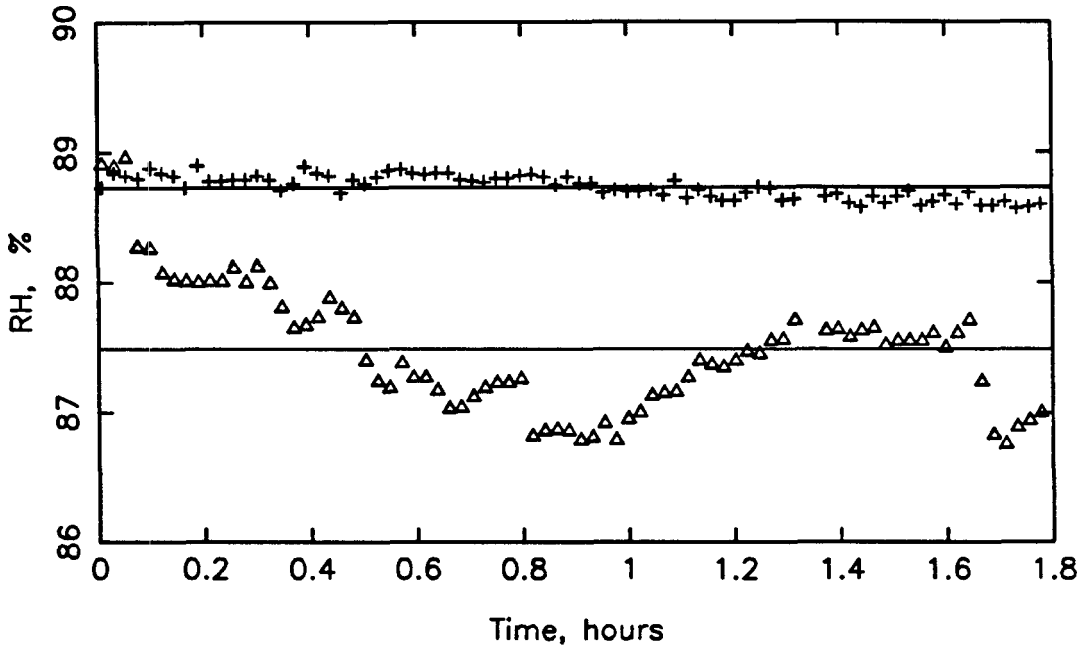

Figure F.9g Experiment 9: Effluent EMC2 and CSTR relative humidity.

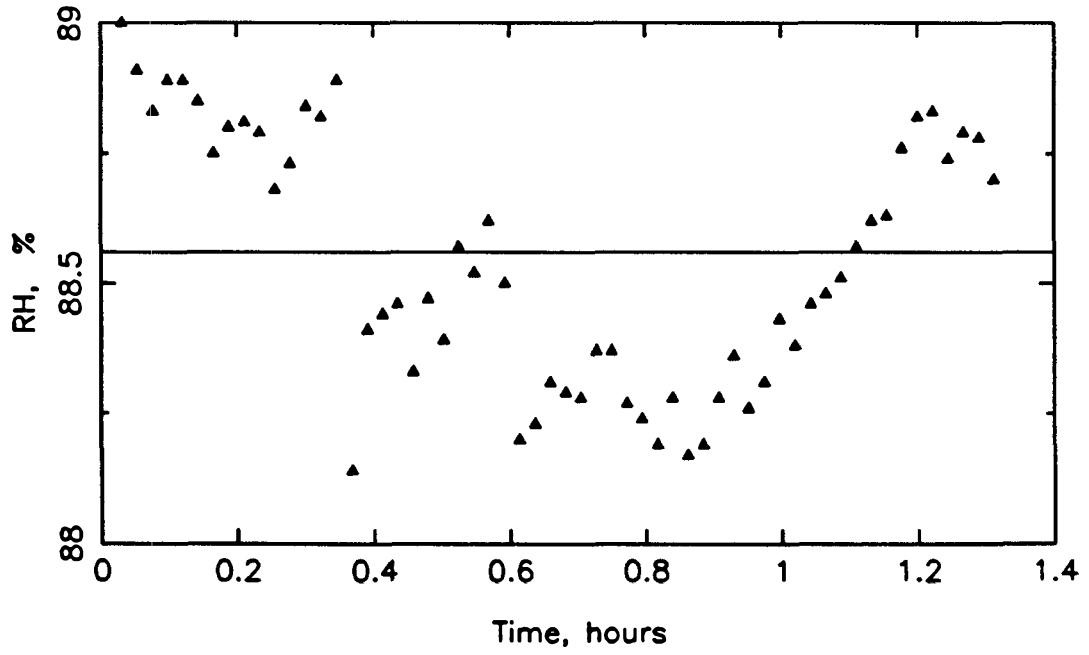

Figure F.9h Experiment 9: Feed EMC2 relative humidity.

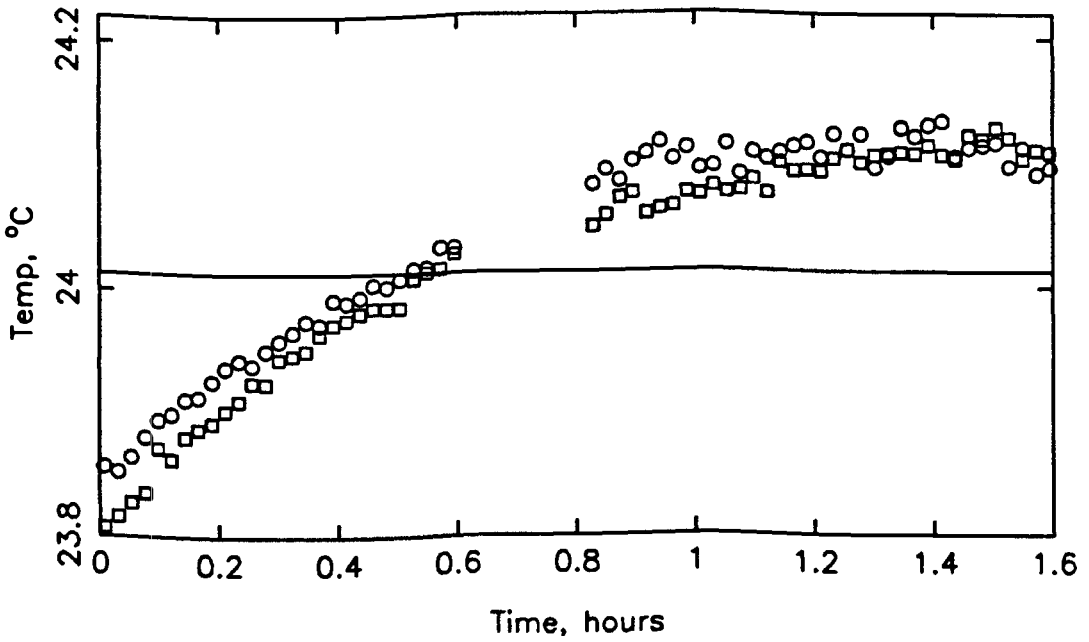

Figure F.10a Experiment 10: Effluent EMC2 inlet and outlet temperatures.

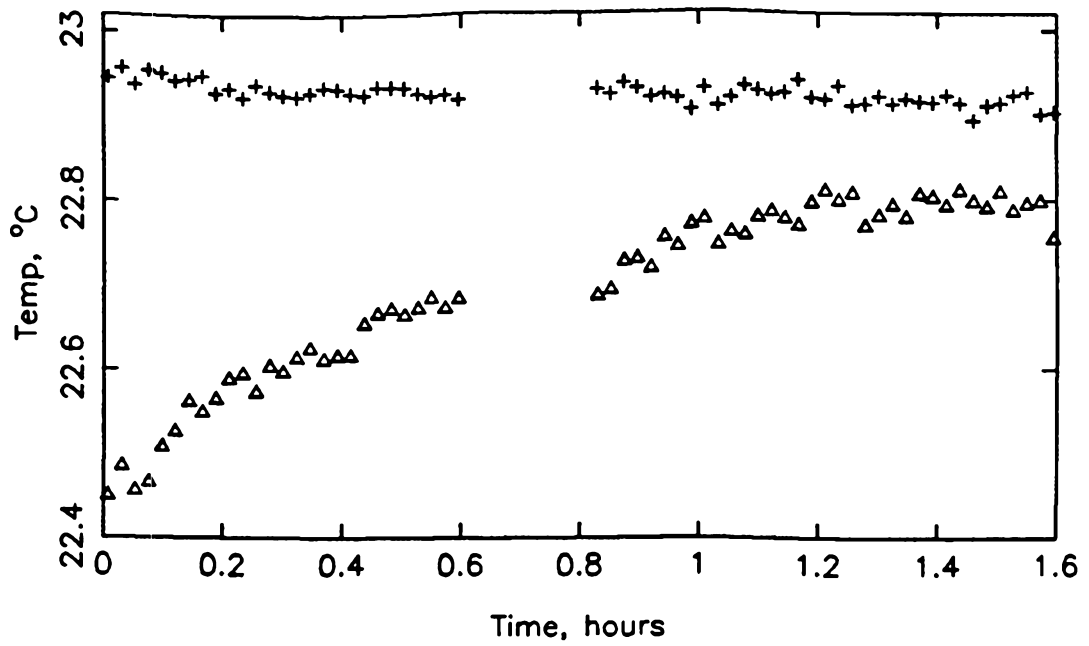

Figure F.10b Experiment 10: Effluent EMC2 and CSTR dew point temperatures.

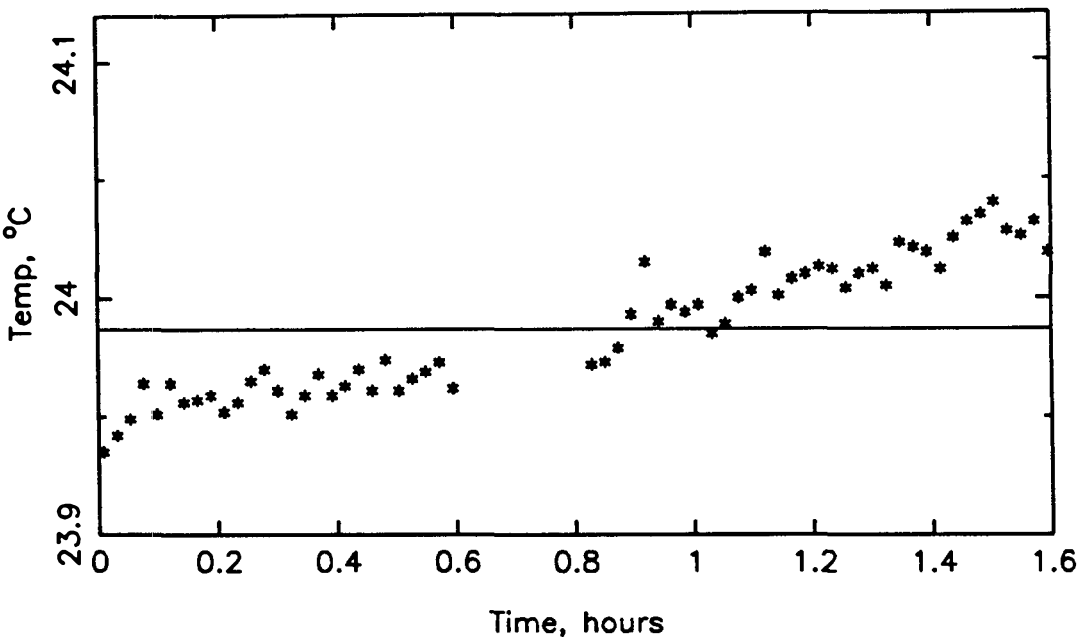

Figure F.10c Experiment 10: Effluent CSTR temperature.

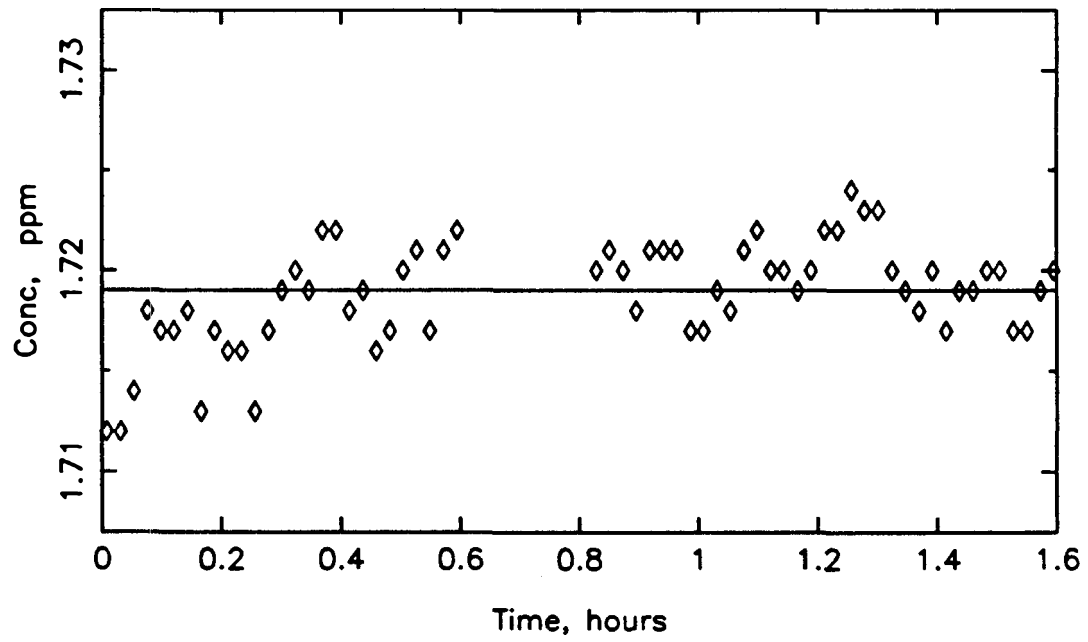

Figure F.10d Experiment 10: Effluent SO_2 concentration.

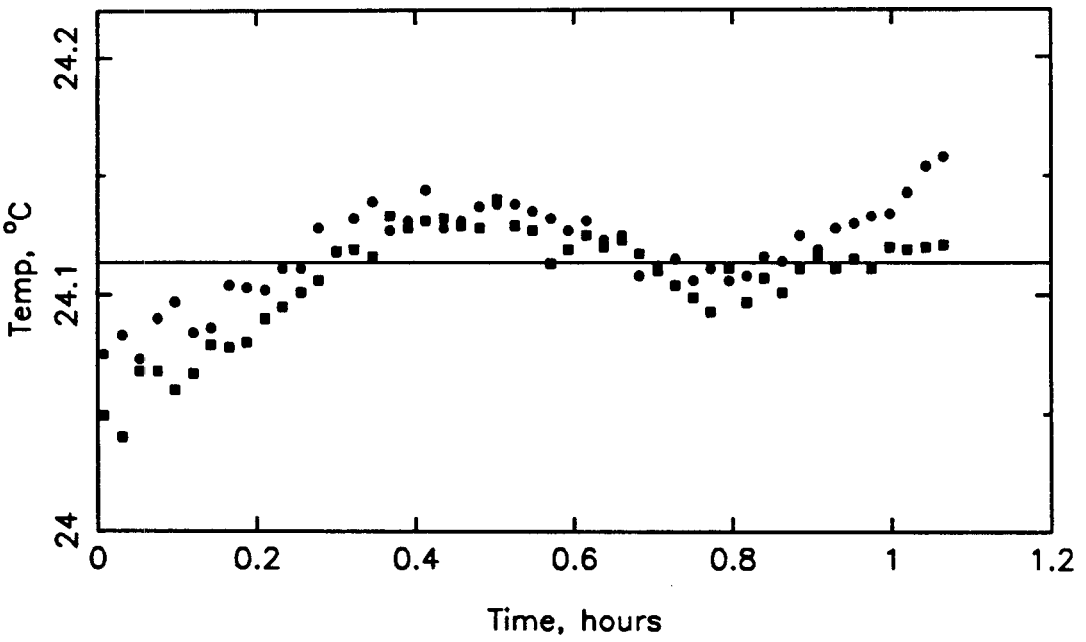

Figure F.10e Experiment 10: Feed EMC2 inlet and outlet temperatures.

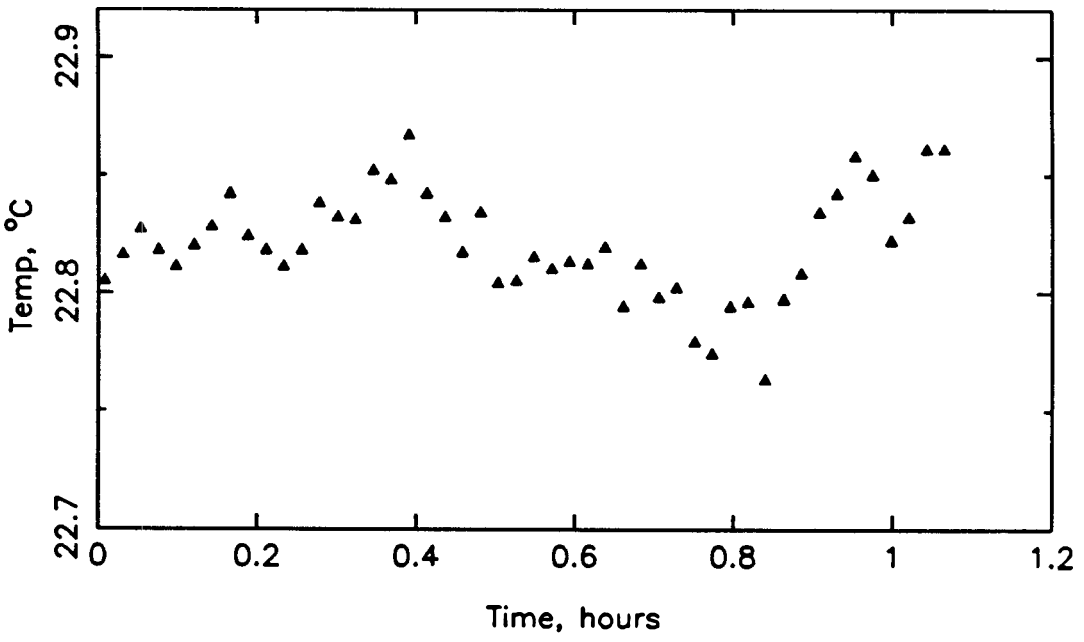

Figure F.10f Experiment 10: Feed EMC2 dew point temperature.

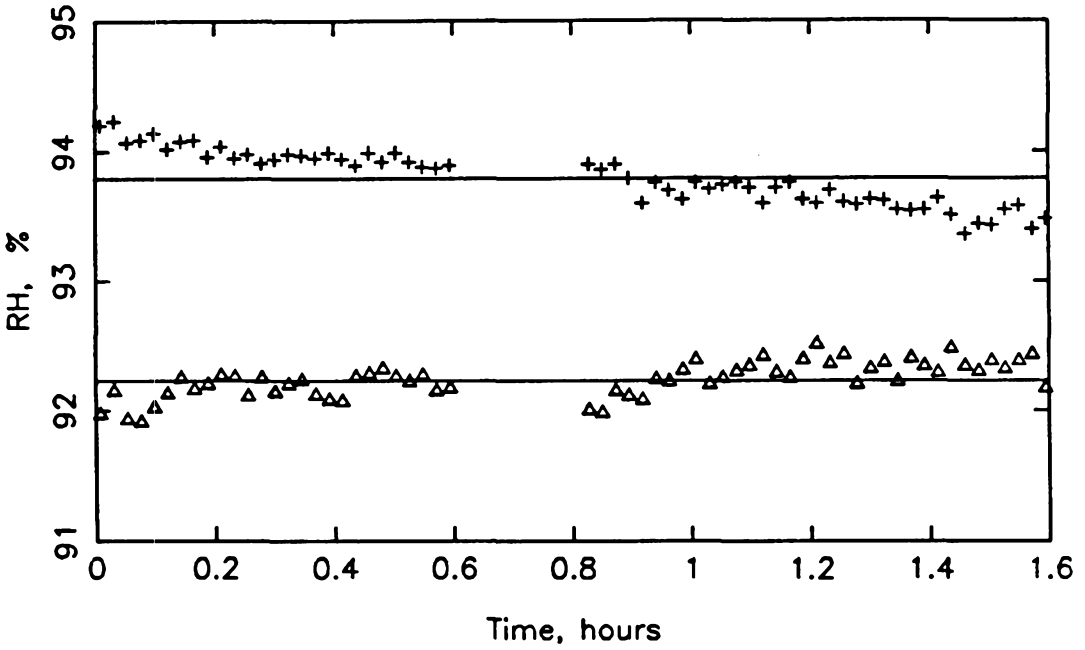

Figure F.10g Experiment 10: Effluent EMC2 and CSTR relative humidity.

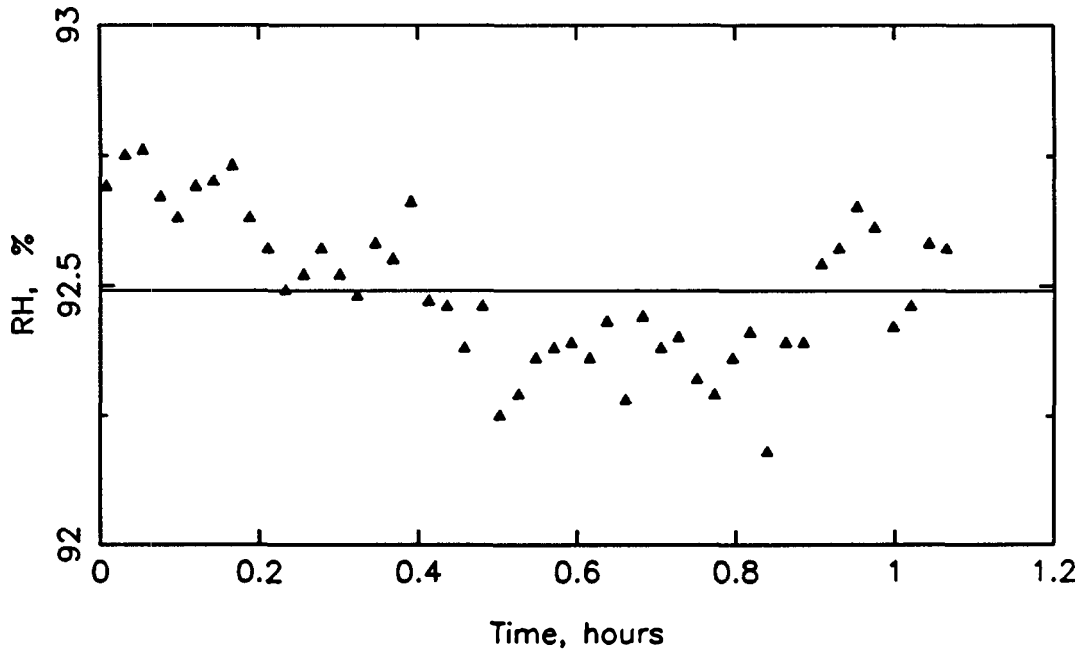

Figure F.10h Experiment 10: Feed EMC2 relative humidity.

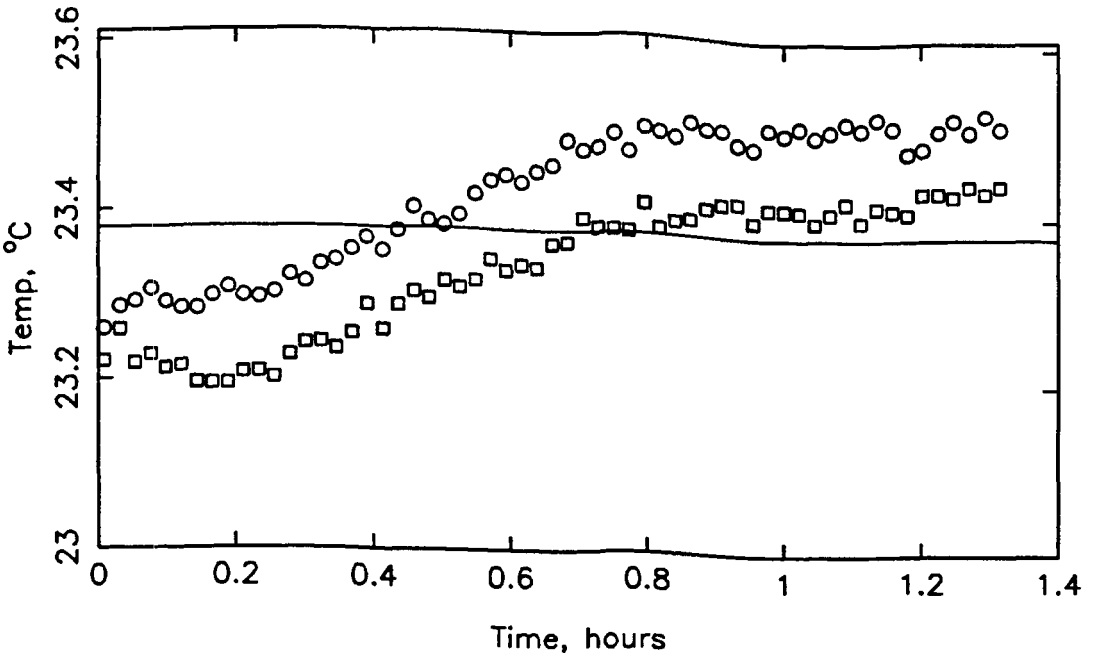

Figure F.11a Experiment 11: Effluent EMC2 inlet and outlet temperatures.

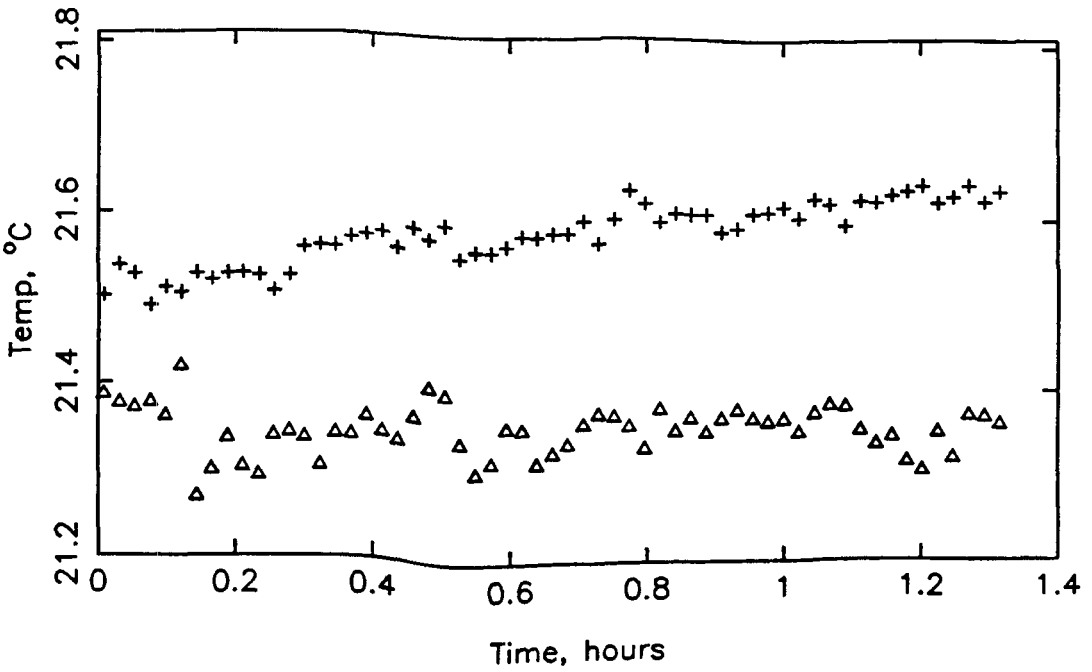

Figure F.11b Experiment 11: Effluent EMC2 and CSTR dew point temperatures.

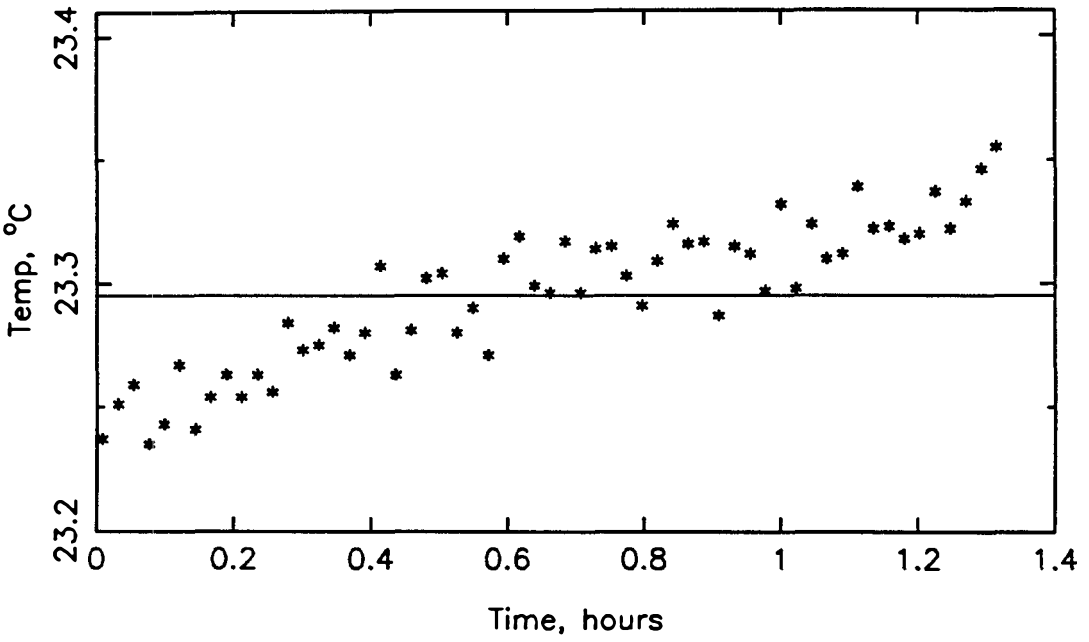

Figure F.11c Experiment 11: Effluent CSTR temperature.

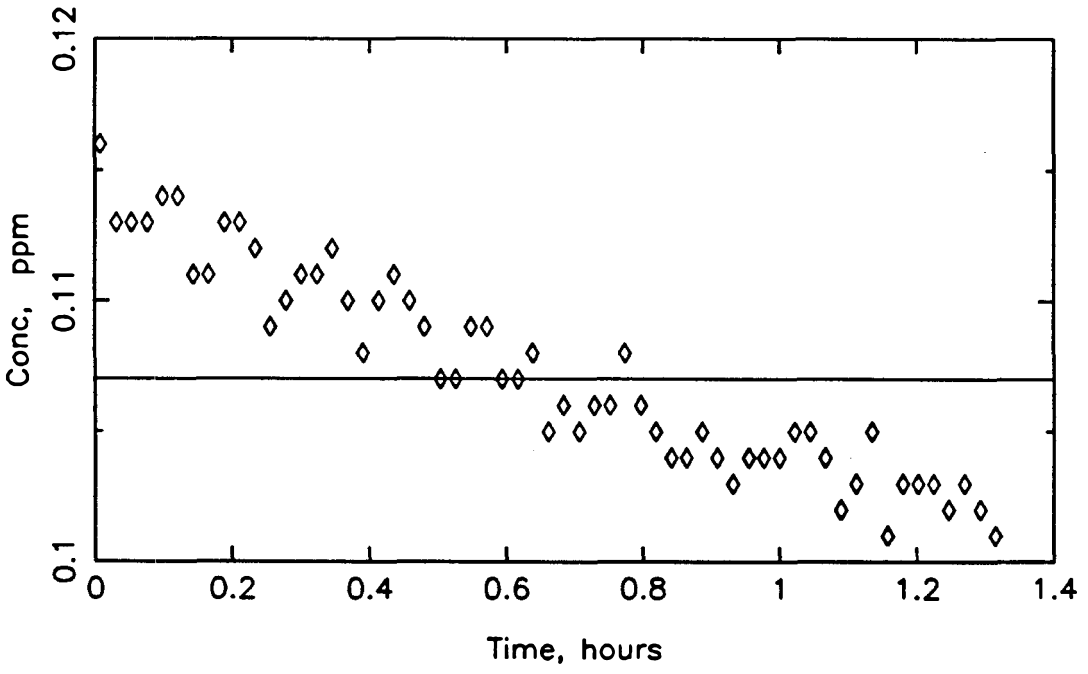

Figure F.11d Experiment 11: Effluent SO_2 concentration.

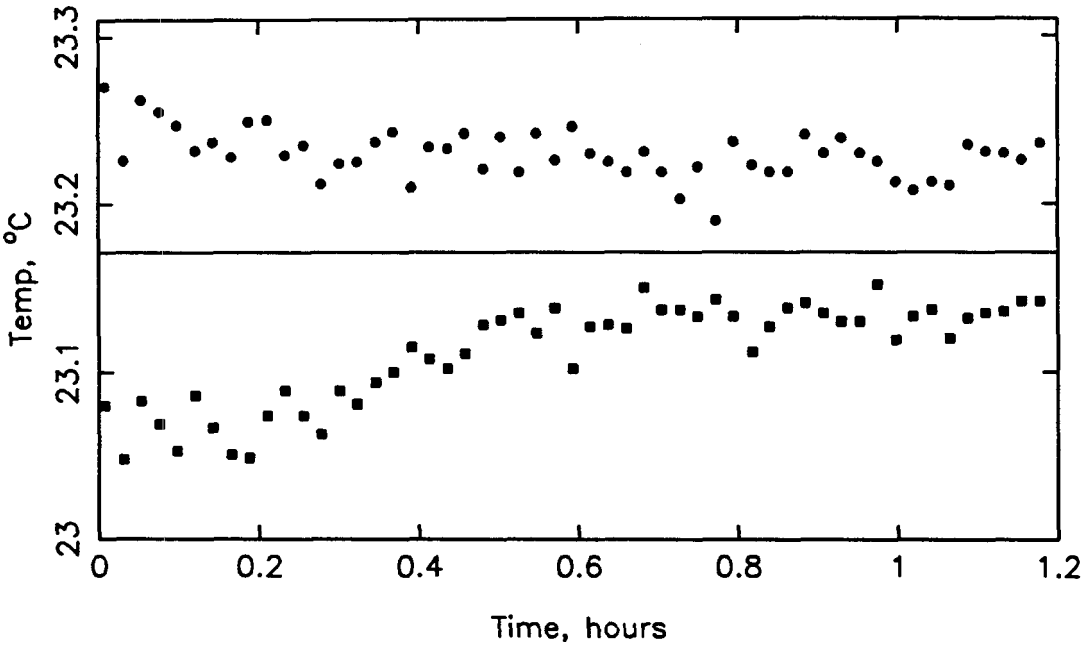

Figure F.11e Experiment 11: Feed EMC2 inlet and outlet temperatures.

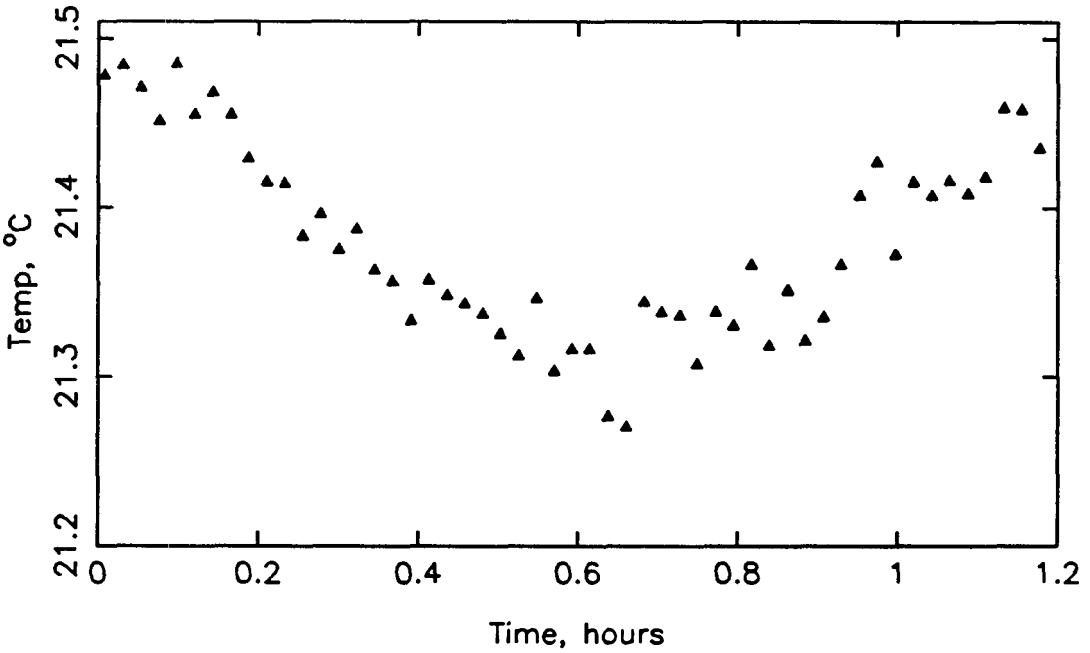

Figure F.11f Experiment 11: Feed EMC2 dew point temperature.

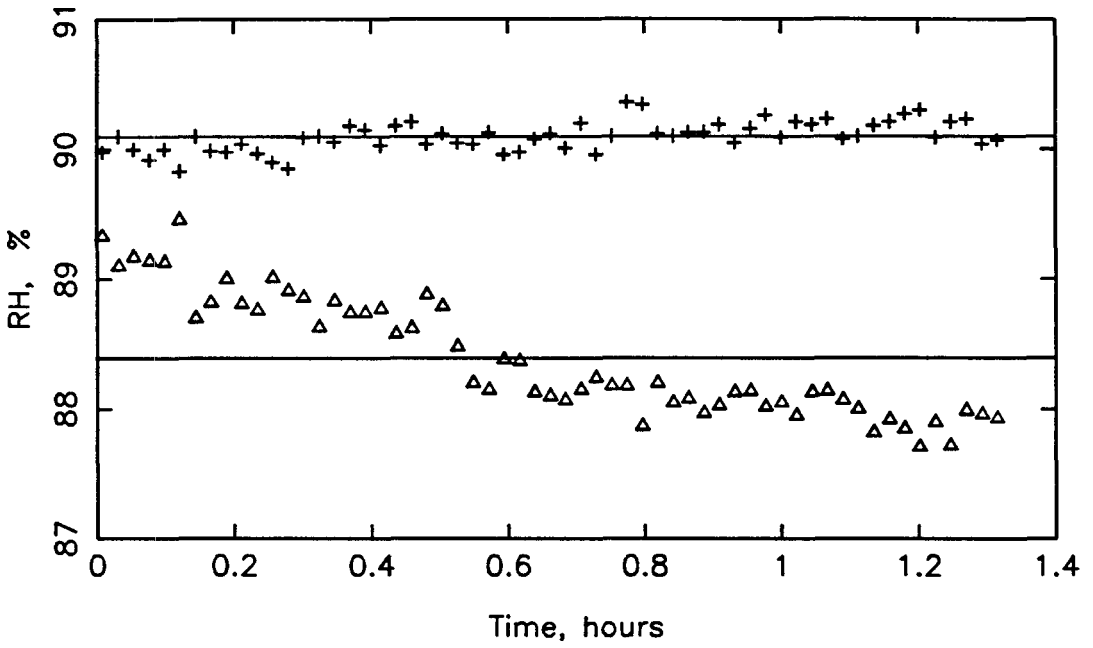

Figure F.11g Experiment 11: Effluent EMC2 and CSTR relative humidity.

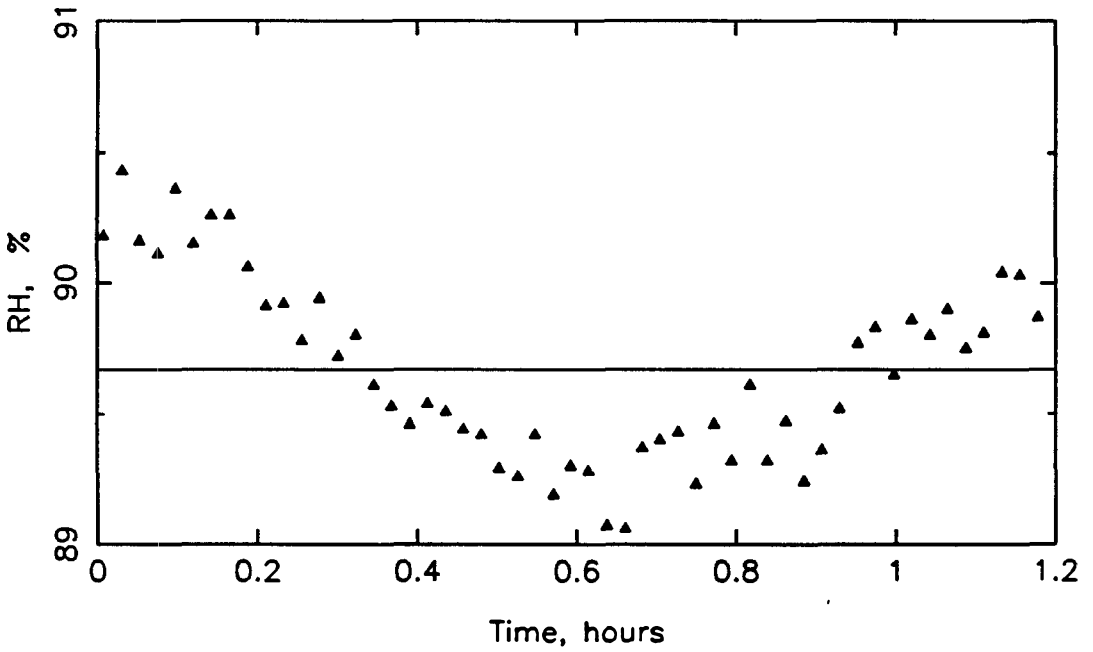

Figure F.11h Experiment 11: Feed EMC2 relative humidity.

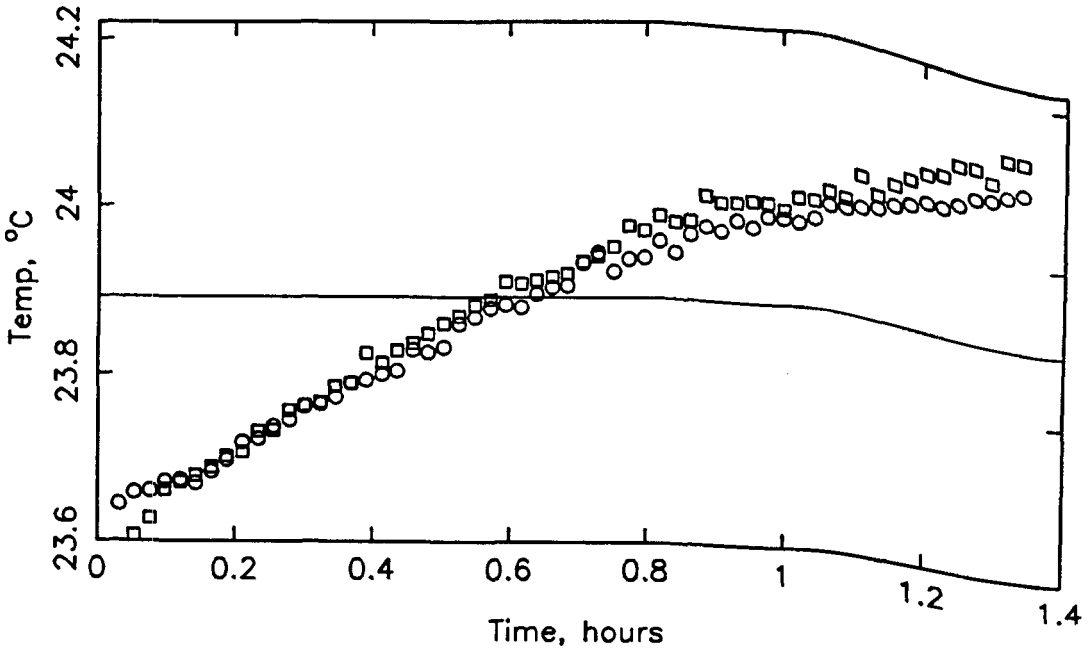

Figure F.12a Experiment 12: Effluent EMC2 inlet and outlet temperatures.

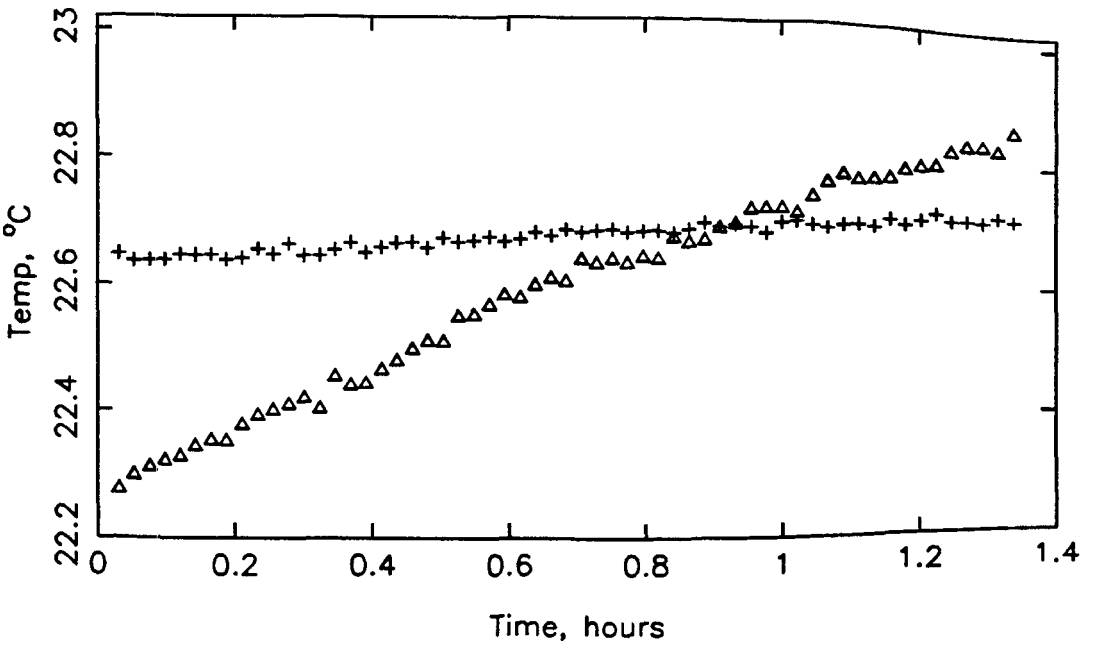

Figure F.12b Experiment 12: Effluent EMC2 and CSTR dew point temperatures.

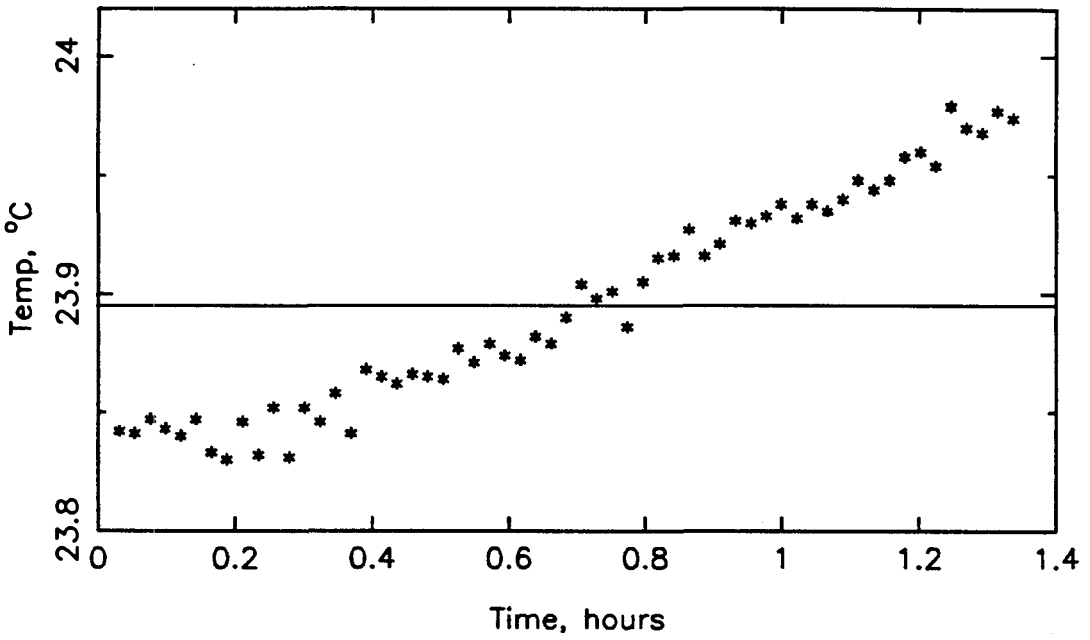

Figure F.12c Experiment 12: Effluent CSTR temperature.

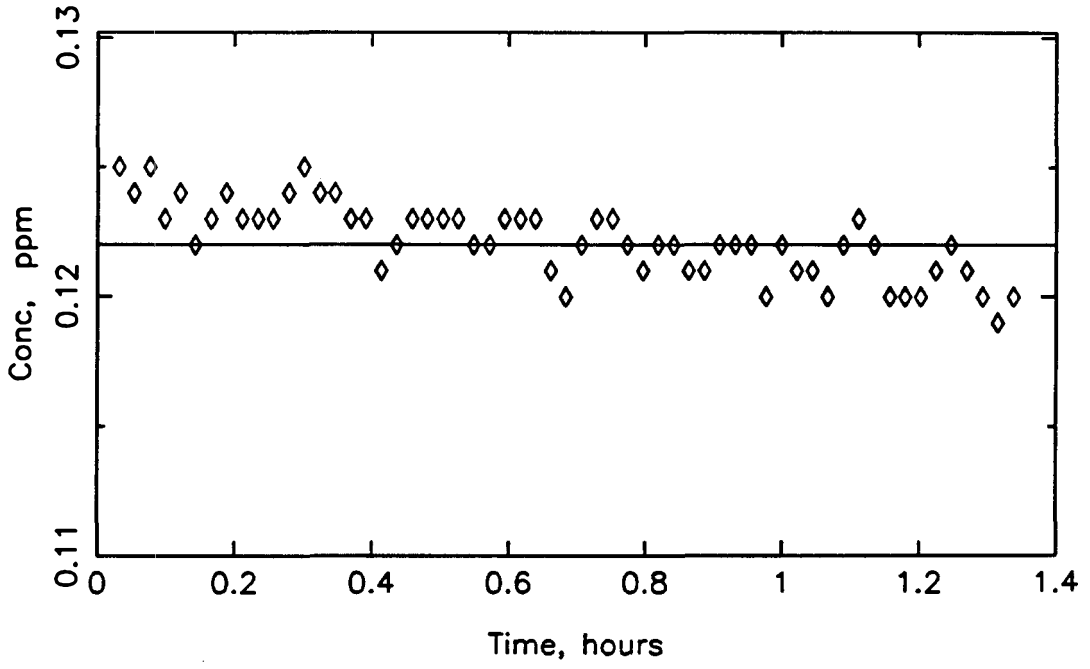

Figure F.12d Experiment 12: Effluent SO_2 concentration.

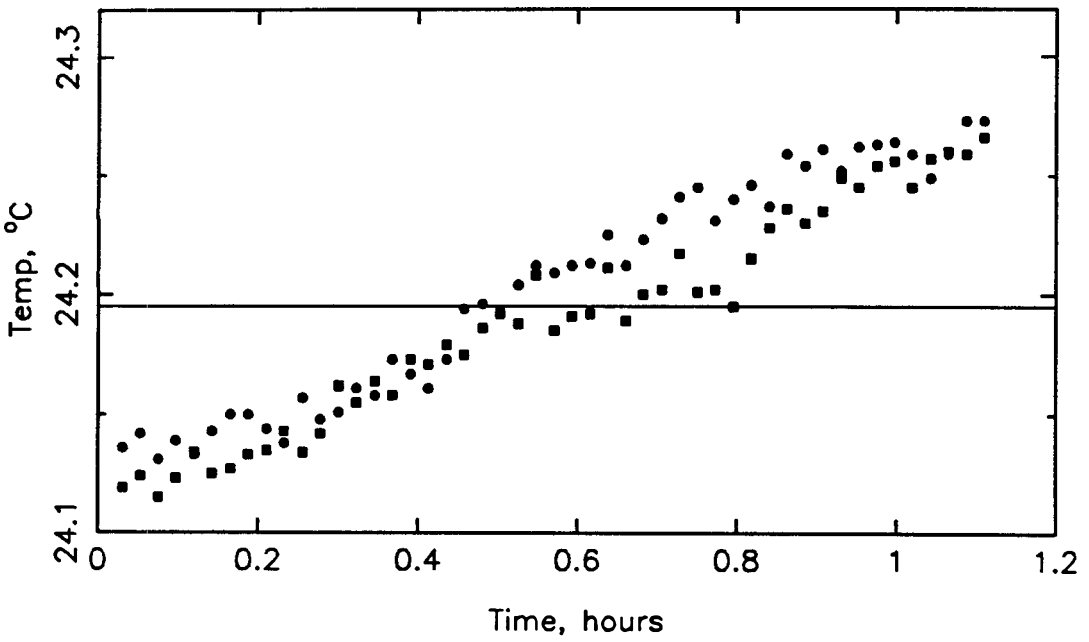

Figure F.12e Experiment 12: Feed EMC2 inlet and outlet temperatures.

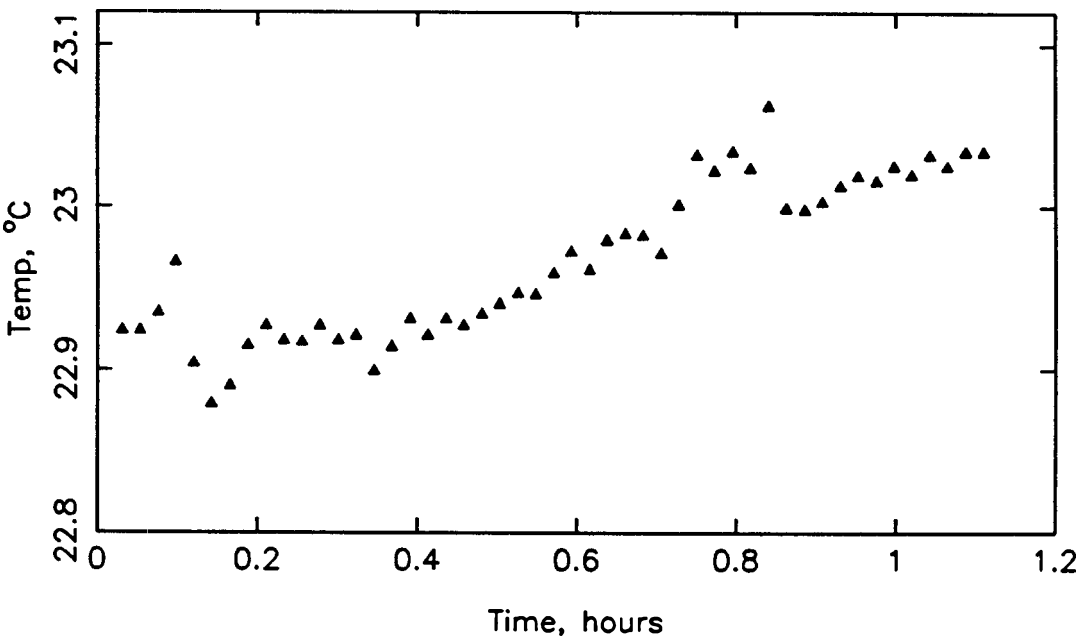

Figure F.12f Experiment 12: Feed EMC2 dew point temperature.

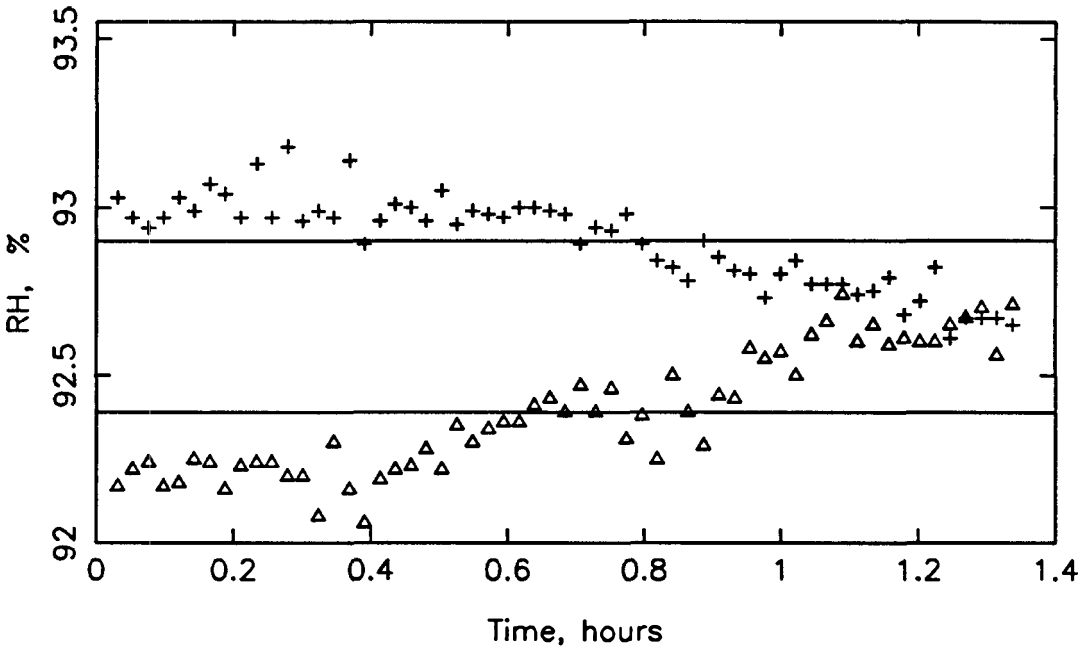

Figure F.12g Experiment 12: Effluent EMC2 and CSTR relative humidity.

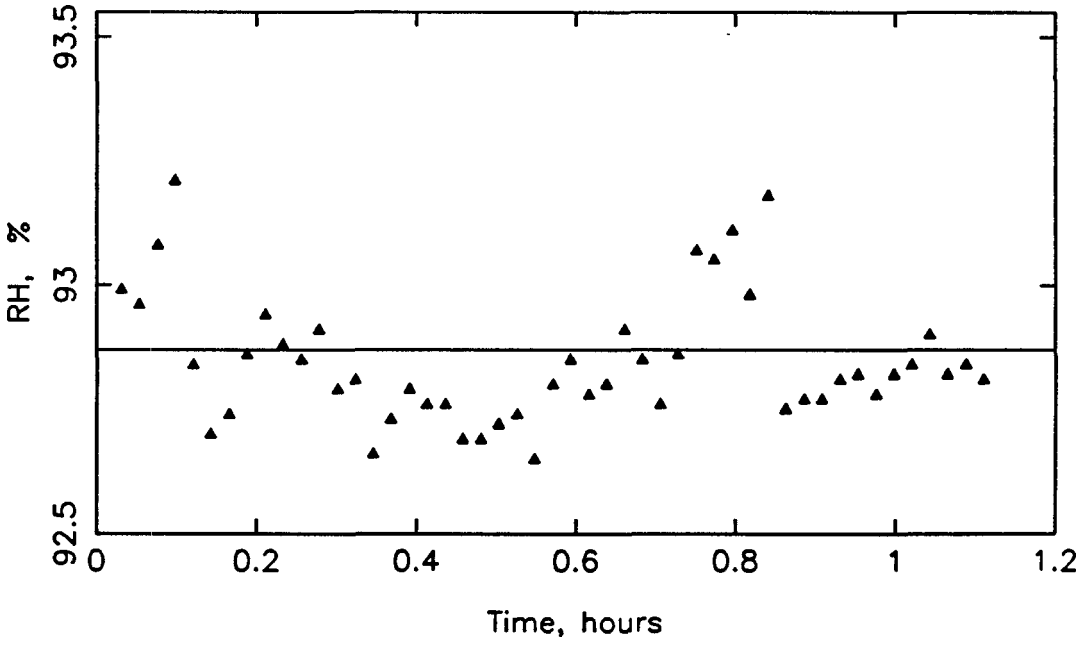

Figure F.12h Experiment 12: Feed EMC2 relative humidity.

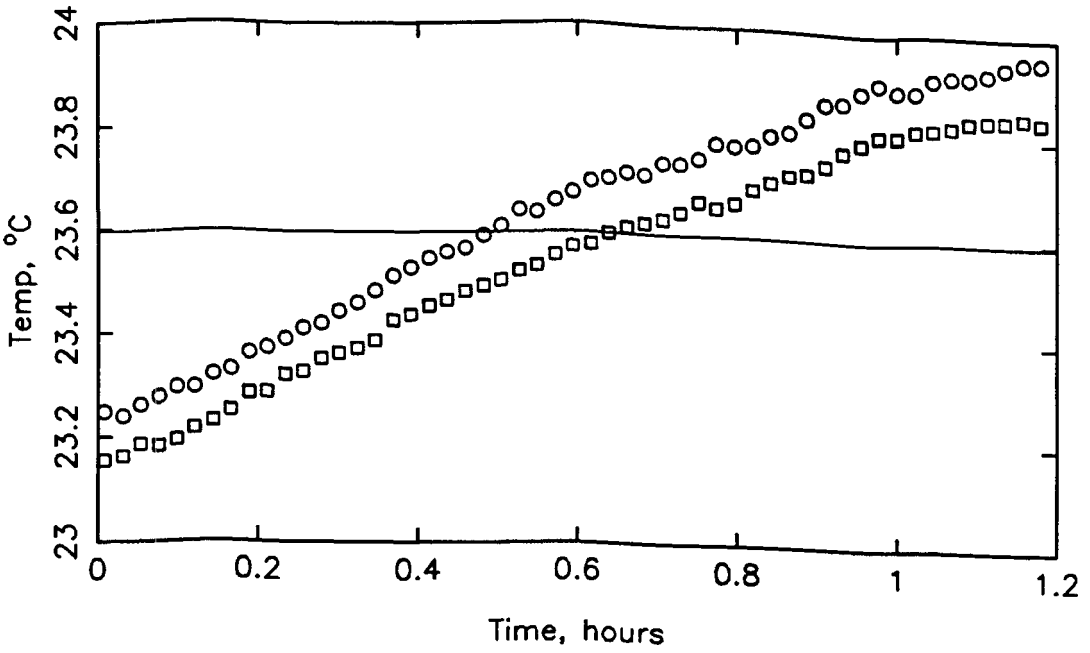

Figure F.13a Experiment 13: Effluent EMC2 inlet and outlet temperatures.

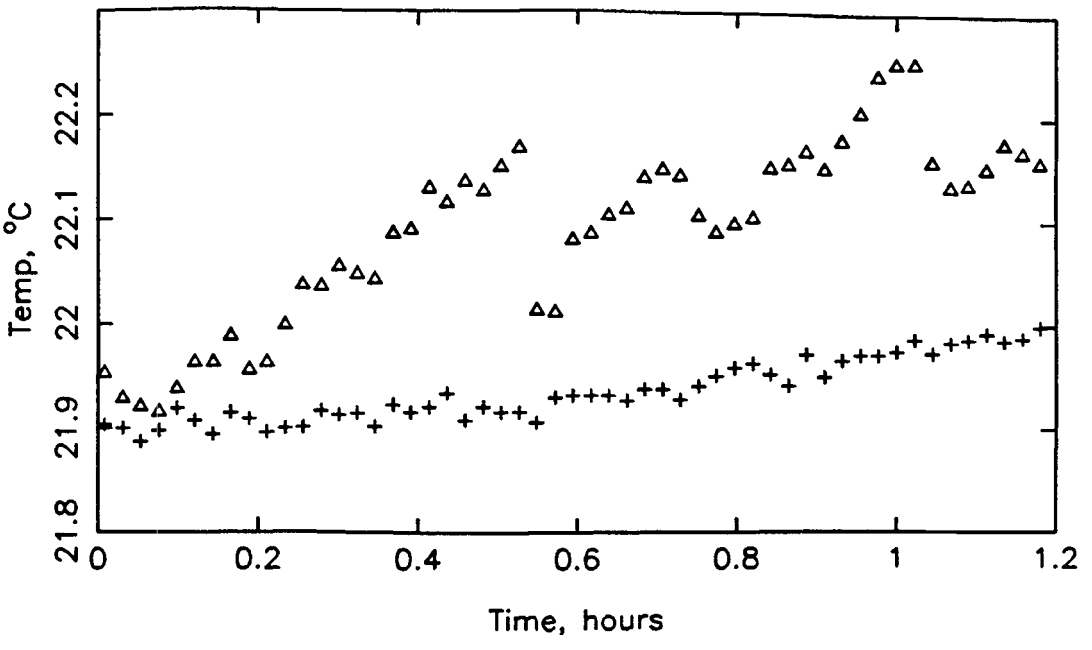

Figure F.13b Experiment 13: Effluent EMC2 and CSTR dew point temperatures.

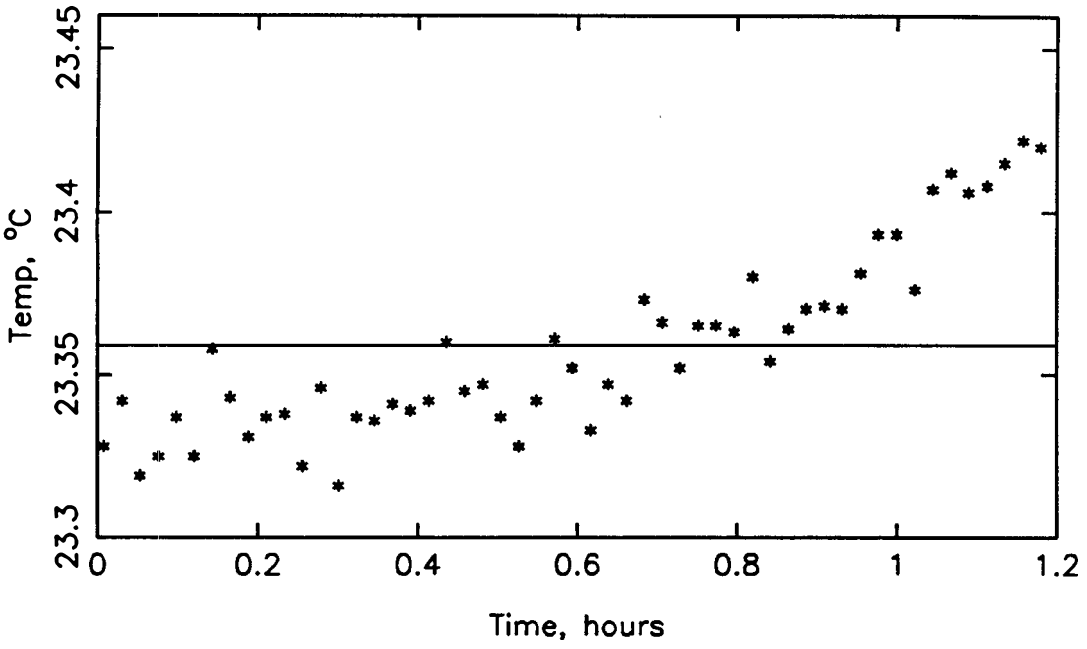

Figure F.13c Experiment 13: Effluent CSTR temperature.

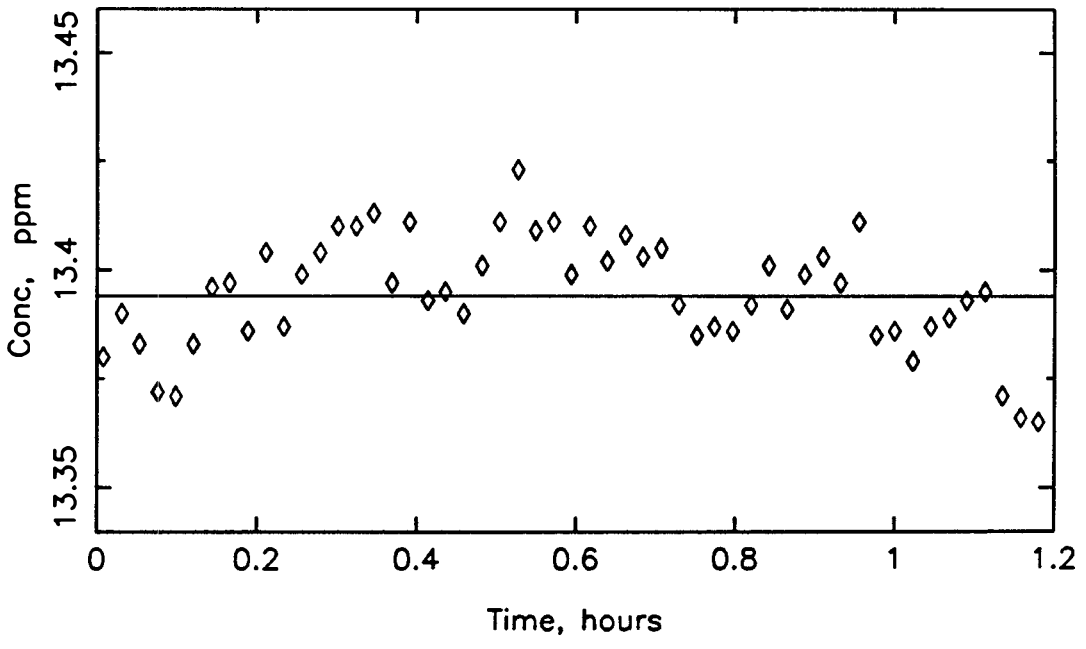

Figure F.13d Experiment 13: Effluent SO_2 concentration.

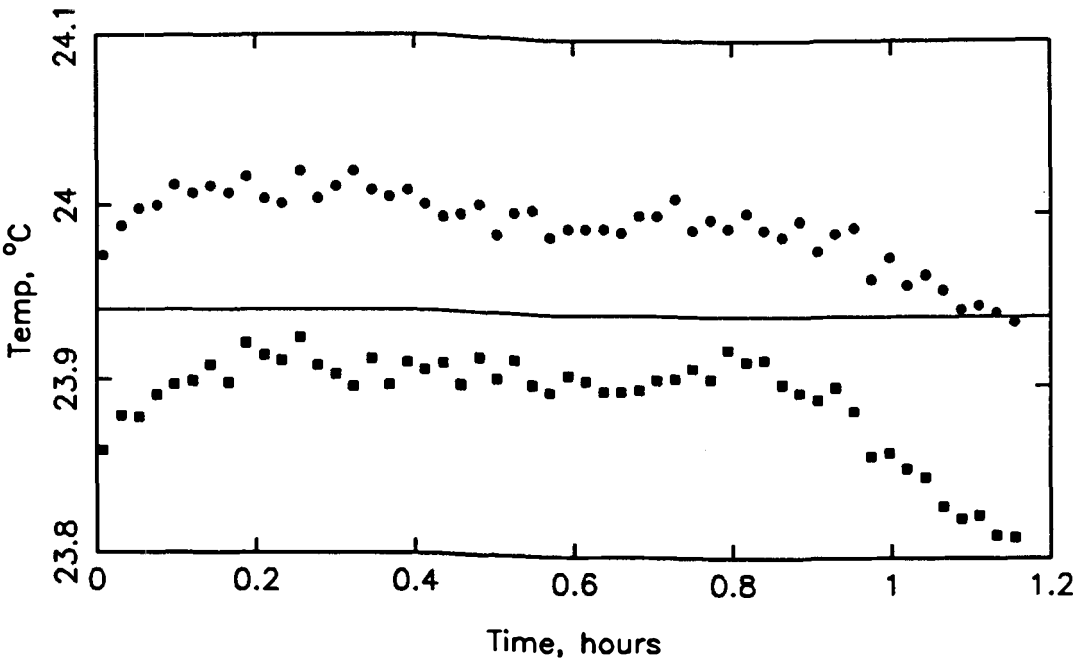

Figure F.13e Experiment 13: Feed EMC2 inlet and outlet temperatures.

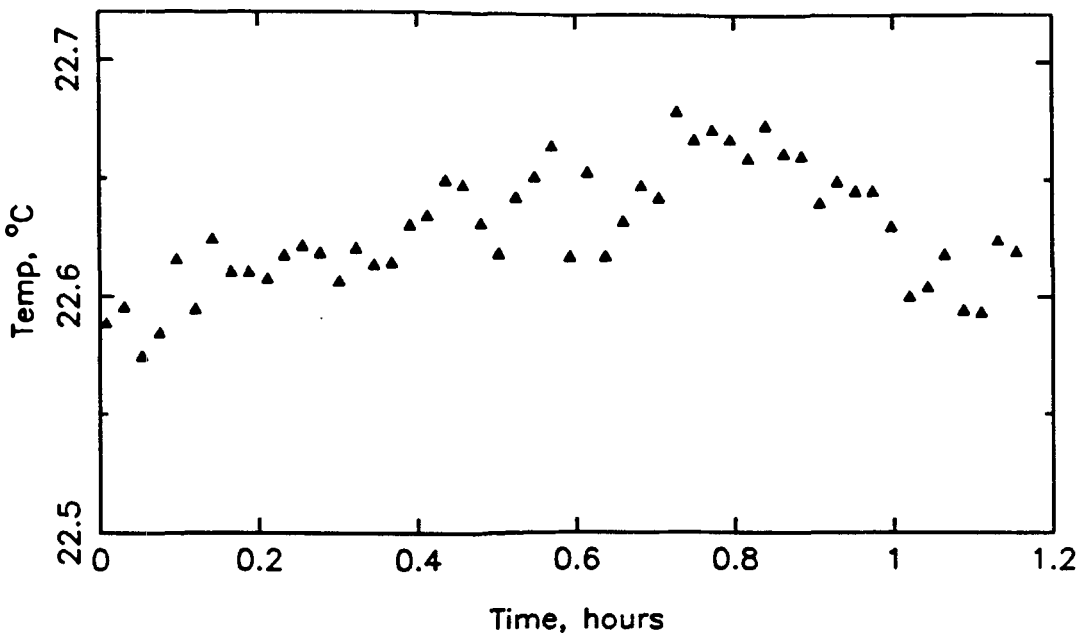

Figure F.13f Experiment 13: Feed EMC2 dew point temperature.

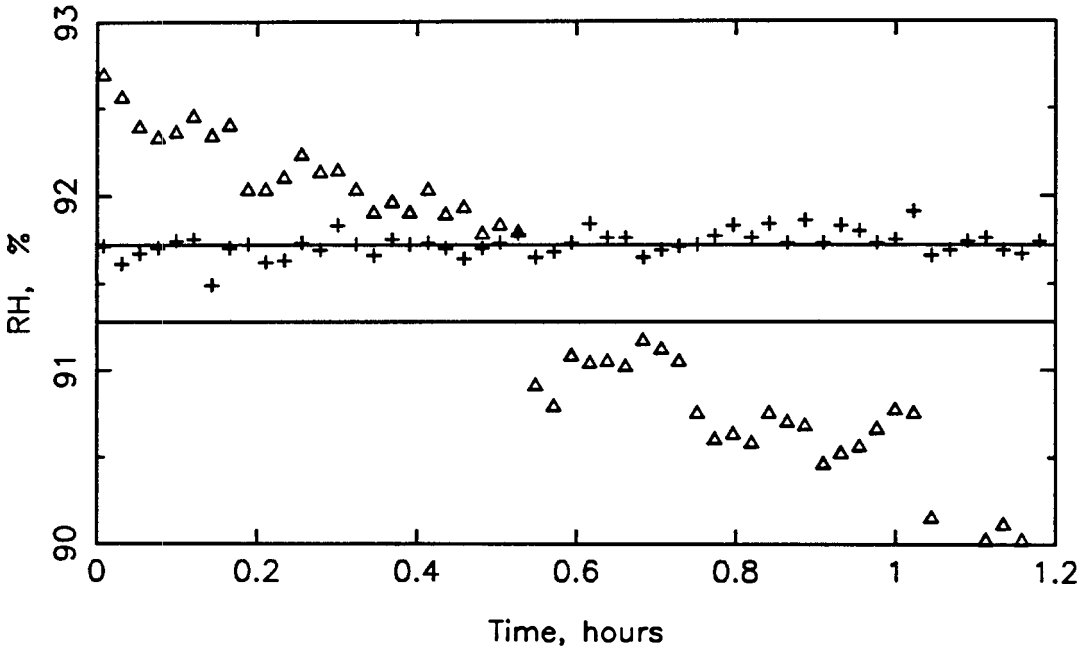

Figure F.13g Experiment 13: Effluent EMC2 and CSTR relative humidity.

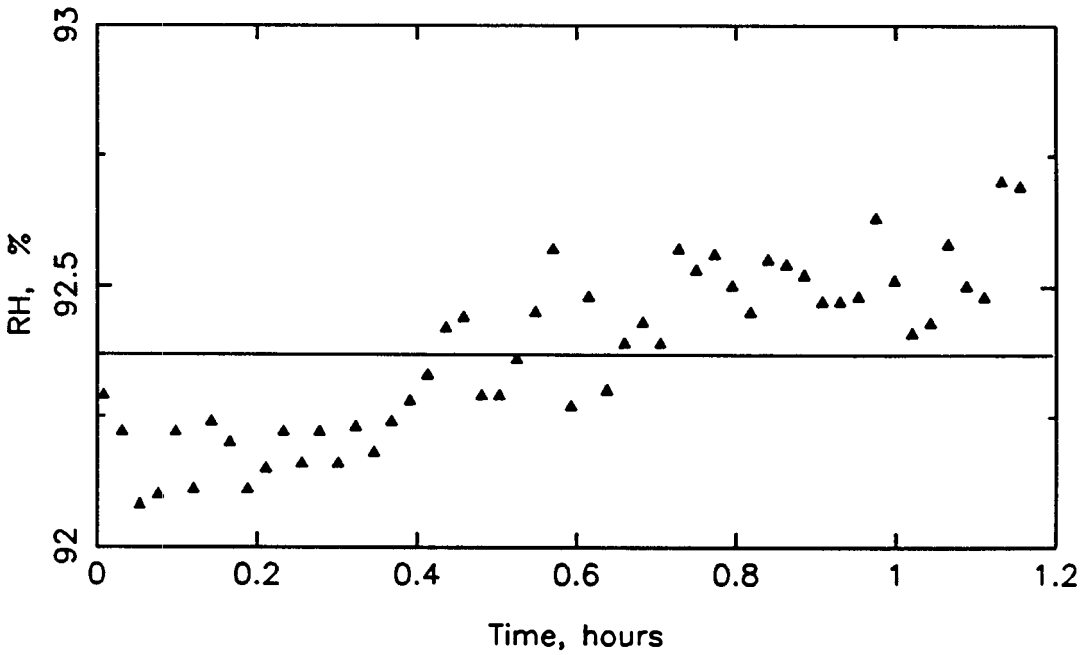

Figure F.13h Experiment 13: Feed EMC2 relative humidity.

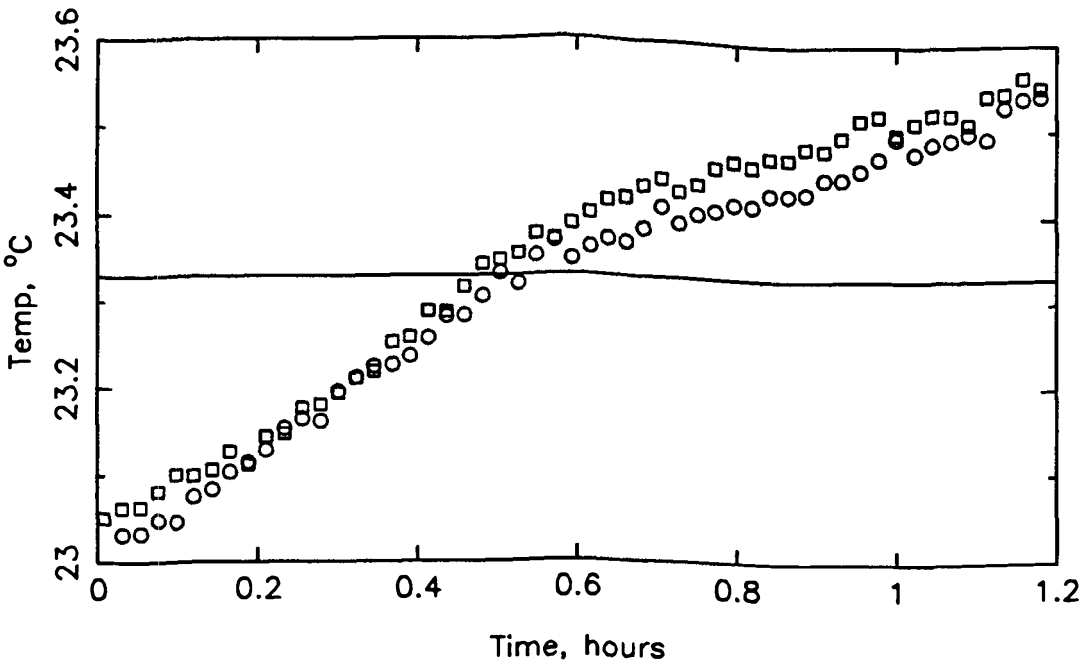

Figure F.14a Experiment 14: Effluent EMC2 inlet and outlet temperatures.

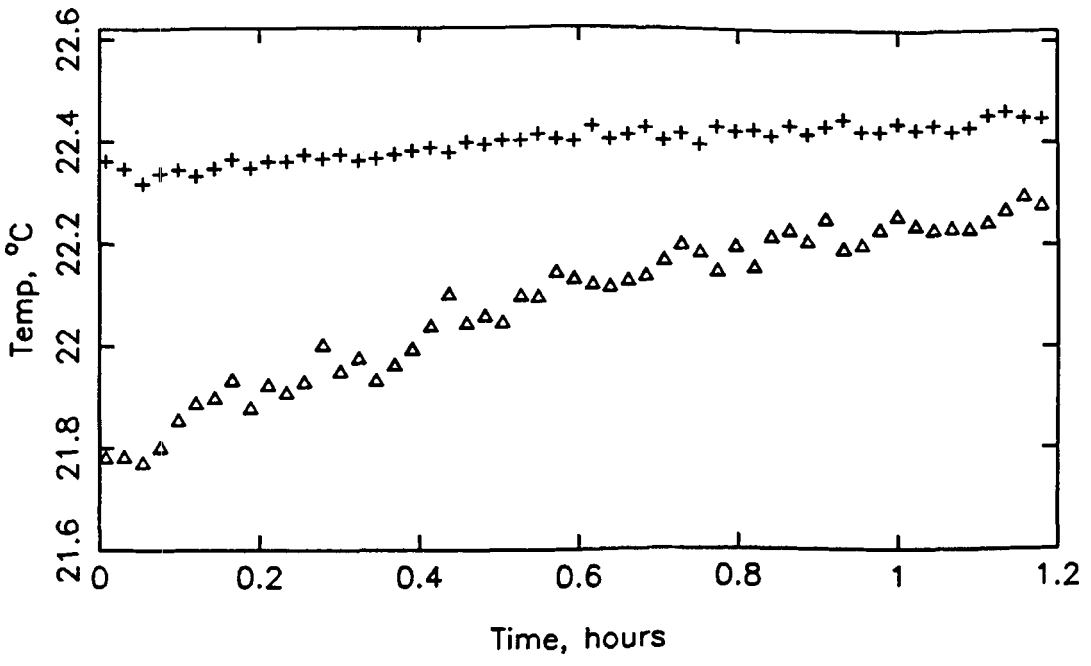

Figure F.14b Experiment 14: Effluent EMC2 and CSTR dew point temperatures.

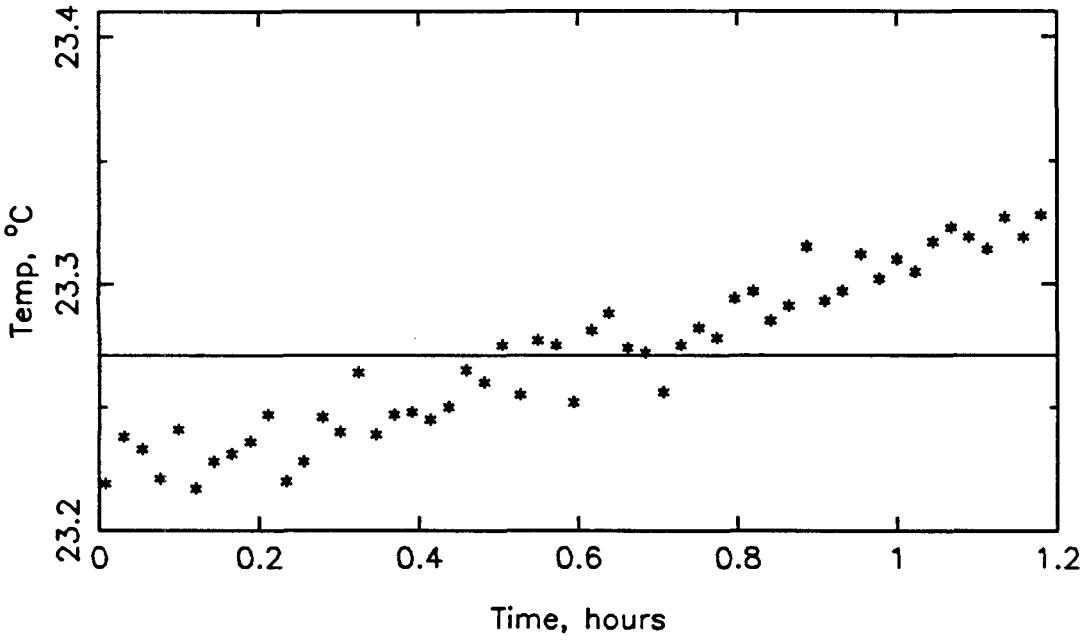

Figure F.14c Experiment 14: Effluent CSTR temperature.

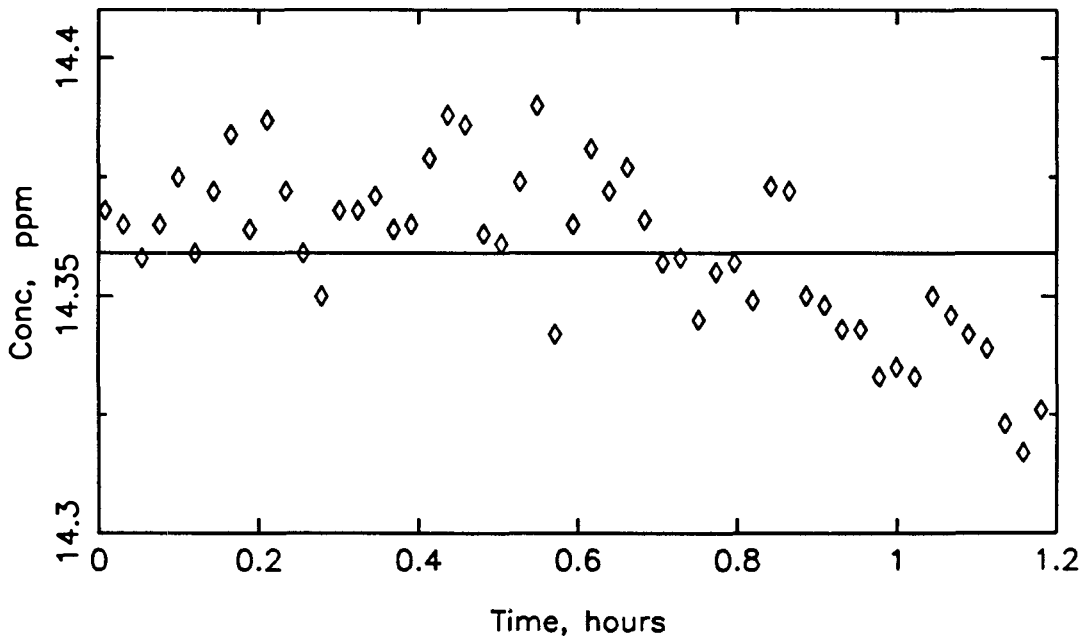

Figure F.14d Experiment 14: Effluent SO_2 concentration.

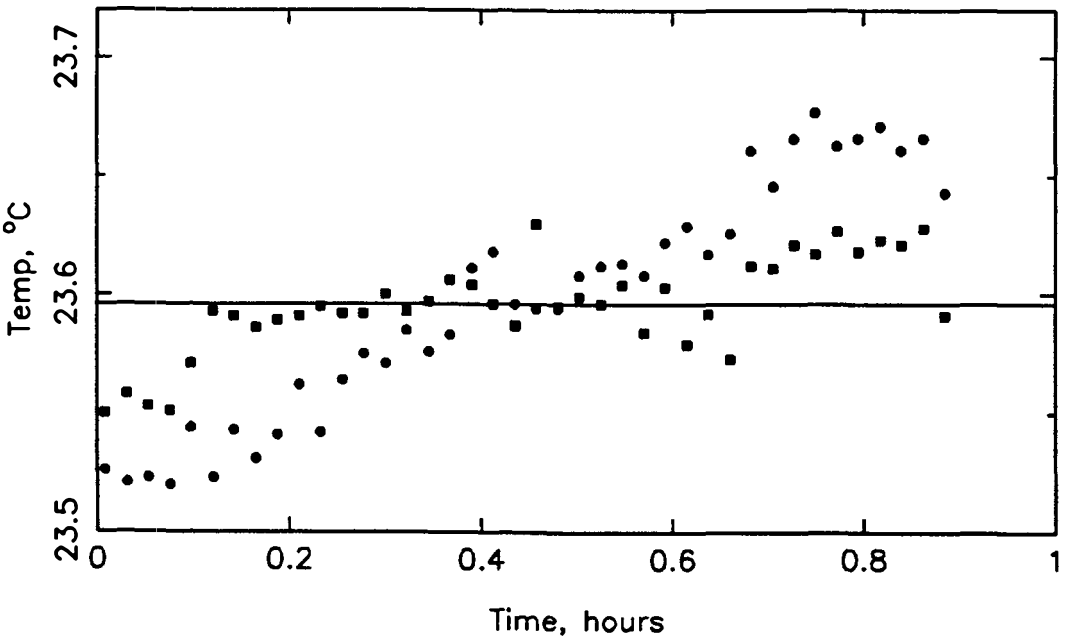

Figure F.14e Experiment 14: Feed EMC2 inlet and outlet temperatures.

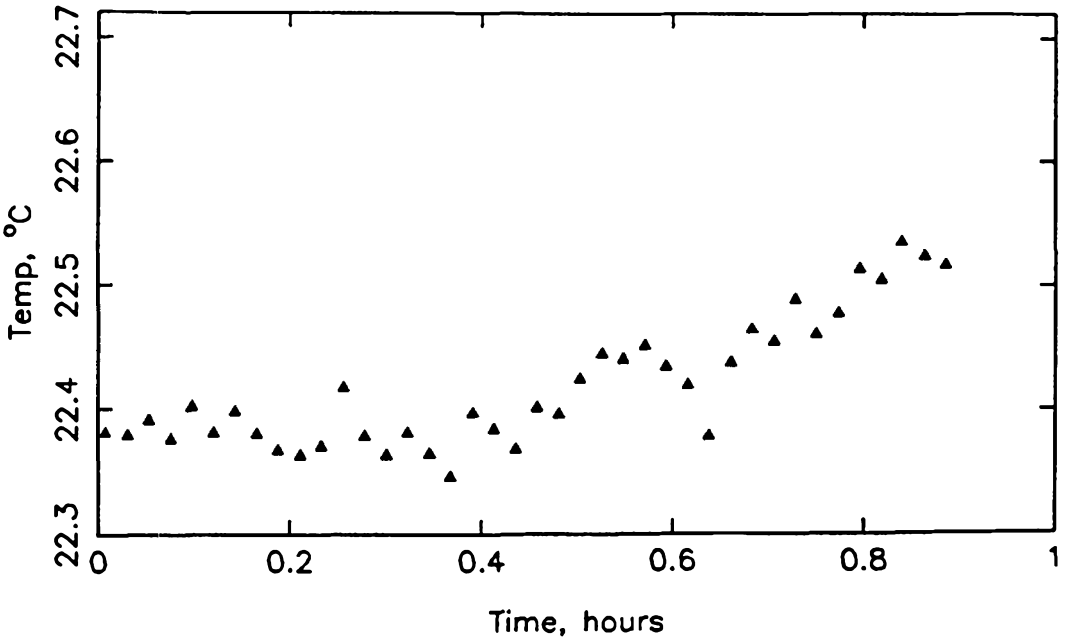

Figure F.14f Experiment 14: Feed EMC2 dew point temperature.

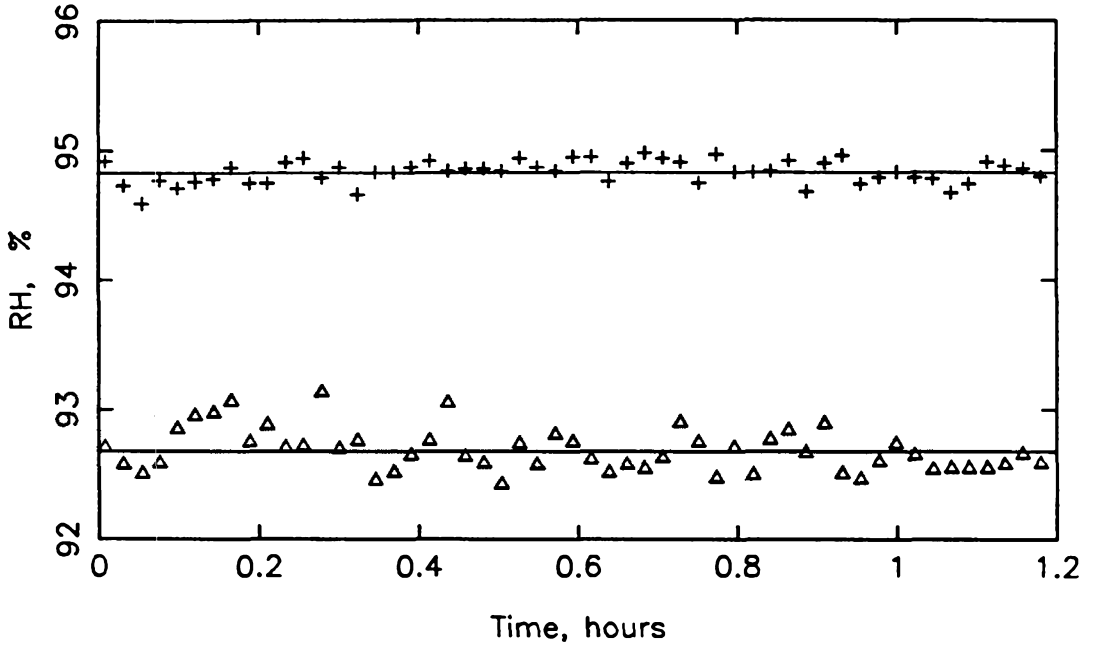

Figure F.14g Experiment 14: Effluent EMC2 and CSTR relative humidity.

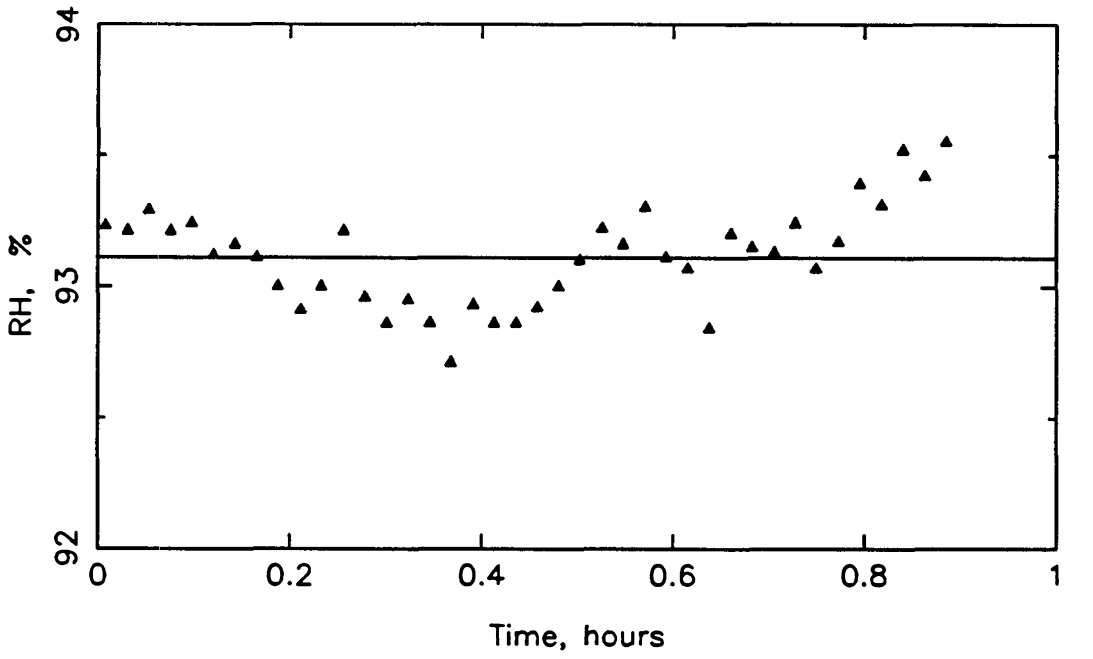

Figure F.14h Experiment 14: Feed EMC2 relative humidity.

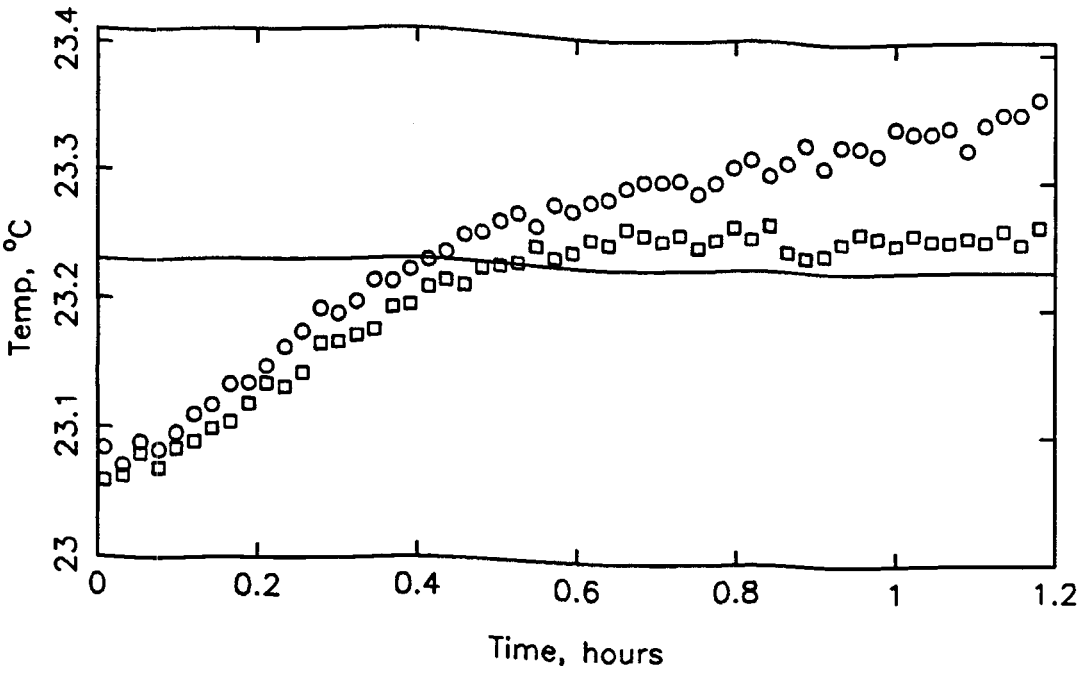

Figure F.15a Experiment 15: Effluent EMC2 inlet and outlet temperatures.

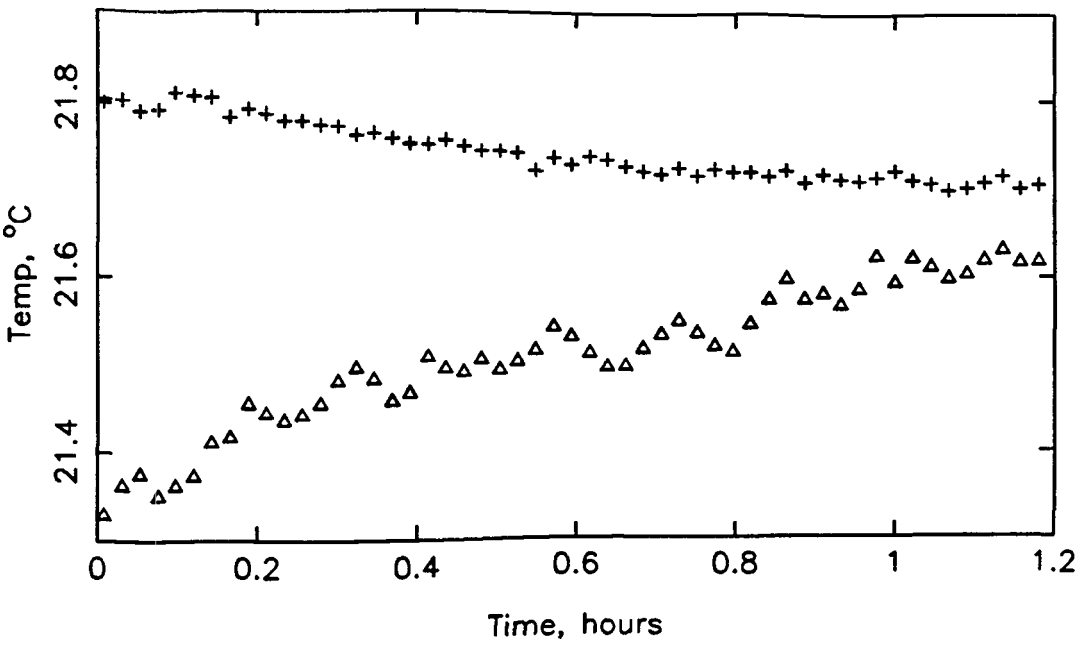

Figure F.15b Experiment 15: Effluent EMC2 and CSTR dew point temperatures.

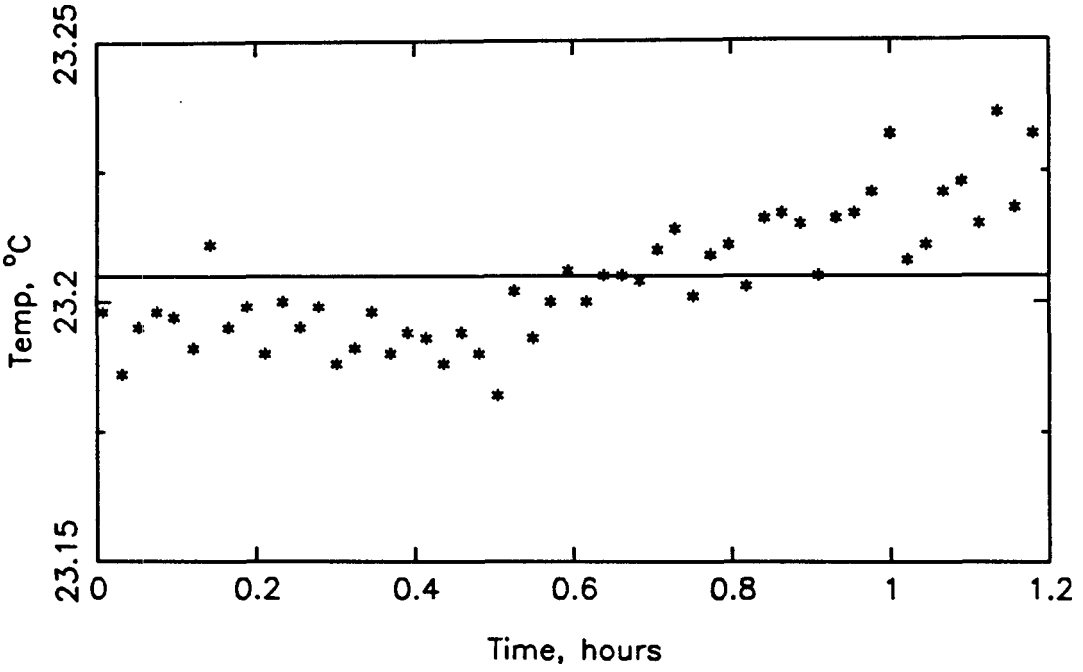

Figure F.15c Experiment 15: Effluent CSTR temperature.

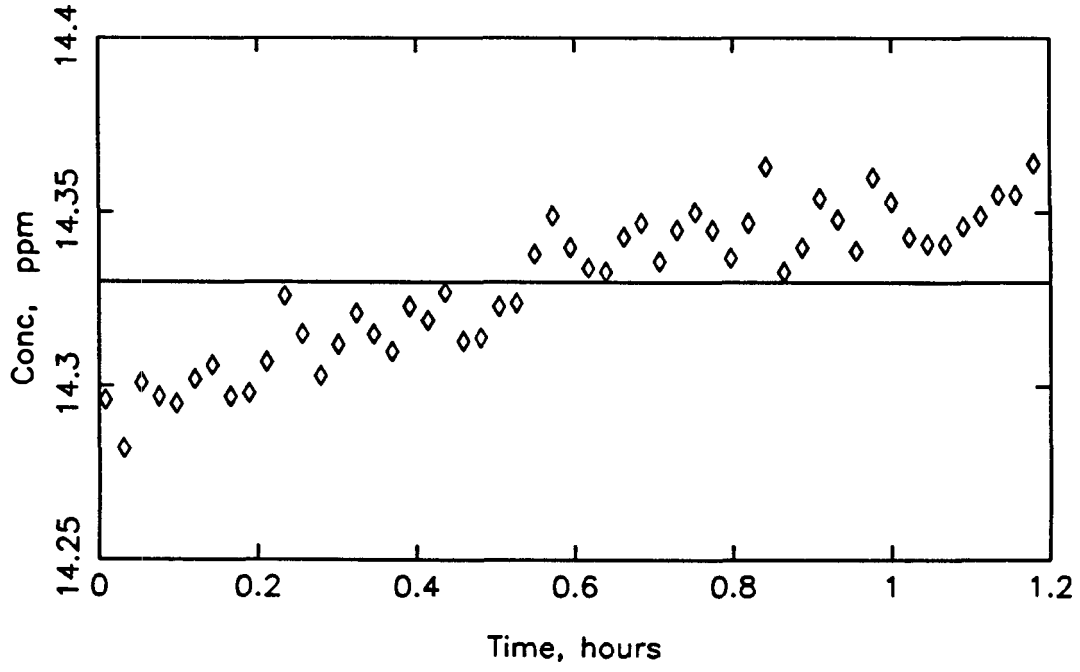

Figure F.15d Experiment 15: Effluent SO_2 concentration.

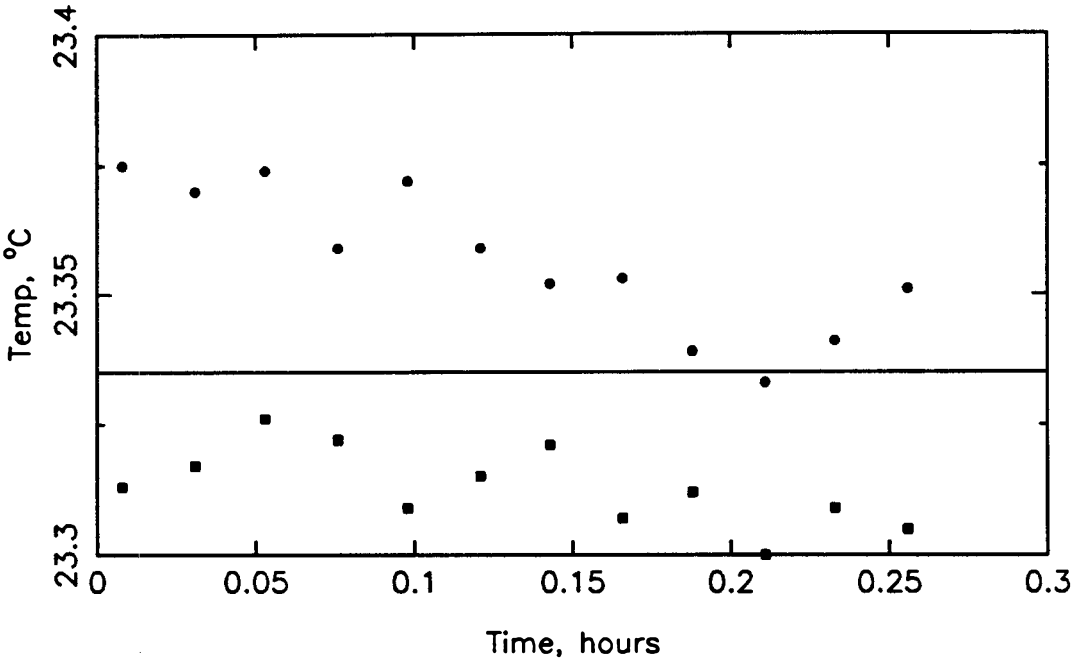

Figure F.15e Experiment 15: Feed EMC2 inlet and outlet temperatures.

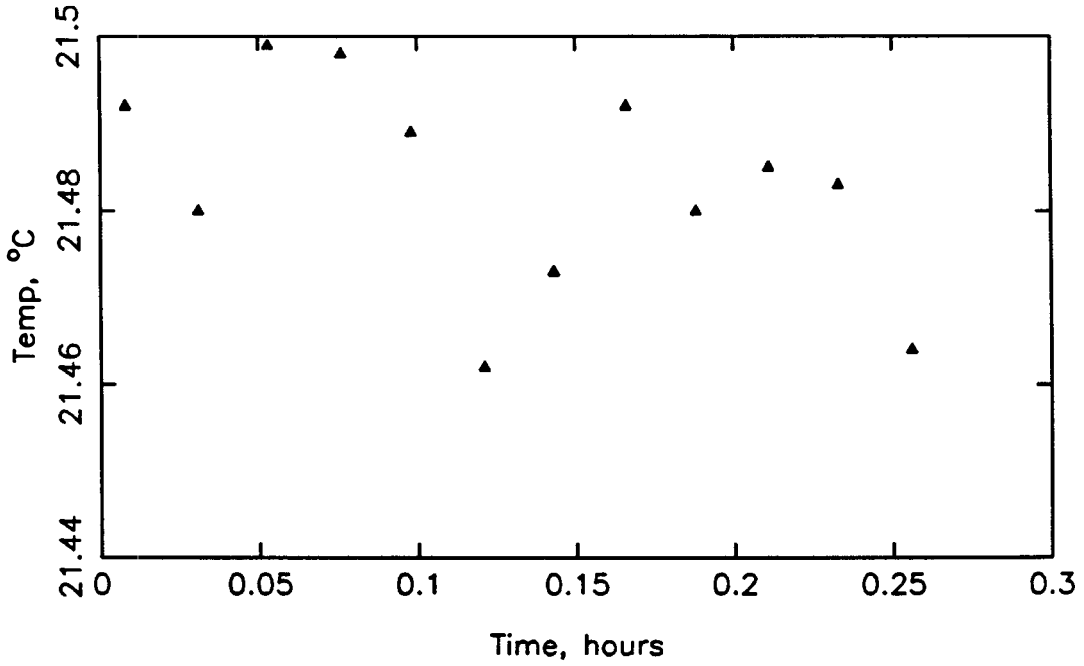

Figure F.15f Experiment 15: Feed EMC2 dew point temperature.

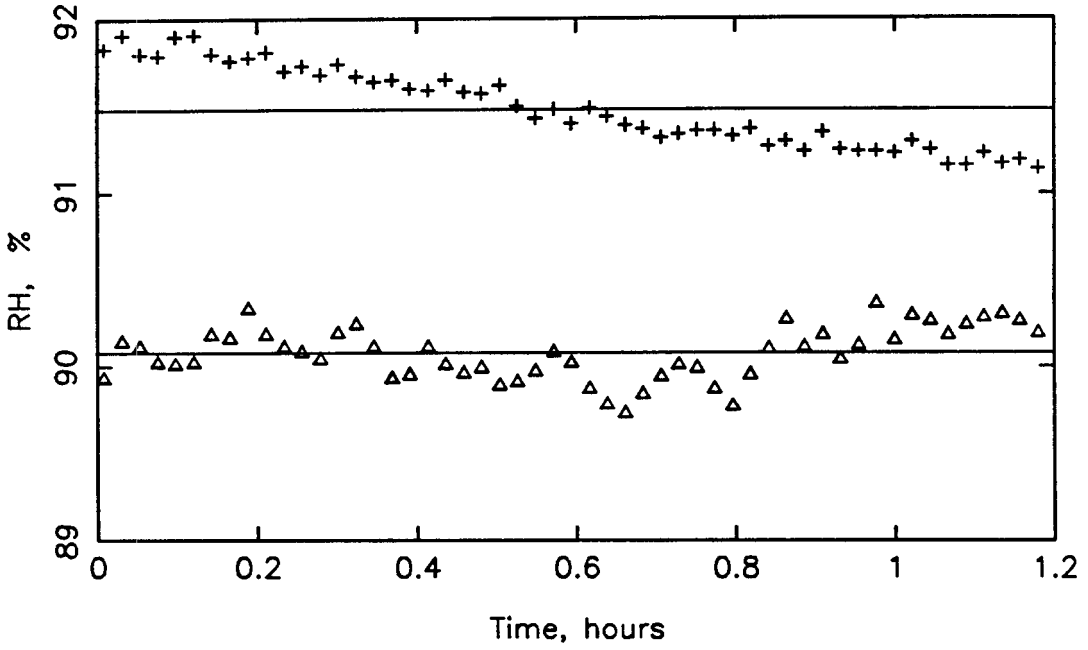

Figure F.15g Experiment 15: Effluent EMC2 and CSTR relative humidity.

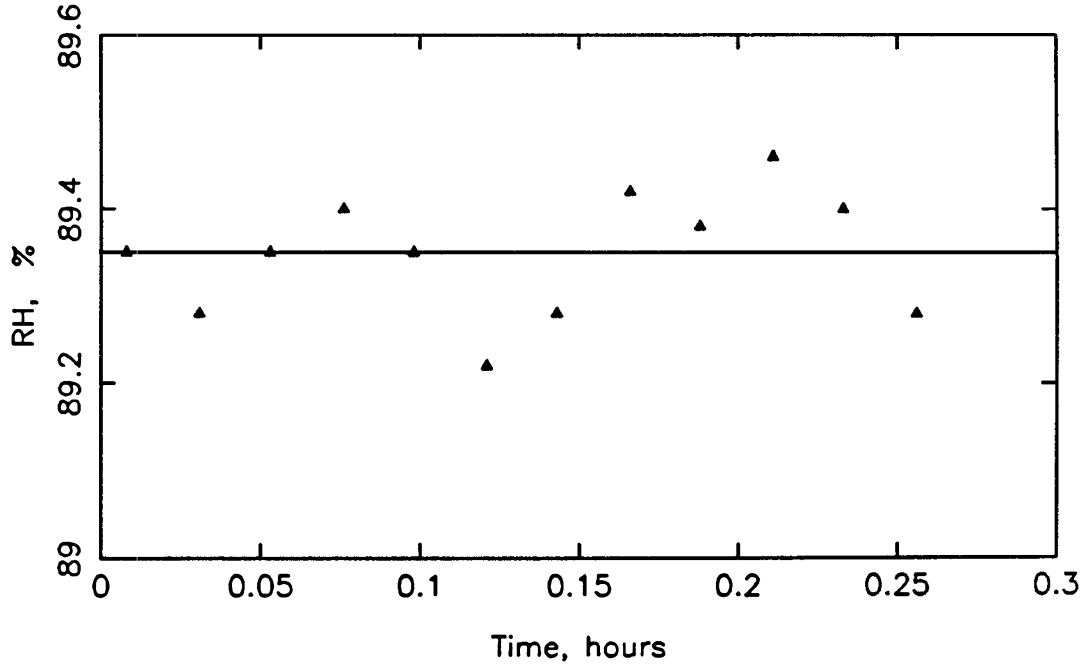

Figure F.15h Experiment 15: Feed EMC2 relative humidity.

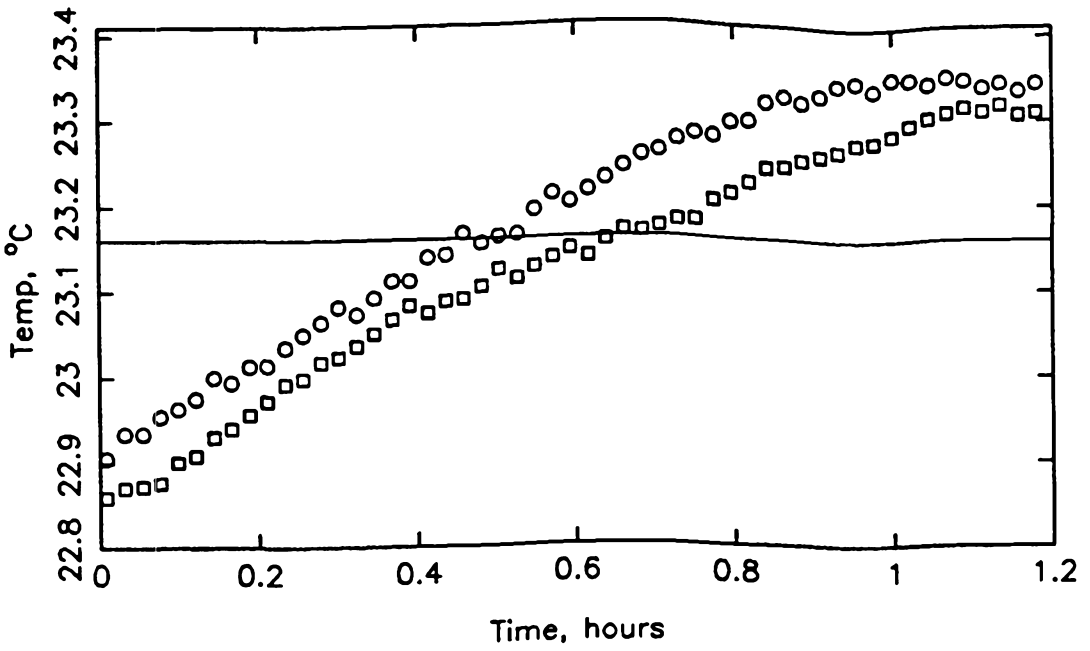

Figure F.16a Experiment 16: Effluent EMC2 inlet and outlet temperatures.

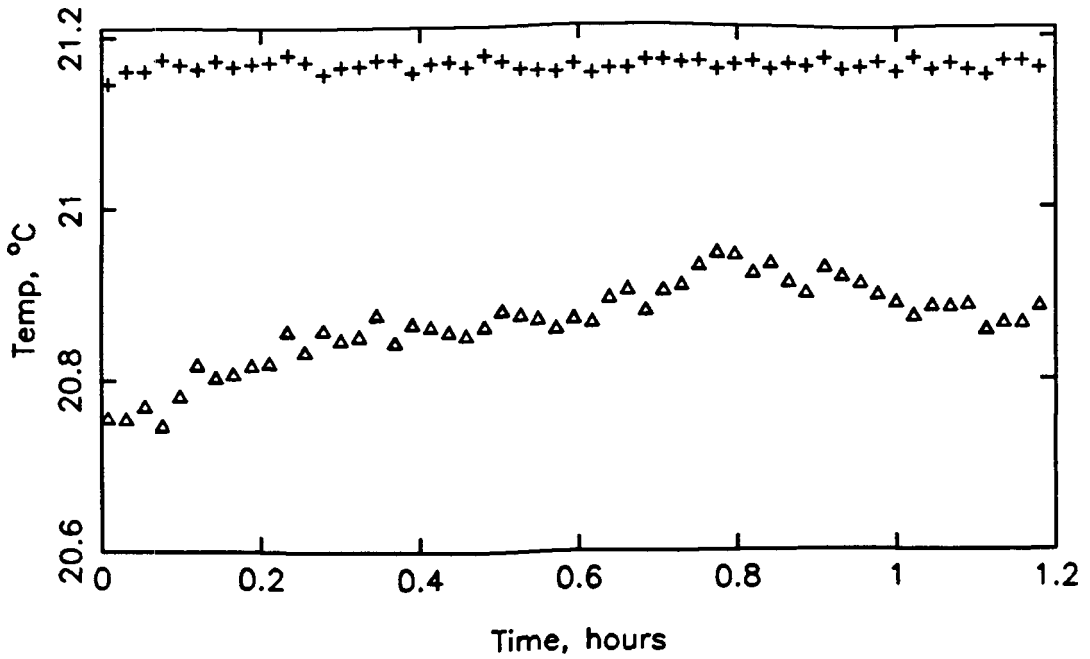

Figure F.16b Experiment 16: Effluent EMC2 and CSTR dew point temperatures.

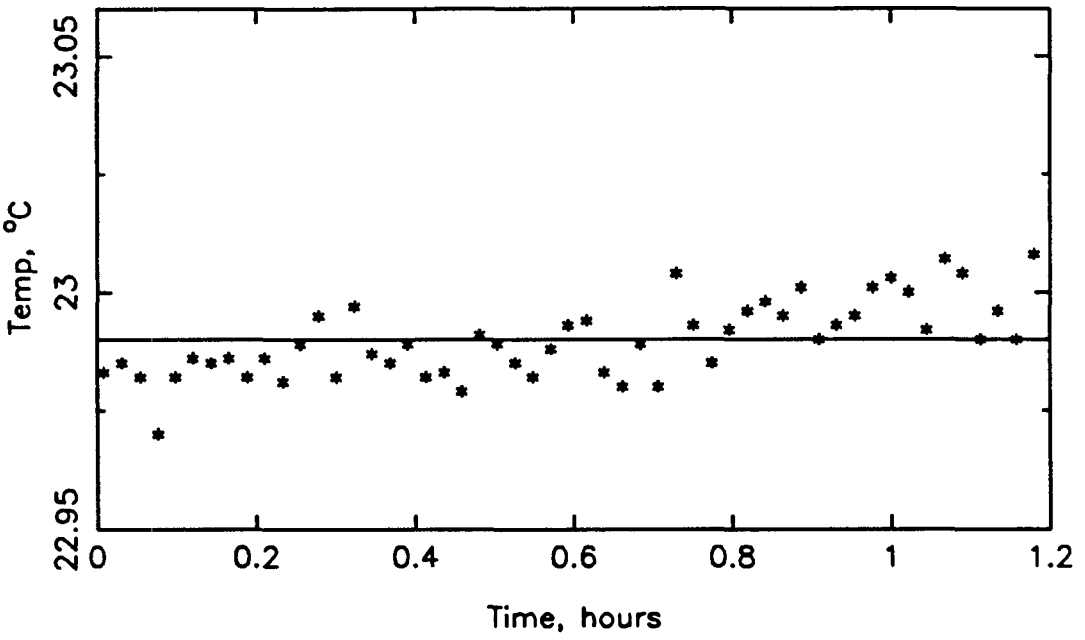

Figure F.16c Experiment 16: Effluent CSTR temperature.

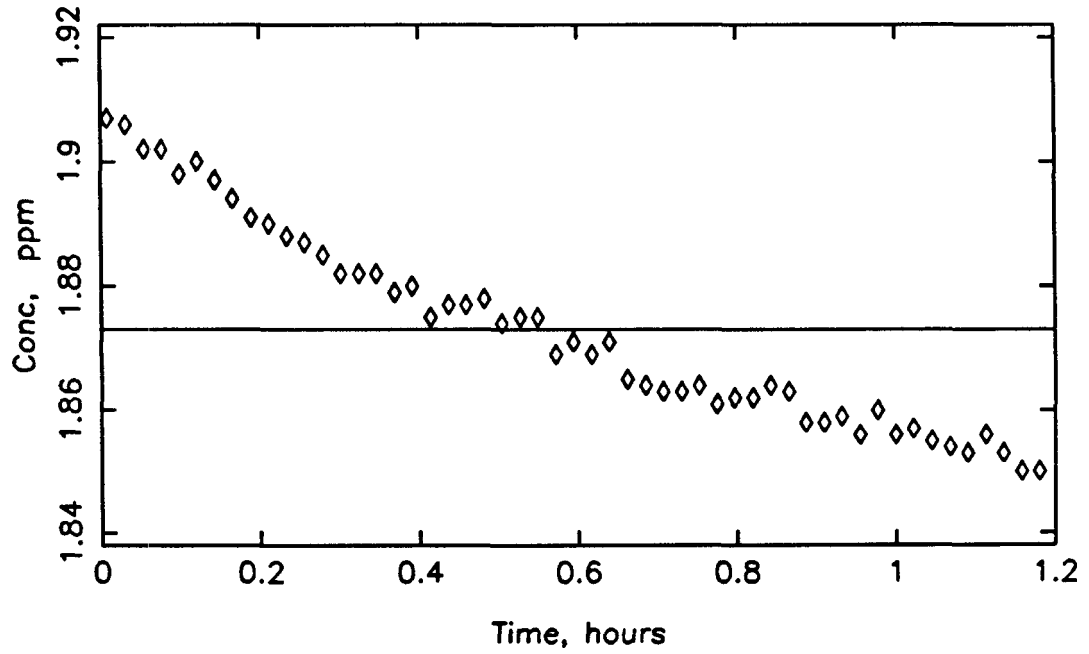

Figure F.16d Experiment 16: Effluent SO_2 concentration.

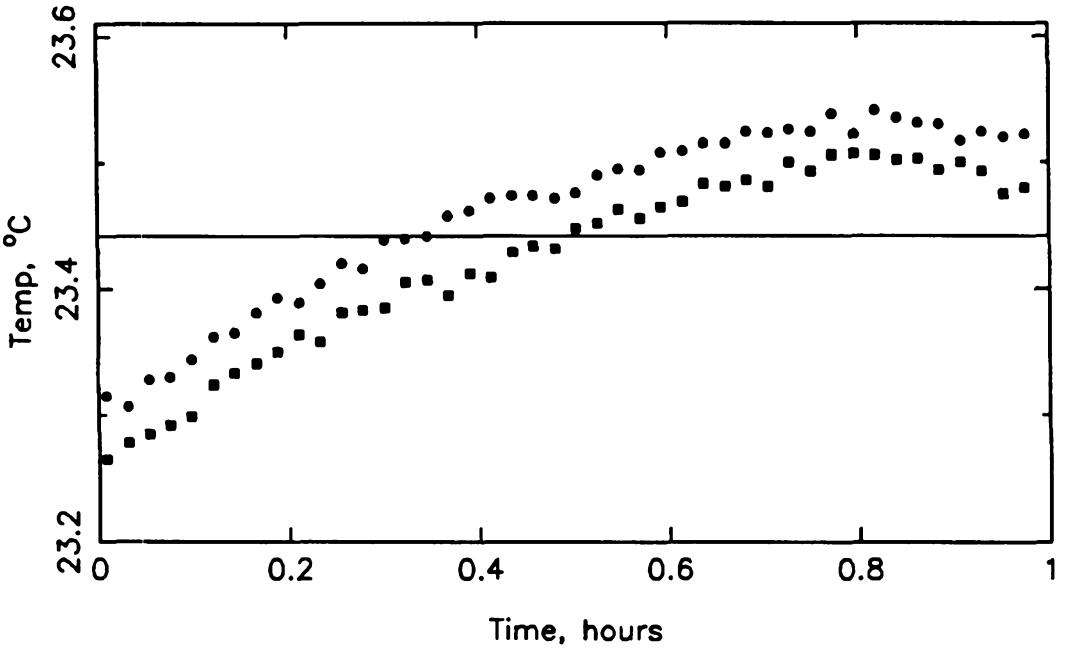

Figure F.16e Experiment 16: Feed EMC2 inlet and outlet temperatures.

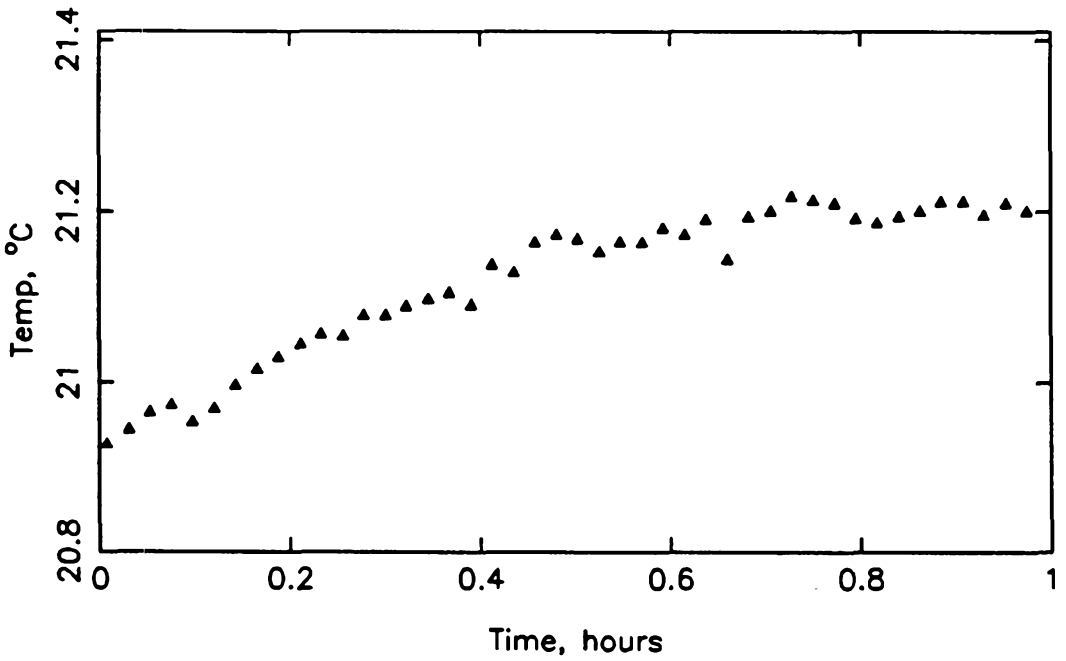

Figure F.16f Experiment 16: Feed EMC2 dew point temperature.

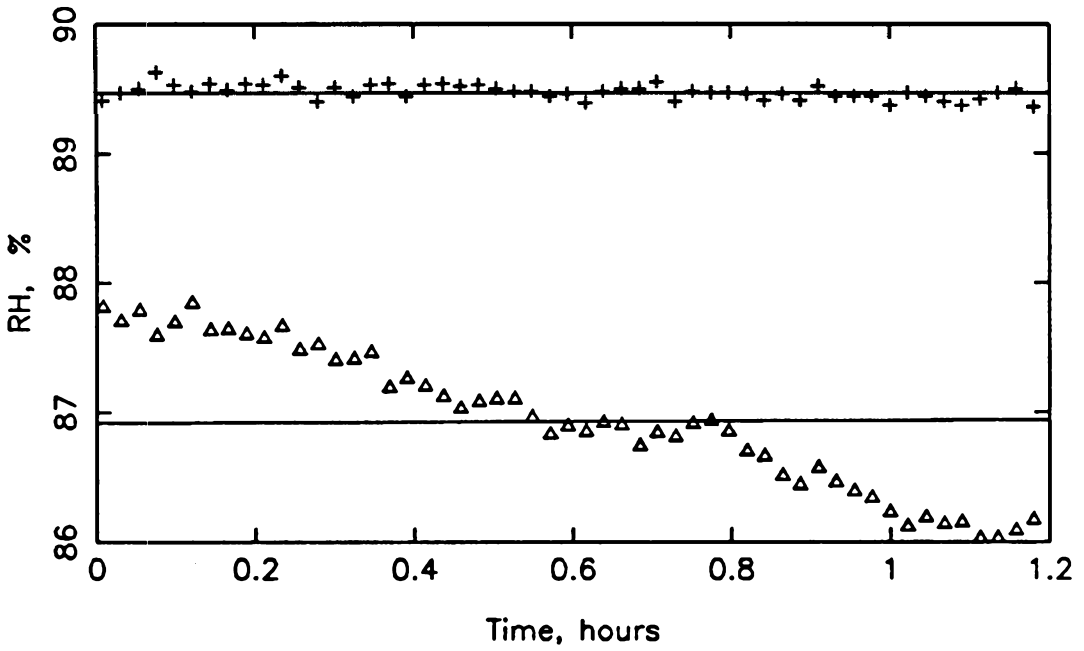

Figure F.16g Experiment 16: Effluent EMC2 and CSTR relative humidity.

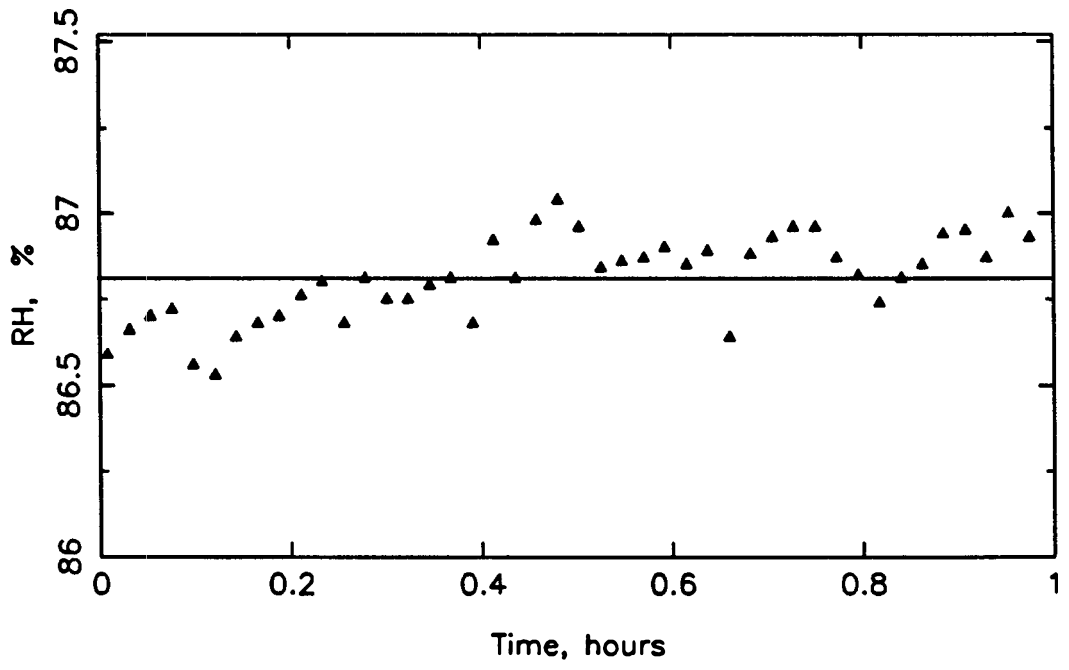

Figure F.16h Experiment 16: Feed EMC2 relative humidity.

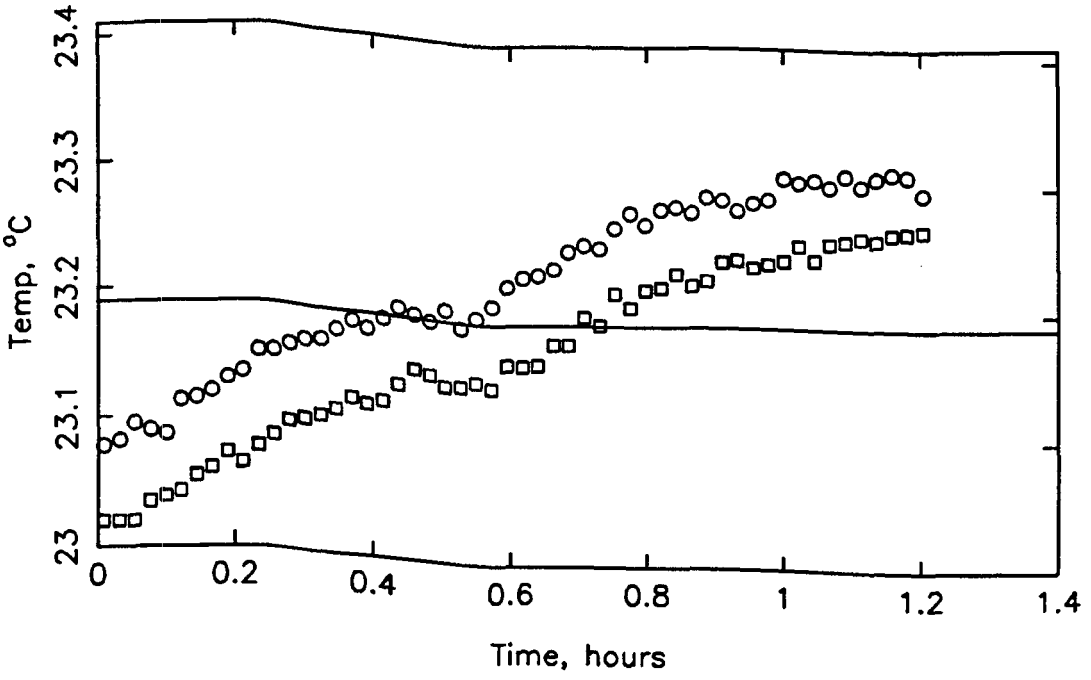

Figure F.17a Experiment 17: Effluent EMC2 inlet and outlet temperatures.

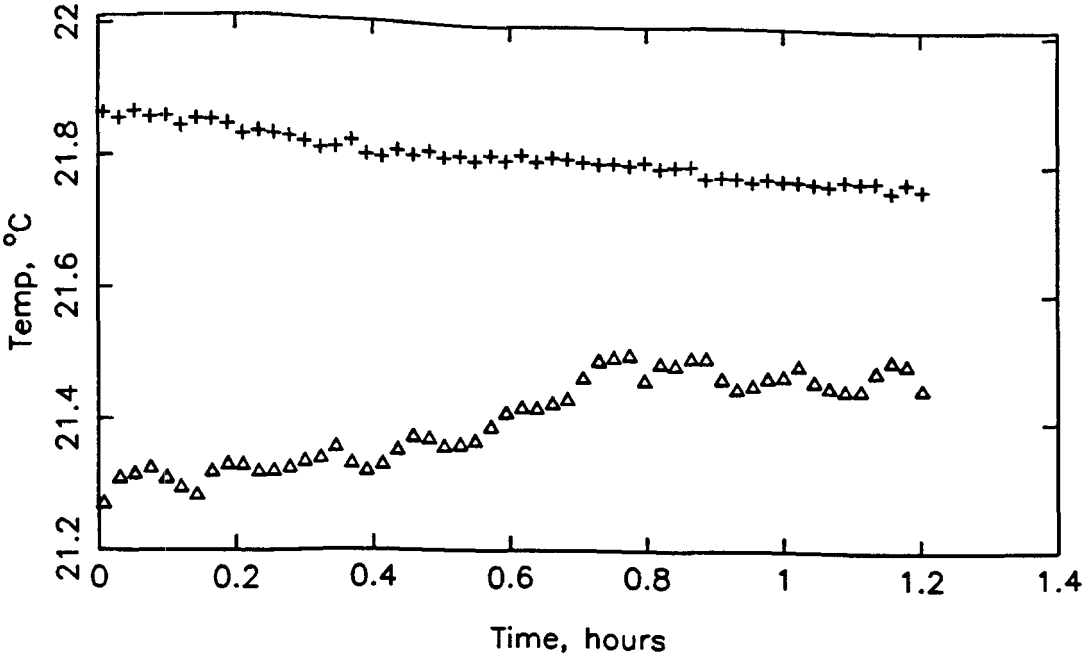

Figure F.17b Experiment 17: Effluent EMC2 and CSTR dew point temperatures.

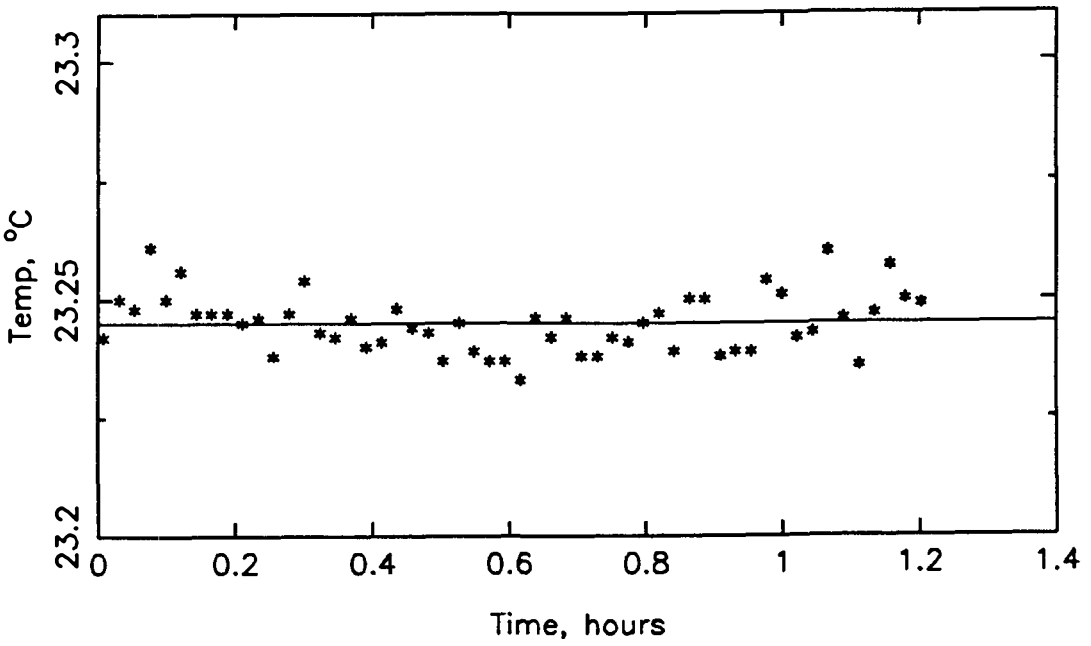

Figure F.17c Experiment 17: Effluent CSTR temperature.

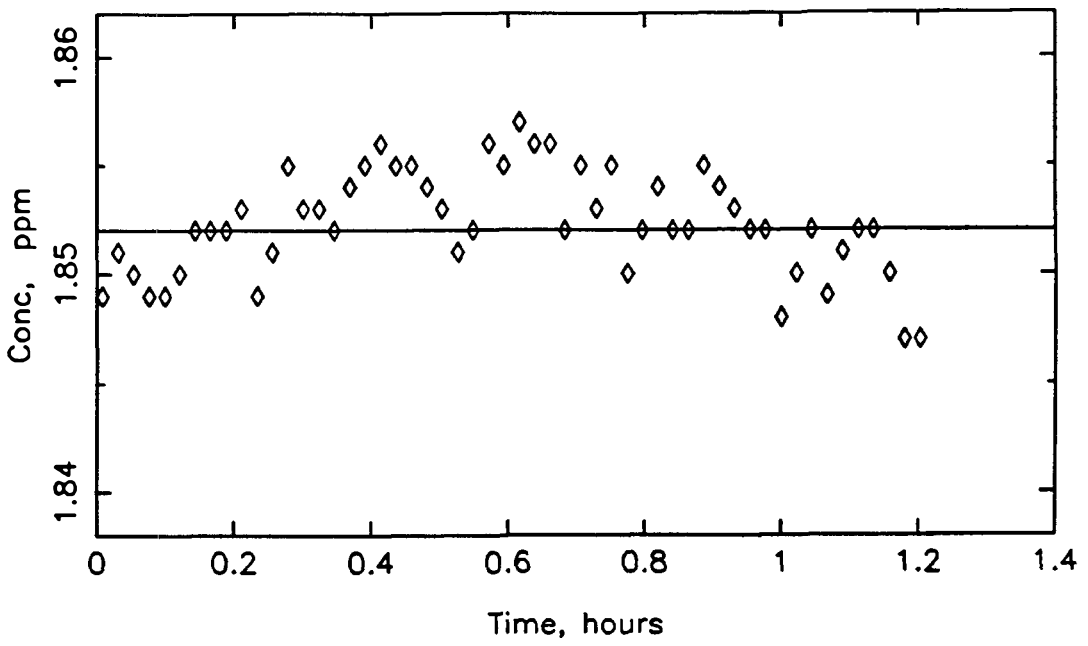

Figure F.17d Experiment 17: Effluent SO_2 concentration.

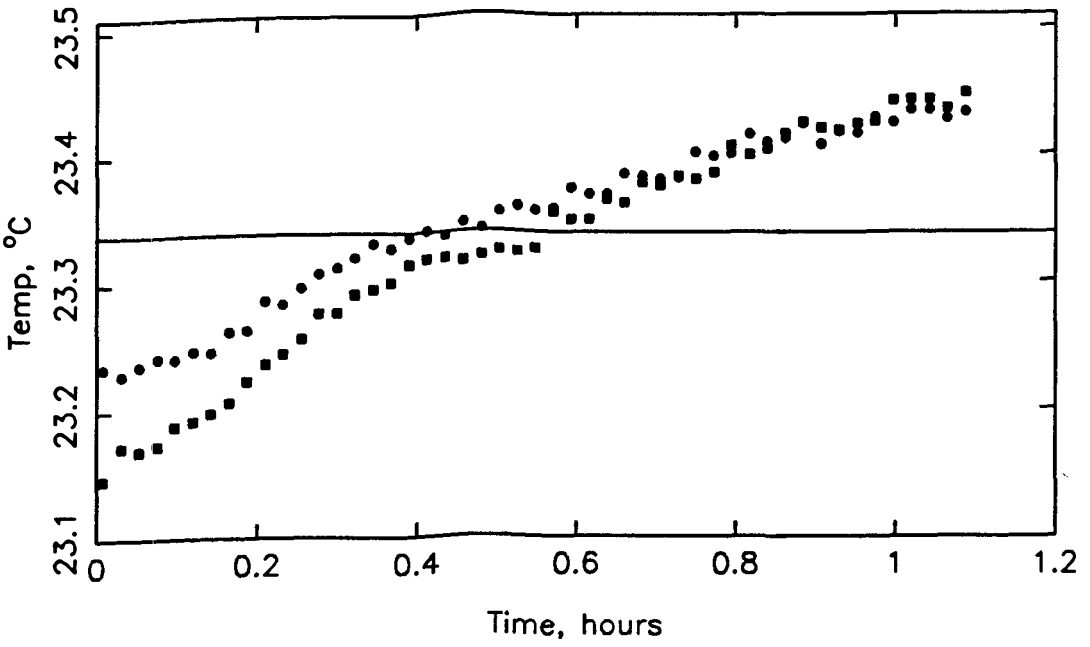

Figure F.17e Experiment 17: Feed EMC2 inlet and outlet temperatures.

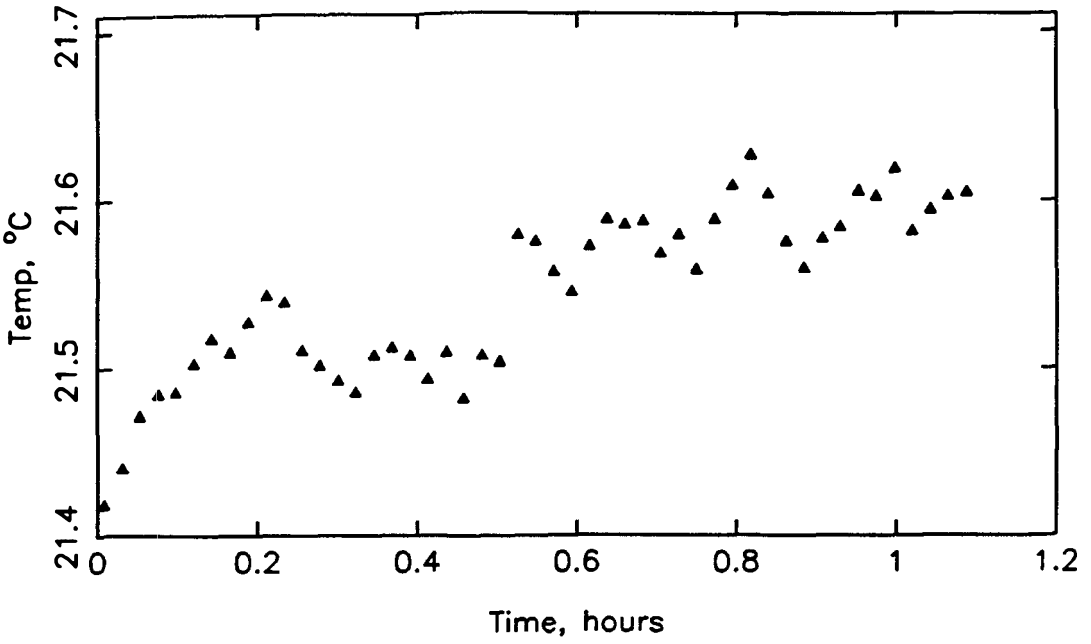

Figure F.17f Experiment 17: Feed EMC2 dew point temperature.

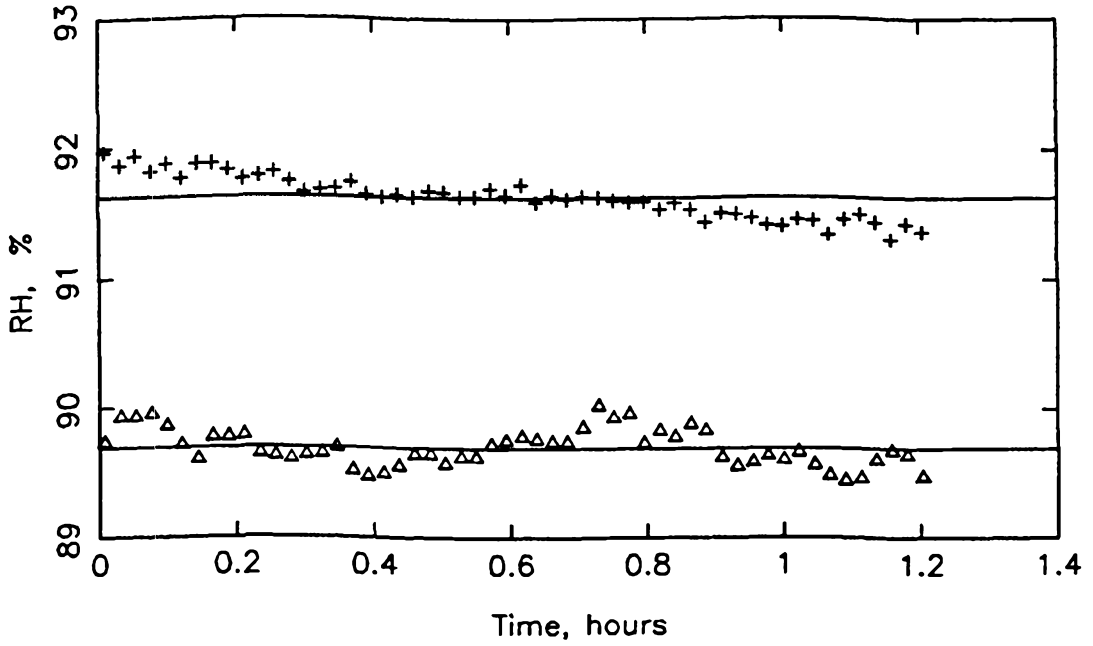

Figure F.17g Experiment 17: Effluent EMC2 and CSTR relative humidity.

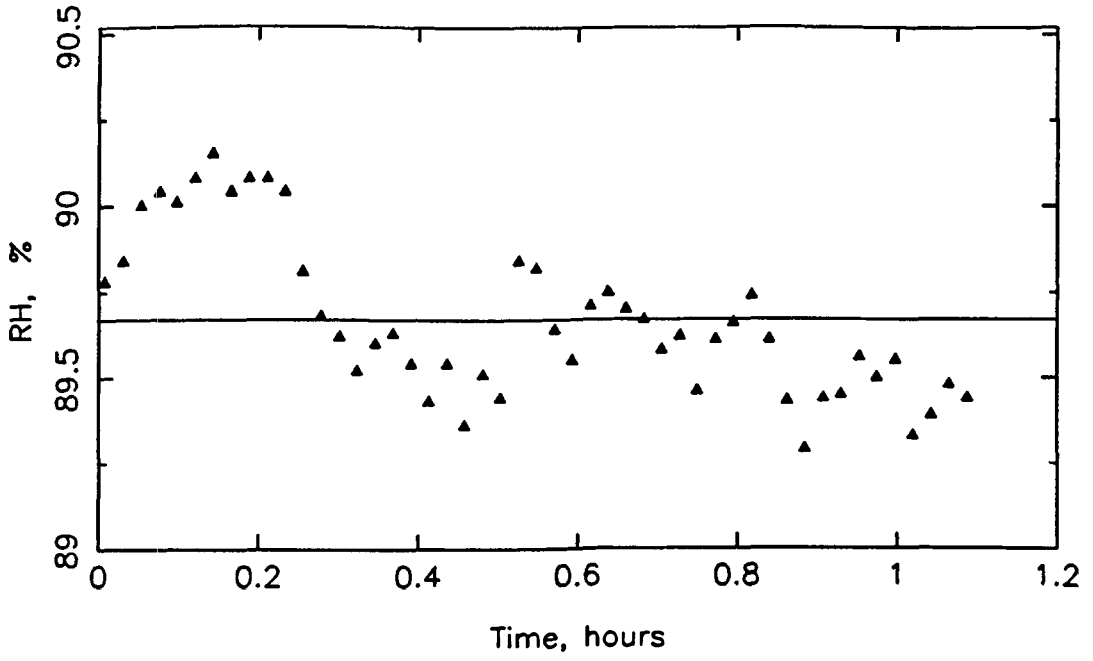

Figure F.17h Experiment 17: Feed EMC2 relative humidity.

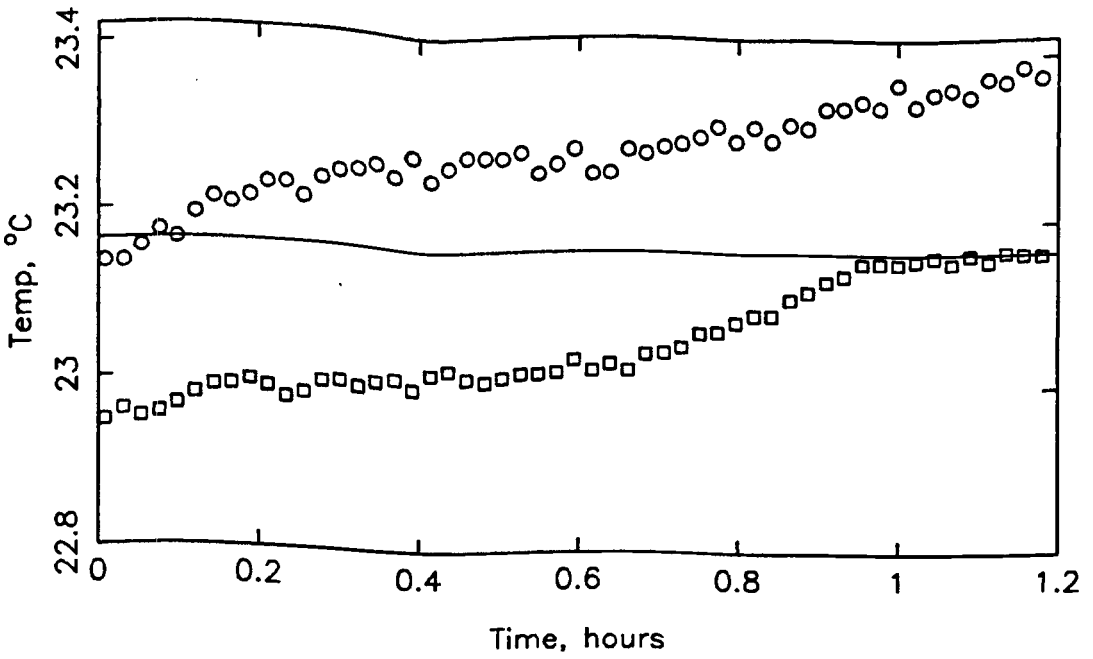

Figure F.18a Experiment 18: Effluent EMC2 inlet and outlet temperatures.

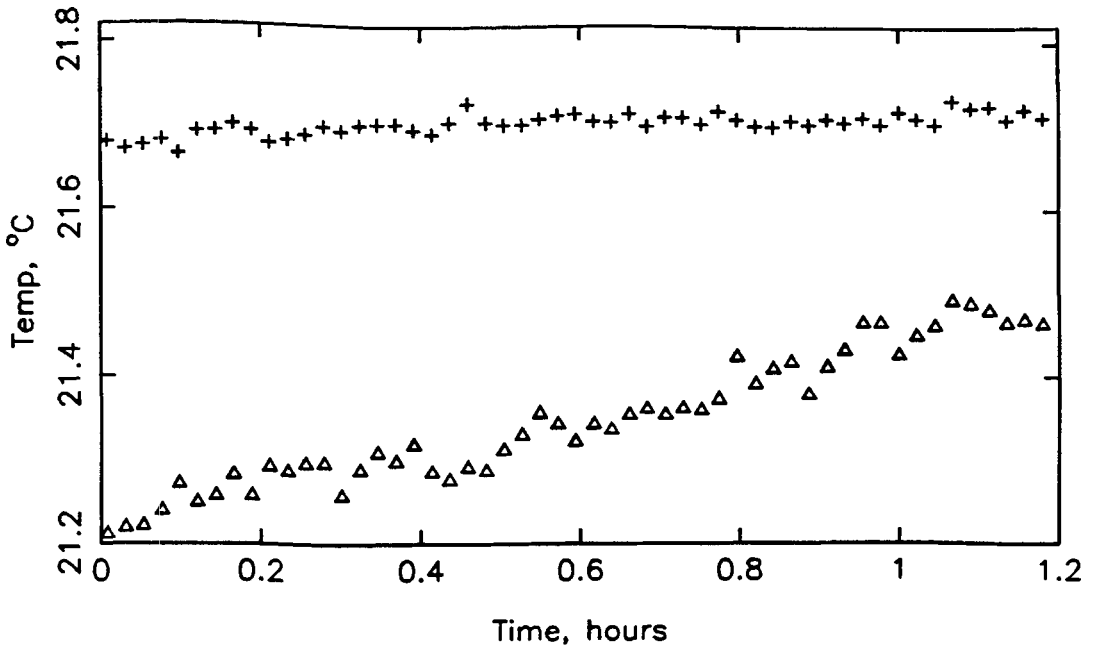

Figure F.18b Experiment 18: Effluent EMC2 and CSTR dew point temperatures.

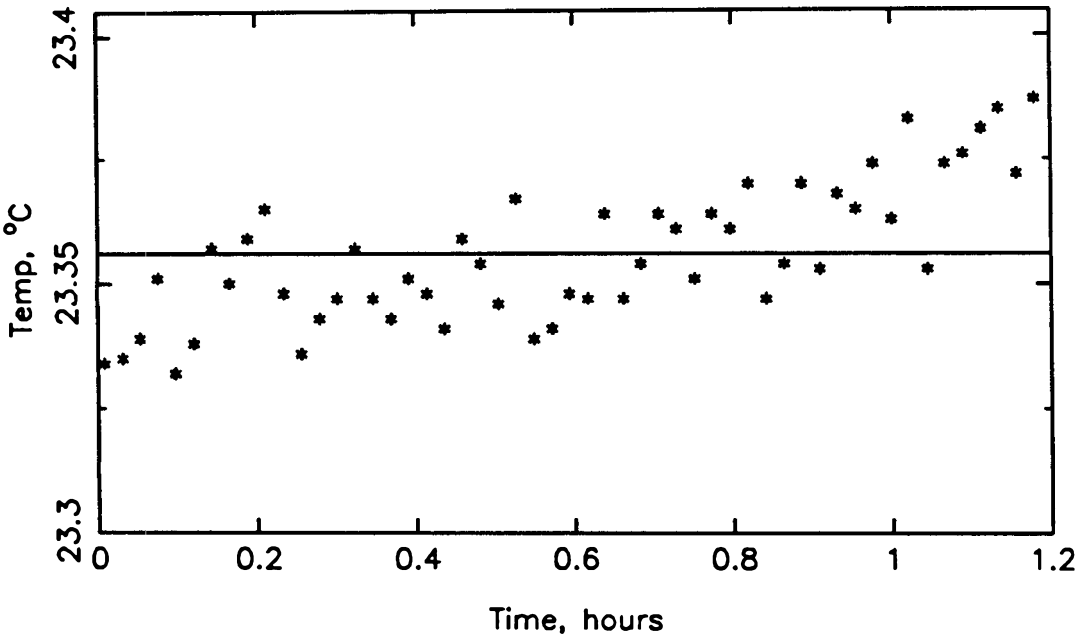

Figure F.18c Experiment 18: Effluent CSTR temperature.

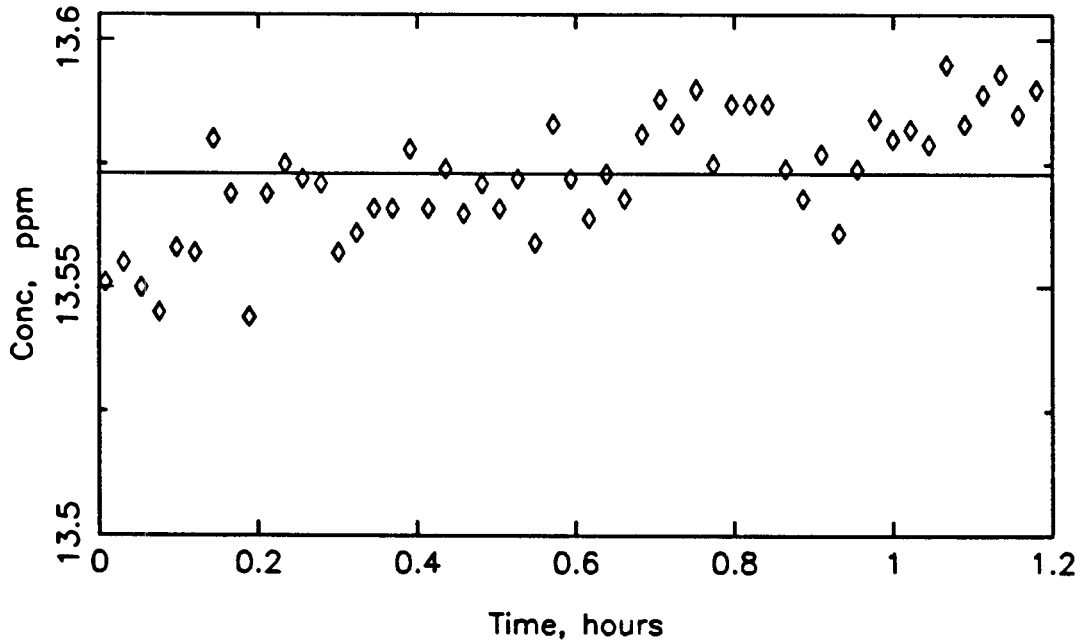

Figure F.18d Experiment 18: Effluent SO_2 concentration.

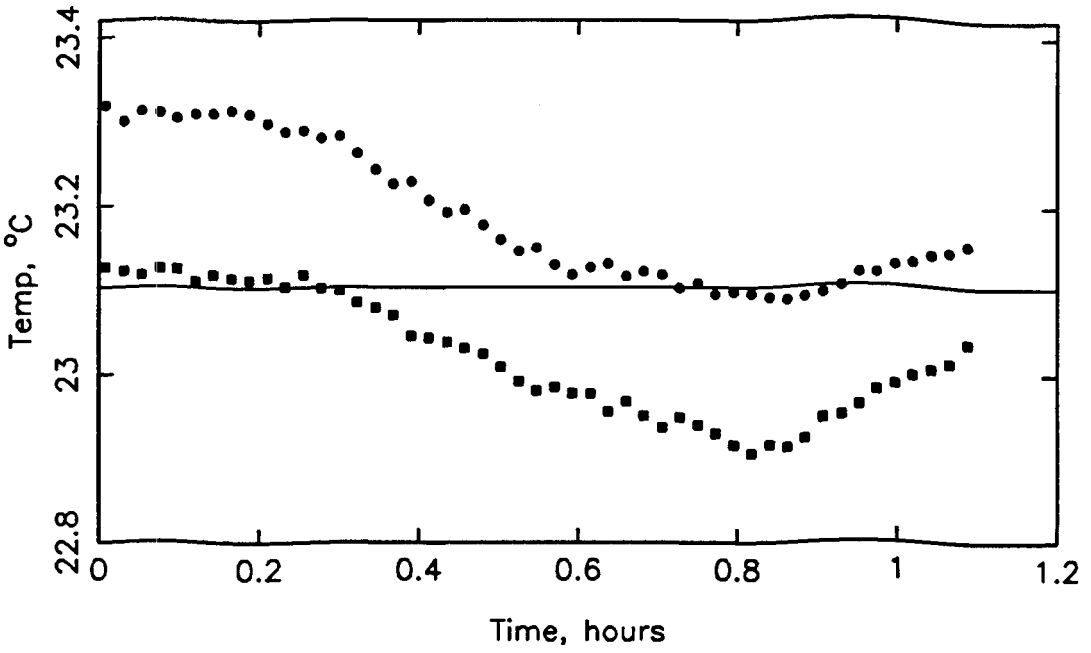

Figure F.18e Experiment 18: Feed EMC2 inlet and outlet temperatures.

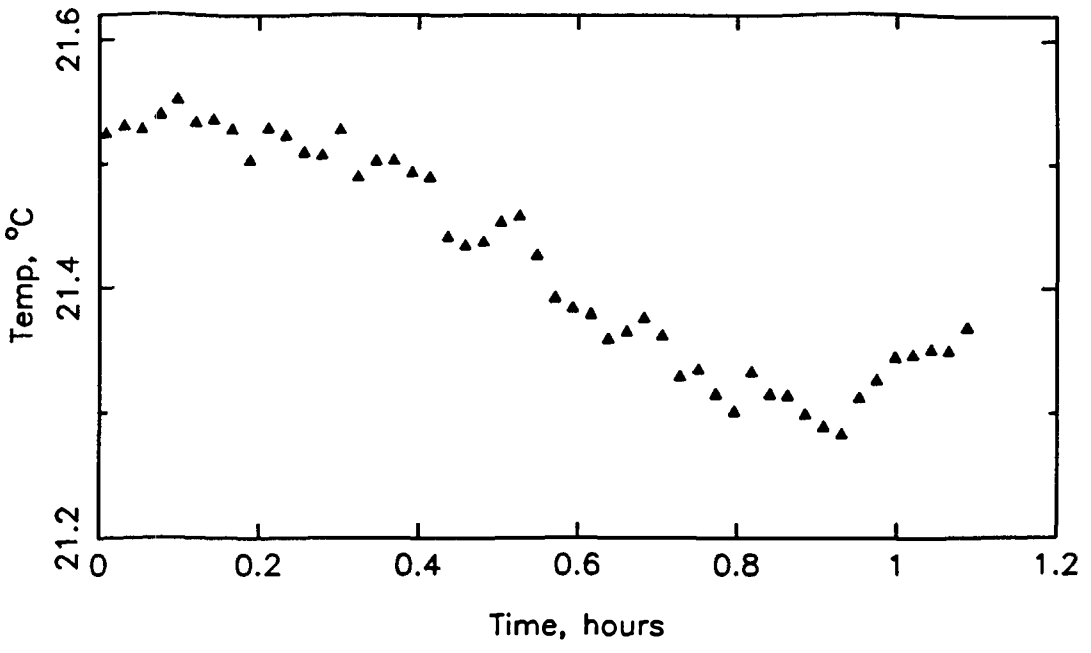

Figure F.18f Experiment 18: Feed EMC2 dew point temperature.

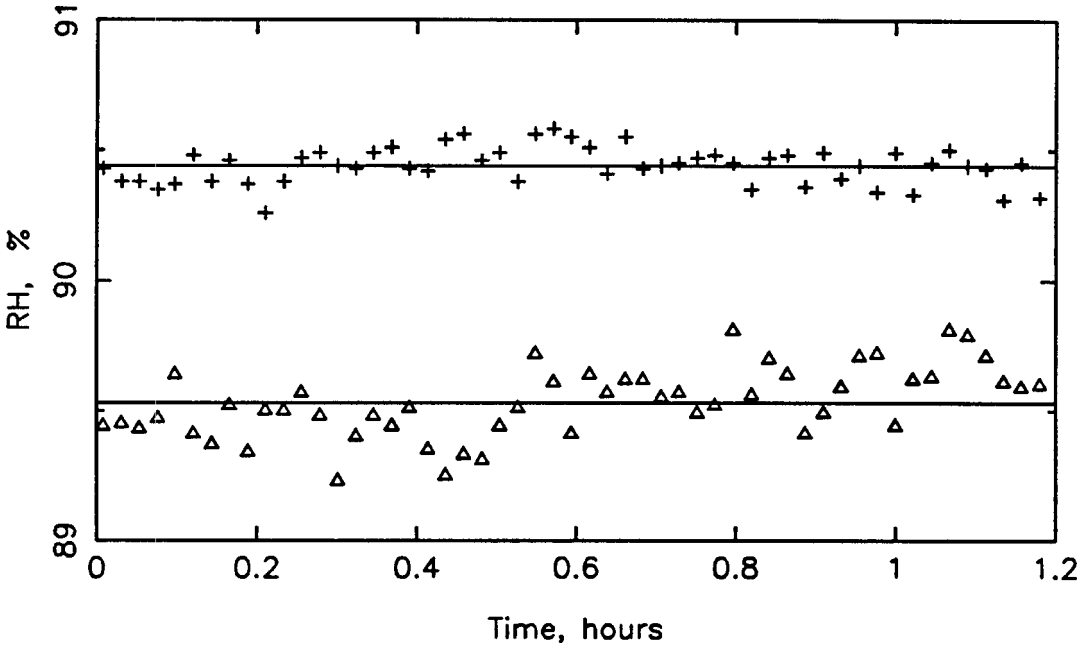

Figure F.18g Experiment 18: Effluent EMC2 and CSTR relative humidity.

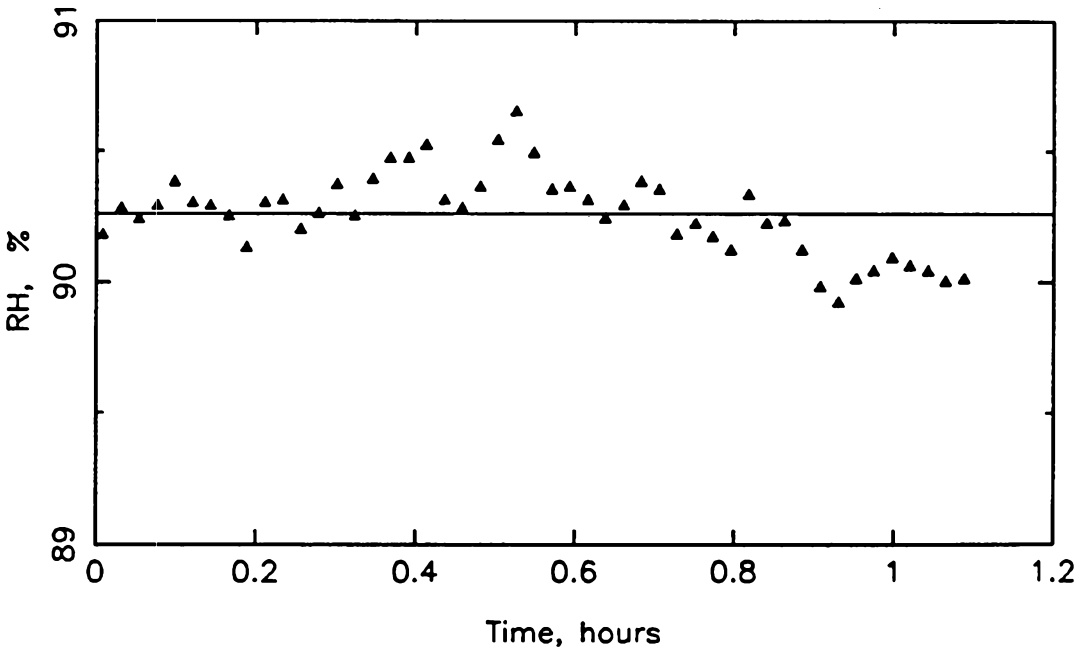

Figure F.18h Experiment 18: Feed EMC2 relative humidity.

APPENDIX G
COMPOSITION DATA GENERATED BY THE CSTR MODEL

The following plots represent the data obtained from the CSTR model runs. Since no rate expression is required to generate the salt, acid, H^+, and S(IV) concentrations and the total and effective ionic strengths, these data are unique only to the CSTR conditions specified when they were generated. The results are plotted as a function of x, the nondimensional particle diameter. For any feed diameter (x_f), the composition of a resulting effluent diameter (D_p) corresponds to the composition at x, where

$$D_p = D_{p,min} \left(\frac{D_{p,max}}{D_{p,min}} \right)^{x_f + x} .$$

However, once the various effluent distributions resulting from the set of monodisperse feeds are added to form the overall CSTR effluent distribution, the chemical composition of a given particle size is no longer unique. Data for Experiments 5, 8, 9, 10, 12, 13, 17, and 18 are presented in Figures G.1 through G.8, respectively.

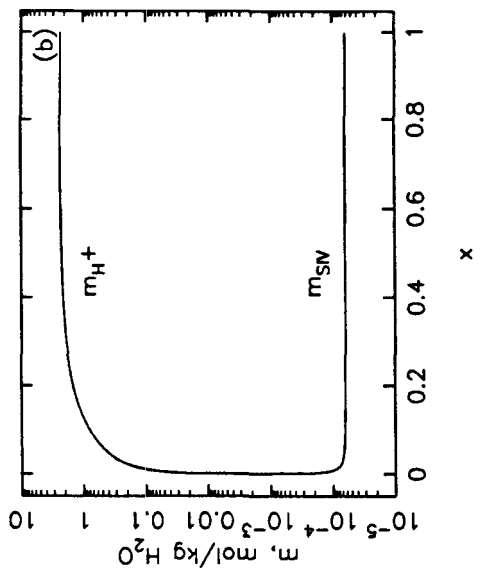

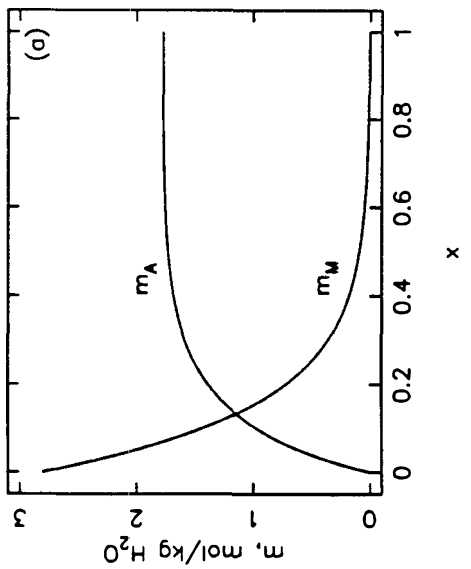

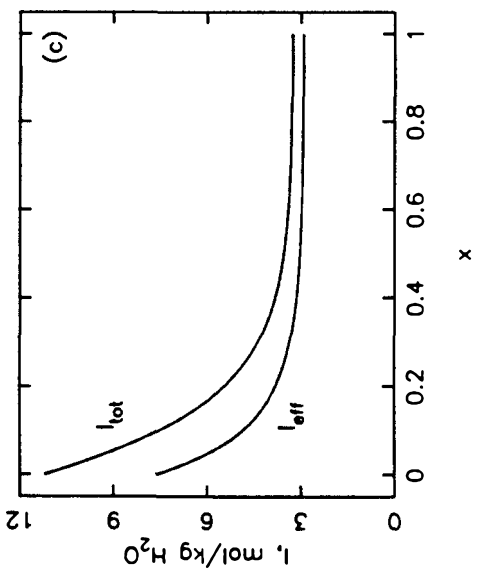

Figure G.1 Experiment 5: $MnSO_4$ aerosol at 50.2 ppm SO_2, T_{CSTR} = 23.62°C, RH_{CSTR} = 92.38% humidity. $D_{p,min} = 0.1$ μm and $D_{p,max} = 1.0$ μm.

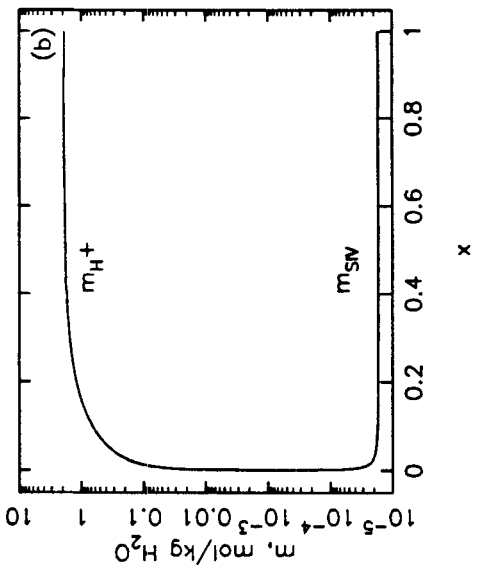

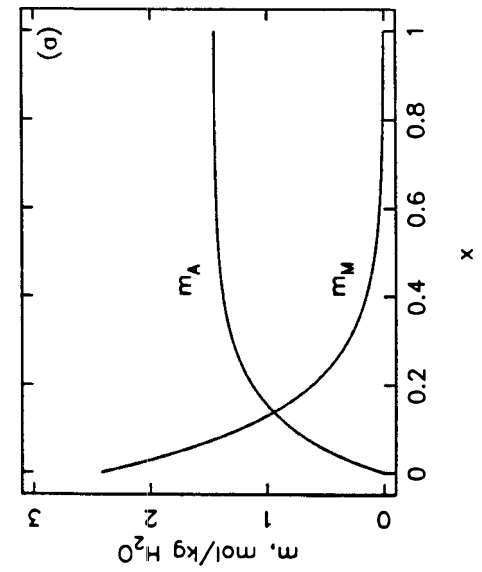

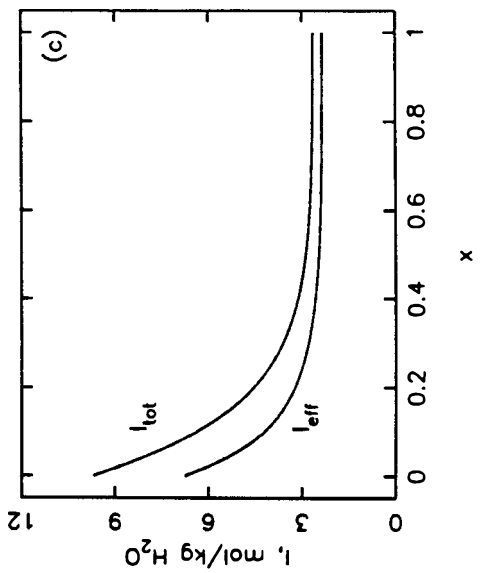

Figure G.2 Experiment 8: $MnSO_4$ aerosol at 13.5 ppm SO_2, T_{CSTR} = 23.62°C, RH_{CSTR} = 94.39% humidity. $D_{p,min}$ = 0.1 μm and $D_{p,max}$ = 1.0 μm.

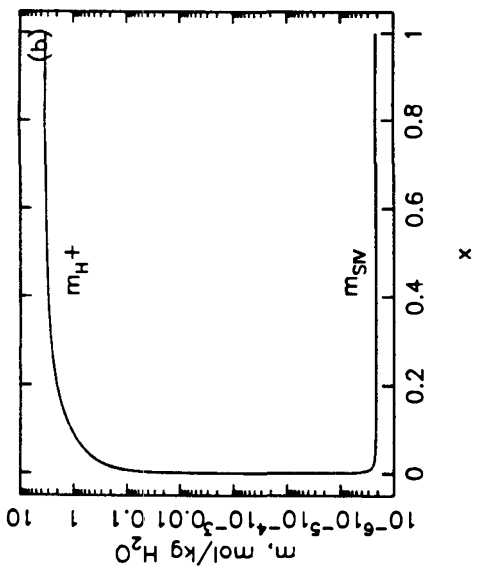

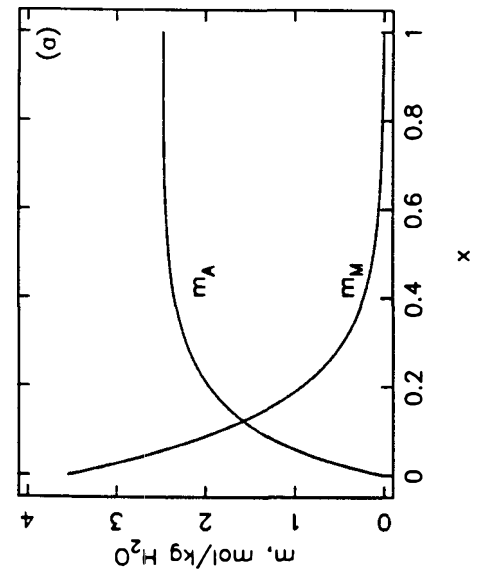

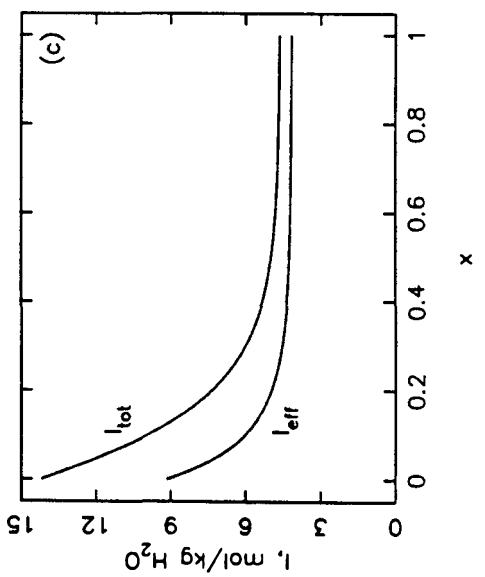

Figure G.3 Experiment 9: $MnSO_4$ aerosol at 1.74 ppm SO_2, T_{CSTR} = 23.24°C, RH_{CSTR} = 88.73% humidity. $D_{p,min} = 0.1$ μm and $D_{p,max} = 1.0$ μm.

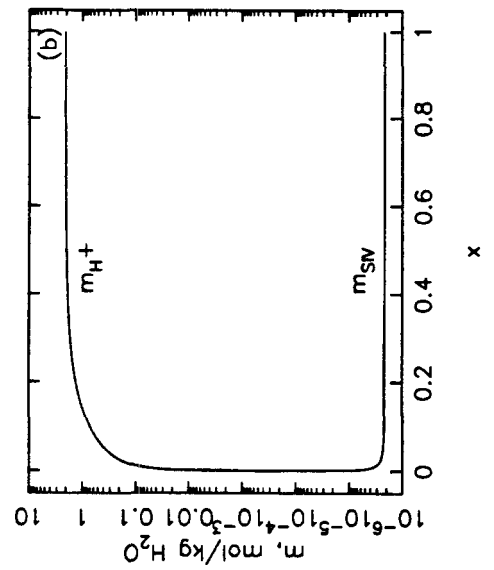

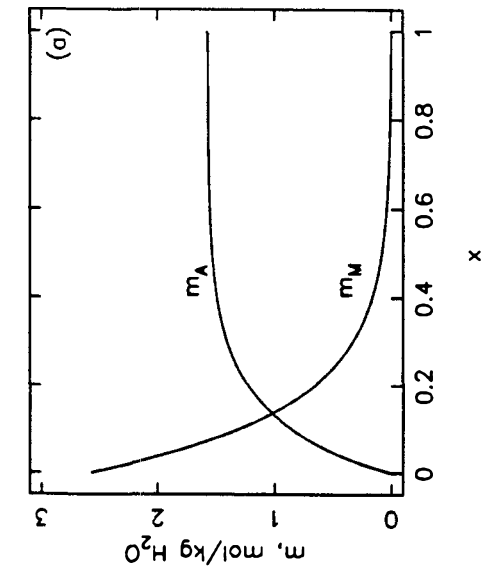

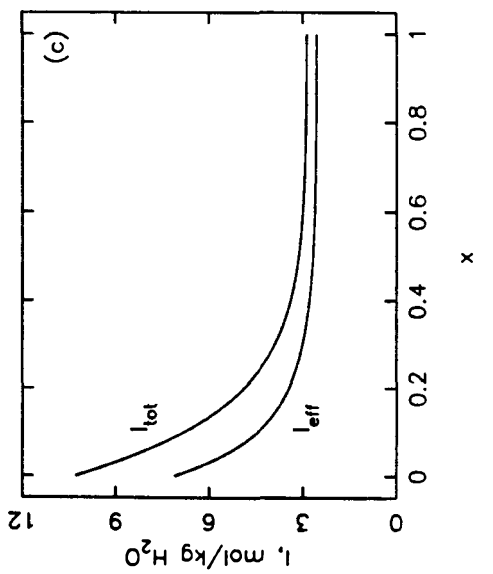

Figure G.4 Experiment 10: $MnSO_4$ aerosol at 1.72 ppm SO_2, T_{CSTR} = 23.99°C, RH_{CSTR} = 93.79% humidity. $D_{p,min} = 0.1$ μm and $D_{p,max} = 1.0$ μm.

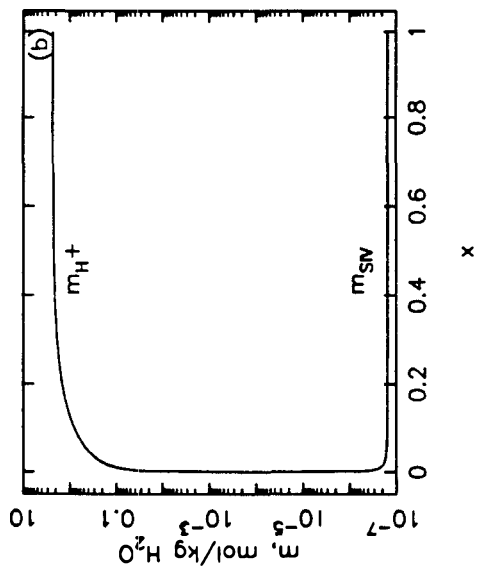

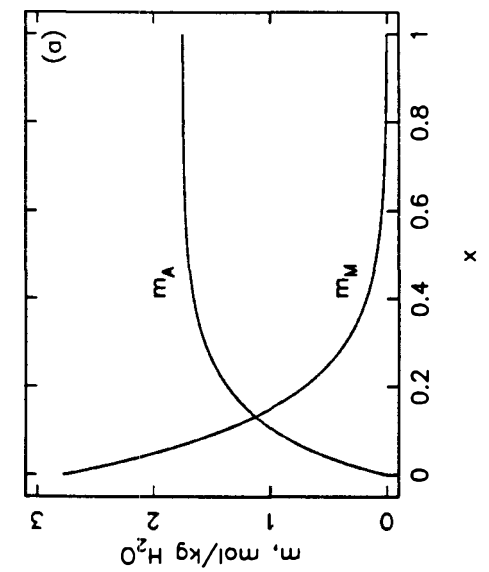

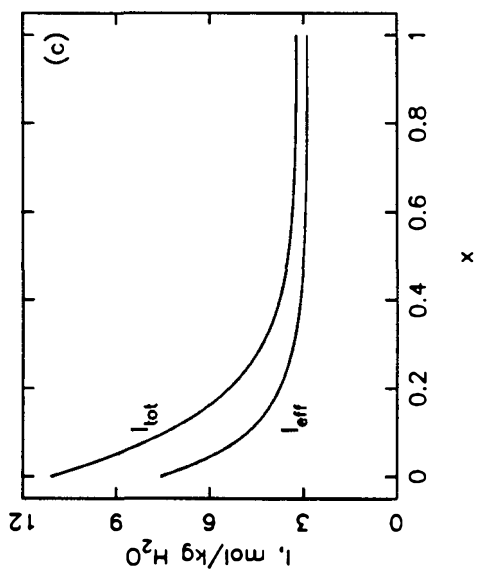

Figure G.5 Experiment 12: $MnSO_4$ aerosol at 0.122 ppm SO_2, T_{CSTR} = 23.90°C, RH_{CSTR} = 92.90% humidity. $D_{p,min} = 0.1$ μm and $D_{p,max} = 1.0$ μm.

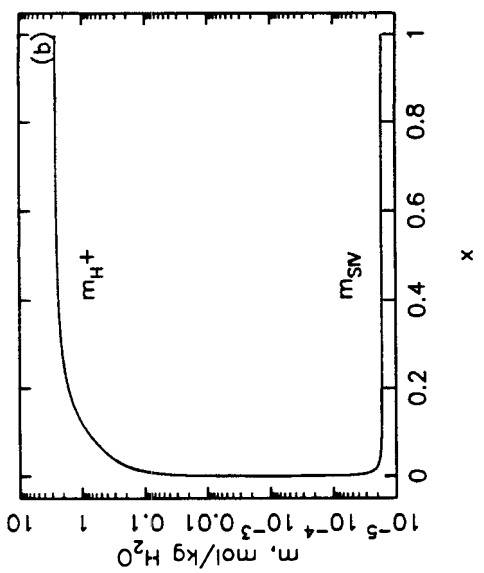

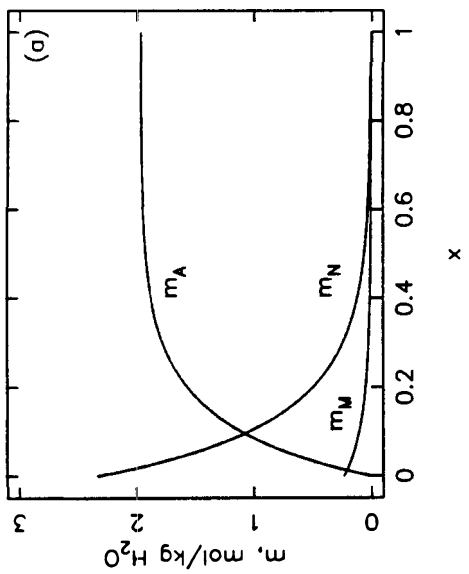

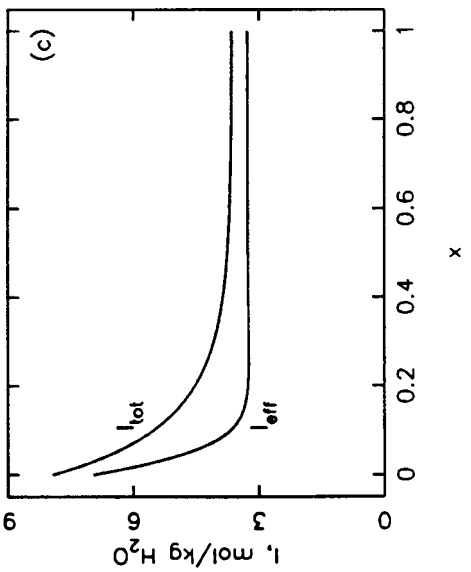

Figure G.6 Experiment 13: 0.10 moles $MnSO_4$/mole Na_2SO_4 aerosol at 13.4 ppm SO_2, $T_{CSTR} = 23.36°C$, $RH_{CSTR} = 91.72\%$ humidity. $D_{p,min} = 0.1$ μm and $D_{p,max} = 1.0$ μm.

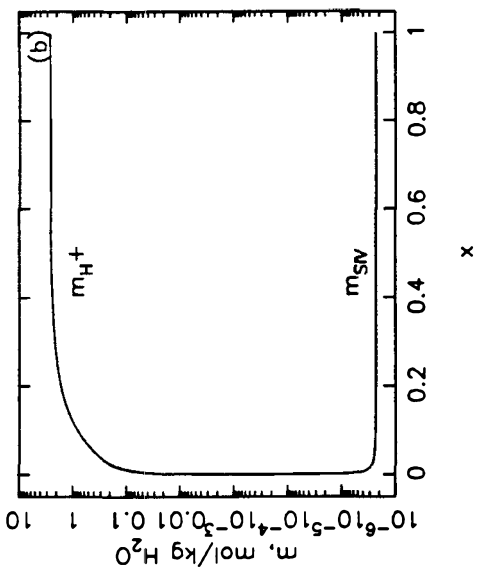

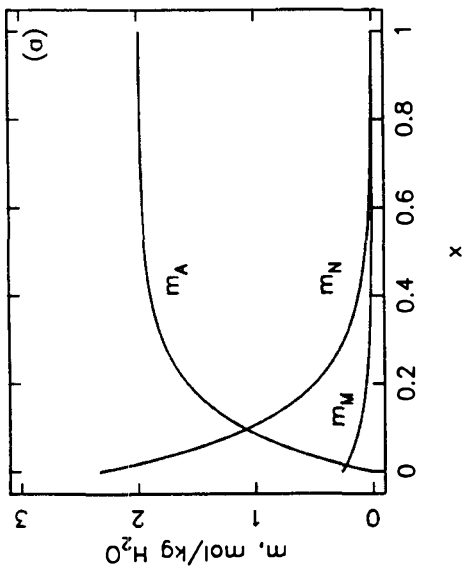

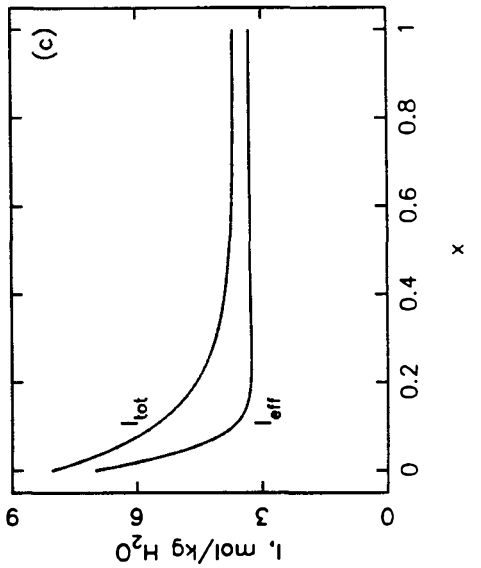

Figure G.7 Experiment 17: 0.11 moles $MnSO_4$/mole Na_2SO_4 aerosol at 1.85 ppm SO_2, $T_{CSTR} = 23.25°C$, $RH_{CSTR} = 91.63\%$ humidity. $D_{p,min} = 0.1$ μm and $D_{p,max} = 1.0$ μm.

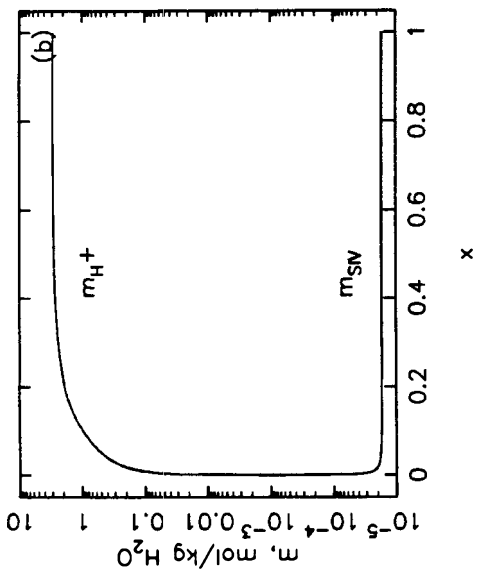

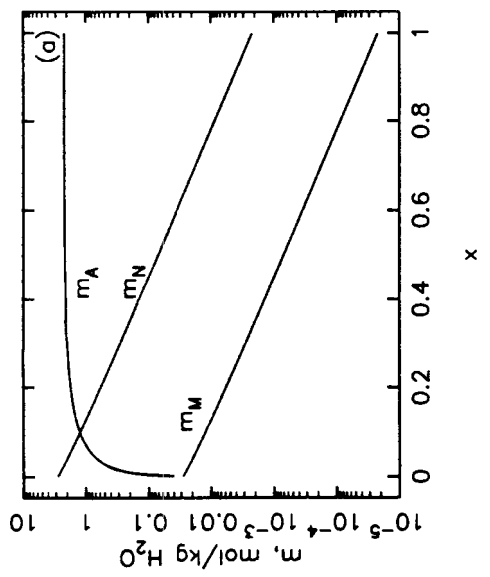

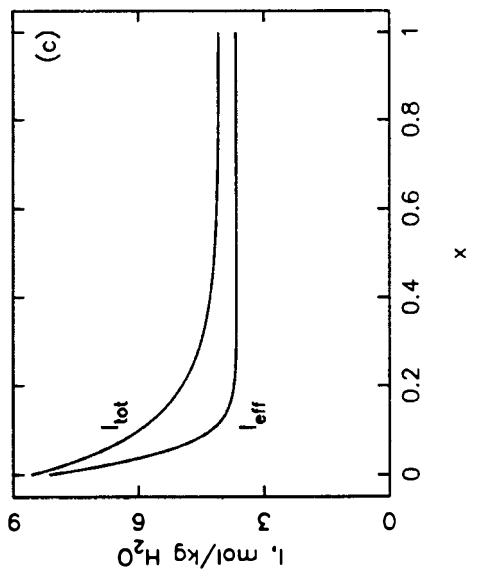

Figure G.8 Experiment 18: 0.01 moles $MnSO_4$/mole Na_2SO_4 aerosol at 13.6 ppm SO_2, $T_{CSTR} = 23.36°C$, $RH_{CSTR} = 90.44\%$ humidity. $D_{p,min} = 0.1$ μm and $D_{p,max} = 1.0$ μm.